Springer Series in Biomaterials Science and Engineering 15

Ning Lin
Juntao Tang
Alain Dufresne
Michael K. C. Tam *Editors*

Advanced Functional Materials from Nanopolysaccharides

Springer

Springer Series in Biomaterials Science and Engineering

Volume 15

Series Editor

Prof. Min Wang, Department of Mechanical Engineering
The University of Hong Kong, Pokfulam Road, Hong Kong
e-mail: memwang@hku.hk

Aims and Scope

The Springer Series in Biomaterials Science and Engineering addresses the manufacture, structure and properties, and applications of materials that are in contact with biological systems, temporarily or permanently. It deals with many aspects of modern biomaterials, from basic science to clinical applications, as well as host responses. It covers the whole spectrum of biomaterials—polymers, metals, glasses and ceramics, and composites/hybrids—and includes both biological materials (collagen, polysaccharides, biological apatites, etc.) and synthetic materials. The materials can be in different forms: single crystals, polycrystalline materials, particles, fibers/wires, coatings, non-porous materials, porous scaffolds, etc. New and developing areas of biomaterials, such as nano-biomaterials and diagnostic and therapeutic nanodevices, are also focuses in this series. Advanced analytical techniques that are applicable in R&D and theoretical methods and analyses for biomaterials are also important topics. Frontiers in nanomedicine, regenerative medicine and other rapidly advancing areas calling for great explorations are highly relevant.

The Springer Series in Biomaterials Science and Engineering aims to provide critical reviews of important subjects in the field, publish new discoveries and significant progresses that have been made in both biomaterials development and the advancement of principles, theories and designs, and report cutting-edge research and relevant technologies. The individual volumes in the series are thematic. The goal of each volume is to give readers a comprehensive overview of an area where new knowledge has been gained and insights made. Significant topics in the area are dealt with in good depth and future directions are predicted on the basis of current developments. As a collection, the series provides authoritative works to a wide audience in academia, the research community, and industry.

More information about this series at http://www.springer.com/series/10955

Ning Lin · Juntao Tang · Alain Dufresne ·
Michael K. C. Tam
Editors

Advanced Functional Materials from Nanopolysaccharides

Springer

Editors
Ning Lin
School of Chemistry, Chemical Engineering and Life Sciences
Wuhan University of Technology
Wuhan, Hubei, China

Juntao Tang
College of Chemistry and Chemical Engineering
Central South University
Changsha, Hunan, China

Alain Dufresne
Grenoble INP
Grenoble, France

Michael K. C. Tam
Department of Chemical Engineering
University of Waterloo
Waterloo, ON, Canada

ISSN 2195-0644 ISSN 2195-0652 (electronic)
Springer Series in Biomaterials Science and Engineering
ISBN 978-981-15-0912-4 ISBN 978-981-15-0913-1 (eBook)
https://doi.org/10.1007/978-981-15-0913-1

This Springer imprint is published by the registered company Springer Nature Singapore Pte Ltd.
The registered company address is: 152 Beach Road, #21-01/04 Gateway East, Singapore 189721, Singapore

Preface

Polysaccharide is a type of carbohydrate molecules composed of long polymeric chains with monosaccharide units as building blocks covalently bound together by glycosidic linkages. The typical polysaccharides in nature are cellulose, chitin, and starch, which commonly exist in the plants, animals, microorganisms, and bacteria. Derived from the strong intra- and inter-molecular hydrogen bonds, the crystalline and amorphous regions by the ordered arrangement and assembly of the linear and highly branched polymeric chains constitute the microstructures of these polysaccharides. Nanopolysaccharides can be produced by the partial or complete removal of amorphous regions, which is a kind of novel materials with the preservation of crystalline region and possesses the nanometer scale (<100 nm) at least one dimension. The typical nanopolysaccharides include the highly crystalline cellulose nanocrystal, chitin nanocrystal, and starch nanocrystal, together with the semi-flexible cellulose nanofibril and chitin nanofibril. As the nanoscaled aggregates of natural polymers, these nanopolysaccharides exhibit numerous advantages in comparison with conventional inorganic and metal nanoparticles, for instance, renewability, low toxicity, biodegradability, biocompatibility, high mechanical modulus but low density, high specific area and surface activity, morphological regulation, etc. Since the first report by Dr. Alain Dufresne on the use of cellulose nanocrystal as the rigid filler to enhance the mechanical property of rubber-based composite, the application of nanopolysaccharides in materials science has attracted a surging number of researchers in this field. With the continuous attempt during last thirty years, the functional materials based on nanopolysaccharides were rapidly developed, involving the exploration of their novel properties and additional added values in diverse applications taking the special functions but not only mechanical enhancement. Focusing on the nanocellulose, nanochitin, and nanostarch, this monograph is the summarization and discussion on the functional materials from these three nanopolysaccharides covering the studies in recent ten years on this topic.

The structural framework of this monograph is organized according to the specific functional applications of nanopolysaccharides with 12 chapters. In each chapter, the strategy of constructing the functional system and the critical concerns

of the functional materials (for instance, the functional mechanism) are summarized and commented on the basis of the reported studies, which are expected to be an inspiration or reference to the readers for their work. The potential functions and applications of a nanomaterial firstly depend on its intrinsic properties, and therefore, Chap. 1 introduces the different preparation routes and main properties of nanocellulose, nanochitin, and nanostarch. The influence of preparation and treatment on the properties of obtained nanopolysaccharides is also discussed in this chapter, which is an important issue for their applications. Chapter 2 covers the surface modification with functional molecules on nanopolysaccharides, involving the surface grafting of selective functional molecules as antibacterial, fluorescent, stimuli-responsive, superhydrophobic molecules, and modifications on drug delivery. Rod-like cellulose nanocrystals and chitin nanocrystals can form the chiral nematic liquid crystal phase in suspensions, which can be preserved in the self-assembly solid materials (films) exhibiting the colorful optical behaviors by the reflective wavelengths to the light. The development of optical materials based on two polysaccharide nanocrystals is an attracting functional application in the structural color field, and the color controlling strategy, structural design, regulating approach, and mechanism explanation on this topic are introduced in Chap. 3. As the nanomaterials from sustainable resources, the energy material-based nanopolysaccharides received much attention with the purpose of replacing conventional synthetic materials, and Chap. 4 focuses on the preparation and application of nanopolysaccharide-based energy storage materials including the dielectric capacitor, supercapacitor and battery. Chapter 5 summarizes the development of nanopolysaccharides in the fields of biomedical applications, served as the biocompatible and non-toxic nanomaterials in the construction systems of drug release and gene delivery, bioimage, biosensor, and biocatalyst, tissue engineering, and bioscaffold. Pickering emulsions stabilized by nanopolysaccharides have drawn increased attentions as they possess the enhanced stability, biocompatibility, and environmental friendliness over traditional surfactant-stabilized emulsions. Chapter 6 offers an overview of Pickering emulsions stabilized by pristine and modified nanopolysaccharides on the definition, instability mechanism, and potential applications.

In view of the resources and environmental concerns, Chap. 7 discusses the binding efficiency of pollutants in nanopolysaccharides, providing the overview of pristine, surface-functionalized nanopolysaccharides, and nanocomposites for applications in removal heavy metal ions, dyes, organic molecules, and toxic gas in various wastewater treatment and gas adsorption processes. The highly crystalline and rigid nanopolysaccharides are the promising additives in the coating applications, for instance, the effect on the barrier, anti-corrosion, UV shielding, scratch-resistant, which are described in Chap. 8. From another point of view, Chap. 9 emphasizes the nanopolysaccharides as barrier components or layers in the packaging composites, discussing the selection and match of the specific nanopolysaccharide with matrix, processing and construction of barrier system, as well as characterization and mechanism of water vapor/oxygen permeability and barrier. Some recent studies reported the introduction of nanopolysaccharides as

functional additives to improve the special properties of materials, which are summarized in Chap. 10 as food, construction and ceramics, and adhesive additives. Besides the academic interests discussed by the previous ten chapters, the high-value applications for reported trial and commercial products on nanocellulose are covered by Chap. 11 with the classification of various reported products by the functions of nanocellulose. The last Chap. 12 makes the conclusion on the functional applications of nanopolysaccharides and proposes the challenges and likely future trends on this topic.

As the ancient but ageless materials, nanopolysaccharides received an incredible enthusiasm and attention from the researchers throughout the world. During last ten years, the functional materials based on nanopolysaccharides have generated an exceptional appeal, and the publications on this topic continued to grow exponentially. Because of the length limitation of monograph, we can only select the latest and classic studies for the description, but the list is far from being complete. I would like to deeply thank all the contributors, and this monograph would not be possible without their intensive and dedicated work.

Wuhan, China
August 2019

Ning Lin

Contents

Editors and Contributors

About the Editors

Dr. Ning Lin is Associate Professor at School of Chemistry, Chemical Engineering and Life Sciences, Wuhan University of Technology, China, where he received his B.S. and M.S. in 2007 and 2011, respectively. Prof. Lin received his Ph.D. in 2014 at the International School of Paper, Print Media and Biomaterials (Pagora) at University Grenoble Alpes in France, and was awarded the State Scholarship Fund by Chinese Scholarship Council (CSC) for his Ph.D. studies. He then completed one-year postdoctoral research. He has more than 30 scientific publications, 3 co-authored book, and 7 patents with H-index 21. Prof. Lin's research interests include chemical modification, design and development of biomass-based nanopolysaccharides (nanocellulose, nanochitin, starch nanocrystals), and functional applications.

Dr. Juntao Tang is Associate Professor at the College of Chemistry and Chemical Engineering at Central South University, China. He received his Ph.D. in Chemical Engineering under the guidance of Prof. Michael Tam at the University of Waterloo, Canada, in 2016 and completed one-year's postdoctoral research. He received the Chinese Government Award for outstanding students abroad in 2015. Prof. Tang has more than 30 journal articles and 2 patents in the fields of colloids and polymer science. His current research interests involve designing and developing functional nanomaterials derived from sustainable resources for advanced applications.

Dr. Alain Dufresne received his Ph.D. in 1991 from INSA Toulouse (Electronics) and was a postdoctoral researcher at Polytechnique Montreal, and a lecturer at INSA Lyon. He was appointed as Associate Professor at Grenoble University in 1993, and then as Professor in 2001. He has been Professor at Grenoble INP since 2003. He was Visiting Professor at UFRJ and Embrapa Fortaleza (Brazil), and UKM (Malaysia). His research interests include the processing and characterization

of renewable nanocomposites. He has published more than 280 peer-reviewed papers. Prof. Dufresne received the 2016 International Nanotechnology Division Award and FiberLean® Technologies Prize awarded by TAPPI and is in the 2016 top 300 most-cited researchers in materials science and engineering/Elsevier Scopus Data. He is also a member of the editorial board of Carbohydrate Polymers, ACS Sustainable Chemistry and Engineering, Fibers, Materials Research, the Ibero-American Journal of Materials and the Journal of Korean Wood Science and Technology, as well as an associate editor of Polimeros: Ciencia e Tecnologia.

Dr. Michael K. C. Tam obtained his B.Eng. and Ph.D. in Chemical Engineering from Monash University, Australia, in 1982 and 1991, respectively. He spent 18 months as a postdoctoral fellow at the Department of Chemical Engineering, McMaster University Canada, and subsequently taught at Nanyang Technological University, Singapore, for 15 years. In June 2007, he joined the Department of Chemical Engineering, University of Waterloo, as a tenured Full Professor, and holds the position of University Research Chair in the field of functional colloids and sustainable nanomaterials. He is an active member of the Waterloo Institute for Nanotechnology. Prof. Tam's research interests include sustainable nanomaterials, colloids, self-assembly systems, polymer–surfactant interactions, and controlled delivery systems. He has published more than 300 journal articles in various fields of polymer science and engineering. His total citations exceed 13,500, and his H-index is 62. He is also an associate editor of ACS Sustainable Chemistry and Engineering.

Contributors

Jianxiang Chen Department of Materials Engineering, Jiangsu University of Technology, Changzhou, Jiangsu, China

Ziyang Chen School of Chemistry, Chemical Engineering and Life Sciences, Wuhan University of Technology, Wuhan, People's Republic of China

Alain Dufresne Grenoble INP, Grenoble Alpes University, Grenoble, France

Ekrem Durmaz Department of Forest Biomaterials, College of Natural Resources, North Carolina State University, Raleigh, NC, USA;
Faculty of Forestry, Kastamonu University, Kastamonu, Turkey

Martin A. Hubbe Department of Forest Biomaterials, College of Natural Resources, North Carolina State University, Raleigh, NC, USA

Muhammad Shahidul Islam Department of Chemical Engineering, Waterloo Institute for Nanotechnology, University of Waterloo, Waterloo, ON, Canada

Feng Jiang Sustainable Functional Biomaterials Laboratory, Department of Wood Science, University of British Columbia, Vancouver, BC, Canada

Kulang Primo Sokiri Kiliona School of Chemistry, Chemical Engineering and Life Sciences, Wuhan University of Technology, Wuhan, People's Republic of China

Daesung Kim Department of Chemical Engineering, Waterloo Institute for Nanotechnology, University of Waterloo, Waterloo, ON, Canada

Nathalie Lavoine Department of Forest Biomaterials, College of Natural Resources, North Carolina State University, Raleigh, NC, USA

Ning Lin School of Chemistry, Chemical Engineering and Life Sciences, Wuhan University of Technology, Wuhan, People's Republic of China

Yan Liu School of Materials Science and Engineering, Wuhan University of Technology, Wuhan, People's Republic of China

Aban Lwal John Lwal School of Chemistry, Chemical Engineering and Life Sciences, Wuhan University of Technology, Wuhan, People's Republic of China

Hale Oguzlu Sustainable Functional Biomaterials Laboratory, Department of Wood Science, University of British Columbia, Vancouver, BC, Canada

Lokendra Pal Department of Forest Biomaterials, College of Natural Resources, North Carolina State University, Raleigh, NC, USA

Chunyue Pan College of Chemistry and Chemical Engineering, Central South University, Changsha, Hunan, People's Republic of China

Zhuqun Shi School of Chemistry, Chemical Engineering and Life Sciences, Wuhan University of Technology, Wuhan, People's Republic of China

Michael K. C. Tam Department of Chemical Engineering, Waterloo Institute for Nanotechnology, University of Waterloo, Waterloo, ON, Canada

Chuang Tang Department of Materials Engineering, Jiangsu University of Technology, Changzhou, Jiangsu, China

Juntao Tang College of Chemistry and Chemical Engineering, Central South University, Changsha, Hunan, People's Republic of China;
College of Chemistry and Chemical Engineering, Central South University, Changsha, China

Han Tao School of Chemistry, Chemical Engineering and Life Sciences, Wuhan University of Technology, Wuhan, People's Republic of China

Ramakrishna Trovagunta Department of Forest Biomaterials, College of Natural Resources, North Carolina State University, Raleigh, NC, USA

Preeti Tyagi Department of Forest Biomaterials, College of Natural Resources, North Carolina State University, Raleigh, NC, USA

Jinyu Wang School of Materials Science and Engineering, Wuhan University of Technology, Wuhan, People's Republic of China

Sunan Wang School of Chemistry, Chemical Engineering and Life Sciences, Wuhan University of Technology, Wuhan, People's Republic of China

Yuxia Wang School of Chemistry, Chemical Engineering and Life Sciences, Wuhan University of Technology, Wuhan, People's Republic of China

Bolang Wu School of Chemistry, Chemical Engineering and Life Sciences, Wuhan University of Technology, Wuhan, People's Republic of China

Defeng Wu Department of Chemistry and Chemical Engineering, Yangzhou University, Yangzhou, Jiangsu, China

Chuanxi Xiong School of Materials Science and Engineering, Wuhan University of Technology, Wuhan, People's Republic of China

Quanling Yang School of Materials Science and Engineering, Wuhan University of Technology, Wuhan, People's Republic of China

Guipeng Yu College of Chemistry and Chemical Engineering, Central South University, Changsha, Hunan, People's Republic of China

Wenchao Yu School of Materials Science and Engineering, Wuhan University of Technology, Wuhan, People's Republic of China

Yang Zhan School of Materials Science and Engineering, Wuhan University of Technology, Wuhan, People's Republic of China

Chenggang Zhang School of Materials Science and Engineering, Wuhan University of Technology, Wuhan, People's Republic of China

Zhen Zhang SCNU-TUE Joint Lab of Device Integrated Responsive Materials (DIRM), National Center for International Research on Green Optoelectronics, South China Normal University, Guangzhou, People's Republic of China

Ge Zhu Grenoble INP, Grenoble Alpes University, Grenoble, France

Abbreviations

13C-NMR	Solid-state ^{13}Carbon nuclear magnetic resonance
1D	One-dimensional
2D	Two-dimensional
2-HEA	2-hydroxyethyl acrylate
3D	Three-dimensional
5CB	4-cyano-4'-pentylbiphenyl
5-FC	5-fluorocytosine
5-FU	5-Fluorouracil
6-MP	6-mercaptopurine
8CB	4-cyano-4'-octylbiphenyl
AAc	Acrylic acid
AAm	Acrylamide
AANI	4-((2-aminoethyl)amino)-9-methyl-1,8-naphthalimide
AC	Activated carbon
ACFs	Activated carbon fibers
ADSCs	Human adipose-derived mesenchymal stem cells
AEOC	Acrylated epoxidized soybean oil
AFM	Atomic force microscopy
AgNP	Silver nanoparticles
AGU	Anhydro-D-glucopyranose unit
AHPC	Ant-derived hierarchical porous carbon
AKD	Alkyl ketene dimer
Aln	Sodium alendronate
ALP	Alkaline phosphatase
AL-PEG-NH_2	Alkaline lignin-aminated polyethylene glycol
AL-PEG-NPs	Alkaline lignin-aminated polyethylene glycol nanoparticles
AMEO	Aminopropyl triethoxysilane
AMIMBr	1-allyl-3-methylimidazolium bromide
AminCl	1-allyl-3-methylimidazolium chloride
AMNPs	CS on Fe_3O_4 magnetic nanoparticles

ApA	Aminopropyl phosphoric acid
APIs	Active pharmaceutical ingredients
APMS	Aminopropyl trimethoxysilane
APS	Ammonium persulfate
APTS	3-(2-Aminoethylamino)propyltrimethoxysilane
ASC	Asymmetric supercapacitor
ATRP	Atom transfer radical polymerization
AuNC	Gold nanoclusters
AuNP	Gold nanoparticle
AWC	Activated wood carbon
B/N-CS	B/N co-doped carbon nanosheets
BA	Butyl acrylate
BC	Bacterial cellulose
BC-NH_2	Bacterial cellulose nanostructured membranes
BDC	1,4-benzenedicarboxylic acid
BG	Bioactive glass
BiB	2-bromoisobutyryl bromide
BIBA	α-bromoisobutyric acid
BMA	Butyl methacrylate
BmimCl	1-butyl-3-methylimidazolium chloride
BN	Boron nitride
BNC	Bacterial nanocelluloses
BNNS	Boron nitride nanosheets
BOPP	Biaxially oriented polypropylene
BSA	Bovine serum albumin
BTMSE	1,2-bis(trimethoxysilyl)ethane
BTNF	$BaTiO_3$ nanofibers
BTNP	$BaTiO_3$ nanoparticles
CA	Cellulose acetate
CAC	Coconut shell activated carbon
$CaCO_3$	Calcium carbonate
CAP	Cellulose acetate phthalate
CB	Bacterial cellulose
CBA	Cystamine bisacrylamide
CD	Carbon dots
CD/5-FC	Cytosine deaminase/5-fluorocytosine
β-CD	β-cyclodextrin
CED	Cupriethylene diamine
CFBs	Hydrogel/nanofibrin composite bandage
CHA	Carbonated hydroxyapatite
CHHPC	Corn husk-derived hierarchical porous carbons
ChNC(s)	Chitin nanocrystal(s)
ChNF	Chitin nanofibers
ChNF(s)	Chitin nanofibril(s)
ChNM	Chitin nanomaterials

CHPTAC	3-chloro-2-hydroxypropyltrimethylammonium chloride
CHX	Chlorhexidine digluconate
CI	Crystallinity index
$ClSO_3H$	Chlorosulfonic acid
CLTOCN/BNNS	Cross-linked TOCN/BNNS
CMB	Carbon microtube bundles
CMC	Carboxymethyl cellulose
CNC(s)	Cellulose nanocrystal(s)
CNC@PR	Cellulose nanocrystal@polyrhodanine
CNF(s)	Cellulose nanofibril(s)
CNFF	Carbon nanofibrous framework
CNGs	Chitin nanogels
CNMs	Cellulose nanomaterials
CNS	Carbon nanosheets
CNTs	Carbon nanotubes
CNWs	CS and chitin nanowhiskers
CO	Carbon monoxide
Co-AF	Co-alginate fibers
CP	Cross-polarization
CPC	CNF-PE-CNF
CQDs	Carbon quantum dots
CRL	Candida rugosa lipase
CS	Chitosan
CSos	Chitosan oligosaccharide
CTA	3-chloro-2-hydroxypropyltrimethylammonium chloride
CTAB	Cetyltrimethylammonium bromide
Cur	Curcumin
CWX	Cellulose (nano)whiskers
DAMO	N-[3-Trimethoxysilylpropyl]ethylenediamine
DAMS	2-aminoethyl 3-aminopropyl trimethoxysilane
DANFC	2,3-dialdehyde nanofibrillated cellulose
DCC	Dicarboxylic acid nanocellulose
DCNC	Dialdehyde nanocellulose
DDS	Drug delivery systems
DES	Deep eutectic solvents
DLC	Drug loading content
DLE	Drug loading efficiency
DLS	Dynamic light scattering
DMAB	Didecyldimethylammonium bromide
DMDHEU	Dimethyloldihydroxyethylene urea
DMF	N,N-Dimethylformamide
DODA	Dimethyldioctadecylammonium
DOX	Doxorubicin
DP	Degree of polymerization
DTAF	5-(4,6-dichlorotriazinyl) aminofluorescein

DTMOS	Dodecyltrimethoxysilane
DuR-BNGs	Dual temperature/acidic pH-responsive bionanogels
EA	Ethyl acrylate
EANI	4-ethoxy-9-allyl-1,8-naphthalimide
EC	Ethyl cellulose
ECH	Epichlorohydrin
ECM	Extracellular matrix
ECNC	Electrosterically stabilized CNC
ECPs	Electronically conducting polymers
EDAC	1-ethyl-3-[3-dimethylaminopropyl]carbodiimide hydrochloride
EDC	N-(3-dimethylaminopropyl)-N'-ethyl-carbodiimide hydrochloride
EDLC	Electrical double-layer capacitors
EGUPy	Copolymers of poly(oligoethylene glycol methacrylate) and methacrylate derivative with 2-ureido-4-pyrimidinone groups
ElPs	Elastin-like polypeptides
EPR	Enhanced permeability and retention
EPTMAC	Epoxypropyltrimethylammonium chloride
ESC(s)	Electrospun-cellulose nanofiber(s)
FA	Folic acid
FITC	Fluorescein isothiocyanate
FITC-DEX	Fluorescein isothiocyanate-dextran
FMOC	Glycidyl-fluorenylmethyloxycarbonyl
FOTS	Trichlorosilane surfactant with fluorinated alkyl
F-PBZ/SiO_2	Bifunctional fluorinated polybenzoxazine and SiO_2 NP
FS	1H,1H,2H,2H-perfluorooctyltriethoxysilane
FTIC-BSA	Bovine serum albumin-fluorescein isothiocyanate conjugate
GA	Gum Arabic
GMA	Glycidyl methacrylate
GNP	Gold nanoparticle
GNR	Gold nanorod
GO	Graphene oxide
GON	Graphene oxide nanosheet
GOx	Glucose oxidase
β-GP	β-glycerophosphate
g-PLA	Grafted PLA
GQD	Graphene quantum dots
GSH	Glutathione
GTMAC	Glycidyltrimethylammonium chloride
H_2SO_4	Sulfuric acid
H_3PO_4	Phosphoric acid
HA	Hyaluronic acid
HaCat	Human immortalized keratinocyte
hASC	Human adipose stem cells

HAT	Hydroxyapatite
hBMSC	Human bone marrow stromal cells
HCHO	Formaldehyde
HCl	Hypochlorite acid
HCM	Hierarchically porous carbon microsphere
HDA	Hexamethylenediamine
HDTMA	Hexadecyltrimethylammonium bromide
HEA	2-hydroxyethyl acrylate
HEA-TDI	2-hydroxyethyl acrylate tolylene-2,4-diisocyanate
HEC	Hydroxyethyl cellulose
HEMA	2-hydroxyethyl methacrylate
HepG2	Human hepatoma carcinoma cells
HFBII	Class II hydrophobin protein
HFD	Heart functional diseases
HIPE	High internal phase Pickering emulsion
HIV	Human immunodeficiency virus
HLB	Hydrophilic-lipophilic balance
HLPC	Honeycomb-like porous carbon
HMC	Human hair-derived micro/mesoporous carbon
HMssEt	Pendant disulfide linkage
HNE	Human neutrophil elastase
HOBC	4'-(hexyloxy)-4-biphenylcarbonitrile
HPAM	Hydrolyzed polyacrylamide
HPC	Hierarchical porous carbon
HPE	Hierarchical polymer electrolyte
HPMC	Hydroxypropyl methylcellulose
HPMCP	Hydroxypropyl methylcellulose phthalate
HPN-CS	Hierarchically porous nitrogen-doped carbon nanosheet
I_1, I_2	Isotropic phase
IBU	Ibuprofen
IC50	Half-maximal inhibitory concentration
IMI	Imipramine hydrochloride
INDO	Indomethacin
IPN	Interpenetrating polymer network
IPSCs	Induced pluripotent stem cells
KETO	Ketoprofen
KPS	Potassium persulfate
L/D	Aspect ratio
LB	Langmuir–Blodgett
LBL	Layer by layer
LCMNs	Lipase-immobilized CS-cross-linked magnetic nanoparticles
LCP/RCP	Left/right-hand circularly polarized
LCST	Lower critical solution temperature
LH	Levamisole hydrochloride
LIB	Lithium-ion battery

LNP	Latex nanoparticle
LNPs	Lignin nanoparticles
LODP	Leveling-off DP
LRBED	Lissamine rhodamine B ethylenediamine
LRV	log10 reduction value
LS	Langmuir–Schaefer
Ly	Lysozyme
MA	Microcystis aeruginosa
MAA	Methacrylic acid
MACMC	Methacrylated carboxymethyl cellulose
MAH	Maleic anhydride
MAS	Magic angle spinning
MB	Methylene Blue
MBA	N,N'-methylenebisacrylamide
MC	Methyl cellulose
MCC	Microcrystalline cellulose
MCF-7	Human breast cancer cells
MDR	Multidrug resistant
MEC	Minimum effective concentration
MF	Microfiltration
MFC	Microfibrillated cellulose
MG63	Human osteosarcoma cells
MMT	Biofunctionalized montmorillonite
MR	Mauran
MRSA	Methicillin-resistant S. aureus
MTCS	Methyltrichlorosilane
MTES	Methyltriethoxysilane
MTX	Methotrexate
M_w	Molecular weight
MWCNT	Multi-walled carbon nanotube
MWCO	Molecular weight cut-off
m-WS	Mesoporous wollastonite
MZ	Quercetin, metronidazole
NA	Cotton-based nanocellulosic aerogels
NaCl	Sodium chloride
NaClO	Sodium hypochlorite
NAD	Nadolo
NaOH	Sodium hydroxide
NAP	Naproxen
NCC	Nanocrystals of cellulose
NCh	Nanochitin
n_e	Extraordinary optical index
NF	Nanofiltration
NFC	Nanofibrillated cellulose
NG	Nanotubular cellulose

nGO	Nanographene oxide
NGs	Nanogels
n-HA	Nanohydroxyapatite
-$NHCOCH_3$	Acetamide groups
NHS	N-hydroxysuccinimide
NIPAm	N-isopropylacrylamide
NMMT	Montmorillonite
NNC	New Natura Concept
n_o	Ordinary optical index
NOx	Nitrogen oxides
NPs	Nanopolysaccharides
NPS-NPs	Nanopolysaccharide-based nanoparticles
NS	Nanostarches
ODDMAC	Octadecyldimethyl(3-trimethoxysilylpropyl)ammonium chloride
OECD	Organisation for Economic Co-operation and Development
OEOMA	Oligo(ethylene oxide)
OSi	Organosilica
OSO_3^-	Sulfate half-ester groups
OTR	Oxygen transmission rate
P(MVE-MA)	Poly(methyl vinyl ether-alt-maleic anhydride)
PA	Phloretic acid
PAAc	Polyacrylic acid
PAAc	Poly(acrylic acid)
PAAm	Polyacrylamide
PAAS	Anionic sodium polyacrylate
PAH	Poly(allylamine hydrochloride)
PAHA	Polyhydroxyamines
PAHCl	Papaverine hydrochloride
PAM	Polyacrylamide
PAMAM	Poly(amidoamine)
PAN	Polyacrylonitrile
PANI	Polyaniline
PAni	Pectin coated on polyaniline
PBA	Poly(n-butyl acrylate)
PBAT	Poly(butylene adipate-co-terephthalate)
PBuA-MAEA LNP	Poly[butyl acrylate-co-2-(methacryloyloxy)-ethyl acetoacetate] latex nanoparticle
PC	Polycarbonate
PCC	Precipitated calcium carbonate
PCL	Polycaprolactone
PCS	Porous carbon sheets
pDADMAC	Poly(diallyldimethylammonium chloride)
PDDA	Poly(diallyldimethylammonium chloride)
PDDA-CNC	Poly(diallyldimethylammonium chloride)

PDDC-HD	Poly(dodecanediol-co-citrate)
PDEAEMA	poly(diethylaminoethyl methacrylate)
PDEGMA	Poly(di-(ethylene glycol) methyl ether methacrylate)
PDMAEMA	Poly(2-(dimethylamino)ethyl methacrylate)
PDMAPM	Poly(dimethylaminopropyl methacrylamide)
PDMC	Poly(2-methacryloyloxyethyl) trimethyl ammonium chloride
PDMS	Polydimethylsiloxane
pDNA	Plasmid DNA
PE	Polyethylene
PEC	Polyelectrolyte complexes
PEDOT:PSS	Poly(3,4-ethylenedioxythiophene): poly(styrenesulfonate)
PEEP	Poly(ethyl ethylene phosphate)
PEG	Poly(ethylene glycol)
PEGDMA	Poly-(ethylene glycol) dimethacrylate
PEGMa	Polyethylene glycolmethacrylate
PEI	Polyethylenimine
PEIs	Polyethyleneimines
PEM	Polymer electrolyte membrane
PEMA LNP	Poly(ethyl methacrylate) latex nanoparticle
PEMA150 LNP	Poly(ethyl methacrylate) latex nanoparticle with diameter of $\sim$150 nm
PEMA50 LNP	Poly(ethyl methacrylate) latex nanoparticle with diameter of $\sim$50 nm
PEO	Poly(ethylene oxide)
PepNA	Nanocellulosic aerogels modified with fluorescent tripeptide
PES	Polyethersulfone
PET	Poly(ethylene terephthalate)
PF	Phenol-formaldehyde
PFTS	1H, 1H, 2H, 2H-Perfluorooctyltriethoxysilane
PG	Polyglycerol
PGA	Polyglycolide
PGCMT	Porous graphitic carbon microtube
PGM	Poly(glycidyl methacrylate)
PGMA	Poly(glycidyl methacrylate)
PHB	Polyhydroxybutyrate
PHEA	Poly(2-hydroxyethyl acrylate)
PHEMA	Poly(2-hydroxyethyl methacrylate)
PHFBA	Poly(2,2,3,4,4,4-Hexafluorobutyl acrylate)
PLA	Polylactide
PLA/CHT	Polylactic acid-chitosan
PLGA	Poly(lactic-co-glycolide)
PMAA	poly(methacrylic acid)
PMMA	Poly(methyl methacrylate)
PMMAZO	Poly{6-[4-(4-methoxyphenylazo)phenoxy] hexyl methacrylate}

PNIPAM	Poly(N-isopropylacrylamide)
PNIPAM-co-PGM	Poly(N-isopropylacrylamide)-co-poly(glycidyl methacrylate)
POEG(M)A	Poly(oligo(ethylene glycol)monomethyl ether (meth) acrylates)
POEGMA	Poly(oligoethylene glycol) methacrylate)
POFC	Poly(1,8-octanediol-co-Pluronic F127 citrate)
PP	Polypropylene
Pp-18	Purpurin-18
PPEGEEMA	Poly [poly(ethylene glycol)ethyl ethermethacrylate]
PPI	Poly(propylene imine)
PPy	Polypyrrole
PrHy	Procaine hydrochloride
PS	Polystyrene
PS-CNCs	Water-soluble photosensitizer cellulose nanocrystal
Pst	Pseudomonas syringae pv. Tomato
PTh	Polythiophene
PTX	Paclitaxel
PU	Polyurethane
PVA	Poly(vinyl alcohol)
PVAm	Polyvinylamine
PVdC	Polyvinylidene chloride
PVDF	Polyvinylidene difluoride
PVDF-HFP	Polyvinylidene fluoride-co-hexafluoropropylene
PVK	Poly(9-vinylcarbazole)
PVP	Polyvinylpyrrolidone
Py-CNCs	CNC fluorescent labeling nanoparticle conjugated to pyrene
QAGs	Quaternary ammonium groups
QC	Quaternized cellulose
QCM-D	Quartz-crystal microbalance with dissipation
QD	Quantum dots
R2R	Roll-to-roll
RBITC	Rhodamine B isothiocyanate
RC	Regenerated cellulose
R-CNC	Rosin-CNC
R-CNFs	Rosin functionalized cellulose nanofibers
RES	Reticuloendothelial system
rGO	Reduced graphene oxide
RH	Relative humidity
RML	Rhizomucor miehei lipase
R-NH_2	Fluorescent dye 4-(2-aminoethylamino)-7H-benz[de]-benzimidazo[2,1-a]isoquinoline-7-one
RO	Reverse osmosis
ROP	Ring-opening polymerization
SAOS	Small-amplitude oscillatory shear
SCA	Cellulose acetate

SCNC	Succinic anhydride-functionalized cellulose nanocrystals
SCs	Supercapacitors
SDS	Sodium dodecyl sulfate
SEM	Scanning electron microscopy
SeNPs	Selenium nanoparticle
SEVA-C	Ethylene vinyl alcohol
sFRP4	Secreted frizzled-related protein-4
SGF	Simulated gastric fluid
SH-SY5Y	Human neuroblastoma
si-ATRP	Surface-initiated atom transfer radical polymerization
SIF	Simulated intestinal fluid
SiO_2@PR	Spherical nanocomposite particles
SIV	Swine influenza virus
SLNs	Solid lipid nanoparticles
SMMT	Biofunctionalized montmorillonite with chitosan sulfate chains
SNCs	Starch nanocrystals
SNPs	Starch nanoparticles
SNR	Silver nanorod
SNs	Starch nanocrystals
SOx	Sulfur oxides
SPCL	Starch with polycaprolactone
SPI	Soy protein isolate
SPLC	Starch with poly(lactic acid)
SPR	Surface plasmon resonance
SS	Single stranded
SSC	Symmetric supercapacitor
ssNMR	Solid-state Nuclear Magnetic Resonance
STPP	Sodium tripolyphosphate
SWCNT	Single-wall carbon nanotubes
TAMS	3-2-(2-aminoethylamino) ethylamino propyl-trimethoxysilane
TC	Tubular cellulose
TCVS	Trichlorovinylsilane
TE	Tissue engineering
TEM	Transmission electron microscopy
TEMPO	(2,2,6,6-Tetramethylpiperidin-1-yl)oxyl
TEOS	Tetraethoxysilane
TGF-β1	Human transforming growth factor
TH	Tetracycline hydrochloride
THF	Tetrahydrofuran
THFS	Trichloro(1H,1H,2H,2H-heptadecafluorodecyl) silane
TINOPAL	Optical whitening agent
TMC	Trimesoyl chloride
TMOS	Tetramethoxysilane

TMSQI	(3-trimethoxysilylpropyl)quinolinium iodide
TOCN	TEMPO-oxidized cellulose nanofiber
TO-CNCs	TEMPO-oxidized CNCs
TPF	Two-photon fluorescence
$TPPC_6$-OH	6-(5'-(4'-phenoxyl)-10',15',20'-triphenylporphyrin-1-hexanol
TPP-OH	(5-4-hydroxylphenyl)-10,15,20-triphenylporphyrin)
UF	Urea formaldehyde
V	Vanadium
VASA	Vacuum-assisted self-assembly
VC	Vitamin C
VOC	Volatile organic compounds
WC	Wood carbon
WVP	Water vapor permeability
WVTR	Water vapor transmission rate
xMuLV	Xenotropic murine leukemia virus
XRD	X-Ray diffraction spectroscopy
ZIF	Zeolitic imidazolate framework

Chapter 1
Preparation and Properties of Nanopolysaccharides

Nathalie Lavoine, Ekrem Durmaz and Ramakrishna Trovagunta

Abstract With the raising environmental awareness of the society, the interest in exploiting nanomaterials from renewable resources is rapidly increasing. Renewable nanotechnology not only features the outstanding properties of common synthetic nanomaterials, but also combines renewability, biodegradability and biocompatibility. These past two decades have seen the emergence of so-called nanopolysaccharides, namely nanoscale particles isolated and/or produced from renewable and abundant materials such as cellulose, chitin and starch. These particles are paving the way for the design of high-performance tailored materials, which can address the current environmental and sustainability concerns of our society. Their potential in replacing plastics from petroleum-based polymers is especially the key driver behind this global and raising research effort. This chapter introduces the different preparation routes and main properties of nanopolysaccharides from cellulose, chitin and starch; three of the most abundant biopolymers available and exploited today. This chapter suggests as well potential applications and usages for these nanoparticles, as a preamble of the following next chapters, which will illustrate much more in details how these nanoparticles can change our society of tomorrow.

Keywords Nanopolysaccharides · Cellulose nanomaterials · Nanocellulose · Nanochitin · Nanostarch · Nanocrystals · Nanofibrils

1.1 Cellulose Nanomaterials

Cellulose is the most abundant polymer derived from biomass with an estimated worldwide production of 10^{12} ton per year [1]. Cellulose is a linear homopolysaccharide composed of glucose units bonded end-to-end through carbons C1

N. Lavoine (✉) · E. Durmaz · R. Trovagunta
Department of Forest Biomaterials, College of Natural Resources, North Carolina State University, Campus Box 8005, Raleigh, NC 27695-8005, USA
e-mail: nmlavoin@ncsu.edu

E. Durmaz
Faculty of Forestry, Kastamonu University, Kastamonu, Turkey

N. Lin et al. (eds.), *Advanced Functional Materials from Nanopolysaccharides*,
Springer Series in Biomaterials Science and Engineering 15,
https://doi.org/10.1007/978-981-15-0913-1_1

and C4 by β-l,4-glycosidic linkage [1]. Two anhydro-D-glucopyranose units (AGU), namely cellobiose, form the repeating units of this polymer. With the presence of three hydroxyl groups per AGU, the linear cellulose chains assemble via strong intra- and inter-molecular hydrogen bonding into larger semi-crystalline units known as elementary fibrils (or microfibrils), which are 3–4 nm wide [2]. Bundles of elementary fibrils form larger units referred to as macrofibrils (of approximately 15–60 nm in width), which in turn assemble into the well-known cellulose fibers (20–50 μm wide and 1–4 mm long) [3].

Cellulose has thus a multi-scale fibrillated structure and a hierarchical organization that can be broken down and isolated for the production of a new family of nanomaterials, called cellulose nanomaterials (CNMs) [4]. CNMs refer to cellulose particles having at least one dimension in the nanoscale range, i.e. between 1 and 100 nm. Similar to synthetic nanomaterials, CNMs exhibit unique characteristic such as low density, high aspect ratio (i.e. length to diameter ratio), large surface area and good mechanical strength [5]. The growing interest in this type of nanomaterials has particularly been fueled by their potential to address related issues to nanomaterials such as sustainability, renewability, biocompatibility and cost efficiency [6]. Therefore, CNMs are being investigated in a wide range of applications, spanning from nanocomposites [5], packaging [7], tissue engineering [8] to functional coatings [9] and printed electronics [10].

The family of CNMs includes cellulose nanoparticles of different sizes, shapes, surface chemistries and thus, properties. CNMs are often divided in two main categories, namely (i) cellulose nanocrystals (CNCs) and (ii) cellulose nanofibrils (CNFs). Over the years, CNMs have taken many names, and the literature reflects these discrepancies in terminologies. CNCs have been referred to as cellulose nanocrystalline, cellulose (nano)whiskers (CWX), and nanocrystals of cellulose (NCC) [11], while CNFs were referred to as microfibrillated cellulose (MFC), microfibrils, and nanofibrillated cellulose (NFC) [2]. Very recently, ISO standards on terms and definitions for cellulose nanomaterials have been established and are now being accepted by the global research community to define these nanomaterials [12].

In this chapter, we will follow the adopted terms and definitions by ISO to refer to both types of particles, namely CNCs for cellulose nanocrystals, and CNFs for cellulose nanofibrils. According to ISO/TS 20477:2017, CNCs are defined as rod-shaped cellulose particles of width ranging from 3 to 50 nm and aspect ratios between 5 and 50 [12]. CNFs are a more 'flexible' type of cellulose particles, with a width ranging from 3 to 100 nm and higher aspect ratios, between 10 and 100 [12]. This chapter will detail the preparation routes of CNMs, from the selection of the cellulosic feedstock to the different processing steps investigated to date. The main properties of the resulting CNMs will be discussed to highlight their usage potential in diverse applications.

1.1.1 Preparation of Cellulose Nanomaterials

1.1.1.1 Sources and Feedstock for the Preparation of Cellulose Nanomaterials

Various biomasses such as woods, plants, animals, bacteria and algae can be used to produce CNMs. Wood was, and is still the foremost source for CNM production. However, the shift towards the use of non-wood cellulosic sources such as agricultural plants and industrial bio-residues is more and more reported [13]. The use of agricultural plants and low-cost industrial bio-residues can offer broader opportunities in applications and may contribute to solve part of the global industrial waste issue [14]. Other sources such as bacteria, tunicates (marine animal) and algae, can also be of interest as they have a faster growth rate than terrestrial plants and trees, and can thus contribute in reducing the increasing feedstock demand for CNMs [15]. However, due to the rarity of tunicates, this source is rather explored for its ability to form 'defect-free' CNCs [16]. The end-use applications can drive the use of a particular source of cellulose for CNMs. For instance, CNMs produced from bacteria generally demonstrate higher biocompatibility compared to wood and plants CNMs, and are thereby preferred for biomedical applications [8, 17].

The primary difference between these biomass feedstocks lies in their biosynthesis process, which affects the chemical composition of the source, the crystalline structure of cellulose and its hierarchical organization, as shown in Table 1.1. Lignocellulosic biomass such as wood and agricultural plants differs in chemical composition from tunicate, bacterial and algae cellulose by the presence of lignin, hemicelluloses and other extractives (Table 1.1). Wood usually consists of about 40% cellulose in mass, while non-wood plants such as hemp and flax have a much higher cellulose content of about 70% [14]. In comparison, non-lignocellulosic sources, such as tunicates and bacteria, contain around 60 and 40–45% of cellulose, respectively. [17] The purity of cellulose in bacteria is however much higher than that of lignocellulosic sources, as no purification process is necessary to extract and release cellulose from other polymers or molecules [15].

Purification of the cellulosic source aims at isolating cellulose from the non-cellulosic components for the production of CNMs [4]. Lignocellulosic biomass typically undergoes a pulping process, which can involve the use of chemicals to remove the non-cellulosic components such as hemicelluloses, lignin and other extractives. In tunicates, the entire epidermis of the animal, named *tunic*, is covered by a composite of cellulose and proteins, which are held together by muco-polysaccharides and lipids [18]. The isolation of cellulose from this tunic can be achieved by combining an acidic prehydrolysis step with an alkaline Kraft cooking procedure (similar to Kraft pulping process), followed by a bleaching treatment to remove the coloration [19]. Similar steps can be used to isolate cellulose from algae [20]. Unlike other biomass, bacteria naturally synthesize cellulose at specific culture conditions, in liquid medium [15]. A *static* culture medium commonly results in the formation and deposition of a thick white gelatinous cellulose pellicle at the air-liquid interface

Table 1.1 Cellulose source characteristics and preparation, and general features of the resulting CNMs

Cellulose sources and resulting CNMs	Wood	Plants and industrial residues	Tunicate	Bacteria	Algae
Growth time	Years	Few months to years	Few months	Few days	Few weeks
Chemical composition	Cellulose, hemicellulose, lignin, others*	Cellulose, hemicellulose, lignin, others*	Cellulose, proteins and lipids, others*	Cellulose	Cellulose, proteins, lipids, others*
Source purification process	Complete or partial removal of hemicellulose, lignin, others[a]	Complete or partial removal of hemicellulose, lignin, others[a]	Isolation of mantel and removal of protein matrix	Culture in liquid medium	Removal of protein, lipids, others[a]
Dominant native cellulose allomorph	Iβ	Iβ	Iβ	Iα	Iα
CNM crystallinity (%)	40–80	40–80	85–100	65–79	>80
CNM width range (nm)	3–100	3–100	3–20	20–40	20–30
CNM aspect ratio (L/D)	10–100	10–100	70–100	>50	>40
Commercialization[c]	+++[c]	++[c]	n/a[b]	+[c]	n/a[b]
References	[4]	[13]	[22]	[23]	[24, 25]

[a]Others can include extractives or ash
[b]n/a information not available
[c]+++ source highly used for commercialization of CNMs, ++ moderate use, + low use

[8], as opposed to a *stirred* culture medium, which produces cellulose as suspended fibers or in irregular pellets form [21].

Depending on the cellulosic source and its purification/extraction steps, the resulting CNMs may thus feature different characteristics as illustrated in Table 1.1.

1.1.1.2 Production Routes of Cellulose Nanomaterials

Cellulose Nanocrystals (CNCs)

Cellulose nanocrystals, or CNCs, are usually produced from a purified cellulosic source by a controlled chemical treatment that aims at removing the disordered regions of cellulose, to leave intact the nanosized cellulose crystals. After treatment,

the resulting suspension is washed by several centrifugation and dialysis steps, and finally subjected to ultrasonification to disperse the CNCs in water [26, 27] (Fig. 1.1). Depending on the selected cellulosic source, slight variations in the preparation steps can be implemented to produce CNCs.

Acid hydrolysis is the most common production route of CNCs [28]. This process involves the penetration of acid hydronium ions into the disordered regions of the cellulose chains, where preferential hydrolytic cleavage of glycosidic linkages takes place. The resulting CNCs possess a higher resistance to acid treatment [26, 27]. Acid hydrolysis is commonly performed in the presence of strong mineral acids (6–8 M) under controlled temperature, time, agitation and acid-to-cellulose ratio [25].

Sulfuric acid is the most extensively used mineral acid for CNC production. Sulfuric acid when used as a hydrolyzing agent, grafts anionic sulfate half ester groups (OSO_3^-) to the surface of cellulose [27] (Fig. 1.1), which will stabilize by electrostatic repulsions the CNCs in aqueous suspension. The colloidal stability of the aqueous suspension prevents the CNCs from aggregating [29]. In addition to sulfuric acid, other acids, such as hydrochloric [30], phosphoric [31] and hydrobromic [32] acids, have also been used for the production of CNCs. Compared to the other acids, the use of hydrochloric acid results in the production of "uncharged" CNCs, which thus aggregate more easily in water [33].

The cellulose source can dictate the hydrolysis conditions to apply for the production of CNCs, but depending on the acid type and concentration, the temperature and time of hydrolysis need to be adapted to prevent the cellulose biomass from burning.

Significant amount of research has focused on optimizing the acid hydrolysis conditions for the production of well-dispersed and defined CNCs. Bondeson et al. [44] demonstrated that a sulfuric acid concentration of 63.5% (w/w) and a hydrolysis time of 2 h were sufficient to produce CNCs from microcrystalline cellulose, having a length between 200 and 400 nm and a width of less than 10 nm, with a production yield of 30% of the initial weight. Shorter, narrower, and less polydisperse CNCs can be obtained by increasing the hydrolysis time (e.g. from 25 to 45 min [45]) and temperature (e.g. from 45 to 72 °C [46]), but at the cost of the production yield. A very narrow range of hydrolysis conditions has indeed been identified for achieving higher production yield (i.e. 66–69 wt%) of wood pulp-CNCs, namely the use of 57–58 wt% sulfuric acid at 64–67 °C and for 134–156 min [47]. One explanation for this narrow range of experimental conditions is linked to the formation of by-products during hydrolysis. Using 64 wt% sulfuric acid and a hydrolysis time of 25 min, a low hydrolysis temperature of 45 °C resulted in the formation of more by-products than at a temperature of 65 °C [48]. The by-products formed at low temperature were oligosaccharides with a high degree of polymerization, which precipitated on the surface of the CNCs during water quenching. Because oligosaccharides of lower degree of polymerization were formed at higher hydrolysis temperature, their precipitation on the CNC surface was lowered, thus resulting in an increased CNC production yield.

As illustrated in Table 1.2, the production yield varies drastically between CNC batches. The cellulose source, hydrolysis conditions and post-treatments grandly

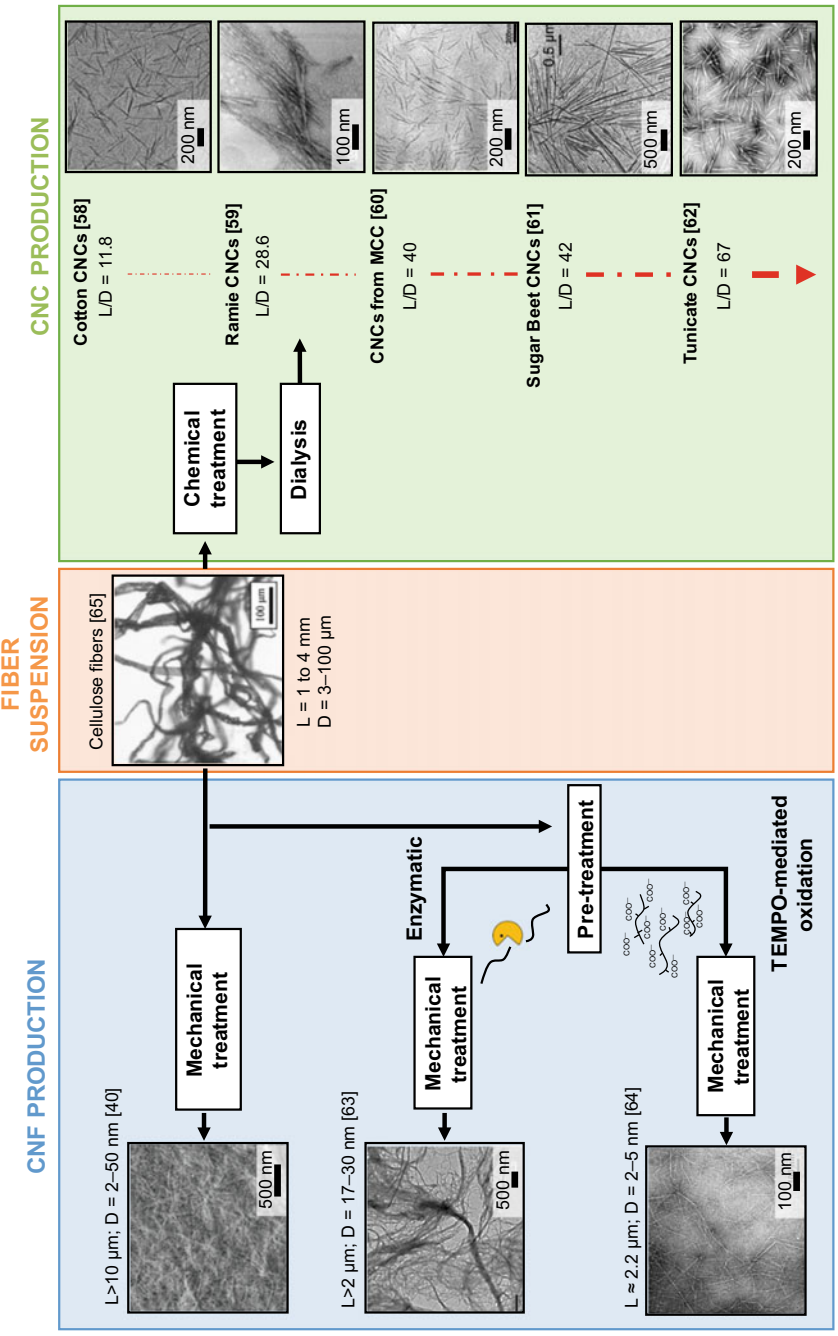

Fig. 1.1 Production routes of cellulose nanocrystals (CNCs) (Reproduced from [34–38]) and cellulose nanofibrils (CNFs) (Reproduced from [39–41]) from cellulosic biomass (Reproduced from [42], [43])

Table 1.2 Influence of acid hydrolysis conditions on morphology of CNCs

Cellulose source	Acid Type and concentration (wt%)	Hydrolysis temperature (°C)	Hydrolysis time (min)	Acid/cellulose ratio (w/v)	Width (nm)	Aspect ratio	Reaction yield (%)	Crystallinity index (%)	References
Bacterial cellulose	37% sulfuric acid 77–85%	60	2880	–	14 ± 7.4	94 ± 79	–	72[a]	[63]
Bamboo	Phosphoric acid	40–60	90–210	30	15–30	–	–	59	[29]
Cotton linter	64% sulfuric acid	50	50	20	33.0 ± 3.3	8.4	33.4	71.7	[64]
Hardwood bleached kraft	64% sulfuric Acid	50	50	20	14.9 ± 3.5	11.5	20	61.5	[64]
Hemp	64% sulfuric acid 22%	45	30	–	15	–	19	87	[65]
MCC	Hydrochloric acid	120	180	60	22 ± 6	–	90.5	87.3	[66]
		110	120	40	295 ± 38	–	94.8		
Rice straw	64% sulfuric acid	45	30–45	8.75	11.2	–	4.83–6.83	91.2	[67]
	50% sulfuric acid	30	180	10	10–12	–	6.5	76	[68]

(continued)

Table 1.2 (continued)

Cellulose source	Acid Type and concentration (wt%)	Hydrolysis temperature (°C)	Hydrolysis time (min)	Acid/cellulose ratio (w/v)	Width (nm)	Aspect ratio	Reaction yield (%)	Crystallinity index (%)	References
Sisal	65% sulfuric acid	60	15	25	4	60	30	–	[69]
Softwood bleached kraft	64% sulfuric acid	50	50	20	16.9 ± 4.5	10.6	20.5	64.9	[64]
		45	25–45	8.75–17.5	4.5–5	23–28	–	–	[45]
Tunicate	48% sulfuric acid	60	20	20	9.4 ± 5.0	148 ± 147	–	80[a]	[63]

[a]Crystallinity index determined by solid-state ^{13}Carbon nuclear magnetic resonance (^{13}C-NMR); X-ray Diffraction spectroscopy (XRD) was used for the other reported values

affect the production yield, but the strategy used to calculate the reported yield has also to be considered for comparison purposes.

Alternative pathways have been explored for the production of CNCs to increase the production yield and go towards more sustainable production routes, as one of the main challenges of acid hydrolysis is the recovery of the acid used. Production routes such as gaseous acid hydrolysis [49], ionic liquid treatment [50] and ammonium persulfate oxidation [51] have thus been proposed, but to date, their efficiency to produce CNCs and their influence on the properties of the resulting CNCs are still under study.

Cellulose Nanofibrils (CNFs)

Unlike CNCs, cellulose nanofibrils (CNFs) contain both crystalline and amorphous (or disordered) regions, and are typically obtained by successive high-shear mechanical treatment of the cellulosic source (Fig. 1.1). As for CNCs, the cellulosic source is purified and/or bleached before being converted to an aqueous suspension of nanoscale cellulose fibers.

CNFs were first reported by Turbak et al. [52] and Herrick et al. [53] in 1983, after subjecting an aqueous softwood pulp suspension several times through a high-pressure homogenizer. The high-shear mechanical action aims at facilitating the transverse cleavage along the longitudinal axis of the cellulose fibers [6] that results in a strong entangled network of nanoscale fibrils [3]. For an effective fibrillation of the cellulose fibers (i.e. fiber delamination instead of fiber shredding), the shear force applied to the fibers has to overcome the interfibrillar hydrogen bonding energy [2]. The production of CNFs is, therefore, commonly performed in aqueous medium to loosen the hydrogen bonding between fibrils and promote delamination. In addition, due to their high water absorption capacity and water affinity, the cellulose fibers need to be processed at very low concentrations (<5 wt%), as their intense fibrillation result in highly viscous suspensions [2].

Mechanical Treatments

High-pressure homogenization, microfluidization and grinding are the three most conventional high-shear mechanical treatments used to convert cellulose fibers to CNFs (Fig. 1.1). Because of differences in mechanical shear and stress applied on the fibers, the CNFs resulting from these three distinct processes will feature different morphological and physical characteristics. For instance, in a high-pressure homogenizer, the cellulose slurry passes through a tiny gap between the homogenizing valve and an impact ring [54, 55], while in a Microfluidizer, the cellulose slurry goes through a micrometer-wide geometry chamber [56, 57]. The grinder has a completely distinct operating mode as the cellulose slurry undergoes shear action between a grooved rotary disk and a static one [58, 59] (Fig. 1.1). A complete understanding of the exact shearing action applied on the fibers is still missing in the

literature, but the resulting materials show clear distinct properties as reported in previous literature reviews [2, 43].

In addition to the conventional high-shear treatments, some 'unconventional' mechanical treatments such as aqueous counter collision [60, 61], cryocrushing [62] and ultrasonification [41] have also been developed and tested to produce CNFs. More information on these processes can be found in the recent review of Nechyporchuk et al. [2].

The production of CNFs by high-shear mechanical treatment is a highly energy intensive process [56, 70]. Most research work has been focusing on ways to reduce the energy consumption to produce CNFs. To date, the most viable option consists in combining the mechanical treatment with either a chemical or an enzymatic pre-treatment (Fig. 1.1). The disintegration energy can as such be reduced from ≈100 kWh/kg for unmodified cellulose fibers to as little as 1–2 kWh/kg [5]. While these physicochemical pre-treatment methods considerably contribute in decreasing the total energy consumption, their use can be costly and result in the chemical modification of cellulose, thus imparting different properties to the CNF that may not be desirable for a given application [70]. Other proposed strategies thus attempt to rely only on the "wise employment" of existing equipment and the combination of several mechanical treatments to reduce the production energy consumption, without deteriorating the properties of the CNFs [58, 71].

Enzymatic and Chemical Pre-treatments

The enzymatic hydrolysis process uses a group of enzymes, the cellulases, to catalyze the hydrolysis of cellulose fibers and promote their fibrillation [72]. The cellulases (endoglucanases, cellobiohydrolases and exoglucanases) selectively hydrolyze the crystalline and amorphous domains of cellulose [72]. A decrease in degree of polymerization (DP) as well as an increase in crystallinity index is a direct consequence of the hydrolysis pre-treatment [72, 73].

Compared with the enzymatic pre-treatment, the chemical pre-treatments act on the surface chemistry of cellulose chains to modify the inter- and intra- hydrogen bonds. Introduction of negatively charged groups on the cellulose fiber surface via carboxylation or carboxymethylation is known to significantly improve the fibers fibrillation by electrostatic repulsions or osmotic pressure effect [74].

TEMPO ((2,2,6,6-Tetramethylpiperidin-1-yl)oxyl)-mediated oxidation is a regioselective oxidation process, which converts the primary alcohol groups on the cellulose surface to carboxyl groups [3], under mild alkaline conditions [75]. A loss in DP is also commonly observed during the TEMPO-oxidation; however, the original DP of cellulose can be maintained when processing the oxidation under weakly acidic or neutral conditions [76]. Owing to the presence of (negatively charged) sodium carboxylate groups on the fibers' surface, a less-energy intensive mechanical treatment can be applied to produce TEMPO-CNFs, with a uniform width of around 3–4 nm [3]. Not only a drastic reduction in energy consumption has been reported (e.g. 1400 MJ/kg using a high-pressure homogenizer versus 7 MJ/kg when combined with TEMPO-oxidation [3]), but also the production of well-dispersed, uniform and

thin CNFs. For more information about this pre-treatment, the readers are referred to this review paper [3].

Carboxymethylation is another chemical pre-treatment of the cellulose fibers, which uses monochloroacetic acid in the presence of isopropanol to graft anionic groups on the cellulose surface [77, 78]. Carboxymethylated CNFs have slightly lower and more uniform dimensions than enzymatically-treated CNFs, when subjected to the same mechanical treatment [77]. Taipale et al. [78] estimated a decrease in energy from 5.5 MWh/t per pass through a Microfluidizer to 2.2 MWh/t per pass after carboxymethylation. Interestingly, the potential of carboxymethylated-CNFs has been highlighted as a pathway to produce CNFs in powder form, while preserving the nanoscale properties and ensuring their re-dispersibility in water [79].

Other chemical approaches have also been developed to produce CNFs, such as phosphorylation [2, 80] or periodate oxidation [81, 82], which all result in CNFs with different surface chemistry, morphology and properties.

The origin of the cellulosic source seems to mainly affect the morphology of CNCs, while the properties of CNFs are mostly influenced by the selected production routes. Further research is however needed to achieve a controlled production of different CNM grades. This challenge has yet not prevented industry and companies from moving forward with the large-scale production and commercialization of CNMs. Over the past decade, researchers and companies have started the transition from lab-scale to industrially-produced CNMs. Current large-scale production of CNMs exploits lignocellulosic biomass and, principally wood, due to its abundance, low cost and ease of process. The main producers of wood pulp CNCs, obtained by sulfuric acid hydrolysis, are CelluForce Inc. (Canada) and GranBio (USA) with a production rate of 300 and 130 t/y, respectively (on dry basis) [83]. Major CNF production plants include, but are not limited to, FiberLean Technologies (UK) with an annual production of 8800 tonne, Borregaard in Norway (1100 t/y), Nippon Paper in Japan (560 t/y) and the University of Maine in the USA, with a production rate of 260 t/y [83].

1.1.2 Properties of Cellulose Nanomaterials

CNMs are produced in water at a very low solid content (<5 wt%). They thus appear as an aqueous gel of high viscosity or as liquid suspension, of different turbidity depending on the size of the nanomaterials, their interactions with each other, and the concentration (Fig. 1.2). Commercially available forms of CNMs, however, are sold as dried powders or under a more concentrated form (Fig. 1.2). CNCs can be purchased as concentrated suspensions of 6–12 wt% or as redispersible freeze/dried powders, while CNFs are available as highly concentrated gels or pastes of 1–25 wt% [84]. Due to redispersibility issues, CNFs are currently not available as freeze-dried or spray-dried forms.

The wet-state properties of CNMs are thus the primary properties to be characterized, but also the most challenging ones. While dried forms of CNMs can sound

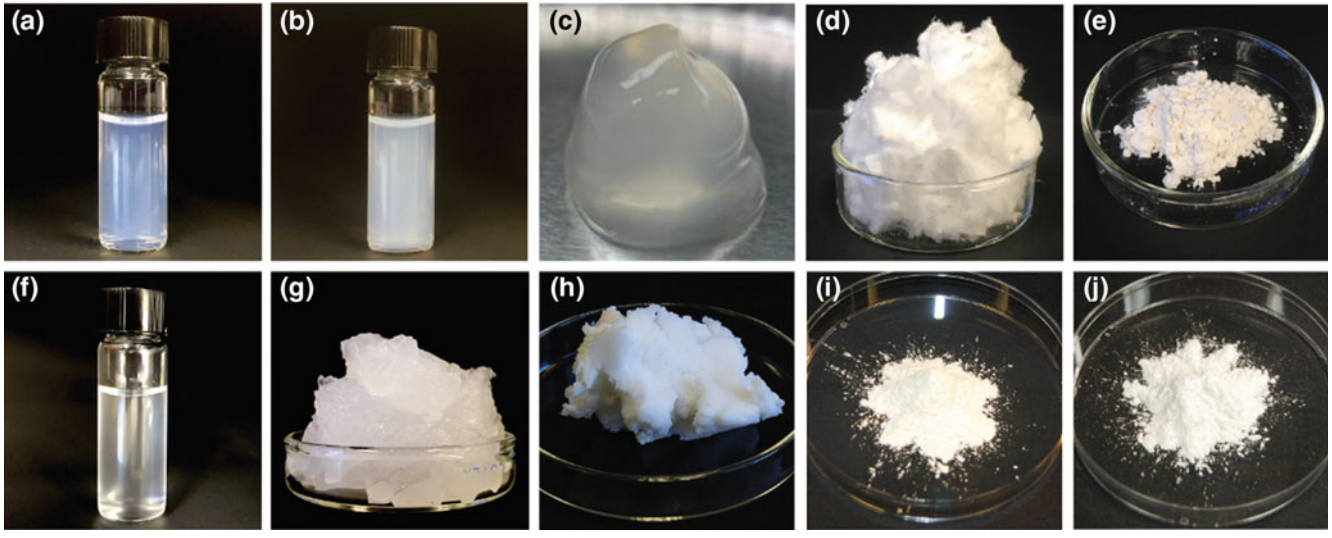

Fig. 1.2 Photographs of cellulose nanomaterials from various producers (Reproduced from [84]). [*Top row*] CNCs produced from cotton or wood pulp by sulfuric acid hydrolysis: **a** lab-made CNCs fully dispersed in water at 1 wt%, **b** lab-made CNCs at 5 wt%, **c** CNCs at 15 wt% from FPInnovations (Canada), **d** 0.5 g of freeze-dried lab-made CNCs, **e** 2 g of spray-dried CNCs from CelluForce (Canada); [*Bottom row*] CNFs from wood pulps: **f** carboxymethylated CNFs produced by RISE Bioeconomy (Sweden) at 0.1 wt%, **g** 2wt% CNF gel from RISE Bioeconomy; **h** 10 wt% Exilva paste produced by Borregaard, **i** 1 g of freeze dried and ground mechanically produced CNFs from the University of Maine (USA), **j** 1 g of spray dried CNFs from University of Maine

easier to characterize, the presence of residual moisture (2–5 wt%) can influence the characterization and analysis of certain properties such as surface specific area [84]. Indirect methods have thus been attempted to help characterizing the properties of CNMs, and consist mostly in converting the aqueous CNMs to dry materials such as films and foams for further analysis.

This section will discuss the main wet-state and dry-state properties of CNMs, and mention some of the techniques implemented to date to characterize these nanomaterials. For more details on CNM characterization, the readers are strongly recommended to read a very recent published review discussing the best practices, methods and techniques for characterizing CNMs [84].

1.1.2.1 Wet-State Properties of CNMs

Morphology of CNMs

'Morphology' can include the size of the particles (length and width), their shape in water, and the state of dispersion, which is also related to the surface chemistry of the particles. While CNCs are stiff crystals with spindle-like morphology of reported lengths 50–350 nm (up to 1 μm for tunicate-CNCs) and width 5–20 nm, CNFs are flexible, with a fibril/fibril morphology of length exceeding one micrometer and width 20–100 nm (3–4 nm width for the elementary fibril) [84].

The measurement of the exact particle size is a convoluted process, especially in the case of CNFs due to their long entangled fibrillar structure [26, 43]. More especially, non-surface charged CNMs remain the most complicated particles to characterize, as aggregation and interaction by hydrogen bonding prevent particle individualization. Microscopic techniques such as scanning electron microscopy (SEM), transmission electron microscopy (TEM) and atomic force microscopy (AFM) are commonly used to study the morphology of CNMs. These techniques remain, however, time-consuming, and cannot give an exact representation of the whole batch of produced CNMs.

The hydrodynamic "apparent particle size" of CNMs can be determined by dynamic light scattering (DLS) [85]. An estimate of the hydrodynamic radius of CNMs based on light scattering effect could be measured, assuming that the particles are spherical in nature [86]. Since CNMs are either rod or fibrillar-like materials, DLS cannot be directly correlated with their particle size (length or cross-section) or with the particle size distribution. Instead, DLS gives information on the dispersion quality and state of aggregation of the CNMs.

Turbidity is another method that can indirectly help assessing the level of dispersion of CNMs by measuring the reduction in transparency of a suspension due to the presence of light-scattering particles [87]. A low turbidity value is linked to less aggregated nanoparticles or smaller particles, and indicates a higher dispersion quality [88]. This method is however sensitive to several physical phenomena and kinetic effects that may not depend solely on the nanoparticle aggregation, and therefore can influence the turbidity value measured [84]. Both turbidity and DLS can provide an

indirect estimation of the particle size and when combined with other microscopic techniques, they can potentially offer more insight on the CNM dimensions [84].

Degree of Polymerization

The degree of polymerization (DP) of CNMs can indirectly be estimated by the intrinsic viscosity method, which uses a cupriethylene diamine (CED) solution as a solvent and a capillary viscometer [89]. The intrinsic viscosity is related to the average DP through the Mark–Houwink–Sakurada equation [1]:

$$[\eta] = 0.57 \times DP_v \tag{1.1}$$

with η, the intrinsic viscosity, and DP_v, the degree of polymerization determined by viscosity measurement [90].

A decrease in DP of cellulose is reported after both acid hydrolysis and high-shear mechanical treatment. The production of CNFs by high-shear mechanical treatment can overall reduce by 27% the DP of cellulose [52, 72]. The TEMPO-mediated oxidation, as pre-treatment, affects however much more the DP of cellulose. For instance, with increasing addition of NaClO, DP values of wood pulp fibers were decreased from 1270 to 500–600 [91]. According to studies on acid hydrolysis of cellulose [92], the DP is expected to rapidly decrease during CNC production, until it reaches the so-called leveling-off DP (LODP) [27]. The LODP can then be correlated to the length of the particles obtained after purification and dispersion of the hydrolysis residue of biomass [93], giving an indirect access to the average length of the CNCs. In the case of TEMPO-oxidized CNFs, a clear linear relationship between the average fibril length and DP was identified as an additional tool to estimate the average lengths of the particles [91].

Degree of Crystallinity

Assessment of the crystallinity degree of CNMs can help improving the extraction/production methods so as to obtain appropriate structures for a given application, in addition to give information on the molecular structure of the materials. The degree of crystallinity in CNCs can range from 54 to 88%, while CNF crystallinity index can span from very low (i.e. 20%) to very high values, such as 90% in the case of bacterial CNFs [94].

X-ray Diffraction (XRD), Solid-state Nuclear Magnetic Resonance (ssNMR) and Raman spectroscopy are three techniques to estimate the cellulose crystallinity in CNMs [84].

XRD is usually performed on powder forms of CNMs. The recorded diffraction spectrum of dried CNMs consists of well-defined peaks with the two most prominent ones being assigned to the (002) plane at $2\theta \approx 22.7°$ and to the (101) and ($10\bar{1}$) plane at $2\theta \approx 14$–$17°$. The crystallinity index of CNMs can be defined and calculated as

the ratio of the total crystalline area to the total diffraction area (i.e. amorphous + crystalline) of CNMs [95]. Deconvolution of the crystalline peaks from the amorphous region can be challenging, therefore XRD is often combined with a peak area approach [96] or a peak intensity approach (also known as the Segal approach) [97] to better evaluate the degree of crystallinity. More details on pros and cons of these approaches can be found in the review article by Park et al. [98].

With the high resolution of ^{13}C CP-MAS NMR spectroscopy, which combines cross-polarization (CP), magic angle spinning (MAS), and high dipolar decoupling devices, the atomic structure of CNMs samples can be obtained by resolving the C1, C4 and C6 carbon peaks [99]. Similar to XRD, the crystallinity index of CNMs (in %), as defined previously, can be calculated after peak analysis. The obtained crystallinity values by NMR are mostly comparable (or lower) than the crystallinity index values calculated from XRD experiments.

Another wet-state property, which directly results from the presence of highly crystalline domains, specifically in the case of CNCs, is called the flow birefringence effect [27]. The birefringence phenomena can be observed under a polarized light, not only for CNCs but also, yet less clearly, with highly diluted CNF suspensions. The evaluation of the birefringence of CNC suspensions can also provide a quick indication on the level of dispersion of the particles (in presence of electrostatic repulsions). A well-dispersed CNC suspension separates into a lower chiral nematic liquid crystalline phase and an upper isotropic phase above a critical concentration of approximately 4.5 wt% [100]. At higher concentration (ca. 10 wt%), the CNCs can take up to 10 days to self-assemble in a clear chiral nematic phase [101]. Interestingly, this birefringence can be preserved after solvent evaporation, which results in colorful-patterned CNC films. The self-assembly of the CNCs can be tuned by e.g. adding salt to the suspension or high-shear mechanical action, to tailor the structural color of the films observed after solvent evaporation [45, 102].

Surface Chemistry and Colloidal Stability

The colloidal stability of CNMs is the result of electrostatic repulsions due to the presence of charged groups at the particle surface. Conductometric titration and zeta potential are the two commonly used methods to determine the surface or 'bulk' charge density of CNMs.

Sulfuric acid-hydrolyzed CNCs are titrated with sodium hydroxide (NaOH), so that the protons of the surface groups, $–OSO_3H$, are consumed by the OH^- groups from the titrant, thereby lowering the conductivity of the suspension. The protons are then progressively replaced with Na^+ counterions with continuous addition of NaOH, which increases back the conductivity due to free OH^- groups in the suspension. The surface charge density of CNCs can be tuned by varying the hydrolysis conditions, but a more accurate control of the surface charge density is commonly achieved by surface desulfation or postsulfation techniques using e.g. sodium hydroxide and chlorosulfonic acid ($ClSO_3H$), respectively [103].

In the case of CNFs, the conductometric titration process can be challenging with the use of conventional titrants such as sodium hydroxide, due to their high surface area and ability to form a gel at high concentration and pH [84]. Access to the *real* surface charge is also debatable, since the CNFs form a tight entanglement. The use of polyelectrolytes, such as poly (diallyldimethyl-ammonium chloride) (pDADMAC), is thus an alternative to conductometric titration to get access to the surface charge density of the nanofibrils, as the charged polymer neutralizes the fibrils surface by adsorption [72].

Further information on the surface charge and colloidal stability of CNMs can be obtained by measuring the zeta potential of the suspensions [104]. Conductometric titrations do not provide any significant insight into particle aggregation and colloidal stability of the system, especially at different pH or ionic strength. CNC suspensions commonly feature zeta potential values between −20 and −50 mV, except for HCl-hydrolyzed CNCs, as these particles are not charged [84]. Depending on the degree of oxidation (e.g. TEMPO-oxidized CNFs), CNFs can have even higher values, approaching −60 mV. Note that these values are only quantitative if the assumptions inherent to Henry's equation are met.

Rheological Properties

The aqueous CNM suspensions showcase a rheological behavior, which can be described in terms of shear-dependent viscoelastic response (e.g. shear-thinning) [105, 106], thus expanding the application of CNMs in industrial processes such as coatings, mixing or pumping [2]. The rheological behavior of CNM suspensions is influenced by the CNM microstructure, the degree of dispersion and the interaction of the particles with the solvent.

A rotational (torsion) rheometer is the most commonly used method for analyzing the rheology of CNMs. The CNM suspensions are sheared between two plates to measure their viscosity and their viscoelastic response at low shear rate (commonly, 0.001–100 s^{-1}). Two testing operating modes can be set to study the rheological properties of CNMs: (i) the steady-shear mode, which gives access to the bulk viscosity, and (ii) the small amplitude oscillatory shear (SAOS) mode, which is used to determine the viscoelastic properties of the suspensions, such as the shear modulus, loss modulus and complex viscosity [107].

Rheology can also be used as a complementary tool to determine the aspect ratio of CNMs [108] and to assess the quality of the CNM dispersion. Typically, a poorly dispersed CNM suspension would result in decrease in viscosity due to limited particle-particle interaction at low shear rates [109].

More information on the rheological properties of CNMs can be found in the following review articles [84, 106].

1.1.2.2 Dry-State Properties of CNMs

CNM 'Powders'

CNMs can be dried into powders by means of different techniques, such as oven drying, freeze-drying, supercritical drying or spray drying. Because of their high surface area, hydrophilic nature and high water holding capacity, the particles typically agglomerate upon drying, and cannot be redispersed upon rehydration. While dewatering and drying of CNMs remain a challenge to overcome, several strategies have been proposed to facilitate their redispersion in water without losing their nanoscale properties. As a result, powder forms of CNMs are, today, available for purchase.

CNCs are more favorable to redispersion due to their lower aspect ratio and morphology. However, only neutralized CNC suspensions in the sodium-salt form can be fully redispersed in water after drying, and at low concentrations (0.5–3 wt%) with sonication [110]. The drying of CNCs with H^+ as counterions (so called acid-form CNCs) results in strong hydrogen bonding and van der Waals interactions between particles, which cannot be redispersed, even at intense sonication [111]. Therefore, the dried sodium-salt form CNCs should contain a residual moisture content of about 4% for full redispersion. Likewise, CNF suspensions in the sodium-salt form (obtained e.g. by addition of sodium chloride) can be partially redispersible [112].

CNM powders are commonly obtained by freeze-drying. This method presents, however, several disadvantages such as long batch times, requirement for liquid nitrogen to prevent ice crystals from forcing aggregation of CNMs and limited scalability. Other methods, such as spray drying, spray freeze-drying and supercritical drying have been proposed for drying the materials, and present many advantages for the optimization of powder properties and yields [84, 111].

Solvent exchange strategies are intensively investigated, especially for the production of highly porous and lightweight CNM materials like aerogels [113], but have also shown promising results for drying CNMs without altering their nanoscale properties [114, 115]. For instance, dried carboxymethylated CNFs have demonstrated full redispersion after solvent exchange with mixed alcohol and drying under stirring at 60 °C [116]. The carboxymethylation pretreatment particularly helped preventing irreversible agglomeration of the fibrils during drying.

Hence, the surface modification and the addition of additives to the CNM suspensions are two other alternatives for producing redispersible dried CNMs. Several works have been exploring these pathways, but will not be detailed in this chapter. For further information, the readers are referred to the following research articles [84, 117–120].

CNM Films

Facing the challenge of characterization of wet-state CNMs, researchers have primarily exploited the film-forming ability of these nanoscale cellulose particles for indirectly assessing their properties. By simple water evaporation or solvent casting, CNMs can form a film, or 'nanopaper', with mechanical, barrier and optical properties of great interest for diverse applications, spanning from barrier packaging [121] to optically transparent papers for electronics [122].

Multiple film-making methods have been tested for the preparation of CNM films, such as solvent casting, vacuum filtration, or spin-coating, but the preparation of very thin films of CNMs, i.e. submonolayer films and 'full surface coverage thin films' (<less than one micron thick), is favored to study the properties of individual particles, fundamental adsorption, swelling, surface forces and optical properties [84]. Production of such thin films can be achieved by spin-coating, Langmuir-Blodgett/Schaeffer deposition or solvent casting [123–125]. Their characterization by microscopy techniques such as AFM, quartz-crystal microbalance with dissipation (QCM-D) and surface plasmon resonance (SPR) can give further insight on the particle size, swelling and adsorption phenomena of the CNMs. The readers are referred to the review article of Foster et al. [84] for further information.

Mechanical Properties of CNM Films

Owing to their entanglement and high aspect ratio, CNFs can more easily form self-standing films than CNCs through interfibrillar hydrogen bonding [43]. Neat CNC films are often too brittle to be characterized.

CNF films of 20–200 μm thick can be prepared by varying the concentration of the suspension regardless of the film-making process [121]. The types of CNFs, the making-process and the drying technique, such as evaporative drying [126], oven drying [127] or hot press [128] can all influence the properties of the films.

Under controlled conditions, i.e. 23 °C and 50% relative humidity (RH), Young's modulus of CNF films can typically range from 1–2 GPa for e.g. hardwood CNF films by casting [129] to 20 GPa for e.g. Korean white pine CNF films obtained after filtration and hot pressing [130]. The testing conditions, in particular temperature and relative humidity, are critical and well known to affect the measured mechanical properties. With a continuous increase of the relative humidity (from 0 to 100%), a consistent decrease by one order of magnitude of the Young's modulus (from 20 to 1.5 GPa), yield stress (from 231 to 14 MPa) and tensile strength (from 360 to 34 MPa) has been observed on TEMPO-oxidized CNF films [131].

Optical Properties of CNM Films

The optical properties of CNM films can be measured by determining the light transmittance with a U.V.-visible spectrometer, in the wavelength range 200–1000 nm. Typically, the transmittance value at 600 nm is reported.

CNF films can be optically transparent if the fibrils are small enough to densely packed, thus reducing the interstices between the fibrils to avoid light scattering [122]. With diameters of 3–4 nm, TEMPO-oxidized CNFs usually result in highly transparent films with transmittance values of above 80% [132]. The presence of hemicelluloses has however been reported to interfere with the colloidal stability of the wood pulp CNFs in water, thus lowering the light transmittance of the films after drying [132]. The filmmaking process can also influence the optical properties of the films. Films prepared by slow filtration, drying and compression are usually not optically transparent, but translucent due to a dense packing of the fibrils [122].

Unlike CNFs, CNCs display a lyotropic liquid crystalline behavior in water, caused by electrostatic repulsion forces between the negatively charged particles, which are indirectly characterized by a cholesteric pitch (*P*) [133]. From a certain concentration threshold, a phase transition from an isotropic liquid phase to a chiral nematic phase is observed. The CNC self-organization is preserved by simple water evaporation, resulting in Bragg reflection of visible light if the pitch length in the solid films approximate the wavelength of visible light [134]. Iridescent CNC films of different colors can be obtained by modifying the pitch length by e.g. adding electrolytes to the CNC suspension, or varying the energy of the ultrasound/sonication treatment to disperse the particles in water [134].

Barrier Properties of CNM Films

In addition to excellent mechanical and optical properties, CNM films feature good gas and liquid barrier properties due to their highly crystalline nature, their ability to form a dense percolating network and their high aspect ratio [135].

Generally, addition of nanoparticles as fillers or coating can significantly reduce the gas permeability of the substrates by increasing the tortuosity [136]. Very low oxygen transmission rates (OTR) can be achieved with neat CNM films, with values as good as or even lower than OTR values of petroleum- and bio-based polymers [137]. For instance, films of CNFs and polyvinylidene chloride (PVdC) of similar thickness (20–30 μm) showed similar OTR values in the range of 17–18 and 9–15 mL/m^2 day, respectively [121]. Because the film structure is one of the most important criteria in the consideration of barrier properties, the density and porosity of the films, and thus the making-process, can significantly influence the gas barrier properties. Compared to casted CNF films (oxygen permeability <1 cm^3 μm/m^2 day kPa at 0% RH [43]), CNF films made by filtration and hot pressing displayed a much lower oxygen permeability of 0.6 cm^3 μm/m^2 day kPa up to 65% RH, and this regardless of the CNF widths (50–100 nm versus 5–20 nm-thick CNFs were tested) [128].

While CNM films show reduced gas permeability in dry atmospheres, this property is often lost in moist atmospheres [136], due to the plasticizing and swelling of the fibrils through the ad- and ab-sorption of water molecules at high relative humidity. Strategies to improve the oxygen barrier of the films at high relative humidity can then involve the chemical surface modification of cellulose [138] or the preparation

of composites, multilayer [139] or hybrid [140] CNM films. However, it is worth noting that, although cellulose is a hydrophilic polymer, CNM films still feature lower water vapor permeability than their macroscale counterpart. The simple conversion from macro- to nanofibrils can already decrease the water vapor transmission rate of the films by 10%, regardless of the cellulose source [141].

For more information on the barrier properties of CNM films, the readers is referred to the two following review articles [43, 136].

1.1.3 Concluding Remarks

With the growing interest in using renewable sources for the development of sustainable materials and energy, research on cellulose nanomaterials has gained prominence these past two decades. In 2019, over 20 known companies and universities can produce and sell, worldwide, large-scale batches of various grades of cellulose nanomaterials, either at wet or dry states.

Cellulose nanomaterials are materials derived from cellulosic biomass, having at least one dimension in the nanometer range. Two main types of nanoscale particles can be defined, namely cellulose nanocrystals (CNCs), which are crystalline rod-like particles, obtained by acid hydrolysis, and cellulose nanofibrils (CNFs), which are produced mechanically and thus, still display both crystalline and disordered regions. Owing to their nanoscale dimension, (semi-)crystalline nature and renewable origin, these particles have unique properties, which are nowadays exploited in a wide range of applications, spanning from biomedical, food, packaging to energy-storage devices and filtration systems. Few of these applications will be illustrated in the following chapters.

1.2 Chitin Nanomaterials

Chitin is a linear polysaccharide made out of units of *N*-acetyl-D-glucose-2-amine, linked together by β-1,4 linkages. Although its chemical structure is identical to that of cellulose, chitin structure differs with the presence of acetamide groups ($-NHCOCH_3$) at the C2 positions (Fig. 1.3). In nature, this biopolymer exists in the cell walls of fungi, the exoskeleton of shellfish, insects and other arthropods and animals.

Although chitin is produced in nature at a rate of 10^{10}–10^{11} ton per year, to date, the main industrial source of chitin is shellfish canning waste (from shrimp and crab shells), in which the chitin content ranges between 8 and 33% [26]. The chitin is extracted from these crustacean wastes by acid treatment, aiming at dissolving the calcium carbonate, followed by an alkaline extraction, which solubilizes the proteins. A bleaching step can additionally be performed to remove leftover pigments, resulting in a colorless chitin product.

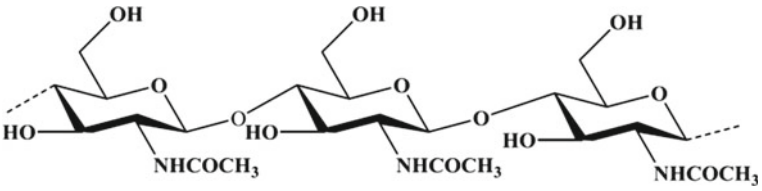

Fig. 1.3 Chemical structure of chitin

Different grades of chitin products with varying purity and color levels can thus be obtained by varying the treatment conditions. The purification and isolation treatment conditions should not only be adapted to the chitin source, which can feature structure differences, but also to the end-use application (e.g. a high purity and transparent chitin product is required for biomedical applications).

Similar to cellulose, chitin has high crystallinity owing to its linear structure, and assembles into nanofibers. Hence, production of chitin nanomaterials, namely chitin nanocrystals (ChNCs) and chitin nanofibers (ChNFs), has been investigated to broaden up the spectrum of application of this waste biomaterial, and will be discussed hereinafter in this chapter.

1.2.1 Hierarchical Structure of Chitin

The exoskeleton material (exo- and endocuticles) of crustaceans displays a hierarchical organization comprised of six structural levels of chitin (Fig. 1.4). The polysaccharide molecules of α-chitin, arranged in antiparallel direction, form the first structural level, namely (A) the α-chitin crystals (the α-configuration is the most abundant and stable form of chitin, but other chain assemblies can lead to β- and γ-chitin, with parallel and alternate parallel/antiparallel chain directions, respectively). The arrangement of 18–25 of these chitin chains in the form of long and narrow crystalline units, which are wrapped by proteins, forms the second structural level, (B) chitin nanofibers of about 2–5 nm diameter and 300 nm in length. These nanofibers then assemble into (C) long chitin-protein fibers of 50–300 nm in diameter. The fourth level is (D) the formation of a planar, branched woven made of entangled chitin-protein fibers. The spacing between fibers is filled with a variety of proteins and minerals. The fifth structural level is referred to as (E) twisted plywood structure or Bouligand pattern, which is made of woven chitin-protein planes. Each plane is oriented differently from each other, which creates a complex structure appearing as fiber arches, when viewed in cross-section (F).

As for cellulose fibers, the hierarchical structure of crustacean exoskeletons can be exploited for the isolation of chitin nanomaterials. Similarly, mechanical and chemical methods are typically applied to either the crustacean shells or commercially available chitin powder for the production of chitin nanofibers and nanocrystals, respectively.

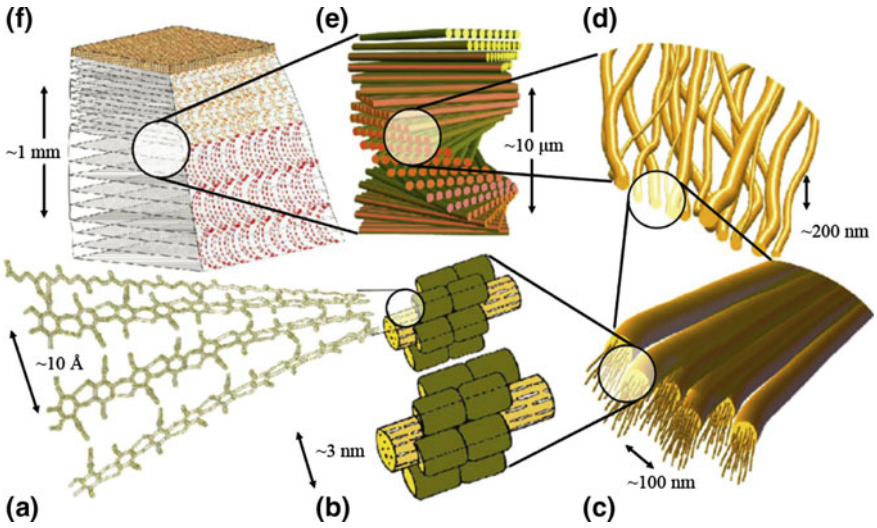

Fig. 1.4 Hierarchical organization of the exoskeleston material of the lobster *Homarus americanus* (**a**–**f**). Reproduced from [142]

1.2.2 Preparation of Chitin Nanocrystals

As for cellulose, the preparation of chitin nanocrystals (ChNCs) involves a hydrolysis step in a strong acid aqueous medium. Chitin has first to be intensively purified from the living organism, i.e. extracted from the protein and calcium carbonate matrix. The polymer is then subjected to an acid hydrolysis using hypochlorite acid (HCl), commonly at 104–105 °C, for few minutes to few hours [26]. During hydrolysis, the disordered and low lateral ordered regions of chitin are preferentially hydrolyzed and dissolved in the acidic solution, while the water-soluble and highly crystalline regions remain intact owing to their higher resistance to the acid attack [26].

The first preparation procedure of ChNC was reported in 1959, by Marchessault et al. [143]. They hydrolyzed purified chitin from crab shells for 1 h using 2.5 N HCl under reflux. After hydrolysis, the excess of acid was removed by decantation and distilled water was added to quench the reaction. They obtained a stable isotropic suspension, at pH 3.5. Since then, ChNCs have been prepared from chitin of different origins, with slight variations in the protocol as highlighted in Table 1.3.

Hydrolysis variables such as reaction time and temperature are usually adjusted to the chitin source, to promote the preparation of a good colloidal suspension. As for cellulose nanocrystals (CNCs), a series of centrifugation/filtration and washing steps is performed after hydrolysis in order to isolate and purify the nanoparticles, followed by a dialysis step, which ensures the removal of any residual acid. Ultrasonication or homogenization treatments can be then used to facilitate the dispersion of ChNC in suspension [151]. Several procedures also consider the use of low pH during ChNC preparation to facilitate the isolation of the particles. At low pH, the surface amino

Table 1.3 Hydrolysis conditions for the preparation of chitin nanocrystals from various chitin sources

Source	Acid	Time (min)	Temperature (°C)	Acid-to-Chitin ratio (mL/g)	Average dimensions of ChNCs (nm)	References
Crab shell	2.5 N HCl	60	104	37.5	n/a	[143]
		3 × 90	104	30	240 (length) 15 (width)	[144]
	3 N HCl	360	120	30	255 ± 56 (length) 31 ± 6 (width)	[145]
Shrimp shell	3 N HCl	3 × 90	90	n/a	200–500 (length) 10–15 (width)	[146]
		3 × 90	90	30	243.5 ± 55.1 (length) 9.7 ± 3.2 (width)	[147]
Riftia tube	3 N HCl	3 × 90	104	n/a	–	[148]
Lobster exoskeleton	3 N HCl	90	100	30	300 (length) 60 (width)	[149]
Cuttlefish bone	5 N HCl	90	90	30	22 (length) 14 (width)	[150]

groups of the chitin fibrils get protonated (NH_3^+), thus easing the individualization of fibrils in water.

The resulting chitin nanocrystals are highly crystalline (57–93%) and typically have a width in the range 10–20 nm, and a length ranging from 200 to 500 nm [26]. While hydrochloric acid is the most commonly used acid for the preparation of ChNCs, the use of sulfuric acid has also been investigated using the same protocol variables applied for the preparation of CNCs, i.e. 64% H_2SO_4 at 60 °C for 90 min. The needle-like ChNCs, isolated from crab shells, had a slightly higher length than their HCl-hydrolyzed counterparts (i.e. 426 ± 10 nm) and a sulfate group content of 135 μmol/g as for CNCs [152].

Other methods such as TEMPO-mediated oxidation, partial deacetylation and ionic liquids, have also been used for the preparation of ChNCs. ChNCs with 10–15 nm in width and 270 nm in length were produced from crab shells by TEMPO-mediated oxidation, using the TEMPO/NaBr/NaClO system, at pH 10 and room temperature [153]. As a result of the dissolution of the amorphous domains, polyuronic

acid is formed, and some of the C6 hydroxyl groups are converted to carboxyl groups. With the presence of surface carboxylate groups, the ChNCs form a highly stable colloidal suspension in water. Compared to the acid hydrolysis route, the yield of ChNCs can reach 90% (against 20–70%), and no *N*-deacetylation of chitin occurs during the reaction [151].

Partial deacetylation of the chitins fibrils with 33% NaOH at 90 °C for 2–4 h followed by mechanical disintegration at pH 3–4 also resulted in the production of ChNCs of 6.2 ± 1.1 nm in width and 250 ± 140 nm in length [154]. The combination of protonated amino groups on the partially deacetylated chitin fibrils surface associated with partial mechanical scission of the fibrils during disintegration promoted the individualization of the chitin fibrils and their conversion to nanocrystals. In addition, the presence of individual chitin nanofibrils of more than 500 nm in length was also detected in the ChNC suspension [154].

As an alternative for the dissolution of the amorphous domains of chitin fibrils, ionic liquids have been used on chitin for the production of ChNCs. Combination of chitin with 1-allyl-3-methylimidazolium bromide (AMIMBr) resulted, after heating, in the formation of a chitin gel, which after regeneration in methanol and subsequent sonication, showed ChNCs of 20–60 nm in width and several hundred nanometers in length [155].

Figure 1.5 shows microscopic images of ChNCs isolated by the four previously discussed production routes. For more information on the preparation of chitin nanocrystals, the readers are referred to the following review articles and book/book chapters [156, 157]

1.2.3 Preparation of Chitin Nanofibers

The preparation of chitin nanofibers (ChNFs) resembles that of cellulose nanofibers, and includes mechanical treatment (e.g. grinder, blender, and homogenizer) as well as chemical methods such as TEMPO-mediated oxidation.

High-shear mechanical treatment of crustacean shells and aqueous chitin powder suspension induces transverse cleavage along the longitudinal axis of the chitin microfibrillar structure, which results in long chitin nanofibers of high aspect ratio [151]. Similar to the production of ChNCs, the use of acidic conditions, i.e. pH 3–4, is recommended to facilitate the isolation of the fibrils by electrostatic repulsions. In particular, the use of monovalent acids at pH 2.5–3.5 and low ionic strengths seem to result in higher fibrillation degree than high ionic strengths and pH values or dispersions prepared with deprotonated polyvalent acids [26]. The degree of nanofibrillation is also influenced by the ionic strength of the system; for instance, excess acid at pH 3 inhibits the fibrillation efficiency.

The use of grinder was applied on never-dried [160] and dried [161] purified chitin from crab or prawn shells, under neutral and acidic conditions, and resulted in the formation of nanofibers of 10–20 nm in width (Fig. 1.6). Compared to cellulose nanomaterials, the production of chitin nanomaterials from dried state is advantageous

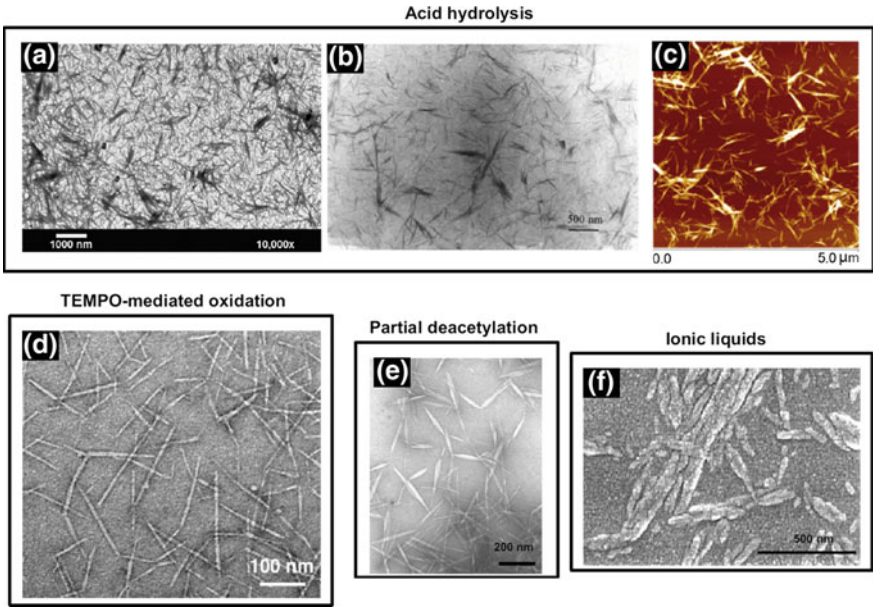

Fig. 1.5 Chitin nanocrystals obtained by acid hydrolysis from **a**, **b** shrimp shells (Transmission Electronic Microscopy (TEM) images) and **c** lobster shells (Atomic Force Microscopy (AFM) image), by **d** TEMPO-mediated oxidation from crab shells (TEM image), by **e** partial deacetylation from crab shells (TEM image) and by **f** ionic liquid method from crab shells (Scanning Electron Microscopy (SEM) image). Reproduced from [158] (**a**), [159] (**b**), [151] (**c**), [153] (**d**), [154] (**e**), and [155] (**f**). Full figure reproduced from [151]

for commercial applications in terms of storage and transportation. Smaller ChNF diameters (4 nm) can for instance be obtained after passing an aqueous dispersion of β-chitin from squid pen through a double-cylinder type homogenizer [162] (Fig. 1.6). Other variations in mechanical treatments have also been investigated, such as the combination of blender and microfluidizer [163], the use of dynamic high pressure homogenization [164] or ultrasonication [165]; all resulting in entangled chitin nanofibers of high aspect ratio (Fig. 1.6). Note that regardless of the process used, the energy consumption required for the production of chitin nanofibers remained very high, as for the production of cellulose nanofibers.

Similar to the production of chitin nanocrystals, ChNFs can be obtained by TEMPO-mediated oxidation. ChNFs of 20–50 nm in width and several microns in lengths were obtained from tubeworm using the TEMPO-mediated system with 2.5–10 mmol of sodium hypochlorite (NaClO) per gram of chitin, at a yield of more than 70% [166]. Interestingly, although a similar procedure was applied to squid pen, the oxidized products could not be converted into chitin nanofibers under any conditions examined by disintegration in water [166].

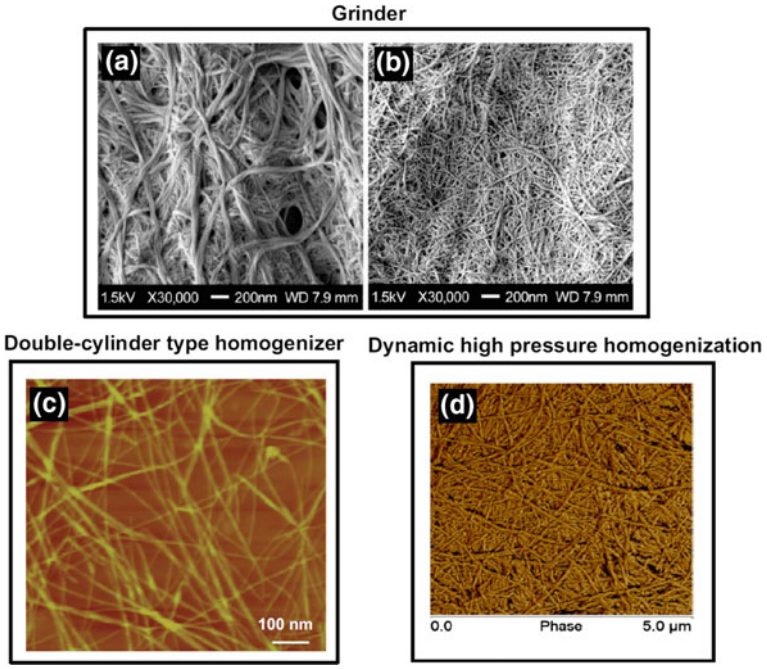

Fig. 1.6 Microscopic images of chitin nanofibers obtained from crab shells using a grinder under **a** neutral conditions and **b** acidic conditions (pH 3) (SEM images) (Reproduced from [160]), **c** from squid pen chitin using a double-cylinder type homogenizer (AFM image) (Reproduced from [162]), and **d** from lobster shells using a dynamic high-pressure homogenizer (AFM image) (Reproduced from [164]). Full picture reproduced from [151]

1.2.4 Main Properties of Chitin Nanomaterials

1.2.4.1 Morphology, Surface Area, and Colloidal Stability

Chitin nanocrystals occur as rod-like nanoparticles, while chitin nanofibers are flexible and entangled fibrils of much higher aspect ratio (length of several micrometers compared to ChNC lengths of hundreds of nanometers). Table 1.3 indicates the width and length of ChNCs obtained by acid hydrolysis from different chitin sources. A very recently published study has investigated the influence of the hydrolysis conditions and suspension treatments on the dimension and colloidal stability of ChNCs [167]. With increasing hydrolysis time (from 90 to 540 min), the length and width of the crystals were both decreased by 60%, with a consequent increase in zeta-potential from 39 ± 5 to 55 ± 9 mV, respectively.

ChNCs have high crystallinity degree (usually >80%), while ChNFs present a more amorphous character, with a crystallinity index around 50–70%. As observed with CNMs, the origin of the chitin source, the purification treatment and production

methods selected influence the crystallinity degree measured on the final nanoparticles.

While protonated amino groups are present on their surface (i.e. in the case of (partially) deacetylated chitin), chitin nanomaterials exhibit positive zeta-potential values [162] (except in the case of chitin nanomaterials obtained via TEMPO-mediated oxidation). Therefore, at lower pH, the surface charge is higher, favoring the repulsive interactions between the particles. The colloidal stability, and thus self-assembly of ChNCs can be controlled by varying the ionic strength and acid concentration of the suspension. An increase in HCl concentration results in higher chiral nematic pitch values between the particles. An increase in the ionic strength of the system can also result in a larger pitch owing to an increase in surface charge, as prevailing effect on the colloidal stability (i.e. the ionic strength of the suspension remains very low). However, with increasing ionic strength value, the pitch can start to substantially drop, as the increase in surface charge becomes limited [167].

Chitin nanomaterials exhibit exceptionally high surface area, up to 400 m^2/g. The technique of dye absorption using Congo red was applied to measure the surface area of α-chitin nanocrystals from shrimp shells, and indicated values near 350 m^2/g as well [146].

1.2.4.2 Chitin Nanopapers

Like CNMs, the mechanical properties of chitin nanomaterials have primarily been investigated on films. The manufacturing techniques of chitin nanopapers also include film casting and vacuum filtration of ChNFs suspensions.

The Young's modulus of deacetylated chitin nanopapers typically ranges from 3 to 9 GPa with tensile strengths varying from 44 to 157 MPa, respectively [168]. Note that the properties of the films highly depend on the thickness and density of the materials (information not always provided by the authors). Overall, compared with cellulose nanopapers, films from ChNFs exhibit inferior mechanical properties, which may be due to the remaining protein content after chitin purification [168]. With increasing protein content from 7 to 12%, a decrease in the mechanical properties of ChNF membranes was indeed observed: from 8.3 to 7.8 GPa for the Young's modulus and from 141 to 107 MPa for the tensile strength, respectively [163]. Membranes with the lowest protein content also showed the highest optical transmittance; the presence of protein in higher amount promoting the agglomeration of chitin nanofibers [163].

Films of chitin nanomaterials also exhibit low oxygen permeability values, but not as low as CNF films. Fan et al. [162] compared the oxygen permeability of chitin nanocrystals and nanofibers coating onto PLA to that of TEMPO-oxidized CNF coating. While all nano-chitin films showed similar oxygen permeability of 1 mL μm/m^2 day kPa, TEMPO-CNF films reached an oxygen permeability value of 0.001 mL μm/m^2 day kPa, under similar dry and coating conditions. One possible explanation is linked to the bulky acetyl groups, protonated or not, which may have disrupted the close packing of the nano-elements in the films, thus resulting in such lower oxygen barrier properties [162].

1.2.4.3 Antibacterial and Antifungal Properties of Chitin Nanomaterials

From nano-chitin, chitosan nanomaterials can be obtained by careful deacetylation using e.g. an aqueous solution of sodium hydroxide. Watthanaphanit et al. [169] prepared chitosan nanocrystals by deacetylation of ChNCs using 50% NaOH and borohydride. A direct consequence was the drastic drop of the molecular weight to 59 kDa, which was much lower than that of chitosan obtained from chitin powder under the same conditions (420 kDa). The degree of deacetylation was 0.50, and the suspension was colloidally stable for concentration in the range 1–13%. Chitosan nanomaterials can also be obtained directly from deacetylation of chitin powder using e.g. 33% NaOH at 90 °C for 2–4 h (much milder conditions), followed by mechanical disintegration (degree of deacetylation of 0.7–0.75) [154], or by direct wet-grinding or homogenization of chitosan powder [170]. The degree of *N*-acetylation is usually determined by the conditions of deacetylation. Note however that the distinction between chitin and chitosan with different degrees of deacetylation is not strict, and therefore, chitin and chitosan are often used interchangeably [171].

Chitosan is a more versatile polysaccharide than chitin. In particular, the presence of a greater number of free amino groups is responsible for its greater antimicrobial activity than chitin (upon protonation of the amino groups). Therefore, chitosan and its nanomaterials have mostly been exploited for applications requiring an antimicrobial activity, such as packaging, medicine and pharmaceutics. Chitosan nanocrystals were for instance incorporated in alginate fibers to impart antibacterial activity against a gram-positive (*Staphylococcus aureus*) and a gram-negative (*Escherichia coli*) to the wet-spun textile for wound dressing application [169]. A recent study highlighted the benefit of using chitosan at the nanoscale for improved antimicrobial activity. Ramezani et al. [172] compared the coating effects of chitosan and chitosan nanoparticles on the quality of silver carp fillets during refrigerated storage. Compared to chitosan, the nanoparticles exhibited higher antimicrobial activity during the whole storage period and were able to inhibit the total volatile basic nitrogen, which is a direct indicator of spoilage [172]. The enhanced antimicrobial activity of chitosan nanoparticles is, however, still debatable. While Qi et al. [173] also reported that the nanoparticles had higher antibacterial activity against *Escherichia coli, Staphylococcus aureus* and *Salmonella typhimurium* on account of their larger surface area and higher affinity with bacterial cells, Sadeghi et al. [174] demonstrated that chitosan nanoparticles had lesser inhibition effect on *S. aureus* than the chitosan polymer in free soluble form. Further studies are thus required to better understand the influence of the preparation routes and particle properties on the antimicrobial activity of the chitosan nanoparticles.

1.2.5 Concluding Remarks

As for CNMs, chitin nanomaterials (ChNM) have been investigated for a wide spectrum of applications [168], spanning from packaging, textiles [175] to electronics [176], wastewater treatment [177] and nanocomposites [26].

Chitin nanopapers offer a great technology platform for utilizing waste of crustacean shells as high-performance products. However, their utilization remains scarce in the literature, or shadowed by the intensive research activities on cellulose nanomaterials. Further work is needed to further understand the different characteristics between cellulose and chitin nanomaterials in order to further improve and highlight the performance of ChNM-based products.

Chitin nanomaterials have yet one unique property, which make them distinct from CNMs: their antibacterial and antifungal properties. In addition to their renewability and biocompatibility nature, chitin and chitosan nanomaterials are ideal biopolymers for the design of high-performance products for packaging, biomedical and pharmaceutical applications.

1.3 Starch Nanomaterials

Starch is a renewable and biodegradable polysaccharide generated by many plants to store energy. Starch participates to structures like root, stem, seed, leave, grain, fruit and tuber of all kinds of herbal sources in the shape of very thin particles of different shapes (ellipsoids, spheres, platelets, polygon and irregular tubules) and dimensions, ranging from 0.1 to 200 μm depending on their botanical origin [178]. Since the 1970s, starch has been of great interest owing to its renewability, biodegradability, and low cost. Various food products such as rice, wheat, corn, maize, cassava, potato contain starch, which constitutes a significant part of the daily calories needed by human beings. But starch is also present in the structure of algae, bacteria, mosses fern and protozoa [179].

Starch is commonly used in the food, adhesive, medical, paper and textile industries, but its native form, as found in nature, cannot be processed as such for industrial applications. Most starches in the native form present, indeed, limitations such as high viscosity, susceptibility to retrogradation, (i.e. reassembly or recrystallization of amylopectin and amylose chains in gelatinized starch [180]), limited digestibility for some and poor solubility in organic solvents, which limit considerably their applications. Natural starch is therefore modified by e.g. hydrolysis, acetylation, oxidation and cross-linking, to achieve preferred characteristics for a given application [181, 182].

Starch has a multi-scale structure, as depicted in Fig. 1.7, composed of (a) 2–100 μm wide granules showing (b) growth rings of 120–500 nm, which are themselves, composed of (d) blocklets of 20–50 nm in diameter. Each blocklet is composed

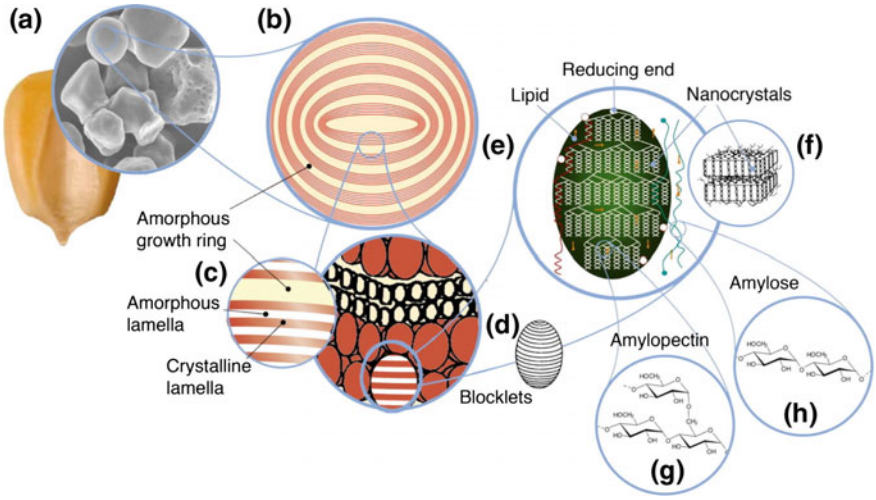

Fig. 1.7 Multiscale structure of starch. Reproduced from [183]

of (c) amorphous and crystalline lamellae (9 nm) which contain (g) amylopectin and (h) amylose chains (0.1–1 nm) [183].

Amylose is a linear polymer made of glucose monomer units linked by α-(1–4) glycosidic bonds and slightly branched by α-(1–6) linkages (molecular weight (M_w) of 1–1.5 million glucose subunits) (Fig. 1.8). Although linear, amylose commonly

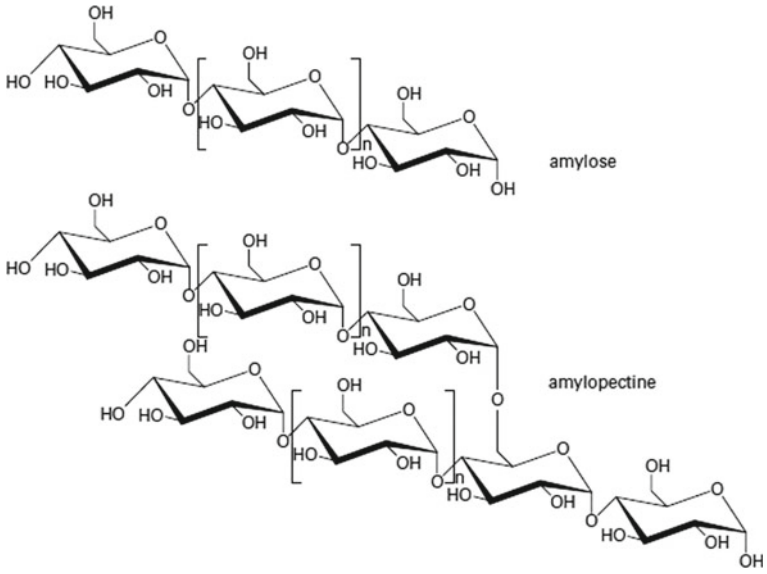

Fig. 1.8 Chemical structure of amylose and amylopectin. Reproduced from [26]

shows an extended helical twist. In most common types of starch, the amylose content ranges between 15–20 wt% [184].

Unlike amylose, amylopectin is a highly branched polymer consisting of short branches of α-D-(1–4) glycopyranose that are interlinked by α-D-(1–6) glycosidic linkages, with a M_w of approximately 50–500 million of glucose subunits (Fig. 1.8) [183]. The amylopectin content in starch is much higher than the amylose ones and ranges between 72 and 82 wt%. The unique regular assembly of amylopectin imparts crystallinity to the starch granules, while the amylose units form amorphous regions, arranged irregularly within the ordered amylopectin regions [185].

Due to notable differences in the amylopectin crystalline lattices, plant starches are generally classified into three types (A, B, and C). Observed differences in the botanical origin of starch result in different crystallinity pattern. For instance, starches obtained from waxy maize [186] and corn [187] display a A-type crystallinity, while pea starch are B-type [188]. The characteristic X-ray diffraction peaks of the A- and B-type crystals are around 15.3°, 17.1°, 18.5°, 23.5° and 5.5°, 17.2°, 22.3°, respectively. Because the C-type crystals are believed to be a combination of A- and B-type crystallinity, the diffraction spectrum will also result in a combination of the A- and B-type diffraction peaks [189].

The semi-crystalline nature of starch (and respective nanoparticles) will be detailed further below in this chapter, but is here exploited for the production of nanosized starch particles, namely nanostarches.

1.3.1 Preparation of Nanostarches

Nanostarches (NS) are nanosized particles (i.e. with at least one dimension below 100 nm) produced from starch by either hydrolysis, regeneration or mechanical treatment (Fig. 1.9). Depending on the botanical origin of starch and production routes, NS can have various shapes, morphology and structure.

Three main types of nanostarch particles can be distinguished, namely (i) starch nanocrystals (SNCs), (ii) starch nanoparticles (SNPs) and (iii) starch nanocolloids. While SNCs are purely crystalline particles, both SNPs and starch nanocolloids refer to predominantly amorphous particles.

1.3.1.1 Production of Starch Nanocrystals (SNCs)

SNCs are commonly obtained by acid hydrolysis of starch using diluted hydrochloric or sulfuric acid, at controlled extraction conditions [183]. The kinetic of hydrolysis occurs in two-steps. A fast hydrolysis step first takes place to remove the amorphous zones of natural starch and is then followed by a slower hydrolysis step that induces the fragmentation of the crystalline zones of starch [190]. After hydrolysis, the SNCs are separated from the acid by centrifugation, and washed thoroughly with distilled

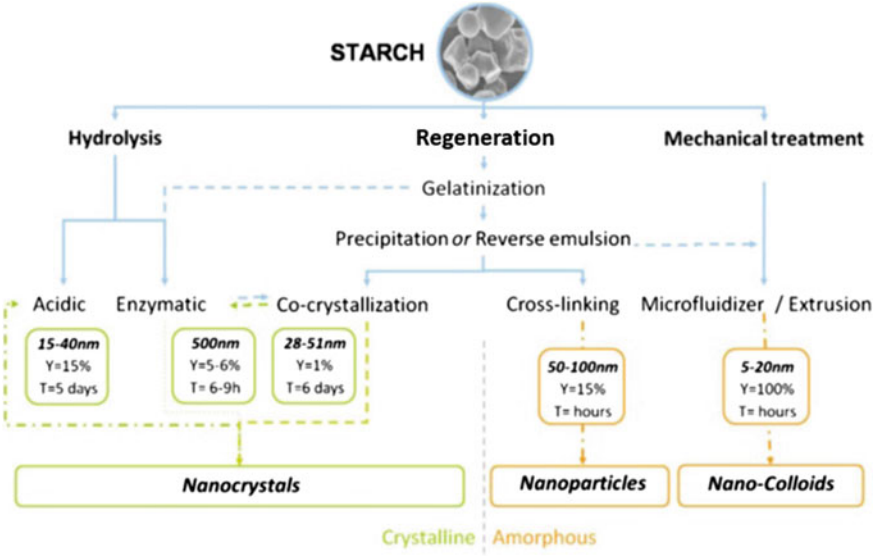

Fig. 1.9 Production routes of nanostarch. Reproduced from [183]

water until pH neutralization. Ultimately, a mechanical treatment using e.g. high shear-dispersing tools can be conducted to homogenize the SNC dispersion.

Nägeli [191] and Lintner [192] conducted one of the first studies on the production of 'crystalline granules' from potato starch by means of acid hydrolysis. By analogy with CNCs, Dufresne et al. [193] succeeded later in producing so-called 'microcrystalline starch' by hydrolyzing potato starch at 35 °C for 15 days using 5% (w/w) hydrochloric acid (HCl). Under these conditions, the microcrystalline starch consisted of agglomerates of particles of a few tens of nanometers in diameter. The term of 'starch nanocrystals (SNCs)' was only proposed few years later by Putaux et al. [194], after analyzing by TEM the crystalline particles obtained after a 6-week hydrolysis of waxy maize starch. Since then, different sources of starch and extraction conditions have been investigated for the production of starch nanocrystals (Table 1.4). For instance, Wang et al. [195] produced rectangular prism-shaped SNCs of 15–30 nm in width and 20–40 nm in length by subjecting *Rhizoma dioscorea* starch to a 2.2 M HCl hydrolysis at 35 °C and for 40 days.

The main drawbacks in using HCl hydrolysis for the production of SNCs lie in the reaction time, which accounts for few days to several weeks, and the very low-reaction yield, which can be as low as 0.5 wt% [196]. SNCs obtained by HCl hydrolysis also show poor colloidal stability due to chemical aggregation between the particles. The production of a more stable SNC suspension was achieved by Angellier et al. [196], who used sulfuric acid (H_2SO_4) to add negative sulfate groups on the particles' surface. The use of H_2SO_4 also resulted in a higher production yield of 15.7% (using 3.16 M H_2SO_4 at 40 °C) and in a shorter hydrolysis time of 5 days only. Using a slightly higher concentration of acid, in combination with a high-shear

Table 1.4 Acid hydrolysis conditions for the production of SNCs and influence on SNC morphology

Starch sources	Acid type	Reaction time (d)	Characterization technique	Reported dimensions (nm)	Reaction yield (%)	Morphology	References
Waxy potato starch	H_2SO_4	5	SEM	200–800	–	Agglomerated SNCs	[209]
Waxy (Alamo)	HCl[b]	5	FE[f]-SEM	50 ± 10	–	Sphere	[210]
Mango kernel starch	HCl/H_3PO_4[c]	5	SEM	67 ± 22	24 ± 3	Platelet	[211]
Amaranth	H_2SO_4	10	SEM/TEM[g]	376	3.6	Lamellar structure	[212]
Cassava	H_2SO_4	5	TEM	47–178	30	Sphere	[213]
Amadumbe	H_2SO_4	5	SEM/AFM	180–280	25	Platelet	[214]
Unripened banana starch Tapioca starch	H_2SO_4/HCl	5–15 h	SEM/TEM	30–70	37–86	Sphere	[197]
Waxy maize	H_2SO_4	5	FE-SEM/AFM	58	–	Platelet	[215]
Waxy corn starch	H_2SO_4	5	TEM	6–8 (*t*); 70–100 (*l*)	–	–	[216]
Pea starch	H_2SO_4	5	SEM/TEM	15–30 (*w*); 60–150 (*l*)	–	–	[188]
Potato starch	H_2SO_4	5	SEM/TEM	10–20 (*w*); 40–70 (*l*)	–	Sphere	[217]

Acid types: [a]sulfuric acid (H_2SO_4), [b]hydrochloric acid (HCl), [c]phosphoric acid (H_3PO_4); *Characterization techniques*: [d]Scanning Electron Microscopy (SEM), [e]Atomic Force Microscopy (AFM), [f]Transmission Electron Microscopy (TEM), [g]Field-Emission SEM (FE-SEM); *Dimensions*: (*w*) width, (*l*) length, (*t*) thickness

mechanical treatment (homogenizer), SNCs from banana and tapioca starches were obtained after few hours only (5–10 h), with a much higher production yield in the range 55–85% [197]. While the authors explained the differences in yield and hydrolysis time by the utilization of chemical method together with a mechanical treatment, it is worth noting that the source of starch differed between studies. The botanical origin of starch may indeed influence the hydrolysis conditions for the extraction of nanocrystals, as it has been observed with cellulose.

By varying the hydrolysis conditions such as the hydrolysis time, temperature and acid concentration, different sizes ranging from tens to hundreds of nanometers, and morphologies (e.g. round [198], square or double helical [199] shapes) of SNCs can be produced (Table 1.4). The dimensions and morphologies of the SNCs are also influenced by the chemical composition and structure of starch. While the distribution of amylose inside the granules and the blocklets only moderately affects the final characteristics of the ensuing SNCs, the amylose/amylopectin content and crystalline structure (A-, B- or C-types) influence much more the size and shape of the resulting SNCs. For a same botanic origin, an increasing amylopectin content and an A-type crystallinity are for example associated with the production of more square-shaped SNCs. For the production of SNCs, a high amylopectin content is thus usually preferred as raw materials [200].

Because of the previously mentioned challenges regarding acid hydrolysis, other approaches have been investigated for the production of SNCs (Fig. 1.9). For instance, Kim et al. [201] produced SNCs from waxy rice starch via a 24 h enzymatic hydrolysis using α-amylase followed by ultrasonication in ethanol. Similar to acid hydrolysis, the amorphous layers are preferably hydrolyzed during the initial high rate hours of the enzymatic hydrolysis.

Another approach, namely the co-crystallization, consists in forming complexes of starch molecules, especially the amylose component, with a guest compound [202]. The amylose helix can form inclusion complexes with a variety of small molecules, such as fatty acids, alcohols, aromas [203, 204], p-aminobenzoic acid, ibuprofen and salicylic acid [205], owing to its hydrophilic outer surface and hydrophobic helical channel. The amylose helices may then pack together in another crystalline structure, knows as V-type, with a number of subtypes [206]. The "V-type" crystallinity is not necessarily related to the crystalline type of native starch [189]. Depending on the guest compounds, various types of V-amylose complexes can be manufactured and are commonly categorized into V_6–V_8 categories according to the structure of the helix formed [207]. For instance, the amylose-*tert*-butanol inclusion complex belongs to the V_7 category as it contains seven fold single helices with larger cavities to accommodate a guest molecule.

Nanoscale starch particles can thus be prepared by complex formation with other components under controlled physical environmental conditions. The co-crystallization approach is yet often combined with an enzymatic hydrolysis in order to increase the crystallinity degree of the resulting SNCs; yet, a large portion of amorphous matrices can still be present [208].

1.3.1.2 Production of Starch Nanoparticles (SNPs) and Nanocolloids

The preparation of SNPs and starch nanocolloids can involve different processes such as starch regeneration by precipitation [218] or reverse emulsion, and mechanical treatment [219] (Table 1.5).

Starch regeneration is the process of gelation of starch into hydrolysates of linear and low molecular weight polymer chains, before its regeneration by means of a secondary process, either (i) solvent precipitation or (ii) reverse emulsion [183]. The regeneration step promotes the crosslinking between the starch particles.

Crosslinking by (i) nanoprecipitation of starch can be done in solvents such as ethanol, after the dissolution of starch in acetone [220], or using physical sources such as U.V. light [221]. Crosslinking by (ii) reverse emulsion consists in dispersing an aqueous phase made of starch and cross-linkers in an oil phase with the presence of emulsifiers. The obtained emulsion is composed of crosslinked starch particles whose size and shape are retained within the dispersed phase [222].

The previously mentioned techniques can also be combined to produce SNPs of different sizes, properties and higher crystallinity. Combination of these different

Table 1.5 Production routes of starch nanoparticles and nanocolloids

Starch sources	Production routes	Reported dimensions (nm)	Ref
Native starch	Acid pretreatment and ultrasound	40–80	[223]
Cassava starch	Nanoprecipitation	500–900	[224]
Oxidized starch			
Native potato starch	Ultrasonic treatment	~75	[225]
Waxy corn starch	Nanoprecipitation	20–200	[189]
		15–80	
		50–225	
		30–110	
		30–150	
Corn starch			
Potato starch			
Tapioca starch			
Pea starch			
Proso millet starch	Recrystallization	30–50	[226]
Pinhão seeds starch	Hydrochloric acid hydrolysis	453	[227]
	Ultrasonication	22	
Waxy maize	Ultrasonication	30–250	[228]
		30–140	
Maize starch			
Corn starch	Extrusion and homogenization	160	[229]

processes can contribute to energy saving and result in increased starch availability and functionality for a broader range of industrial applications.

Unlike SNPs, starch nanocolloids are principally produced (and thus defined) by mechanical treatment of starch, in a similar way to the production of CNFs from lignocellulosic biomass (Fig. 1.9). Compared to the previous chemical strategies, mechanical routes usually result in the production of much smaller starch particles. Liu et al. [219] obtained starch nanocolloids of 10–20 nm in diameter after passing a starch solution through a microfluidizer under a pressure of 207 MPa and over 20 cycles. Although this process resulted in a very high yield (>95%), the crystallinity of starch was drastically impacted, resulting in nanoscale amorphous particles. Another mechanical treatment investigated for the production of starch nanocolloids is ultrasonication. The particle dimension of the starch nanocolloids can be controlled by varying the ultrasonication time [230].

As a less energy-intensive and more eco-friendly route, extrusion has been used for producing starch nanocolloids of below 400 nm in diameter [231]. As the extrusion is performed under semi-dry conditions (around 65% solid content), the production yield is much higher than some of the other mechanical methods. During extrusion, starch is exposed to high pressure, heat and mechanical shear, resulting in significant structural alterations of starch such as melting, gelatinization, and fragmentation. It was noted that, during extrusion, complete gelatinization would not happen due to the limited water content in starch. However, at high extrusion temperatures, starch granules soften, melt, and become less resistant to high shear forces, which may cause the loss of crystallinity. Partial or complete destruction of the crystalline structure of the raw starch granule was indeed reported, confirming the starch fragmentation during extrusion [232]. Song et al. [229] produced starch nanocolloids of 300 nm in diameter at 100 °C without any crosslinker, using extrusion. With the addition of suitable crosslinkers, the starch particle dimension can be further decreased (e.g. to around 160 nm) and lower extrusion temperature can also be used (e.g. 75 °C).

Milling is another preferred mechanical route to obtain starch nanocolloids (or nanoparticles) due to its ease of operation and low wear contamination. Without using any chemical stabilizers, Patel et al. [233] produced SNPs of 245 nm after 90 min milling under stirring. While the crystallinity of SNPs was reported to decrease with increasing milling process, this method can be considered for large-scale preparation of SNPs at high yield in limited time.

Strategies to produce nanostarch are diverse and multiple, and result in particles of various shapes, dimensions, crystallinities and thus, properties. To date, no unique route is proposed, and further works are needed for a better control of the particles' morphology and structure, and to reduce the time and energy demand of the processing routes. Yet, large-scale production and commercialization of nanostarch are already in place.

1.3.2 Characterization and Properties of Nanostarches

1.3.2.1 Morphology

The morphology of NS differs with respect to the botanical origin of starch and the selected production route (Fig. 1.10).

Overall, the reported dimensions of NS range from 20 to 200 nm for the lengths (or diameters) and from 5 to 10 nm for the thickness (or width). The morphology of waxy maize SNCs was for the first time observed by TEM, in 2003 (Fig. 1.11 [194]).

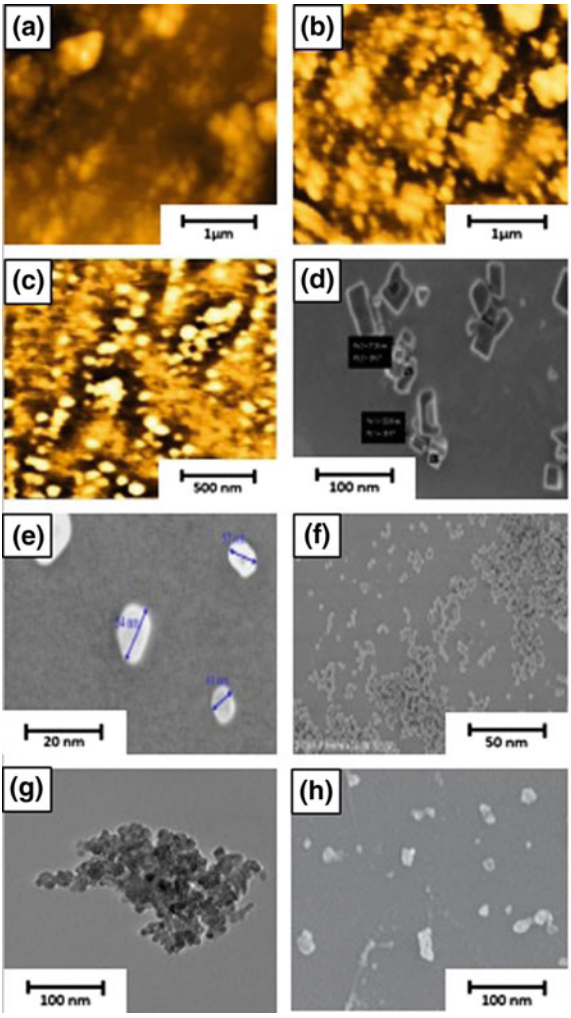

Fig. 1.10 Microscopic images of nanostarches. **a** Corn starch (AFM); **b** Cassava starch (AFM); **c** Yam starch (AFM) (Reproduced from [234]); **d** Waxy maize sulfuric acid hydrolyzed SNCs (FESEM) (Reproduced from [215]); **e** Waxy maize SNPs by ultrasound (FESEM) (Reproduced from [228]) **f** Core–Shell Starch (SEM) (Reproduced from [235]); **g** Waxy barley starch (TEM) (Reproduced from [236]); **h** Waxy maize starch (SEM) (Reproduced from [237])

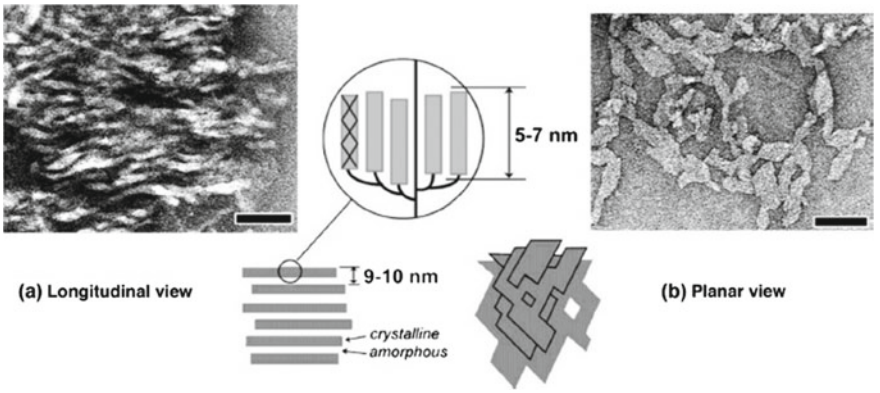

Fig. 1.11 Transmission Electron Microscopy (TEM) images of waxy maize SNCs obtained after a 6-week hydrolysis. **a** Longitudinal view of the lamellar fragments; **b** planar view of the individual platelets. Reproduced with the permission from [183] Copyright © 2014 Elsevier Ltd.

After 6 weeks of acid hydrolysis, the thus-produced SNCs displayed a lamellar morphology consisting of stack of elongated elements, with a width of 5–7 nm.

Since then, nanostarch of various shapes, spanning from polyhedron to well-defined spheres have been produced (Fig. 1.10). Le Corre et al. [200] researched the influence of botanic origin on the morphology of SNCs. No correlation between the SNC morphology and botanic origin or amylose content was observed, but a direct link with the crystalline type (A, B, or C-types) was highlighted, as shown on Fig. 1.12. Waxy maize and wheat starch, both A-type, displayed respectively parallel

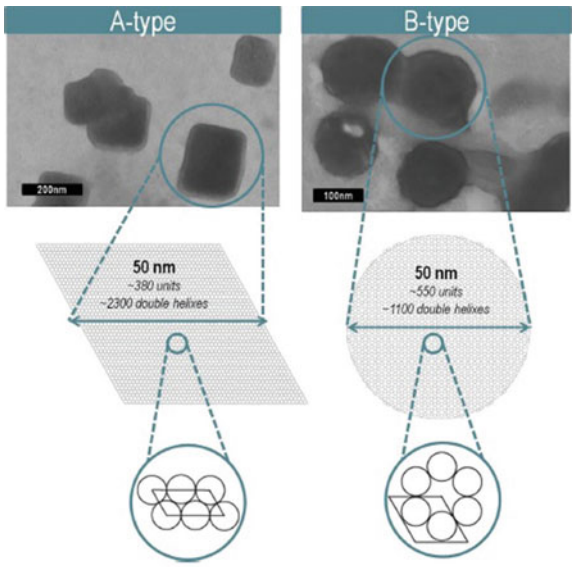

Fig. 1.12 Influence of the two main crystalline structures (A- and B-types) on the morphology of starch nanocrystals. Reproduced from [183]

epipedic and square-like nanocrystals (i.e. square-like particles), while high amylose maize and potato SNCs, both B-type starch, were more rounded particles [183]. The C-type starch usually refers to a mixture of both A and B types and therefore has not been correlated to any specific nanocrystal shape [238].

The crystalline structure also seems to affect the resistance of starch to acid hydrolysis, and therefore influence the particle size. For instance, Le Corre et al. [200] reported that the sizes of SNCs prepared from B- and C-type starches were much bigger than those prepared from A-type starches, probably due to their greater resistance to the hydrolysis.

1.3.2.2 Crystallinity

The crystal structure of nanostarches is usually related to that of the starch they are made from, and consequently varies with the botanical origin (as discussed previously).

Commonly, the degree of crystallinity of SNCs ranges between 45 and 50% [200] (Table 1.6). The amylose content in native starch is reported to be the most significant factor influencing the degree of crystallinity, or crystallinity index (CI), of NS [239]. By varying the acid hydrolysis time from 4 to 6 days, and thus varying the amylose content, the CI of waxy maize NS increased from 48 to 63% respectively [240]. After 10 days of hydrolysis, the CI of NS increased further to 79%, but the production yield was then decreased to 10%.

Table 1.6 Crystallinity properties of nanostarches

Starch sources	Amylose content of starch (%)	Production method	Crystal structure	Crystallinity index (%)	References
Corn starch	27 ± 1	Acid hydrolysis and Ultrasonication	–	36.6	[245]
Proso millet starch	3	Recrystallization	B-type	49	[226]
Tapioca starch	18.9	Nanoprecipitation	V-type	19.3	[189]
Waxy corn starch	0.8			7.1	
Corn starch	26.5			23.2	
Potato starch	28.0			26.3	
Pea starch	40.0			31.5	
Short amylose from waxy corn starch	–	Enzymatic hydrolysis and recrystallization	B and V-type	55.41	[237]
Waxy corn starch	–	TEMPO-mediated oxidation	Amorphous character	1.72	[246]
Waxy corn starch	1%	Acid hydrolysis	A-type	50	[194]

The production methods, such as nanoprecipitation or enzymatic hydrolysis, can also drastically influence the crystal structure of NS, and in this case, the starch source and amylose: amylopectin ratio will not be the determining factors anymore that dictate the crystallinity and structure of the particles. SNPs produced by nanoprecipitation showed, indeed, a so-called V-type crystallinity by XRD spectroscopy which was defined by the emergence of new diffraction peaks at 13.5° and 20.8° [189], due to the re-assembly of the polymer chains in a more single-helical structure. Similarly, a decrease and change in crystallinity can be observed after an enzymatic hydrolysis. A polymorphic transition from V-type to B-type has for instance been observed [241], which suggests that the crystalline regions of the amylose complexes may be disrupted by hydrolysis [208]. Likewise, an enzymatic treatment can also act on the amorphous zones in a V-type amylose structure, and result in an increase in crystallinity degree [242]. In some cases, however, the crystalline structure of the starch is not affected by the enzymatic hydrolysis at all, and only a broadening of some diffraction peaks can be observed.

1.3.2.3 Surface Chemistry

With the conversion of macroscale native starch to nanoscale starch, both the specific surface area and total surface energy of the particles increase, resulting in highly reactive surface NS with a greater number of hydroxyl groups compared to native starches.

SNCs have a polar constituent as high as the dispersive one, as expected from an OH-rich surface [243]. For 1 g of freeze-dried SNCs, a surface charge density of 0.0025 mol of reactive hydroxyl groups has been estimated by the Connolly surface methodology, which represents ~14% of the total weight.

As mentioned earlier, the nature of the acid used for the hydrolysis affects the surface chemistry of the NS. Compared to SNCs produced using hydrochloric acid, the SNCs resulting from sulfuric acid hydrolysis display enhanced colloidal stability in water, due to the presence of negative sulfate ester groups, as opposed to hydroxyl groups [244]. In addition to sulfate ester groups, the presence of carboxyl groups has also been detected in H_2SO_4-hydrolyzed SNCs due to the adsorption of formic and levulinic acids; both byproducts resulting from the degradation of glucose during the acid hydrolysis process (Fig. 1.13). H_2SO_4-SNCs have thus higher zeta-potential values than HCl-SNCs (e.g. −23 mV against −5 mV at pH 6.5, respectively).

1.3.2.4 Rheological Properties

The rheological properties of NS in aqueous suspension have been investigated to broaden their utilization, but also in reference to the common usage of starch in the pulp and paper coating industry.

Aqueous dispersions of starch nanocrystals typically display a shear-thinning behavior for a shear rate range of 0.1–10,000 s^{-1} [200], and this, regardless of the

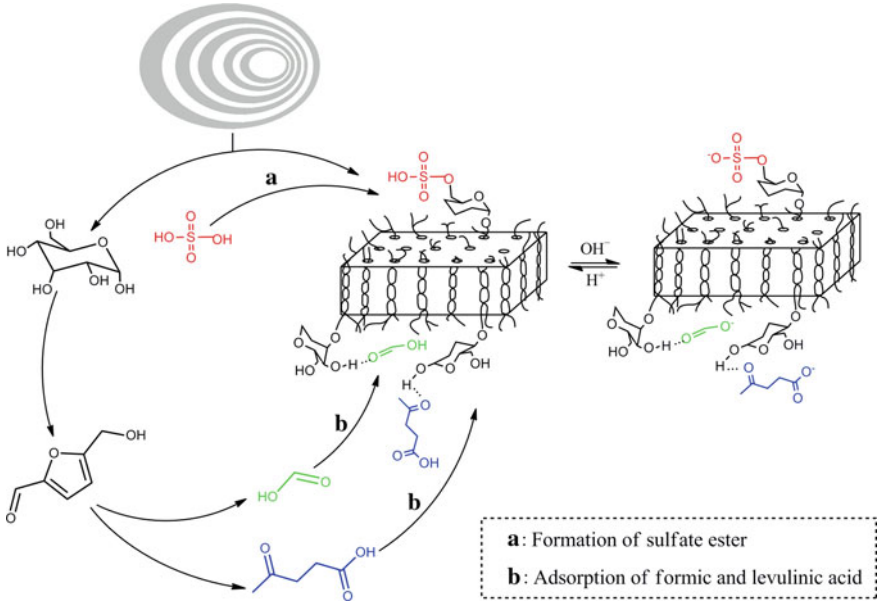

Fig. 1.13 Proposed reactions occurring during acid hydrolysis of starch, resulting in the formation of sulfate esters and carboxyl groups on the surface of SNCs. Reproduced from [244]

solid content, morphology and physical properties of the particles. Suspensions of starch nanoparticles of 600 nm in diameter or lower, have also shown a similar shear-thinning behavior [183].

Overall, most of the studies reporting the rheological behavior of starch nanoparticles demonstrated that the rheological nature of SNPs, in particular, is similar to their counterpart native starches (i.e. increase in viscosity upon heating), besides some variations in the gelatinization temperature.

Nanostarches are typically produced in water, and therefore, to extend the storage life of the particles and reduce the volume/weight of the final product, attempts have been made to dry the particles. Spray drying and vacuum freeze-drying are the two most commonly used methods for removing the water in the production of NS [247, 248]. Since these two systems operate differently (i.e. different particle temperature and rate of water removal), the ensuing dry products display distinct properties, especially in size, morphology, degree of crystallization and re-dispersibility. The re-dispersing behavior of NS can impact on their application, and therefore the effect of drying on the rheological properties of these particles has been investigated.

Preliminary studies reported that vacuum-freeze dried NS showed a less thixotropic behavior than the spray-dried NS, with a stronger elastic structure, while spray-dried NS possessed more stiffness, shorter relaxation time and less irrecoverable creep deformation [249]. The addition of sodium chloride (NaCl) to the re-dispersed nanostarches also acted quite differently on the shear viscosity of both types of re-dispersed suspensions, suggesting that a careful selection of the drying

method is required for a given application [250]. Further works are yet still needed to understand further the particle interaction and structure variation of the starch nanoparticles after drying and re-dispersion in water.

1.3.2.5 Biodegradability and Toxicity

There are still very few research studies focusing on the biodegradability of NS. The first reported studies show that compared with native starch and cellulose nanocrystals (CNCs), SNCs demonstrate a considerably faster degradation in the first seven days. After 28 days of biodegradability testing following the Organisation for Economic Co-operation and Development (OECD) standard, 58% of SNCs were successfully degraded against e.g. 54% for CNCs [251]. These promising results encourage the use of nanostarch for the development of biodegradable materials.

The main driving force behind the use of biodegradable and renewable nanomaterials is to address the toxicity issue of synthetic nanoparticles [230]. SNPs were tested in contact with mouse embryonic fibroblast cells in a wide range of concentration (0–250 g/mL), and showed no alteration of the cell viability after 24 h [252]. Similarly, surface modified SNPs (e.g. propyl SNPs) did not show any important decrease in cell viability at doses as high as 2 mg of nanoparticles per mL of growth medium [253]. Cationic SNPs of 50 nm in diameter, prepared by reverse emulsion, did not show any cytotoxicity either in addition to demonstrate good biodegradability and biocompatibility [254].

The first studies on cytotoxicity and biodegradability of NS highlight the potential of starch nanoparticles, with and without chemical modifications, to be used in food packaging, biomedical and pharmaceutical applications.

1.3.3 Concluding Remarks

Similar to chitin and cellulose, starch nanoparticles can be produced from native starch by either chemical or mechanical treatments. Different types of particles can be obtained with diverse morphologies and specificities. While chitin and cellulose nanocrystals have an elongated rod-like morphology, starch nanocrystals occur as platelet-like nanoparticles, which may limit their application as e.g. reinforcement fillers of polymeric matrices, but may open the door to new applications.

The studies on the non-cytotoxicity and good biodegradability of these nanoparticles pave the way for application in e.g. food industry, medicine and pharmaceutics. Compared to CNMs, research progress on nanostarches grows slower and further works are still needed to fully understand the potential of these nanoparticles. Some commercial applications are yet already available such as the EcoSphere® biolatex® coating binder for paper and paperboard developed by the Canadian company EcoSynthetix.

1.4 General Conclusion

The synthesis of nanoparticles from polysaccharides has been the subject of intense research efforts over the past twenty years. Huge advancements have been made to exploit the unique properties of these nanomaterials for a wide spectrum of applications, spanning from composites, paper and board products, adhesives, coatings to construction, electronics, energy-storage devices, cosmetics and biomedical applications (among others). Research has indeed revealed that these nanomaterials have not only unique properties but also comparable and competitive ones to well-known synthetic nanomaterials, which make them the ideal candidate to address the sustainability challenges of our society.

Cellulose, chitin and starch are three abundant and renewable polymers, featuring in nature a hierarchical structure with distinct properties. The preparation routes to isolate the nanomaterials from these three biopolymers are yet quite similar, and include two main strategies, namely (i) an acid hydrolysis to isolate the pure crystalline particles, or (ii) a high-shear mechanical treatment aiming at extracting nanoscale particles of amorphous/crystalline nature, which, in the case of cellulose and chitin, display a highly fibrillary structure. Variations in synthesis approaches have also been proposed, mainly for energy and cost reduction purposes, which result in nanoparticles of different morphology and properties. To date, researchers are still attempting to correlate the most appropriate preparation route for a given application.

Among those three polymers, research on cellulose nanomaterials is the most advanced, and as a result of these intense research initiatives, several organizations mostly located in North America, North Europe and Japan can produce CNMs at pilot and industrial scales. Cellulose nanomaterials seem, indeed, to feature better and more tunable properties than chitin and starch nanomaterials, which may have pushed forward their development for a broader range of applications. Further works are yet needed to fully exploit and discover the unique properties of chitin and starch nanomaterials (e.g. the antimicrobial properties of chitin) for target applications.

Acknowledgements The authors would like to acknowledge the Scientific and Technological Research Council of Turkey (Türkiye Bilimsel ve Teknolojik Araştırma Kurumu, Project #1059B141800332) for financial support, and Dr. Saim Ateş from Kastamonu University, Faculty of Forestry, Department of Forest Industrial Engineering for his collaboration and support.

References

1. Klemm D, Heublein B, Fink H-P et al (2005) Cellulose: fascinating biopolymer and sustainable raw material. Angew Chem Int Ed Engl 44:3358–3393
2. Nechyporchuk O, Belgacem MN, Bras J (2016) Production of cellulose nanofibrils: a review of recent advances. Ind Crops Prod 17:2311–2320
3. Isogai A, Saito T, Fukuzumi H (2011) TEMPO-oxidized cellulose nanofibers. Nanoscale 3:71–85

4. Moon RJ, Martini A, Nairn J et al (2011) Cellulose nanomaterials review: structure, properties and nanocomposites. Chem Soc Rev 40:3941–3994
5. Siró I, Plackett D (2010) Microfibrillated cellulose and new nanocomposite materials: a review. Cellulose 17:459–494
6. Moon RJ, Schueneman GT, Simonsen J (2016) Overview of cellulose nanomaterials, their capabilities and applications. JOM 1–12
7. Li F, Mascheroni E, Piergiovanni L (2015) The potential of nanocellulose in the packaging field: a review. Packag Technol Sci 28:475–508
8. Dugan JM, Gough JE, Eichhorn SJ (2013) Bacterial cellulose scaffolds and cellulose nanowhiskers for tissue engineering. Nanomedicine 8:287–298
9. Brodin FW, Gregersen ØW, Syverud K (2014) Cellulose nanofibrils: challenges and possibilities as a paper additive or coating material—a review. Nord Pulp Pap Res J 29:156–166
10. Hoeng F, Denneulin A, Bras J (2016) Use of nanocellulose in printed electronics: a review. Nanoscale 8:13131–13154
11. Mariano M, El Kissi N, Dufresne A (2014) Cellulose nanocrystals and related nanocomposites: review of some properties and challenges. J Polym Sci, Part B: Polym Phys 52:791–806
12. ISO (2017) Nanotechnologies—standard terms and their definition for cellulose nanomaterial ISO/TS 20477:2017. In: International organization for standardization ISOTC/ 229 nanotechnologies
13. García A, Gandini A, Labidi J et al (2016) Industrial and crop wastes: a new source for nanocellulose biorefinery. Ind Crops Prod 93:26–38
14. Jonoobi M, Oladi R, Davoudpour Y et al (2015) Different preparation methods and properties of nanostructured cellulose from various natural resources and residues: a review. Cellulose 22:935–969
15. Jozala AF, de Lencastre-Novaes LC, Lopes AM et al (2016) Bacterial nanocellulose production and application: a 10-year overview. Appl Microbiol Biotechnol 100:2063–2072
16. Favier V, Chanzy H, Cavaillé JY (1995) Polymer nanocomposites reinforced by cellulose whiskers. Macromolecules 28:6365–6367
17. Brown EE, Laborie M-PG (2007) Bioengineering bacterial cellulose/poly(ethylene oxide) nanocomposites. Biomacromol 8:3074–3081
18. Hirose E (2009) Ascidian tunic cells: morphology and functional diversity of free cells outside the epidermis. Invertebr Biol 128:83–96
19. Zhao Y, Li J (2014) Excellent chemical and material cellulose from tunicates: diversity in cellulose production yield and chemical and morphological structures from different tunicate species. Cellulose 21:3427–3441
20. Seo YB, Lee YW, Lee CH, You HC (2010) Red algae and their use in papermaking. Bioresour Technol 101:2549–2553
21. Krystynowicz A, Czaja W, Wiktorowska-Jezierska A et al (2002) Factors affecting the yield and properties of bacterial cellulose. J Ind Microbiol Biotechnol 29:189–195
22. Iwamoto S, Kai W, Isogai A, Iwata T (2009) Elastic modulus of single cellulose microfibrils from tunicate measured by atomic force microscopy. Biomacromol 10:2571–2576
23. Kose R, Mitani I, Kasai W, Kondo T (2011) "Nanocellulose" as a single nanofiber prepared from pellicle secreted by gluconacetobacter xylinus using aqueous counter collision. Biomacromol 12:716–720
24. Imai T, Sugiyama J (1998) Nanodomains of I α and I β cellulose in algal microfibrils. Macromolecules 31:6275–6279
25. Kargarzadeh Hanieh (2017) Handbook of nanocellulose and cellulose nanocomposites. Wiley-VCH Verlag GmbH & Co., KGaA, Weinheim, Germany
26. Dufresne A (2017) Nanocellulose: from nature to high performance tailored material. In: Nanocellulose. De Gruyter, Berlin, Boston
27. Habibi Y, Lucia LA, Rojas OJ (2010) Cellulose nanocrystals: chemistry, self-assembly, and applications. Chem Rev 110:3479–3500
28. Rånby BG, Banderet A, Sillén LG (1949) Aqueous colloidal solutions of cellulose micelles. Acta Chem Scand 3:649–650

29. Lu Q, Lin W, Tang L et al (2014) A mechanochemical approach to manufacturing bamboo cellulose nanocrystals. J Mater Sci 50:611–619
30. Araki J, Wada M, Kuga S, Okano T (1998) Flow properties of microcrystalline cellulose suspension prepared by acid treatment of native cellulose. Colloids Surf A Physicochem Eng Asp 142:75–82
31. Camarero Espinosa S, Kuhnt T, Foster EJ et al (2013) Isolation of thermally stable cellulose nanocrystals by phosphoric acid hydrolysis. Biomacromol 14:1223–1230
32. Lee SY, Mohan DJ, Kang IA et al (2009) Nanocellulose reinforced PVA composite films: effects of acid treatment and filler loading. Fibers Polym 10:77–82
33. Araki J, Wada M, Kuga S (2001) Steric stabilization of a cellulose microcrystal suspension by poly(ethylene glycol) grafting. Langmuir 17:21–27
34. Fleming K, Gray D, Prasannan S et al (2000) Cellulose crystallites: a new and robust liquid crystalline medium for the measurement of residual dipolar couplings. J Am Chem Soc 122:5224–5225
35. Habibi Y, Goffin A-L, Schiltz N et al (2008) Bionanocomposites based on poly(ε-caprolactone)-grafted cellulose nanocrystals by ring-opening polymerization. J Mater Chem 18:5002–5010
36. Kvien I, Tanem BS, Oksman K (2005) Characterization of cellulose whiskers and their nanocomposites by atomic force and electron microscopy. Biomacromol 6:3160–3165
37. Saïd Azizi Samir MA, Alloin F, Paillet M et al (2004) Tangling effect in fibrillated cellulose reinforced nanocomposites. Macromolecules 37:4313–4316
38. Anglès MN, Dufresne A (2000) Plasticized starch/tunicin whiskers nanocomposites. Struct Anal Macromol 33:8344–8353
39. Siqueira G, Bras J, Dufresne A (2009) Cellulose whiskers versus microfibrils: influence of the nature of the nanoparticle and its surface functionalization on the thermal and mechanical properties of nanocomposites. Biomacromol 10:425–432
40. Hassan ML, Hassan EA, Oksman KN (2011) Effect of pretreatment of bagasse fibers on the properties of chitosan/microfibrillated cellulose nanocomposites. J Mater Sci 46:1732–1740
41. Saito T, Nishiyama Y, Putaux J-L et al (2006) Homogeneous suspensions of individualized microfibrils from tempo-catalyzed oxidation of native cellulose. Biomacromol 7:1687–1691
42. Agoda-Tandjawa G, Durand S, Berot S et al (2010) Rheological characterization of microfibrillated cellulose suspensions after freezing. Carbohydr Polym 80:677–686
43. Lavoine N, Desloges I, Dufresne A et al (2012) Microfibrillated cellulose—its barrier properties and applications in cellulosic materials: a review. Carbohydr Polym 90:735–764
44. Bondeson D, Mathew A, Oksman K (2006) Optimization of the isolation of nanocrystals from microcrystalline cellulose by acid hydrolysis. Cellulose 13:171–180
45. Beck-Candanedo S, Roman M, Gray DG (2005) Effect of reaction conditions on the properties and behavior of wood cellulose nanocrystal suspensions. Biomacromol 6:1048–1054
46. Elazzouzi-Hafraoui S, Nishiyama Y, Putaux J-L et al (2008) The shape and size distribution of crystalline nanoparticles prepared by acid hydrolysis of native cellulose. Biomacromol 9:57–65
47. Dong S, Bortner MJ, Roman M (2016) Analysis of the sulfuric acid hydrolysis of wood pulp for cellulose nanocrystal production: a central composite design study. Ind Crops Prod 93:76–87
48. Bouchard J, Méthot M, Fraschini C et al (2016) Effect of oligosaccharide deposition on the surface of cellulose nanocrystals as a function of acid hydrolysis temperature. Cellulose 23:3555–3567
49. Fang W, Arola S, Malho J-M et al (2016) Noncovalent dispersion and functionalization of cellulose nanocrystals with proteins and polysaccharides. Biomacromol 17:1458–1465
50. Man Z, Muhammad N, Sarwono A et al (2011) Preparation of cellulose nanocrystals using an ionic liquid. J Polym Environ 19:726–731
51. Leung ACW, Hrapovic S, Lam E et al (2011) Characteristics and properties of carboxylated cellulose nanocrystals prepared from a novel one-step procedure. Small 7:302–305

52. Turbak AF, Snyder FW, Sandberg KR (1983) Microfibrillated cellulose, a new cellulose product: properties, uses, and commercial potential. J Appl Polym Sci Appl Polym Symp 37
53. Herrick FW, Casebier RL, Hamilton JK et al (1983) Microfibrillated cellulose: morphology and accessibility. J Appl Polym Sci: Appl Polym Symp 37:797
54. Iwamoto S, Nakagaito AN, Yano H et al (2005) Optically transparent composites reinforced with plant fiber-based nanofibers. Appl Phys A Mater Sci Process 81:1109–1112
55. Nakagaito AN, Yano H (2004) The effect of morphological changes from pulp fiber towards nano-scale fibrillated cellulose on the mechanical properties of high-strength plant fiber based composites. Appl Phys A Mater Sci Process 78:547–552
56. Spence KL, Venditti RA, Rojas OJ et al (2011) A comparative study of energy consumption and physical properties of microfibrillated cellulose produced by different processing methods. Cellulose 18:1097–1111
57. Qing Y, Sabo R, Zhu JY et al (2013) A comparative study of cellulose nanofibrils disintegrated via multiple processing approaches. Carbohydr Polym 97:226–234
58. Kriechbaum K, Munier P, Apostolopoulou-Kalkavoura V et al (2018) Analysis of the porous architecture and properties of anisotropic nanocellulose foams: a novel approach to assess the quality of cellulose nanofibrils (CNFs). ACS Sustain Chem Eng
59. Hu C, Zhao Y, Li K et al (2015) Optimizing cellulose fibrillation for the production of cellulose nanofibrils by a disk grinder. Holzforschung 69:993–1000
60. Kondo T, Kose R, Naito H et al (2014) Aqueous counter collision using paired water jets as a novel means of preparing bio-nanofibers. Carbohydr Polym 112:284–290
61. Kose R, Kondo T (2011) Favorable 3D-network formation of chitin nanofibers dispersed in water prepared using aqueous counter collision. FIBER 67:91–95
62. Chakraborty A, Sain M, Kortschot M (2005) Cellulose microfibrils: a novel method of preparation using high shear refining and cryocrushing. Holzforschung 59:102–107
63. Sacui IA, Nieuwendaal RC, Burnett DJ et al (2014) Comparison of the properties of cellulose nanocrystals and cellulose nanofibrils isolated from bacteria, tunicate, and wood processed using acid, enzymatic, mechanical, and oxidative methods. ACS Appl Mater Interfaces 6:6127–6138
64. Van Hai L, Son HN, Seo YB (2015) Physical and bio-composite properties of nanocrystalline cellulose from wood, cotton linters, cattail, and red algae. Cellulose 22:1789–1798
65. Luzi F, Fortunati E, Puglia D et al (2014) Optimized extraction of cellulose nanocrystals from pristine and carded hemp fibres. Ind Crops Prod 56:175–186
66. Yu H, Qin Z, Liang B et al (2013) Facile extraction of thermally stable cellulose nanocrystals with a high yield of 93% through hydrochloric acid hydrolysis under hydrothermal conditions. J Mater Chem A 1:3938–3944
67. Lu P, Hsieh Y-L (2012) Preparation and characterization of cellulose nanocrystals from rice straw. Carbohydr Polym 87:564–573
68. Agustin MB, Ahmmad B, Alonzo SMM et al (2014) Bioplastic based on starch and cellulose nanocrystals from rice straw. J Reinf Plast Compos 33:2205–2213
69. Garcia de Rodriguez NL, Thielemans W, Dufresne A (2006) Sisal cellulose whiskers reinforced polyvinyl acetate nanocomposites. Cellulose 13:261–270
70. Tejado A, Alam MN, Antal M et al (2012) Energy requirements for the disintegration of cellulose fibers into cellulose nanofibers. Cellulose 19:831–842
71. Naderi A, Lindström T, Sundström J (2015) Repeated homogenization, a route for decreasing the energy consumption in the manufacturing process of carboxymethylated nanofibrillated cellulose? Cellulose 22:1147–1157
72. Henriksson M, Henriksson G, Berglund LA et al (2007) An environmentally friendly method for enzyme-assisted preparation of microfibrillated cellulose (MFC) nanofibers. Eur Polym J 43:3434–3441
73. Nechyporchuk O, Pignon F, Belgacem MN (2015) Morphological properties of nanofibrillated cellulose produced using wet grinding as an ultimate fibrillation process. J Mater Sci 50:531–541

74. Bäckström M, Bolivar S, Paltakari J (2012) Effect of ionic form on fibrillation and the development of the fibre network strength during the refining of the kraft pulps. O Pap 73:57–65
75. Saito T, Kimura S, Nishiyama Y et al (2007) Cellulose nanofibers prepared by TEMPO-mediated oxidation of native cellulose. Biomacromol 8:2485–2491
76. Saito T, Hirota M, Tamura N et al (2009) Individualization of nano-sized plant cellulose fibrils by direct surface carboxylation using TEMPO catalyst under neutral conditions. Biomacromol 10:1992–1996
77. Aulin C, Ahola S, Josefsson P et al (2009) Nanoscale cellulose films with different crystallinities and mesostructures—their surface properties and interaction with water. Langmuir 25:7675–7685
78. Taipale T, Österberg M, Nykänen A et al (2010) Effect of microfibrillated cellulose and fines on the drainage of kraft pulp suspension and paper strength. Cellulose 17:1005–1020
79. Eyholzer C, Borges de Couraça A, Duc F et al (2011) Biocomposite hydrogels with carboxymethylated, nanofibrillated cellulose powder for replacement of the nucleus pulposus. Biomacromol 12:1419–1427
80. Ghanadpour M, Carosio F, Larsson PT et al (2015) Phosphorylated cellulose nanofibrils: a renewable nanomaterial for the preparation of intrinsically flame-retardant materials. Biomacromol 16:3399–3410
81. Larsson PA, Berglund LA, Wågberg L (2014) Ductile all-cellulose nanocomposite films fabricated from core–shell structured cellulose nanofibrils. Biomacromol 15:2218–2223
82. Liimatainen H, Visanko M, Sirviö JA et al (2012) Enhancement of the nanofibrillation of wood cellulose through sequential periodate–chlorite oxidation. Biomacromol 13:1592–1597
83. Miller J (2019) Nanocellulose: packaging applications and markets. RISI
84. Foster EJ, Moon RJ, Agarwal UP et al (2018) Current characterization methods for cellulose nanomaterials. Chem Soc Rev 47:2609–2679
85. Cranston ED, Gray DG (2006) Morphological and optical characterization of polyelectrolyte multilayers incorporating nanocrystalline cellulose. Biomacromol 7:2522–2530
86. Bhattacharjee S (2016) DLS and zeta potential—what they are and what they are not? J Control Release 235:337–351
87. Revol J-F, Bradford H, Giasson J et al (1992) Helicoidal self-ordering of cellulose microfibrils in aqueous suspension. Int J Biol Macromol 14:170–172
88. Isogai A, Saito T, Shimizu M et al (2016) Fast and robust nanocellulose width estimation using turbidimetry. Macromol Rapid Commun 37:1581–1586
89. Iwamoto S, Nakagaito AN, Yano H (2007) Nano-fibrillation of pulp fibers for the processing of transparent nanocomposites. Appl Phys A Mater Sci Process 89:461–466
90. Smith DK, Bampton RF, Alexander WJ (1963) Use of new solvents for evaluating chemical cellulose for the viscose process. Ind Eng Chem Process Des Dev 2:57–62
91. Shinoda R, Saito T, Okita Y et al (2012) Relationship between length and degree of polymerization of TEMPO-oxidized cellulose nanofibrils. Biomacromol 13:842–849
92. Battista OA (1950) Hydrolysis and crystallization of cellulose. Ind Eng Chem 42:502–507
93. Håkansson H, Ahlgren P (2005) Acid hydrolysis of some industrial pulps: Effect of hydrolysis conditions and raw material. Cellulose 12:177–183
94. Thomas B, Raj MC, Athira KK et al (2018) Nanocellulose, a versatile green platform: from biosources to materials and their applications. Chem Rev 118:11575–11625
95. French AD (2014) Idealized powder diffraction patterns for cellulose polymorphs. Cellulose 21:885–896
96. Garvey CJ, Parker IH, Simon GP (2005) On the interpretation of X-ray diffraction powder patterns in terms of the nanostructure of cellulose I fibres. Macromol Chem Phys 206:1568–1575
97. Segal L, Creely JJ, Martin AE et al (1959) An empirical method for estimating the degree of crystallinity of native cellulose using the X-ray diffractometer. Text Res J 29:786–794
98. Park S, Baker JO, Himmel ME et al (2010) Cellulose crystallinity index: measurement techniques and their impact on interpreting cellulase performance. Biotechnol Biofuels 3:10
99. Yamamoto H, Horii F, Odani H (1989) Structural changes of native cellulose crystals induced by annealing in aqueous alkaline and acidic solutions at high temperatures. Macromolecules 22:4130–4132

100. Revol JF, Godbout L, Dong XM et al (1994) Chiral nematic suspensions of cellulose crystallites; phase separation and magnetic field orientation. Liq Cryst 16:127–134
101. Reid MS, Villalobos M, Cranston ED (2017) Benchmarking cellulose nanocrystals: from the laboratory to industrial production. Langmuir 33:1583–1598
102. Frka-Petesic B, Sugiyama J, Kimura S et al (2015) Negative diamagnetic anisotropy and birefringence of cellulose nanocrystals. Macromolecules 48:8844–8857
103. Lin N, Dufresne A (2014) Surface chemistry, morphological analysis and properties of cellulose nanocrystals with gradiented sulfation degrees. Nanoscale 6:5384–5393
104. Uetani K, Yano H (2012) Zeta potential time dependence reveals the swelling dynamics of wood cellulose nanofibrils. Langmuir 28:818–827
105. Pääkkö M, Ankerfors M, Kosonen H et al (2007) Enzymatic hydrolysis combined with mechanical shearing and high-pressure homogenization for nanoscale cellulose fibrils and strong gels. Biomacromol 8:1934–1941
106. Nechyporchuk O, Belgacem MN, Pignon F (2016) Current progress in rheology of cellulose nanofibril suspensions. Biomacromol 73:2311–2320
107. Macosko CW (1994) Rheology: principles, measurements, and applications. AIChE J 41:10
108. Boluk Y, Lahiji R, Zhao L et al (2011) Suspension viscosities and shape parameter of cellulose nanocrystals (CNC). Colloids Surf A Physicochem Eng Asp 377:297–303
109. Bröckel U, Meier W, Wagner G et al (2013) Product design and engineering: formulation of gels and pastes. Wiley-VCH Verlag GmbH & Co., KGaA, Weinheim
110. Beck S, Bouchard J, Berry R (2012) Dispersibility in water of dried nanocrystalline cellulose. Biomacromol 13:1486–1494
111. Peng Y, Gardner DJ, Han Y (2012) Drying cellulose nanofibrils: in search of a suitable method. Cellulose 19:91–102
112. Missoum K, Bras J, Belgacem MN (2012) Water redispersible dried nanofibrillated cellulose by adding sodium chloride. Biomacromol 13:4118–4125
113. Sehaqui H, Zhou Q, Berglund LA (2011) High-porosity aerogels of high specific surface area prepared from nanofibrillated cellulose (NFC). Compos Sci Technol 71:1593–1599
114. Hanif Z, Jeon H, Tran TH et al (2017) Butanol-mediated oven-drying of nanocellulose with enhanced dehydration rate and aqueous re-dispersion. J Polym Res 25:191
115. Jiang F, Hsieh Y-L (2014) Assembling and redispersibility of rice straw nanocellulose: effect of tert-butanol. ACS Appl Mater Interfaces 6:20075–20084
116. Eyholzer C, Bordeanu N, Lopez-Suevos F et al (2010) Preparation and characterization of water-redispersible nanofibrillated cellulose in powder form. Cellulose 17:19–30
117. Fairman E (2014) Avoiding aggregation during drying and rehydration of nanocellulose. University of Maine
118. Jongaroontaprangsee S, Chiewchan N, Devahastin S (2018) Production of nanofibrillated cellulose with superior water redispersibility from lime residues via a chemical-free process. Carbohydr Polym 193:249–258
119. Velásquez-Cock J, Gómez HBE, Posada P et al (2018) Poly (vinyl alcohol) as a capping agent in oven dried cellulose nanofibrils. Carbohydr Polym 179:118–125
120. Nie S, Zhang K, Lin X et al (2018) Enzymatic pretreatment for the improvement of dispersion and film properties of cellulose nanofibrils. Carbohydr Polym 181:1136–1142
121. Syverud K, Stenius P (2008) Strength and barrier properties of MFC films. Cellulose 16:75–85
122. Nogi M, Iwamoto S, Nakagaito AN et al (2009) Optically transparent nanofiber paper. Adv Mater 21:1595–1598
123. Cranston ED, Gray DG (2009) Model cellulose I surfaces: a review. In: Model cellulosic surfaces. American Chemical Society, pp 3–75
124. Habibi Y, Foulon L, Aguié-Béghin V et al (2007) Langmuir-Blodgett films of cellulose nanocrystals: preparation and characterization. J Colloid Interface Sci 316:388–397
125. Ahola S, Salmi J, Johansson L-S et al (2008) Model films from native cellulose nanofibrils. Preparation, swelling, and surface interactions. Biomacromol 9:1273–1282
126. Kumar V, Bollström R, Yang A et al (2014) Comparison of nano- and microfibrillated cellulose films. Cellulose 21:3443–3456

127. Fujisawa S, Okita Y, Fukuzumi H et al (2011) Preparation and characterization of TEMPO-oxidized cellulose nanofibril films with free carboxyl groups. Carbohydr Polym 84:579–583
128. Österberg M, Vartiainen J, Lucenius J et al (2013) A fast method to produce strong NFC films as a platform for barrier and functional materials. ACS Appl Mater Interfaces 5:4640–4647
129. Stelte W, Sanadi AR (2009) Preparation and characterization of cellulose nanofibers from two commercial hardwood and softwood pulps. Ind Eng Chem Res 48:11211–11219
130. Jang J-H, Lee S-H, Endo T et al (2013) Characteristics of microfibrillated cellulosic fibers and paper sheets from Korean white pine. Wood Sci Technol 47:925–937
131. Benítez AJ, Torres-Rendon J, Poutanen M et al (2013) Humidity and multiscale structure govern mechanical properties and deformation modes in films of native cellulose nanofibrils. Biomacromol 14:4497–4506
132. Fukuzumi H, Saito T, Iwata T et al (2009) Transparent and high gas barrier films of cellulose nanofibers prepared by TEMPO-mediated oxidation. Biomacromol 10:162–165
133. Gray DG (2016) Recent advances in chiral nematic structure and iridescent color of cellulose nanocrystal films. Nanomaterials 6:213
134. Beck S, Bouchard J, Berry R (2011) Controlling the reflection wavelength of iridescent solid films of nanocrystalline cellulose. Biomacromol 12:167–172
135. Dufresne A (2013) Nanocellulose: a new ageless bionanomaterial. Mater Today 16:220–227
136. Nair SS, Zhu J, Deng Y et al (2014) High performance green barriers based on nanocellulose. Sustain Chem Process 2:1–7
137. Aulin C (2009) Novel oil resistant cellulosic materials. KTH Royal Institute
138. Missoum K, Belgacem MN, Bras J (2013) Nanofibrillated cellulose surface modification: a review. Materials (Basel) 6:1745–1766
139. Dai L, Long Z, Chen J et al (2017) Robust guar gum/cellulose nanofibrils multilayer films with good barrier properties. ACS Appl Mater Interfaces 9:5477–5485
140. Liu A, Walther A, Ikkala O et al (2011) Clay nanopaper with tough cellulose nanofiber matrix for fire retardancy and gas barrier functions. Biomacromol 12:633–641
141. Spence KL, Venditti RA, Rojas OJ et al (2011) Water vapor barrier properties of coated and filled microfibrillated cellulose composite films. Bioresour 6(4)
142. Raabe D, Romano P, Sachs C et al (2005) Discovery of a honeycomb structure in the twisted plywood patterns of fibrous biological nanocomposite tissue. J Cryst Growth 283:1–7
143. Marchessault RH, Morehead FF, Walter NM (1959) Liquid crystal systems from fibrillar polysaccharides. Nature 184:632–633
144. Gopalan Nair K, Dufresne A (2003) Crab shell chitin whisker reinforced natural rubber nanocomposites. Processing and swelling behavior. Biomacromolecules 4:657–665
145. Hariraksapitak P, Supaphol P (2010) Preparation and properties of α-chitin-whisker-reinforced hyaluronan–gelatin nanocomposite scaffolds. J Appl Polym Sci 117:3406–3418
146. Goodrich JD, Winter WT (2007) α-Chitin nanocrystals prepared from shrimp shells and their specific surface area measurement. Biomacromol 8:252–257
147. Larbi F, García A, del Valle LJ et al (2018) Comparison of nanocrystals and nanofibers produced from shrimp shell α-chitin: from energy production to material cytotoxicity and pickering emulsion properties. Carbohydr Polym 196:385–397
148. Morin A, Dufresne A (2002) Nanocomposites of chitin whiskers from Riftia tubes and poly (caprolactone). Macromolecules 35:2190–2199
149. Salaberria AM, Diaz RH, Labidi J et al (2015) Role of chitin nanocrystals and nanofibers on physical, mechanical and functional properties in thermoplastic starch films. Food Hydrocoll 46:93–102
150. Jung H-S, Kim MH, Park WH (2019) Preparation and structural investigation of novel β-chitin nanocrystals from cuttlefish bone. ACS Biomater Sci Eng 5:1744–1752
151. Salaberria AM, Labidi J, Fernandes SCM (2015) Different routes to turn chitin into stunning nano-objects. Eur Polym J 68:503–515
152. Oun AA, Rhim J-W (2018) Effect of isolation methods of chitin nanocrystals on the properties of chitin-silver hybrid nanoparticles. Carbohydr Polym 197:349–358

153. Fan Y, Saito T, Isogai A (2008) Chitin nanocrystals prepared by TEMPO-mediated oxidation of α-chitin. Biomacromol 9:192–198
154. Fan Y, Saito T, Isogai A (2010) Individual chitin nano-whiskers prepared from partially deacetylated α-chitin by fibril surface cationization. Carbohydr Polym 79:1046–1051
155. Kadokawa J, Takegawa A, Mine S et al (2011) Preparation of chitin nanowhiskers using an ionic liquid and their composite materials with poly(vinyl alcohol). Carbohydr Polym 84:1408–1412
156. Mincea M, Negrulescu A, Ostafe V (2012) Preparation, modification, and applications of chitin nanowhiskers: a review. Rev Adv Mater Sci 30:225–242
157. Lin N, Huang J, Dufresne A (2012) Preparation, properties and applications of polysaccharide nanocrystals in advanced functional nanomaterials: a review. Nanoscale 4:3274–3294
158. Ang-atikarnkul P, Watthanaphanit A, Rujiravanit R (2014) Fabrication of cellulose nanofiber/chitin whisker/silk sericin bionanocomposite sponges and characterizations of their physical and biological properties. Compos Sci Technol 96:88–96
159. Sriupayo J, Supaphol P, Blackwell J et al (2005) Preparation and characterization of α-chitin whisker-reinforced poly(vinyl alcohol) nanocomposite films with or without heat treatment. Polymer (Guildf) 46:5637–5644
160. Ifuku S, Nogi M, Abe K et al (2009) Preparation of chitin nanofibers with a uniform width as α-chitin from crab shells. Biomacromol 10:1584–1588
161. Ifuku S, Nogi M, Yoshioka M et al (2010) Fibrillation of dried chitin into 10–20 nm nanofibers by a simple grinding method under acidic conditions. Carbohydr Polym 81:134–139
162. Fan Y, Fukuzumi H, Saito T et al (2012) Comparative characterization of aqueous dispersions and cast films of different chitin nanowhiskers/nanofibers. Int J Biol Macromol 50:69–76
163. Mushi NE, Butchosa N, Salajkova M et al (2014) Nanostructured membranes based on native chitin nanofibers prepared by mild process. Carbohydr Polym 112:255–263
164. Salaberria AM, Fernandes SCM, Diaz RH et al (2015) Processing of α-chitin nanofibers by dynamic high pressure homogenization: characterization and antifungal activity against A. niger. Carbohydr Polym 116:286–291
165. Lu Y, Sun Q, She X et al (2013) Fabrication and characterisation of α-chitin nanofibers and highly transparent chitin films by pulsed ultrasonication. Carbohydr Polym 98:1497–1504
166. Fan Y, Saito T, Isogai A (2009) TEMPO-mediated oxidation of β-chitin to prepare individual nanofibrils. Carbohydr Polym 77:832–838
167. Narkevicius A, Steiner LM, Parker RM et al (2019) Controlling the self-assembly behavior of aqueous chitin nanocrystal suspensions. Biomacromol 20:2830–2838
168. Huang W (2018) Chitin nanopapers, chap 6. In: Huang WBT-N (ed) Micro and nano technologies. William Andrew Publishing, pp 175–200
169. Watthanaphanit A, Supaphol P, Tamura H et al (2010) Wet-spun alginate/chitosan whiskers nanocomposite fibers: Preparation, characterization and release characteristic of the whiskers. Carbohydr Polym 79:738–746
170. Liu D, Wu Q, Chang PR et al (2011) Self-assembled liquid crystal film from mechanically defibrillated chitosan nanofibers. Carbohydr Polym 84:686–689
171. Elieh-Ali-Komi D, Hamblin MR (2016) Chitin and chitosan: production and application of versatile biomedical nanomaterials. Int J Adv Res 4:411–427
172. Ramezani Z, Zarei M, Raminnejad N (2015) Comparing the effectiveness of chitosan and nanochitosan coatings on the quality of refrigerated silver carp fillets. Food Control 51:43–48
173. Qi L, Xu Z, Jiang X et al (2004) Preparation and antibacterial activity of chitosan nanoparticles. Carbohydr Res 339:2693–2700
174. Sadeghi AMM, Dorkoosh FA, Avadi MR et al (2008) Preparation, characterization and antibacterial activities of chitosan, N-trimethyl chitosan (TMC) and N-diethylmethyl chitosan (DEMC) nanoparticles loaded with insulin using both the ionotropic gelation and polyelectrolyte complexation methods. Int J Pharm 355:299–306
175. Yang H-C, Wang W-H, Huang K-S et al (2010) Preparation and application of nanochitosan to finishing treatment with anti-microbial and anti-shrinking properties. Carbohydr Polym 79:176–179

176. Jin J, Lee D, Im H-G et al (2016) Chitin nanofiber transparent paper for flexible green electronics. Adv Mater 28:5169–5175
177. Olivera S, Muralidhara HB, Venkatesh K et al (2016) Potential applications of cellulose and chitosan nanoparticles/composites in wastewater treatment: a review. Carbohydr Polym 153:600–618
178. Pérez S, Bertoft E (2010) The molecular structures of starch components and their contribution to the architecture of starch granules: a comprehensive review. Starch–Stärke 62:389–420
179. Altuna L, Herrera ML, Foresti ML (2018) Synthesis and characterization of octenyl succinic anhydride modified starches for food applications. A review of recent literature. Food Hydrocoll 80:97–110
180. Wang S, Li C, Copeland L et al (2015) Starch retrogradation: a comprehensive review. Compr Rev Food Sci Food Saf 14:568–585
181. Gao W, Lin X, Lin X et al (2011) Preparation of nano-sized flake carboxymethyl cassava starch under ultrasonic irradiation. Carbohydr Polym 84:1413–1418
182. Marinich JA, Ferrero C, Jiménez-Castellanos MR (2009) Graft copolymers of ethyl methacrylate on waxy maize starch derivatives as novel excipients for matrix tablets: physicochemical and technological characterisation. Eur J Pharm Biopharm 72:138–147
183. Le Corre D, Angellier-Coussy H (2014) Preparation and application of starch nanoparticles for nanocomposites: a review. React Funct Polym 85:97–120
184. Zia F, Zia KM, Zuber M et al (2015) Starch based polyurethanes: a critical review updating recent literature. Carbohydr Polym 134:784–798
185. Sajilata MG, Singhal RS, Kulkarni PR (2006) Resistant starch–a review. Compr Rev Food Sci Food Saf 5:1–17
186. Valodkar M, Thakore S (2010) Isocyanate crosslinked reactive starch nanoparticles for thermoresponsive conducting applications. Carbohydr Res 345:2354–2360
187. Gong B, Liu W, Tan H et al (2016) Understanding shape and morphology of unusual tubular starch nanocrystals. Carbohydr Polym 151:666–675
188. Zheng H, Ai F, Chang PR et al (2009) Structure and properties of starch nanocrystal-reinforced soy protein plastics. Polym Compos 30:474–480
189. Qin Y, Liu C, Jiang S et al (2016) Characterization of starch nanoparticles prepared by nanoprecipitation: influence of amylose content and starch type. Ind Crops Prod 87:182–190
190. Kim H-Y, Park SS, Lim S-T (2015) Preparation, characterization and utilization of starch nanoparticles. Colloids Surf B Biointerfaces 126:607–620
191. Nägeli W (1874) Beiträge zur näheren kenntniss der stärkegruppe. Justus Liebigs Ann Chem 173:218–227
192. Lintner CJ (1886) Studien uber diastase. J für Prakt Chemie 34:378–386
193. Dufresne A, Cavaillé J-Y, Helbert W (1996) New nanocomposite materials: microcrystalline starch reinforced thermoplastic. Macromolecules 29:7624–7626
194. Putaux J-L, Molina-Boisseau S, Momaur T et al (2003) Platelet nanocrystals resulting from the disruption of waxy maize starch granules by acid hydrolysis. Biomacromol 4:1198–1202
195. Wang S, Yu J, Jin F, Yu J (2008) The new insight on ultrastructure of C-type starch granules revealed by acid hydrolysis. Int J Biol Macromol 43:216–220
196. Angellier H, Choisnard L, Molina-Boisseau S et al (2004) Optimization of the preparation of aqueous suspensions of waxy maize starch nanocrystals using a response surface methodology. Biomacromol 5:1545–1551
197. Saeng-on J, Aht-Ong D (2017) Production of starch nanocrystals from agricultural materials using mild acid hydrolysis method: optimization and characterization. Polym Renew Resour 8:91–116
198. Romdhane A, Aurousseau M, Guillet A et al (2015) Cross flow microfiltration of starch nanocrystal suspensions. Can J Chem Eng 93:412–418
199. Kim JH, Park DH, Kim J-Y (2017) Effect of heat-moisture treatment under mildly acidic condition on fragmentation of waxy maize starch granules into nanoparticles. Food Hydrocoll 63:59–66

200. LeCorre D, Bras J, Dufresne A (2011) Influence of botanic origin and amylose content on the morphology of starch nanocrystals. J Nanoparticle Res 13:7193–7208
201. Kim J-Y, Park D-J, Lim S-T (2008) Fragmentation of waxy rice starch granules by enzymatic hydrolysis. Cereal Chem 85:182–187
202. Wei B, Cai C, Tian Y (2018) Nano-sized starch: preparations and applications BT—functional starch and applications in food. In: Jin Z (ed). Springer Singapore, Singapore, pp 147–176
203. Biais B, Le Bail P, Robert P et al (2006) Structural and stoichiometric studies of complexes between aroma compounds and amylose. Polymorphic transitions and quantification in amorphous and crystalline areas. Carbohydr Polym 66:306–315
204. Rondeau-Mouro C, Le BP, Buléon A (2004) Structural investigation of amylose complexes with small ligands: inter- or intra-helical associations? Int J Biol Macromol 34:251–257
205. Lay Ma UV, Floros JD, Ziegler GR (2011) Formation of inclusion complexes of starch with fatty acid esters of bioactive compounds. Carbohydr Polym 83:1869–1878
206. Kong L, Ziegler GR (2014) Molecular encapsulation of ascorbyl palmitate in preformed V-type starch and amylose. Carbohydr Polym 111:256–263
207. Le Bail P, Rondeau C, Buléon A (2005) Structural investigation of amylose complexes with small ligands: helical conformation, crystalline structure and thermostability. Int J Biol Macromol 35:1–7
208. Kim J-Y, Lim S-T (2009) Preparation of nano-sized starch particles by complex formation with n-butanol. Carbohydr Polym 76:110–116
209. Hao Y, Chen Y, Li Q et al (2019) Synthesis, characterization and hydrophobicity of esterified waxy potato starch nanocrystals. Ind Crops Prod 130:111–117
210. Del Buono D, Luzi F, Benincasa P et al (2019) Extraction of nanostructured starch from purified granules of waxy and non-waxy barley cultivars. Ind Crops Prod 130:520–527
211. Silva APM, Oliveira AV, Pontes SMA et al (2019) Mango kernel starch films as affected by starch nanocrystals and cellulose nanocrystals. Carbohydr Polym 211:209–216
212. Sanchez de la Concha BB, Agama-Acevedo E, Nuñez-Santiago MC et al (2018) Acid hydrolysis of waxy starches with different granule size for nanocrystal production. J Cereal Sci 79:193–200
213. Costa ÉK de C, de Souza CO, da Silva JBA et al (2017) Hydrolysis of part of cassava starch into nanocrystals leads to increased reinforcement of nanocomposite films. J Appl Polym Sci 134:45311
214. Mukurumbira A, Mariano M, Dufresne A et al (2017) Microstructure, thermal properties and crystallinity of amadumbe starch nanocrystals. Int J Biol Macromol 102:241–247
215. Bel Haaj S, Thielemans W, Magnin A et al (2016) Starch nanocrystals and starch nanoparticles from waxy maize as nanoreinforcement: a comparative study. Carbohydr Polym 143:310–317
216. Namazi H, Dadkhah A (2010) Convenient method for preparation of hydrophobically modified starch nanocrystals with using fatty acids. Carbohydr Polym 79:731–737
217. Chang PR, Ai F, Chen Y et al (2009) Effects of starch nanocrystal-graft-polycaprolactone on mechanical properties of waterborne polyurethane-based nanocomposites. J Appl Polym Sci 111:619–627
218. Ma X, Jian R, Chang PR, Yu J (2008) Fabrication and characterization of citric acid-modified starch nanoparticles/plasticized-starch composites. Biomacromol 9:3314–3320
219. Liu D, Wu Q, Chen H, Chang PR (2009) Transitional properties of starch colloid with particle size reduction from micro- to nanometer. J Colloid Interface Sci 339:117–124
220. Tan Y, Xu K, Li L et al (2009) Fabrication of size-controlled starch-based nanospheres by nanoprecipitation. ACS Appl Mater Interfaces 1:956–959
221. Mostafa K, Ameen H, Morsy M et al (2019) Production of high-performance textiles via pioneering strengthening approach using starch nanoparticles. J Ind Text 0:1–15
222. Antonietti M, Landfester K (2002) Polyreactions in miniemulsions. Prog Polym Sci 27:689–757
223. Shabana S, Prasansha R, Kalinina I et al (2019) Ultrasound assisted acid hydrolyzed structure modification and loading of antioxidants on potato starch nanoparticles. Ultrason Sonochem 51:444–450

224. de Oliveira NR, Fornaciari B, Mali S et al (2018) Acetylated starch-based nanoparticles: synthesis, characterization, and studies of interaction with antioxidants. Starch–Stärke 70:1700170
225. Chang Y, Yan X, Wang Q et al (2017) High efficiency and low cost preparation of size controlled starch nanoparticles through ultrasonic treatment and precipitation. Food Chem 227:369–375
226. Gong M, Li X, Xiong L et al (2016) Retrogradation property of starch nanoparticles prepared by pullulanase and recrystallization. Starch–Stärke 68:230–238
227. Gonçalves PM, Noreña CPZ, da Silveira NP et al (2014) Characterization of starch nanoparticles obtained from Araucaria angustifolia seeds by acid hydrolysis and ultrasound. LWT Food Sci Technol 58:21–27
228. Bel Haaj S, Magnin A, Pétrier C et al (2013) Starch nanoparticles formation via high power ultrasonication. Carbohydr Polym 92:1625–1632
229. Song D, Thio YS, Deng Y (2011) Starch nanoparticle formation via reactive extrusion and related mechanism study. Carbohydr Polym 85:208–214
230. Sun Q (2018) Starch Nanoparticles. In: Starch in food, structure, function and applications, 2nd edn, pp 691–745
231. Giezen F, Jongboom R, Gotlieb K et al (2000) Process for producing biopolymer nanoparticles. US Patent 9011741, p. 17
232. Lai LS, Kokini JL (1991) Physicochemical changes and rheological properties of starch during extrusion (a review). Biotechnol Prog 7:251–266
233. Patel CM, Chakraborty M, Murthy ZVP (2016) Fast and scalable preparation of starch nanoparticles by stirred media milling. Adv Powder Technol 27:1287–1294
234. Minakawa AFK, Faria-Tischer PCS, Mali S (2019) Simple ultrasound method to obtain starch micro- and nanoparticles from cassava, corn and yam starches. Food Chem 283:11–18
235. Wang Y, Hu Q, Li T et al (2018) Core–shell starch nanoparticles and their toughening of polylactide. Ind Eng Chem Res 57:13048–13054
236. Sessini V, Raquez J-M, Kenny JM et al (2019) Melt-processing of bionanocomposites based on ethylene-co-vinyl acetate and starch nanocrystals. Carbohydr Polym 208:382–390
237. Sun Q, Li G, Dai L et al (2014) Green preparation and characterisation of waxy maize starch nanoparticles through enzymolysis and recrystallisation. Food Chem 162:223–228
238. Jiping P, Shujun W, Jinglin Y et al (2007) Comparative studies on morphological and crystalline properties of B-type and C-type starches by acid hydrolysis. Food Chem 105:989–995
239. Kaur J, Kaur G, Sharma S et al (2018) Cereal starch nanoparticles—a prospective food additive: a review. Crit Rev Food Sci Nutr 58:1097–1107
240. Duan B, Sun P, Wang X, Yang C (2011) Preparation and properties of starch nanocrystals/carboxymethyl chitosan nanocomposite films. Starch–Stärke 63:528–535
241. Godet MC, Bouchet B, Colonna P et al (1996) Crystalline amylose-fatty acid complexes: morphology and crystal thickness. J Food Sci 61:1196–1201
242. Gelders GG, Duyck JP, Goesaert H et al (2005) Enzyme and acid resistance of amylose-lipid complexes differing in amylose chain length, lipid and complexation temperature. Carbohydr Polym 60:379–389
243. Angellier H, Molina-Boisseau S, Dufresne A (2005) Mechanical properties of waxy maize starch nanocrystal reinforced natural rubber. Macromolecules 38:9161–9170
244. Wei B, Xu X, Jin Z et al (2014) Surface chemical compositions and dispersity of starch nanocrystals formed by sulfuric and hydrochloric acid hydrolysis. PLoS ONE 9:1–7
245. Amini AM, Razavi SMA (2016) A fast and efficient approach to prepare starch nanocrystals from normal corn starch. Food Hydrocoll 57:132–138
246. Sun Q, Fan H, Xiong L (2014) Preparation and characterization of starch nanoparticles through ultrasonic-assisted oxidation methods. Carbohydr Polym 106:359–364
247. Jain AK, Khar RK, Ahmed FJ et al (2008) Effective insulin delivery using starch nanoparticles as a potential trans-nasal mucoadhesive carrier. Eur J Pharm Biopharm 69:426–435
248. Patil VV, Dandekar PP, Patravale VB et al (2010) Freeze drying: Potential for powdered nanoparticulate product. Dry Technol 28:624–635

249. Shi A, Li D, Wang L, Adhikari B (2012) Rheological properties of suspensions containing cross-linked starch nanoparticles prepared by spray and vacuum freeze drying methods. Carbohydr Polym 90:1732–1738
250. Shi A, Wang L, Li D, Adhikari B (2013) Suspensions of vacuum-freeze dried starch nanoparticles: influence of NaCl on their rheological properties. Carbohydr Polym 94:782–790
251. Kümmerer K, Menz J, Schubert T et al (2011) Biodegradability of organic nanoparticles in the aqueous environment. Chemosphere 82:1387–1392
252. Liu C, Ge S, Yang J et al (2016) Adsorption mechanism of polyphenols onto starch nanoparticles and enhanced antioxidant activity under adverse conditions. J Funct Foods 26:632–644
253. Dandekar P, Jain R, Stauner T et al (2012) A hydrophobic starch polymer for nanoparticle-mediated delivery of docetaxel. Macromol Biosci 12:184–194
254. Huang Y, Liu M, Gao C et al (2013) Ultra-small and innocuous cationic starch nanospheres: preparation, characterization and drug delivery study. Int J Biol Macromol 58:231–239

Chapter 2
Surface Modification with Grafting Functional Molecules on Nanopolysaccharides

Kulang Primo Sokiri Kiliona, Aban Lwal John Lwal, Han Tao and Ning Lin

Abstract Numerous active hydroxyl groups and charges derived from the hydrolysis provide the surface chemistry and possible modification of nanopolysaccharides. Taking the strategy of surface grafting functional molecules, nanopolysaccharides can possess the specific function serving as the nanoparticle carriers in diverse applications. This chapter introduces several typical cases of surface modification with functional molecules on nanopolysaccharides, including grafting the antibacterial molecules, fluorescent molecules, stimuli-responsive molecules, as well as the superhydrophobic modification and drug-delivery modification. The emphasis of this chapter is put on the summarization of various functional species grafted on nanopolysaccharides and then discussion on how to achieve this modification in each case. We conclude the strategies of functional modifications on nanopolysaccharides and comment their different advantages based on the comparison of reported studies, while leaving the description of functional materials production and their functional applications in the following chapters.

Keywords Antibacterial modification · Fluorescent modification · Stimuli-responsive modification · Drug delivery · Superhydrophobicity

2.1 Surface Grafting of Antibacterial Molecules on Nanopolysaccharides

The growing concerns in the fight against microbial (bacterial) resistance on antibiotics have caught the attention of many scientists and academic researchers to continue in the pursuit to provide a remedy to the human population from health risks associated with food contamination. As a matter of concern to these alarming health risks, researchers have explored various antimicrobial drug species in an attempt to improve food quality during handling, packaging and storage. Shelf life and safety

K. P. S. Kiliona · A. L. J. Lwal · H. Tao · N. Lin (✉)
School of Chemistry, Chemical Engineering and Life Sciences,
Wuhan University of Technology, Wuhan 430070, People's Republic of China
e-mail: ninglin@whut.edu.cn

N. Lin et al. (eds.), *Advanced Functional Materials from Nanopolysaccharides*,
Springer Series in Biomaterials Science and Engineering 15,
https://doi.org/10.1007/978-981-15-0913-1_2

of food is the first priority the food industry undertakes to ensure that economic losses incurred by spoilage, health risks to the human population. In the medical field, wound dressing requires a material that can prevent infection of wounds from bacteria. Therefore, the need to resolve the widespread of microorganisms from deteriorating food quality and human health has let to extensive studies of antibacterial species that have potency in killing bacteria. The commonly known examples of such bacteria include *Mycobacterium smegmatis*, *Escherichia coli*, *Staphylococcus aureus*, *M. lysodeikticus*, *Corynebacterium* sp., *Pseudomonas mendocina*, *Bacillus subtilis*, *Pseudomonas aeruginosa*, *Candida albicans*, *Aspergillus niger*, *Salmonella infantis*, and etc. This section summarizes the antibacterial species and the strategies of grafting antibacterial species on nanopolysaccharides.

Generally, the functional modification of nanopolysaccharides with antibacterial agents have been widely developed by different strategies. However, the practical performance depends entirely on the uniform dispersion which improves the distribution of the antibacterial species on their surfaces and availability of their surface groups which promote adsorption of antibacterial species.

2.1.1 Antibacterial Species

The antibacterial species ranging from inorganic metals or metal oxides, small organic molecules to cationic polymers of high molecular weights have been under intensive utilization for surface modification of nanopolysaccharides in an attempt to fight bacterial infections. The Gram-negative and Gram-positive bacteria are generally considered for different assays and analysis. Notably, metal or metal oxides such as silver nanoparticles, zinc oxide nanoparticles and coper oxide nanoparticles are well known antibacterial agents. The possession of the positive charges by these inorganic nanoparticles play a crucial role in disrupting bacterial cells. When these nanoparticles come into direct contact with bacteria, electrostatic interaction occurs between the positively charged antibacterial species and the negatively charged bacterial cell wall (both Gram-positive and Gram-negative types). Consequently, the active physical contact (binding) to the cell membrane causes morphological (structural) changes and destruction leading to the death of cells [1–7]. Several selected antibacterial agents reported in the studies on this topic are illustrated in Fig. 2.1 and the rest are listed below and they include; aminosilanes, quaternary ammonium compounds such as [Aminopropyl trimethoxysilane (APMS), 2-aminoethyl 3-aminopropyl trimethoxysilane (DAMS) and 3-2-(2-aminoethylamino) ethylamino propyl-trimethoxysilane (TAMS), *N*,*N*-Dimethyl decylamine, *N*,*N*-Dimethyl hexadecylamine], chitosan, rhodamines, cationic porphyrin, while other antibacterial agents such as chromophoric nitro radical (nitroaniline hybrid), lysozymes, rosin acids, chlorhexidine digluconate, carvacrol, and allicin are few examples of antiacterial compounds that possess features relatively different from the other types mentioned before. Table 2.1 summarizes the typical antimicrobial agents reported

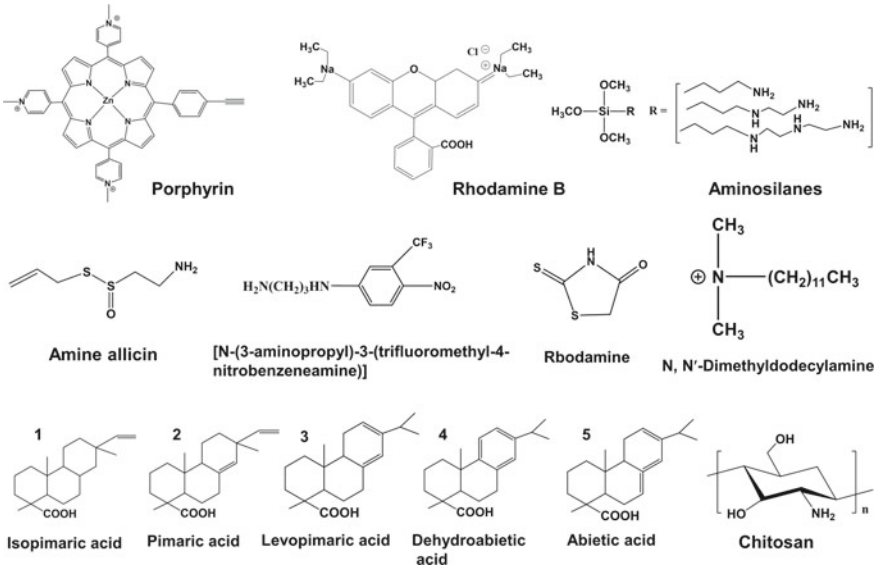

Fig. 2.1 The chemical structures of reported antibacterial agents (1–5 are representative examples of rosin acids) introduced on the surface modifications of nanopolysaccharides

on the surface modification of nanopolysaccharides, the types of bacteria evaluated against, the method of evaluation and their efficacy in fighting bacteria.

In the view of introducing antibacterial properties to nanopolysaccharides, several issues should be noted on the selection of targeted antibacterial agents: (i) their accessibility (groups or surface charges) to be functionalized on the surface of nanopolysaccharides through covalent attachment or adsorption; (ii) their particle sizes (steric hindrance) to diffuse from the surface of nanopolysaccharides, (iii) their ability to penetrate into impermeable bacterial cell wall and killing kinetics.

2.1.2 Strategies of Grafting Antibacterial Species on Nanopolysaccharides

In the cases of CNC, the modification strategies of grafting the antibacterial species on the nanocrystals depends mainly on the surface active groups and charges. For example, the presence of surface hydroxyl groups (–OH) the sulfate groups ($–OSO_3H$) and carboxylic groups (–COOH) provide the negative charges resulting from hydrolysis of CNC with hydrochloric acid (HCl), sulfuric acid (H_2SO_4) and 2,2,6,6-tetramethylpiperidine-1-oxyl radical (TEMPO) oxidation respectively. These surface reactive groups are readily available for chemical reaction resulting in covalent attachment and electrostatic interaction with other functional molecules.

Table 2.1 Summarization of antibacterial species on the modification of nanopolysacchrides (NPs) (CNC: cellulose nanocrystals, CNF: cellulose nanofibrils, ChNC: chitin nanocrystals, ChNF: chitin nanofibrils, SNC: starch nanocrystals) evaluated against specific type of bacteria and their killing kinetics

NPs	Antibacterial species/molecules	Type of bacteria	Action on bacteria (killing kinetics)	References
CNC	*N,N*-Dimethyl-dodecylamine and *N,N*-Dimethyl hexadecylamine	*Staphylococcus aureus* and *Escherichia coli*	Binding of positively charged quaternary ions on negatively charged cell membrane of bacteria	[8]
	Nitroaniline hybrid	*Staphylococcus aureus* and *Pseudomonas aeruginosa*	Cell proliferation	[9]
	Lysozyme from hen egg white and T4 bacteriophage	*M lysodeikticus and Corynebacterium* sp., and *Escherichia coli Ps, mendocina, and Corynebacterium* sp.	Covalent binding and attachment of hydrophobic peptide residue to bacteria C-terminus	[10]
	Rosin acids	*Bacillus subtilis* and *Escherichia coli*	Protonation of rosin and subsequent binding to the bacterial membrane	[11]
	Ag nanoparticles	*Escherichia coli* and *Staphylococcus aureus*	Binding of silver to the bacterial cell wall	[1]
		Escherichia coli and *Staphylococcus aureus*	Binding of silver to the bacterial cell wall	[2]
		Escherichia coli and *Bacillus subtilis*	Disruption of the bacterial cell membrane	[3, 4]
	ZnO nanoparticles	*Escherichia coli* and *Staphylococcus aureus*	–	[12]
	Chlorhexidine digluconate	*Bacillus subtilis*	–	[13]
	Chitosan	*Escherichia coli*	Cell membrane damage by CNC and susceptibility to protonated chitosan	[14]
	Polyrhodanine	*Escherichia coli* and *Bacillus subtilis*	Cell lysis as a result of interaction between positive charges of polyrhodanine and negative bacterial cell membrane	[1]
	Amine-allicin	*Staphylococcus aureus*	–	[15]

(continued)

Table 2.1 (continued)

NPs	Antibacterial species/molecules	Type of bacteria	Action on bacteria (killing kinetics)	References
	Allicin and lysozyme	*Candida albicans Aspergillus niger Staphylococcus aureus,* and *Escherichia coli*	–	[2]
	Cationic porphyrin	*Mycobacterium smegmatis Escherichia coli* and *Staphylococcus aureus*	Uptake of photosensitizer and subsequent production of singlet oxygen in a close proximity leading to bacterial cell death	[16]
CNF	(3-trimethoxysilyl propyl)quinolinium iodide (TMSQI)	*Escherichia coli Pseudomonas aeruginosa,* and *Staphylococcus aureus*	Electrostatic interaction that disrupt the membrane integrity leading to leakage of intracellular constituents and subsequent death of the cell upon contact	[6]
	Carvacrol	*Bacillus subtilis*	Interaction with the lipid bilayer of cytoplasmic membrane which caused disruption and leakage of cell component	[10]
	Aminosilanes (APMS DAMS TAMS)	*Bacillus subtilis Staphylococcus aureus* and *Escherichia coli*	Direct binding of cationic alkyl chain on bacterial cell wall resulting to cell lysis and death	[17]
	Quaternary ammonium compound (ODDMAC)	*Escherichia coli Pseudomonas aeruginosa,* and *Staphylococcus aureus*	–	[18]
	Ag nanoparticles	*Staphylococcus aureus* and *Escherichia coli*	Binding of silver to the bacterial cell wall	[5, 19]
		Staphylococcus aureus Candida albicans Salmonella infantis and *Listeria monocytogenes*	–	[20]
	Ag nanoclusters	*Escherichia coli*	–	[21]

(continued)

Table 2.1 (continued)

NPs	Antibacterial species/molecules	Type of bacteria	Action on bacteria (killing kinetics)	References
ChNC	Ag nanoparticles	*Staphylococcus aureus* and *Escherichia coli*	Contact active physical disruption (1–10 nm attachment range)	[22]
	ZnO/Ag nanoparticles	*Listeria monocytogenes* and *Escherichia coli*	Direct interaction with bacterial cell membrane causing structural changes and destruction of the bacteria	[7]
	Lysozyme	*Escherichia coli Staphylococcus aureus,* and *Bacillus subtilis*	–	[18]
	Chitin nanocrystals	*Listeria monocytogenes* and *Escherichia coli*	Electrostatic interaction that causes disruption and leakage of intracellular materials of the bacterial cell	[19]
ChNF	Chitin nanofibrils	*Staphylococcus aureus* and *Escherichia coli*	Interaction of cation groups of chitosan with anionic bacterial cells leading to leakage of cell constituents	[20]
	Chitin nanofibrils	*Listeria monocytogenes*	Flocculation bacteria leading to loss of nutrients and oxygen (mass transfer limitation) in addition to the interaction of cation groups of CNF with anionic bacterial cells leading to leakage of cell constituents	[23]
	N-halamine	*Staphylococcus aureus* and *Escherichia coli*	Oxidative transfer of chlorine to the receptors of the micro-organisms (bacteria) that inhibit enzymatic or metabolic process, causing death	[24]
	Ag nanoparticles	*Escherichia coli*	–	[25]
SNC	Graphene	*Staphylococcus aureus* and *Escherichia coli*	Ability to inactivation and control bacterial proliferation	[26]

Regarding the surface introduction of metals and metals oxides such as silver nanoparticles (AgNP), zinc oxide (ZnO) and copper oxide (CuO) as antibacterial agents, the mechanism for functional modification of CNC is attributed to its large surface area in which interaction between surface anionic groups with metal cationic ions occurs. Homogeneous dispersion of the nanoparticles in the suspension enable uniform distribution of the metal nanoparticles which enhances the antibacterial activity. In the case of surface grafting of AgNP, nucleation of Ag^+ on the surface of CNC could be achieved by use of Tollens's reagent $(Ag–NH_3)_2OH$ and glucose as a reducing agent [1]. In a related report, the modified CNC with complexation of silver nanoparticles (AgNP) was further used as the nanofiller in polylactide (PLA) and poly(butylene adipate-co-terephthalate (PBAT) matrices, producing biocompatible nanocomposites with the promising antibacterial activity against *E. coli and S. aureus* [2]. In another study, the CNC was modified with polydopamine and anchored with AgNP by in situ reduction reaction from silver nitrate, which was efficient against *E. coli and B. subtilis* bacteria [3]. The robust coating of AgNP onto the CNC surface was achieved by charge transfer and hydrogen bonding based on the "bridge" of polydopamine, resulting in the good dispersion, stability, and compatibility with minimal agglomeration. Yu et al. reported the Fisher esterification and precipitation method to graft ZnO on the surface of CNC based on the electrostatic interactive property of ZnO nanoparticles [12]. This simple and facile one-pot synthesis route induced electrostatic interaction between the –COO and Zn^{2+}. Figure 2.2 illustrates

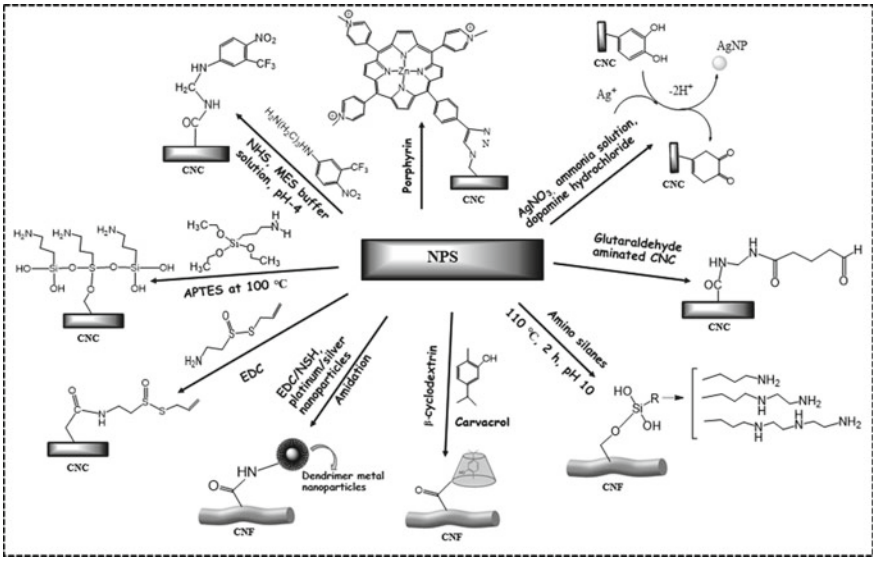

Fig. 2.2 Generalized schematic illustration of different grafting strategies of antibacterial agents on nanopolysaccharides in the typical cases of cellulose nanocrystals (CNC) and cellulose nanofibrils (CNF)

the summarization of grafting strategies of antibacterial species on the surface of cellulose nanocrystals and nanofibrils.

The surface grafting of organic antibacterial molecules on CNC involves several different strategies. In situ polymerization approach for surface modification of CNC with polyrhodamine using ferric chloride as an initiator was reported [27]. The polyrhodamine contains tertiary amide groups which can be used as an effective antibacterial agent, initiated by ferric chloride deposited onto the sulfated CNC surface. Chloroacetylation of CNC nanoparticles using chloroacetic anhydride in presence of ethyl acetate was reported to be another simple approach to graft quaternary ammonium on the CNC surface. Nevertheless, surface grafting of *N*,*N*-dimethyl decylamine and *N*,*N*-dimethyl hexadecylamine onto the chloroacetylated CNC was reported [8]. This reaction occurred by direct substitution of chlorine with the alkyl groups, and the length of the alkyl chains grafted on the CNC surface determined the inhibition of the bacteria. Because of the toughness of the bacterial cell wall that can build resistance to some drugs, the concentration of the antibacterial species is the key factor in elimination of bacterial. For example polyrhodanine with concentration of (0.5–1.0 and 1.0–2.0 mg/mL) grafted on CNC could eliminate E. coli and S. subtilis [27].

Different from the rigid and rod-like CNC, cellulose nanofibrils (CNF) is the typical semi-flexible nanomaterial possessing large specific surface area and high aspect ratio for the functional modifications. The fibrous network and entanglement of CNF offer excellent mechanical properties enabling the formation of functional materials. Regarding grafting antibacterial agents on the surface of CNF, the electrostatic adsorption is widely used approach. In the case of grafting quaternary ammonium compounds as antibacterial agents on the surface CNF, the adsorption-curing process in presence of potassium iodide was reported as a simple procedure to introduce the (3-trimethoxysilylpropyl)quinolinium iodide (TMSQI) [6] and octadecyldimethyl(3-trimethoxysilylpropyl)ammonium chloride (ODDMAC) [18] on CNF with the enhanced efficiency of antibacterial activities. Recently, the host-guest inclusion strategy was reported to introduce the antibacterial molecules on the surface of CNF [13]. The TEMPO-oxidized CNF was firstly functionalized with β-Cyclodextrin (β-CD) in which the hydrophobic cavities were able to entrap the antibacterial molecule carvacrol by simple impregnation and drying treatment.

The pristine nanochitin such as chitin nanocrystals (ChNC) and chitin nanofibrils (ChNF) possesses the amino groups bearing positive charges as the cationic biopolymer. Delivery of the cationic biopolymer to the negative bacterial cell wall causes electrostatic interaction between the negative bacterial cell wall and the positively charged chitin nanocrystals. Specific example of starch-based nanocomposite reinforced with chitin nanocrystals was reported to be effective against *Listeria monocytogenes and Escherichia coli* [28]. To increase the content of the amino groups in ChNC and postive charges, the partial deacetylation (>50%) can be performed on the ChNC with NaOH to produce chitosan nanocrystals, a well-known antibacterial biomaterial. Similarly, carboxymethyl cellulose-based nanocomposites with the addition of CNF can interact with gram-positive bacterial and display the ability to

proliferate the bacterial cell wall [29]. Furthermore, Jiang et al. reported the immobilization of lysozyme on the surface of ChNC aided by the hydrophobic interaction, which was evaluated against *Escherichia coli Staphylococcus aureus,* and *Bacillus subtilis* and was found to be effective with minimal inhibition [30].

The combined properties of nanopolysaccharides and antibacterial molecules together play a crucial role for the effectiveness of bacterial elimination. The surface charges, the rode-like shape of CNC and ChNC, and particles size of the antibacterial molecules are the key points during the modification process. The reduction of the inorganic nanoparticles into size that can penetrate into the bacterial cell wall is very crucial. It should be noted that the modification process should preserve the structural morphology of modified nanopolysaccharides in order to maintain the stability as well as the thermal behavior and their effectiveness in killing bacteria. Therefore, the grafting content of antibacterial species such as inorganic nanoparticles, short chains of organic molecules and other high- or low-weight polymers should be taken into consideration for the enhancement of their performance.

2.2 Surface Grafting of Fluorescent Molecules on Nanopolysaccharides

Since fluorescent molecules are associated with different photophysical and photochemical properties, their applications have been widely studied in the fields of biosensor, imaging, recognition, detection, etc. Some fluorescent molecules such as rhodamine B, carbon dots, gold nanoparticle, graphene quantum dots have been extensively studies to discover new nanomaterials such as chemosensors with high sensibility and selectivity.

2.2.1 Fluorescent Species

Nowadays, the varieties of florescent molecules reported in the combination with nanopolysaccharides can be generally divided as two parts, including the organic fluorescent molecules of fluorescein isothiocyanate (FITC), 5-(4,6-dichlorotriazinyl) aminofluorescein (DTAF), rhodamine B isothiocyanate (RBITC), lissamine rhodamine B ethylenediamine (LRBED) porphyrin pendant, amino fullerene Alexa Fluor G6 poly(amidoamine) dendrimer and inorganic nanoparticles of quantum dot (QD), graphene quantum dots (GQD), gold nanoparticle (AuNP). The studies on fluorescent labelling of nanopolysaccharides have been dominated by nanocellulose (CNC and CNF), in comparison with nanochitin and nanostarch as presented in Table 2.2. Grafting organic fluorescent molecules onto the surface CNC may involve direct reaction of the fluorescent molecules with pristine CNC or may require premodification (treatment) of the nanocrystals and then the grafting of fluorescent

Table 2.2 Summarization of fluorescent molecules grafted on the surface of nanopolysaccharides (NPs) and the mechanisms of attachment in the modification process

NPs	Fluorescent molecules	Mechanism of grafting/attachment of fluorescent on NPs surfaces	References
CNC	Porphyrin pendant (TPPOH)	Extended esterification and dicyclohexylcarbodiimide reaction	[31]
	Graphene quantum dot	Cross-linking via host-guest chemistry	[32]
	Quantum dot	Carbodiimde coupling reaction using one-step covalent attachment	[33]
	Lissamine rhodamine B ethylenediamine Rhodamine B isothiocyanate	Covalent attachment	[34]
	Rhodamine B isothiocyante	Covalent conjugation	[35]
	Amino fullerene	Covalent grafting	[36]
	Rhodamine B isothiocyante	Electrostatic adsorption and covalent bonding.	[37]
	Gold nanocluster	Evaporation-induced corporative assembly	[38]
	Quantum dot	Anionic ring-opening polymerization	[39]
	Carbazol-9-yl-acetic acid and Coumarin-3-carboxylic acid	One-step esterification reaction	[40]
	4-Ethoxy-9-allyl-1,8-naphthalimide	Surface initiated atom transfer radical polymerization	[41]
	G6 Poly(amidoamine) dendrimer	Carbodiimide-mediated amidation process	[42]
	Alexa Fluor 633 hydrazide bis(triethylammonium) salt	–	[43]
	Alexa Fluor	Reductive amination reaction	[44]
	Thiolated fluorescein-substituted lysine	Nucleophile-based thiol-ene Michael addition reaction.	[45]
	5-(4,6-Dichlorotriazinyl) aminofluorescein	One-step labelling reaction	[46]
	Perylene fluorophore	Supramolecular assembly	[47]
	Rhodamine B isothiocyanate, fluorescein isothiocyanate	Covalent conjugation	[48]
	Quinolone fluorophore	–	[49]
CNF	Terthienyl pendant	Cross-coupling between carbamate and ester linkages	[50]
	S-doped carbon quantum dot	One-pot hydrothermal method	[51]

(continued)

Table 2.2 (continued)

NPs	Fluorescent molecules	Mechanism of grafting/attachment of fluorescent on NPs surfaces	References
	7-Mercapto-4-methylcoumarin, fluorescein diacetate 5-maleimide	Diels-Alder and Thiol-Michael cycloaddition	[52]
	Carbon dot	Covalent attachment via EDC/NHS coupling	[53]
	9,9-Dihexylfluorene-2,7 bis(trimethyleneborate)	Chemical assembly	[54]
ChNC	Imidazoisoquinolinone dye	Chemical cross-linking	[55]

molecules. The binding mechanism of the florescent molecules depends on the reaction methods and reaction conditions. Figure 2.3 shows a summary of chemical structures of fluorescent molecules reported for the functionalization of nanopolysaccharides to synthesize nanohybrid materials with distinct fluorophore functionalities.

The research emphasis on grafting fluorescent molecules on nanopolysaccharides is the development of novel approach with environmentally friendly (green chemistry), low cost with high grafting efficiency to achieve the desired results. Based on the structural properties of the florescent molecules, the grafting efficiency and the ease of modification varies. Physical adsorption and electrostatic interaction is a common phenomenon for grafting inorganic fluorescent nanoparticles. In the case of grafting inorganic nanoparticles (graphene quantum dots) on CNC, the carboxylate

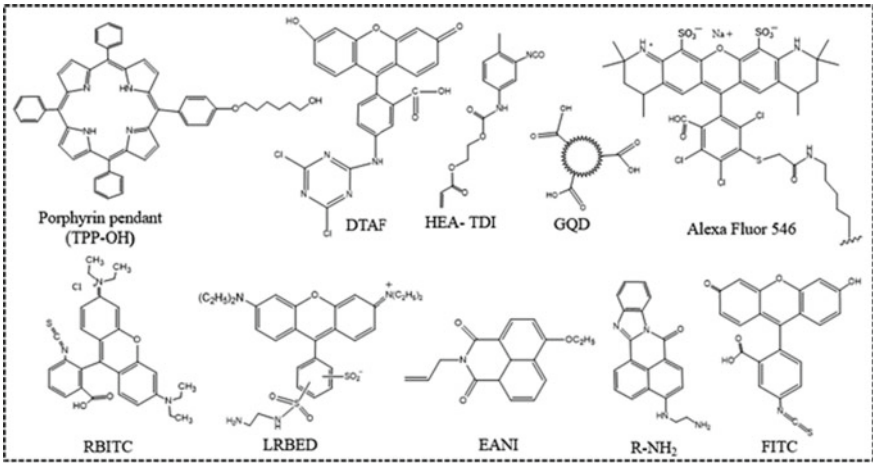

Fig. 2.3 Schematic illustration of chemical structures of various fluorescent molecules. TPPOH: (5-4hydroxylphyney)-10,15,20-triphenylporphyrin) DTAF: 5(4,6-Dichlorotriazinyl) amino fluorescein LRBED: Lissamine rhodamine B ethylenediamine EANI: (4-Ethoxy-9-allyl-1,8-naphthalimide) RBITC: Rhodamine B isocyanate HEATDI: (2-hydroxyethyl acrylate tolylene-2,4-diisocyanate) RNH_2: Fluorescent dye 4-(2-aminoethylamino)-7H-benz[de]-benzimidazo[2,1-a]isoquinoline-7-one FITC: fluorescein isothiocyanate

groups present in the quantum can form hydrogen bonding with half-ester sulfate and hydroxyl groups of CNC by taking advantage of host-gust chemistry and carbodiimide coupling. However, other organic fluorescent molecules require pretreatment in order to enhance their grafting efficiency on the fluorescent modification of CNC.

2.2.2 *Strategies of Grafting Fluorescent Molecules on Nanopolysaccharides*

Grafting of fluorescent molecules on the surface of nanopolysaccharides depend majorly on the availability of the functional surface groups, surface charges and the method of extraction of the various nanopolysaccharides. For example, CNC extracted by sulfuric acid hydrolysis contains the sulfate and hydroxyl groups on surface, while hydrochloric acid and TEMPO-mediated oxidation of nanocellulose provides nanomaterial bearing hydroxyl groups and carboxyl groups on the surface respectively. As a comparison, the presence of the amino groups on nanochitin with the surface positive charges in acidic conditions distinguishes it from cellulose. In addition, the mechanical disintegration for the preparation of cellulose and chitin nanofibrils can result into a fibrous network which differ greatly from the crystallite on the basis of surface area, aspect ratio and flexibility while maintaining similar tunable surface properties in the grafting of fluorescent molecules.

Generally, grafting of inorganic fluorescent nanoparticles can be achieved by physical adsorption through hydrogen bonding, electrostatic interaction and chemical cross-linking by covalent bonding where the CNCs sulfate groups with negative charges induces electrostatic repulsion and enhancement of fluorescent molecules. Figure 2.4 shows the typical grafting strategies for fluorescent molecules on the surface of CNC. The covalent attachment of QD on the surface of carboxylated CNC was reported by employing carbodiimide coupling reaction [33]. Another grafting strategy include immobilization of double bonds (of short chains polymer brushes) on the CNC surface for subsequent grafting of fluorescent molecules. Herein the amide bonds have been reported for grafting of dendrimer G6 poly(amidoamine) on the surface of TEMPO-mediated CNC which demonstrated a pH-responsive and fluorescent emission properties [42]. The amidation process required that the primary hydroxyl group of CNC was firstly converted into carboxyl groups through TEMPO-oxidation and then making use of *N*-(3-dimethylaminopropyl)-*N′*-ethyl-carbodiimide hydrochloride (EDC) and *N*-hydroxysuccinimide (NHS) systems for the grafting of dendrimer displaying brighter fluorescence emission at pH 3.0. Another facile procedure for esterification reaction can be combined on the surface of the carboxylated CNC, succinic anhydride and dichlorohexyl carbodiimide for subsequent grafting of porphyrin pendants fluorescent nanoprobe [31]. The linkage of these pendants and the carboxylated CNCs backbone improved the solubility of porphyrin in water and the nanomaterial was investigated for selective detection of mercury ions. Surface-initiated activators generated by electron transfer for atom transfer

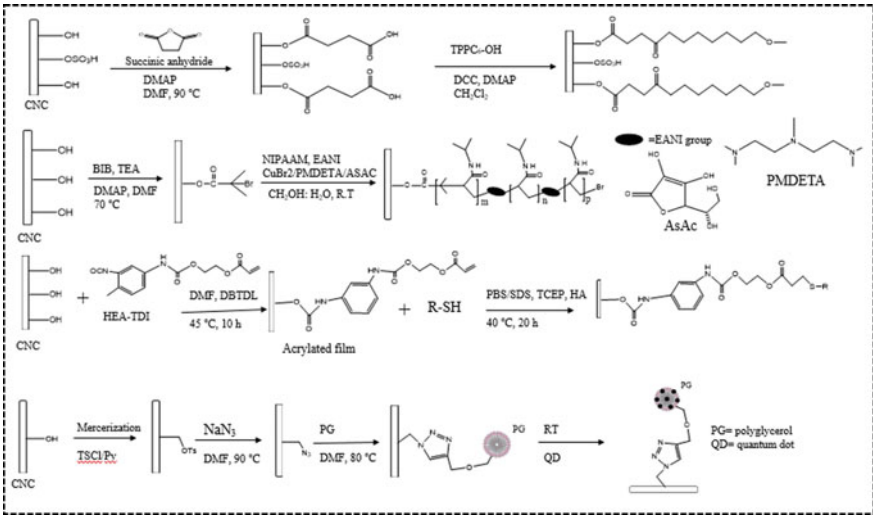

Fig. 2.4 Schematic illustration of four cases of grafting strategies for fluorescent molecules on CNC **a** esterification reaction of porphyrin pendants ($TPPC_6$–OH) with carboxylated CNC; **b** grafting of polymer brush of poly(*N*-isopropylacrylamide (PNIPAM) on the CNC surface via surface-initiated activators generated by atom transfer radical polymerization (ATRP) for subsequent encapsulation of fluorescent dye (EANI); **c** facile immobilization of (2-hydroxyethyl acrylate tolylene-2,4-diisocyanate) (HEATDI) on CNC surface for grafting thiolated fluorogenic peptide and fluorescein-substituted lysine denoted as (RSH); **d** grafting of polyglycerol (PG) on tosylated CNC for subsequent loading of QD via hydrogen bond formation

polymerization have been reported for the synthesis of thermo-responsive fluorescent CNC by grafting polymer brushes of poly(*N*-isopropylacrylamide) for encapsulation of fluorescent porphyrin pendants (4-etthoxy-9-allyl-1,8-naphthalimide) (EANI) [41]. Comparatively, an extended esterification reaction of carboxylated CNC with porphyrin pendants (6-(5′-(4′-phenoxyl)-10′,15′,20′-triphenylporphyrin-1-hexanol ($TPPC_6$–OH) was reported to provide the covalent linkage between the polymeric backbone and the fluorophore producing the high sensibility and selectively in metal detection [32].

Regarding the inorganic fluorescent molecules, the typical case is quantum dot (QD), which exhibits stable fluorescent behaviors, tunable florescence life time decay by photonic stopband, and emission spectrum with high efficiency. However, based on the linkage between two nanoparticles for the obtained hybrid fluorescent nanoparticles, the inorganic nanoparticles are prone to self-aggregation during the surface grafting on nanopolysaccharides and therefore requires versatile modification steps.

2.3 Surface Grafting of Stimuli-Responsive Molecules on Nanopolysaccharides

Stimuli-responsive nanomaterials derived from nanopolysaccharides have received considerable attention due to their diverse functionality and application in biomedical [56, 57], flexible electronics [58], tissue engineering [59, 60] and intelligent packaging [61]. Surface grafting of organic stimuli-responsive molecules on nanopolysaccharides to impart stimuli-responsive characteristics have been achieved with the emphasis on their responsiveness to physical, mechanical and chemical factors such as temperature, shear stress/mechanical compression, pressure, pH, polarity and ionic strength, humidity. In view of most studies reported for nanocellulose on this topic, this section discusses the grafting of stimuli-responsive molecules on cellulose nanocrystals (CNC) and cellulose nanofibrils (CNF).

2.3.1 Stimuli-Responsive Molecules

Most recent studies revealed that elastomers precursors such as ethyl acrylate (EA), 2-hydroxyethyl acrylate (2-HEA) and polyethylene acrylate grafted on the surface of CNC can produce versatile nanomaterials with stimuli-responsive features such birefringence change triggered by mechanical stress offering functional application in optical materials and sensors [62, 63]. Dual functionalization of CNC with numerous polymer brush (chains) of poly(acrylic acid) (PAA) and biosynthetic polypeptides, poly(oligoethylene glycol) methacrylate (POEGMA) and poly(methacrylic acid) (PMAA) N-isopropylacrylamide (PNIPAM) and poly(acrylic acid) (PAAc) have been reported [64–66]. Esterification reaction involving stimuli-responsive molecules such as 4-pentonoic acid and stearoyl chloride can also be grafted on nanocellulose [67, 68]. Poly(oligo(ethylene glycol)monomethyl ether (meth)acrylates) (POEG(M)A), poly(*N*-isopropylacrylamide) (PNIPAM), poly(glycidyl methacrylate) (PGM), poly-(ethylene glycol) dimethacrylate (PEGDMA), poly(N-isopropylacrylamide)-co-poly(glycidyl methacrylate) (PNIPAM-co-PGM) *N*-isopropylacrylamide (NIPAm), 4-((2-amnioethyl)amino)-9-methyl-1,8-naphthalimide (AANI) are few examples of molecules bearing stimuli-responsive properties when combined with cellulose nanocrystals and nanofibrils. Table 2.3 shows summarization of stimuli-responsive molecules grafted on cellulose nanocrystal (CNC) and cellulose nanofibrils (CNF) and the possessing properties after the modification.

Table 2.3 Stimuli-responsive molecules grafted on nanocellulose

Nanocellulose	Modification agent	Stimuli-responsiveness	Proposed area of application	References
CNC	Elastomer precursors (EA 2-HEA)	Colour change after mechanical stress	Versatile sensors for visual mechanical stress	[62]
	PNIPAM, Polyacrylic acid	Formation of core-corona structure due to temperature and pH	–	[65]
	PDMAEMA PDEGMA	Liquid-to-gel transition triggered by temperature	Injectable biomedical systems	[70]
	Elastomer (Polyethylene acrylate)	Birefringence triggered by aligned mechanical stress	Optical material	[63]
	Polystyrene, poly(4-vinylpyridine), and poly(*N*-isopropyl acrylamide	Drug control and release triggered by pH and temperature	Drug encapsulation control release	[69]
	POEGMA	Increased stiffness upon exposure to warm water under lower critical solution temperature (LCST)	Biomedical implants	[71]
	ANNI	Sensitivity to solvent polarity and ionic strength	Sensing nanomaterial	[72]
	NIPAAM, Acrylic acid	Change in phase transition triggered by temperature and pH	Controlled drug release	[73]
	Stearoyl chloride	Optical colors and correlated fluorescence triggered by UV and temperature	Optical material	[67]
	4-Pentenoic acid	Formation of free radicals induced by UV-light	Biomedical	[68]

(continued)

Table 2.3 (continued)

Nanocellulose	Modification agent	Stimuli-responsiveness	Proposed area of application	References
	PMAA POEGMA	pH-controlled reversible of emulsification-demulsification	Harvesting of lipophilic compound and oil-water separation	[64]
	PAA	pH and temperature sensitivity	Supramolecular engineering	[66]
	PDMAEMA, PDEAEMA PDMAPAAm	Reversible switching of the surface properties of CNC using CO_2 and pH	–	[74]
	HEA PEGDMA	Change of microgel pitch and dimension in response to temperature and ionic strength	Catalysis	[75]
	Rhodamine spiroamide (aminoethyl rhodamine)	Optical colour change triggered by pH UV-light, temperature (heat)	Multifunctional optical material	[76]
CNF	PNIPAM-co-PGM	Temperature-dependent reaction	Catalysis	[77]
	NIPAm ALPEG	Modulus increase/decrease of the hydrogels in response to pH, gelation in response to temperature	Food and biomedical application	[78]
	Elastomer	Transition of the hydrogel between fluid and solid due to shear stress, pH and cations	Tissue engineering 3D bio- printing	[79]

Abbreviations: *PAA* polyacrylic acid, *POEGMA* poly(oligoethylene glycol) methacrylate, *PMAA* poly(methacrylic acid), *PNIPAM* poly(*N*-isopropylacrylamide, *ElPs* elastin-like polypeptides, *AL-PEG-NPs* alkaline lignin-aminated polyethylene glycol, *PNIPAM-co-PGM* poly(*N*-isopropylacrylamide)-co-poly(glycidyl methacrylate), *AANI* 4-((2-amnioethyl)amino)-9-methyl-1,8-naphthalimide, *PDMAEMA* poly(2-(dimethylamino)ethyl methacrylate), *PDEGMA* poly(di-(ethylene glycol) methyl ether methacrylate), *PDEAEMA* poly(diethylaminoethyl methacrylate, *PDMAPM* poly(dimethylaminopropyl methacrylamide)

2.3.2 *Strategies of Grafting Stimuli-Responsive Molecules on Nanopolysaccharides*

For the bio-based nanomaterials to respond to external factors that can trigger responsiveness to stimulus, certain conditions must be made and this caused the urge for development of modification strategies to graft special molecules such as peptides, elastomers precursors and biopolymers. Polymerization reaction is a commonly known strategy for grafting polymer chains onto the surface of nanopolysaccharides. Surface-initiated atom transfer radical polymerization, distillation precipitation polymerization and nitroxide and azo initiated polymerization has been widely reported for grafting stimuli-responsive molecules on the surface of cellulose crystals and nanofibrils. Dual functionalization of CNC with polyacrylic acid and p-maleidophenylisocyanate containing maleimide reactive groups via thiol-imide chemistry and surface initiated atom transfer radical polymerization (si-ATRP) was also reported [69]. By taking the advantage of the imide bonds and the radical initiator 2-bromoisobutyryl bromide (BiB) on the CNC surface, poly(tert-butylacrylate) can be grafted by si-ATRP to tune the CNC as the pH and thermo-responsive multifunctional nanomaterial. Similarly, nitroxide mediated polymerization reaction to graft poly(dimethylaminoethyl methacrylate) (PDMAEMA), poly(diethylaminoethyl methacrylate) (PDEAEMA) and poly(dimethylaminopropyl methacrylamide) (PDMAPM) can also be achived on the surface of CNC via surface transfer polymerization [70].

Fluorescent molecules such as rhodamine spiroamide (aminoethyl rhodamine) immobilized on TEMPO-oxidized CNC produced a multifunctional optical material that exhibiting the responsive to pH, ultra violet light and temperature or heat [76]. Recently, the organic nanoparticle of self-assembled alkaline lignin-aminated polyethylene glycol (AL-PEG-NPs) was reported on the grafting of nanocellulose to develop the stimuli-responsive nanomaterials [78, 80, 81]. Figure 2.5 shows a schematic diagram demonstrating a simplified example of grafting mechanisms of stimuli-responsive molecules on the surface of nanocellulose. In each step shown in the figure, the detailed reaction conditions have not been included and can be accessed from Table 2.3.

Atom transfer radical polymerization was reported for the synthesis of cationic PDMAEMA/PDEGMA. The positive charges of the cationic polymers cross-linked with the negative charges of the carboxylic groups of the TEMPO-oxidized CNC through electrostatic interaction. The cross-linking improved the mechanical properties of the block copolymer with reversible liquid-to-gel transition with the increased viscosity of systems. This thermos-responsive biobased nanomaterial was expected to be potentially used in injectable biomedical systems. The self-assembly of alkaline lignin–aminated polyethylene glycol (AL-PEG-NH_2) into nanoparticles (AL-PEG-NPs) endowed the reinforcement of the fabricated thermos-responsive hydrogels from TEMPO-oxidized CNF. Hydrogen bonding predominates in this interaction between the NIPAm-grated CNF and AL-PEG-NPs which on the other hand can

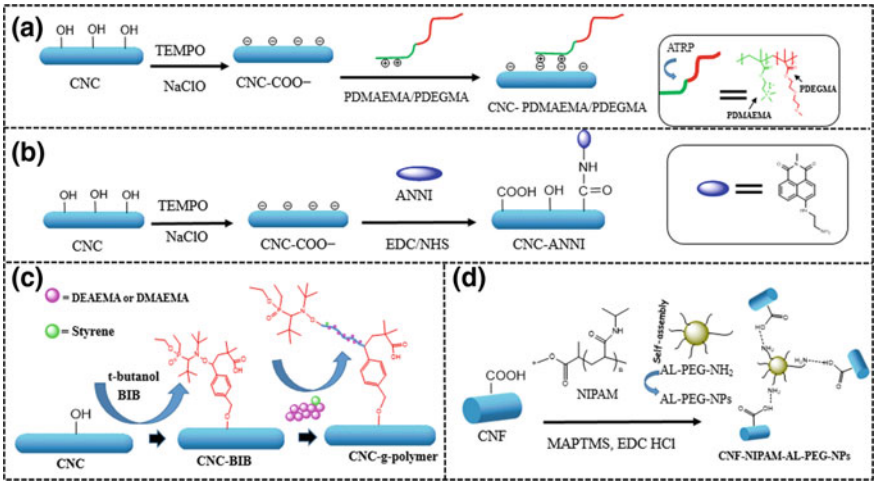

Fig. 2.5 Schematic illustration of strategies for grafting stimuli-responsive molecules on nanocellulose with the typical cases of **a** attachment of quaternized poly(2-(dimethylamino)ethyl methacrylate) (PDMAEMA) and poly(di-(ethylene glycol) methyl ether methacrylate) (PDEGMA) TEMPO-mediated CNC, **b** grafting of 4-((2-amnioethyl)amino)-9-methyl-1,8-naphthalimide (AANI), **c** grafting of polymers on CNC using surface-initiated nitroxide mediated polymerization **d** grafting of N-isopropylacrylamide (NIPAm) and self-assembled alkaline lignin-aminated polyethylene glycol (AL-PEG-NPs) on CNF

easily be weaken by the change of pH to slightly alkaline conditions, and therefore displaying the pH sensitivity. The synthesized hydrogels were reported to be promising applications because of the mechanical performance and the stimuli-responsiveness.

2.4 Surface Modification on Nanopolysaccharides Served as Drug Delivery

2.4.1 Drug Molecules in Nanopolysaccharides-Based Drug Delivery

The development of nanopolysaccharides-based drug delivery systems has become one of hotspots in the research field of biomedical application due to their unique properties supporting both in vitro and in vivo release of drugs. The choice for nanopolysaccharides as suitable drug delivery systems is based on their intrinsic characteristics such as biocompatibility, biodegradability, non-toxicity, surface functionalities and excellent mechanical performance as scaffolds and their ability to directly entrap drug species or graft other drug carrier such β-cyclodextrin [82] and

dendrimer [83] which possess hydrophobic cavities suitable for drug molecules. The typical drug molecues are reported for the modification on nanopolysaccharides include: methotrexate (MTX), 5-fluorouracil (5-FU), levamisole hydrochloride (LH), curcumin (Cur) folic acid (FA), doxorubicin (DOX), vitamin C (VC), procaine hydrochloride (PrHy), imipramine hydrochloride (IMI), quercetin, metronidazole (MZ), nadolo (NAD), ketoprofen (KETO), indomethacin (INDO), 5-fluorocytosine (5-FC), naproxen (NAP) and ibuprofen (IBU). Figure 2.6 shows three typical modification strategies on CNC for the trapping of drug molecules in the application of drug delivery.

To achieve the trapping of targeted drug molecules, surface modification is generally performed on nanopolysaccharides, with the typical pre-modification on nanopolysaccharides for subsequent physical binding (adsorption), direct chemical grafting of drug molecules or grafting of other molecules to entrap the drugs to avoid the drug from leakage. For instance, chitosan oligosaccharide with active amino groups was reported to be grafted on the surface of CNC for subsequent loading and delivery of cationic drugs procaine hydrochloride and imipramine hydrochloride [87]. The chemical grafting of fatty acids (stearic and oleic acid) on the surface of nanostarch for loading and delivery of indomethacin drug was also reported [88]. Table 2.4 summarizes recent reports on the use of nanopolysaccharides as drug delivery with various surface modifications and entrapped drugs and interaction.

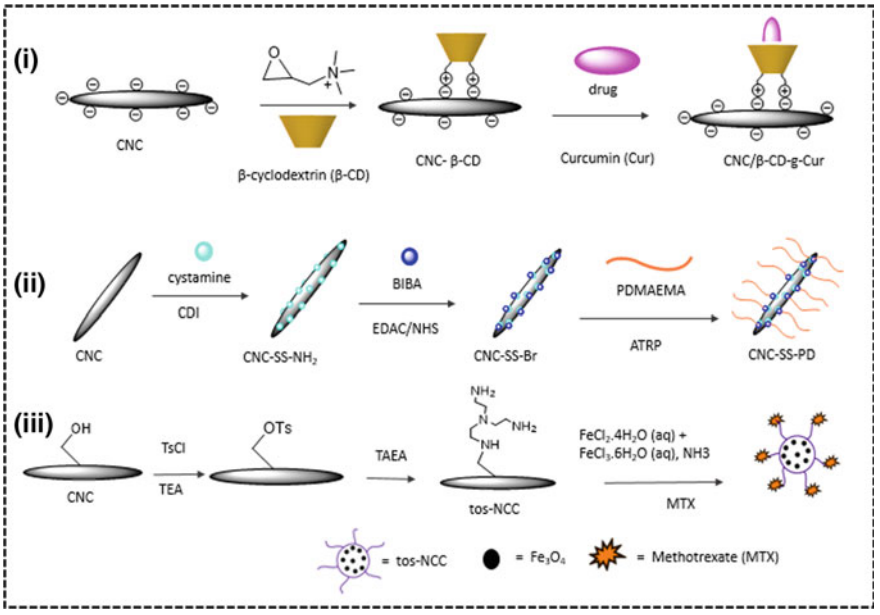

Fig. 2.6 Specific surface modification strategies on nanopolysacchrides for the application of drug delivery (i) β-CD-grafted CNC for encapsulation of curcumin drug; (ii) immobilization of PDMAEMA brushes on CNC using ATRP for transfection of gene; (iii) tosylated CNC functioned with Fe_3O_4 for the loading of MTX

Table 2.4 Diverse modification agents for nanopolysaccharides (NPs)-based delivery systems with specific model drugs, entrapping interactions and potential application

NPs	Modification agent	Model drug	Entrapping interaction	Potential application	References
CNC	HEMA and MAA as monomers KPS and MBA as initiator and cross-linker	5-FU and LH	Induced apoptosis that destroys the mutated cells	Colon cancer	[89]
	Tris(2-aminoethyl)amine Fe_3O_4 nanoparticles	MTX	Endocytosis	Breast cancer	[90]
	CHPTAC	DOX	Shrinkage of cell nuclei and apoptotic of liver cells	Liver cancer	[91]
	β-Cyclodextrin	Curcumin	Endocytosis of intracellular membrane through ERP	Colorectal and prostatic cancer	[82]
	PEEP by CuAAC click reaction	DOX	Endocytosis	Cervical cancer (HeLa)	[92]
	PEI	SiRNA	Apoptosis triggered by external and internal stimuli	–	[93]
	PPI-dendrimer	DOX FA	–	–	[83]
	PDMAEMA, BIBA and DTT	CD/5-FC	Cytotoxicity of 5-FU that suppress the growth of tumor cell	Antitumor and gene delivery	[94]
	Epichlorohydrin and FITC	FA	Caveolae and Clathrin mediated endocytosis	Brain tumors	[95]
	CTAB	Curcumin	–	–	[96]
	Chitosan oligosaccharide	Vitamin C	–	–	[97]
	Chitosan oligosaccharide	PrHy IMI	Electrostatic repulsion	Local analgesic	[98]

(continued)

Table 2.4 (continued)

NPs	Modification agent	Model drug	Entrapping interaction	Potential application	References
	Chitosan oligosaccharide	PrHy	Electrostatic repulsion	Local analgesic	[84]
	Sodium alendronate (Aln) ApA	–	–	Bone therapies and theranostics	[85]
	PLGA PVA	FTICBSA	–	Bone therapy	[86]
CNF	FITCDEX Ly BSA	MZ NAD KETO	Diffusion	–	[98]
	Fe_3O_4–Ag_2O quantum dots (QD)	Etoposide and MTX	–	Anticancer	[99]
	Polyvinyl chloride (PVC)	Quercetin	Fickan diffusion mechanism	–	[100]
	(GTMAC)	Furosemide	–	–	[101]
	HFBII	NAP and IBU	–	–	[102]
Nanostarch	Oleic acid stearic acid and sodium tripolyphosphate as cross-linker	INDO	–	Oral drug delivery	[88]

Abbreviations: *PDMAEMA* poly(2-(dimethylamino)ethyl methacrylate), *BIBA* α-bromoisobutyric acid, *CD/5-FC* cytosine deaminase/5-fluorocytosine, *HEMA* 2-hydroxyethyl methacrylate, *MAA* methacrylic acid, *KPS* potassium persulphate, *MBA N,N′*-methylenebisacrylamide, *CTAB* cetyltrimethyl ammonium bromide, *PLGA* poly(lactide-co-glycolide), *GTMAC* glycidyltrimethylammonium chloride, *HFBII* Class II hydrophobin protein, *PEEP* poly(ethyl ethylene phosphate), *CHPTAC* 3-chloro-2-hydroxypropyltrimethylammonium chloride, *PPI* poly(propylene imine), *PEI* polyethyleneime, *PVA* poly(vinyl alcohol), *Aln* sodium alendronate, *ApA* aminoropyl phosphoric acid, *FTICBSA* bovine serum albumin-fluorescein isothiocynate conjugate, *FITCDEX* fluorescein isothiocyanate-dextran, *Ly* lysozyme

2.4.2 *Strategies of Surface Modification on Nanopolysaccharides for Drug Delivery*

The modification of nanopolysaccharides to serve as drug delivery vehicles involves direct grafting of the targeted drug molecules on the surface or/and grafting of intermediate molecules capable of entrapping drug molecules. The modification strategies have been categorized into three parts viz. (i) grafting of modification agent for potential drug delivery without the introduced model drugs; (ii) direct grafting of model drugs onto the surface of nanopolysaccharides; and (iii) grafting other molecules such as β-cyclodextrin and dendrimers to entrap the drug molecules. Figure 2.6 illustrates several typical approaches for surface modification on nanopolysaccharides in drug

delivery. Cellulose nanocrystals mediated by TEMPO-oxidation were successfully modified by grafting cationic chitosan oligosaccharide (CSos) for loading and delivery of Vitamin C (VC) [97]. This grafting was performed by the chemical reaction between the carboxylic groups of the TEMPO-oxidized CNC and the amino groups of the CSos. In the further application, the electrostatic interaction between the positive charges of surface modified nanocrystals and the negatives charges of VC can enhance the drugs entrapment.

In another case, the chitosan bearing the amino groups was combined with the carboxylated nanocellulose and then coated with sodium alignate to produce the nanocomposite for drug delivery. To promote the binding and release of anticancer drug (5-FU) and a biomodulator (LH), the obtained nanocomposite was further modified by grafting 2-hydroxylethylmethacrylate (HEMA) and methacrylic acid (MAA). Therefore, the hydrophilic moieties of HEMA and MAA can bind the drug molecules through electrostatic interaction for the sustained release of drugs [85]. Polymerization reaction techniques were also reported to be applied to graft polymers taking the excellent compatibility with both drug molecules and nanocellulose. Immobilization of polymer brushes of poly-(2-(dimethylamino)ethyl methacrylate) (PDMAEMA) using atom transfer radical polymerization (ATRP) for the delivery of prodrug and evaluation against suicide gene has been reported [94]. The mechanism in this modification strategy involved the reaction between CNC with cystamine to impart disulfide bonds followed by the introduction of an initiation (BIBA) for subsequent ATRP reaction and immobilization of the suicide gene. The presence of the disulfide bonds played an important role for the cleavage of the PDMAEMA brushes from CNC for the release of the suicide gene under the reducing conditions. Similarly, the ring opening polymerization (ROP) is another useful technique for the grafting of propargyl-terminated polyethylene phosphate on the surface of azide-modified CNC via click reaction for the subsequent loading and delivery of doxorubicin.

It is worth noting that some model drugs are poorly water soluble and therefore the development of delivery systems that can endow controlled release and sustainability is a challenge. The availability of hydrophobic cavities in β-cyclodextrin play an important role and it regarded as the choice for trapping nonpolar drugs on CNC. To graft the cyclodextrin, an etherification reaction of CNC with epoxypropyltrimethyl ammonium is required for subsequent reaction of the quaternized CNC with cyclodextrin. Another strategy for the grafting of cationic polymer brushes on the surface of CNC takes the advantage of disulfide bonds from thiol-imide groups. These bonds are responsible for covalent attachment of the drug molecules which can be detached change of the pH media Similar case involving PDMAEMA has recently been reported to be applied in combination with gold nanoparticle and poly [poly (ethylene glycol)ethyl ethermethacrylate] (PPEGEEMA) for gene transfection in HepG2 and HEK 293 cell line [103]. In addition, the use of CNF with numerous network and amphiphilic properties are potential adsorbents to improve stability of the hydrophobic drugs [100].

2.5 Superhydrophobic Modification on Nanocellulose

Superhydrophobic materials have attracted considerable interest such as exhibiting the significant adsorption and separation properties towards oil and organic pollutants [104]. Superhydrophobic materials are referred to materials with the water contact angel higher than 120º. Nanocellulose in general is known for their inherent sensitivity towards moisture and high hydrophilicity due to the presence of numerous hydroxyl groups on their surface, hence the high wettability. There ae two factors that govern the wettability of a solid surface; (i) surface energy and (ii) surface roughness. These factors are essential when considering the modification of nanocellulose, since achieving surfaces with low energy and roughness can ensure tailoring them into superhydrophobic molecules to provide the adsorption and separation properties. Utilization of some chemicals (with low surface energy) such as fluorocarbons and silicone can ensure the obtain of hydrophobic nanocellulose through reducing the surface energy.

2.5.1 Superhydrophobic Molecules

Superhydrophobic modifying agents are basically classified into, agents to serve in reduction of the surface energy and others to enhance surface roughness [105]. There is a good number of fluorine and silicon derivatives serve as modification agents to tailor the surface of nanocellulose with superhydrophobic properties which results in compatibility with other hydrophobic chemicals or materials. Amino propyl trimethoxysilane (APMS) [106], alkyl ketened dimer (AKD), trichloro(1*H*,1*H*,2*H*,2*H*-heptad-cafluorodecyl) silane (THFS) [107], methyltrichlorosilane (MTCS) [108] are typical examples summarized in Table 2.5 by emphasizing the methods and results of corresponding water contact angels obtained.

2.5.2 Strategies of Grafting Superhydrophobic Molecules on Nanocellulose

The strategies to graft superhydrophobic molecules on nanocellulose include the direct covalent attachment of modified agents and indirect modification of nanocellulose with the pretreatment to introduce the active groups. Figure 2.7 illustrates the strategies of several typical cases on the surface superhydrophobilization to CNF. Generally, chemical modification was achieved directly with superhydrophobic particles covalently attached to the surface of CNF as reported with the water contact angels in the range of 130°–170°. The existing hydroxyl groups on the surface of CNF provided reaction sites for the saline molecules obtained from its various low surface energy derivatives as mentioned before, for instance FTOS, FS and APTS, silane

Table 2.5 The reported superhydrophobic molecules grafted on nanocellulose

Nanocellulose	Superhydrophobic agent	Method	Water contact angle	References
CNC	Tetraethyl orthosilicate (TEOS)	In situ growth of SiO_2	159°	[109]
	2*H*,2*H*,3*H*,3*H*-Perfluorononanoyl chloride and 2*H*,2*H*,3*H*,3*H*-perfluoroundecanoyl chloride	Dispersion and precipitation techniques under nitrogen atmosphere	150°	[110]
	Dodecyltrimethoxysilane (DTMOS)	Chemical grafting/KH560 linker	140°	[111]
CNF	Trichlorovinylsilane (TCVS)	In situ polycondensation and thiol-ene click reaction	166° 167°	[112]
	Methyltriethoxysilane (MTES)	Silylation reaction	151.8°	[113]
	Bifunctional fluorinated polybenzoxazine and SiO_2 NP (F-PBZ/SiO_2)	In situ polymerization	161°	[114]
	Trichlorosilane surfactant with fluorinated alkyl (FOTS)	Chemical vapor deposition	169° 163°	[115]
	1*H*,1*H*,2*H*,2*H*-Perfluorooctyltriethoxysilane (PFTS), 3-(2-Aminoethylamino) propyltrimethoxysilane (APTS)	Dipping and coating	160°	[116]
	Methyltrichlorosilane (MTCS)	In situ siloxanes growth	159.6°	[117]
	1*H*,1*H*,2*H*,2*H*-Perfluorooctyltriethoxysilane (FS) and 3- (2 –aminoethylamino)-propyltrimethoxysilane	Direct chemical modification in water	160°	[118]
	Silane (polysiloxane)	Covalent attachment	>130°	[119]
	Trichloro(1*H*,1*H*,2*H*,2*H*-heptadecafluorodecyl) silane (THFS)	Fluorinated silane functionalization	160°	[107]
	Fluorine plasma (trifluoromethane)	Electrospinning plasma treatment	>150°	[120]

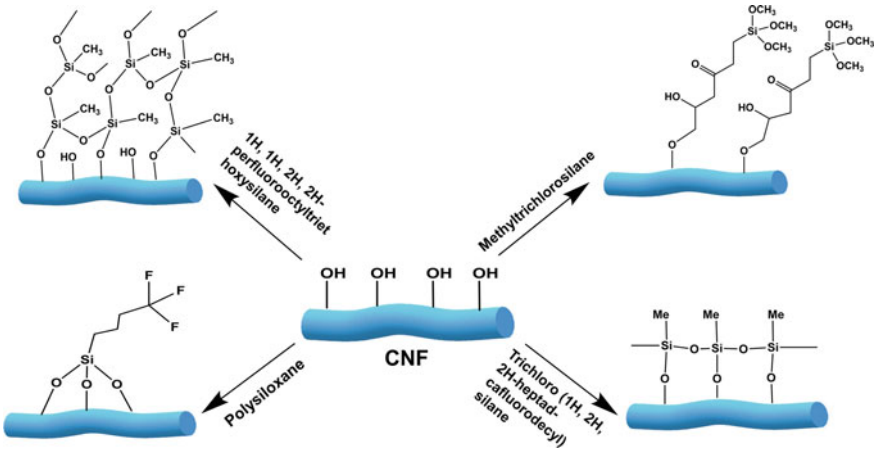

Fig. 2.7 Typical superhydrophobic modification on cellulose nanofibrils (CNF)

and THFS to be covalently attached onto the surface of CNF and therefore render its superhydrophobic property. The typical superhydrophobic molecules introduced on the grafting of CNF are silicone and fluorine-based molecules.

2.6 Concluding Remarks

The combination with functional molecules and nanopolysaccharides is a promising approach to advance the high-added value of these natural nanomaterials and expand their applications in diverse fields. This chapter describes five typical functional modifications on nanopolysaccharides with the grafting of antibacterial, fluorescent molecules, stimuli-responsive species, and surface modifications for drug delivery and superhydrophobicity. The emphasis of each topic is put on the grafting strategies of different functional agents on nanopolysaccharides. Generally, all the cases of surface modification with grafting functional molecules on nanopolysaccharides can be summarized as three approaches, (i) covalent linkage between grafted species and nanopolysaccharides; (ii) electrostatic or ionic adsorption based on the surface charges of nanopolysacchrides and charged molecules; and (iii) physical adsorption or self-assembly (hydrogen bonding or hydrophilic/hydrophobic interaction) of functional species on nanopolysaccharides. The novel grafting strategy aiming to obtain the high grafting efficiency at the facile step and manipulation to introduce the functional molecules on nanopolysaccharides as well as the achievement of multi-functional modification will be the challenges of future study on this topic.

Acknowledgements The authors would like to acknowledge the support of the National Natural Science Foundation of China (51603159).

References

1. Wang SW, Sun JS, Jia YX et al (2016) Nanocrystalline cellulose-assisted generation of silver nanoparticles for nonenzymatic glucose detection and antibacterial agent. Biomacromol 17:2472–2478
2. Ma PM, Jiang L, Yu MM et al (2016) Green antibacterial nanocomposites from poly(lactide)/poly(butylene adipate-co-terephthalate)/nanocrystal cellulose silver nanohybrids. ACS Sustain Chem Eng 4:6417–6426
3. Shi ZQ, Tang JT, Chen L et al (2015) Enhanced colloidal stability and antibacterial performance of silver nanoparticles/cellulose nanocrystal hybrids. J Mater Chem B 3:603–611
4. Drogat N, Granet R, Sol V et al (2011) Antimicrobial silver nanoparticles generated on cellulose nanocrystals. J Nanopart Res 13:1557–1562
5. Kebede MA, Imae T, Sabrina (2017) Cellulose fibers functionalized by metal nanoparticles stabilized in dendrimer for formaldehyde decomposition and antimicrobial activity. Chem Eng J 311:340–347
6. Hassanpour A, Asghari S, Lakouraj MM (2017) Synthesis, characterization and antibacterial evaluation of nanofibrillated cellulose grafted by a novel quinolinium silane salt. RSC Adv 7:23907–23916
7. Oun AA, Rhim JW (2017) Preparation of multifunctional chitin nanowhiskers/ZnO-Ag NPs and their effect on the properties of carboxymethyl cellulose-based nanocomposite film. Carbohydr Polym 169:467–479
8. Vasanthan N, Bespalova Y, Kwon D (2017) Surface modification and antimicrobial properties of cellulose nanocrystals. Paper presented at 254th National meeting and exposition of the American-chemical-society (ACS) on chemistry's impact on the global economy, Washington DC, 20–24 Aug 2017
9. Chauhan P, Yan N (2017) Novel nitroaniline-cellulose nanohybrids: nitro radical photo-release and its antibacterial action. Carbohydr Polym 174:1106–1113
10. Abouhmad A, Dishisha T, Amin MA et al (2017) Immobilization to positively charged cellulose nanocrystals enhances the antibacterial activity and stability of hen egg white and T4 lysozyme. Biomacromol 18:1600–1608
11. de Castro DO, Bras J, Gandini A et al (2016) Surface grafting of cellulose nanocrystals with natural antimicrobial rosin mixture using a green process. Carbohydr Polym 137:1–8
12. Yu HY, Chen GY, Wang YB et al (2014) A facile one-pot route for preparing cellulose nanocrystal/zinc oxide nanohybrids with high antibacterial and photocatalytic activity. Cellulose 22(1):261–273
13. Lavoine N, Desloges I, Manship B et al (2015) Antibacterial paperboard packaging using microfibrillated cellulose. J Food Sci Technol 52(9):5590–5600
14. Tyagi P, Mathew R, Opperman CH et al (2018) High strength antibacterial chitosan-cellulose nanocrystals composite tissue paper. Langmuir 35:104–112
15. Jafary R, Mehrizi MK, Hekmatimoghaddam SH et al (2015) Antibacterial property of cellulose fabric finished by allicin-conjugated nanocellulose. J Text I 106:683–689
16. Feese E, Sadeghifar H, Gracz HS et al (2011) Photobactericidal porphyrin-cellulose nanocrystals: synthesis, characterization, and antimicrobial properties. Biomacromol 12:3528–3539
17. Saini1 S, Quinot D, Lavoine N et al (2017) Beta-Cyclodextrin-grafted TEMPO-oxidized cellulose nanofibers for sustained release of essential oil. J Mater Sci 52:3849–3861
18. Andresen M, Stenstad P, Moretro T et al (2007) Nonleaching antimicrobial films prepared from surface-modified microfibrillated cellulose. Biomacromol 8:2149–2155
19. Nguyen HL, Jo YK, Cha M et al (2016) Mussel-inspired anisotropic nanocellulose and silver nanoparticle composite with improved mechanical properties, electrical conductivity and antibacterial activity. Polymers-Basel 8:102–115
20. Bober P, Liu J, Mikkonen KS et al (2014) Biocomposites of nanofibrillated cellulose, polypyrrole, and silver nanoparticles with electroconductive and antimicrobial properties. Biomacromol 15:3655–3663

21. Díez I, Eronen P, Österberg M et al (2011) Functionalization of nanofibrillated cellulose with silver nanoclusters: fluorescence and antibacterial activity. Macromol Biosci 11(9):1185–1191
22. Li ZH, Zhang M, Cheng D et al (2016) Preparation of silver nanoparticles immobilized onto chitin nanochitin nanocrystals and their application to cellulose paper for imparting antimicrobial activity. Carbohydr Polym 151:834–840
23. Shankar S, Reddy JP, Rhim JW et al (2015) Preparation, characterization, and antimicrobial activity of chitin nanofibrils reinforced carrageenan nanocomposite films. Carbohydr Polym 117:468–475
24. Dutta AK, Egusa M, Kaminaka H et al (2015) Facile preparation of surface N-halamine chitin nanofiber to endow antibacterial and antifungal activitie. Carbohydr Polym 115:342–347
25. Nata IF, Wu TM, Chen JK et al (2014) A chitin nanofibril reinforced multifunctional monolith poly(vinyl alcohol) cryogel. J Mater Chem B 2(26):4108–4113
26. González K, García-Astrain C, Santamaria-Echart A et al (2018) Starch/graphene hydrogels via click chemistry with relevant electrical and antibacterial properties. Carbohydr Polym 202:372–381
27. Tang JT, Song Y, Tanvir S et al (2015) Polyrhodanine coated cellulose nanocrystals: a sustainable antimicrobial agent. ACS Sustain Chem Eng 3:1801–1809
28. Qin Y, Zhang S, Yu J et al (2016) Effects of chitin nano-whiskers on the antibacterial and physicochemical properties of maize starch films. Carbohydr Polym 147:372–378
29. Li MC, Wu QL, Song KL et al (2016) Chitin nanofibers as reinforcing and antimicrobial agents in carboxymethyl cellulose films: influence of partial deacetylation. ACS Sustain Chem Eng 4:4385–4395
30. Jiang SS, Qin Y, Yang J et al (2017) Enhanced antibacterial activity of lysozyme immobilized on chitin nanowhiskers. Food Chem 221:1507–1513
31. Chen JD, Zhou ZX, Chen ZX et al (2017) A fluorescent nanoprobe based on cellulose nanocrystals with porphyrin pendants for selective quantitative trace detection of Hg^{2+}. New J Chem 41:10272–10280
32. Khabibullin A, Alizadehgiashi M, Khuu N et al (2017) Injectable shear-thinning fluorescent hydrogel formed by cellulose nanocrystals and graphene quantum dots. Langmuir 33(43):12344–12350
33. Abitbol T, Marway HS, Kedzior SA et al (2017) Hybrid fluorescent nanoparticles from quantum dots coupled to cellulose nanocrystals. Cellulose 24(3):1287–1293
34. Leng T, Jalcubek ZJ, Mazloumi M et al (2017) Ensemble and single particle fluorescence characterization of dye-labeled cellulose nanocrystals. Langmuir 33(32):8002–8011
35. Gorgieva S, Vivod V, Maver U et al (2017) Internalization of (bis)phosphonate-modified cellulose nanocrystals by human osteoblast cells. Cellulose 24(10):4235–4252
36. Herreros-Lopez A, Carini M, Da Ros T et al (2017) Nanocrystalline cellulose-fullerene: novel conjugates. Carbohydr Polym 164:92–101
37. Ding QJ, Zeng JS, Wang B et al (2017) Influence of binding mechanism on labeling efficiency and luminous properties of fluorescent cellulose nanocrystals. Carbohydr Polym 175:105–112
38. Qu D, Zhang JN, Chu G et al (2016) Chiral fluorescent films of gold nanoclusters and photonic cellulose with modulated fluorescence emission. J Mater Chem C 4:1764–1768
39. Parsamanesh M, Tehrani AD (2016) Synthesize of new fluorescent polymeric nanoparticle using modified cellulose nanowhisker through click reaction. Carbohydr Polym 136:1323–1331
40. Sîrbu E, Eyley S, Thielemans W (2016) Coumarin and carbazole fluorescently modified cellulose nanocrystals using a one-step esterification procedure. Can J Chem Eng 94(11):2186–2194
41. Wu WB, Huang F, Pan SB et al (2015) Thermo-responsive and fluorescent cellulose. J Mater Chem A 3:1995–2005
42. Chen L, Cao W, Grishkewich N et al (2015) Synthesis and characterization of pH-responsive and fluorescent poly (amidoamine) dendrimer-grafted cellulose nanocrystals. J Colloid Interface Sci 450:101–108

43. Colombo L, Zoia L, Violatto MB et al (2015) Organ distribution and bone tropism of cellulose nanocrystals in living mice. Biomacromol 16(9):2862–2871
44. Grate JW, Mo KF, Shin Y et al (2015) Alexa fluor-labeled fluorescent cellulose nanocrystals for bioimaging solid cellulose in spatially structured microenvironments. Bioconjug Chem 26(3):593–601
45. Schyrr B, Pasche S, Voirin G et al (2014) Biosensors based on porous cellulose nanocrystal-poly(vinyl alcohol) scaffolds. ACS Appl Mater Interfaces 6(15):12674–12683
46. Abitbol T, Palermo A, Moran-Mirabal JM et al (2013) Fluorescent labeling and characterization of cellulose nanocrystals with varying charge contents. Biomacromol 14(9):3278–3284
47. Hassan ML, Moorefield CM, Elbatal HS et al (2012) Fluorescent cellulose nanocrystals via supramolecular assembly of terpyridine-modified cellulose nanocrystals and terpyridine-modified perylene. Mater Sci Eng B 177(4):350–358
48. Mahmoud KA, Mena JA, Male KB et al (2010) Effect of surface charge on the cellular uptake and cytotoxicity of fluorescent labeled cellulose nanocrystals. ACS Appl Mater Interfaces 2(10):2924–2932
49. Zhou J, Butchosa N, Jayawaredena S et al (2015) Synthesis of multifunctional cellulose nanocrystals for lectin recognition and bacterial imaging. Biomacromol 16:1426–1432
50. Ikai T, Suzuki D, Kojima Y et al (2016) Chiral fluorescent sensors based on cellulose derivatives bearing terthienyl pendants. Polym Chem 7:4793–4801
51. Yang G, Wan X, Su Y et al (2016) Acidophilic S-doped carbon quantum dots derived from cellulose fibers and their fluorescence sensing performance for metal ions in an extremely strong acid environment. J Mater Chem A 4:12841–12849
52. Navarro JRG, Conzatti G, Yu Y et al (2015) Multicolor fluorescent labeling of cellulose nanofibrils by click chemistry. Biomacromol 16:1293–1300
53. Junka K, Guo J, Filpponen I et al (2014) Modification of cellulose nanofibrils with luminescent carbon dots. Biomacromol 15:876–881
54. Niu Q, Gao K, Wu W (2014) Cellulose nanofibril based graft conjugated polymer films act as a chemosensor for nitroaromatic. Carbohydr Polym 110:47–52
55. Zhou J, Butchosa N, Jayawardena HSN et al (2014) Glycan-functionalized fluorescent chitin nanocrystals for biorecognition applications. Bioconjugate Chem 25:640–643
56. Shahid UNM, Deshpande AP, Rao CL (2015) Electro-mechanical properties of hydrogel composites with micro- and nano-cellulose fillers. Smart Mater Struct 24:095013
57. Qian Z, Wang Z, Zhao N et al (2018) Aerogels derived from polymer nanofibers and their applications. Macromol Rapid Comm 39:1700724
58. Sabo R, Yermakov A, Law CT et al (2016) Nanocellulose-enabled electronics energy harvesting devices smart materials and sensors: a review. J Renew Mater 4:297–312
59. Natterodt J, Petri-Fink A, Weder C et al (2017) Cellulose nanocrystals: surface modification applications and opportunities at interfaces. Chimia Int J Chem 71:376–383
60. Calvo-Correas T, Garrido P, Alonso-Varona A et al (2018) Biocompatible thermoresponsive polyurethane bionanocomposites with chitin nanocrystals. J Appl Polym Sci 136:47430
61. Li Y, Ying Y, Zhou Y et al (2019) A pH-indicating intelligent packaging composed of chitosan-purple potato extractions strength by surface-deacetylated chitin nanofibers. Int J Biol Macromol 127:376–384
62. Kose O, Tran A, Lewis L et al (2019) Unwinding a spiral of cellulose nanocrystals for stimuli-responsive stretchable optics. Nat Commun 10:510
63. Kose O, Boott CE, Hamad WY et al (2019) Stimuli-responsive anisotropic materials based on unidirectional organization of cellulose nanocrystals in an elastomer. Macromolecules 52:5317–5324
64. Tang J, Berry RM, Tam KC (2016) Stimuli-responsive cellulose nanocrystals for surfactant-free oil harvesting. Biomacromol 17:1748–1756
65. Zeinali E, Haddadi-Asl V, Roghani-Mamaqani H (2018) Synthesis of dual thermo- and pH-sensitive poly(N-isopropylacrylamide-co-acrylic acid)-grafted cellulose nanocrystals by reversible addition-fragmentation chain transfer polymerization. J Biomed Mater Res A 106:231–243

66. Malho JM, Brand J, Pecastaings G et al (2018) Multifunctional stimuli-responsive cellulose nanocrystals via dual surface modification with genetically engineered elastin-like polypeptides and poly(acrylic acid). ACS Macro Lett 7:646–650
67. Wang Y, Heim LO, Xu Y et al (2015) Transparent stimuli-responsive films from cellulose-based organogel nanoparticles. Adv Funct Mater 25:1434–1441
68. Smyth M, Rader C, Bras J et al (2017) Characterization and mechanical properties of ultraviolet stimuli-responsive functionalized cellulose nanocrystal alginate composites. J Appl Polym Sci 135:45857
69. Zhang Z, Cheng M, San Gabriel M et al (2019) Polymeric hollow microcapsules (PHM) via cellulose nanocrystal stabilized pickering emulsion polymerization. J Colloid Interface Sci 555:489–497
70. Gicquel E, Martin C, Gauthier Q et al (2019) Tailoring rheological properties of thermoresponsive hydrogels through block copolymer adsorption to cellulose nanocrystals. Biomacromol 20:2545–2556
71. Cudjoe E, Khani S, Way AE et al (2017) Biomimetic reversible heat-stiffening polymer nanocomposites. ACS Cent Sci 3:886–894
72. Wu W, Song R, Xu Z et al (2018) Fluorescent cellulose nanocrystals with responsiveness to solvent polarity and ionic strength. Sens Actuators B 275:490–498
73. Haqani M, Roghani-Mamaqani H, Salami-Kalajahi M (2017) Synthesis of dual-sensitive nanocrystalline cellulose-grafted block copolymers of N-isopropylacrylamide and acrylic acid by reversible addition-fragmentation chain transfer polymerization. Cellulose 24:2241–2254
74. Garcia-Valdez O, Brescacin T, Arredondo J et al (2017) Grafting CO_2-responsive polymers from cellulose nanocrystals via nitroxide-mediated polymerisation. Polym Chem 8:4124–4131
75. Cho S, Li Y, Seo M et al (2016) Nanofibrillar stimulus-responsive cholesteric microgels with catalytic properties. Angew Chem Int Ed 128:14220–14224
76. Zhao L, Li W, Plog A et al (2014) Multi-responsive cellulose nanocrystal–rhodamine conjugates: an advanced structure study by solid-state dynamic nuclear polarization (DNP) NMR. Phys Chem Chem Phys 16:26322–26329
77. Li Y, Zhu L, Wang B et al (2018) Fabrication of thermoresponsive polymer-functionalized cellulose sponges: flexible porous materials for stimuli-responsive catalytic systems. ACS Appl Mater Interfaces 10:27831–27839
78. Lu J, Zhu W, Dai L et al (2019) Fabrication of thermo- and pH-sensitive cellulose nanofibrils-reinforced hydrogel with biomass nanoparticles. Carbohydr Polym 215:289–295
79. Sanandiya ND, Vasudevan J, Das R et al (2019) Stimuli-responsive injectable cellulose thixogel for cell encapsulation. Int J Biol Macromol 130:1009–1017
80. Anirudhan TS, Sekhar VC, Shainy F et al (2019) Effect of dual stimuli responsive dextran/nanocellulose polyelectrolyte complexes for chemophotothermal synergistic cancer therapy. Int J Biol Macromol 135:776–789
81. Low LE, Tan LTH, Goh BH et al (2019) Magnetic cellulose nanocrystal stabilized pickering emulsions for enhanced bioactive release and human colon cancer therapy. Int J Biol Macromol 127:76–84
82. Ndong Ntoutoume GMA, Granet R, Mbakidi JP et al (2016) Development of curcumin–cyclodextrin/cellulose nanocrystals complexes: New anticancer drug delivery systems. Bioorg Med Chem Lett 26:941–945
83. Golshan M, Salami-Kalajahi M, Roghani-Mamaqani H et al (2017) Poly(propylene imine) dendrimer-grafted nanocrystalline cellulose: Doxorubicin loading and release behavior. Polymer 117:287–294
84. Akhlaghi SP, Berry RC, Tam KC (2013) Surface modification of cellulose nanocrystal with chitosan oligosaccharide for drug delivery applications. Cellulose 20:1747–1764
85. Gorgieva S, Vivod V, Maver U et al (2017) Internalization of (bis)phosphonate-modified cellulose nanocrystals by human osteoblast cells. Cellulose 24:4235–4252
86. Rescignano N, Fortunati E, Montesano S et al (2014) PVA bio-nanocomposites: a new take-off using cellulose nanocrystals and PLGA nanoparticles. Carbohydr Polym 99:47–58

87. Akhlaghi SP, Tiong D, Berry RM et al (2014) Comparative release studies of two cationic model drugs from different cellulose nanocrystal derivatives. Eur J Pharm Biopharm 88:207–215
88. Simi CK, Emilia Abraham T (2007) Hydrophobic grafted and cross-linked starch nanoparticles for drug delivery. Bioprocess Biosyst Eng 30:173–180
89. Anirudhan TS, Binusreejayan B, Christa J (2017) Multi-polysaccharide based stimuli responsive polymeric network for the in vitro release of 5-fluorouracil and levamisole hydrochloride. New J Chem 41:11979–11990
90. Rahimi M, Shojaei S, Safa KD et al (2017) Biocompatible magnetic tris(2-aminoethyl)amine functionalized nanocrystalline cellulose as a novel nanocarrier for anticancer drug delivery of methotrexate. New J Chem 41:2160–2168
91. You J, Cao J, Zhao Y et al (2016) Improved mechanical properties and sustained release behavior of cationic cellulose nanocrystals reinforced cationic cellulose injectable hydrogels. Biomacromol 17:2839–2848
92. Wang H, He J, Zhang M et al (2015) A new pathway towards polymer modified cellulose nanocrystals via a "grafting onto" process for drug delivery. Polym Chem 6:4206–4209
93. Ndong Ntoutoume GMA, Grassot V, Brégier F et al (2017) PEI-cellulose nanocrystal hybrids as efficient siRNA delivery agents—synthesis, physicochemical characterization and in vitro evaluation. Carbohydr Polym 164:258–267
94. Hu H, Yuan W, Liu FS et al (2015) Redox-responsive polycation-functionalized cotton cellulose nanocrystals for effective cancer treatment. ACS Appl Mater Interfaces 7:8942–8951
95. Dong S, Cho HJ, Lee YW et al (2014) Synthesis and cellular uptake of folic acid-conjugated cellulose nanocrystals for cancer targeting. Biomacromol 15:1560–1567
96. Zainuddin N, Ahmad I, Kargarzadeh H et al (2017) Hydrophobic kenaf nanocrystalline cellulose for the binding of curcumin. Carbohydr Polym 163:261–269
97. Akhlaghi SP, Berry RM, Tam KC (2014) Modified cellulose nanocrystal for vitamin C delivery. AAPS Pharm Sci Tech 16:306–314
98. Paukkonen H, Kunnari M, Laurén P et al (2017) Nanofibrillar cellulose hydrogels and reconstructed hydrogels as matrices for controlled drug release. Int J Pharm 532:269–280
99. Fakhri A, Tahami S, Nejad PA (2017) Preparation and characterization of Fe_3O_4–Ag_2O quantum dots decorated cellulose nanofibers as a carrier of anticancer drugs for skin cancer. J Photochem Photobiol B 175:83–88
100. Li C, Wang ZH, Yu DG et al (2014) Tunable biphasic drug release from ethyl cellulose nanofibers fabricated using a modified coaxial electrospinning process. Nanoscale Res Lett 9:258
101. Svagan AJ, Müllertz A, Löbmann K (2017) Floating solid cellulose nanofibre nanofoams for sustained release of the poorly soluble model drug furosemide. J Pharm Pharmacol 69:1477–1484
102. Paukkonen H, Ukkonen A, Szilvay G et al (2017) Hydrophobin-nanofibrillated cellulose stabilized emulsions for encapsulation and release of BCS class II drugs. Eur J Pharm Sci 100:238–248
103. Hu H, Hou XJ, Wang XC et al (2016) Gold nanoparticle-conjugated heterogeneous polymer brush-wrapped cellulose nanocrystals prepared by combining different controllable polymerization techniques for theranostic applications. Polym Chem 7:3107–3116
104. Arslan O, Aytac Z, Uyar T (2016) Superhydrophobic, hybrid, electrospun cellulose acetate nanofibrous mats for oil/water separation by tailored surface modification. ACS Appl Mater Interfaces 8:19747–19754
105. Song J, Orlando RJ (2013) Approaching super-hydrophobicity from cellulosic materials: a review. Nord Pulp Pap Res J 28:216–238
106. Reverdy C, Belgacem N, Moghaddam MS et al (2018) One-step superhydrophobic coating using hydrophobized cellulose nanofibrils. Colloid Surf A 544:152–158
107. Bashar MM, Zhu H, Yamamoto S et al (2017) Superhydrophobic surfaces with fluorinated cellulose nanofiber assemblies for oil–water separation. RSC Adv 7:37168–37174

108. Orsolini P, Antonini C, Stojanovic A et al (2017) Superhydrophobicity of nanofibrillated cellulose materials through polysiloxane nanofilaments. Cellulose 25:1127–1146
109. Huang J, Lyu S, Chen Z et al (2019) A facile method for fabricating robust cellulose nanocrystal/SiO_2 superhydrophobic coatings. J Colloid Interface Sci 536:349–362
110. Khanjani P, King AWT, Partl GJ et al (2018) Superhydrophobic paper from nanostructured fluorinated cellulose esters. ACS Appl Mater Interfaces 10:11280–11288
111. Lin W, Hu X, You X et al (2018) Hydrophobic modification of nanocellulose via a two-step silanation method. Polymers 10:1035
112. Guo J, Fang W, Welle A et al (2016) Superhydrophobic and slippery lubricant-infused flexible transparent nanocellulose films by photoinduced thiol-ene functionalization. ACS Appl Mater Interface 8:34115–34122
113. Zhou S, Liu P, Wang M et al (2016) Sustainable, reusable, and superhydrophobic aerogels from microfibrillated cellulose for highly effective oil/water separation. ACS Sustain Chem Eng 4:6409–6416
114. Shang Y, Si Y, Raza A et al (2012) An in situ polymerization approach for the synthesis of superhydrophobic and superoleophilic nanofibrous membranes for oil-water separation. Nanoscale 4:7847–7854
115. Mertaniemi H, Laukkanen A, Teirfolk J-E et al (2012) Functionalized porous microparticles of nanofibrillated cellulose for biomimetic hierarchically structured superhydrophobic surfaces. RSC Adv 2:2882–2886
116. Gu L, Jiang B, Song J et al (2018) Effect of lignin on performance of lignocellulose nanofibrils for durable superhydrophobic surface. Cellulose 26:933–944
117. Chen S, Song Y, Xu F (2018) Highly transparent and hazy cellulose nanopaper simultaneously with a self-cleaning superhydrophobic surface. ACS Sustain Chem Eng 6:5173–5181
118. Baidya A, Ganayee MA, Ravindran SJ et al (2017) Organic solvent-free fabrication of durable and multifunctional superhydrophobic paper from waterborne fluorinated cellulose nanofiber building blocks. ACS Nano 11:11091–11099
119. Gopakumar MH, Arumughan D, Pottathara V et al (2019) Robust superhydrophobic cellulose nanofiber aerogel for multifunctional environmental applications. Polymers 11:495
120. Thorvaldsson A, Edvinsson P, Glantz A et al (2012) Superhydrophobic behaviour of plasma modified electrospun cellulose nanofiber-coated microfibers. Cellulose 19:1743–1748

Chapter 3
Tunable Optical Materials Based on Self-assembly of Polysaccharide Nanocrystals

Yuxia Wang, Ziyang Chen, Juntao Tang and Ning Lin

Abstract Rod-like polysaccharide nanocrystals, cellulose nanocrystal (CNC) and chitin nanocrystal (ChNC), can form the chiral nematic liquid crystal phase in suspensions, which can be preserved in the self-assembly solid materials (films) exhibiting colorful optical behaviors origin from the reflective wavelengths of the light. This chapter covers the studies on the topic of CNC and ChNC-based optical-tunable materials during last ten years including the self-assembly mechanism and liquid crystal behaviors of CNC nanoparticles in suspensions, preparation of optical films based on the pristine CNC and surface-modified CNC, summarization of diverse treatments and approaches to regulate the pitch and optical properties of self-assembly films (external energy fields and additives), and fabrication of mesoporous materials based on the strategy of CNC template. Finally, the self-assembly properties and optical applications of ChNC are discussed in the last section as the comparison with those studies introduced in CNC. The development of optical materials based on polysaccharide nanocrystals is an attracting functional application in the structural color field, and this chapter provides the summarization on the controlling strategy, structural design, regulating approach and mechanism explanation aiming to create the novel inspiration.

Keywords Cellulose nanocrystals · Chitin nanocrystals · Self-assembly · Optical materials

Y. Wang · Z. Chen · N. Lin (✉)
School of Chemistry, Chemical Engineering and Life Sciences, Wuhan University of Technology, Wuhan 430070, People's Republic of China
e-mail: ninglin@whut.edu.cn

J. Tang
College of Chemistry and Chemical Engineering, Central South University, Changsha 410083, China

N. Lin et al. (eds.), *Advanced Functional Materials from Nanopolysaccharides*,
Springer Series in Biomaterials Science and Engineering 15,
https://doi.org/10.1007/978-981-15-0913-1_3

3.1 Liquid Crystal Behaviors and Regulation Factors of Cellulose Nanocrystal Suspensions

Liquid crystal phase is an intermediate state between solid and liquid, with liquid fluidity and anisotropic arrangement similar to solid crystals. According to the different structures, liquid crystal phase can be classified as nematic phase, smectic phase and chiral nematic phase (also known as cholesteric phase), with the gradual increase of order degrees. The orientation of the particles in liquid crystal phase is ordered, but their positions are generally disordered. Most of the particles in the liquid crystal phase are anisotropic rod-like or sheet-like morphologies. The rod-like cellulose nanocrystals (CNC) can disperse stably in water and self-assemble into an ordered alignment at high concentrations, which makes this type of nanoparticle easier to form liquid crystal phase in suspensions [1]. During the solvent evaporation, the initial state of CNC suspension with low concentration is the isotropic, while the anisotropic liquid crystal phase of suspension will form with the slow evaporation of solvent and the gradual increase of concentration. There is a two-phase coexistence state in this treatment. Based on the classic colloid DLVO theory, the stability of CNC nanoparticles in the suspension is resulted from the balance between van der Waals attraction and repulsion, accompanied by the steric effect and electrostatic repulsion between the charged particles [2].

3.1.1 Liquid Crystal Formation of CNC Suspensions

The formation of chiral nematic liquid crystal phase for the CNC nanoparticles in the suspension is based on the phase transition. Specifically, at the low concentrations, the CNC nanoparticles disperse in the suspension at random in orientation and are observed to be isotropic phase. With the gradual increase of the concentration, some nanoparticles will be locally clustered into small anisotropic regions as the tactoid in the suspension. When reaching to the first critical value, the tactoids will be merged into a whole anisotropic chiral nematic phase, with the coexistence of the initial isotropic phase in the top of the suspension. The volume ratio of isotropic phase gradually decreases with the continuous removal of the solvent and increase of the concentration. Finally, at the second critical concentration, the isotropic phase disappears and the suspension becomes a complete chiral nematic phase [1]. At this state, the typical feature of fingerprint pattern can be observed by a polarizing microscope [3], as shown in Fig. 3.1. The formation of CNC lyotropic liquid crystal behavior in the suspension is an entropy-driven process at the thermodynamics, which is determined by the equilibrium of oriental entropy and translational entropy of nanoparticles. According to this theory, the attractive force is not essential in the formation of ordered phase for the system, while the phase separation is only determined by the aspect ratio (L/D) of the nanoparticles (Eqs. 3.1 and 3.2) [4].

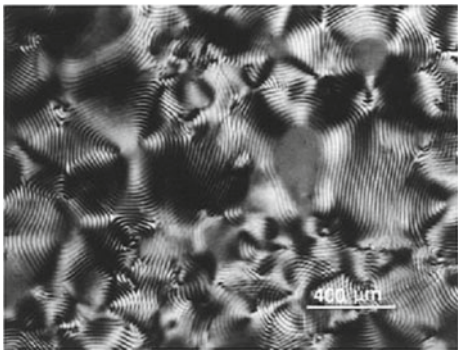

Fig. 3.1 The fingerprint pattern of CNC chiral nematic liquid crystal in aqueous suspension observed by the polarized optical microscope. Reproduced from [3]

$$\Phi_i = 3.3399\ \mathrm{D/L} \tag{3.1}$$

$$\Phi_a = 4.4858\ \mathrm{D/L} \tag{3.2}$$

where φ_i represents the critical volume fraction for the initial formation of a chiral nematic phase; φ_a is the critical volume fraction for the complete formation of the anisotropic phase. The suspension will separate into two coexisting phases when the CNC concentration is in between two critical concentrations.

The CNC suspensions at high concentrations can form the chiral nematic phases with a multilayer structure. The helical direction of the CNC chiral nematic phase is reported as the left-handed, dominated by the intrinsic left-handed helix of cellulose [5, 6]. The CNC nanoparticles in a single layer have the same orientation, defined as the orientation vector n. The vector n of each layer rotates at a certain angle along the axis m perpendicular to the layers, and the length of rotation axis m that rotates 360° is defined as the chiral nematic pitch p. Observed by the polarizing microscope for the fingerprint pattern of chiral lineal structure, the width of a single stripe corresponds to 1/4 of the pitch p [1], typically in the micron range in suspensions. The CNC chiral nematic suspensions can exhibit the special optical properties depending on the varied pitches of the formed chiral nematic structure, together with the polarization and propagation direction of the incident light [7]. When the light propagates along the direction perpendicular to the m axis, the fingerprint pattern resulting from the periodic changes in refractive index and rotation of its orientation vector n can be observed. When the light propagates along the m axis, the left-circular polarized light can be reflected within a specific wavelength range. The reflected wavelength is determined by the chiral nematic pitch and refractive index of the solid film, which can be predicted by the following equation [7, 8].

$$\lambda = n_{av} P \sin\theta \tag{3.3}$$

where λ is the reflected wavelength; $n_{av} = (n_e + n_o)/2$ represents the local average refractive index of the extraordinary optical index n_e and the ordinary optical index

n_o; P is the chiral nematic pitch and θ is the angle between the incident light and the surface of the liquid crystal phase.

It was reported that rod-like CNC nanoparticles can self-assemble into hierarchical chiral nematic architectures in the shrinking aqueous droplets with micron size [9]. This limited spherical geometry greatly affected the self-assembly process, leading to the concentric arrangement of chiral nematic order within droplets. The variations of chiral nematic pitch of droplets and macro capillary were compared in Fig. 3.2. With the increase of CNC concentrations, the initial pitch of droplets and capillary was nearly the same. However, at the concentration of 19 wt%, a different change of pitch of droplets was observed, and the trend line of droplets changed from original c^{-1}–c^{-3} curve. Another study reported liquid crystal phase behavior of CNC nanoparticles in the continuous constraint condition of micro droplet [10], the micron-sized isotropic core and concentric chiral nematic shell formed by the phase separation of droplets were observed. The further decrease of the droplet volume led to a distortion of concentric arrangement of chiral nematic phase. This core-shell droplet could be prepared in one step by limiting and inducing phase separation of CNC suspension, and the thickness of chiral nematic shell is controllable.

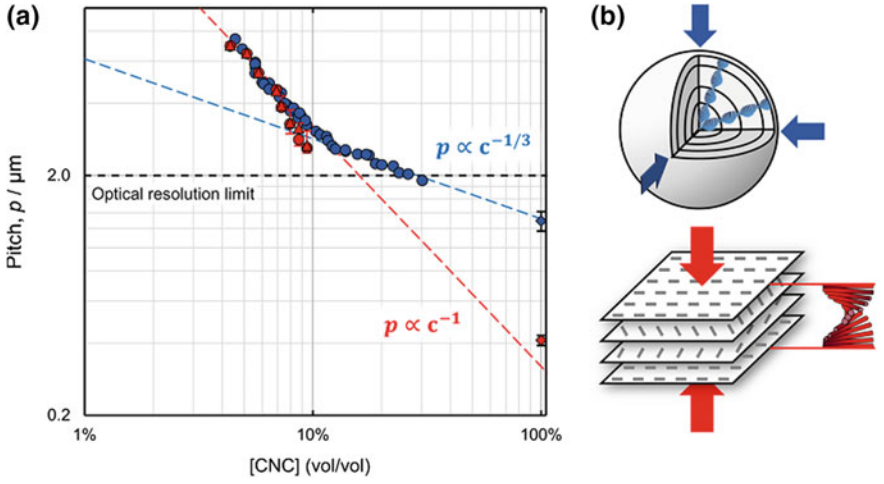

Fig. 3.2 **a** Diagram of pitch evolution (red circles and red triangles are pitch of macro capillary measured by laser diffraction and microscopy; blue circles are pitch of pitch in droplets), **b** schematics illustrating the different chiral nematic structures of different 3-dimensional contraction. Adapted from [9]

3.1.2 Influence and Regulation of Liquid Crystal Behaviors of CNC Suspensions

3.1.2.1 Inherent Properties and Concentration of CNC

The size, aspect ratio and surface charge of CNC nanoparticles will affect the liquid crystal behavior of the suspension. The high aspect ratio and sufficient surface charge can promote the formation of the phase separation and ordered phase [11]. At same concentration with isotropic-chiral nematic coexistence, the CNC suspensions prepared from wood have higher volume fraction of anisotropic phase comparing to those prepared from cotton, and the increasing of wood CNC concentration was reported to result in an increase of volume fraction of anisotropic phase and a decrease of chiral nematic pitch, while cotton CNC suspensions only showed an increase of the volume fraction of anisotropic phase with pitch barely decreases [12]. For the same CNC source, when the size of rod-like CNC decreases, the critical concentration of the suspension to form chiral nematic phase from isotropic suspension increases, together with the reduction of the concentration range of biphasic coexistence. The chiral nematic phase affected by the size decrease of CNC will further induce a decrease in its pitch [13]. Regarding the spherical CNC, its suspension tends to form the colloid rather than liquid crystal phase at high concentration. If the polydispersity of particles is high enough (> 49%), the suspension can form liquid crystal phase when the concentration of spherical CNC is as high as 3.9 wt%. At the higher concentration of 7.1 wt%, the observed liquid crystal structure for the suspension containing spherical CNC is gradually transferred as the birefringence glass phase [14]. The similar phenomenon was also reported in the study of post-sulfated modification treatment on the hydrochloric acid-hydrolyzed CNC suspension, which lost the mobility at the concentration of 7.1 wt% and formed the birefringent glassy phase [15].

According to the DLVO theory, the decrease of the distance between nanoparticles will lead to the increase of electrostatic repulsion force, thus increases the dislocation of parallel arrangement and the twisted angle. Therefore, the volume fraction of rod-like CNC is another critical factor to affect its arrangement in the suspensions, which will further determine the phase transition behavior and chiral nematic structure of CNC nanoparticles in the suspension. Generally, the higher volume fraction of CNC in the suspension results in the smaller distance among the nanoparticles. With the increase of the CNC volume fraction in the suspension from 2.5 to 6.5 vol.%, the chiral nematic pitch decreases from 15 to 2 μm, as well as the increase of the twisted angle between adjacent CNC particles from 1° to 4° [16]. Figure 3.3 shows the phase transition of the acid-hydrolyzed CNC in the aqueous suspension. With the gradual increase of CNC concentration, the suspension transfers from isotropic to isotropic-anisotropic biphase, and finally becomes completely anisotropic [3].

Different from the electrostatic stability of traditional sulfate half-esters groups from the sulfuric acid hydrolysis, the CNC prepared by the ammonium persulfate

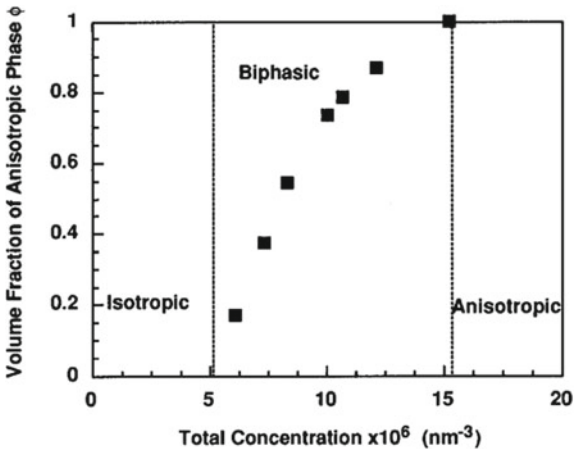

Fig. 3.3 The diagram of phase transition of sulfuric acid-hydrolyzed CNC aqueous suspension with varied concentrations. Reproduced from [3]

oxidation was reported to homogeneously disperse in the suspension by the presence of surface carboxyl groups, which can also form the chiral nematic liquid crystal phase above the critical concentration [17]. Another approach to introduce the negatively-charged carboxyl groups on the surface of CNC was the TEMPO oxidation. The obtained TEMPO-oxidized CNC in suspensions exhibited the similar lyotropic liquid crystal behavior and formed the anisotropic phase when the CNC concentration reaches to the critical value (4.1 wt%) [18]. When the concentration of TEMPO-oxidized CNC in suspensions reached 9.0 wt%, the clear fingerprint pattern can be observed by the polarized light microscope with the pitch of 6.0 μm. As the contrast, the critical concentration of CNC suspension prepared by sulfuric acid hydrolysis was reported as 4.8 wt% [18]. In fact, the aspect ratio of CNC prepared by the TEMPO oxidation is larger together with the higher surface charge density, which can reduce the critical concentration to form a liquid crystal phase and increase the chiral nematic pitch. Further study indicated that the nematic tactoids were firstly formed in isotropic suspension of TEMPO-oxidized CNC, with the subsequent chiral nematic tactoids developed by relaxation and equilibrium from nematic tactoids and eventually merging into a bulk chiral nematic phase [19]. The cationic modified CNC by epoxypropyltrimethyl ammonium chloride can achieve the charge reversal as positive surface and reduce the total surface charge density, which was reported to inhibit the formation of chiral nematic liquid crystal phase in the suspension. However, the nematic phase can be observed for the cationic CNC at the edge of formed thixotropic gels [20].

3.1.2.2 Surface Grafting of Polymeric Chains on CNC

Several studies reported the influence of polymer grafting on the CNC to the formation of its chiral nematic phase in the suspension. As summarized in Table 3.1, the suspensions containing various polymer-grafted CNCs generally exhibit the similar

Table 3.1 Polymer grafting on the surface of CNC and the influence on liquid crystal behaviors

Grafted polymer	Grafting method	Solvent	Critical concentration of first phase transition	Phase behavior	References
PEG	Amidation	Water	5 wt%	Liquid crystal behavior, $p =$ 4.0 μm	[21]
PMMAZO	ATRP	Chlorobenzene	5.1 wt%, nematic phase in chlorobenzene	Both lyotropic and thermotropic liquid crystal behavior, smectic to nematic at 95 °C, nematic to isotropic at 135 °C	[22]
PS	ATRP	DMF	5.7 wt%, in DMF	Both lyotropic and thermotropic liquid crystal behaviors, $p =$ 1–2 μm at 5.7 wt% in DMF	[23]
PDMAEMA	ATRP	Methanol	4.7 wt%	Temperature-dependent, $p =$ 1–2 μm at 4.7 wt%	[24]
PEO	Alkaline epoxide ring-opening	Water	5 wt%	Liquid crystal behavior, flower petal texture	[25]
PAM	Free radical graft copolymerization	Water	3 wt%	Liquid crystal behavior	[26]
Jeffamine polyetheramine M2070	Peptidic coupling	Water	1.7 vol.%	Liquid crystal behavior, $p =$ 6.1–16.5 μm at concentration decrease from 5.2 to 1.7 vol.%	[27]

Abbreviations: *PEG* (poly(ethylene glycol)), *PMMAZO* (poly{6-[4-(4-methoxyphenylazo)phenoxy] hexyl methacrylate}), *PS* (poly(styrene)), *PDMAEMA* (Poly(2-(dimethylamino)ethyl methacrylate)), *PEO* (poly(ethylene oxide)), *PAM* (polyacrylamide), *ATRP* (atom transfer radical polymerization), *THF* (tetrahydrofuran), *DMF* (*N*,*N*-dimethylformamide)

liquid crystal behaviors as that of sulfuric acid hydrolyzed CNC suspension. The chiral nematic phase will appear when the CNC concentration increases to the critical value. Moreover, the functional properties of grafted polymers can be introduced to the modified CNC. For example, if the grafted polymers are thermotropic, such as poly{6-[4-(4-methoxyphenylazo) phenoxy] hexyl methacrylate} (PMMAZO) and poly(styrene) (PS), the modified CNC suspensions will exhibit the thermotropic liquid crystal phase transition behavior, while retaining the original lyotropic liquid crystal behavior. The PMMAZO-grafted CNC suspension was reported to be the phase transition from smectic to nematic at 95 °C and the nematic to isotropic at 135 °C. The nematic phase appeared when the concentration of PMMAZO-grafted CNC was higher than 5.1 wt% in chlorobenzene [22]. In the case PS-grafted CNC suspension, the liquid crystal phase transition of this system was reported at 172 and 212 °C, with the critical concentration of formation for the chiral nematic sphere at 5.7 wt% and then a complete chiral nematic phase [23]. When the solubility of grafted polymer is affected by the temperature, the liquid crystal structure of modified CNC suspension (for instance poly(2-(dimethylamino)ethyl methacrylate) (PDMAEMA) modified CNC) will exhibit the temperature-dependency with the decrease of the chiral nematic pitch above the critical temperature and increase below the critical temperature [24].

3.1.2.3 Ionic Strength

Ionic strength is considered to be another important factor affecting the formation of chiral nematic phase of CNC suspension. Regarding the sulfuric acid-hydrolyzed CNC, the increase of electrolyte concentration will reduce the chiral nematic pitch, but the introduction of excessive electrolyte may induce the instability and flocculation of nanoparticles in the suspension [3]. The presence of electrolytes reduces the thickness of the electrostatic double layer for the charged CNC, and therefore increases the chiral interaction and reduces the chiral nematic pitch. For the isotropic and bi-phase CNC suspensions, the addition of electrolytes can increase the critical concentration of isotropic and bi-phase transformation (Fig. 3.4a). In addition, at the same CNC concentration, the volume fraction of anisotropic phase in the suspension is reduced with the addition of electrolytes (Fig. 3.4b).

The properties of counterions are different for the phase separation of sulfate groups stabled CNC suspension. The critical concentrations of chiral nematic formation for the inorganic counterions were reported as $H^+ < Na^+ < K^+ < Cs^+$ for sulfated CNC suspensions. Regarding the organic counterions, the larger sizes of organic counterions leads to the higher critical concentrations of phase separation for sulfated CNC suspensions, due to the balance between hydrophobic attraction and spatial repulsion [28].

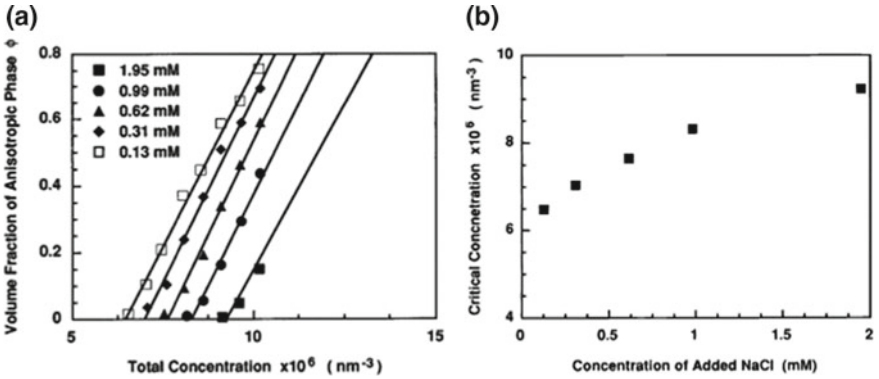

Fig. 3.4 **a** The volume fraction of anisotropic phase versus total concentration of CNC at different NaCl concentrations, **b** the critical concentration of phase transition versus NaCl concentrations. Reproduced from [3]

3.1.2.4 External Energy-Fields

The imposed external energy, such as the ultrasonic or magnetic field, can affect the formation of the ordered phase for the CNC suspensions. Long ultrasonic time and strong inputting energy can induce the high critical concentration of the ordered phase for CNC suspensions. One explanation is that the ultrasonic treatment will disperse the microcrystallites in CNC suspensions, and therefore reduce the average aspect ratio and affect the critical pitch of phase separation [11]. Another explanation on the ultrasonic influence to the arrangement of CNC nanoparticles in the suspension was reported as the change of electrostatic double layer of CNC by this treatment [29].

The presence of magnetic field can also promote the formation of the ordered phase for the CNC suspensions with the electrostatic double layer. When 2 T magnetic field was exposed, the CNC suspension was reported to exhibit a uniform orientation and chiral nematic axis arranged along the magnetic field direction [30]. Another study reported the cooperative ordering of the CNC nanoparticles in magnetic field, which exhibited the sigmoidal profile S curve for the correlation length and orientation order parameters as well as the distance among the nanoparticles with the increase of magnetic field intensity and duration [31]. Reaching the critical concentration ranged from 4.13 to 5.50 wt%, the CNC suspension suffering 1.2 T magnetic field showed the partial ordered arrangement within 2 min, followed by a slower cooperative ordering. An almost perfect orderly arrangement achieved within 200 min, with the nearly perfect arrangement under the low magnetic field intensity for a long duration.

3.1.2.5 Additives

The introduction of additives into the CNC suspensions can regulate their phase separation behaviors, with the typical small molecule, macromolecule and surfactant. The effect of blue dextran on the phase behavior of sulfuric acid-hydrolyzed CNC suspensions was reported [32]. For the bi-phase suspension, the added blue dextran tended to enter isotropic phase (Fig. 3.5a), and the biphasic region expanded due to a mutual exclusion between them. The addition of blue dextran to the completely anisotropic suspension will induce a phase separation forming an isotropic dextran-rich phase and an anisotropic dextran-poor phase. The presence of blue dextran can distort the ordered chiral nematic structure of the CNC suspension. However, the dextran molecules without the charge did not cause phase separation in the complete anisotropic phase of the CNC suspension, thus its phase separation behavior was reported to be ascribed to the anionic dye molecule (Cibacron blue, 3G-A) attached to the dextran [33]. The anionic dye ligands improved the ionic strength of the system, and increased the CNC critical concentration for phase separation. Under this condition, the phase equilibrium of the suspension shifted from complete anisotropic phase to biphase coexistence region. In the further studies, various anionic dyes were reported to separate CNC suspensions from completely anisotropic phases into isotropic-chiral nematic biphase, including the Acid Red-66, Acid Red-112 and Phloxine B [34]. The ionic strength required for phase separation induced by anionic dyes was lower than that by electrolytes, which may be resulted from the polyvalence and larger hydration radius of anionic dyes. The addition of both dextran and blue dextran into CNC suspension caused an isotropic-isotropic-chiral nematic

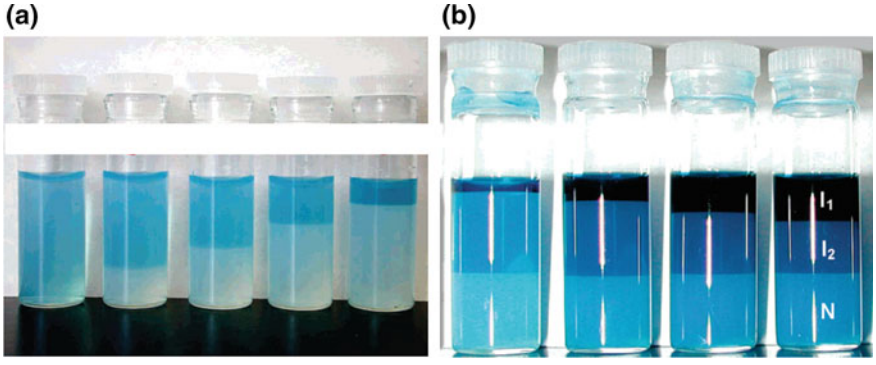

Fig. 3.5 **a** Photograph of suspensions with the same blue dextran concentration (0.07 mg/mL) and increasing CNC concentrations (6.5, 8.8, 9.4, 11.0, 13.3 wt%) from left to right, showing the preferential partitioning of blue dextran into the isotropic phase (Reproduced from [32]); **b** Triphase isotropic (I_1)-isotropic (I_2)-chiral nematic (chiral nematic phase) equilibrium for CNC suspensions of 8.7 wt% and containing dextran T-2000 with constant content (number density of 5.3×10^{-6} nm^{-3}) and increasing content blue dextran 2000 (number densities of 0.45 to 2.50×10^{-6} nm^{-3}) from left to right, showing the preferential partitioning of blue dextran into the isotropic (I_1) phase (Reproduced from [35])

triphase equilibria in suspensions [35], as shown in Fig. 3.5b. The concentration of dextran required for triphase equilibrium was reported to be strongly influenced by the molecular weight of dextran.

The combination of nematic droplets of 4-cyano-4′-pentylbiphenyl (5CB) with chiral nematic CNC suspension was reported to generate various types of coupled structure [36]. Different anisotropic structure can be obtained by controlling the diameter-to-pitch ratio of 5CB droplets and chiral nematic phase of CNC. At high diameter-to-pitch ratio, the spheres with nematic 5CB core and concentric chiral nematic CNC shell were observed. Another study reported the surface adsorption of macromolecule (xyloglucan oligosaccharide-poly(ethylene glycol)-polystyrene triblock copolymer) on the sulfuric acid-hydrolyzed CNC, which exhibited the formation of the isotropic-chiral nematic biphase in the toluene [37]. When the concentration of the modified CNC reached to 20 wt% (with the neat CNC of 11 wt%), the chiral nematic pitch of suspension was 17 μm. With the introduction of the surfactant (Beycostat NA) as dispersant, the CNC nanoparticles can homogeneously dispersed in toluene and cyclohexane. This CNC suspension at the 36 wt% concentration in cyclohexane was observed the sign of chiral nematic phase and fingerprint pattern with the 80% volume fraction of anisotropy phase [5]. In this system, due to the presence of surfactant and the dielectric constant of solvent, the electrostatic double layer on the surface of CNC nanoparticles no longer exists, and the helically twisted shape of rod-like CNCs was reported to be the key to form the ordered phase. The further study reported the different phase separation behaviors of CNC with various aspect ratios in cyclohexane and the improved dispersion by the surfactant (Beycostat NA). The suspensions containing high aspect ratio of CNC nanoparticles did not occur the phase separation, but formed an anisotropic gel at high concentration in cyclohexane. The pitch of the formed chiral nematic phase was as low as 2 μm, much lower than that in aqueous suspension, which was due to the strong chiral interactions between CNC nanoparticles in nonpolar media [38].

3.2 Solid Self-assembly Films of Cellulose Nanocrystals and Optical Properties

3.2.1 Optical Films Based on Pristine CNC

The isotropic CNC suspension can form an anisotropic chiral liquid crystal phase by the slow evaporation to remove the solvent. A dry solid film retaining the chiral structure of CNC nanoparticles can be obtained by the further solvent evaporation. The whole process was reported to go through three stages: phase separation, gel vitrification and solid film formation [39]. The chiral nematic pitch in the solid film will be reduced from micron range in the liquid phase to nanometer range. Therefore, the wavelength of the reflected left-circularly polarized light will be reduced to the nanometer range. If the reflected peak wavelength is in the visible light range

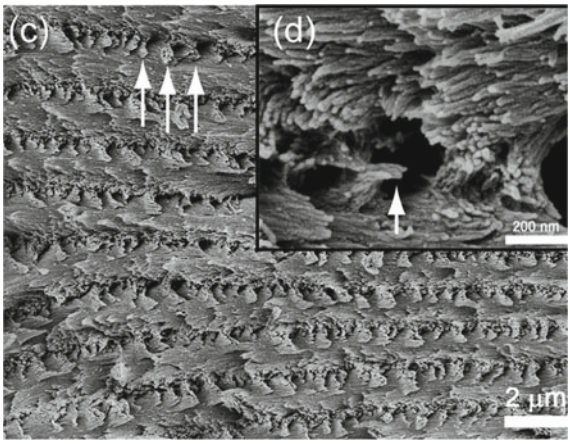

Fig. 3.6 SEM images of a fracture surface of CNC self-assembly film. Reproduced from [41]

(400–760 nm), the obtained CNC film will exhibit the visible colors to the naked eye with special optical performances. It should be noted that the CNC self-assembly films show the different reflections to the left and right hand circularly polarized (LCP/RCP) light in areas with different CNC concentrations. The RCP light was reported to appear in areas with lower CNC concentrations and higher film height than that of LCP light [40].

The fracture surface of CNC self-assembly films observed by scanning electron microscopy (SEM) shows the pitch, chirality, rotation axis direction and other details of chiral nematic structure, as shown in Fig. 3.6. A regular fan-like pattern was observed exhibiting the characteristic of the left-handed helicoidal alignment of CNC nanoparticles, and the rotation axis was perpendicular to the surface of the film [41].

The optical properties of CNC self-assembly films depend on their microstructure affected by the preparation conditions and pitches vary from a few microns to tens of microns. In fact, the observation by scanning electron microscope reported that the area of the single color had a uniform chiral nematic pitch, while the pitch suddenly changed at the border of different colors because of the discontinuity and defects of the orientation order [42]. The initial concentration of suspension, morphology of CNC nanoparticles, and evaporation conditions, including temperature, humidity, and evaporation time, will affect the microstructure of the resultant solid films with the chiral nematic structure [7]. As for the influence of initial suspension concentration on the pitch of film, it was found that the relationship between the CNC suspension concentration c and the pitch p was consistent with following formula (Eq. 3.4) within the concentration range of 0.5–2.0 wt% [43]:

$$\ln \frac{1}{\mathrm{P}} = \mathrm{k}\ \ln\ \mathrm{c} + \mathrm{A} \tag{3.4}$$

where A is a constant determined by solvent, temperature and molecular mass of polymer; k is determined by the solvent and is usually less than 2. The CNC suspension with a high initial concentration tends to form a uniform chiral nematic alignment [39, 44]; meanwhile, the reflection wavelength exhibits a small red-shift comparing with the self-assembly films obtained from the low CNC concentration suspensions [44, 45]. The chiral nematic pitch of self-assembly film is also determined by the size of rod-like CNC nanoparticles in the suspension at the positive correlation with the low pitch for small nanoparticles [46]. The size distribution of CNC nanoparticles in the suspension also plays an effect on the uniformity of chiral nematic alignment. The temperature and humidity in the evaporation treatment are other important influence factors to regulate the microstructure of the CNC self-assembly film. High temperature and low humidity in the evaporation were reported to reduce the chiral nematic pitches of films, and therefore can regulate the reflection of different colors [47, 48]. In fact, under the high environmental humidity, the water molecules can diffuse through the voids and are adsorbed on the surface and interface between CNC nanoparticles, which will enlarge the interspacing and increase the chiral nematic pitch of CNC nanoparticles, thus exhibiting the reflection wavelength redshift. The homogeneity of the resultant films was reported to be improved by extending the evaporation duration of CNC suspensions after the onset of liquid crystal phase. An intermediate stage between the phase separation and gel vitrification, called tactoid annealing was hypothesized to explain the differences in the structure of chiral nematic order of solid CNC films resulting from different evaporation durations. The hypothesis of this intermediate stage is of great significance for controlling the structure of CNC films and regulating their optical properties [39].

Asymmetrical confined drying conditions were reported to prepare large and uniform chiral nematic CNC films within a capillary [49]. The interface between isotropic and chiral nematic phase was perpendicular to the long axis of the capillary, which benefited the fast growth of chiral pseudolayers. In contrast to the traditional dish-cast approach with slow and heterogeneous drying, the formation of ordered films using capillary was reported to only take few hours and the films exhibited highly oriented order over the large area and narrower optical reflectance peak.

Some pre- or post-treatments can be performed on the preparation of CNC self-assembly films to regulate the chiral pitch and optical performances. With the desulfurization treatment by heating in water bath, the surface charges and electrostatic interactions of sulfuric acid-hydrolyzed CNC nanoparticles are reduced in the suspension [50]. The iridescent films prepared from this desulfurized CNC suspension exhibited the blue shift of reflected colors, with the obtained red, green and blue films from 12, 21 and 30 h of desulfurization. A recent study reported the preparation of iridescent CNC films with predefined patterns by the treatment of differential heating during the evaporation for the CNC aqueous suspension [51]. The reflection peak of the film dried at higher temperature showed a red-shift, corresponding to a larger pitch, and this part has a smaller density and a larger thickness. Increasing the temperature difference can improve the clarity of the pattern and make the reflected wavelength redshift. The differential heating caused by the difference of the relative rates of heat transfer of different materials transferred to the suspension, thus

formed the watermark-like pattern. Pattern formation was reported to occur in the final stage of drying and was caused by differences in evaporation rates and thermal motion between areas of different temperature. Self-assembly of CNCs to form a chiral nematic phase was reported to be strongly influenced by the properties of the substrate and evaporation rate. The CNC suspension tended to reduce the contact with the highly hydrophobic substrates, which can form the thick opaque film similar as the nacre with large pitches. For the high-hydrophilicity substrates, the CNC suspension can spread and adhere to the substrates, and the obtained film was thin and blue color [52]. The influence of the interrelated effects of liquid crystal behavior, flow alignment and microstructural relaxation on the self-assembly and optical properties of CNC self-assembly films was also reported [53]. The optical contrast measurement by the cross-polarized light microscope showed that the ordered structure of liquid crystal CNC suspension was better than that of isotropic or biphasic coexistence suspension after shearing, but CNC gels showed the lower alignment under constant shearing rate. The anisotropic films with the optical properties can be obtained by combining greater initial alignment and slower relaxation of sheared liquid crystal. The evaporation duration and formation process can also be applied to control the optical behaviors of CNC self-assembly films.

Semi-sphere photonic CNC films with chiral nematic structure were reported to be fabricated by the self-assembly of CNC in semi-spherical cavities [54]. The structure and optical properties of the obtained films were strongly influenced by the curvature of cavities, the composition of precursor CNC suspensions and the phase of suspension. The effects of curvature of films combining with the restricted mobility of CNC in drying process can change the pitch and helical axis inclination, resulting in broadband reflectance properties of the semi-sphere CNC films.

The “coffee-stain” effect of CNC suspension droplets dried deposition on the plane was proposed to explain the microstructural change and nanoparticles self-assembly during the evaporation process [55]. During the drying process of droplets, CNC nanoparticles transport to the outer edge of droplets where the contact line is fixed, and deposit down due to their relatively poor surface fluidity, and finally form a solid film with thick outer edge and thin center region with concentric colored rings. The concentration gradient on the ring leads to the color gradient of the film and the reflected wavelength red shift near the outer ring. The rod-like CNC nanoparticles may also undergo some fractionation during the evaporation process, with longer rods gather at the edges, leading to the larger pitch and red-shift wavelength. Another study reported that the “coffee-ring” effect of CNC suspension droplets with low initial concentration was weaker after drying. The Marangoni flow inside the droplet was too small to offset the capillary flow that made the CNC nanoparticles depositing on the edge [56]. Variation of the surface tension of the droplets will increase the Marangoni flow (compared with the capillary flow), and finding the balance between the colloid stability and the Marangoni flow can make the preparation of uniform iridescent films success. Meshed substrate can provide a complex topology for the formation of CNC self-assembly films, under the confinement and support of the framework of meshes [57]. With the “coffee-ring effect”, CNC nanoparticles can form a defect-free and continuous rim on the basis of the mesh frame at a lower initial concentration

(0.2 wt%). Recently, Picard et al. proposed a model quite different from traditional theory of slow evaporation for the formation of CNC self-assembly iridescence films [58]. This model regarded that the CNC nanoparticles in suspension can form a smectic liquid crystal during the evaporation, which was a multi-layer structure of CNC nanoparticles with a long axis perpendicular to the layer plane. The dried films retained the multi-layers' structure of the smectic phase, with a submicron range for each layer. The iridescent color of obtained films was attributed to the optical interference of the multi-layer structure rather than the traditional chiral nematic liquid crystal structure.

3.2.2 Optical Films and Pitches Regulation Based on Surface Modification of CNC

As mentioned before, the surface modification to CNC will affect its liquid crystal properties, and therefore can be applied to regulate the chiral nematic pitch and control the optical properties of the self-assembly film. Various surface modification on CNC, the liquid crystal properties and obtained self-assembly films are summarized in Table 3.2. The surface modification on the CNC was regarded to increase the interlayer distance among nanoparticles, due to the decrease of intermolecular interactions

Table 3.2 Surface modification of CNC and the ordered structure of solid films

Surface modification	Solvent of suspension	Interlayer distance/reflection peak/pitch	References
Acetylation with acetic anhydride	Acetone	Interlayer distance 50–150 nm	[59]
Butyration with butyric anhydride	Acetone	Interlayer distance 70 nm	[60]
TEMPO oxidation	Water	Reflection peak 687 nm	[61]
Desulfation with NaOH	Water	Reflection peak 565 nm	
Acetylation with acetic anhydride	Anhydrous pyridine	Reflection peak 720 nm	
Cationization with EPTMAC	Water	Reflection peak 534 nm	
Neutralization with Na^+	Water	Pitch 420–1000 nm	[62]
Acetylation with acetic anhydride	Water	Pitch 504–619 nm	
Grafting with PAAm	Water	Reflection peak 530–580 nm	[63]
Alkali treatment with NaOH	Water	Reflection peak 450–550 nm	[64]

caused by the replacement of hydroxyl groups and presence of groups pendants. In the cases of surface acetylation and butyration to CNC, the modified nanocrystals were reported to form a smectic phase with the interlayer spacing in the suspensions, only observing the chiral nematic structure in some domains [59, 60]. Generally, the surface modification on CNC can retain the chiral nematic structure of the suspension in the self-assembly film on both the surface and entire. The surface modification can affect the repulsion among the CNC nanoparticles, and therefore change the long-range ordered chiral nematic structure in suspensions and films. In the case of the methyl(triphenyl) phosphonium cations modified CNC, the drying rate on chiral nematic phase and pitch of the self-assembly film was reported, which demonstrated the smaller pitch but more uniform structure of the obtained films based on a slower evaporation rate due to the increase of the inhibition to electrostatic repulsion and compact arrangement of CNC nanoparticles from the hydrophobic modification [62]. It is worth noting that the swelling treatment may be influence to the optical properties of the films from the modified CNC self-assembly. In some cases, the films fabricated by the surface modified CNC exhibited the clear color change from green yellow to red when soaked in ethanol; or the immersion in water with the swelling behavior can cause the reflected peak wavelength moving to the near-infrared region and therefore exhibiting the transparent films [61]. The color change caused by the swelling may be reversible, which means the recovery of films to their original color after drying. The optical properties of CNC films were also reported to be regulated by the alkali post-treatment after vacuum assisted drying [64]. The alkali treatment resulted in the reduction of CNC crystallinity, which changed from type I to II. The chiral nematic structure of the films can be retained after the alkali treatment, with the decrease of the pitch and blue shift of reflected wavelength.

Regarding the surface grafting macromolecules on CNC, a study reported the preparation of CNC-g-polyacrylamide optical film by the slow evaporation inducing nanoparticles' self-assembly with chiral nematic structure and reflecting light of specific wavelength [63]. With the addition of different amounts of acrylamide monomer for polymerization, the varied polymer grafting chains on the surface of CNC regulated the pitches of films, and therefore changed the reflection peak wavelength. It was reported that the more monomer added with the longer polyacrylamide chain grafted on CNC resulted in the larger pitches and reflection peak wavelength for the obtained films. Furthermore, these films exhibited the increase of chiral nematic pitches and red shift of the reflected color when swelling in water.

3.2.3 Providing External Energy Fields to Regulate Pitch and Optical Properties

To impose the energy on the CNC suspension or apply an energy field during the evaporation process is an effective method to regulate the chiral nematic structure and optical properties of the self-assembly film. The typical treatments to provide the

external energy fields into the CNC suspension include the ultrasonic field, magnetic field, electric field and shearing field.

3.2.3.1 Ultrasonic Field

The first study on the fabrication of optical tunable iridescent CNC films by the ultrasonic treatment was reported in 2011 [29]. The introduced ultrasonic energy induced the increase of chiral nematic pitch and a red shift of the reflection peak wavelength for the CNC self-assembly films. As shown in Fig. 3.7, the colors of the CNC films gradually shifted from blue-purple to red with the applied increasing ultrasonic energy of 0, 250, 700, 1800, and 7200 J/g. In the further study, the chiral nematic pitch of CNC self-assembly film was controlled by the ultrasonic treatment in coordination with the addition of electrolyte (NaCl). The pitch increase of the suspension and film was ascribed to the change of electrostatic interaction. The CNC nanoparticles were surrounded by a layer of binding water or an oligosaccharide gel. Ions generated in the hydrolysis process were bound in the layer, which did not be removed in the purification step. The introduction of ultrasonic energy made the ions in the binding water layer or gel layer transferring to the suspension, and further leading to the increase of electrostatic double layer and the reduction of chiral interaction between nanoparticles, so as to increase the pitch of chiral aligned phase [29]. In another case, when the surface protons on the sulfuric acid-hydrolyzed CNC were replaced by neutral monovalent cations such as Na^+, with good redispersibility, the inputting of ultrasonic energy can restore the optical properties of the salt-form CNC suspension to form an iridescent film with the red shift of reflection wavelength [65].

Recently, several studies reported the combination of vacuum drying with the ultrasonic treatment to prepare the CNC self-assembly films with the preservation of chiral nematic structure for the fast drying. When the vacuum degree was increased for the evaporation, the drying duration was shortened and the reflected wavelength of the obtained film was increased. The gel CNC was different under the condition of fast evaporation of higher vacuum degree, which were "locked in" the chiral nematic structure with the longer pitch, resulting in a thicker and less dense film [66]. In another case, the iridescent CNC films with high orientation can be prepared by the vacuum-assisted self-assembly with the long ultrasonic pretreatment [67]. As shown

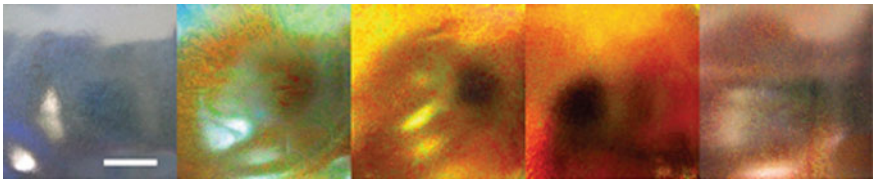

Fig. 3.7 Photograph of CNC self-assembly films with the applied increasing ultrasonic energies of 0, 250, 700, 1800, and 7200 J/g from left to right, scale bar is 1 cm. Reproduced from [29]

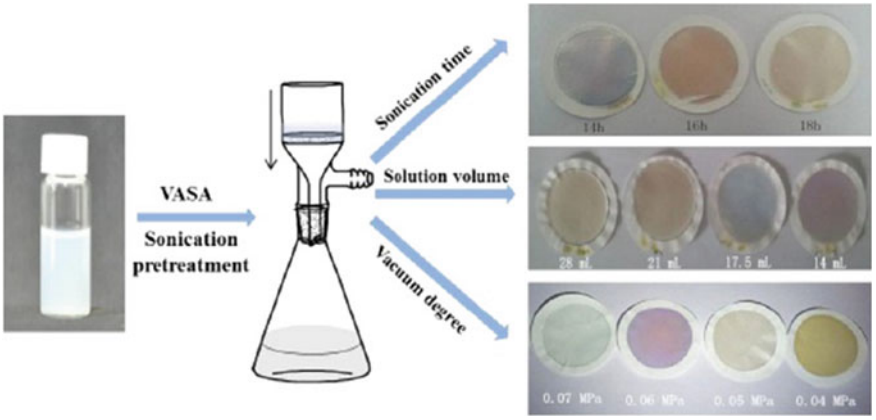

Fig. 3.8 The CNC iridescent films prepared by various sonication durations, solution volumes and vacuum degrees after the vacuum-assisted self-assembly (VASA) and sonication treatments. Reproduced from [67]

in Fig. 3.8, the colors of the CNC films can be controlled by controlling the ultrasonic duration, suspension volume and vacuum degree.

3.2.3.2 Magnetic Field

The sulfuric acid-hydrolyzed CNC was proved to process the negative diamagnetic anisotropy, due to its surface charge from surface sulfate or carboxylgroups. An early study reported the influence of magnetic field on the self-assembly of singer layers of CNC adsorbed with poly (allyl amine hydrochloride) coating [68]. The poly (allyl amine hydrochloride) coated silicon wafers were soaked vertically in CNC suspension for the adsorption and alignment in the presence of magnetic field of 7 T, and then rinsing and drying to obtain the CNC adsorbed film. After soaking for 24 h, the degree of order for the modified CNC self-assembly film was significantly improved. The axis of chiral nematic phase was parallel to the plane of the film, so there was a twist elastic energy barrier to make CNC nanoparticles that were not parallel to the surface occurring reorientation and then adsorb on the surface of the film. A recent study reported the preparation of CNC self-assembly films with tunable optical properties by the generated magnetic field (about 0.5–1.2 T) from commercial neodymium (NdFeB) magnets [69]. The imposed magnetic field can induce the long-range orientation order of chiral nematic phase for CNC nanoparticles in the suspension and retain this structure in the solid film after drying. The orientation of the thin film can be controlled by adjusting the spatial configuration of the magnets with respect to the suspensions. By providing a patterned multi-area magnetic field to the suspension during the evaporation process, the iridescent films with watermark-like pattern can be prepared, as shown in Fig. 3.9.

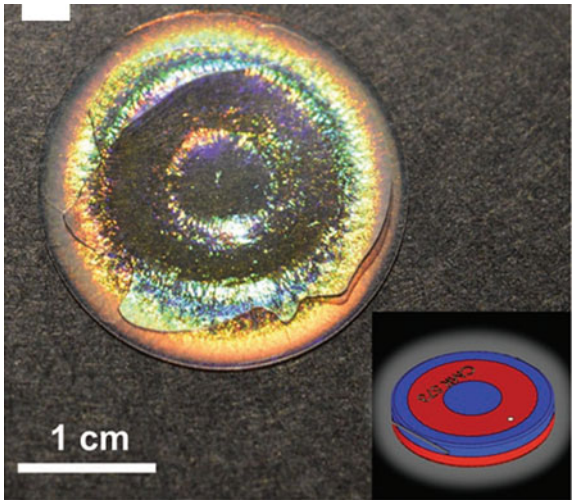

Fig. 3.9 Patterned iridescent CNC film obtained by casting with the presence of patterned magnet. Reproduced from [69]

3.2.3.3 Electric Field

The alternating-current electric field can assist in the self-assembly and orientation of CNC nanoparticles in the suspension. When an alternating voltage was applied to the CNC suspension deposited on a thin gap of coplanar patterned metallic electrodes, the CNC nanoparticles were reported to form the highly homogeneous orientation. The electric field induced the electron polarization of CNC nanoparticles, and the dipole moment parallel to the direction of the nanorods was stronger than that in the vertical direction. Therefore, the rod-like CNC nanoparticles were arranged along the direction of the electric field. The influence of electric field strength on orientation was studied by changing the widths of electrode gap and voltage. It was reported that the homogeneity of CNC orientation can be improved by different electric field strengths with the change of the widths of electrode gap and voltage [70]. In the further study, the AC electric field induced a perfect orientation of CNC nanoparticles parallel to the external magnetic field under certain voltage and frequency conditions, which was reported to be related to the dielectric constant of CNC and its polarization rate in aqueous solutions [71].

Recently, Bruno et al. reported the application of electric field to control the iridescent characteristics of concentrated CNC in the apolar solvent (toluene), in which the pitch, the homogeneity and structural color of the obtained films can be controlled accurately at the macroscopic scale [72]. The use of the apolar solvent can enable the surfactant coated CNC nanoparticles to maintain chiral structure without forming a gel when the concentration was up to 35 wt%. Meanwhile, the organic solvent has a better matching of refractive index with CNC, which can reduce Rayleigh scattering and enhance transparency and light diffraction caused by the intrinsic birefringence of CNC. In addition, the dispersion of CNC nanoparticles in the apolar solvent made it possible to use the high voltages, and therefore promoted the alignment parallel to the

direction of the electric field of these rod-like nanoparticles. The CNC nanoparticles in suspensions can unwind and form the pure nematic phase under the high electric fields, as shown in Fig. 3.10. The effect of electric field annealing was reported to prepare highly disoriented or uniform chiral nematic phase of CNC nanoparticles in zero field with fast or slow field loop. When the electric field changed at a low frequency (f < 0.1 Hz), the time-modulated electric field can dynamically tune the iridescent color, and the faster and larger electric field modulation can generate the switchable stable structure color-white scattering sample.

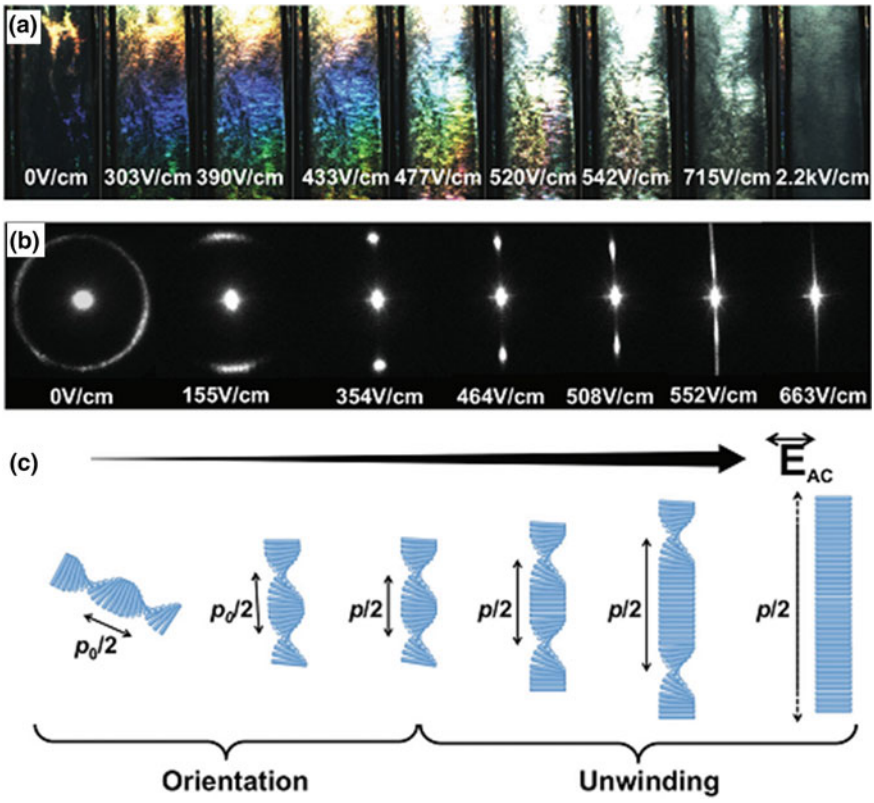

Fig. 3.10 **a** The iridescence evolution of chiral nematic suspension with the increase of electric field, showing enhancement of light intensity, red-shift and disappearance of color; **b** evolution of laser diffraction pattern with the increase of electric field, indicating chiral nematic orientation, pitch increase and chiral nematic unwinding; **c** schematic of the evolution of CNC alignment at the increasing electric field. Reproduced from [72]

3.2.3.4 Shearing Field

The shearing force is another factor to induce and regulate the self-assembly of CNC nanoparticles in the suspension and therefore can affect the optical performances of the solid films. The CNC ultrathin film with an ordered orientation was prepared by depositing on a solid supporting by the convective and shear assembly [73]. The surface charge and surface energy of different substrates were reported to influence to the alignment degree of CNC nanoparticles. Compared with the substrates with the positive charge, the CNC alignment on the substrates with negative charge was more accessible. At a certain withdrawal rate, the multi-layer membrane formed by high concentration suspension exhibited the higher alignment than that of the monolayer formed by low concentration. However, when the withdrawal rate increases, the order of the films increased first and then decreased. In all of the forces including hydrodynamic (shear and drag), surface tension (capillary forces) and electrostatic interaction, the shearing force is dominant the highest alignment. A recent study reported the influence of weak circular shear flow in the drying process of CNC films with a superior structural periodicity through the entire film depth [74]. The explanation was that the circular shear flow subtracting the concentration gradient and the subsequent delayed kinetic arrest of the surface layer resulting in a uniform and equilibrium chiral nematic alignment with a vertical helical structure throughout the sample. Although this was weak effect on the optical properties of the film, the introduction of shear flow can improve the uniformity of the structure and the surface adhesion, which can be of great significance for the application of optical coatings. The influence of the initial pH of CNC suspensions on the preparation of oriented films from aqueous suspensions by shearing was also reported [75]. Under the acidic condition (pH = 2), the longitudinal axis of CNC nanoparticles preferred to be perpendicular to the shear direction; while under the neutral condition (pH = 6.7), CNC nanoparticles were more likely to be parallel to the shear direction. The chiral nematic phase was formed in the drying process of acidic suspensions, while there was almost no presence in neutral suspensions, which was attributed to the difference of sulfate counterions on the CNC surface. Therefore, in neutral suspension without mesomorphic structure, CNC nanoparticles were allowed to be arranged separately in parallel with the shear direction, thus producing a common uniaxial orientation in dry films. As for the acidic suspensions, the nematic planar domains deformed under the action of winding-up force, and therefore the nematic directions were perpendicular to shear direction resulting in the transverse orientation pattern of CNC nanoparticles in the films.

3.2.4 *Optical Films and Pitches Regulation Based on Additives to CNC Suspensions*

The introduction of additives to the CNC suspension, such as electrolytes, small molecules, polymers, is an effective approach to regulate the chiral nematic pitch and optical properties of the self-assembly films. In addition, the presence of different additives can also provide the film a variety of special properties from the additives components, resulting in the multi-functional CNC materials.

3.2.4.1 Electrolytes

The effects of electrolytes on the liquid crystal phase of CNC suspensions were reported early in 1996 [3]. Generally, the increase of the electrolytes concentration in the sulfuric acid-hydrolyzed CNC suspension will lead to the reduction of chiral nematic pitch. However, the introduction of superfluous electrolytes may make the suspension unstable. In fact, the addition of electrolytes can decrease the thickness of the electrostatic double layer of CNC nanoparticles, and therefore affects the chiral interaction and reduces the chiral nematic pitch of the suspension. As mentioned before, the critical concentration of isotropic-biphase transition will increase with the addition of electrolytes for the isotropic and biphase suspensions. A recent study reported that with the same CNC concentration, the addition of electrolytes results in a decrease of volume fraction of anisotropic phase. This phenomenon can be retained in the dried films with the change of film's pitch by the introduction of electrolytes [43]. The introduction of NaCl electrolyte as the additive was used to increase the ionic strength and reduce the chiral nematic pitch of the CNC assembly film. The pitches of the obtained films decreased linearly with the increase of NaCl concentrations and varied reflective wavelengths measured by circular dichroism. Another study reported the replacement of the surface counterions on CNC with Li^+, the isotropic contraction of disordered phase occurred in the drying process of the suspension, rather than the self-assembly into chiral centripetal phase of CNC with H^+ counterions [76].

3.2.4.2 Small Molecules

The introduction of small molecules in the CNC suspension is another effective method to regulate the pitch and optical property of the self-assembly films. Table 3.3 summarized the reported studies of CNC-based self-assembly films with the additives of various small molecules. Generally, the added small molecules will deposit together with the CNC nanoparticles in the drying process to form the composite solid films and increased the pitch. In addition, the presence of additional components can provide the CNC self-assembly films new functions, for instance the fluorescence and hygroscopicity.

Table 3.3 The CNC-based self-assembly films with the introduction of various small molecules as the additives to regulate the optical performances

Small molecular additives	Content of small molecules (wt%)	Pitch (μm)		Color or/and reflective peak wavelength (nm)	Other functions	References
TINOPAL	0.17 (50 ppm in 3 wt% CNC)	3.3 ± 1.1		–	Fluorescence	[77]
	0.33 (100 ppm in 3 wt% CNC)	5.1 ± 2.1		–		
	0.50 (150 ppm in 3 wt% CNC)	7.1 ± 2.2		–		
D-(+)-glucose	0.16	11.0 ± 0.2	In suspension	Blue	–	[78]
	0.37	5.7 ± 0.3		Blue-green		
	0.49	6.4 ± 0.2		Red		
	0.57	7.4 ± 0.3		Transparent		
	0.66	7.2 ± 0.3		–		
Copper chloride	0.1 mol/gCNC	1.194 ± 0.010		428	Ammonia sensing	[79]
	0.3 mol/gCNC	1.220 ± 0.006		434		
	0.5 mol/gCNC	1.270 ± 0.004		442		
	0.7 mol/gCNC	1.365 ± 0.014		454		
	0.9 mol/gCNC	1.486 ± 0.022		490		
	1.1 mol/gCNC	–		448		
	1.5 mol/gCNC	–		436		
HOBC	–	0.119 ± 0.004		–	Thermo-response	[80]
Glycerol	10	–		–	Plasticizer and hygroscopic agent	[81]
	20	0.278 ± 0.008		Green 542		

(continued)

Table 3.3 (continued)

Small molecular additives	Content of small molecules (wt%)	Pitch (μm)	Color or/and reflective peak wavelength (nm)	Other functions	References
	30	–	Orange		
	40	0.424 ± 0.016	Red 691		
	50	0.620 ± 0.040	Colorless 834		
Glycerol	10.52	~0.275	Blue ~430	Plasticizer and hygroscopic agent	[82]
	19.05	~0.320	Blue ~490		
	26.09	~0.350	Green ~550		
	32.00	~0.380	Yellow ~590		
	37.04	0.402	Red 610		
AmimCl	5 wt% solution	–	Light blue	Plasticizer	[83]
	10 wt% solution	–	Green		
	15 wt% solution	0.516	Yellow		
	20 wt% solution	–	Orange		
	25 wt% solution	–	Red		
	30 wt% solution	–	Light brown		
BminCl	–	–	–	Plasticizer	[84]

Abbreviations: *HOBC* (4′-(hexyloxy)-4-biphenylcarbonitrile), *AminCl* (1-allyl-3-methylimidazolium chloride), *BmimCl* (1-butyl-3-methylimidazolium chloride)

The addition of optical whitening agent (TINOPAL) into the CNC suspension increased the chiral nematic pitch of CNC self-assembly film, with the decrease of chiral nematic region and homogeneity. In addition, preserving the chiral nematic structure, the CNC film also exhibited a strong fluorescence when excited by the UV light, which was the potential of overt encryption as anti-counterfeiting application [77]. Another study reported the effect of glucose on the chiral nematic structure of CNC suspension during the drying process [78]. During the evaporation process, the influences of glucose on the pitch of CNC self-assembly included two stages, viz. (i) CNC concentration increased and pitch decreased with the evaporation of suspension; (ii) the formation of the gel or glass phase prevented the further decrease of pitch. At the second stage, the addition of glucose will reduce the concentration of CNC and lead to an increase of the pitch, thus resulting in an overall red shift of the spectrum of the solid film. The metal ions Cu(II) was also reported to be doped in the CNC self-assembly film [79]. The addition of copper ion resulted in the slightly red shift of the reflected wavelength for the obtained film. The loaded copper ion exhibited the strong chelation action with the CNC nanoparticles with the surface negative charges. Based on this chelation interaction, the fabricated hybrid film was reported to be sensitive to the ammonia, as which can be merged into the CNC nematic layer and trigger the sensing of copper ions chelated on CNC nanoparticles, thus causing the red shift of reflected wavelength and effective colorimetric transition. A novel multifunctional film possessing the iridescence, conductive and thermal response was reported by the combination of 4′-(hexyloxy)-4-biphenylcarbonitrile (HOBC) and CNC self-assembly [80]. As a thermotropic nematic liquid crystal, HOBC was compounded by coating on the CNC film. The chiral nematic structure of composite film with the penetration of HOBC through CNC layers exhibited the special thermo-optical properties. The transition from opaque (OFF state) to transparent (ON state) occurred in the range of 56–60 °C for the composite film with the preservation of liquid crystal phase for both CNC and HOBC components.

As a plasticizer and hygroscopic agent, glycerol was also reported as an additive to regulate the chiral namatic pitch of CNC self-assembly film [81]. The addition of glycerol induced the red shift of the reflected wavelength for the obtained film. The reflected wavelength and color can be controlled by changing the content of added glycerol, with the transition of colors from the blue-purple range for the pure CNC film to near infrared region for the composite films. In addition, due to the hygroscopicity of glycerol molecules, the reversible color transition of the composite films can also be regulated by the humidity conditions (Fig. 3.11a, b). In another study, the CNC/glycerol self-assembly films also exhibited the color response to the external pressure [82]. As shown in Fig. 3.11c, the shift of wavelength and the applied pressure were in a monotonic relationship, exhibiting the blue shift of wavelength induced by the higher pressure. This pressure response can also be superimposed with the humidity response effect, as shown in Fig. 3.11d.

Ionic liquid is another type of small molecule as the optical-tunable additive for the CNC self-assembly film. With the assistant of vacuum filtration process, the composite film of CNC/1-allyl-3-methylimidazolium chloride (AmimCl) can be prepared with the strong ionic interaction between CNC and AmimCl components [83]. By

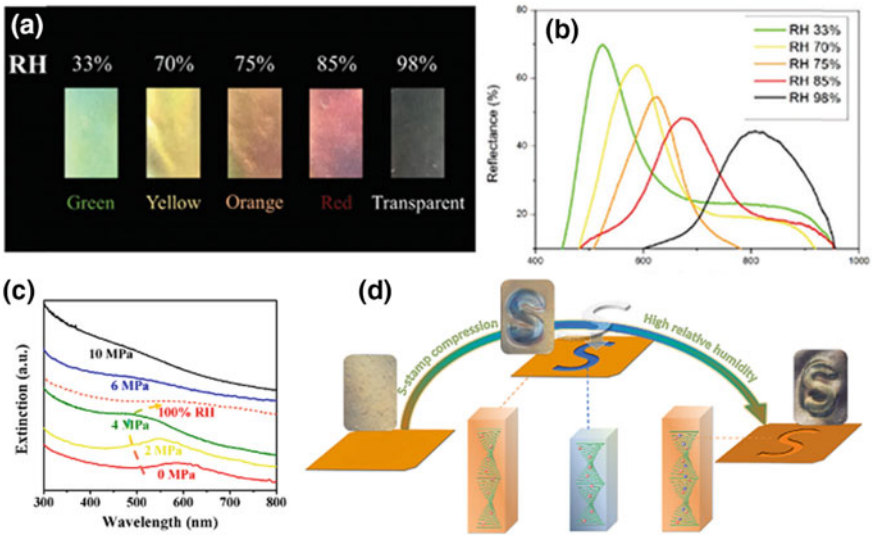

Fig. 3.11 Color appearances (**a**) and reflection spectra (**b**) of the CNC films containing 20 wt% glycerol at different relative humidity (RH) (Reproduced from [81]); color-pressure response (**c**) and color-pressure/humidity response (**d**) of the CNC/glycerol films. Reproduced from [82]

the uniform penetration of AmimCl molecules into the CNC self-assembly layers, the color of the films can be regulated by changing the concentration of AmimCl. With the high concentrations of added AmimCl in the suspensions, the obtained films exhibited a red shift of reflected wavelengths. Another study reported a dipping and pulling method to prepare CNC self-assembly films with the tunable colors by the introduction of 1-butyl-3-methylimidazolium chloride (BminCl) [84]. The presence of BminCl can screen the electrostatic repulsion between CNC nanoparticles, resulting in the close packing of nanoparticles on the substrate. By controlling the pulling speed of the substrate (3–9 μm/min), the obtained films exhibited different colors with the thickness of 100–300 nm. It was worth noting that attributed to the amine groups functionalization, the obtained optical films had a color sensitive to aldehyde gases, which can be potentially used as the colorimetric sensor.

3.2.4.3 Macromolecules

In comparison with the small molecules, the macromolecules hold the larger spatial dimensions and therefore can be effectively as the additives to penetrate into the chiral nematic structure and enlarge the pitch of CNC self-assembly. Generally, two approaches can be used in the preparation of optical CNC films with the introduction of macromolecules. The first approach is similar as the compounding treatment using the small molecules as additives in the CNC self-assembly films,

viz. dissolving the macromolecule in the CNC suspension and mixing two components homogeneously, then depositing the macromolecule with CNC by evaporation process. The second approach includes a polymerization process with the addition of targeted monomer and initiator into the CNC suspension. The anisotropic chiral nematic phase of CNC nanoparticles and monomers were formed before the synthesis of the penetrated/surrounded polymers. These composites films take both the optical-tunable performance and the multifunctional properties originated from the intrinsic properties of introduced macromolecules. Table 3.4 summarized the reported studies of CNC-based optical films with the physical compounding of macromolecules as the additives.

Water-soluble polymers are typical macromolecules introduced into the CNC aqueous suspensions to prepare the optical composite films, such as polyethylene glycol (PEG), polyacrylate sodium (PAAS), polyvinyl alcohol (PVA) etc. Generally, the polymer solution is mixed with the CNC aqueous suspension, and slowly evaporated to form the composite films after the stirring or ultrasonic treatment. In these cases, PEG is the widely used additive in the CNC suspension to develop the smooth, flexible and optical-tunable films [85–87]. Similar as the effect of other additives, the addition of PEG commonly increased the pitches of CNC-based chiral nematic films. However, the introduction of superfluous PEG may destroy the chiral nematic structure of CNC, due to the weakening of the interaction between CNC nanoparticles and nematic layers, the destruction of the long-term orientation for chiral nematic phase and micro-phase separation [86]. Ascribed to the flexibility of PEG chains, the brittleness of CNC self-assembly film can be improved as the flexible and bendable materials based on the plasticization of added PEG. In addition, a recent study reported the improvement of adhesion strength between the CNC self-assembly film and neutral polymer matrix without destroying the chiral nematic structure by the introduction of PEG as the compatibilizer [86]. As shown in Fig. 3.12, the hygroscopic effect of PEG can endow the CNC self-assembly film with a reversible color response to humidity, resulting from the penetration of water molecules into the chiral structure of the film and therefore change of pitch. When the mass ratio of CNC to PEG was 80/20, the composite film exhibited the green color at relative humidity (RH) of 50%. With the increase of RH, the film changed into olive, brown, orange and dark red successively, and finally became transparent at RH 100%. This color change was reported to be reversible and can preserve this reversible humidity response property under multiple cycles [87].

The effect of introducing the water-soluble PVA in the CNC aqueous suspension was reported to be similar as that of the PEG, with the increase of pitch for the CNC chiral nematic film due to the introduction of PVA additive [88]. Another study reported the addition of the supramolecular copolymer poly(oligoethylene glycol methacrylate) into the CNC suspension to adjust the optical properties and humidity response of the obtained film. The chiral nematic pitch of the CNC self-assembly films increased linearly with the added polymer content, attributed to the enhancement of hydrogen bonding in the system. After the treatment of moisture absorption, the large amount of hydrogen bonds formed in the film caused a blue shift of reflected wavelength [89]. The addition of poly(vinyl pyrrolidone) (PVP) also increased the

Table 3.4 The reported studies of CNC-based optical films with the physical compounding of polymers as the additive (without CNC-based templating mesoporous materials)

Approach to introduce the polymer	Polymer as the additive	M_n of added polymers (kDa)	Ratio of CNC/polymer	Concentration of CNC (wt%) and solvent	Pitch (nm)	Color	Reflective wavelength (nm)	References
Direct mixing	PEG	0.2	40	5.3, water	–	–	585 ± 25	[85]
			20		–	–	615 ± 5	
			10		–	–	623 ± 25	
	PAAS	5	12.5		450	Green	600	
	PEG	20	95/5	2, water	1360 ± 8	Bluish green	442	[86]
			90/10		1562 ± 12	Yellowish green	460	
			70/30		1716 ± 6	Yellowish brown	545	
			60/40		1586 ± 108	–	494	
			50/50		1758 ± 210	–	516	
	PEG	20	90/10	3, water	260	Blue	~400	[87]
			80/20		340	Green	~500	
			70/30		400	Red	665 ± 17	
	PVA	85–126	90/10	0.5, water	740 ± 90	–	590	[88]
			80/20		812 ± 50	–	641	
			70/30		880 ± 58	–	688	
			60/40		972 ± 100	–	726	
	EGUPy	55–65	60/40	1, water	–	–	750	[89]
	PVP	58	90/10	3, water	–	Orange	597	[90]

(continued)

Table 3.4 (continued)

Approach to introduce the polymer	Polymer as the additive	M_n of added polymers (kDa)	Ratio of CNC/polymer	Concentration of CNC (wt%) and solvent	Pitch (nm)	Color	Reflective wavelength (nm)	References
			80/20		–	Red	717	
			70/30		–	Colorless	865	
	OSi/PEG	0.4 (PEG)	48.7/21.3/30.0	– , water	286	Blue	200	[91]
			46.0/24.0/30.0		357	Green	557	
			43.9/26.1/30.0		–	Red	688	
			37.4/32.6/30.0		660	Colorless	915	
	PS	116	36	3.5, DMF	–	–	About 700	[92]
			46		–	Dark red	About 800	
			54		–	–	About 940	
			59		–	–	About 1135	
	PMMA	98.3	46		–	Red	About 680	
	PVK	167	46		–	–	About 600	
	PC	35.8	46		–	–	About 500	
	PEMA LNP	–	~ 73/27	2.5, water	220 ± 80	–	–	[93]
	PEMA50 LNP	–	75/25	2.5, water	180 ± 80	–	–	[94]
	PEMA150 LNP	–	75/25		220 ± 80	–	–	
	HDA/PBuA-MAEA LNP	–	89.3/0.7/10	5.0, water	239 ± 27	–	About 700	[95]
			84.3/0.7/15		–	–	About 750	

(continued)

Table 3.4 (continued)

Approach to introduce the polymer	Polymer as the additive	M_n of added polymers (kDa)	Ratio of CNC/polymer	Concentration of CNC (wt%) and solvent	Pitch (nm)	Color	Reflective wavelength (nm)	References
			75.3/0.7/24		290 ± 15	–	–	
			89.93/0.07/10		–	–	About 800	
			88. 6/1.4/10		–	–	About 650	
Mixing and in situ polymerization	PHEMA	–	>7.1/92.9	5.0, water	–	–	2800	[96]
	PAAm	–	66/34	3.0, water	–	Blue	About 490	[97]
	PHEMa	–	66/34		–	–	About 420	
	PEGMa	–	66/34		–	–	About 500	
	PNIPAM	–	66/34		–	–	About 490	
	PAAc	–	66/34		–	–	About 370	
	PHEA	–	–	8.2, water	5400–6900	–	–	[98]
	PDDC-HD	–	–	1.0, water	–	Green to red	490–800	[50]

Abbreviations: *PEG* (poly(ethylene glycol)), *PAAS* (anionic sodium polyacrylate), *PVA* (poly(vinyl alcohol)), *EGUPy* (copolymers of poly(oligoethylene glycol methacrylate) and methacrylate derivative with 2-ureido-4-pyrimidinone groups), *PVP* (polyvinylpyrrolidone), *OSi* (organosilica), *PS* (polystyrene), *PMMA* (poly(methyl methacrylate)), *PVK* (poly(9-vinylcarbazole)), *PC* (polycarbonate), *PEMA LNP* (poly(ethyl methacrylate) latex nanoparticle), *PEMA50 LNP* (poly(ethyl methacrylate) latex nanoparticle with diameter of ~50 nm), *PEMA150 LNP* (poly(ethyl methacrylate) latex nanoparticle with diameter of ~150 nm), *HDA* (hexamethylenediamine), *PBuA-MAEA LNP* (poly[butyl acrylate-co-2-(methacryloyloxy)-ethyl acetoacetate] latex nanoparticle), *PHEMA* (poly(2-hydroxyethyl methacrylate)), *PAAm* (polyacrylamide), *PEGMa* (polyethylene glycol methacrylate), *PNIPAM* (poly(*N*-isopropyl acrylamide)), *PAAc* (polyacrylic acid), *PHEA* (poly(2-hydroxyethyl acrylate)), *PDDC-HD* (poly(dodecanediol-co-citrate))

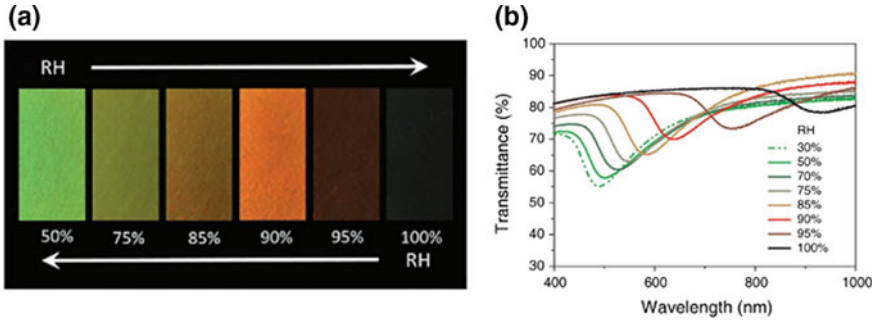

Fig. 3.12 **a** Reversible structural color change of the CNC/PEG (80/20, w/w) film at the varied RH; **b** the influence of RH to the reflectance peaks of CNC/PEG (80/20, w/w) film. Adapted from [87]

reflected wavelength peak of CNC composite films [90]. Chiral nematic structure and structural color were reported to be maintained even at the PVP content up to 70 wt%. Due to the wide solubility of PVP in organic solvents, composite films displayed different swelling and change of structural color when dipping in different solvents, and composite films with higher content of PVP exhibited more distinguishable color difference. Besides the uncharged polymers mentioned before, the anionic PAAS was also reported to be added in the self-assembly film to decrease the pitch [85]. In this study, the ultrasound treatment with a high energy (5 kJ/g) was firstly applied to the CNC suspension to achieve the maximum reflected wavelength of 1006 nm. Then, the PAAS solution with different concentrations of 0–160 μmol/g was added into the CNC suspension to reduce the reflected wavelength and chiral nematic pitch of the film. The obtained films exhibited the stronger and narrower colors in the visible spectrum with obvious fingerprint patterns. Due to the negative charges on the surface of sulfuric acid-hydrolyzed CNC nanoparticles, the introduced anion PAAS was more likely to move out of the nanocrystals. This movement may result in the difference of PAAS concentration around and within CNC nanoparticles and further induce a difference in osmotic pressure, which caused the reduction of chiral nematic pitch.

Recently, the CNC composite optical films with sandwich structure were reported to be prepared by a nematic CNC layer embedded between two chiral nematic composite layers of CNC/organosilica/PEG [91]. The reflected color of chiral nematic layers can be tuned from blue to near-IR region by increasing the content of organosilica. The PEG component acted as a plasticizer. The sandwich structure featured the polarization-independent reflection with reflectivity approaching 100%, which was almost twice that of the corresponding single chiral nematic CNC composite film.

Preparation of mesoporous chiral nematic cellulose films by contemplating with the polymer additive was also reported [99]. The precursor of urea formaldehyde (UF) was firstly mixed with CNC suspension and performed a polymerization reaction after formation of CNC/UF composite film. Then, the UF component in composites was removed by the alkaline treatment, to obtain the mesoporous chiral nematic CNC

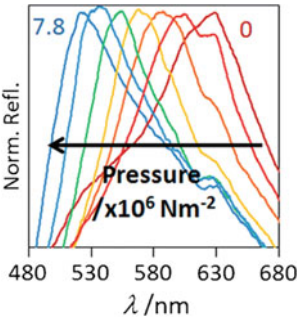

Fig. 3.13 Pressure response of mesoporous CNC film at 0, 0.4, 0.8, 1.6, 2.7, 5.9, and 7.8×10^6 N m^{-2}, showing a blue shift of reflected wavelength with the increase of pressure. Reproduced from [99]

films. The increase of polymer content will lead to the red shift, and the increase of ion strength will lead to the blue shift for the CNC self-assembly films. In addition, the introduction of mesoporosity was reported to be effective to regulate the increase of pitch for the obtained films. The obtained mesoporous CNC film was responsive to the polar solvent, which exhibited the red shifts when rapid swelling in polar solvent (ethanol) with the reflected wavelengths increasing from 330 nm for the dry film to 820 nm for the wet film. Changing the solvent ratio of ethanol/water mixture can also change the color of the film, ranging from 430 nm in pure ethanol to 840 nm in pure water of the reflected wavelengths. In addition, this mesoporous CNC film was also responsive to the macroscopic pressure, causing the blue shift due to the pressure transferring to nanoscale layers, as shown in Fig. 3.13. This pressure-induced-color change was reversible, which can return back to its original colorless state after the removal of external pressure.

Dispersions of neutral sulfated CNC in the polar organic media and preparation of chiral nematic composite films by composite with polystyrene (PS), poly(methyl methacrylate) (PMMA), polycarbonate (PC), and poly(9-vinylcarbazole) (PVK) were reported [92]. It should be noted that in order to achieve the homogeneous dispersion of CNC nanoparticles in the organic solvent (DMF), the surface H^+ of sulfuric acid-hydrolyzed CNC was replaced by the neutral salts (Li^+, Na^+, K^+, NH^{4+}, NMe^{4+}, NBu^{4+}), to allow the formation of chiral nematic liquid crystal phase in organic suspensions. Anisotropic iridescent films were obtained by the dissolution of various polymers mentioned before. At the same polymer content, different kinds of polymer composite films exhibited the different reflecting wavelengths, from about 800 nm for PS composites, to about 680 nm for PMMA composite, about 600 nm for PVK composite and about 500 nm for PC composites. When adding the same polymer, the increase of the polymer contents induced a red shift of reflected wavelength for the composite films. In addition, the introduction of salt will increase the ionic strength of suspensions and therefore cause a blue shift in the reflected wavelength of the CNC self-assembly films.

Besides the liquid compounding with CNC and polymers, several novel methods were reported to develop the self-assembly composite materials with the purposes of enhancing the compatibility between CNC nanoparticles and polymeric additives, accurately controlling the color change of the obtained films and providing

some functional applications. The 2-hydroxyethyl methacrylate (HEMA) monomer mixed with CNC suspension together with the crosslinker and initiator was conducted a polymerization reaction to regulate the optical behaviors of the composite films by the adjusting of total PHEMA concentration [96]. It was reported that the composites obtained by direct polymerization from the initial CNC suspension did not exhibit the obvious chiral nematic phase. After the phase separation at higher concentrations, the dispersed fingerprint pattern can be observed in the films polymerized from the isotropic upper layer. Meanwhile, the uniform fingerprint pattern can be observed in the materials obtained from the anisotropic lower layer, indicating the existence of chiral nematic phase in this region. The similar method of in situ polymerization and compounding to prepare the CNC-based composite self-assembly hydrogels was also reported for the monomers of acrylamide (AAm), *N*-isopropylacrylamide (NIPAm), acrylic acid (AAc), 2-hydroxyethylmethacrylate (HEMa), polyethylene glycol methacrylate (PEGMa), and 2-hydroxyethyl acrylate (HEA) [97, 98]. By changing the composition of polymer precursors, evaporation durations and concentrations, the composite hydrogels with different chiral nematic structures can be fabricated. In addition, the chiral nematic pitch and corresponding reflected color can be regulated by the swelling treatment of these composite hydrogels in the solvent. For instance, when the blue CNC/PAAm composite hydrogel was immersed in water, it will immediately swell and exhibit the red shift of the reflected wavelength. After 150 s swelling, the composite hydrogel reached to the equilibrium in the near-infrared region. This change in color was reported to be reversible and influenced by the different solvents, for example changing the swelling media in ethanol will cause a blue shift in reflected wavelengths.

Recently, a novel process for the fabrication of optical composite films was reported including three separated steps of first preparation of chiral nematic CNC films by self-assembly, then immersing of CNC films in polymer precursors and drying, and finally conducting the polymerization of monomers [50]. In this study, a polysilicate elastomer with shape memory, hydroxyl-dominant poly(dodecanediol-co-citrate) (PDDC-HD) was used. The prepolymer was reported to penetrate into the chiral nematic structure of CNC film during the immersing treatment, which increased the pitch and red shift of the maximum average reflected wavelength by about 20%. This process can significantly preserve the original chiral nematic structure of CNC nanoparticles in the self-assembly composite films.

Kumacheva et al. reported the combination of rubber and CNC nanoparticles to produce the self-assembly films using the fluorescent labeled spherical latex nanoparticle (LNP). The combination of two nanoparticles with different morphologies was reported as the entropically driven coassembly in both aqueous suspensions and solid films [93]. In the suspension, the phase separation can be observed into a LNP-rich isotropic phase and a CNC-rich anisotropic phase, and large amount of LNP was also observed in the anisotropic phase. After the drying treatment, the composite self-assembly films exhibited the alternation of planar disordered layers of LNP-rich and CNC-rich chiral nematic regions, with nearly homogeneous fluorescence, birefringence and circular dichroic properties. The effects of LNP concentration, particle size, surface charge and glass transition temperature on the structure and properties

of CNC/rubber self-assembly films were reported in the further study [94]. The chiral nematic phase of CNC was retained when the 50% content of negative charged LNP added, and the obtained composite films exhibited the macroscopic uniform fluorescence, birefringence and circular dichroic properties. However, the addition of positive charged LNP will cause the flocculation of CNC nanoparticles in suspensions and destroy the chiral nematic structure of the composite films. In terms of size effect, the destruction degree of the larger LNP was reported to be greater than that of the smaller LNP to the chiral nematic phase. Regarding the effect of LNP glass transition temperature (T_g), the thermal treatment above the T_g of LNP can improve the ordering of CNC nanoparticles arrangement in the composite films, due to the combination of the rubbery-state LNP and ordered CNC matrix. The reactive LNP was also reported to be introduced in the CNC self-assembly with in situ chemical crosslinking to retain the photonic properties and enhance the mechanical performance [95].

3.2.5 Optical Films and Pitches Regulation from CNC Compounding with Other Nanoparticles

In recent years, the combination of CNC and other nanoparticles was reported as a novel approach to develop the coassembly films. The nanoparticles used for the additives generally include the metal and carbon-based nanoparticles, with diverse morphologies such as the sphere, nanorod, nanotube, and nanosheet. Most of these nanoparticles can be combined with CNC suspensions to form the chiral nematic optical materials, and taking various properties from the additional nanoparticles.

3.2.5.1 Metal and Inorganic Nanoparticles

Gold nanoparticles are the popular additives to be introduced in the CNC chiral nemaic films to develop the optical materials. Due to the entropic/excluded-volume effect, when compounding with the CNC nanoparticles, the gold nanorod (GNR) will gradually align along with the ordered orientation of CNC [100]. The alignment of GNR was reported to transit from the initial disordered isotropic phase to the left-handed chiral nematic phase. In addition, the isotropic-chiral nematic biphase of GNR-CNC co-dispersions was obtained, which was in accordance with the theoretical prediction of bidispersed rod-like nanoparticles with different aspect ratios. The ordered arrangement of GNR also resulted in the strong polarization sensitivity of surface plasmon resonance (SPR) effects, providing the potential applications of biocompatible composites with SPR properties. In another study, the chiral plasmonic films were reported to be prepared by the photonic properties of CNC matrix and plasmonic properties of GNR, exhibiting stronger plasmonic chiroptical activity [101]. When the GNR content in the composite films was lower than 0.93 wt%,

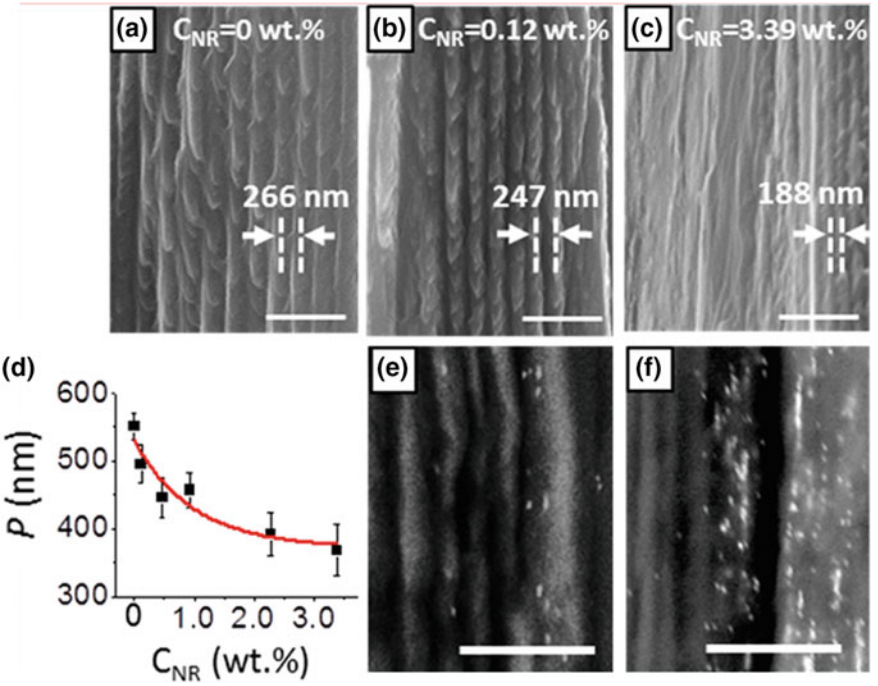

Fig. 3.14 SEM images of the cross-sectional morphologies of CNC slef-assembly films with different GNR contents at 0 (**a**), 0.12 wt% (**b**) and 3.39 wt% (**c**); **d** plot of chiral nematic pitch as a function of the GNR content; **e**, **f** SEM images of the cross-sectional morphologies of the GNR-CNC self-assembly films acquired with the backscattered electron detector (GNR appear as bright spots). Scale bars are 1 μm. Reproduced from [101]

these films can preserve a complete chiral nematic structure. The increase of GNR content caused the reduction of chiral nematic pitch of films, as shown in Fig. 3.14, the decrease of pitches from 551 nm to 368 nm with the increase of GNR contents from 0 to 3.39 wt% in the composite films.

In the further studies, the gold nanoparticle (GNP) was also reported to be introduced in the CNC suspensions by the co-assembly method to form a free-standing chiral plasmonic composite film, which can also retain the optical properties from the chiral nematic structure of CNC matrix as well as the plasmonic resonance of GNP [102, 103]. The obtained composite films exhibited a distinct chiroptical activity induced by the plasmon and a strong resonance plasmonic-photonic coupling. With the changing of the incidence angle of light or utilizing the response properties of CNC matrix, the switchable optical activity can be observed for the composite films. The chiral nematic CNC films with gold nanoclusters (AuNC) exhibited modulated fluorescence emission because of the stopband- and band edge-photoemission coupling effects between CNC and fluorescent AuNC nanoparticles [104]. The intensity of fluorescence emission can be enhanced by the slow photon effect of band-edge, while the stopband will inhibit it.

The silver nanorod (SNR) is another metal nanoparticle to be added in the CNC self-assembly films to prepare the photonic–plasmonic coupled hybrid materials [105]. The SNR was reported to self-assemble with CNC nanoparticles to form the chiral nematic phase, with the combination of advantages of plasmonic SNR and photonic CNC nanoparticles. The plasmonic properties of doped SNR can be controlled by adjusting the photonic local density of optical states of CNC matrix.

Because of the unique property of 4f–4f inner-shell electron transitions, the rare-earth doped nanoparticles have good hydrothermal stability and rich water emission spectra. With the chiral assembly arise from co-deposit with CNC nanoparticles and rare-earth nanoparticles, the hybrid composites holding the chiral electron transition with circularly polarized excitation properties can be produced [106]. It was reported that YVO_4: Eu^{3+} nanoparticles can adhere onto the surface of CNC nanoparticles to prepare the chiral nematic luminescent films. The low content of YVO_4: Eu^{3+}nanoparticles can load on CNC nanoparticles and self-assemble into chiral nematic phase. Another study reported the combination of photonic CNC films with lanthanide-doped $NaYF_4$ upconverting nanoparticles [107]. The introduction of $NaYF_4$: Yb, Er hexagonal nanorods can effectively convert the near-infrared light into the visible light due to distinct energy transfer pathways owing to the interactions between dopant and matrix. The chiral nematic upconverting photonic composite films produced by co-assembly of $NaYF_4$: Yb, Er hexagonal nanorods and CNC nanoparticles exhibited the visible up-conversion of near-infrared light and retained the adjustable photonic chiral activity.

The mesoporous chiral nematic CNC film can be prepared by the composite with inorganic silica to regulate the pitch and then removing the silica by the alkaline or acid treatment [108]. The optical properties and mesoporosity of the obtained CNC self-assembly films can be controlled by changing the CNC/silica ratio or different substrates during the evaporation process.

3.2.5.2 Carbon-Based Nanoparticles

The addition of carbon nanoparticles can provide the additional conductivity to the CNC self-assembly films. One-dimensional multi-walled carbon nanotube (MWCNT) was reported to be added into the chiral nematic CNC suspension to obtain the hybrid nanopaper with the photonic properties and good conductivity [109]. With the increase of MWCNT content, the circular dichroism signal of the obtained nanopaper gradually shifted from the positive to negative, indicating that the chiral structure of nanopapers changed from left-handed to right-handed. In another study, the oxidized carbon nanotube was added into the CNC suspension to prepare the hybrid optical film by the evaporation-induced self-assembly [110]. With the increase of oxidized carbon nanotube content, the reflection spectrum of the hybrid films shifted to the higher wavelengths with the increase of pitches. In addition, the CNC and oxidized carbon nanotube can coordinate to form an ordered alignment and exhibit the anisotropic conductivity for the prepared films. Two-dimensional

graphene oxide nanosheet (GON) was also reported to compound with CNC nanoparticles to prepare the hybrid films with the chiral smectic structure based on a binary composite colloid [111]. The formation of chiral smectic structure in the suspensions and films can be achieved by adjusting the GON/CNC ratio and colloid concentration.

3.3 Optical Materials Based on Templates of CNC Self-assembly

In view of its rod-like morphology, CNC nanoparticles can form the chiral nematic structure in both suspensions and self-assembly films as introduced before. On the basis of this property, CNC can be used as a template to take the inorganic nanoparticles on the surface and preserve the chiral nematic structure in the resultant mesoporous materials. This idea was first reported in 2003 by a study on the use of CNC as the template in the synthesis of mesoporous silica films [112]. The birefringent CNC/silica composite was firstly obtained by the slow evaporation, and then performed the calcination to remove the CNC component for the preparation of the mesoporous silica materials. The rod-like CNC nanoparticles provided the template of liquid crystal structure retained in the calcined silica films. Unfortunately, only the localized helical structure was reported to be observed in the silica materials rather than the long-term ordered chiral nematic structure.

In the further studies, the mesoporous silica films with tunable chiral nematic structures and optical performances were reported [45, 113]. The silica precursortetraethoxysilane ($Si(OEt)_4$, TEOS) or tetramethoxysilane, ($Si(OMe)_4$, TMOS) was mixed with the CNC suspension to achieve the chiral nematic structure at pH 2.4 for the composite compounding. The CNC/silica self-assembly composite films with varied ratios of compositions were fabricated after the slow evaporation treatment. As shown in Fig. 3.15, the obtained films with the higher silica precursor content exhibited the longer peak reflected wavelengths, which was preserved for the calcinated mesoporous materials. The reflection peaks of the mesoporous silica films showed the blue-shift of about 300 nm. Two possible reasons proposed to explain this optical behavior, including the decrease of the chiral nematic pitch from the contraction of obtained films, and the decrease of average refractive index resulting from the removal of CNC nanoparticles during the calcination.

Diverse treatments were reported to regulate the self-assembly, pitch and optical performances of the CNC-templated mesoporous silica films, including the pH condition, ionic strength, hydrophilicity and hydrophobicity of substrates, evaporation rate and additives. As mentioned before, the optimal pH condition for the formation of chiral nematic structure in the composite CNC/silica was 2.4, which was close to the isoelectric point of colloidal silica to restrain the polymerization of TMOS. The addition of extra acid or base in the CNC/TMOS mixture may lead to the disruption of ordered alignment and chiral nematic phase. The introduction of acid molecules into the CNC suspension induced the formation of the nematic

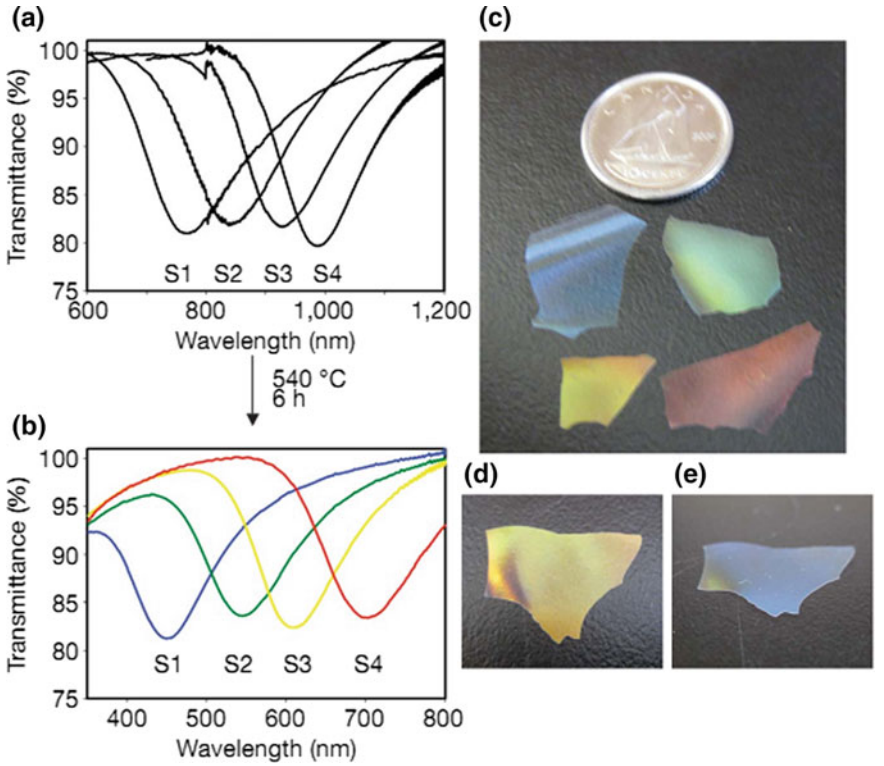

Fig. 3.15 Transmission spectra of CNC/silica composite films (**a**) and mesoporous silica films after the calcination (**b**) with the gradual increase of the silica content from S1 to S4 samples; photograph of mesoporous silica films S1 to S4 with different reflected colors (**c**) and the different colors of sample S3 at normal incidence (**d**) and oblique incidence (**e**). Reproduced from [113]

phase rather than chiral nematic structure, because of the inhibition of chiral interactions between CNC nanoparticles at the low pH condition. When adjusting the pH to the higher values (pH = 7 and 12.5), a disordered structure was observed for the composite films, indicating the disruption of chiral nematic structure from the changing in the rate of silica condensation. By the regulation of ionic strength is another method to tailor the pitch of chiral nematic structure and optical properties of the CNC/silica self-assembly films. For instance, the addition of ionic compounds $HAuCl_4$ was reported to induce a blue-shift of CNC/TMOS films from 975 to 450 nm [114]. It should be noted that the addition of excessive ionic strength may prevent the effective self-assembly and formation of chiral nematic structure of the CNC/TMOS mixture. The effect of various substrates on the optical properties of CNC-templated mesoporous silica films was also reported [52]. Various hydrophilic substrates taking the mesoporous silica films exhibited different iridescent colors changing from blue to red. While the evaporation on highly hydrophobic substrates provided the hazy nacre-like iridescence for the obtained mesoporous silica films. The evaporation rate

was reported as another factor to regulate the self-assembly and optical properties of the CNC/TMOS films [52]. The reflected peak wavelength of CNC-templated mesoporous silica films exhibited the blue-shift at the low-rate evaporation, while a red-shift was observed for the films at the quick evaporation. Finally, with the introduction of small molecules, such as the monosaccharides or polyols (glucose, sucrose, glycerol), was reported to cause a red-shift in the reflected peak for both CNC/silica composite films and calcined silica films [115].

Mesoporous organosilica films were reported to be prepared by the similar method as that of mesoporous silica [116]. The 1,2-bis(trimethoxysilyl)ethane (BTMSE) was used as the organosilica precursor to mix with the chiral nematic self-assembly of CNC nanoparticles. In order to prevent the decomposition of organosilica, acid hydrolysis was performed to remove CNC nanoparticles instead of the calcination. The reflected peaks of CNC/organosilica composites exhibited a red-shift with the increase of BTMSE content, which can be adjusted from 700 to 900 nm by changing the BTMSE content. In the further study, the thermotropic liquid crystalline, 4-cyano-4′-octylbiphenyl (8CB), was introduced into the mesoporous organosilica films exhibiting the thermochromic reflection with the reversible transformation of colorless and transparent films at around 40 °C [117].

Preparation of mesoporous silica materials by using CNC as the template can also be realized in the three-dimensional structural materials, such as the microsphere and aerogel. Silica macrospheres with chiral nematic structure based on the CNC self-assembly were reported to be manufactured by a double-matrix templating method [118]. In the proposed procedure, the CNC suspension and TMOS were mixed with polyacrylamide (PAAm) precursors, and the tactoids growed in the aqueous micro-droplets with a sol-gel transition of TMOS. Then, the photopolymerizaiton of PAAm was initiated to capture the tactoids with chiral nematic order in solid microspheres. After the condensation of silanol groups and drying process, the microspheres were calcined to remove the CNC and polymer components to obtain the mesoporous silica microspheres. These silica microspheres exhibited the high surface area, mesoporosity, micro-optical and chiral separation properties. In the case of silica aerogels, the chiral nematic order was achieved by the calcination of CNC/silica aerogels obtained from the critical point drying of silica/cellulose hydrogel [119]. The lower pH and higher proportion of TMOS precursor can induce the larger pitch for the chiral nematic aerogels.

Besides the silica-based mesoporous materials, several metal particles were also reported to produce the ordered mesoporous materials by the CNC templating method [114], including the titania [120–122], germanium (Ge) and its oxide (GeO_2) [123], Y_2O_3: Eu^{3+} [124], magnesium [125] mesoporous materials. The presence of silica was necessary for the preservation of the chiral nematic order and the introduction of mesoporosity. These chiral nematic mesoporous materials were reported to be potential applications in the photovoltaics, sensing, photo catalysis, optoelectronics, chiral separation and enantioselective adsorption. With the carbonization of CNCs and the etching of silica, the free-standing mesoporous carbon films can be obtained from the CNC/silica chiral nematic mesoporous materials as intermediates. The mesoporous carbon films retained both the chiral nematic order and high specific surface area,

which was reported to be widely used as an efficient electrode in supercapacitor or electrocatalysis [126]. Porous nitrogen-doped carbon films with chiral nematic arrangement can also be prepared by the template of CNC [127].

In addition to small molecules, polymers were also reported to generate mesoporous chiral nematic materials by using CNCs as template. Mark J. MacLachlan and coworkers prepared mesoporous phenol-formaldehyde (PF) resin and conducted a series of studies on it. Mesoporous chiral nematic PF resin with flexibility, tunable optical properties and responsive swelling behavior was prepared [128]. The reflected peak could be adjusted by both increasing the proportion of PF precursor, which leads to a red shift, and adding salts, which results in a blue shift. The mesoporous PF resin swelled rapidly and showed a fast response of red-shift of reflected peak when immersion in solvents of different polarities. Mesoporous bilayer resins were generated by a simple layer-by-layer fabrication method: CNC/PF composites with different compositions successively self-assembled to form chiral nematic films through evaporation, one of which serves as the substrate of the latter one [129]. Mesoporous chiral nematic bilayer films had two different pitches and selectively reflect light of two different wavelengths. Thus, the layers underwent a differential swelling when exposed to different solvents, causing reversible curling of the films, which made them appealing for applications of soft robotics. When swelling in polar solvents, the red-shift of mesoporous PF resins could be manipulated by acidification or formaldehyde treatment [130]. The acidification decreased the concentration of surface methylol groups of the film, made the film became less hydrophilic, and the effects of formaldehyde treatment was the opposite. Treated resins showed a differential swelling in polar solvents, resulting in changes of chiral nematic pitch and the reflected color. Acid and formaldehyde could be further used as inks to write on the film, producing latent images that only appear upon swelling of the film.

Some applications of mesoporous films prepared by the CNC templating method were reported. Silver (Ag) nanoparticles were directly synthesized in mesoporous silica films. Chiral nematic arrangement of silver nanoparticles originated from CNC self-assembly can produce the optical activities for silica/Ag composites in the vicinity of the surface plasmon resonance [131]. In another study, both gold and silver nanoparticles contained in chiral nematic mesoporous silica films exhibited the induced circular dichroism signals related to their plasmon resonances, which was sensitive to the changes in the environment, and therefore can be used in sensing applications [114]. Similar processing was performed on the mesoporous silica materials loaded with CdS quantum dots [132]. In this study, the water-soluble poly(acrylic acid)/mercaptopropionic acid-stabilized CdS quantum dot was mixed with CNC/silica suspension to proceed the co-assembly of chiral nematic alignment. After the calcination, the freestanding chiral nematic mesoporous CdS-loaded silica film can be obtained with the iridescence and luminescence. By changing the loading levels of CdS quantum dots, these CdS/silica films exhibited various iridescent colors and green-yellow emission brightness.

3.4 Self-assembly and Optical Materials of Chitin Nanocrystals

Chitin nanocrystals (ChNC) prepared by acid hydrolysis have the similar rod-like morphology and liquid crystal phase behavior as cellulose nanocrystals. When the concentration of ChNC suspension increased to the critical value, the phase separation into the isotropic-chiral nematic biphase will occur, which can be preserved for the retention of chiral nematic alignment in dry films [133]. The early study reported the critical concentration of ChNC suspension at 5 wt% under the pH 3.6 reaching a biphase equilibrium, with the pitch of the lower chiral nematic phase of 16 μm and the pitch of the tactoids in the upper isotropic phase of 20 μm [134]. The surface $-NH_3^+$ is the origin of the electrostatic repulsion of ChNC nanoparticles in suspensions. The increase of concentrations of acid and salt molecules will compress the electrical double layer of ChNC and cause the screening effect, which therefore resulted in the increase of the critical concentration for phase separation.

Several factors play the important influence on the liquid crystal behaviors of ChNC suspensions, including the surface charges, concentration, ionic strength, pH, and temperature. N-sulfonation was performed on the surface modification of the ChNC suspension to regulate its surface charges and liquid crystal behaviors [135]. With the low N-sulfonation degree (0.3) and pH 4.0, the modified ChNC occurred a phase separation into isotropic-chiral nematic coexistence above the critical concentration of 4 wt% in the suspension. The anisotropic phase was reported to disappear for the same sample with the extent of surface N-sulfonation below than 0.7, which was explained by the change of surface charge density from different extents of N-sulfonation. At the higher N-sulfonation degree of 0.8, the formation of tactoids from the self-assembly of ChNC nanoparticles can be observed in suspensions. This study also reported the critical surface charge density (0.40 e/nm^2) of ChNC nanoparticles for the formation of chiral nematic phase in suspensions. When the surface charge density of ChNC nanoparticles below this critical value, only the nematic phase was formed in the suspension. The effects of concentration, ionic strength, pH, and temperature on the liquid crystal behaviors of ChNC suspensions were further reported [136]. With the increase of ChNC concentration, the suspensions exhibited a nematic gel-like behavior rather than chiral nematic structure, because of the formation of the ChNC network. With the increase of ionic strength and pH, the electrostatic repulsive force of ChNC nanoparticles was reduced with the increase of the attractive interaction, resulting in the formation of stable gels. A recent study reported the critical concentration of 5 wt% for the formation of the namatic phase and the critical concentration of 10 wt% for the anisotropic birefringent gel of ChNC nanoparticles in suspensions [137]. Liu et al. reported the lyotripic liquid crystal behaviors of ChNC nanoparticles prepared by the H_2O_2-hydrolysis with the switching of surface charges from positive to negative [138]. The gel transition of ChNC nanoparticles in the suspension was reported to happen at a critical concentration of 1.30 wt%, which indicated the gradual formation of nanofibers to nanobelts and finally to multi-layered lamellae during the self-assembly of ChNC in suspensions. The spacing of periodic

lines of dried ChNC film was reported as 4.4 μm, much less than the chiral nematic pitch of HCl-hydrolyzed ChNC (30 μm) [133].

Similar as the reports in CNC-based self-assembly materials, the external energy field and additives are effective strategies to regulate the liquid crystal behaviors and optical properties of obtained ChNC films. The optically anisotropic ChNC/poly(acrylic acid) composite film was fabricated with the existence of high magnetic field (5 T) [139]. The photo initiated free-radical polymerization was applied to lock the ordered liquid crystal phase of ChNC nanoparticles. These rod-like nanoparticles were observed to form a uniplanar orientation with the long axis perpendicular to the direction of magnetic field. In another study, the small molecule of acrylic acid was added in the ChNC suspensions to investigate the liquid crystal behavior of aqueous mixtures [140]. With the introduction of acrylic acid, a higher ChNC concentration was required for the formation of complete chiral nematic phase in mixture comparing with that of the pure ChNC in water. At a limited range of ChNC concentrations (6.22–6.41 wt%) with the addition of acrylic acid, the mixing suspensions were observed a stable birefringence glassy phase with the nematic order, which provided a clear-cut boundary between the isotropic and anisotropic phases.

Finally, ChNC can also be used as the template to induce the ordering self-assembly of inorganic particles to form the optical mesoporous materials. The fabrication of the anisotropic ChNC-templating calcium carbonate ($CaCO_3$) hybrid materials was reported [141]. The lyotropic nematic liquid crystal phase of ChNC/$CaCO_3$was preserved in the DMSO/DMF solution at the critical concentration of 15 wt% [142]. This nematic solution was soaked in methanol to transform as a free-standing gel, which can be manually stretched in methanol and dried to obtain anisotropic solid films with the alignment of ChNC nanoparticles parallel to the direction of stretching stress. The growth of rod-like $CaCO_3$ crystals was observed to arrange within the films along the direction of ChNC template.

A series studies on the preparation of ChNC-templating silica mesoporous films were also reported [143, 144]. The aqueous mixture of ChNCs and silica precursor can precipitate based on the electrostatic interactions and/or rapid siloxane condensation, thus the solvent exchange with the alcoholic suspensions of ChNC/silica precursor was used to avoid the precipitation [143]. In this study, a strong magnetic field was applied during the evaporation to align ChNC nanoparticles perpendicular to the magnetic direction. Another study reported the use of alternating current electric field to assist the alignment of ChNC/silica precursors in water-ethanol suspensions [145]. When the mixed suspensions form chiral nematic phase, the applied electric fields can induce a fast reorientation to uniform the nematic phase. In the preparation of mesoporous silica materials with the ChNC template, the initial concentration of ChNC determined the porosity and chiral nematic structure of films was reported as 0.35 (volume fraction) [144]. The removal of ChNC component was generally realized by the calcination and sulfuric acid hydrolysis for superfluous organosilica [146]. The mesoporous nitrogen-doped carbon films with layered nematic arrangement from ChNC template can be obtained by carbonization and etching of ChNC/silica composites, which was widely used as the supercapacitor

electrode materials [147]. Several other mesoporous materials such as silica–titania [148, 149] and alumina [150] can also be prepared by the strategy of ChNC template.

3.5 Concluding Remarks

The development of self-assembly optical application is a hot topic in the study of rod-like polysaccharide nanocrystals of functional materials during last ten years. The early studies focused on the regulation of pitches and optical behaviors of the self-assembly films, typically by the changing the surface properties of polysaccharide nanocrystals and applying of external energy fields or diverse additives. Recent studies reported the multifunctional development of the polysaccharide nanocrystals self-assembly materials, viz. the combination of optical properties with electric, magnetic, catalytic, adsorbing properties. With the preservation of polysaccharide nanocrystals' chiral nematic structure, the introduction of functional additives into the suspensions is an effective approach to achieve the regulation of pitches and optical properties and provide the additional functional properties. In this field, the future study should accurately control the self-assembly and optical behaviors of polysaccharide nanocrystals with the establishment of microstructure-reflective wavelength relationship. In addition, the development of easy-handling preparation method for these optical materials is another significant requirement with the purpose of driving the industrial production and application.

Acknowledgements The authors would like to acknowledge the support of the National Natural Science Foundation of China (51603159).

References

1. Dufresne A (2017) Nanocellulose: from nature to high performance tailored materials, 2nd edn. Berlin/Boston, Walter de Gruyter GmbH
2. Buining PA, Philipse AP, Lekkerkerker HNW (1994) Phase behavior of aqueous dispersions of colloidal boehmite rods. Langmuir 10:2106–2114
3. Min Dong X, Kimura T, Revol J-F et al (1996) Effects of ionic strength on the isotropic–chiral nematic phase transition of suspensions of cellulose crystallites. Langmuir 12:2076–2082
4. Onsager L (1949) The effects of shape on the interaction of colloidal particles. Ann NY Acad Sci 51:627–659
5. Heux L, Chauve G, Bonini C (2000) Nonflocculating and chiral-nematic self-ordering of cellulose microcrystals suspensions in nonpolar solvents. Langmuir 16:8210–8212
6. Khandelwal M, Windle A (2014) Origin of chiral interactions in cellulose supra-molecular microfibrils. Carbohydr Polym 106:128–131
7. Parker RM, Guidetti G, Williams CA et al (2017) The self-assembly of cellulose nanocrystals: hierarchical design of visual appearance. Adv Mater 30:e1704477
8. Dreher R, Meier G (1973) Optical properties of cholesteric liquid crystals. Phys Rev A 8:1616–1623

9. Parker RM, Frka-Petesic B, Guidetti G et al (2016) Hierarchical self-assembly of cellulose nanocrystals in a confined geometry. ACS Nano 10:8443–8449
10. Li Y, Jun-Yan Suen J, Prince E et al (2016) Colloidal cholesteric liquid crystal in spherical confinement. Nat Commun 7:12520
11. Dong XM, Revol J-F, Gray DG (1998) Effect of microcrystallite preparation conditions on the formation of colloid crystals of cellulose. Cellulose 5:19–32
12. Schutz C, Van Rie J, Eyley S et al (2018) Effect of source on the properties and behavior of cellulose nanocrystal suspensions. ACS Sustain Chem Eng 6:8317–8324
13. Beck-Candanedo S, Roman M, Gray DG (2005) Effect of reaction conditions on the properties and behavior of wood cellulose nanocrystal suspensions. Biomacromol 6:1048–1054
14. Wang N, Ding E, Cheng R (2008) Preparation and liquid crystalline properties of spherical cellulose nanocrystals. Langmuir 24:5–8
15. Araki J, Wada M, Kuga S et al (2000) Birefringent glassy phase of a cellulose microcrystal suspension. Langmuir 16:2413–2415
16. Schutz C, Agthe M, Fall AB et al (2015) Rod packing in chiral nematic cellulose nanocrystal dispersions studied by small-angle X-ray scattering and laser diffraction. Langmuir 31:6507–6513
17. Castro-Guerrero CF, Gray DG (2014) Chiral nematic phase formation by aqueous suspensions of cellulose nanocrystals prepared by oxidation with ammonium persulfate. Cellulose 21:2567–2577
18. He J, Liu S, Li L et al (2017) Lyotropic liquid crystal behavior of carboxylated cellulose nanocrystals. Carbohydr Polym 164:364–369
19. Nystrom G, Arcari M, Adamcik J et al (2018) Nanocellulose fragmentation mechanisms and inversion of chirality from the single particle to the cholesteric phase. ACS Nano 12:5141–5148
20. Hasani M, Cranston ED, Westman G et al (2008) Cationic surface functionalization of cellulose nanocrystals. Soft Matter 4:2238–2244
21. Araki J, Wada M, Kuga S (2001) Steric stabilization of a cellulose microcrystal suspension by poly(ethylene glycol) grafting. Langmuir 17:21–27
22. Xu Q, Yi J, Zhang X et al (2008) A novel amphotropic polymer based on cellulose nanocrystals grafted with azo polymers. Eur Polym J 44:2830–2837
23. Yi J, Xu Q, Zhang X et al (2008) Chiral-nematic self-ordering of rod-like cellulose nanocrystals grafted with poly(styrene) in both thermotropic and lyotropic states. Polymer 49:4406–4412
24. Yi J, Xu Q, Zhang X et al (2009) Temperature-induced chiral nematic phase changes of suspensions of poly(N, N-dimethylaminoethyl methacrylate)-grafted cellulose nanocrystals. Cellulose 16:989–997
25. Kloser E, Gray DG (2010) Surface grafting of cellulose nanocrystals with poly(ethylene oxide) in aqueous media. Langmuir 26:13450–13456
26. Ye D, Yang J (2015) Ion-responsive liquid crystals of cellulose nanowhiskers grafted with acrylamide. Carbohydr Polym 134:458–466
27. Azzam F, Heux L, Jean B (2016) Adjustment of the chiral nematic phase properties of cellulose nanocrystals by polymer grafting. Langmuir 32:4305–4312
28. Min Dong XG, Gray D (1997) Effect of counterions on ordered phase formation in suspensions of charged rod-like cellulose crystallites. Langmuir 13:2404–2409
29. Beck S, Bouchard J, Berry R (2011) Controlling the reflection wavelength of iridescent solid films of nanocrystalline cellulose. Biomacromol 12:167–172
30. Orts WJ, Godbout L, Marchessault RH et al (1998) Enhanced ordering of liquid crystalline suspensions of cellulose microfibrils: a small angle neutron scattering study. Macromolecules 31:5717–5725
31. De France KJ, Yager KG, Hoare T et al (2016) Cooperative ordering and kinetics of cellulose nanocrystal alignment in a magnetic field. Langmuir 32:7564–7571
32. Edgar CD, Gray DG (2002) Influence of dextran on the phase behavior of suspensions of cellulose nanocrystals. Macromolecules 35:7400–7406

33. Beck-Candanedo S, Viet D, Gray DG (2006) Induced phase separation in low-ionic-strength cellulose nanocrystal suspensions containing high-molecular-weight blue dextrans. Langmuir 22:8690–8695
34. Beck-Candanedo S, Viet D, Gray DG (2006) Induced phase separation in cellulose nanocrystal suspensions containing ionic dye species. Cellulose 13:629–635
35. Beck-Candanedo S, Viet D, Gray DG (2007) Triphase equilibria in cellulose nanocrystal suspensions containing neutral and charged macromolecules. Macromolecules 40:3429–3436
36. Chu G, Vasilyev G, Vilensky R et al (2018) Controlled assembly of nanocellulose-stabilized emulsions with periodic liquid crystal-in-liquid crystal organization. Langmuir 34:13263–13273
37. Zhou Q, Brumer H, Teeri TT (2009) Self-organization of cellulose nanocrystals adsorbed with xyloglucan oligosaccharide–poly(ethylene glycol)–polystyrene triblock copolymer. Macromolecules 42:5430–5432
38. Elazzouzi-Hafraoui S, Putaux J-L, Heux L (2009) Self-assembling and chiral nematic properties of organophilic cellulose nanocrystals. J Phys Chem B 113:11069–11075
39. Tran A, Hamad WY, MacLachlan MJ (2018) Tactoid annealing improves order in self-assembled cellulose nanocrystal films with chiral nematic structures. Langmuir 34:646–652
40. Hewson D, Vukusic P, Eichhorn SJ (2017) Reflection of circularly polarized light and the effect of particle distribution on circular dichroism in evaporation induced self-assembled cellulose nanocrystal thin films. AIP Adv 7:065308
41. Majoinen J, Kontturi E, Ikkala O et al (2012) SEM imaging of chiral nematic films cast from cellulose nanocrystal suspensions. Cellulose 19:1599–1605
42. Dumanli AG, van der Kooij HM, Kamita G et al (2014) Digital color in cellulose nanocrystal films. ACS Appl Mater Interfaces 6:12302–12306
43. Pan J, Hamad W, Straus SK (2010) Parameters affecting the chiral nematic phase of nanocrystalline cellulose films. Macromolecules 43:3851–3858
44. Klockars KW, Tardy BL, Borghei M et al (2018) Effect of anisotropy of cellulose nanocrystal suspensions on stratification, domain structure formation, and structural colors. Biomacromol 19:2931–2943
45. Hiratani T, Hamad WY, MacLachlan MJ (2017) Transparent depolarizing organic and inorganic films for optics and sensors. Adv Mater 29. https://doi.org/10.1002/adma.201606083
46. Korolovych VF, Cherpak V, Nepal D et al (2018) Cellulose nanocrystals with different morphologies and chiral properties. Polymer 145:334–347
47. Dumanli AG, Kamita G, Landman J et al (2014) Controlled, bio-inspired self-assembly of cellulose-based chiral reflectors. Adv Opt Mater 2:646–650
48. Shrestha S, Diaz JA, Ghanbari S et al (2017) Hygroscopic swelling determination of cellulose nanocrystal (CNC) films by polarized light microscopy digital image correlation. Biomacromol 18:1482–1490
49. Cherpak V, Korolovych VF, Geryak R et al (2018) Robust chiral organization of cellulose nanocrystals in capillary confinement. Nano Lett 18:6770–6777
50. Espinha A, Guidetti G, Serrano MC et al (2016) Shape memory cellulose-based photonic reflectors. ACS Appl Mater Interfaces 8:31935–31940
51. Beck S, Bouchard J, Chauve G et al (2013) Controlled production of patterns in iridescent solid films of cellulose nanocrystals. Cellulose 20:1401–1411
52. Nguyen TD, Hamad WY, MacLachlan MJ (2013) Tuning the iridescence of chiral nematic cellulose nanocrystals and mesoporous silica films by substrate variation. Chem Commun (Camb) 49:11296–11298
53. Haywood AD, Davis VA (2016) Effects of liquid crystalline and shear alignment on the optical properties of cellulose nanocrystal films. Cellulose 24:705–716
54. Rofouie P, Alizadehgiashi M, Mundoor H et al (2018) Self-assembly of cellulose nanocrystals into semi-spherical photonic cholesteric films. Adv Funct Mater 28:1803852
55. Mu X, Gray DG (2015) Droplets of cellulose nanocrystal suspensions on drying give iridescent 3-D “coffee-stain” rings. Cellulose 22:1103–1107

56. Gencer A, Schutz C, Thielemans W (2017) Influence of the particle concentration and marangoni flow on the formation of cellulose nanocrystal films. Langmuir 33:228–234
57. Tardy BL, Ago M, Guo J et al (2017) Optical properties of self-assembled cellulose nanocrystals films suspended at planar-symmetrical interfaces. Small 13:1702084–1702110
58. Picard G, Simon D, Kadiri Y et al (2012) Cellulose nanocrystal iridescence: a new model. Langmuir 28:14799–14807
59. Abraham E, Kam D, Nevo Y et al (2016) Highly modified cellulose nanocrystals and formation of epoxy-nanocrystalline cellulose (CNC) nanocomposites. ACS Appl Mater Interfaces 8:28086–28095
60. Abraham E, Nevo Y, Slattegard R et al (2016) Highly hydrophobic thermally stable liquid crystalline cellulosic nanomaterials. ACS Sustain Chem Eng 4:1338–1346
61. Lizundia E, Nguyen T-D, Vilas Jose L et al (2017) Chiroptical, morphological and conducting properties of chiral nematic mesoporous cellulose/polypyrrole composite films. J Mater Chem A 5:19184–19194
62. Natarajan B, Emiroglu C, Obrzut J et al (2017) Dielectric characterization of confined water in chiral cellulose nanocrystal films. ACS Appl Mater Interfaces 9:14222–14231
63. Lu T, Pan H, Ma J et al (2017) Cellulose nanocrystals/polyacrylamide composites of high sensitivity and cycling performance to gauge humidity. ACS Appl Mater Interfaces 9:18231–18237
64. Nan F, Nagarajan S, Chen Y et al (2017) Enhanced toughness and thermal stability of cellulose nanocrystal iridescent films by alkali treatment. ACS Sustain Chem Eng 5:8951–8958
65. Beck S, Bouchard J, Berry R (2012) Dispersibility in water of dried nanocrystalline cellulose. Biomacromol 13:1486–1494
66. Tang H, Guo B, Jiang H et al (2013) Fabrication and characterization of nanocrystalline cellulose films prepared under vacuum conditions. Cellulose 20:2667–2674
67. Chen Q, Liu P, Nan F et al (2014) Tuning the iridescence of chiral nematic cellulose nanocrystal films with a vacuum-assisted self-assembly technique. Biomacromol 15:4343–4350
68. Cranston ED, Gray DG (2006) Formation of cellulose-based electrostatic layer-by-layer films in a magnetic field. Sci Technol Adv Mater 7:319–321
69. Frka-Petesic B, Guidetti G, Kamita G et al (2017) Controlling the photonic properties of cholesteric cellulose nanocrystal films with magnets. Adv Mater 29:1701469
70. Habibi Y, Heim T, Douillard R (2008) Ac electric field-assisted assembly and alignment of cellulose nanocrystals. J Polym Sci, Part B: Polym Phys 46:1430–1436
71. Aguié-Béghin V, Molinari M, Hambardzumyan A et al (20010) Preparation of ordered films of cellulose nanocrystals. ACS Symp Ser 1019:115–136
72. Frka-Petesic B, Radavidson H, Jean B et al (2017) Dynamically controlled iridescence of cholesteric cellulose nanocrystal suspensions using electric fields. Adv Mater 29:1606208–1606228
73. Hoeger I, Rojas OJ, Efimenko K et al (2011) Ultrathin film coatings of aligned cellulose nanocrystals from a convective-shear assembly system and their surface mechanical properties. Soft Matter 7:1957
74. Ličen M, Majaron B, Noh J et al (2016) Correlation between structural properties and iridescent colors of cellulose nanocrystalline films. Cellulose 23:3601–3609
75. Tatsumi M, Teramoto Y, Nishio Y (2015) Different orientation patterns of cellulose nanocrystal films prepared from aqueous suspensions by shearing under evaporation. Cellulose 22:2983–2992
76. Liu Y, Stoeckel D, Gordeyeva K et al (2018) Nanoscale assembly of cellulose nanocrystals during drying and redispersion. ACS Macro Lett 7:172–177
77. Zhang YP (2012) Nanocrystalline cellulose for covert optical encryption. J Nanophotonics 6:063516
78. Mu X, Gray DG (2014) Formation of chiral nematic films from cellulose nanocrystal suspensions is a two-stage process. Langmuir 30:9256–9260
79. Dai S, Prempeh N, Liu D et al (2017) Cholesteric film of Cu(Ii)-doped cellulose nanocrystals for colorimetric sensing of ammonia gas. Carbohydr Polym 174:531–539

80. Santos MV, Tercjak A, Gutierrez J et al (2017) Optical sensor platform based on cellulose nanocrystals (CNC)—4′-(hexyloxy)-4-biphenylcarbonitrile (HOBC) bi-phase nematic liquid crystal composite films. Carbohydr Polym 168:346–355
81. Xu M, Li W, Ma C et al (2018) Multifunctional chiral nematic cellulose nanocrystals/glycerol structural colored nanocomposites for intelligent responsive films, photonic inks and iridescent coatings. J Mater Chem C 6:5391–5400
82. He YD, Zhang ZL, Xue J et al (2018) Biomimetic optical cellulose nanocrystal films with controllable iridescent color and environmental stimuli-responsive chromism. ACS Appl Mater Interfaces 10:5805–5811
83. Liu P, Guo X, Nan F et al (2017) Modifying mechanical, optical properties and thermal processability of iridescent cellulose nanocrystal films using ionic liquid. ACS Appl Mater Interfaces 9:3085–3092
84. Song W, Lee JK, Gong MS et al (2018) Cellulose nanocrystal-based colored thin films for colorimetric detection of aldehyde gases. ACS Appl Mater Interfaces 10:10353–10361
85. Bardet R, Belgacem N, Bras J (2015) Flexibility and color monitoring of cellulose nanocrystal iridescent solid films using anionic or neutral polymers. ACS Appl Mater Interfaces 7:4010–4018
86. Gu M, Jiang C, Liu D et al (2016) Cellulose nanocrystal/poly(ethylene glycol) composite as an iridescent coating on polymer substrates: structure-color and interface adhesion. ACS Appl Mater Interfaces 8:32565–32573
87. Yao K, Meng Q, Bulone V et al (2017) Flexible and responsive chiral nematic cellulose nanocrystal/poly(ethylene glycol) composite films with uniform and tunable structural color. Adv Mater 29. https://doi.org/10.1002/adma.201701323
88. Wang B, Walther A (2015) Self-assembled, iridescent, crustacean-mimetic nanocomposites with tailored periodicity and layered cuticular structure. ACS Nano 9:10637–10646
89. Zhu B, Merindol R, Benitez AJ et al (2016) Supramolecular engineering of hierarchically self-assembled, bioinspired, cholesteric nanocomposites formed by cellulose nanocrystals and polymers. ACS Appl Mater Interfaces 8:11031–11040
90. Gao Y, Jin Z (2018) Iridescent chiral nematic cellulose nanocrystal/polyvinylpyrrolidone nanocomposite films for distinguishing similar organic solvents. ACS Sustain Chem Eng 6:6192–6202
91. De La Cruz JA, Liu Q, Senyuk B et al (2018) Cellulose-based reflective liquid crystal films as optical filters and solar gain regulators. ACS Photonics 5:2468–2477
92. Cheung CCY, Giese M, Kelly JA et al (2013) Iridescent chiral nematic cellulose nanocrystal/polymer composites assembled in organic solvents. ACS Macro Lett 2:1016–1020
93. Therien-Aubin H, Lukach A, Pitch N et al (2015) Coassembly of nanorods and nanospheres in suspensions and in stratified films. Angew Chem Int Ed Engl 54:5618–5622
94. Therien-Aubin H, Lukach A, Pitch N et al (2015) Structure and properties of composite films formed by cellulose nanocrystals and charged latex nanoparticles. Nanoscale 7:6612–6618
95. Vollick B, Kuo P-Y, Thérien-Aubin H et al (2017) Composite cholesteric nanocellulose films with enhanced mechanical properties. Chem Mater 29:789–795
96. Tatsumi M, Teramoto Y, Nishio Y (2012) Polymer composites reinforced by locking-in a liquid-crystalline assembly of cellulose nanocrystallites. Biomacromol 13:1584–1591
97. Kelly JA, Shukaliak AM, Cheung CC et al (2013) Responsive photonic hydrogels based on nanocrystalline cellulose. Angew Chem Int Ed Engl 52:8912–8916
98. Cho S, Li Y, Seo M et al (2016) Nanofibrillar stimulus-responsive cholesteric microgels with catalytic properties. Angew Chem Int Ed Engl 55:14014–14018
99. Giese M, Blusch LK, Khan MK et al (2014) Responsive mesoporous photonic cellulose films by supramolecular cotemplating. Angew Chem Int Ed Engl 53:8880–8884
100. Liu Q, Campbell MG, Evans JS et al (2014) Orientationally ordered colloidal co-dispersions of gold nanorods and cellulose nanocrystals. Adv Mater 26:7178–7184
101. Querejeta-Fernandez A, Chauve G, Methot M et al (2014) Chiral plasmonic films formed by gold nanorods and cellulose nanocrystals. J Am Chem Soc 136:4788–4793

102. Lukach A, Therien-Aubin H, Querejeta-Fernandez A et al (2015) Coassembly of gold nanoparticles and cellulose nanocrystals in composite films. Langmuir 31:5033–5041
103. Chu G, Wang X, Yin H et al (2015) Free-standing optically switchable chiral plasmonic photonic crystal based on self-assembled cellulose nanorods and gold nanoparticles. ACS Appl Mater Interfaces 7:21797–21806
104. Qu D, Zhang J, Chu G et al (2016) Chiral fluorescent films of gold nanoclusters and photonic cellulose with modulated fluorescence emission. J Mater Chem C 4:1764–1768
105. Chu G, Yin H, Jiang H et al (2016) Ultrafast optical modulation of rationally engineered photonic–plasmonic coupling in self-assembled nanocrystalline cellulose/silver hybrid material. J Phys Chem C 120:27541–27547
106. Chu G, Wang X, Chen T et al (2015) Chiral electronic transitions of YVO_4: Eu^{3+}nanoparticles in cellulose based photonic materials with circularly polarized excitation. J Mater Chem C 3:3384–3390
107. Nguyen T-D, Hamad WY, MacLachlan MJ (2017) Near-IR-sensitive upconverting nanostructured photonic cellulose films. Adv Opt Mater 5:1600514
108. Schlesinger M, Hamad WY, MacLachlan MJ (2015) Optically tunable chiral nematic mesoporous cellulose films. Soft Matter 11:4686–4694
109. Ren Y, Wang T, Chen Z et al (2016) Liquid crystal behavior induced assembling fabrication of conductive chiral MWCNTs@NCCnanopaper. Appl Surf Sci 385:521–528
110. Sun J, Zhang C, Yuan Z et al (2017) Composite films with ordered carbon nanotubes and cellulose nanocrystals. J Phys Chem C 121:8976–8981
111. Pan H, Zhu C, Lu T et al (2017) A chiral smectic structure assembled from nanosheets and nanorods. Chem Commun (Camb) 53:1868–1871
112. Dujardin E, Blaseby M, Mann S (2003) Synthesis of mesoporous silica by sol–gel mineralisation of cellulose nanorod nematic suspensions. J Mater Chem 13:696–699
113. Shopsowitz KE, Qi H, Hamad WY et al (2010) Free-standing mesoporous silica films with tunable chiral nematic structures. Nature 468:422–425
114. Kelly JA, Shopsowitz KE, Ahn JM et al (2012) Chiral nematic stained glass: controlling the optical properties of nanocrystalline cellulose-templated materials. Langmuir 28:17256–17262
115. Kelly JA, Yu M, Hamad WY et al (2013) Large, crack-free freestanding films with chiral nematic structures. Adv Opt Mater 1:295–299
116. Shopsowitz KE, Hamad WY, MacLachlan MJ (2012) Flexible and iridescent chiral nematic mesoporous organosilica films. J Am Chem Soc 134:867–870
117. Giese M, De Witt JC, Shopsowitz KE et al (2013) Thermal switching of the reflection in chiral nematic mesoporous organosilica films infiltrated with liquid crystals. ACS Appl Mater Interfaces 5:6854–6859
118. Wang PX, Hamad WY, MacLachlan MJ (2016) Polymer and mesoporous silica microspheres with chiral nematic order from cellulose nanocrystals. Angew Chem Int Ed 55:12460–12464
119. Xu YT, Dai Y, Nguyen TD et al (2018) Aerogel materials with periodic structures imprinted with cellulose nanocrystals. Nanoscale 10:3805–3812
120. Ivanova A, Fattakhova-Rohlfing D, Kayaalp BE et al (2014) Tailoring the morphology of mesoporous titania thin films through biotemplating with nanocrystalline cellulose. J Am Chem Soc 136:5930–5937
121. Ivanova A, Fravventura MC, Fattakhova-Rohlfing D et al (2015) Nanocellulose-templated porous titania scaffolds incorporating presynthesized titania nanocrystals. Chem Mater 27:6205–6212
122. Shopsowitz KE, Stahl A, Hamad WY et al (2012) Hard templating of nanocrystalline titanium dioxide with chiral nematic ordering. Angew Chem Int Ed Engl 51:6886–6890
123. Xu J, Nguyen TD, Xie K et al (2015) Chiral nematic porous germania and germanium/carbon films. Nanoscale 7:13215–13223
124. Chu G, Xu W, Qu D et al (2014) Chiral nematic mesoporous films of Y_2O_3: Eu^{3+} with tunable optical properties and modulated photoluminescence. J Mater Chem C 2:9189–9195

125. Nguyen T-D, Kelly JA, Hamad WY et al (2015) Magnesiothermic reduction of thin films: towards semiconducting chiral nematic mesoporous silicon carbide and silicon structures. Adv Funct Mater 25:2175–2181
126. Asefa T (2012) Chiral nematic mesoporous carbons from self-assembled nanocrystalline cellulose. Angew Chem Int Ed Engl 51:2008–2010
127. Wang Y, Liu T, Lin X et al (2018) Self-templated synthesis of hierarchically porous N-doped carbon derived from biomass for supercapacitors. ACS Sustain Chem Eng 6:13932–13939
128. Khan MK, Giese M, Yu M et al (2013) Flexible mesoporous photonic resins with tunable chiral nematic structures. Angew Chem Int Ed Engl 52:8921–8924
129. Khan MK, Hamad WY, Maclachlan MJ (2014) Tunable mesoporous bilayer photonic resins with chiral nematic structures and actuator properties. Adv Mater 26:2323–2328
130. Khan MK, Bsoul A, Walus K et al (2015) Photonic patterns printed in chiral nematic mesoporous resins. Angew Chem Int Ed Engl 54:4304–4308
131. Qi H, Shopsowitz KE, Hamad WY et al (2011) Chiral nematic assemblies of silver nanoparticles in mesoporous silica thin films. J Am Chem Soc 133:3728–3731
132. Nguyen T-D, Hamad WY, MacLachlan MJ (2014) CdS Quantum dots encapsulated in chiral nematic mesoporous silica: new iridescent and luminescent materials. Adv Funct Mater 24:777–783
133. Revol JF, Marchessault RH (1993) In vitro chiral nematic ordering of chitin crystallites. Int J Biol Macromol 15:329–335
134. Li J, Revol JF, Naranjo E et al (1996) Effect of electrostatic interaction on phase separation behaviour of chitin crystallite suspensions. Int J Biol Macromol 18:177–187
135. Li J, Revol JF, Marchessault RH (1997) Effect of N-sulfonation on the colloidal and liquid crystal behavior of chitin crystallites. J Colloid Interface Sci 192:447–457
136. Tzoumaki MV, Moschakis T, Biliaderis CG (2010) Metastability of nematic gels made of aqueous chitin nanocrystal dispersions. Biomacromol 11:175–181
137. Liu Y, Liu M, Yang S et al (2018) Liquid crystalline behaviors of chitin nanocrystals and their reinforcing effect on natural rubber. ACS Sustain Chem Eng 6:325–336
138. Liu D, Chang Y, Tian D et al (2018) Lyotropic liquid crystal self-assembly of H_2O_2-hydrolyzed chitin nanocrystals. Carbohydr Polym 196:66–72
139. Nge TT, Hori N, Takemura A et al (2003) Synthesis and orientation study of a magnetically aligned liquid-crystal line chitin/poly(acrylic acid) composite. J Polym Sci, Part B: Polym Phys 41:711–714
140. Nge TT, Hori N, Takemura AK et al (2003) Phase behavior of liquid crystalline chitin/acrylic acid liquid mixture. Langmuir 19:1390–1395
141. Matsumura S, Kajiyama S, Nishimura T et al (2015) Formation of helically structured chitin/$CaCO_3$ hybrids through an approach inspired by the biomineralization processes of crustacean cuticles. Small 11:5127–5133
142. Nishimura T, Ito T, Yamamoto Y et al (2008) Macroscopically ordered polymer/$CaCO_3$ hybrids prepared by using a liquid-crystalline template. Angew Chem 120:2842–2845
143. Alonso B, Belamie E (2010) Chitin-silica nanocomposites by self-assembly. Angew Chem Int Ed Engl 49:8201–8204
144. Belamie E, Boltoeva MY, Yang K et al (2011) Tunable hierarchical porosity from self-assembled chitin–silica nano-composites. J Mater Chem 21:16997
145. Boltoeva MY, Dozov I, Davidson P et al (2013) Electric-field alignment of chitin nanorod-siloxane oligomer reactive suspensions. Langmuir 29:8208–8212
146. Nguyen TD, Shopsowitz KE, MacLachlan MJ (2013) Mesoporous silica and organosilica films templated by nanocrystalline chitin. Chemistry 19:15148–15154
147. Nguyen T-D, Shopsowitz KE, MacLachlan MJ (2014) Mesoporous nitrogen-doped carbon from nanocrystalline chitin assemblies. J Mater Chem A 2:5915

148. Sachse A, Hulea V, Kostov KL et al (2012) Efficient mesoporous silica-titania catalysts from colloidal self-assembly. Chem Commun (Camb) 48:10648–10650
149. Sachse A, Hulea V, Kostov KL et al (2015) Improved silica-titania catalysts by chitin biotemplating. Catal Sci Technol 5:415–427
150. Sachse A, Cardoso L, Kostov KL et al (2015) Mesoporous alumina from colloidal biotemplating of al clusters. Chemistry 21:3206–3210

Chapter 4
Nanopolysaccharides in Energy Storage Applications

Chenggang Zhang, Yan Liu, Wenchao Yu, Yang Zhan, Jinyu Wang, Chuanxi Xiong, Zhuqun Shi and Quanling Yang

Abstract In the recent decades, shortages of energy and resource, together with pollution of environment, have become the biggest problems on earth. Thus, construction of novel renewable and biodegradable materials based on nanopolysaccharides, such as nanocellulose, nanochitin or nanochitosan, and nanostarch, and exploration of their energy related applications, have received more and more attention. In this chapter, we review the preparation of nanopolysaccharide-based energy materials as well as their applications in the fields of energy storage, e.g. dielectric capacitor, supercapacitors, batteries, etc.

Keywords Nanopolysaccharides · Dielectric capacitor · Supercapacitors · Batteries

4.1 Introduction

Energy, resource, and environment have become three significant issues in the world. Development of environment-friendly, renewable, biodegradable, and high-performance energy storage materials is in great demand for construction of a low-carbon society. The ongoing surge in demand for high-performance energy storage systems inspires the relentless pursuit of advanced materials and structures.

Nowadays, the most promising energy storage materials are dielectric capacitor, supercapacitors, and batteries (Fig. 4.1) [1]. Dielectric capacitors can release the stored energy in an extremely short period of time to create intense power pulses and this capacity enables many pulsed power applications such as medical defibrillators,

C. Zhang · Y. Liu · W. Yu · Y. Zhan · J. Wang · C. Xiong · Q. Yang (✉)
School of Materials Science and Engineering, Wuhan University of Technology, Wuhan 430070, People's Republic of China
e-mail: yangql@whut.edu.cn

Z. Shi (✉)
School of Chemistry, Chemical Engineering and Life Sciences, Wuhan University of Technology, Wuhan 430070, People's Republic of China
e-mail: zqshi2016@whut.edu.cn

N. Lin et al. (eds.), *Advanced Functional Materials from Nanopolysaccharides*,
Springer Series in Biomaterials Science and Engineering 15,
https://doi.org/10.1007/978-981-15-0913-1_4

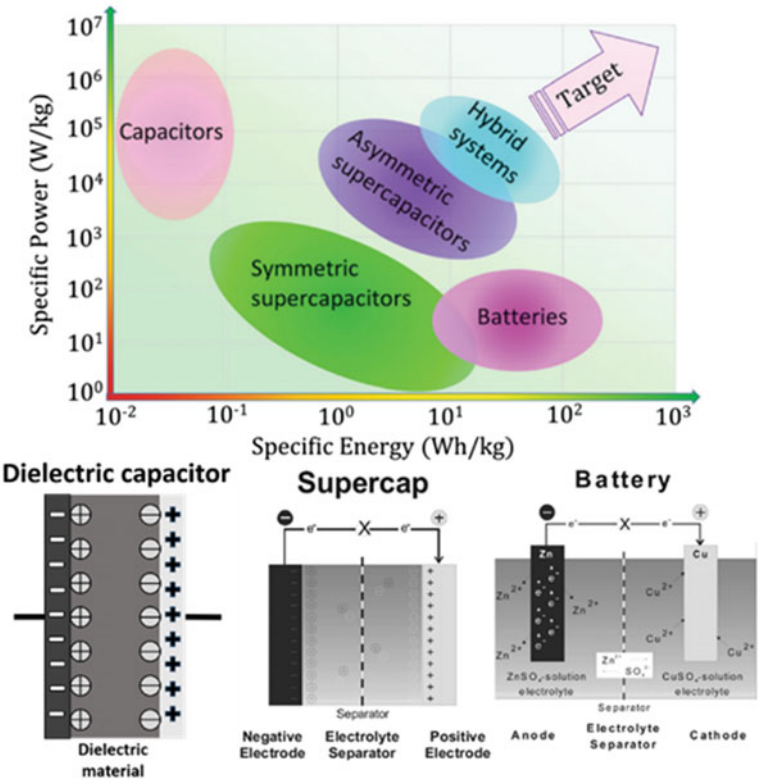

Fig. 4.1 Simplified Ragone plot of the energy storage domains for the dielectric capacitor, supercapacitors and batteries. Reproduced from [1]

transversely excited atmospheric lasers, and advanced electromagnetic systems [2]. They possess high specific power density; however, the specific energy densities of them are usually low. Supercapacitors (SCs) can provide relative high power density and energy density due to the surface charge storing mechanisms and enable many portable/wearable electronic devices including mobile phones, laptops, cameras, smart watch, activity trackers and many more [3, 4]. Batteries with long-cycle life can provide high energy density by storing charge in bulk electrodes through faradaic reactions and can be applied in electric vehicles and portable electronic devices [5]. However, the specific power densities of the batteries are usually relatively low compared with dielectric capacitors and supercapacitors.

Components of energy storage systems are based on inorganic/metal compounds, carbonaceous substances, and petroleum-derived hydrocarbon chemicals [6, 7]. Nowadays for energy storage systems, petroleum-derived synthetic polymers or traditional porous carbon materials are used as matrix, frame or active material [8, 9]. These traditional materials could not meet the requirements of the rapidly developing energy storage systems. Besides the performance and safety enhancements,

the major challenges for the future development of energy storage systems are the reduction of costs, the utilization of green materials, and the development of easily recyclable and up-scalable systems [9].

Nanopolysaccharides are widespread and important in nature, including starch, cellulose, peptidoglycan, chitin and so on. Nanopolysaccharides have enormous industrial importance, especially in the energy field. Cellulose as one of the most important polysaccharides, is commonly applied as electrical insulators, mainly in oil-filled power transformers and paper-insulated power cables [10]. Native cellulose is widely used in the field of dielectric due to its chemical stability, flexibility, low cost and good dielectric property and the dielectric properties of cellulose can be further improved by a series of treatments. Besides in the dielectric field, nanopolysaccharides, such as cellulose and starch, can also be used in the fields of supercapacitors, lithium-ion batteries (LIBs), and post-LIBs as a green material due to its unique 1D structure. Especially, nanocellulose has the high aspect ratio with length of several micrometers and width of a few nanometers, and the chemical functionalities of nanocellulose are also promising for the further applications [11]. Herein, the research of nanopolysaccharides has drawn more and more attention. There will be an introduction about the application of nanopolysaccharides in energy storage system, especially in the fields of dielectric capacitors, supercapacitors and batteries.

4.2 Dielectric Capacitor

Dielectric capacitor is a device with the function of energy storage. It can store energy because of dipole moment. The charged particles in a dielectric are tightly bound by the internal or intermolecular forces of atoms and molecules, so that the charge does not move between the poles and only moves in microscopic scales to form polarization after applied electric field. At the macro level, the two sides of dielectric capacitor have different charges and generate internal electric field. Traditional dielectric materials include ceramics, transformer oil, ferroelectric polymers and so on, and are widely used in electronic devices. The existing polymer-based dielectric materials mainly involve thermoplastic polymers and thermosetting polymers, such as polyvinylidene difluoride (PVDF) [2], biaxially oriented polypropylene (BOPP), epoxy resin, and polyimide. Currently, BOPP is the most widely used flexible dielectric capacitor in the economical electronic devices. However, all of them are nonbiodegradable and nonrenewable.

Cellulose, as environment-friendly, renewable and biodegradable material, has been applied to all sides [12, 13]. Cellulose is an important dielectric material [14–17]. Paper, a kind of cellulose material, is used as dielectric material in insulation system of various power plants after immersion in oil [18]. Cellulose was also used as dielectric layer for applications in green electronics, due to its ultrathin high-k [19–21]. Ji et al. [22] prepared flexible and transparent cellulose nanofiber (CNF) films embed ultralong metal nanofibers, and applied them to flexible touchscreen panels (Fig. 4.2a, c) with high dielectric constants (above 9.2) and high transmittance of 90%. Yang

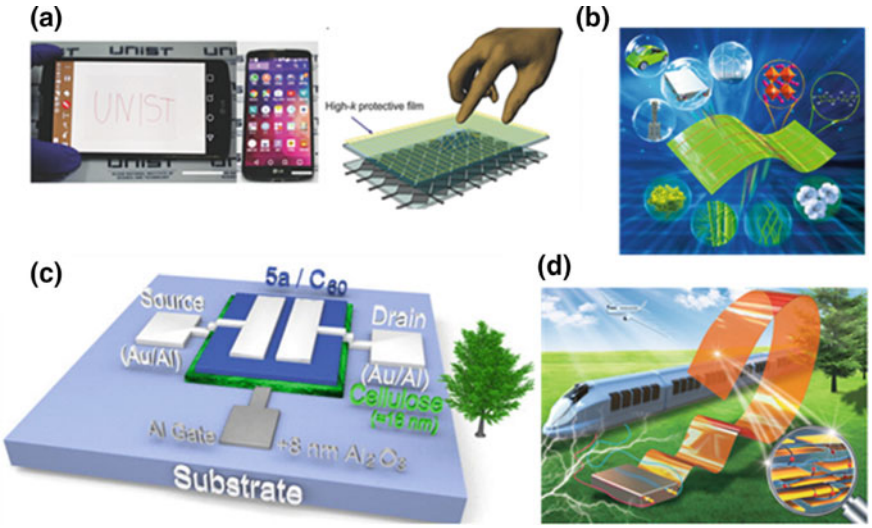

Fig. 4.2 High dielectric performances of flexible and transparent cellulose-based hybrid films. Reproduced from [19, 22–24]

et al. [23, 24] prepared cellulose-based dielectric capacitor with high discharged energy storage in the electronic devices, as shown in Fig. 4.2b, d. Cellulose can also be used as a reinforcing material to enhance the dielectric constant [25–27].

However, the availability of the biodegradable cellulose as a matrix for flexible dielectric capacitor has rarely been demonstrated so far. Zeng et al. tried introducing conducting particles into cellulose matrix to prepare dielectric materials. They reported a kind of flexible dielectric paper based on CNF and carbon nanotubes (CNT). They used CNT to improve the dielectric constant of CNF papers [28]. The obtained composite paper possessed a high dielectric constant of 3198 at 1.0 kHz, as shown in Fig. 4.3, but low dielectric energy storage capability (0.81 J cm^{-3}). Kafy et al. prepared cellulose-based nanocomposite by incorporating graphene oxide (GO) nanoplatelets modified with hexamethylene diisocyanate grafting agent useful for such versatile applications [20], and the schematic mechanism is shown in Fig. 4.4. Raghunathan et al. [29] reported that they coated regenerated cellulose with polypyrrole to enhance dielectric properties. While the high dielectric loss and low breakdown strength of these composite films limited the practical application. Therefore, increasing breakdown strength is the key to solve the disadvantage of the cellulose-based dielectric capacitor. Jia et al. [30, 31] used barium titanate as a filler for improving the dielectric property of cyanoethyl cellulose and possessed a high dielectric constant of 147.30 at 100 Hz. While the constant loss of cyanoethyl cellulose composites films was still high. Wu et al. [32] prepared a collapsible, strong, and highly thermally conductive film based on oriented functionalized boron nitride nanosheets and cellulose nanofiber, with low dielectric constant of 4.86 and low dielectric loss of 0.07 at 1000 Hz, respectively.

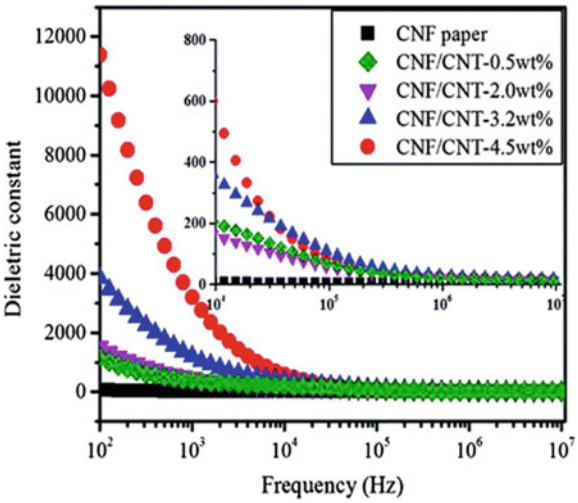

Fig. 4.3 Chemical network structure of cellulose, attributing the hydrogen bonding linkages (dashed lines). The inset illustrates the Fourier transform infrared spectra (measured in attenuated mode) of native cellulose. Reproduced from [28]

To improve the breakdown strength and reduce the dielectric loss, Yang et al. introduce inorganic nanosheets with high breakdown strength to the cellulose matrix [23, 33]. Boron nitride nanosheets (BNNS) [34] were added to 2,2,6,6-tetramethylpiperidine-1-oxyl radical (TEMPO)-oxidized cellulose nanofibrils (TOCNs) [35, 36] to prepare dielectric films followed by cross-linking through immersion in $CaCl_2$ solution [23]. The breakdown strength of these cross-linked TOCN/BNNS (CLTOCN/BNNS) composite films increased obviously compared with the original TOCN/BNNS films and the CLTOCN/BNNS films showed high discharged energy density and high charge-discharge efficiency, as shown in Fig. 4.5. The highest breakdown strength of these composite films was 380 MV m^{-1} and the relevant highest energy density was 3.9 J cm^{-3}.

Furthermore, regenerated cellulose (RC) showed higher strength and thermal stability compared with raw cellulose [37] after dissolution and regeneration. The transition from cellulose I to cellulose II has taken place in the RC film formation process [38]. Yang et al. prepared a series of nanocomposites with nanolayered structure from BNNS and RC [33]. The energy density of the composite film could reach 4.1 J cm^{-3}, twice as much as commercial BOPP [39], as shown in Fig. 4.6. And the thermal conductivity (TC) of the composites was also studied. RC possessed a TC of 0.035 W m^{-1} K^{-1}, and a much higher TC of 2.97 W m^{-1} K^{-1} was obtained after incorporation of 30 wt% BN. This is about 84 times higher than that of the RC film and makes it possible for cellulose to work in a high temperature environment. Meanwhile, ceramic nanofillers, i.e. $BaTiO_3$ nanoparticles (BTNP) and $BaTiO_3$ nanofibers (BTNF), were also incorporated in cellulose matrix to prepare the flexible composite films. The flexible and biodegradable cellulose-based dielectric films exhibited an ultrahigh discharged energy density of 13.14 J cm^{-3} at breakdown strength of 370 MV m^{-1} [24], the highest of reported biomass-based films (Table 4.1). At 300 MV/m^{-1}, RC-2BTNF possess high discharged energy density

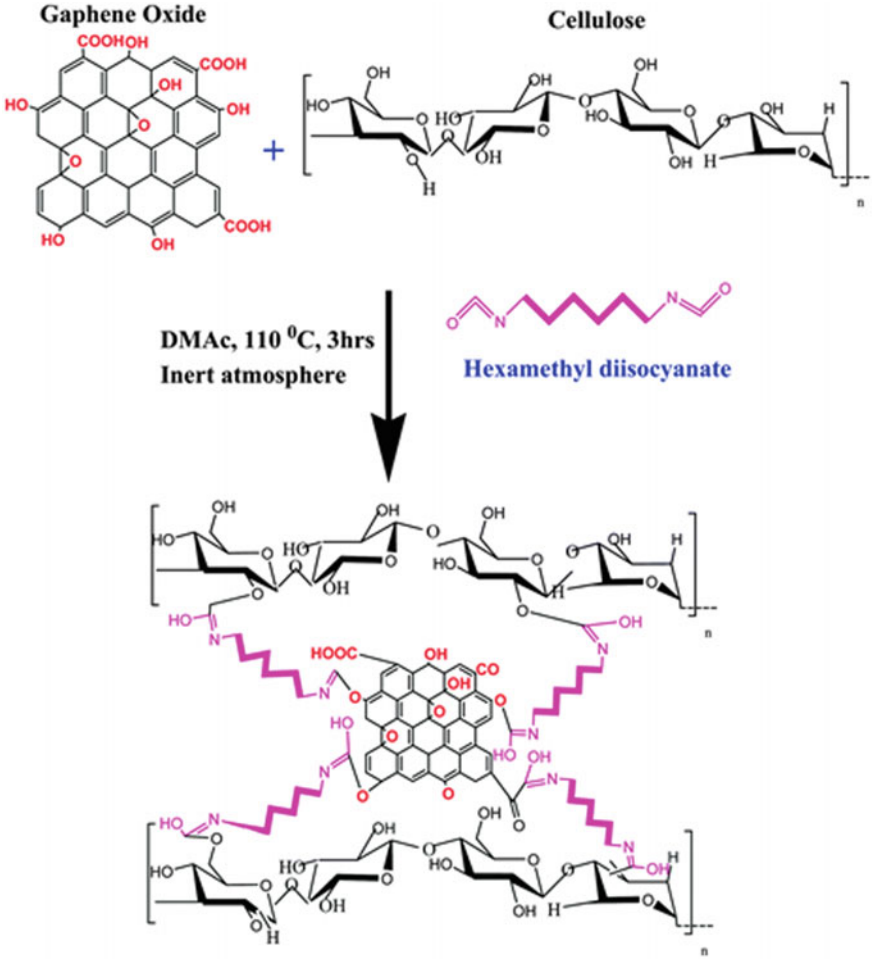

Fig. 4.4 Reaction mechanism of cellulose with GOs grafted using hexamethylene diisocyanate. Reproduced from [20]

(9.45 J cm^{-3}), higher those of reported polymer-based dielectric films (closed to actual electric field strength when film capacitors work), as shown in Fig. 4.7.

Cellulose exhibits good dielectric properties and paper as a dielectric material has been used as capacitor in power plants or transformers for a long time, while there are still not many researches on the dielectric properties of cellulose so far. The hydrophilicity of cellulose hinders their further practical applications. Therefore, future research should be focused to improve the hydrophobicity of cellulose-based dielectric capacitor and keep their high dielectric properties at high humid condition. Cellulose could be a good choice as dielectric materials instead of synthetic polymers after solving the problem of moisture absorption.

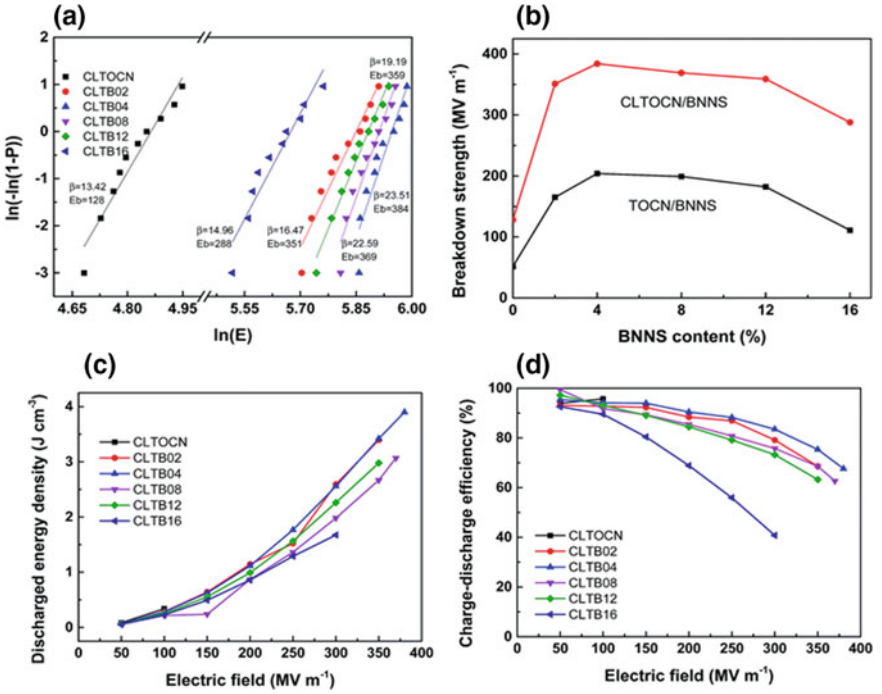

Fig. 4.5 **a** Weibull plots of CLTOCN/BNNS composite films, **b** breakdown strengths of TOCN/BNNS and CLTOCN/BNNS composite films with different volume fractions of BNNSs, **c** discharged energy densities, and **d** efficiency of CLTOCN/BNNS films with different volume fractions of BNNSs. Reproduced from [23]

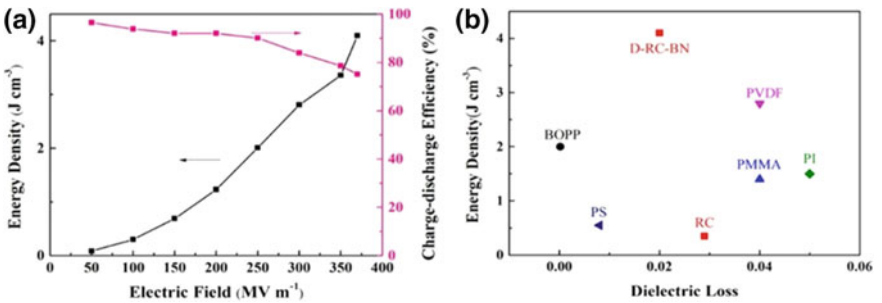

Fig. 4.6 **a** Energy density and charge-discharge efficiency of the RC-BN10 film pre-pared via regeneration in acetone followed by vacuum drying with various applied electric fields at 100 Hz. **b** Energy density versus dielectric loss of RC-BN10 and other dielectric polymers. Reproduced from [33]

Table 4.1 Dielectric properties of the reported cellulose-based materials [18, 20–23]

Samples	Dielectric constant (at 100 Hz)	Dielectric loss (at 100 Hz)	Breakdown strength (MV m^{-1})	Discharged energy density(J cm^{-3})
TOCN-BN	8	0.03	380	3.9
RC-BN	7.2	0.02	370	4.1
RC-CNT	3000	1	42.5	0.81
C-GO	150	5	30	0.012
RC-PPy	16,000	1000	–	–
RC-BTNF	12.3	0.02	370	13.14

Abbreviations TOCN-BN: TEMPO-oxidized cellulose nanofibril/boron nitride composites; RC-BN: Regenerated cellulose/boron nitride composites; RC-CNT: Regenerated cellulose/carbon nanotube composites; C-GO: Cellulose/graphene oxide composites; RC-PPy: Regenerated cellulose/polypyrrole composites; RC-BTNF: Regenerated cellulose/barium titanate composites

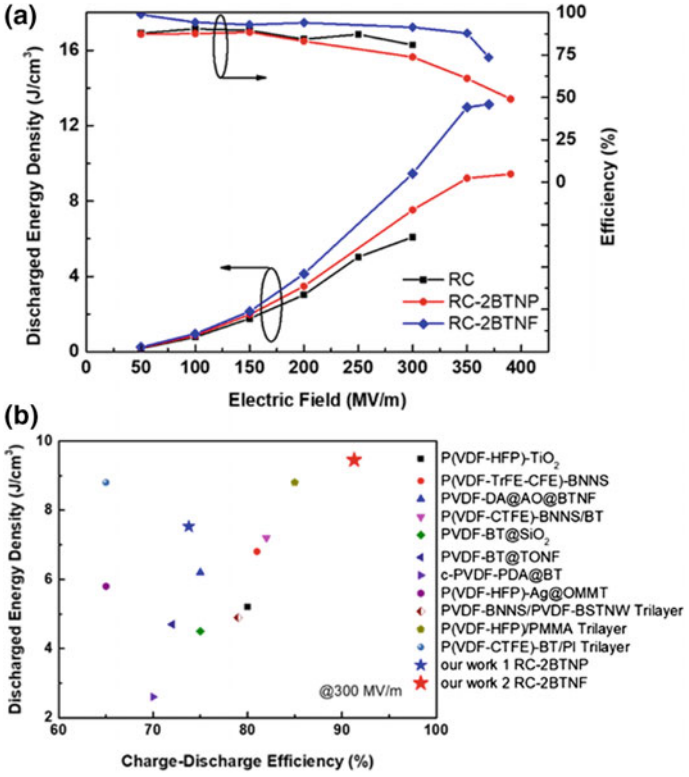

Fig. 4.7 **a** Energy density and charge-discharge efficiency of the RC, RC-2BTNP, RC-2BTNF films. **b** Discharge energy density versus efficiency of RC-2BTNP, RC-2BTNF and other dielectric polymer composites at 300 MV m^{-1}. Reproduced from [24]

4.3 Supercapacitors

Conventional capacitors can only store a small amount of energy, mainly due to the limitation of the distance between the electrodes and the limited surface area. Compared to general capacitors, the effective capacity of supercapacitors is several orders of magnitude higher due to that the electrode materials of supercapacitors usually have a relatively large specific surface area, the charge is stored at the interface between the electrolyte and the electrode and the distance of electrolyte ion transport is greatly reduced. Compared with batteries, supercapacitors have the advantages of high power density, fast charge and discharge rate and long cycle life. Supercapacitors are mainly composed of positive and negative electrodes, separator and electrolyte. Supercapacitors can be divided into electrical double layer capacitors (EDLC) and pseudo capacitors according to the different energy storage mechanism [40]. The energy storage of EDLC is achieved by the adsorption and desorption of electrolyte ions between the electric double layers. Since no chemical reaction occurs during the whole energy storage process, the electrochemical properties of EDLC are related to the properties of electrode materials (conductivity, specific surface area, pore structure, etc.) and the wettability between electrode material and electrolyte, and the electric field between the electric double layers. In contrast, pseudocapacitors store charge through a fast reversible redox reaction, which mostly use transition metal oxides and conducting polymers (the relatively high theoretical capacities) as electrode materials. The main problems of these materials are poor cycling stabilities and mass transport limitations.

For a long time, nanopolysaccharides and its derivatives have played an important role in traditional industries such as food additives, textiles and construction [41]. Nanopolysaccharide is a flexible insulating material. If the surface of nanopolysaccharide is covered with a conductive layer or conductive fillers are blended, it is effective to improve the conductivity of nanocomposites and it can be used as an active material for energy storage applications. Hence, biocompatibility, wide availability, intrinsic mechanical strength and flexibility of nanocomposites can be applied to the development of supercapacitors and batteries. Numerous nanopolysaccharide-based supercapacitors, where nanopolysaccharide is used as a flexible substrate for structural reinforcement or as a composite framework, have shown promising electrochemical properties. The produced electrode combines flexibility and excellent mechanical properties, and nanopolysaccharides hold great promise for the design of portable energy storage device devices, especially for supercapacitors that will meet our growing demand for energy, power and sustainability.

Cellulose Nanofibers (CNFs) can be extracted by high-speed shearing, high pressure or ultrasonic treatment; the cross-sectional dimension of it is usually 3–20 nm. CNF-based electrode materials have pore structures which are extremely easy to adsorb electrolyte and CNF is an ideal framework supporting material for energy storage material. They mainly utilize capacitive nanomaterials (such as electronically conducting polymers (ECPs), metal oxides, and carbon materials) to manufacture electrode materials forming compact films and hydrogels. At present, the preparation

of self-doped porous carbon electrodes using various biomass materials as carbon sources has become a hot topic in the field of energy storage and conversion. In particular, the biomass material can be used as a carbon source by a number of specific methods to prepare an electrode material in which nano-scale porous carbon can be obtained with high specific surface area, hetero atom doping, or complex with a transition metal oxide.

4.3.1 Carbon/CNF Composites

Carbon-based conductive materials like graphene and carbon nanotubes (CNTs) can be introduced into the interconnected CNF fiber network to form strong, highly conductive networks suitable for supercapacitors due to the exceptional mechanical, chemical and thermal stability.

As active materials in electrodes, CNTs not only are highly conductive and flexible, but also can increase the effective surface area in the composites. Nevertheless, CNTs tend to aggregate into bundles due to the hydrophobicity of the sidewalls. Recently, it mainly solves the problem by chemical or physical means to improve its dispersion in water and these methods used for the preparation of CNTs-based supercapacitors may cause environmental pollution and decreased conductivity. Shao and co-workers [42] prepared a CNFs/CNTs hybrid aerogel in which CNFs played a role in dispersion and supported the porous structure. These aerogel composite electrodes can reach a capacitance as high as 178 F g^{-1} (based on the mass of CNTs) at a scan rate of 5 mV s^{-1} in the flexible, all-solid-state supercapacitors (Fig. 4.8a). Wågberg and co-workers [43] reported a compressible, three-dimensional (3D) supercapacitor based on layer-by-layer (LbL) assembly of SWCNTs on cross-linked CNF aerogels. A cationic polyethyleneimine (PEI) layer and an anionic (–COOH-functionalized) SWCNT layer were used as active materials with a layer of PEI/polyacrylic acid as the separator and electrolyte. The 3D supercapacitor showed almost perfect cyclic performance and the specific electrode capacitance was calculated to be 419 ± 17 F g^{-1} (Fig. 4.8b–c).

Reduced graphene oxide (rGO) aerogel has the advantages of light weight, porosity, large specific surface area, good electrical conductivity and mechanical properties; their porous structures enhance the electrolyte absorption properties and provide a charge conduction path of the active material carried on the graphene sheet layer. A CNF-rGO hybrid aerogel [44] was prepared by supercritical CO_2 drying using CNFs as the dispersing agent for the rGO. These aerogel composite electrodes achieved a specific capacitance of 207 F g^{-1} at a scan rate of 5 mV s^{-1} (Fig. 4.8d). Zheng et al. [45] reported a flexible all-solid-state supercapacitor based on CNF/rGO/CNT electrodes and H_2SO_4/PVA gel as the electrolyte. The resultant compressible CNF/rGO/CNT hybrid electrode can reach a specific capacitance as high as 252 F g^{-1} at a discharge current density of 0.5 A g^{-1}. In addition, the device exhibited significant cycling stability, and the capacitance remained above 99.5% after 1000 charge and discharge cycles with a current density of 1 A g^{-1} (Fig. 4.8e).

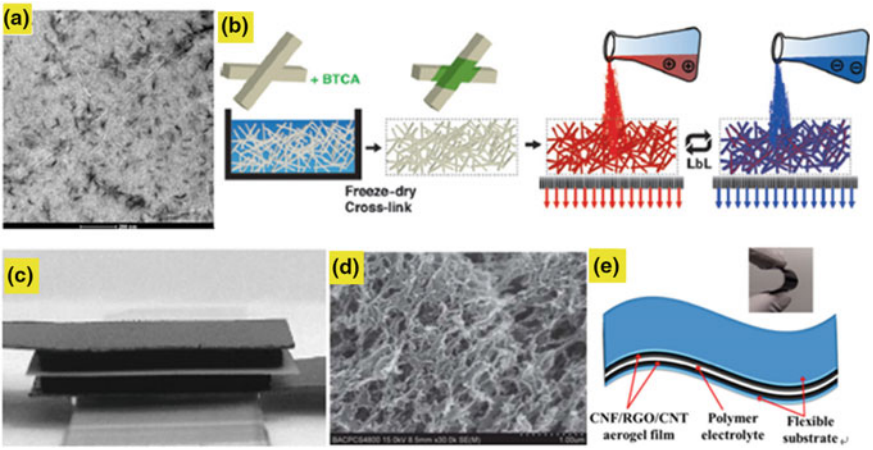

Fig. 4.8 **a** TEM image of the CNFs/CNTs suspension. Reproduced from [42]. **b** Representations of the cross-linking in NFC, and aerogel construction and the LbL assembly on aerogels. **c** Photograph of a supercapacitor device with two (PEI/SWCNT) $_5$ aerogels sandwiched with a spacer and connected to an anode and cathode graphite foil at top and bottom. Reproduced from [43]. **d** SEM of CNFs-RGO (10%) hybrid aerogel. Reproduced from [45]. **e** Schematic diagram of the all-solid-state supercapacitor where the polymer-gel electrolyte serves as the electrolyte and the separator. Inset shows the flexibility of the device. Reproduced from [44]

4.3.2 ECP/CNF Composites

Since the 1970s, it has been found that the polymer materials itself or the structures of it after doping have conductive function, and the high conjugate of the large π-health in the main chain provides unique optical, electrical and electrochemical properties. The main conductive polymer materials, such as polyacetylene, polyaniline (PANI), polypyrrole (PPy), polythiophene (PTh). Compared to carbon-based supercapacitors, ECP have a higher specific capacitance due to their store charge in the holes of the material by redox reactions to increase stored energy and reduce self-discharge. But the main problem with ECP based supercapacitors is generally considered to be their poor cycling stabilities. CNFs are appealing substrates for ECPs because of their ability to form mechanically flexible, robust structures when covered with the polymers.

Conductive polymer monomers are attached to the interior or surface of the nanocellulose network by chemical oxidation or electrochemical to obtain CNF/ECP composites. Zhang et al. [46] deposited Ag particles on the surface of the CNF aerogel to obtain a fast electron transport channel, and then coated the PANI nanoparticles on the surface of the Ag particles to obtain a supercapacitor electrode material with high capacitance performance. The assembled supercapacitor has a specific capacitance of 176 mF cm^{-2} and electrochemical performance does not change even if bent at will (Fig. 4.9a). Shen et al. [47] prepared freestanding and highly conductive electrodes by mixing multi-walled carbon nanotubes, PPy and CNFs obtained from

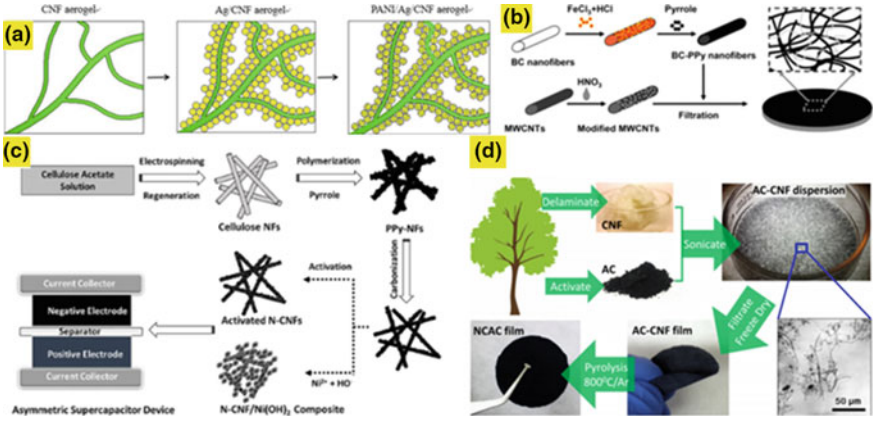

Fig. 4.9 **a** Fabrication process of Ag/PANI/CNF aerogel electrodes. Reproduced from [46]. **b** Schematic of the synthesis procedure of BC/PPy nanofibre/MWCNTs hybrid membrane. Reproduced from [47]. **c** Schematic illustration of the procedure to prepare NF electrode materials and the supercapacitor device. Reproduced from [48]. **d** The concept of sustainable energy storage solution using components from renewable resources: cellulose nanofibers (CNF) and activated carbon (AC). The photomicrograph in the right bottom corner highlights the flocculent structure of AC-CNF in aqueous dispersion. Reproduced from [49]

bacterial nanocellulose (BC), which were studied in a standard three-electrode system in LiCl solution, had a high capacitance of 2.43 F cm^{-2} at a mass of 11.2 mg cm^{-2} (Fig. 4.9b). Moreover, device prepared by the electrode can offer large capacitance (590 mF cm^{-2}) and excellent cycling stability (94.5% of initial capacity after 5000 cycles).

In addition to being used as a mechanical reinforcement of the active conductive material, nanocellulose can also be used as a carbon source to obtain a carbonized fiber layer for use as a supercapacitor electrode. Cai et al. [48] coated PPy on nanocellulose for carbonization as a negative electrode material, and then mixed the carbonized material with $Ni(OH)_2$ as a positive electrode, successfully assembled asymmetric supercapacitors with high energy density, specific capacitance, and outstanding cycle life (Fig. 4.9c). The $Ni(OH)_2$ nanoparticles on the carbon nanofibers can infiltrate the electrolyte well, and carbon matrix imparts high conductivity to the electrode, synergistically promotes the redox reaction and improves the capacitance performance. The specific capacitances of the positive and negative electrodes are 1045 and 236 F g^{-1} relatively, the energy density achieved 51 W h kg^{-1}, the power density is 117 kW kg^{-1} and the capacitance retention rate reaches 84% after 5000 cycles. Moreover, Li et al. [49] mixed CNF and activated carbon (AC) to form films, which were used as supercapacitor electrodes after carbonization at 800 °C for 2 h in an argon atmosphere. There is a strong interaction between CNF and AC after carbonization and this network structure has good ion transport efficiency. Compared to pure AC electrodes, it has higher current density and cycle stability, and the capacitance retention rate achieves 92% after 10,000 cycles (Fig. 4.9d).

4.3.3 Biomass-Derived Porous Carbon

In recent years, biomass-derived carbon electrode materials for energy storage have attracted great attention due to their wide availability, regeneration and low cost. More importantly, their inherently uniform and precise biological structure can be used as a template for the fabrication of electrode materials with controlled and well-defined geometries. At the same time, the basic elements of biomass are carbon, phosphorus, sulfur and nitrogen. The special natural ordered layered structure and the rich surface properties of biomass-derived carbon materials are compatible with electrochemical reaction processes such as ion transfer and diffusion [50].

4.3.3.1 One-Dimensional Biomass-Based Carbon Electrode

One-dimensional (1D) biomass nanostructures, which typically include fibrous and tubular structures among other morphologies have been identified as the most viable structures for high performance supercapacitors and other various applications due to the excellent mechanical properties, abundant reactive hydroxyl groups on the surface and high aspect ratio etc.

Cellulose is the most abundant renewable green resource on earth, it has all the advantages of biomass materials for supercapacitors, such as high carbon content, abundant chemical reaction sites, advantageous mechanical properties, high specific surface areas. Cai et al. [51] produced nitrogen-doped carbon nanofibers by electrospinning a cellulose acetate solution with subsequent deacetylation and pyrolysis. The corresponding electrode showed specific capacitance of 241.4 F g^{-1} at 1 A g^{-1} with high capacitance retention of 84.1% even at 10 A g^{-1}, indicating good rate capability and non-kinetic limited performance (Fig. 4.10a). Lignin is a by-product of the pulp and paper industry. Similarly, it is used for high value for supercapacitors. Berenguer et al. [52] demonstrated that interconnected porous lignin-carbon fibers could be easily controlled by an appropriate heating rate during stabilization. When lignin fibers were thermally stabilized at a slightly faster heating rate, their partial softening and interconnection at contact points between the fibers occurred during carbonization. The fiber-fiber interconnections facilitated charge transfer and higher capacitance. Furthermore, the control of the porous structure of the fibers for electrical double layer capacitors (EDLCs) plays a key role. Jin et al. [53] reported a series of activated carbon fibers (ACFs) made from one-step carbonization and water vapor activation of wood fibers. A longer activation time created more mesopores that are connected reciprocally, which are important for the accessibility of the inner micropores by the electrolyte. The sample with an optimal structure exhibited outstanding specific capacitance of 280 F g^{-1} at 0.5 A g^{-1} and high capacitance retention of 99.3% after 2000 cycles. Particularly, compared to nanofibers, the hollow tubular structure can be used as a buffer tank for electrolytes and has a higher specific surface area to provide a more active contact site. Liu et al. [54] reported a method that

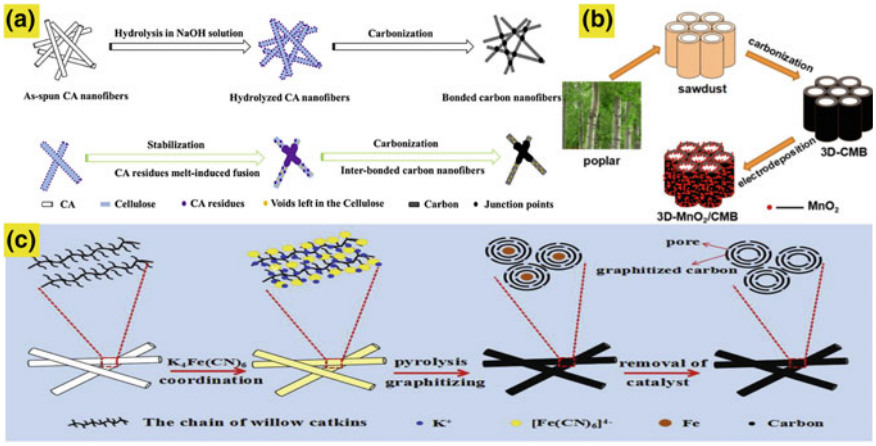

Fig. 4.10 **a** Schematic illustration of carbon nanofiber preparation and formation mechanism of inter-boned carbon nanofibers. Reproduced from [51]. **b** Schematic of the synthesis of 3D-MnO_2/CMB. Reproduced from [55]. **c** Schematic preparation procedure of PGCMT materials. Reproduced from [56]

activated carbon fibers with a hierarchical nanostructure were prepared by the pretreatment of fibers in NaOH/urea solution and a subsequent carbonization process. The hierarchically porous structure and the well retained hollow microstructure could simultaneously minimize the diffusion/transfer resistance of the electrolyte and electrons and maximize the surface area utilization for charge accumulation. It exhibited enhanced electrical double layer capacitance of 221.7 F g^{-1} at 0.3 A g^{-1} and excellent cycling stability with 95.4% retention after 6000 cycles at 2 A g^{-1}. Based on the above methods, the introduction of transition metal oxides can significantly increase the specific capacitance. Zhang et al. [55] reported 3D MnO_2/carbon microtube bundles that contained carbon microtube bundles (CMB) produced from sawdust and 3D nanostructured MnO_2 through anodic electrodeposition. The structure provides multiple channels for electron transport and allows multiple active sites to contact the electrolyte. The as-obtained electrode derived from the composite exhibited high specific capacitance of 617.6 F g^{-1} at the current density of 1 A g^{-1} and excellent cycle performance (Fig. 4.10b). Zhang et al. [56] used $K_4Fe(CN)_6$ to treat willow catkins and obtained porous graphitic carbon by carbonization. The enhanced conductivity of the porous graphitic carbon microtube (PGCMT) provided sufficient space for the deposition of MnO_2 and effectively alleviated MnO_2 accumulation. PGCMT/MnO_2 showed good rate capability with capacitance retention of 61.8% even at 50 A g^{-1} (Fig. 4.10c).

4.3.3.2 Two-Dimensional Biomass-Based Carbon Electrode

Two-dimensional (2D) carbonaceous materials with abundant sp^2 hybridizations show great potential in energy storage and conversion. The following advantages are the reasons: abundant active sites on the surface, high aspect ratio, rich active surface edge and their in-plane defect active sites facilitate charge storage and the internal free space of two-dimensional porous carbon nanosheets can greatly buffer the volume changes during the charge/discharge cycles etc.

In recent years, some 2D graphene-based carbon nanosheets have been successfully prepared from renewable and inexpensive biomass by an efficient process for decreasing the cost and expanding the applications of biomass-based materials. Purkait et al. [57] prepared few-layered graphene-like nanosheets by KOH activation of peanut shells and a subsequent mechanical exfoliation method. The resulting carbonaceous material with graphene-like nanosheets possessed abundant micropores as well as mesopores. The cell assembled with the few-layered graphene-like nanosheet electrode exhibited the highest energy density of 58.13 W h kg^{-1} and the energy density up to 37.5 kW kg^{-1} without any binder in 1 M H_2SO_4 as the electrolyte (Fig. 4.11a). Heteroatom doping can effectively reduce charge transfer resistance and enhance wettability, thereby increasing the capacitive performances. So, many biomass materials are widely used in the electrode materials of supercapacitors due to the self-doping characteristics of heteroatoms. Qian et al. [58] prepared self-doped nitrogen porous carbon flakes via carbonization of Chinese human hair fibers. The resulting materials not only inherited the natural lamellar structure of the human hair, but also developed a micro/mesoporous structure with relatively high self-doped nitrogen content in the resulting carbon. The optimized nitrogen-doped

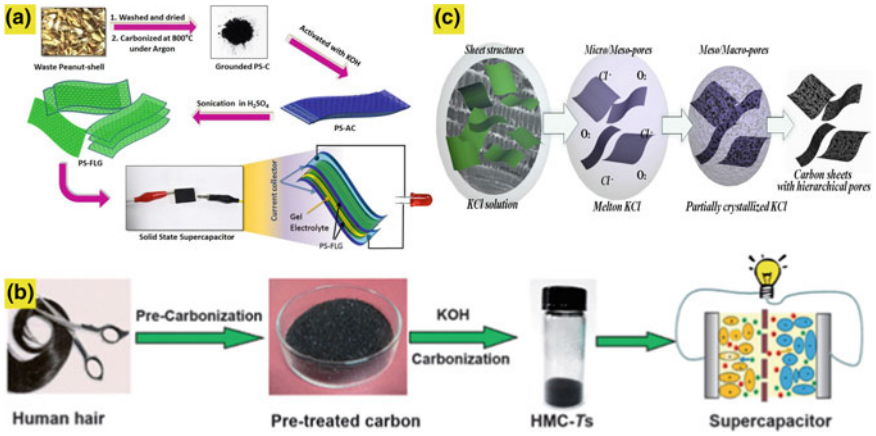

Fig. 4.11 **a** Schematic representation for the synthesis of PS-FLG active material and its subsequent integration into a solid-state device. Reproduced from [57]. **b** Flow diagram for the fabrication of HMCs. Reproduced from [58]. **c** Illustration on the formation of carbon sheets with hierarchical pore structures in the molten salt sealing strategy. Reproduced from [59]

porous carbon flakes exhibited specific capacitance of 340 F g^{-1} in 6 M KOH at current density of 1 A g^{-1} and good stability with capacitance retention of 98% over 20,000 cycles (Fig. 4.11b). Not long ago, Wang et al. [59] reported highly porous carbon sheets with high specific areas and self-doped nitrogen fabricated by the one-step carbonization of fresh clover stems with potassium chloride as the dual function agent. Potassium chloride not only protects the carbon structure produced from high temperature air, but also achieves a high specific surface area by constructing a hierarchical porous structure in a one-step carbonization process. The electrode from carbon sheet displayed high specific capacitance of 436 F g^{-1} at 1 A g^{-1} and excellent rate capacity with 290 F g^{-1} capacitance at 50 A g^{-1} (Fig. 4.11c). Agaric has rich chitin and volumetric swelling performance; it is beneficial for carbon precursor to form self-doped nitrogen carbon materials with high specific surface areas and optimized pore structures. Hu et al. [60] reported the preparation of hierarchically porous nitrogen-doped carbon nanosheets (HPN-CS) from agaric through a one-step method. Due to the unique volumetric swelling property of agaric, potassium hydroxide and urea in the solution easily infiltrate into the cell walls of agaric to form an inbuilt activating agent. Ling et al. [61] reported a facile yet sustainable approach for the large-scale production of B/N co-doped carbon nanosheets by assembling long-range-order gelatin molecules in a 2D boric acid template, followed by pyrolysis. The obtained B/N co-doped carbon electrode delivered extraordinary specific capacitance of 358 F g^{-1} at 0.1 A g^{-1}, excellent rate performance, and good stability over 15,000 cycles. It is also a feasible method to use the hydrophobicity of materials for self-assembly and then carbonization to produce desired structure. You et al. [62] report a method of hydrophobization-induced interfacial-assembly to produce an unprecedented type of nanosheets from marine chitin. Combining emulsifying and carbonization can further convert these 2D precursors to carbon nanosheets, the electrode from carbon nanosheets showed 237.0 F g^{-1} at 1 A g^{-1}, together with a high capacity retention of ≈74% at a current density of 10 A g^{-1}. After 10,000 charge–discharge cycles at 5 A g^{-1}, these carbon nanosheets still have a capacity retention up to 95%.

4.3.3.3 Three-Dimensional Biomass-Based Carbon Electrode

A 3D microstructure with well-interconnected mesopores, micropores and macropores provides a continuous electron pathway for good electrical contact. Among them, micropores are beneficial for energy storage and macropores shorten ion transport pathways; this is essential for designing high performance electrode materials. Therefore, how to design a well-structured 3D material is worth exploring.

Intrinsic structure and pores of biomass can be inherited well during the preparation of carbon materials. So direct carbonization of biomass and then activation is a simple way to get 3D carbon materials. Ma et al. [63] reported an advanced high-value 3D hierarchical porous carbon obtained by the direct pyrolysis of KOH-pre-treated corn husks. The obtained 3D hierarchical porous carbon exhibited superior capacitive performances including high specific capacitance of 356 F g^{-1}, high rate performance

(retention of 84.3% from 1 to 20 A g^{-1}), high energy density of 21 W h kg^{-1} (in Na_2SO_4 aqueous electrolyte), and good cycling stability (95% capacitance retention after 2500 cycles). Liang et al. [64] demonstrated a novel 3D honeycomb-like porous carbon (HLPC) prepared by carbonizing pomelo peels, followed by KOH activation. The as-obtained HLPC exhibited excellent specific capacitance of 342 F g^{-1} at 0.2 A g^{-1} and good cycling performance with 98% retention over 1000 cycles at 10 A g^{-1} in 6 M KOH. How to get excellent mechanical properties of carbon materials is a problem and challenge. Duan et al. [65] prepared nanofibrous microspheres by using chitin solution dissolved in NaOH/urea aqueous solvent at low temperature, and subsequently fabricated the novel elastic nitrogen-doped carbon microspheres by pyrolyzing the chitin microspheres. Moreover, the carbon microspheres exhibited an outstanding rate capability with a capacitance retention of ~50% when increase the scan rate from 5 to 10,000 mV s^{-1} as well as good cycling stability for supercapacitor applications (Fig. 4.12a). Based on above method, increasing specific capacitance by introducing conductive polymer, such as PANI etc. Gao et al. [66] prepared hierarchically porous carbon microspheres (HCM) by directly pyrolyzing the chitin microspheres derived from chitin/chitosan blend solution, in which chitosan was used as a nanopore/nanochannel forming agent to construct microspheres. In order to apply HCM as a hybrid electrode material to supercapacitors, polyaniline (PANI) nanoclusters were further deposited on the surface of HCM. Symmetric supercapacitor (SSC) based on HCM-PANI exhibited excellent rate capability with 64% retention as the scan rate increased from 2 to 500 mV s^{-1} (Fig. 4.12b). The porous

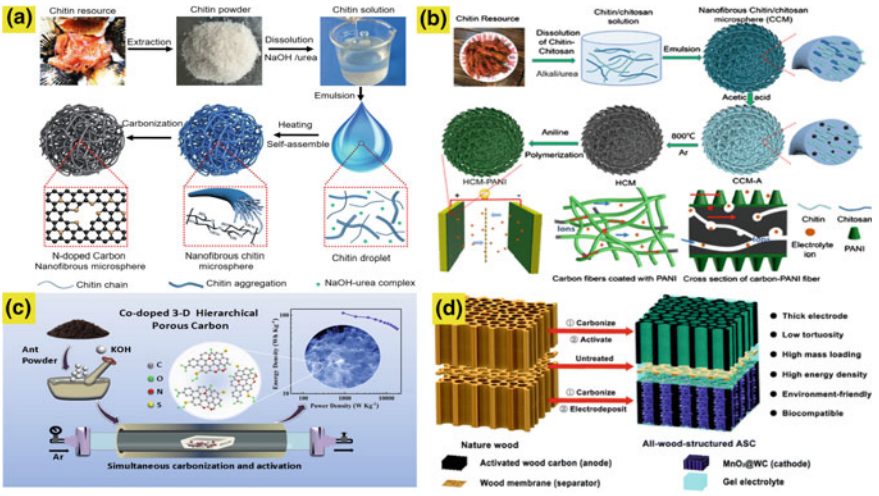

Fig. 4.12 **a** Graphical illustration of the formation process for the nanofibrous carbon microspheres. Reproduced from [65]. **b** Graphical illustrations of the formation process, two-electrode system and porous structure of the nanofibers for HCM-PANI. Reproduced from [66]. **c** Schematic illustration of the production processes for the 3-D hierarchical porous carbons. Reproduced from [67]. **d** Graphical illustration of the design concept and construction process of the all-wood-structured supercapacitor. Reproduced from [69]

structure with abundant active sites can also be generated by direct carbonization without the additional activation agents. Zhao et al. [67] reported the production of HPCs using ant powder as the precursor. The exoskeleton of ant contains chitin and helps to create a tough 3D scaffold frame, while the high protein and fatty acid composition forms highly porous carbon co-doped with heteroatoms. Thereby, the obtained carbon afforded high specific capacitance of 352 F g^{-1} at 0.1 A g^{-1}, good rate retention of 80% from 1 to 10 A g^{-1}, and high cycling stability (5% loss over 10,000 cycles) (Fig. 4.12c). Combine with pseudo-active materials as novel nanocomposite electrode materials to improve the specific capacitance is a promising method in the coming years. Yu et al. [68] prepared well-ordered PANI nanowire arrays aligned on both the inner and outer surfaces of the hierarchical porous carbon (HPC). An asymmetric supercapacitor based on HPC/PANI as the positive electrode and HPC as the negative electrode was successfully assembled within a voltage window of 0–1.8 V in 1 M Na_2SO_4 aqueous electrolyte, achieving high specific capacitance (134 F g^{-1}), high energy density (60.3 W h kg^{-1}) and excellent cycling stability (good capacitance retention of 90.6% after 5000 cycles). Assembling high-performance supercapacitor materials into devices is a challenge and opportunity in ordinary life. Chen et al. [69] designed an all-wood-structured asymmetric supercapacitor (ASC) based on an activated wood carbon (AWC) anode and a MnO_2/wood carbon (MnO_2@WC) cathode. For the cathode, the uniform growth of the MnO_2 nanosheets on and even inside the wood carbon channels was realized by a typical electro deposition method, which could be attributed to the multi-channeled structure along the tree growth direction of the wood carbon that could facilitate efficient ion penetration throughout its entire surface. The combination of the two electrode materials enabled the all-wood-structured ASC device to demonstrate remarkably high energy/power densities (Fig. 4.12d).

Table 4.2 summaries the electrochemical properties of the reported biomass-based materials. Nanopolysaccharides is expected to be used in flexible supercapacitors due to its excellent mechanical properties and large specific surface area. However, there are still some shortcomings in large-scale applications. And the application of carbon materials derived from biomass materials is still a huge challenge because of its weakness in mechanical properties. Even if the electronic devices could be obtained through modification, the cost and time of producing materials cannot be ignored. In addition, the energy density of supercapacitors is generally not high, and the energy density and power density can be improved by adjusting the structure of the electrode material and the properties of the active material, which is a long-term challenge.

4.4 Batteries

As an emerging energy storage device, supercapacitors have a lot of advantages, such as high power density, fast charge and discharge rate, and long cycle life. However, even many methods have been reported to improve the energy density of

Table 4.2 Electrochemical properties of the reported nanopolysaccharide-based materials [43–69]

Samples	Specific capacitance	Capacitance retention	Energy density	Power density
CNF/rGO	207 F g^{-1} (at 5 mV s^{-1})	99.1% (at 3.4 mA cm^{-2} after 5000 cycles)	20 μW h cm^{-2}	15.5 mW cm^{-2}
CNF/rGO/CNT	252 F g^{-1} (at 0.5 A g^{-1})	99.5% (at 1 A g^{-1} after 1000 cycles)	28.4 μW h cm^{-2}	9.5 mW cm^{-2}
CNF/Ag/PANI	212 F g^{-1} (at 10 mV s^{-1})	–	10.6 W h kg^{-1}	225 kW kg^{-1}
CNFs/PPy/SWCNTs	590 mF cm^{-2} (at 1 mA cm^{-2})	94.5% (at 1 mA cm^{-2} after 5000 cycles)	–	–
CNF/PPy/$Ni(OH)_2$	172 F g^{-1} (at 1 mV s^{-1})	84% (at 100 mV s^{-1} after 5000 cycles)	51 W h kg^{-1}	0.9 kW kg^{-1}
CNF/AC	84 F g^{-1} (at 0.1 A g^{-1})	92% (at 2 A g^{-1} after 10,000 cycles)	25 W h kg^{-1}	100 W kg^{-1}
ACFs	221.7 F g^{-1} (at 0.3 A g^{-1})	95.4% (at 2 A g^{-1} after 6000 cycles)	–	–
CMBs/MnO_2	617.6 F g^{-1} (at 1 A g^{-1})	80% (at 10 A g^{-1} after 1000 cycles)	–	–
HMC	340 F g^{-1} (at 1 A g^{-1})	98% (at 2 A g^{-1} after 20,000 cycles)	29 W h kg^{-1}	2243 W kg^{-1}
PCSs	420 F g^{-1} (at 0.5 A g^{-1})	99.4% (at 5 A g^{-1} after 30,000 cycles)	58.4 W h kg^{-1}	500 W kg^{-1}
B/N-CS	230 F g^{-1} (at 0.1 A g^{-1})	113% (at 5 A g^{-1} after 15,000 cycles)	8 W h kg^{-1}	6 kW kg^{-1}
CNSs	237.0 F g^{-1} (at 1 A g^{-1})	95% (at 5 A g^{-1} after 10,000 cycles)	–	–
CHHPCs	196 F g^{-1} (at 1 A g^{-1})	95% (at 5 A g^{-1} at after 2500 cycles)	21 W h kg^{-1}	875 W kg^{-1}
CNFF	219 F g^{-1} (at 5 mV s^{-1})	96% (at 50 mV s^{-1} after 10,000 cycles)	5.8 W h kg^{-1}	1.9 kW kg^{-1}
HCM-PANI	76 F g^{-1} (at 0.2 A g^{-1})	90.6% (at 50 mV s^{-1} after 10,000 cycles)	8.9 W h kg^{-1}	1644 W kg^{-1}
AHPCs	352 F g^{-1} (at 0.1 A g^{-1})	95% (at 10 A g^{-1} after 10,000 cycles)	107 W h kg^{-1}	900Wkg^{-1}
HPC/PANI	134 F g^{-1} (at 1 A g^{-1})	91.6% (at 1 A g^{-1} after 5000 cycles)	60.3 W h kg^{-1}	0.9 kW kg^{-1}
AWC/MnO_2@WC	3.6 F cm^{-2} (at 1 mA cm^{-2})	93% (at 10 mA cm^{-2} after 10,000 cycles)	1.6 mW h cm^{-2}	1044 mW cm^{-2}

Abbreviations CNF/rGO: Cellulose nanofiber/reduced graphene oxide; CNF/rGO/CNT: Cellulose nanofiber/reduced graphene oxide/carbon nanotube; CNF/Ag/PANI: Cellulose nanofiber/Ag/polyaniline; CNFs/PPy/SWCNTs: Cellulose nanofibers/polypyrrole/single-wall carbon nanotubes; CNF/PPy/$Ni(OH)_2$: Cellulose nanofiber/polypyrrole/$Ni(OH)_2$; CNF/AC: Cellulose nanofiber/activated carbon; ACFs: Activated carbon fibers; CMBs/MnO_2: Carbon microtube bundles/MnO_2; HMC: Human hair derived micro/mesoporous carbon; PCSs: Porous carbon sheets; B/N-CS: B/N co-doped carbon nanosheets; CNSs: Carbon nanosheets; CHHPCs: Corn husk derived hierarchical porous carbons; CNFF: Carbon nanofibrous framework; HCM-PANI: Hierarchically porous carbon microspheres/polyaniline; AHPCs: Ant-derived hierarchical porous carbons; HPC/PANI: Hierarchical porous carbon/polyaniline; AWC/MnO_2@WC: Activated wood carbon/MnO_2@wood carbon

supercapacitors, they are still lower compared with batteries. Usually they are used together in some fields. Interestingly, renewable and biodegradable materials based on nanopolysaccharides can also be used as electrode material for batteries as the same as supercapacitors.

For example, cellulose has long been widely used in energy field, especially in the lithium-ion battery (LIB) field. Compared with other polymer material, nanocellulose has multiple appealing properties that suitable for LIB, such as high specific modulus (~100 GPa $(g\ cm^{-3})^{-1}$), excellent stability in most solvents, and stability over a wide electrochemical window, etc. [70]. Meanwhile, the inexpensive and environmentally friendly nature of nanocellulose and its derivatives as well as simple fabrication techniques have also drawn much attention in sustainable energy storage. In terms of LIB, nanocellulose is usually used as a substrate material, separator, and electrolyte for energy storage [71–73]. On the other hand, nanopolysaccharides such as sodium alginate, chitin and chitosan also have a similar application for its unique structure. Here, we will make some specific discussion on these three aspects.

4.4.1 Nanopolysaccharides-Based Electrode

Due to the convenience of fabricating unique structure with a high porosity, low density and high specific surface area through nanocellulose, nanocellulose has been extensively used as active substrate or flexible electrode in lithium ion battery electrodes by simple carbonization [74].

For example, in Li's work [75], they fabricated an NCF-GO gel alignment fiber by simply mixing and drying, then the conductive NCF-GO fiber was fabricated by a carbonization process. As shown in Fig. 4.13, GO acted as a template for NFC carbonization, changing the morphology of the carbonized NFC from micro-spheres to sheets while improving the carbonization of NFC, so that this obtained material has a high conductivity about 649 ± 60 S cm^{-1}, and showed a stable discharge capacity of 312 mAh g^{-1} at a constant current density of 25 mA g^{-1} (Fig. 4.14).

In Wu's work [76], they proposed an alternative low-cost, flexible and free-standing electrode fabricate routine through a straightforward carbonization followed by infiltration, which could be stacked to achieve high discharge capacity while with a high loading about 1.3–3.5 mg. It benefited from the high connectivity and conductivity of the pores within the cellulose sheet. All active material particles within the electrodes remained electrically connected and accessible to Li^+ ions (Fig. 4.15).

And in Tu's contribution [77], a natural polymer of Gum Arabic was introduced to conductive carbon nanocellulose fiber (CNF) networks to build free-standing CNF-GA composite films via a solution-coating method. These as-obtained films can thus effectively impede the shuttle effect, and the well-conductive performance of the CNF network can improve the sulfur utilization, ensuring a compatibility with high-sulfur-loading cathodes (Fig. 4.16). In consequence, the sulfur cathodes with the CNF-GA interlayers, in which CNF can offered a 3D network structure and GA

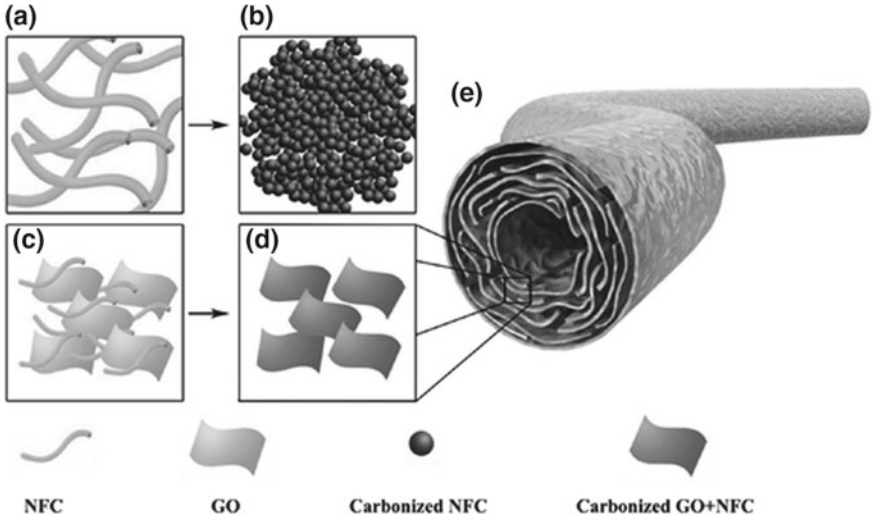

Fig. 4.13 **a**–**b** Schematic to show the morphology of NFC changed from fibers (before carbonization) to sphere particles after carbonization. In the (GO + NFC) microfiber, only sheets formed after carbonization, no particles observed as shown in (**c**–**d**). **e** is the structure of a c(GO + NFC) microfiber. The c(GO + NFC) microfiber shows a hollow structure with building blocks well aligned along the fiber direction. Reproduced from [75]

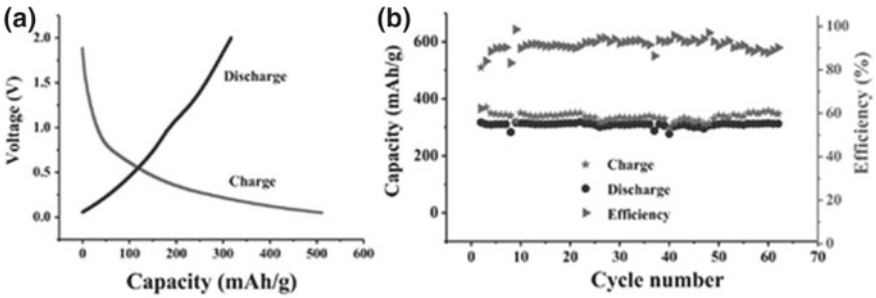

Fig. 4.14 **a** Charge and discharge voltage profile of fiber battery for the second cycle. **b** Charge/discharge capacity and corresponding Coulombic efficiency cycled at a constant current density of 25 mA g^{-1}. Reproduced from [76]

can afford a strong chemical interaction toward poly-sulfides and thereby effectively suppress the shuttling behavior, demonstrated that won a high discharge capacity.

As a renewable biopolymer with rich amino and hydroxyl groups, chitosan has been utilized as both structural agent and carbon precursor for electrode material [78, 79]. In Han's work [80], A conformal and continuous chitosan coating layer were spontaneously formed on Fe_3O_4 particles due to the strong coordination between

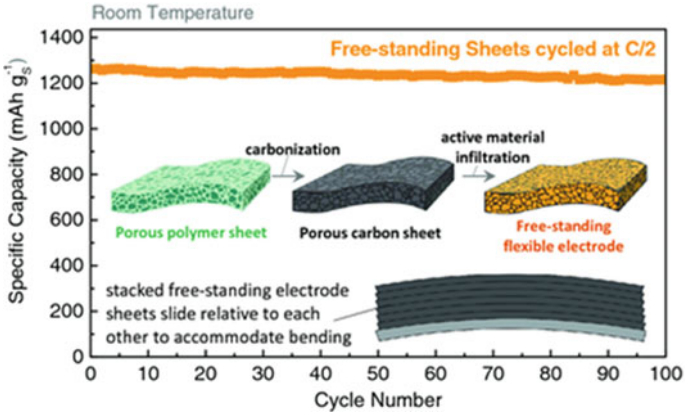

Fig. 4.15 Schematic illustrations of method to prepare the free-standing electrodes and long cycle stability of single and stacked electrodes at C/2. Reproduced from [76]

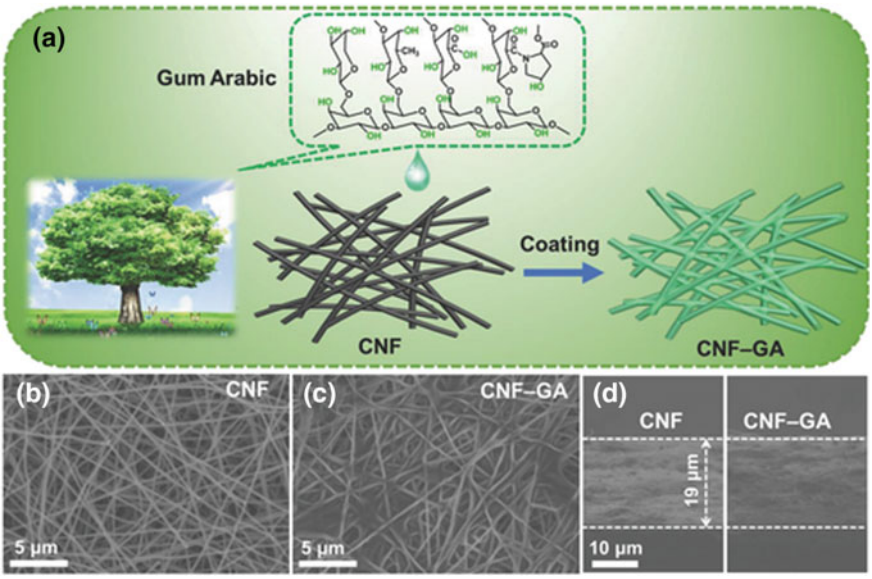

Fig. 4.16 **a** Schematic illustration of the fabrication process of the CNF-GA composite. **b**, **c** Top-view SEM images of CNFs (**b**) and CNF-GA composite (**c**). **d** Cross-sectional SEM images of the CNF. Reproduced from [77]

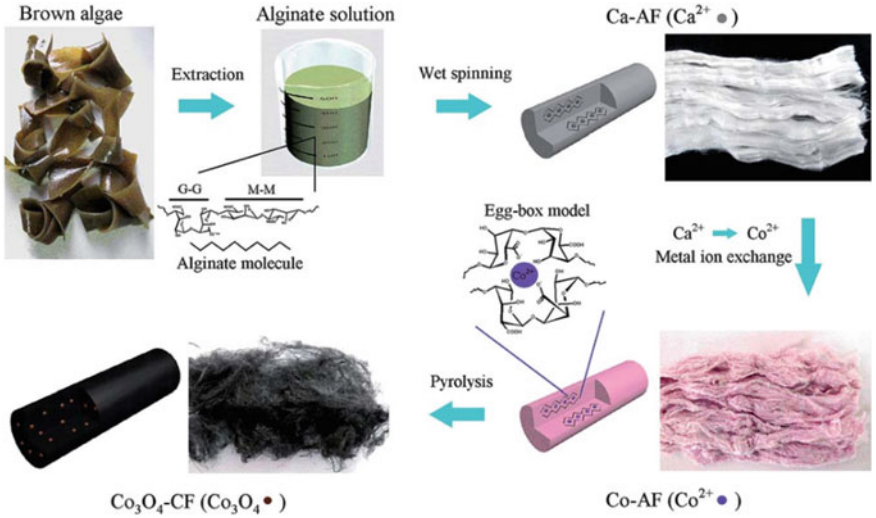

Fig. 4.17 The synthesis process Co_3O_4-CF by pyrolysis of wet spun cobalt alginate fibres. Reproduced from [82]

hydroxyl and amino groups of chitosan and Fe^{3+}, which then converted into N-doped carbon under calcination, and the as prepared Fe_3O_4@C nanocomposites shows dramatically enhanced electrochemical performance.

In addition, abundant sea biomass resources also have attracted much attention because of their potential application in renewable energy [81]. Carbonaceous microfibres with a diameter of ~5–8 μm which are embedded with Co_3O_4 NPs (30–50 nm) were synthesized by pyrolysis of wet spun Co-alginate fibres (Co-AF) as shown in Fig. 4.17 [82].

In conclusion, nanopolysaccharides play a great role in fabricating a conductive electrode especially flexible material. It usually acts as a temple and then composites with other conductive material. The low-cost and richness of raw material makes it a potential development in the future.

4.4.2 Nanopolysaccharides-Based Separator

Separators are important part of lithium-ion batteries and play a great role in the interior of batteries. The separator can prevent the direct contact between the positive and negative electrodes inside the battery, and can ensure the smooth transfer of lithium ions at the electrode. Commercial microporous poly-olefins (such as polypropylene and polyethylene) separators have been widely used in lithium-ion batteries, but such separators exhibit lower ionic conductivity due to poor porosity and aspirating properties. Therefore, the charge and discharge performance requirements of lithium ion

batteries cannot be fully satisfied. Compared with traditional separators, nanocelluloses have high porosity, excellent heat resistance, wettability, biocompatibility, and outstanding mechanical properties, thus it can be used as important candidates for metal ions battery separator, and porosity material have been studied extensively [83–85].

In 1996, the study of Isao Kuribayashi showed composite cellulosic separators that consist of fibrilliform cellulosic fibers embedded in a microporous cellulosic matrix soaked in an aprotic solvent provide a promising alternative to polyolefin separators in the future development of rechargeable lithium-ion batteries, and it reduce the possibility of separator meltdown under exposure to beat generated by overcharging or internal short-circuiting in applications such as load-levelling at electric power plants or lightweight electric vehicles [86]. However, due to the large pore size of the microfibers and the uneven distribution of the pore size, the electrochemical performance of the microfibers was far from the requirements of commercial production. Then, in Zhang's study (Fig. 4.18) [87], a cellulose nanofiber/PET nonwoven composite separator was successfully fabricated, using a wet-laid nonwoven (papermaking) process, which showed a more excellent wettability and porosity compared with the PP separator. In addition, when the CNF and polypropylene separators were placed at 180 °C for 1 h, the CNF separator did not shrink while the PP film shrank more than 50%. It showed that the CNF diaphragm have a higher melting point than the PP separator. Above all, comparing the cycle performance of lithium ion batteries assembled by these two kinds of separators, the discharge capacity and capacitance retention rate of lithium ion batteries assembled by CNF separators were higher than those of PP separators. After 100 cycles, the discharge capacity still has retention rate about 91.7%. Recently, Lee et al. (Fig. 4.19) [88] have built a separator using nanoporous CNF as a top layer, and using microporous polyvinylpyrrolidone (PVP)/polyacrylonitrile (PAN) as a support layer. This unique bilayer hierarchical/asymmetric porous structure contributed to balance leakage current and ion transport rate. Most recently, in Pan's work (Fig. 4.20) [89], a thin, thermally stable, flexible, and hydrophilic cellulose nanofiber layer, fabricated by using a straightforward paper-making process, was laminated on each side of a plasma-treated polyethylene (PE) separator, and then this trilayer separator was used

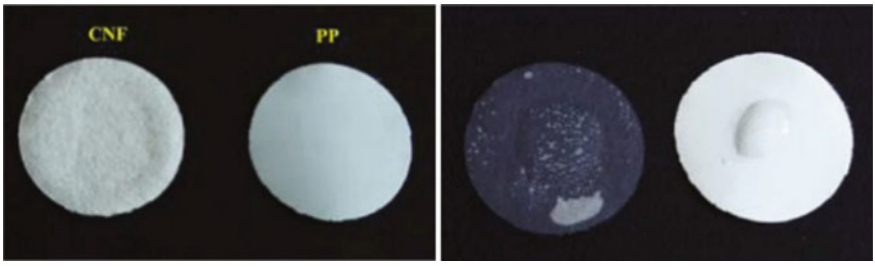

Fig. 4.18 Photographs of electrolyte (EC/DEC) wettability of PP separator and CNF separator. Reproduced from [87]

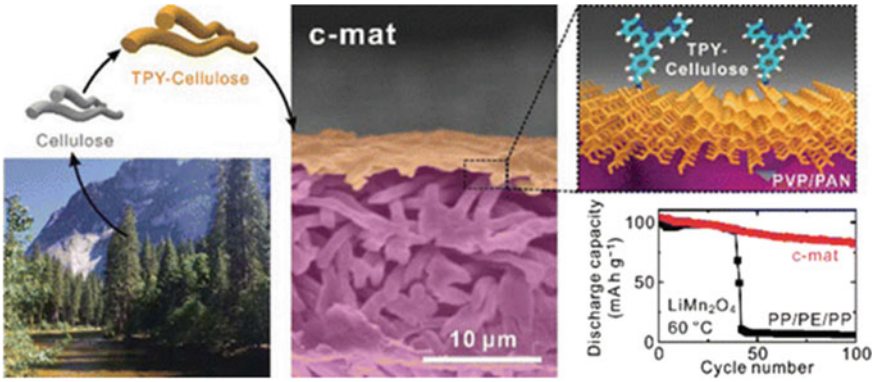

Fig. 4.19 Functionalized nanocellulose-integrated heterolayered nanomats as battery separators: illustration of the fabrication process and rate and cycling performance. Reproduced from [88]

to assemble a cell, which could maintain dimensional stability even at 200 °C when the internal PE layer was melted and blocked the ion transport through the separator.

On the other hand, bacterial cellulose (BC) also has been applied as matrix material for separator of LIB [90, 91]. In Xu's work (Fig. 4.21) [91], a BC/Al_2O_3 nanofibrous composite membrane as a LIB separator was properly prepared by coating Al_2O_3 on BC nanofibers through a simple in situ thermal decomposition method.

4.4.3 Nanopolysaccharides-Based Electrolyte

Similar to the requirements of the separator, the high porosity, mechanical properties, thermal stability of nanocellulose material and other outstanding properties also made it attractive much attention in the development of electrolyte of LIB. Chiappone's group has fabricated a methacrylic-based thermoset gel-polymer electrolyte membrane by a very easy method in 2011 [92]. In this work, the electrolyte membrane was obtained by simple reliable free radical photo-polymerization and reinforced with microfibrillated cellulose particles, which was demonstrated have high flexibility, and well suited for flexible and/or non-planar electronics application (Fig. 4.22).

Soon thereafter, Willgert et al. successfully prepared a highly flexible nanocellulose composite paper and used it as a lithium ion battery electrolyte with an ionic conductivity of up to 5×10^{-5} S cm^{-1} [93]. Experiments showed that this electrolyte material did not have obvious decomposition and had good electrochemical stability.

Recently, Dong's work demonstrated for the first time an ultra-strong bacterial cellulose supported poly (methyl vinyl ether-alt-maleic anhydride) as a multifunctional polymer electrolyte for a 4.45 V-class $LiCoO_2$/lithium Metal battery [94]. This

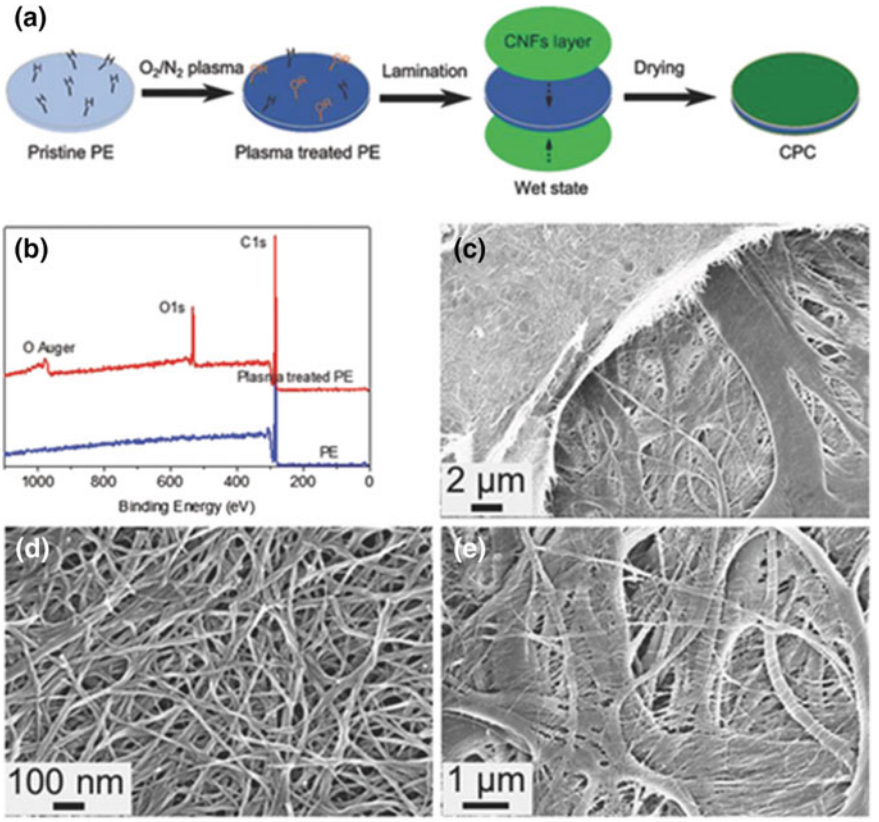

Fig. 4.20 **a** Schematic illustration of the manufacturing of the CPC separator. **b** O1s and C1s XPS spectra of pristine PE and plasma-treated PE, respectively and **c** SEM images of the CNFs/PE interface, **d** the CNFs layer and **e** the PE layer of the CPC separator, respectively. Reproduced from [89]

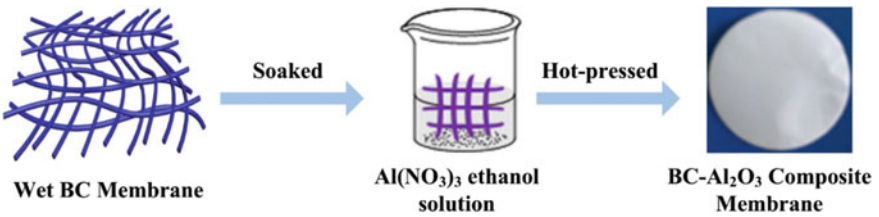

Fig. 4.21 Schematic of the fabrication process of BC-based composite membrane. Reproduced from [91]

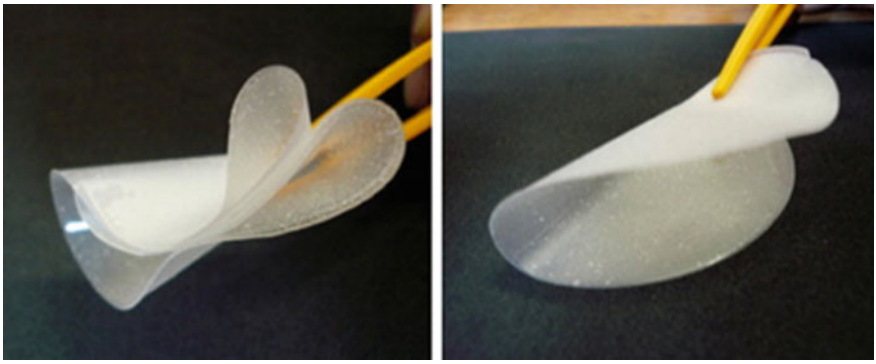

Fig. 4.22 Appearance and rate performance of methacrylic-based thermo-set gel-polymer electrolyte membranes. Reproduced from [92]

polymer electrolyte displayed both a higher ionic conductivity and a wider electrochemical window, and obtained superior capacity retention (85% after 700 cycles) and excellent rate capability (15C) even at 60 °C (Fig. 4.23).

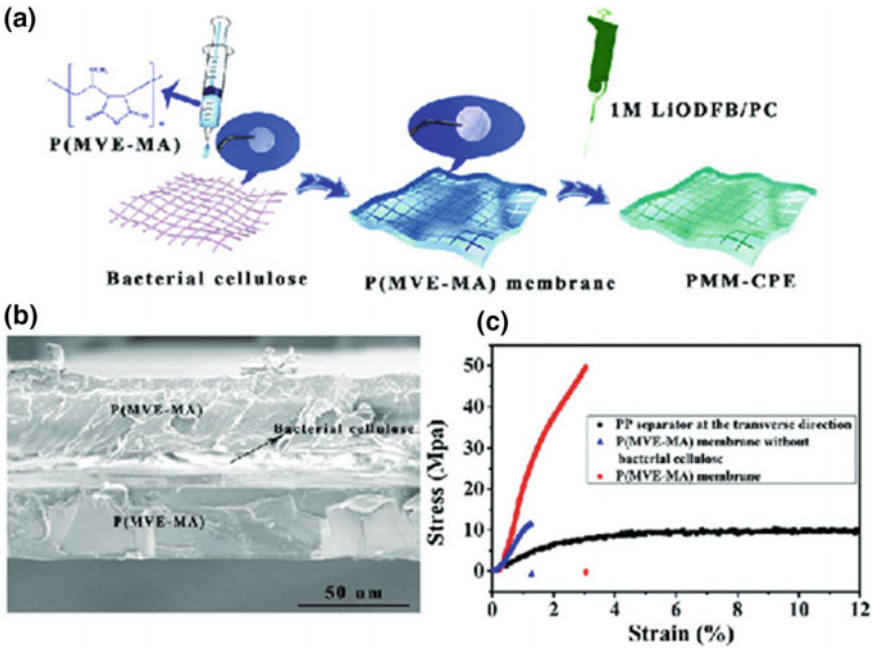

Fig. 4.23 **a** A schematic representation of the PMM-CPE fabrication process. **b** Side-view SEM image of the P(MVE-MA) membrane. **c** Stress-strain curves of the PP separator in the transverse direction, the P(MVE-MA) membrane without bacterial cellulose and the P(MVE-MA) membrane with bacterial cellulose. Reproduced from [94]

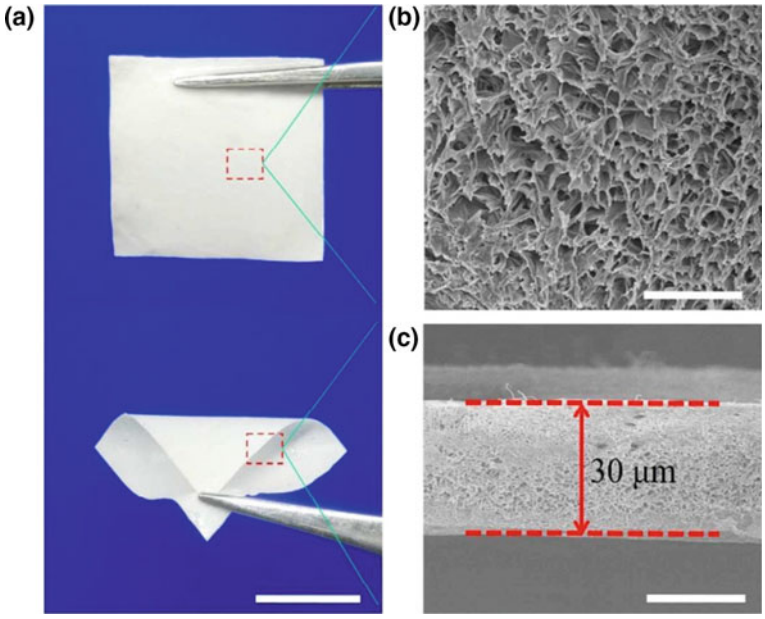

Fig. 4.24 Morphology and structure of HPE film. **a** Optical, **b** SEM, **c** cross-section SEM image of the HPE film. Reproduced from [97]

Meanwhile, there has been a growing interest in utilizing gelatin as solid or gel electrolytes for solid-state devices owing to its environmental friendliness, high inorganic salt solubility, and abundance in nature [95, 96]. Recently, Li's group fabricated a safe solid-state rechargeable and wearable ZIB with a novel hierarchical gelatin and PAM based electrolyte [97]. They synthesized the hierarchical polymer electrolyte by grafting polyacrylamide (PAM) onto gelatin chains that were filled in the network of polyacrylonitrile (PAN) electrospun fiber membrane (Fig. 4.24). As a result, the hierarchical polymer electrolyte (HPE) film with a highly porous three-dimensional (3D) architecture and a high level of water retention in the polymeric network were obtained, and it exhibited an ultra-high ionic conductivity while maintaining excellent flexibility and remarkable mechanical strength.

It can be seen from the above results that polysaccharides play an irreplaceable role in LIB due to its unique structure, when it was applied to electrode materials, separators or electrolyte substrates. However, its industrial production is still a tough problem, which extremely limits its application in energy storage field and requires a lot of work to advance. In addition, nanocellulose can also be widely used in acoustic equipment, transducers, sensors, infrared detectors and other fields.

4.5 Concluding Remarks

With the development of energy storage systems and the depletion of conventional fossil fuels, the use of renewable energy and materials is attracting increasing attention. Cellulose, as the largest reserves of carbon-based material, is a good choice in energy storage because of its good properties. Meanwhile, electronics are developed to be flexible, wearable, lightweight and high-performance, and cellulose will be highly anticipated to bring unprecedented benefits in the structure and performance of energy storage materials and systems, which lie far beyond those achievable with conventional synthetic materials. We envision that cellulose will move us closer toward a new environment-friendly smart energy era, which will find widespread use of cellulose-based materials in various fields.

Acknowledgements This work was supported by the National Natural Science Foundation of China (No. 51703177, 21704079), the Fundamental Research Funds for the Central Universities (WUT: 2018III009, 2018IVB022, 2018IVB041), and Key laboratory of Processing and Quality Evaluation Technology of Green Plastics of China National Light Industry council, Beijing Technology and Business University (No. PQETGP2019007).

References

1. Winter M, Brodd RJ (2014) What are batteries, fuel cells and supercapacitors? Chem Rev 104:4245–4270
2. Li Q, Yao F-Z, Liu Y et al (2018) High-temperature dielectric materials for electrical energy storage. Annu Rev Mater Res 48:3.1–3.25
3. Wen L, Li F, Cheng H-M (2016) Carbon nanotubes and graphene for flexible electrochemical energy storage: from materials to devices. Adv Mater 28:4306–4337
4. Dubal D, Chodankar N, Kim D-H et al (2018) Towards flexible solid-state supercapacitors for smart and wearable electronics. Chem Soc Rev 47:2065–2129
5. He J, Manthiram A (2019) A review on the status and challenges of electrocatalysts in lithium-sulfur batteries. Energy Storage Mater 20:55–70
6. Sun Y, Liu N, Cui Y (2016) Promises and challenges of nanomaterials for lithium-based rechargeable batteries. Nat Energy 1:16071
7. Wang X, Lu X, Liu B et al (2014) Flexible energy-storage devices: design consideration and recent progress. Adv Mater 26:4763
8. Zhou Y, Li Q, Dang B et al (2018) A scalable, high-throughput, and environmentally benign approach to polymer dielectrics exhibiting significantly improved capacitive performance at high temperatures. Adv Mater 30:1805672
9. Chen W, Yu H, Lee SY et al (2018) Nanocellulose: a promising nanomaterial for advanced electrochemical energy storage. Chem Soc Rev 47:2837–2872
10. Bras DL, Stromme M, Mihranyan A (2015) Characterization of dielectric properties of nanocellulose from wood and algae for electrical insulator applications. J Phys Chem B 119:5911–5917
11. Kim JH, Lee D, Lee YH et al (2018) Nanocellulose for energy storage systems: beyond the limits of synthetic materials. Adv Mater 31:1804826
12. Vicente A, Araújo A, Mendes M et al (2018) Multifunctional cellulose-paper for light harvesting and smart sensing applications. J Mater Chem C 6:3143–3181
13. Moon R, Martini A, Nairn J et al (2011) Cellulose nanomaterials review: structure, properties and nanocomposites. Chem Soc Rev 40:3941–3994

14. Sahin H, Ay N (2004) Dielectric properties of hardwood species at microwave frequencies. J Wood Sci 50:375–380
15. Ishida Y, Yōshino M, Takayanagi M et al (1959) Dielectric studies on cellulose fibers. J Appl Polym Sci 1:227–235
16. Rout S, Anwar S, Tripathy B et al (2019) Nanosilver coated coir based dielectric materials with high K and low Df for embedded capacitors and insulating material applications—a greener approach. ACS Sustain Chem Eng 7:3824–3837
17. Yang Q, Zhang C, Shi Z et al (2018) Luminescent and transparent nanocellulose films containing europium carboxylate groups as flexible dielectric materials. ACS Appl Nano Mater 1:4972–4979
18. Tang C, Liao R, Chen G et al (2011) Research on the feature extraction of DC space charge behavior of oil-paper insulation. Sci China Technol Sci 54:1315–1324
19. Petritz A, Wolfberger A, Fian A et al (2013) Cellulose as biodegradable high-k dielectric layer in organic complementary inverters. Appl Phys Lett 103:153303–153308
20. Kafy A, Sadasivuni K, Kim HC et al (2015) Designing flexible energy and memory storage materials using cellulose modified graphene oxide nanocomposites. Phys Chem Chem Phys 17:5923–5931
21. Irimia-Vladu M, Troshin P, Reisinger M et al (2010) Biocompatible and biodegradable materials for organic field-effect transistors. Adv Funct Mater 20:4069–4076
22. Ji S, Jang J, Cho E et al (2017) High dielectric performances of flexible and transparent cellulose hybrid films controlled by multidimensional metal nanostructures. Adv Mater 29:1700538
23. Yang J, Xie H, Chen H et al (2018) Cellulose nanofibril/boron nitride nanosheet composites with enhanced energy density and thermal stability by interfibrillar cross-linking through Ca^{2+}. J Mater Chem A 6:1403–1411
24. Zhang C, Yin Y, Yang Q et al (2019) Flexible cellulose/$BaTiO_3$ nanocomposites with high energy density for film dielectric capacitor. ACS Sustain Chem Eng 7:10641–10648
25. Jayamani E, Hamdan S, Rahman M et al (2014) Comparative study of dielectric properties of hybrid natural fiber composites. Procedia Eng 97:536–544
26. Mehta M, Parsania P et al (2006) Fabrication and evaluation of some mechanical and electrical properties of jute-biomass based hybrid composites. J Appl Polym Sci 100:1754–1758
27. Sreekumar P, Saiter J, Joseph K et al (2012) Electrical properties of short sisal fiber reinforced polyester composites fabricated by resin transfer molding. Compos Part A Appl Sci Manuf 43:507–511
28. Zeng X, Deng L, Yao Y et al (2016) Flexible dielectric papers based on biodegradable cellulose nanofibers and carbon nanotubes for dielectric energy storage. J Mater Chem C 4:6037–6044
29. Raghunathan S, Narayanan S, Poulose A et al (2016) Flexible regenerated cellulose/polypyrrole composite films with enhanced dielectric properties. Carbohydr Polym 157:1024–1032
30. Jia C, Shao Z, Fan H et al (2015) Preparation and dielectric properties of cyanoethyl cellulose/$BaTiO_3$ flexible nanocomposite films. RSC Adv 5(20):15283–15291
31. Jia C, Shao Z, Fan H et al (2016) Barium titanate as a filler for improving the dielectric property of cyanoethyl cellulose/antimony tin oxide nanocomposite films. Compos Part A Appl Sci Manuf 86:1–8
32. Wu K, Fang J, Ma J et al (2017) Achieving a collapsible, strong and highly thermally conductive film based on oriented functionalized boron nitride nanosheets and cellulose nanofiber. ACS Appl Mater Interfaces 9(35):30035–30045
33. Lao J, Xie H, Shi Z et al (2018) Flexible regenerated cellulose/boron nitride nanosheet high-temperature dielectric nanocomposite films with high energy density and breakdown strength. ACS Sustain Chem Eng 6:7151–7158
34. Chen H, Liu B, Yang Q et al (2017) Facile one-step exfoliation of large-size 2D materials via simply shearing in triethanolamine. Mater Lett 199:24–127
35. Okita Y, Saito T, Isogai A (2010) Entire surface oxidation of various cellulose microfibrils by TEMPO-mediated oxidation. Biomacromolecules 11:1696–1700
36. Saito T, Nishiyama Y, Putaux J et al (2006) Homogeneous suspensions of individualized microfibrils from TEMPO-catalyzed oxidation of native cellulose. Biomacromolecules 7:1687–1691

37. Cai J, Zhang L, Liu S et al (2008) Dynamic self-assembly induced rapid dissolution of cellulose at low temperatures. Macromolecules 41:9345–9351
38. Zhang L, Mao Y, Zhou J et al (2005) Effects of coagulation conditions on the properties of regenerated cellulose films prepared in NaOH/urea aqueous solution. Ind Eng Chem Res 44:522–529
39. Huang X, Jiang P, Tanaka T (2011) A review of dielectric polymer composites with high thermal conductivity. IEEE Electr Insul M 27:8–16
40. Sarangapani S (1996) Materials for electrochemical capacitors. J Electrochem Soc 143:3791–3799
41. Isogai A, Saitot T, Fukuzumih H (2011) TEMPO-oxidized cellulose nanofibers. Nanoscale 3(1):71–85
42. Gao KZ, Shao ZQ, Jia L et al (2013) Cellulose nanofiber-graphene all solid-state flexible supercapacitors. J Mater Chem A 1:63–67
43. Hamedi Karabulut M, Marais E et al (2013) Nanocellulose aerogels functionalized by rapid layer-by-layer assembly for high charge storage and beyond. Angew Chem Int Ed 52(46):12038–12042
44. Zheng Q, Zhang H, Mi H et al (2016) High-performance flexible piezoelectric nanogenerators consisting of porous cellulose nanofibril (CNF)/poly(dimethylsiloxane) (PDMS) aerogel films. Nano Energy 26:504–512
45. Zheng Q, Cai Z, Ma Z et al (2015) Cellulose nanofibril/reduced graphene oxide/carbon nanotube hybrid aerogels for highly flexible and all-solid-state supercapacitors. ACS Appl Mater Interfaces 7(5):3263–3271
46. Zhang X, Lin Z, Chen B et al (2014) Solid-state flexible polyaniline/silver cellulose nanofibrils aerogel supercapacitors. J Power Sources 246(3):283–289
47. Li S, Huang D, Yang J et al (2014) Freestanding bacterial cellulose–polypyrrole nanofibres paper electrodes for advanced energy storage devices. Nano Energy 9:309
48. Cai J, Niu H, Li Z et al (2015) High-performnace supercapacitor electrode materials form cellulose-derived carbon nanofibers. ACS Appl Mater Interfaces 7(27):14946
49. Li Z, Liu J, Jiang K et al (2016) Carbonized nanocellulose sustainably boosts the performance of activated carbon in ionic liquid supercapacitors. Nano Energy 25:161–16940
50. Bi Z, Kong Q, Cao Y et al (2019) Biomass-derived porous carbon materials with different dimensions for supercapacitor electrodes: a review. J Mater Chem A 7(27):16028–16045
51. Cai J, Niu H, Wang H et al (2016) High-performance supercapacitor electrode from cellulose-derived, inter-bonded carbon nanofibers. J Power Sources 324:302–308
52. Berenguer R, García-Mateos F, Ruiz-Rosas R et al (2016) Biomass-derived binderless fibrous carbon electrodes for ultrafast energy storage. Green Chem 18(6):1506–1515
53. Jin Z, Yan X, Yu Y et al (2014) Sustainable activated carbon fibers from liquefied wood with controllable porosity for high-performance supercapacitors. J Mater Chem A2(30):11706–11715
54. Liu Y, Shi Z, Gao Y et al (2016) Biomass-swelling assisted synthesis of hierarchical porous carbon fibers for supercapacitor electrodes. ACS Appl Mater Interfaces 8(42):28283–28290
55. Zhang X, Meng X, Gong S et al (2016) Synthesis and characterization of 3D MnO_2/carbon microtube bundle for supercapacitor electrodes. Mater Lett 179:73–77
56. Zhang X, Zhang K, Li H et al (2017) Porous graphitic carbon microtubes derived from willow catkins as a substrate of MnO_2 for supercapacitors. J Power Sources 344:176–184
57. Purkait T, Singh G, Singh M et al (2017) Large area few-layer graphene with scalable preparation from waste biomass for high-performance supercapacitor. Sci Rep UK 7(1)
58. Qian W, Sun F, Xu Y et al (2013) Human hair-derived carbon flakes for electrochemical supercapacitors. Energy Environ Sci 7(1):379–386
59. Wang C, Wu D, Wang H et al (2017) Nitrogen-doped two-dimensional porous carbon sheets derived from clover biomass for high performance supercapacitors. J Power Sources 363:375–383
60. An Y, Li Z, Yang Y et al (2017) Synthesis of hierarchically porous nitrogen-doped carbon nanosheets from agaric for high-performance symmetric supercapacitors. Adv Mater Interfaces 4(12):1700033

61. Ling Z, Wang Z, Zhang M et al (2015) Sustainable synthesis and assembly of biomass-derived B/N Co-doped carbon nanosheets with ultrahigh aspect ratio for high-performance supercapacitors. Adv Funct Mater 26(1):111–119
62. You J, Li M, Ding B et al (2017) Crab chitin-based 2D soft nanomaterials for fully biobased electric devices. Adv Mater 29(19):1606895
63. Ma F, Song S, Wu G et al (2015) Facile self-template large scale preparation of biomass-derived 3D hierarchical porous carbon for advanced supercapacitors. J Mater Chem A3:18154–18162
64. Liang Q, Ye L, Huang Z et al (2014) A honeycomb-like porous carbon derived from pomelo peel for use in high-performance supercapacitors. Nanoscale 6(22):13831–13837
65. Duan B, Gao X, Yao X et al (2016) Unique elastic N-doped carbon nanofibrous microspheres with hierarchical porosity derived from renewable chitin for high rate supercapacitors. Nano Energy 27:482–491
66. Gao L, Xiong L, Xu D et al (2018) Distinctive construction of chitin derived hierarchically porous carbon microspheres/polyaniline for high rate supercapacitors. ACS Appl Mater Interfaces 10(34):28918–28927
67. Zhao G, Chen C, Yu D et al (2018) One-step production of O-N-S Co-doped three-dimensional hierarchical porous carbons for high-performance supercapacitors. Nano Energy 47:547–555
68. Yu P, Zhang Z, Zheng L et al (2016) A novel sustainable flour derived hierarchical nitrogen-doped porous carbon/polyaniline electrode for advanced asymmetric supercapacitors. Adv Energy Mater 6(20):1601111
69. Chen C, Zhang Y, Li Y et al (2017) All-wood, low tortuosity, aqueous, biodegradable supercapacitors with ultra-high capacitance. Energy Environ Sci 10(2):538–545
70. Chen C, Hu L (2018) Nanocellulose toward advanced energy storage devices: structure and electrochemistry. Acc Chem Res 51(12):3154–3165
71. Wang Z, Tammela P, Strømme M et al (2017) Cellulose-based supercapacitors: material and performance considerations. Adv Energy Mater 7(18):1700130
72. Chen W, Yu H, Lee S et al (2018) Nanocellulose: a promising nanomaterial for advanced electrochemical energy storage. Chem Soc Rev 47(8):2837–2872
73. Ling S, Chen W, Fan Y et al (2018) Biopolymer nanofibrils: structure, modeling, preparation, and applications. Prog Polym Sci 85:1–56
74. Jost K, Durkin DP, Haverhals L et al (2015) Natural fiber welded electrode yarns for knittable textile supercapacitors. Adv Energy Mater 5(4):1401286
75. Li Y, Zhu H, Shen F et al (2014) Highly conductive microfiber of graphene oxide templated carbonization of nanofibrillated cellulose. AdvFunct Mater 24(46):7366–7372
76. Wu F, Zhao E, Gordon D et al (2016) Infiltrated porous polymer sheets as free-standing flexible lithium-sulfur battery electrodes. Adv Mater 28(30):6365–6371
77. Tu S, Chen X, Zhao X et al (2018) A polysulfide-immobilizing polymer retards the shuttling of polysulfide intermediates in lithium–sulfur batteries. Adv Mater 30(45):e1804581
78. Wang YY, Hou BH, Lu HY et al (2015) Porous N-doped carbon material derived from prolific chitosan biomass as a high-performance electrode for energy storage. RSC Adv 5(118):97427–97434
79. Yang Y, Cui J, Zheng M et al (2012) One-step synthesis of amino-functionalized fluorescent carbon nanoparticles by hydrothermal carbonization of chitosan. Chem Commun 48(3):380–382
80. Han C, Xu L, Li H et al (2018) Biopolymer-assisted synthesis of 3D interconnected Fe_3O_4@carbon core@shell as anode for asymmetric lithium ion capacitors. Carbon 140:296–305
81. Park HR, Jung KA, Lim SR et al (2014) Quantitative sustainability assessment of seaweed biomass as bioethanol feedstock. Bioenergy Res 7(3):974–985
82. Li D, Yang D, Zhu X et al (2014) Simple pyrolysis of cobalt alginate fibres into Co_3O_4/C nano/microstructures for a high-performance lithium ion battery anode. J Mater Chem A 2(44):18761–18766
83. Xiao S, Yang Y, Li M et al (2014) A composite membrane based on a biocompatible cellulose as a host of gel polymer electrolyte for lithium ion batteries. J Power Sources 270:53–58

84. Pan R, Wang Z, Sun R et al (2017) Thickness difference induced pore structure variations in cellulosic separators for lithium-ion batteries. Cellulose 24(7):2903–2911
85. Zhao D, Chen C, Zhang Q et al (2017) High performance, flexible, solid-state supercapacitors based on a renewable and biodegradable mesoporous cellulose membrane. Adv Energy Mater 7(18):1700739
86. Kuribayashi I (1996) Characterization of composite cellulosic separators for rechargeable lithium-ion batteries. J Power Sources 63(1):87–91
87. Zhang H, Wang X, Liang Y (2015) Preparation and characterization of a lithium-ion battery separator from cellulose nanofibers. Heliyon 1(2):e00032
88. Kim JH, Gu M, Lee DH et al (2016) Functionalized nanocellulose-integrated heterolayered nanomats toward smart battery separators. Nano Lett 16(9):5533–5541
89. Pan R, Xu X, Sun R et al (2018) Nanocellulose modified polyethylene separators for lithium metal batteries. Small 1704371
90. Li F, Wang G, Wang P et al (2017) High-performance lithium-sulfur batteries with a carbonized bacterial cellulose/TiO_2 modified separator. J Electroanal Chem 788:150–155
91. Xu Q, Wei C, Fan L et al (2017) A bacterial cellulose/Al_2O_3 nanofibrous composite membrane for a lithium-ion battery separator. Cellulose 24(4):1889–1899
92. Chiappone A, Nair JR, Gerbaldi C et al (2011) Microfibrillated cellulose as reinforcement for Li-ion battery polymer electrolytes with excellent mechanical stability. J Power Sources 196(23):10280–10288
93. Willgert M, Leijonmarck S, Lindbergh G et al (2014) Cellulose nanofibril reinforced composite electrolytes for lithium ion battery applications. J Mater Chem A 2(33):13556–13564
94. Dong T, Zhang J, Xu G et al (2018) A multifunctional polymer electrolyte enables high-voltage lithium metal battery ultra-long cycle-life. Energy Environ Sci 11:1197–1203
95. Choudhury NA, Sampath S, Shukla AK (2008) Gelatin hydrogel electrolytes and their application to electrochemical supercapacitors. J Electrochem Soc 155(1):A74–A81
96. Benedetti TM, Carvalho T, Iwakura DC et al (2015) All solid-state electrochromic device consisting of a water soluble viologen dissolved in gelatin-based ionogel. Sol Energy Mater Sol Cells 132:101–106
97. Li H, Han C, Huang Y et al (2018) An extremely safe and wearable solid-state zinc ion battery based on a hierarchical structured polymer electrolyte. Energy Environ Sci 11(4):941–951

Chapter 5
The Use of Nano-Polysaccharides in Biomedical Applications

Daesung Kim, Muhammad Shahidul Islam and Michael K. C. Tam

Abstract Nano-polysaccharides (NPs) are materials that have been used to sustain the ecological systems without us knowing their importance. In recent years, NPs are being exploited in various applications, such as in the treatment of diseases and the delivery of therapeutics, offering solutions that impact society. Nanocellulose, chitin/chitosan, and starch nanoparticles possess attractive properties for biomedical applications as they are biocompatible, biodegradable, negligible cytotoxicity, abundant surface functional groups that can be utilized for further chemical modifications. This chapter discusses the synthesis, characterization and applications of nano-polysaccharides in medical related applications, such as controlled drug release and gene delivery, bioimaging, biosensor, biocatalyst, antibacterial, and tissue engineering.

Keywords Drug delivery · Biotechnology · Antibacterial action · Cell cultivation

5.1 Drug Release and Gene Delivery Applications

5.1.1 Introduction

The method of administering a pharmaceutical compound in humans or animals is known as drug delivery and the form in which the drug is delivered is called drug delivery systems. A pharmaceutical drug is a chemical compound used for the treatment, cure, diagnosis, or prevention of a disease or a condition in human or animal species. In order to achieve a desired therapeutic effect, the active pharmaceutical ingredients (APIs) or drugs must achieve a critical concentration in the plasma, called minimum effective concentration (MEC) for a drug dose called minimum efficacious dose [1]. However, the efficacy of many drugs depends on their route of delivery and

D. Kim · M. S. Islam · M. K. C. Tam (✉)
Department of Chemical Engineering, Waterloo Institute for Nanotechnology, University of Waterloo, 200 University Avenue West, Waterloo, ON N2L 3G1, Canada
e-mail: mkctam@uwaterloo.ca

N. Lin et al. (eds.), *Advanced Functional Materials from Nanopolysaccharides*, Springer Series in Biomaterials Science and Engineering 15,
https://doi.org/10.1007/978-981-15-0913-1_5

the delivery system. Drug delivery systems (DDS) are new strategies involving multidisciplinary approaches that combine pharmaceutics and biopharmaceutics, pharmaceutical and chemical engineering, molecular biology and biotechnology, polymer science, and bioconjugate chemistry that have been developed in recent years [2]. The main advantages of modified DDS over the conventional systems are the site specific delivery of the loaded APIs ensuring fewer adverse effects, eliminating variation of bioavailability (maintaining drug concentrations in the acceptable therapeutic range), enhanced patient compliance, and reproducible pharmacokinetics (especially absorption) within the cell of interest [2].

Over the last couple of decades, "Nano" has become a popular prefix, surpassing material science and is now commonly found in products in tissue engineering, medical sciences, computers, cosmetics, building materials, food and beverages, smartphones, and many other sectors. Nanoscale DDS have enabled targeted and controlled release of conventional drugs, vaccines, recombinant proteins, and nucleic acids. They can be rationally designed from biological or synthetic materials and applied in various drug delivery routes, such as inhalable, implantable, injectable, topical, transdermal, and oral [3]. Liposomes, solid lipids nanoparticles (SLN), dendrimers, polymers, silicon or carbon materials, and magnetic nanoparticles (NP) are the examples of nanocarriers that have been utilized as the DDSs [4]. The goals [1] of such nanoscale DDS are the followings:

- **Targeting:** to maintain the therapeutic drug level at the desired sites and to reduce systemic absorption of the API and its toxic effect in healthy tissues.
- **Improved solubility:** to facilitate drug administration by injection.
- **Controlled drug release:** to ensure a zero-order release kinetics maintaining a consistent therapeutic concentration at the target site.
- **Reduced clearance:** to increase the half-life of drug.
- **Drug stability:** to reduce degradation of APIs by physiological factors.
- **Therapeutic effect:** improving the delivery of drugs across the blood–cochlear and blood–brain barriers (BBB).

In the last decade, natural polysaccharide-based nanoparticles, commonly known as nanopolysaccharides, are being exploited as DDS for various APIs, conjugates, therapeutics (e.g. lipids, proteins, peptides) and/or diagnostic agents due to their omnipresence in nature, sustainability, unique physicochemical properties, renewability, biocompatibility, biodegradability, and being low or nontoxic in nature in vivo [5–7]. The presence of reactive functional groups on such nanopolysaccharide backbone permits a wide range of modification performed on functional nanopolysaccharide-based nanoparticles (NPS-NPs) having distinct morphologies, such as nanospheres, nanocapsules, nanomicelles, nanoliposomes, and nanodrugs [5–8]. These NPS-NPs also possess different sizes and surface charges making them useful in novel DDS and diagnostic systems [2, 5–7].

5.1.2 Polysaccharides for DDS Application

Polysaccharides possess various derivable groups on their polymer chains, resulting in diverse structures of varying sizes and molecular weights; linear or branched structures; multi-functional groups (e.g. hydroxyl, carboxyl and amino groups), chirality, solubility, low toxicity, biocompatible and non-immunogenic [9]. They can be modified by (1) oxidation of primary alcohols to aldehyde and carboxylic acids, (2) nucleophilic extraction of hydroxyl groups to form ester and ether bonds, (3) enzymatic oxidation of primary alcohols, (4) amide linkage between carboxyl group and nucleophiles using coupling agents, and (5) nucleophilic reactions of amines, such as in chitosan [2].

These diverse polysaccharide-based NPs could be applied in theranostic (the integrated approach of therapeutics and diagnostics) nanomedicines over other types of synthetic NPs. For example, polysaccharides, being natural biopolymers, the NPS-NPs reduce the concerns of toxicity, biodegradability, and physiological stability [5]. Moreover, studies have shown that polysaccharide-based NPs reduced the likelihood of uptake by cellular phagocytic systems, thereby prolonging the in vivo residence time, and increase the probability of accumulation of such NPs at the target sites [5]. Due to the mucoadhesive properties of the polysaccharide-based materials, the in vivo residence time is also enhanced. Lastly, the modifiable functional groups of NPS-NPs can be tuned and manipulated for the conjugation of molecules to enhance the targeting, therapeutic and imaging, characteristics for theranostic nanomedicine [5].

To discuss all the nano-polysaccharides for drug delivery applications is beyond the scope of this chapter, and thus readers are encouraged to refer to review articles on such topics of interest [4, 5, 10–13]. In this chapter, only cellulose, and chitosan derived nanoparticle for drug delivery applications will be discussed.

5.1.2.1 Cellulose and Cellulose Nanocrystals (CNCs) for Drug Delivery

Cellulose is among one of the most abundant and sustainable material extracted from plants and agriculture biomasses [14]. It consists of a high molecular weight polysaccharide chain with repeating anhydro-D-glucopyranose units (AGU) connected via a β-1,4 glycosidic linkage [15, 16]. Recently, cellulosic polymers have gained renewed attention due to their attractive characteristics, such as low toxicity, biodegradability, biocompatibility, amphiphilicity, low binding to protein, etc. The use of cellulose micellar systems, its derivatives or NPs for drug delivery of poorly water-soluble APIs have been reported [17].

The unique rod-shaped CNCs is extracted from plants and agriculture biomass via acid catalyzed hydrolysis using concentrated acids, such as sulfuric acid yielding CNCs with a diameter of between 2 and 50 nm and length of 100–2000 nm. When sulfuric acid is used, the CNCs surfaces are decorated with anionic sulfate ester groups [14, 15]. These CNCs are electrostatically stable [14], thus they have gained

increasing attention and exploited for specific applications [15]. Due to their special features, CNCs are extremely useful for the design and preparation of novel functional nanomaterials [18, 19].

In the pharmaceutical industries, cellulose and its derivatives are commonly used as "excipients" to modify the release rate of the APIs to achieve the systemic therapeutic concentration. Microcrystalline cellulose (MCC) are frequently used in the pharmaceutical industries with other excipients to produce various dosage forms of APIs for oral drug administration. Derivatives of cellulose, such as carboxymethyl cellulose (CMC), cellulose acetate phthalate (CAP), hydroxy propyl methyl cellulose (HPMC), hydroxy propyl methyl cellulose phthalate (HPMCP), ethyl cellulose, and methyl cellulose (MC) have also been used in topical, oral and injectable formulations. For example, HPMC is widely used as a viscosity modifier, whereas CAP and HPMCP are used as enteric coating and control release formulations [20]. Additionally, Seprafilm^{TM} in which the principal component is CMC, is used for application in surgical sites, enhancing the prevention of post-surgical adhesion. Nevertheless, such cellulose/derivative-based formulations lack control of drug release in nanoparticulate or molecular level via binding interactions with the drug because of the low surface charge density present compared to the total surface area [21].

Nanogels composed of cellulose or modified cellulose have been employed as anticancer drug carriers, considering the anatomical features of the tumor and the stability of the nanogel structures [22, 23]. Li et al. [22] reported on nanogels (NGs) fabricated with lysozyme (Ly) and carboxymethylcellulose (CMC) via a green self-assembly process to evaluate the capabilities of NGs' anticancer drug carrier and delivery, where they used methotrexate (MTX) as the hydrophobic anticancer drug, and the drug encapsulation property was investigated. For such evaluation, they used human hepatoma cells (HepG2) and adriamycin resistant human breast cancer cells (MCF-7) . Usually, NGs are capable of encapsulating drugs to improve their bioavailability, control their delivery and reducing their side effects [24]. Lysozyme (Ly) has molecular weight of 14 kD, isoelectric point of 10.7, and possesses gel property like most globular proteins [25]. CMC has several negatively charged carboxymethyl groups and is readily soluble in water, thus it is a good drug carriers due to its biocompatibility, biodegradability and low immunogenicity [22].

Li et al. [22] reported that the synthesized NGs at the mass ratio of 5:2 (Ly to CMC) possessed a spherical morphology of radius of 84 ± 3 nm, and an average zeta potential of -38 ± 3 mV. They concluded that the NGs are efficient nanocarriers or delivery systems for various biological molecules based on the favorable cellular uptake of fluorescein isothiocyanate (FITC) labelled–NGs within the perinuclear space of the HepG2 and MCF-7 cells. By extending the incubation time, the fluorescence intensity of the NGs in the cells was increased, confirming that the internalization of NGs by the cells was enhanced [22]. The drug loading was driven by electrostatic forces between the carboxyl groups of MTX and amino groups of Ly, and the hydrophobic interactions between MTX and Ly. They reported a drug loading efficiencies ranging from 9.3 to 14.2% and entrapment efficiencies of 37–40% when the MTX concentration was increased from 250 to 350 μg/mL [22]. However, the encapsulation of drug molecules did not alter the average size of the delivery vehicle.

Finally, they concluded that the encapsulation of drug molecules enhanced the efficacy and activity according to in vitro cytotoxicity studies. The toxicity of MTX-NGs was greater in both cell lines than in free MTX due to the rapid penetration and uptake of smaller sized drug loaded–NGs. The nanocarriers remained localized within the cells and the drug was released gradually. Such controlled release of drug molecules in the cells can prolong and enhance the efficacy of cancer drugs leading to the desired cytotoxicities [22]. In another study, Li et al. [26] reported the efficacy of the same Ly–CMC NGs systems to encapsulate and protect curcumin for its antioxidant effects and provided new insights to protect the biomolecule from such systems fabricated with protein/polysaccharide complexes. Their results revealed that Ly–CMC NGs could be promising vehicles to deliver and protect sensitive bioactive molecules against unfavorable environments [26].

Zhu et al. [27] reported similar NG systems of Ly–CMC to evaluate the anticancer drug (5-Fluorouracil, 5-FU) delivery/release from such systems and reported that at a weight ratio of Ly:CMC = 2:1, the nanogels possessed the highest encapsulation efficiency and loading capacity for the anticancer drug, 5-FU (30.48 and 10.16%, respectively). As well, in vitro experiments for the release of 5-FU in simulated intestinal fluid (SIF) and simulated gastric fluid (SGF) revealed that the nanogels displayed a sustained release profile, and the drug release in SGF was lower than in SIF (33.9 and 58.6% in a period of 16 h, respectively), indicating that the 5-FU could be protected in the stomach so that they were released in the intestines [27].

Qian et al. [28] prepared redox-sensitive NGs (MACMC–CBA) having a disulfide linkage (–S–S–), using methacrylated carboxymethyl cellulose (MACMC) and cystamine bisacrylamide (CBA). Morphologically the NGs possessed a spherical shape having a diameter of approx. 192 ± 2 nm, and zeta-potential of −25.7 ± 1.6 mV. These redox sensitive NGs were stable in a high ionic strength environment, but they disintegrated in a medium containing the endogenous amino acid, glutathione, GSH (a reducing agent/antioxidant) which is abundant in cancer cells. Here, doxorubicin (DOX) was encapsulated within the NGs by electrostatic forces between the positive amino groups ($–N^+H_3$) of DOX and negative carboxyl groups ($–COO^-$) on the MACMC. The loading content and encapsulation efficiency were reported to be 36 and 83% respectively, and the DOX-loaded NGs were found to be internalized by the carcinoma cells via endocytosis delivering the DOX molecules into the nucleus. Here, the evaluation of the in vitro cytotoxicities for cancer cells in human neuroblastoma (SH-SY5Y) and murine hepatic carcinoma (H22) cell lines revealed a dose dependent cytotoxicity for the DOX delivered using these NGs. At 16 μg/mL of DOX loaded NGs, 70% of SH-SY5Y and 65% of H22 cell proliferation were suppressed. These results of antitumor effects were significantly superior compared to free DOX. The results also suggested that due to the presence of GSH in the cytoplasm (a reductive environment) a relatively faster release of DOX from the NGs was observed, inducing the suppression of cell proliferation that resulted to an improved antitumor efficacy. Furthermore, the cell viability of the NGs themselves was approx. 97% (for SH-SY5Y cell lines) and 93% (for H22 cell lines) at a maximum concentration up to 400 μg/mL, confirming that the MACMC–CBA NGs are nontoxic and compatible with human cells [2, 28].

Rahimian et al. [29] described the preparation of NGs from hydroxypropyl cellulose (HPC)-grafted copolymers prepared using the atom transfer radical polymerization (ATRP) method on two methacrylate monomers with disulfide linkage (HMssEt) and oligo(ethylene oxide) (OEOMA). The HPC-g-P(HMssEt-co-OEOMA) NGs exhibited both the reductive and thermo-responsive properties, and the thermal properties were controlled by the pendant hydrophobic/hydrophilic balance. Due to the micellization of the self-assembled NGs in aqueous environment, the in situ disulfide-crosslinkers from the thiol-disulfide exchange reaction yielded disulfide-crosslinked nanogels with excellent colloidal stability on dilution. The nanogels exhibited responsive degradation triggered by reduction in the cellular environment containing a reducing agent, such as the GSH. Such reduction responsive NGs offer many possibilities in targeting drug delivery for enhanced aqueous colloidal stability in biological pH and faster release profile [29].

Similarly, Wen and Oh [30] reported on the carboxymethyl cellulose, CMC (pH responsive) and oligo(ethylene oxide)-copolymers (thermo-responsive; OEOMA, MEO2MA etc.) based novel bio-nanogels that are dual responsive (temperature/acidic pH-responsive), and these bionanogels (DuR-BNGs) possessed a narrow size distribution, significant colloidal stability, and negligible interactions with proteins. When the DOX loaded DuR-BNGs were examined in acidic pH at temperature above the lower critical solution temperature, LCST, they exhibited synergistic release of DOX due to the acidic pH-sensitivity of $–COO^-$ groups on the CMC as well as temperature-induced volume change of grafted thermo-responsive copolymers. The evaluation of DOX-loaded DuR-BNGs for the in vitro cytotoxicity through MTT assay on HEK 293 T kidney and HeLa cancer cells reveled >90% of the cell viability at concentrations up to 1.0 mg/mL indicating the nontoxic nature of such BNGs. Furthermore, the competitive and rapid decrease of the Hela cell viability for the DOX loaded DuR-BNGs compared to free DOX over a range of concentrations suggested that cellular proliferation was inhibited due to the effective and rapid release of DOX from DuR-BNGs, and likewise, the authors concluded that this novel DuR-BNGswere colloidally-stable, and thus are promising candidates as drug vehicles for cancer therapy [30].

CNC is well-suited for targeted drug delivery due to its unique physicochemical properties that are favorable for cellular internalization [21]. Due to their excellent colloidal stability, CNCs are excellent candidates for the encapsulation and delivery of biomolecules. Many studies have been conducted with CNCs for loading of several drugs (charged/neutral), and the controlled release of APIs as well as the transport of DNAs to target cells [19]. Notably, the poly(ethyl ethylene phosphate) (PEEP) modified cellulose nanocrystals (CNCs) (CNC-g-PEEP) were synthesized by Wang et al. through a “grafting to” process for the loading and delivery of DOX to cancer cells [31] (Fig. 5.1).

Wang et al. employed the electrostatic interactions to encapsulate the DOX by the aqueous dispersion of negatively-charged CNC-g-PEEP nanocrystals and the DOX was released from such NPs after internalization within the cancer cell, and the drug release was rapid at pH 5.0 compared to pH 7.4. In addition, the PEEP-g-CNCs possessed excellent cytocompatibility with both L929 and HeLa cell lines [31].

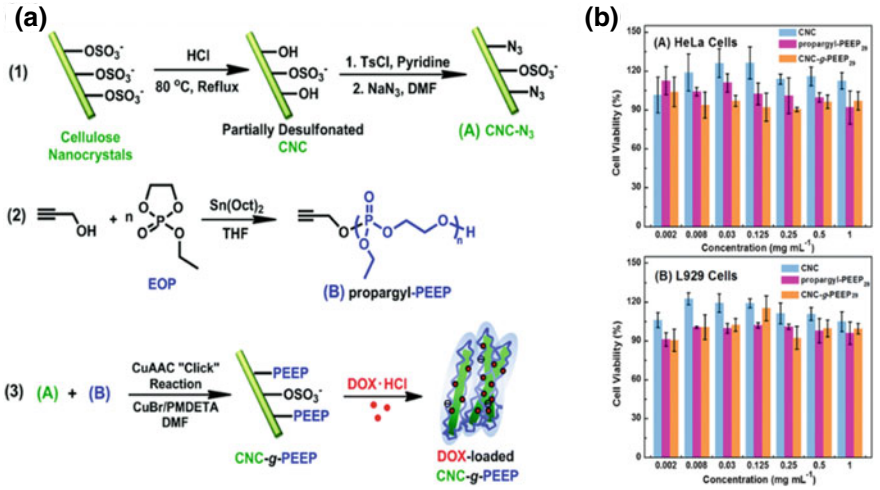

Fig. 5.1 **a** Schematic describing the synthesis of CNC-g-PEEP via CuAAC "click" reaction to prepare DOX-loaded nanocrystals. **b** Cell viability of (**A**) HeLa cells and (**B**) L929 cells incubated with CNC, propargyl-PEEP29 and CNC-g-PEEP29 at different concentrations for 48 h, respectively. Reproduced from [31]

The slow release at the biological pH (7.4) is believed to be beneficial for such nanocrystals/NPs during systemic circulation as most of the drug would be retained within the NPs, ensuring the avoidance of some undesirable side effects to healthy tissues/cells. The fluorescence measurements indicated that the drug loading capacity (DLC) and drug loading efficiency (DLE) for the modified nanocrystals (CNC-g-PEEP) were 13 and 27%, respectively. Moreover, the DOX-loaded NPs showed a notable higher cell viability (less cytotoxic) against HeLa cells compared to free DOX due to the prolonged DOX release from the DOX-PEEP-g-CNCs as a result of the disruption of electrostatic interactions. Here, the DOX loaded NPs exhibited anticancer activity, having the IC50 value (inhibitory concentration to produce 50% cell death) of 9.95 mg DOX equiv. L^{-1} for HeLa cells compared to 6.38 mg DOX equiv. L^{-1} for free DOX [31].

You et al. [32] developed injectable hydrogels comprising of quaternized cellulose (QC) and cationic CNCs (CCNC) crosslinked by β-glycerophosphate (β-GP) that immediately gelled with increasing temperature, where the CCNCs were evenly distributed throughout the hydrogels offering a dual role within the hydrogel: performing as a filler and a crosslinker. Such hydrogels exhibited higher mechanical strength, greater resistance to degradation and sustained release profile due to the crosslinking resulting from the strong interaction between the two components/chains of the hydrogel [32]. The erosion rate is a critical parameter for injectable hydrogels to be considered as the drug delivery vehicle and here, it was reported that hydrogels with CCNC content of 1, 1.5, and 2.5 wt% possessed a disintegration time of approx. 6, 13, and 18 days, suggesting a proportional resistance to in vitro degradation rate

of the hydrogels. They also loaded DOX onto these QC/CCNC/β-GP hydrogels for in vivo studies to evaluate liver cancer tumor growth in H22 cell xenografted mice. It was reported that the sustained release of DOX from the hydrogels increased the efficacy of the chemotherapy and thus suppressed the tumor growth over a prolong time period compared to free DOX, leading to significantly increased survival rate. The authors reported that the highest CCNC loaded hydrogel could release the drug in a sustained manner for at least 17 days and the rate of delivery for the DOX from such hydrogels was about 29.4 μg/day [32]. The in vitro cytotoxicity of the hydrogels evaluated by the MTT assay revealed that such injectable forms of the hydrogels possessed low cytotoxicity and greater biocompatibility at a higher concentration of 5 mg/mL, with mild inflammatory reaction [32].

Dufresne and coworkers developed CCNCs and sodium alginate based hydrogel possessing double membranes (an outer and a rate controlling inner membrane) as the modified release drug delivery (MRDD) vehicle to control the release of two different drug molecules: an antibiotic, ceftazidime and an epidermal human growth factor [33]. When CCNCs crosslinks the alginates to form the inner layer of the hydrogels, they produce a steric effect due to greater interactions between the two constituents, leading to the controlled release of drugs encapsulated within the hydrogels. The goal of the double membrane on such hydrogels was to achieve a faster disintegration of the outer membrane leading to a burst release of the drug component, followed by a modified release in a controlled manner from the inner rate controlling membrane. In that work, the authors investigated the burst release from the outer alginate membrane using an antibiotic, followed by the expected sustained release of the other drug component from the inner alginate/CCNC membrane at physiological pH [33].

Folic acid (FA) has high affinity and thus binds to folate receptors (FR), and the FRs are well recognized biomarkers in a wide range of cancer cells due to its overexpression within such tumor tissues. Dong et al. [34] reported on the fabrication of folic acid-conjugated CNCs for the site specific delivery of anticancer drugs to FR-positive (FR+) neoplastic cells. Here the CNC was conjugated to the folic acid and fluorescein isothiocyanate (FITC) to produce FITC-CNC-FA nanoparticles that selectively and directly bind to the FR+ cells. They established that the cellular internalization through the caveolae-mediated endocytosis of FITC-CNC-FA nanoparticles to the rat (C6) and human (DBTRG-05MG and H4) brain tumor cells was 46, 976 and 1452 times higher when compared to FITC-CNC, signifying their potential ability to target the FR+ noeplastic cells. Additionally, their excellent cytocompatibility (no cytotoxicity) combined with the proven specific FR-mediated cellular internalization establish the FA-conjugated CNCs as the promising nanoparticles for the site specific delivery of anticancer drugs to cancer cells [34].

Rosilo et al. [35] prepared cationic CNCs with pendant quaternary ammonium groups through the facile synthesis by surface-initiated atom-transfer radical polymerization (si-ATRP) of poly(N,N-dimethylaminoethyl methacrylate), PDMAEMA and subsequent quaternization of the pendant amino groups of the DMAEMA chains. Such cationic CNCs displayed excellent aqueous dispersibility and colloidal stability

as confirmed by an overall ζ-potential of +38 mV. This allowed them to bind and concentrate the virus capsid from a solution to form micrometer sized aggregates. This study revealed the feasibility of using CNC-based systems as transduction enhancers for viral or other anionic particle delivery applications [35].

The cytosine deaminase (CD)/5-fluorocytosine (5-FC) system is a widely studied suicide gene therapy approach. CD is a gene encoding enzyme that can convert the prodrug, 5-FC (nontoxic to human due to lack of CD) into the active anticancer drug, 5-fluorouracil (5-FU) [36]. Xu and coworkers studied and developed a CNC system fabricated with cleavable polymeric (PDMAEMA) side chains for plasmid DNA (pDNA) delivery to neoplastic cells, [37] where the needle-like shape of CNCs played a significant role in enhancing the transfection efficiency (TE). The PDMAEMA grafted CNCs complexed with the enzyme/prodrug system (CD/5-FC) yielded a system that could be cleaved by a reducing agent, glutathione (GSH) thereby releasing the condensed pDNA from the system. The in vitro cytotoxicity through the MTT assay for the CNC-SS-PD/pDNA complexes in COS7 and HepG2 cells at various N/P ratios demonstrated that the high molecular weight polycations (chain length of PDMAEMA) exhibited higher cytotoxicity, as the polycation pendant chains of CNC-SS-PDs could quickly be displaced from the CNCs after cellular internalization through the cleavage of the disulfide bonds triggered by GSH, thus the CNC was reported to be nontoxic in such delivery vehicles. They reported outstanding transfection efficiencies (reflecting equivalent antitumor activities) of biocleavable vectors in HepG2 cells partly because of the rod-like shape of CNCs. From the in vivo anti-tumor data obtained from the female balb/c-nu mice (tumor induced through injecting HepG2), they concluded that the CNC-based carriers could effectively suppress and regress the tumor growth [37]. In another work by Xu and coworkers [38], they designed gold nanoparticle (AuNP) conjugated to CNC with polymer brushes for DNA delivery. In that work, the PDMAEMA and poly [poly (ethylene glycol) ethyl ether methacrylate] (PPEGEEMA) grafted CNCs were mixed with pDNA, and the complex was then conjugated with AuNPs for imaging application. This multifunctional CNCs with cationic PDMAEMA chains condensed the DNA to form polycomplexes, and the steric stabilization rendered by the uncharged PPEGEEMA brushes reduced its binding with anionic cell membranes, resulting in an overall low cytotoxicity, proving the system as an ideal vehicle for DNA delivery applications [38].

In a recent review [21], a comprehensive assessment on rainbow trout and nine other aquatic species revealed no serious environmental concerns of CNC based on ecotoxicological characterization [21]. As a drug delivery vehicle, the CNC prepared from commercial softwood was used to attach tetracycline and doxorubicin, which could rapidly be detached within a day. Furthermore, the idea of binding cationic surfactant, CTAB to the surface of the pristine CNC made it possible to design CNC based delivery agents to encapsulate substantial quantities of several hydrophobic anticancer drugs that could be released in a sustained manner over a 2 day period [21].

5.1.2.2 Chitosan and Derivatives for Drug Delivery

Chitosan, a 2-amino-2-deoxy-β-D-glucan is a ubiquitous and abundant natural cationic polysaccharide. This biopolymer is generally derived via the alkaline N-deacetylation of chitin, an abundant polysaccharide found in the exoskeleton of crustaceans, insects, and fungi [39–42]. Chitosan is a linear polysaccharide, comprising of glucosamine (2-amino-2-deoxy-β-d-glucopyranose) and N-acetyl glucosamine (2-acetamide-2-deoxy-β-d-glucopyranose) units via β-(1 → 4) linkages, distributed throughout the polymer backbone, and the chemical compositions depend on the methods of preparing the chitosan from chitin [42, 43]. After deacetylation, chitosan is soluble in acidic medium, acquiring positive charges arising from the protonation of amino groups on the glucosidic residue along the polymer backbone [39, 42]. The primary amine groups impart special properties, making CS a very useful material for pharmaceutical applications [41]. In addition to these characteristics, chitosan possesses many other intrinsic properties, such as low toxicity, biocompatibility, biodegradability, and mucoadhesivity [39, 40–42, 44, 45]. The primary and secondary hydroxyl groups in the C-2 and C-6 positions and the primary amine groups in the C-2 position allows specific chemical modifications of chitosan to yield a wide range of derivatives [40, 45]. Due to these favorable properties, chitosan and its derivatives have received increasing scientific interests and they are widely explored and exploited for applications in food, medical and pharmaceutical applications [45–52].

Polyelectrolytes are macromolecules possessing a wide range of neutral and charged functional groups [53]. In the absence of chemical cross-linker, just through the simultaneous mixing of oppositely charged polyelectrolytes in solution, polyelectrolyte complexes (PEC) are formed. The main interactions driving the formation of polyelectrolyte complexes are strong reversible electrostatic and dipole–dipole association, as well as hydrogen and hydrophobic interactions [54]. The protonation of amino groups produces a cationic polyelectrolyte in acidic medium, and the interactions with other negative polyelectrolytes form the PECs.

Due to the small size of NPs, the systemic circulation times are relatively long and the uptake by the reticuloendothelial system (RES) is low. Hence, they could be directed to the tumor sites via the random and leaky vascular tissues through a well-known phenomenon called enhanced permeability and retention (EPR) effect [55]. Such passive targeting still suffers from a major limitation, where the drug concentration at tumor site is below the therapeutic level, resulting in poor efficacy and negative systemic effects [40, 56]. In this regard, site specific targeting can be attained by fabricating chitosan derivatives with tumor-targeting ligands, such as antibodies, peptides, hyaluronic acid, biotin, folic acid, and avidin that bind to corresponding receptors that are unique to cancer cells [40].

Son et al. reported on the synthesis of CS–DOX conjugates with the cis-aconityl linkage to yield well-defined nanoparticles of size range of between 250 and 300 nm. The DOX loading was as high as 38 wt% and the CS–DOX conjugates were found to preferentially accumulate in the tumor tissue due to the EPR effect. The predominant reason of such accumulation was due to the cis-aconityl spacer which showed

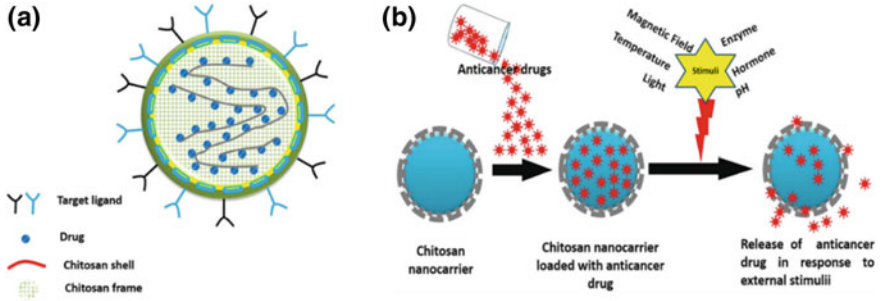

Fig. 5.2 **a** Description of the chitosan nanostructure and drug encapsulation. **b** Release of anticancer drugs from chitosan nanocarriers in response to external or internal stimuli. Reproduced from [43]

pH-responsive behavior resulting in hydrolysis in the acidic environment of endosomes/lysosomes and thus the release of the drug to the cytoplasm [39]. A schematic of stimuli-responsive chitosan-based drug delivery is illustrated in Fig. 5.2.

Similarly, Lee et al. [57] successfully conjugated paclitaxel (PTX), an anticancer drug to CS to produce CS–PTX using a biodegradable succinate linker. As the linker is resistant to gastric pH (acidic) and it can be cleaved at the physiological pH of the blood stream, such conjugate is suitable for oral administration [57]. Lee et al. [58] reported on a novel delivery system for insulin based on low molecular weight chitosan (6 kDa), where a disulfide (–S–S–) linkage was established between the insulin and the chitosan to form the conjugates. Insulin could be released from these conjugates via the breakdown of the S–S bond in the presence of glutathione (GSH), the concentration of which was much higher inside cells and tumors. The bioavailability of insulin at 43% from the in vivo studies demonstrated the significantly enhanced GI absorption of the insulin after oral administration [58].

Gong et al. [59] studied and produced conjugates of 6-MP (6-mercaptopurine) and carboxymethyl-chitosan through an α,β-unsaturated linker, where the linker was found to be sensitive to GSH (a reducing agent) concentration. As the concentration of GSH in cancer cells is almost 4 times higher than in normal cells, therefore such conjugates have the potential for the delivery of 6 MP [59]. Table 5.1 also summarizes some notable drug conjugates based on CS.

Recently, Yang et al. [60, 61] fabricated a chitosan based polymeric delivery system for an anti-HIV drug, Stavudine (d4T). However, intolerable adverse reactions and poor cellular internalization efficiency limit its clinical application. Here, chitosan–O-isopropyl-5′-O-d4T monophosphate was conjugated via the phosphoramidate linkage for effective delivery. In vitro drug release studies at pH 1.1 and 7.4 suggested that the chitosan–d4T conjugates were capable to preferentially release d4T 5′-O-isopropyl monophosphate (a nanoprodrug) compared to free d4T for prolonged periods. Such release profile of the nanoprodrug from the conjugates could bypass the metabolism of d4T resulting in an increased selectivity of anti-HIV action. Additionally, the conjugated NPs could prevent the coupled drug from leakage from the nanoparticles prior to entering the target viral compartment and provide a modest

Table 5.1 Notable drug conjugates based on CS for drug delivery applications

Chitosan derivative	Molecular weight	Drug delivered	Linkage	Cleave condition
Glyco-chitosan	250 kDa	Dox	cis-Aconityl	pH sensitive
Chitosan	6 kDa	Paclitaxel	Succinate	pH sensitive
Chitosan	3, 6, 9 and 13 kDa	Insulin	Disulfide linkage	GSH sensitive
Carboxymethyl-chitosan	200 and 340 kDa	6-MP	α,β unsaturated linkage	GSH sensitive
Chitosan	Low molecular weight	d4T	Phosphoramidate	Prolonged release period

controlled release of d4T 5′-O-isopropyl monophosphate, proving that such conjugated nanoprodrug may be used for targeting with an improved efficacy and reduced adverse effects in anti-HIV treatment [60, 61].

Very recently, Yu and coworkers [45] published an excellent review highlighting the recent advances of chitosan drug delivery systems crossing the blood-brain barrier (BBB) for the treatment of brain disease. A wide range of chitosan nanoparticles can improve the treatment of various brain related diseases due to its biocompatibility, biodegradability, low toxicity, controlled release, mucoadhesion, modifiability and effective uptake by nasal mucosal and tumor cells. The intranasal delivery of drugs and chitosan nanoparticles could enhance the nasal residence time and uptake by the mucosa due to the positively charged surface [45]. In another recent review by Sah and coworkers [62], they discussed the chitosan based devices developed for drug delivery applications for the effective treatment of various periodontal disorders. Chitosan-based NPs have been found to be potential candidates in improving periodontal drug delivery. Due to their sizes, the nanoparticles tend to diffuse into areas below the gumline that are usually inaccessible by other drug delivery vehicles. Thus, they concluded that the chitosan based NP systems that possess the add-on properties of mucoadhesion, biodegradability, drug release in a controlled manner, good penetrability and retention in and around the periodontal pocket, and ease of delivery could be a feasible approach for periodontal drug delivery.

5.2 Bioimage, Biosensor and Biocatalyst Applications

5.2.1 Polysaccharide-Based Nanomaterials for Bioimaging Applications

Bioimaging is a powerful tool in the biomedical sectors, enabling the non-invasive visualization of biological process, subcellular structure, cells, or entire multicellular

organisms using various sources, such as light, fluorescence, electron, ultrasound, X-ray, and magnetic resonance. The image acquisition of biological substances using fluorescent probes and fluorescent labeled materials is generally considered as a bioimaging technique since this is the most well-known method aside from conventional light microscopy and MRI imaging. The bioimaging based on fluorescent nanoparticles or probes can be classified into three major classes according to Wolfbeis [63]: (1) Using unmodified fluorescent nanoparticles or pure fluorophores. This fluorescence imaging probe does not have any recognition sites of chemical species, and the plain fluorescent materials are internalized into random cells, providing images of cellular structure or tissue. (2) Targeted bioimaging is considered as the second fluorescence bioimaging functionalized with receptors, ligands, antibodies or oligomers to accomplish immobilization or internalization at specific site, such as tumor, genes, mitochondria or membranes to provide a more effective treatment for tumor with minimal damage to healthy cells. (3) Fluorescent nanoparticles or probes with sensing abilities to detect and image tissues under various conditions, such as temperature, pH, glucose, calcium (II), or oxygen concentration are suitable systems for theranostics. This section will explore the use of polysaccharide-based nanocomplex for bioimaging applications, mostly based on fluorescent probes or labeled materials.

5.2.1.1 Chitosan-Based Bioimaging Materials

Fluorescent-labeled Chitosan (CS)-based nanoparticles have been extensively used for bioimaging applications due to abundance of amine groups on the glucose units that enable the facile conjugation with fluorescence dye. These fluorescent bioimaging systems have been used for various cancer theranostic applications that possessed both chemotherapy and cellular bioimaging capabilities. Ghoshal et al. synthesized CS-alginate nanoparticles embedded with silver nanoclusters for cancer theranostics. Also, secreted frizzled-related protein-4 (sFRP4) was loaded to block Wnt/β-cateniun signaling in cancer cells that can provide anti-cell proliferative effect. As shown in Fig. 5.3, bioimaging using confocal microscope confirmed the complete cellular uptake by Hela cells after 8 h, demonstrating the utility of silver nanoparticle enabled bioimaging, cellular uptake, and tracking of nanoparticles [64]. Mauran (MR), the sulfated bacterial exopolysaccharide extracted from halophilic bacterium, *Halomonas maura* was synthesized with CS to prepare a nanohybrid system for cancer chemotherapy and bioimaging. MR/CS nanoparticles labelled with fluorescent dye possessed excellent characteristics, such as biocompatible, biodegradable, and nontoxicity for live cellular imaging of cell binding and uptake capabilities [65]. Another cancer-theranostic nanoparticles for melanoma treatment were achieved by coating CS on magnetic iron oxide. CS-Fe_3O_4 nanoparticles exhibited an excellent magnetic resonance imaging (MRI) capability and the in vitro hyperthermia effects under near-infrared (NIR) laser irradiation with good stability and negligible cytotoxicity [66].

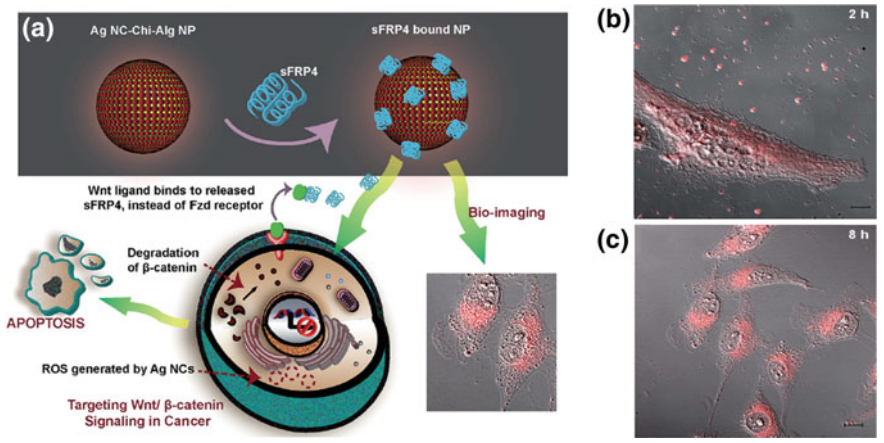

Fig. 5.3 **a** The illustration of CS-Alginate-Ag-sFRP4 for cancer theranostics nanoparticles. **b**, **c** A bioimaging of luminescent NPs acquired by using confocal microscope. **b** Incomplete cellular internalization of nanoparticles after 2 h, **c** complete cellular uptake by Hela cells after 8 h. Scale bar represents 10 μm. Reproduced from [64]

Carbon dots (CD) and quantum dots (QD) have been used in biomedical imaging applications. The fluorescent CD conjugated CS nanoparticles, synthesized in a single step for bioimaging and drug delivery revealed intracellular cellular uptake as determined by fluorescence microscopy and flow cytometry [67]. CD was used in combination with PEG-CS nanogels for two-photon fluorescence (TPF) imaging as a result of CD absorption for NIR and up-conversion photoluminescence properties. The embedded CD in PEG-CS nanogel was suitable for confocal and TPF imaging as well as fluorescent pH-sensing due to the pH-responsive swelling properties of CS [68]. Carboxylated 4,4-difluoro-4-bora-3a,4a-diaza-s-indacene (BODIPY-COOH) was conjugated to CS nanoparticles for fluorescent probe and the CS nanoparticles increased the cell viability by reducing the toxicity of BODIPY-COOH. It could also provide fluorescent imaging, however the system is quite toxic to both A549- and BEAS 2B cell lines [69].

5.2.1.2 CNCs-Based Bioimaging Materials

CNCs extracted from acid hydrolysis of cellulose nanofiber have been investigated for various biomedical applications due to its advantages: biocompatible, biodegradable, higher mechanical strength, high stability in water, and non-toxicity. CNCs are promising candidates for bioimaging applications and various fluorescence-CNC biomarkers were reported using different compounds. Dong and Roman (2007) reported a facile method for nanocellulose-based bioimaging application by covalently conjugating FITC onto CNC surface. They decorated epoxide ring on the surface of CNCs, then treating with hydrogen peroxide and ammonium hydroxide

to generate primary amino groups as they can react with isothiocyanate group of FITC. The content of FITC was confirmed by UV-vis and prepared solution was stable in colloidal system [70]. Mahmoud et al. reported that the surface charge of fluorescent labeled CNCs played a significant role in cellular uptake and cytotoxicity from studies using two types of fluorescent probes [FITC and rhodamine B isothiocyanate (RBITC)]. Positively charged CNC-RBITC exhibited good cellular uptake behavior but negatively charged FITC-CNCs showed no significant internalization and they induced the surrounding cells to rupture [71]. Photoluminescent and biocompatible hybrid materials comprising of TEMPO oxidized CNCs (TO-CNCs) and carbon quantum dots (CQDs) were prepared via carbodiimide-assisted coupling chemistry between the amine group of CQDs and carboxyl group of TO-CNCs. The bioimaging of TO-CNC@CQD hybrid nanomaterials showed an enhanced cellular internalization on both HeLa and RAW 264.7 cells due to the amine groups on CQDs conjugated to the cell surface [72]. Cotton derived CNCs were labeled with 5-(4, 6-dichlorotriazinyl) aminofluorescein (DTAF) of different surface charge density in a one-pot reaction. Three CNC samples (anionic CNCs from sulfuric acid hydrolysis, a partially de-sulfated CNCs, and uncharged CNCs via HCl hydrolysis) showed that the degree of labelling was influenced by the sulfur content on CNC surface, and the amount of DTAF bound to CNCs increased with the reduction of the surface charge density. HCl-hydrolyzed CNCs became less agglomerated after labelling with DTAF but other labelled CNCs showed similar colloidal stability compared to unlabeled CNCs. Also, the uniformity of CNC dispersion in electrospun PVA fibers was studied using DTAF-labelled CNCs. Good dispersion indicating that DTAF-labelled CNCs could be used as optical markers for the dispersion quality of CNC-based composites [73]. For another CNC-based bioimaging applications, water-soluble photosensitizer (PS-CNCs) prepared using CNCs and polyaminated chlorin p6 was reported. Purpurin-18 (Pp-18) was prepared from Spirulina maxima chlorophyll and reacted with different polyethyleneimines (PEIs) resulting in a color change from purple to green. The cancer cell targeting function of PS-CNCs was tested for their antitumor activity against a human immortalized keratinocyte (HaCat) cell line, and the data showed half maximal inhibitory concentration (IC_{50}) was in the nanomolar range indicating high potentials in biomedical applications [74]. Modern Alexa Flour dyes that have advantages of superior brightness and photostability over conventional fluorescence probe were conjugated to CNCs using two approaches for bioimaging applications. The first approach is to modify CNC surface with aldehyde groups that can bind to terminal amino-groups on Alexa Flour dyes. A second approach is to modify Alexa Fluor dye to possess a chloro-substituted triazine ring at the linker end, which can then react with the acetonitrile of CNCs. Fluorescent CNCs with Alexa Flour dyes could be processed into solid deposits in microfluidic structure and the disappearance in the presence of enzymes or microbes were observed by fluorescence microscopy [75].

5.2.2 *Polysaccharide-Based Materials for Biosensor Applications*

A biosensor is an analytical device for detecting specific chemical substances or biological elements, such as glucose, oligonucleotides, and gene fragments. It is composed of a bio-receptor, bio-transducer, and an electronic system. Bio-receptor plays a role in detecting specific compounds through various interactions, such as antibody/antigen, enzymatic, nucleic acid, epigenetics, cells, and tissue interactions. High selectivity is a key requirement for bioreceptors. A bio-transducer is an essential component to measure the interaction from bio-receptor site and its measurement methods can be categorized into electrochemical, optical, electronic, piezoelectric, gravimetric, or pyroelectric. Polysaccharide-based nanomaterials are being used to prepare biosensors since they are biocompatible, biodegradable, non-toxic, and stable. In this section, electrochemical and optical biosensors using nanopolysaccharide will be highlighted and discussed.

Various polysaccharide-based nanocomposites, such as pectin, starch, and cellulose have been extensively used with nano-based sensing agents, such as graphene oxide (GO) and quantum dots (QD) to improve the functionality of the biosensors. By using polysaccharide, the stability and biocompatibility of biosensor system are enhanced.

Pectin coated on polyaniline (PAni) nanoparticles are used in amperometric glucose sensor as it possessed high sensitivity (79.49 μA mM^{-1} cm^{-2}), linear range (0.06–4 mM), and low detection limit (43.5 μM) at a working potential of 0.6 V. Not only does pectin stabilized PAni nanoparticles in the colloidal system, the pectin also provided sites for the covalent immobilization of the enzyme to PAni [76]. Oxidized starch functionalized with poly ((2-dimethylaminoethyl) methacrylate) (OS-g-PDMAEMA) and CdTe/ZnS QDs was used as an optical nano-sensor for tetracycline hydrochloride (TH) drugs. It was reported that modified QDs with OS-g-PDMAEMA exhibited high sensitivity and selectivity in the linear range from 9.14 to 7.23 nM with the detection limit of 2.74×10^{-1} mol L^{-1} by selectively quenching at 520 nm region in the presence of TH [77]. Cotton based nanocellulosic aerogels (NA) modified with fluorescent tripeptide (PepNA) were studied for protease detection that can be applied to chronic wound treatment. Proteolytic enzymes were conjugation to the NA through the esterification of cellulose surface hydroxyl group with the glycidyl-fluorenylmethyloxylcarbonyl (FMOC) and tripeptide that was coupled with the immobilized glycine. PepNA biosensor was capable of detecting human neutrophil elastase (HNE) at concentration present in the arterial chronic wound fluid (0.1 U/mL) with a limited sensitivity concentration of 0.13 U/mL. It displayed four times greater detection capability for HNE than free peptide substrates [78].

Chitin/CS have the most widely studied polysaccharide-based materials for biosensing applications. Multifunctional therapeutic systems consisting of chitin nanogels (CNGs) conjugated to QD were examined for BSA protein delivery as well

as for bioimaging and biosensor applications. BSA-QD-CNG integrated regulated protein delivery, cellular imaging, and optical pH-sensing in a single nanocomplex [79]. Amperometric glucose biosensor prepared from CS nanoparticles extracted from gladius of squid, *Uroteuthis duvaucelii* was functionalized with Glucose oxidase (GOx) on Au electrode. The sensor displayed good amperometric response towards glucose with a proportional detection range from 0.001 to 1 mM with a short response time (within 2 s), high sensitivity, low detection limit, and good stability [80]. GO-CS nanocomposite labeled with single stranded (ss) DNA was used as an electrochemical biosensor for typhoid diagnosis, and it could distinguish complementary, non-complementary, and one base mismatch sequences with the detection range (10 fM–50 nM) and lower detection limit of 10 fM in PBS and 100 fM in spiked serum. The introduction of GO in biosensor increased the electron transfer and electrochemical capabilities, while CS provided biocompatible surface for DNA immobilization [81]. Another electrochemical DNA-based biosensor comprised of cuprous oxide and nano-CS was fabricated for the detection of Hg^{2+} ions in aqueous solution, and Cu_2O@NCs biosensors possessed high sensitivity and stability with a range of 1–100 nmol L^{-1} and detection limit of 0.15 nmol L^{-1}. In addition, they found the Cu_2O@NCs modified with DNA dramatically improved the sensitivity for Hg^{2+} detection over pure Cu_2O@NCs biosensors [82]. Li et al. developed an immunosensor containing thiol graphene and thiol CS with gold nanoparticles (thGP-thCTS-AuNPs) for carcinoembryonic antigen detection with two linear ranges (0.3–0.8 and 8.0–100 ng mL^{-1}) and detection limit of 0.03 ng mL^{-1}. thGP-thCTS-AuNPs nanocomposite revealed improved selectivity, high sensitivity, and good stability for immunosensor [83].

CNCs functionalized with inorganic substances have been explored as biosensors due to the abundance of functional groups and good stability. CNCs modified with pH responsive compounds were studied for pH sensor applications. Nielsen et al. proposed two methods to decorate dual fluorescent compounds on the surface of CNCs. First strategy was to conjugate FITC and RBITC in 0.1 M NaOH solution with hydroxyl groups of CNCs. Prepared fluorescent-labeled CNCs had absorbance at 490 nm (FITC) and 540 nm (RBITC). A second strategy was to use thiol-ene Michael addition and conjugate with succinimidyl ester dye. Both modified CNCs exhibited pH-responsive characteristics by emitting different spectra at various pHs [84]. Another CNC-based pH probe was prepared by grafting Poly (amidoamine) (PAMAM) dendrimer through carbodiimide-mediated amidation process and the pH-responsive functionality was confirmed by zeta potential, UV-vis, and ITC [85]. Nonenzymatic glucose sensor was prepared by synthesizing CNCs with poly(diallyldimethylammonium chloride) (PDDA-CNC) and AuNPs. 5AU/PDDA-CNC (5 wt% Au loading) showed the best glucose sensing capabilities with high sensitivity of 62.8 $\mu A\ mM^{-1}\ cm^{-2}$, low detection limit of 2.4 μM, and a linear detection range from 0.004 to 6.5 mM [86]. The transformation of CNCs into fluorescent labelled nanoparticle conjugated to pyrene (Py-CNCs) was achieved via a three step covalent binding process for the detection of Fe^{3+} in biological, chemical, or environmental system. Py-CNCs possessed excellent selectivity for Fe^{3+} over a wide concentration range with the electron/energy transfer process occurring

Table 5.2 The polysaccharide-based nano-biosensor applications

Polysaccharides	Modified materials	Application	Range	Limit of detection	Reference
Chitin	QD	Optical pH sensor	N/A	N/A	[79]
CS	AuNP	Glucose sensor	0.001–1 mM	1.1 μM	[80]
CS	GO	Typhoid diagnosis	10 fM–50 nM	10 fM	[81]
CS	Cu_2O	Hg_2^+ sensor	1–100 nM	0.15 nM	[82]
Thiol CS	AuNPs, Thiol GO	Antigen sensor	(1) 0.3–0.8 ng mL^{-1} (2) 8.0–100 ng mL^{-1}	0.03 ng mL	[83]
CNCs	PDDA, AuNPs	Glucose sensor	0.004–6.5 mM	2.4 μM	[86]
Pectin	PAni NPs	Glucose sensor	0.06–4 mM	43.5 μM	[76]
Starch	PDMAEMA, CdTe/ZnS QDs	TH drug sensor	9.14–7.23 nM	0.274 M	[77]
CNCs	Py	Fe_3^+ detection	–	–	[87]
CNCs	FITC, RBITC	pH probe	–	–	[84]
CNCs	PAMAM	pH probe	–	–	[85]
NC aerogel	PepNA	Protease sensor	–	0.13 U/mL	[78]

between Py fluorophore and redox active metal ions induced fluorescent quenching [87] (Table 5.2).

5.2.3 Polysaccharide-Based Nanomaterials for Biocatalysts

Biocatalysts are biological substances that initiate, modify, and promote the rate of chemical reactions. Biocatalysts can have several advantages over conventional chemo-catalysts for biomedical and healthcare applications: (1) they are more biocompatible, (2) display higher catalytic activity and chemo-selectivity for various compounds, and (3) produced via green chemical process under milder reaction in physiological conditions. There are various types of biocatalysts, such as microbes (yeast or other anaerobic bacteria), lipases, proteases, cellulases, and amylases. Enzymes are the most popular biocatalytic source with lipases (triacylglycerol ester hydrolases, EC 3.1.1.3) receiving broad attentions for use as versatile biocatalysts in food, chemical, pharmaceutical, and biotechnology industries due to its favorable stereoselectivity and enantioselectivity to catalyze a myriad of reactions. This section will examine nano-polysaccharide (mainly chitin/CS nanoparticles and nanocellulose) for biocatalyst applications.

CS have been extensively used as biocatalyst owing to its high mechanical strength, biocompatibility, non-toxicity, and abundant surface hydroxyl and amino groups that promote the crosslinking reaction with various enzymes, such as lipase, amylase, and laccase. Lipase-immobilized CS-crosslinked magnetic nanoparticles

(LCMNs), prepared by crosslinking CS nanoparticles through glutaraldehyde with thin layer coating of magnetic (Fe_3O_4) were investigated as biocatalyst particles for immobilizing lipase from *Candida antarctica* Lipase B. LCMNs exhibited superior biocatalytic and separation properties with efficient storage stability and reusability due to the tightly crosslinked and covalently immobilized structure of CS network [88]. Another lipase immobilization technique was reported to improve eugenyl benzoate synthesis using *Rhizomucor miehei* lipase (RML) as a biocatalyst crosslinked with CS and chitin nanowhiskers (CNWs) through 1-ethyl-3-[3-dimethylaminopropyl] carbodiimide hydrochloride (EDAC). Crosslinked CS/CNWs dramatically enhanced the RML catalytic activity with higher yields of eugenyl benzoate leading to a more cost effective approach than free RML [89]. Nano-biocatalyst for starch hydrolysis based on amylase immobilization was prepared by coating CS on Fe_3O_4 magnetic nanoparticles (AMNPs), which improved the catalytic activity at varying temperatures and pHs [90]. Super-magnetic nano-biocatalysts consisting of Fe_3O_4 and CS functionalized with halloysite nanotubes (Fe_3O_4-HNTs-CS) were used to immobilize laccase from *Trametes versicolor* since the anti-proliferative laccase is important for laccase-based anticancer treatment. The anti-proliferative properties of Fe_3O_4-HNTs-CS-Lac were examined against various cancer cell lines of liver (HegG2), lung (H460), cervix (Hela), and stomach (AGS), and exhibited highly efficient anti-proliferative properties and significant cytotoxicity against all cancer cell lines by inducing apoptosis as shown in Fig. 5.4 [91].

Nanocelluose (NC)-based materials have been investigated as novel biocatalysts for lipase immobilization. NC-CS nanocomposite was prepared by crosslinking NC extracted from oil palm frond leaves with CS polymer to immobilize Candida rugosa lipase (CRL) to catalyze esterification reaction to produce butyl butyrate. It was

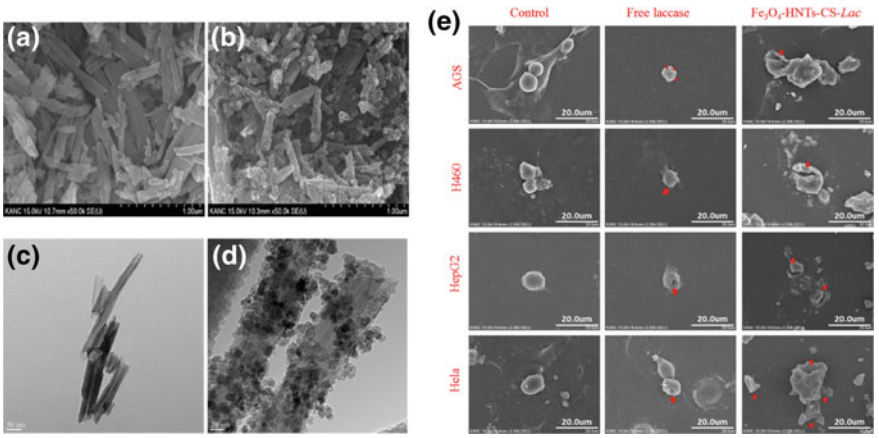

Fig. 5.4 The FE SEM image of **a** pure HNTs, **b** Fe_3O_4-HNTs-CS, and FE HR TEM image of **c** pure HNTs, **d** Fe_3O_4-HNTs-CS, **e** the change of morphologies of various cancer cell lines (AGS, H460, HepG2, and Hela cells) by laccase and Fe_3O_4-HNTs-CS-laccase. Red arrows indicate an apoptosis. Reproduced from [91]

confirmed that CRLs were attached to NC-CS composite (5.2 mg/g) and CRL/NC-CS catalyzed the conversion of ≥80% of butyl butyrate within 6 h. The addition of NC improved the mechanical strength of CS and extended the stability of CRLs for catalytic reaction [92]. Another NC-based nanobiocatalyst was developed by fusing polypyrrole/graphene oxide into a NC network offering a porous skeleton to immobilize CRL through physical adsorption. NC/ppy/GO nanobiocatalyst displayed enhanced catalytic efficiency and colloidal stability of immobilized CRL compared to free lipase. The immobilized lipase formulation possessed an excellent reusability profile as it maintained 85% of its original catalytic capacity after 10 cycles [93].

Nanocomposite composed of cellulose and nano-magnetites was fabricated for catalytic synthesis of Friedel-Crafts reaction between isatins and indoles on the surface of chitosan and cellulose. Grafting carboxymethyl cellulose or carboxymethyl chitosan to magnetite nanoparticles increased the reaction efficiency and yields due to proton-donating and proton-accepting capacity of hydroxyl groups on the cellulose [94]. Such systems are used to treat fruit and vegetable waste (FVW), which is one of the serious problems in developing countries. Yuan et al. developed nano-magnetic catalysts with immobilized cellulases using modified chitosan and Fe_3O_4. The β-glucosidase content of immobilized cellulases improved the FVW degradation efficiency compared to free cellulases, suggesting that immobilized cellulases could be used for cellulose hydrolysis, anthocyanin recycling or other industrial applications [95].

Bioprocessing technologies have been extensively studied as biocatalyst application, however current technologies could not be scaled to the industrial level due to poor productivity and high production cost. One of the major problems in pharmaceutical and food industries is the costly pasteurization process that reduces the nutritional quality of food products. Therefore, many trials to develop biocatalysts to improve the fermentation process in order to control the number of microbes through cell entrapment and immobilization. Nano-tubular cellulose was fabricated to remove microbes in cold pasteurization process of liquid foods, and to reduce the activation energy E_a that improved the low temperature performance during fermentation. The structure of nano-tubular cellulose revealed good stability for cold pasteurization process and it promoted the alcoholic fermentation activity [96]. Another cellulosic nano/micro-porous composites (tubular cellulose, TC) were developed as filter materials to remove yeast and bacteria from drinking water as well as biocatalyst for alcoholic fermentation. The microbial removal load varied from 99.2–88.2 to 92–77% for yeast and bacteria, respectively. In addition, TC filters with good immobilization capabilities for *Saccharomyces cerevisiae* to promote the alcoholic fermentation of grape could contribute to satisfactory fermentation rates, high ethanol content, ethanol productivity, and volatile by-products formation [97].

5.3 Antibacterial Applications

5.3.1 Introduction

Over the last decade, the development of nanosized antimicrobial agents from the natural and sustainable resources has attracted increasing interests, where research on the development of nano-antimicrobial agents has intensified. The demand for non-petroleum based, carbon neutral biodegradable products from sustainable resources having low environmental, animal/human health and safety risks is gaining more attention in the field of nanotechnology [98]. It has been reported that environmental, contagious, food-borned, nosocomial or other forms of microbial infection have resulted in millions of deaths, raising health-care cost, and impacting the economy of many countries [99, 100]. Several strategies have been adopted to minimize such mortality and morbidity. However, researchers are still seeking for more efficient nano-antimicrobial agents from natural sources that possess minimal side effects. The safety issues, unavoidable side effects of existing antimicrobial agents have led to new regulations that restrict their use. Thus, the development of new anti-microbial compounds via "green synthesis (solvent free)" of renewable and sustainable materials as replacement is being pursued vigorously. By modifying natural nano-biopolysaccharides, new systems with attractive antimicrobial characteristics are being explored for many applications, such as in textiles, disinfection in hospitals and active antibacterial packaging in food systems. Among several nano-biopolysaccharides that display good antimicrobial property are chitosan and cellulose based systems, and they will be discussed in this section.

5.3.2 Mechanism of Antibacterial Action in Biopolysaccharides

The mechanism of antimicrobial activity of the biopolysaccharides (for example chitosan) is not clearly understood. For the sake of simplicity, we will briefly discuss the mechanism of action of antibacterial activity displayed by chitosan in order to illustrate the important features of future anti-microbial compounds. When biopolysaccharides are modified with quaternary ammonium groups (QAGs) that possess cationic charges, they are imbued with antibacterial characteristic due to the charged interactions. Several review papers have reported on the mechanism of the antibacterial property of chitosan, a polycationic biopolymer [101–105]. Several important factors that impact the antimicrobial activity of chitosan are molecular weight (M_w), degree of deacetylation, type of microorganism and environmental factors including ionic strength, divalent ions, and pH [101–105]. Gram-negative bacterial cell walls are comprised of lipopolysaccharides which are negatively charged, whereas gram-positive bacterial cell walls consist of mixture of anionic teichoic and lipoteichoic acids [102]. Thus, interactions between positively charged QAGs

($-N^+R_3$) on the chitosan structure and the negatively charged cell membrane (and cytoplasmic constituents) of bacteria that alter the cell permeability and compromising the integrity of the cytoplasmic membranes. This causes the leakage of intracellular matrix, amino acids, vitamins, etc. from the cellular compartment resulting in the disruption of normal cellular metabolic processes that resulted in cell death [106, 107]. Figure 5.5 shows a schematic illustrating the possible mode of action of cationic biopolysaccharides possessing QAGs on both gram positive and negative bacteria.

5.3.2.1 Chitosan and Derivatives as Antimicrobial Agent

Chitosan, first reported by Rouget, is an abundant biopolysaccharide (after cellulose) on the earth's surface [39–42]. Since it is nontoxic, biodegradable, biocompatible, and microbe resistant, it has gained increasing attention for their use in textile finishing to impart novel functionalities to the textiles, such as deodorant, aroma, insect repellent, fire retardant, UV blocking, water resistant and antimicrobial surfaces [111]. Due to its low solubility at neutral pH conditions and weak binding to textile fibers, its application is hindered [112], such as its use as antibacterial agent. Thus, research efforts are being devoted over the last decade to modify chitosan into various derivatives in order to circumvent these limitations.

Chitosan as Antibacterial Finishing Agent on Textiles

Several studies on the preparation of antibacterial finishing of natural and synthetic textile materials have been reported recently. For example, Li et al. [113] coated cotton fabric with core-shell nanoparticles consisting of poly (n-butyl acrylate) (PBA) core and chitosan shell to impart the desired antibacterial property. They reported that untreated fabric possessed an antibacterial activity of less than 5% while the finished cotton displayed a bacterial reduction rate of 99% against *S. aureus*. The core-shell nanoparticles with a reported diameter of 300 nm, was evaluated and characterized using the FTIR and ^{1}H-NMR and the core-shell particles were deposited onto the cotton using a pad-dry cure method [113].

Jung et al. [114] adopted the electrospinning method to produce antibacterial poly (ethylene terephthalate) PET/chitosan nanofiber mats. The PET/chitosan nanofiber mats possessed enhanced bacterial inhibition against *S. aureus* and *K. pneumoniae* compared to only PET nanofiber mats. Ivanova and Philipchenko [115] also disclosed a simple method to produce superhydrophobic antibacterial textiles by spraying chitosan nanoparticle dispersions onto the cotton fabrics. Joshi and co-workers [116] reported on the antimicrobial properties of cotton coated with chitosan and poly(sodium-4-styrene sulfonate) via the layer-by-layer self-assembly approach. The use of ultrasonication together with a non-ionic detergent during washing enhanced the durability of antibacterial activity by up to several laundering cycles. Liu and co-workers [117] reported the conjugation of chitosan–gelatin microcapsules onto

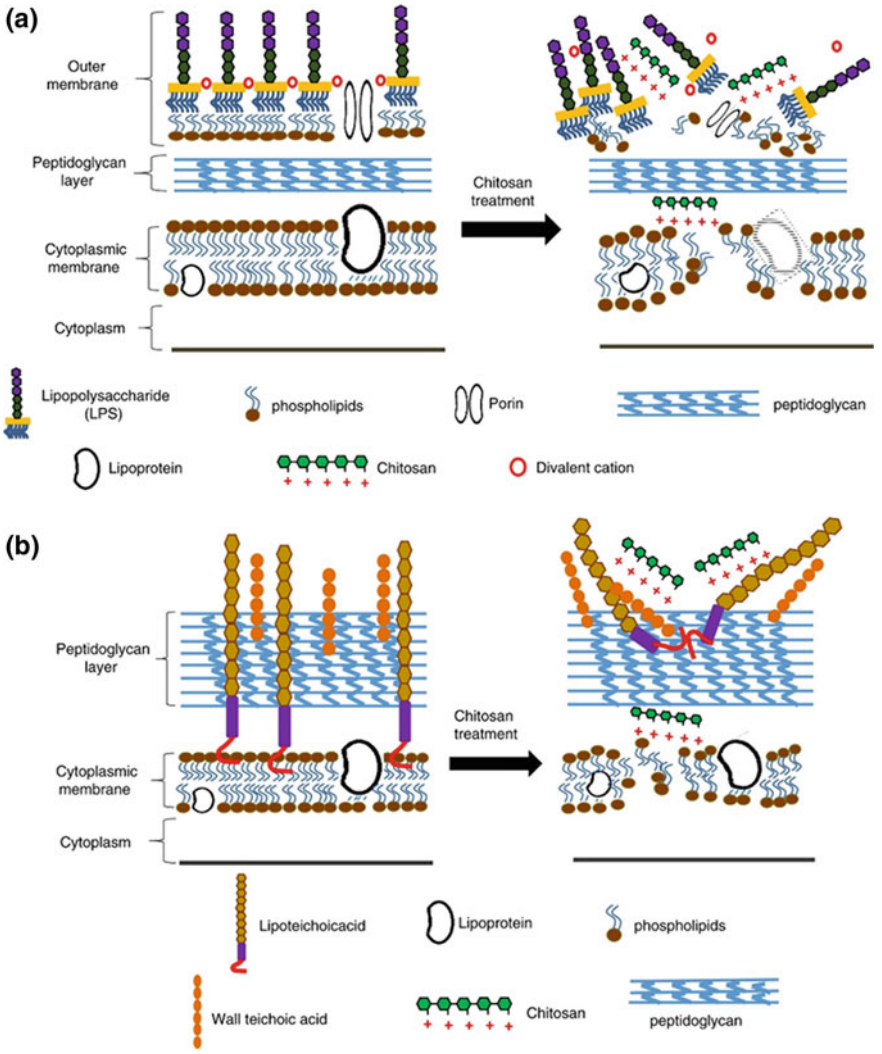

Fig. 5.5 Impact of chitosan against **a** Gram-negative bacteria and **b** Gram-positive bacteria at pH below the pK_a of chitosan. The biopolymer acquires a cationic charge, promoting electrostatic interaction with negative lipopolysaccharide on cell envelope and the outer membrane of Gram-negative bacteria, and the lipoteichoic and teichoic acids of the cytoplasmic membrane of Gram-positive bacteria. These electrostatic interactions disrupt the integrity of the cell envelope, disrupting the membrane potential and induces the leakage of cells, that leads to cell death [108–110]. Reproduced from [101]

cotton using a 2D resin, dimethyloldihydroxyethylene urea (DMDHEU), to prepare antibacterial cotton. They reported a retention of more than 65% antibacterial activity against *S. aureus* and *E. coli* after 25 washing cycles, and the treated fabrics possessed good antibacterial activity, and a better washing durability [117].

Alonso et al. [118] described the preparation of a novel functional fabric by grafting chitosan-based microcapsules consisting of an essential oil from grapefruit seed oil extract onto UV irradiated cellulose fabrics through a cost-effective and non-toxic process, and the durable fragrance and antibacterial properties of such novel functional fabrics were investigated. Interestingly, the results showed that chitosan-based microcapsules containing the essential oil, displayed 100% reduction of *E. coli* and *S. aureus* after 48 h of incubation time. Additionally, the pleasant fragrance of the grapefruit seed extract oil was retained on the fabrics for six months [118]. Abdel-Mohsen et al. [119] developed multifunctional cotton fabrics with a novel finishing formulation consisting of the chitosan-based graft co-polymer, methoxypolyethylene glycol-N-chitosan (MPEG-N-CTS). Here, citric acid was used as a cross-linker between the synthesized copolymer and the cellulose to form ester bonds. The authors reported that the treated cotton retained the antibacterial activities against *S. aureus* and *E. coli* for more than 20 washing cycles.

Janjic et al. [120] reported the production of antibacterial chitosan-coated Lyocell fibers by grafting chitosan onto oxidized (periodate oxidation) cellulose fibers of Lyocell, without using synthetic cross-linking agents. They reported that the higher periodate concentrations significantly increased the dialdehyde content on the Lyocell fibers, which provided a better fixation for the chitosan. The in vitro experimental data for the antibacterial activity of such chitosan-coated Lyocell fibers against *S. aureus* and *E. coli* showed stronger bactericidal effects. They concluded that chitosan of a higher molecular weight was more effective in killing bacteria than a lower molecular weight chitosan [120]. In a recent study, Sheikh and Bramhecha [121] evaluated the wrinkle-free, antibacterial, flame retardant and antioxidant properties of linen fabrics treated with chitosan-citric acid and various phytic acid-thiourea compounds. The coated linen possessed good antibacterial properties against *E. coli* and *S. aureus*, while the coated linen displayed 65.5% reduction of *S. aureus* and 67.9% of *E. coli* after several washing cycles [121].

Chitosan as Antibacterial Coating in Food Packaging

Active antimicrobial packaging protects the internal environment over the shelf-life of the product. It modifies the inner environment of food package, thereby changing the condition of the packaged food system, extending its shelf-life, enhance sensory qualities, and maintain microbial colony [122–124]. It has gained popularity due to the desire for high-quality and safe food products by consumers [125]. Due to its inherent film forming properties and antimicrobial characteristics, chitosan is a good material for packaging films [126]. In order to develop such packaging systems, chitosan and its derivatives have been used as sustainable antibacterial biopolymers over the past decades. The production and evaluation of chitosan-based antimicrobial

films was recently reviewed for active food packaging applications [127]. Chitosan films are attractive food packaging materials due to their intrinsic antimicrobial properties [128]. Several recent review papers describe the use of chitosan-based coatings of fruits and vegetables with antimicrobial agents, such as essential oils, acid, and nanoparticles [129–132].

It was reported that the microbial spoilage of baby carrots was delayed after the application of a chitosan-based coating that maintained the overall quality of the product [133]. Chitosan films containing propolis extract (a resin-like material made by bees), high in polyphenols, was capable of inhibiting the growth of *S. aureus*, *Salmonella enterica*, *E. coli*, and *P. aeruginosa* [134]. Incorporating thin young apple polyphenols enhanced the mechanical properties of chitosan films, while imparting antibacterial characteristics on *E. coli* and *S. aureus*, and molds [135]. Furthermore, the antimicrobial characteristics and stiffness of chitosan films were found to improve significantly through the incorporation of turmeric extract (containing phenolic compounds) by cross-linking with sodium sulphate [136]. The film was reported to be antibacterial against *Salmonella* and *S. aureus* based on the plate counting agar technique [136].

Poly(vinyl alcohol) (PVA) and chitosan films with bifunctional nanosized cellulose fillers displayed antibacterial activity against *Salmonella enterica* and *S. aureus* [137]. A significant reduction in the microbial growth of *Pseudomonas spp*. was observed in chitosan films loaded with silver-montmorillonite nanoparticles [138]. Oleic acid was found to enhance the antimicrobial properties of chitosan/clay composite films [139]. Zhang et al. [140] reported that sodium lactate augmented chitosan-PVA/montmorillonite films possessed excellent antibacterial activity against *E. coli* making it a potential ingredient in food packaging [140]. Moghadas et al. [141] reported that the nanohybrid films based on chitosan and biofunctionalized montmorillonite (MMT) containing chitosan sulfate chains (SMMT) as the macromolecular intercalant, displayed bacteriostatic action against gram-negative *E. coli* [141]. In another study, PVA containing CS was prepared via a simple solution casting and electro-spraying method and the PVA-CS film possessed strong antibacterial action against *E. coli* and *S. aureus* [142]. Stroescu et al. [143] reported the preparation of a novel chitosan film, where vanillin was incorporated as cross-linker for chitosan and the emulsifier, Tween 60 was used to aid the flavor release from the film. These vanillin-imino-chitosan films possessed good antimicrobial activity against *E. coli* [143]. Strong antibacterial activity was reported for chitosan and gelatin films containing 1% *Ziziphora clinopodioides* essential oil +1% pomegranate peel extract +1% cellulose nanocrystals [144].

The use of chitosan as an edible coating, where a thin film is directly coated on the surface of the product for protection has been widely investigated [102]. Edible coatings/films form a protective barrier around the fruits and vegetables and they can be consumed together with the coated product [131, 145]. In addition to antimicrobial properties, these films are also a moisture and gas barrier, resulting in a reduction in the weight loss and respiration rate with a consequential delay in spoilage of the produce [146]. Numerous publications have reported on the antimicrobial and barrier

properties of edible chitosan films, and readers are encouraged to preview additional information from these sources.

5.3.2.2 Cellulose and Derivatives as Antimicrobial Agents

Nanocelluloses are gaining increasing attention in their antibacterial systems due to their remarkable physical properties, unique surface chemistry, and excellent biological functions [147]. Four types of nanocellulose, namely CNC, cellulose nanofiber (CNF), bacterial cellulose (BC), and electrospun-cellulose nanofibers (ESC) have been reported [148]. A schematic describing the synthesis and use of nanocellulose-based antimicrobial compounds is described in Fig. 5.6.

Nanocellulose can be modified at the three active hydroxyls on C-2, C-3, and C-6 positions of glucopyranose ring via oxidation, esterification, or etherification, thereby introducing new functional groups for a given application [148]. The most common functional groups that possess antimicrobial properties are aldehyde and QAG, where these nanocelluloses displayed good antibacterial activity and biocompatibility [148].

Jiang et al. [150] prepared 2,3-dialdehyde NFC (DANFC) by selective oxidization of the hydroxyl into aldehyde groups on the C6 position of nanocellulose using sodium periodate. They found that the antimicrobial activity of DANFC against both *S. aureus* and multidrug resistant (MDR) *S. aureus*/methicillin-resistant *S. aureus* (MRSA) increased with increasing aldehyde content. DANFC displayed good biocompatibility with mammalian cells and exhibited good blood compatibility. From the study on the healing effect of DANFC in animal model, epithelial parakeratosis was observed in both the traditional gauze group and DANFC group, however hair follicles and cuticular pegs appeared first in the wound tissue treated with DANFC mat on day-14. Thus, DANFC could accelerate wound healing by maintaining a sterile environment due to its antibacterial properties, which also promotes the formation of blood vessels and epithelium [150]. The other feasible method to convert

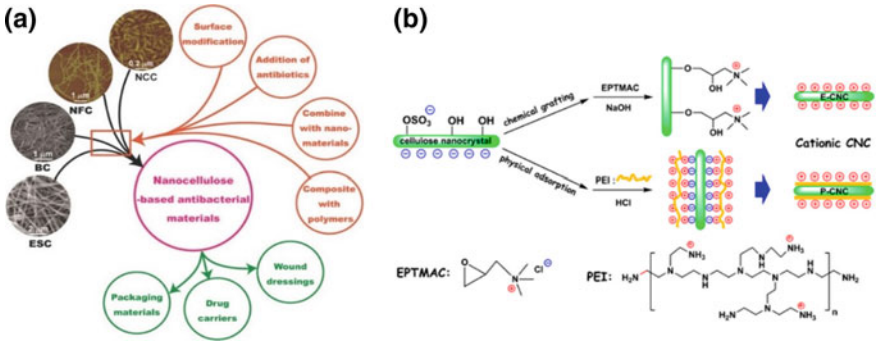

Fig. 5.6 **a** The synthesis and use of nanocellulose-based antimicrobial materials. Reused with permission from [148]. **b** Example of one of the synthetic pathway to prepare cationic CNC via chemical grafting and physical adsorption strategies. Reproduced from [33, 149]

the hydroxyl group at C6 position on nanocellulose to aldehyde and carboxyl functional groups is using TEMPO (2,2,6,6-tetramethylpiperidine-1-oxyl) reagent [151, 152]. Besides the above methods, one additional approach is to graft methacrylate monomers through the surface-initiated single-electron-transfer living radical polymerization, surface-initiated ATRP, and free radical polymerization [35, 153–157], followed by the quaternization of the tertiary amine groups. Besopalova et al. [158] reported the surface modification of CNC using chloroacetylation and the subsequent reaction with tertiary amines (N,N-dimethyl ethylamine, N,N-dimethyl hexylamine, N,N-dimethyl decylamine, N,N-dimethyl dodecylamine and N,N-dimethyl hexadecylamine) to produce cationic CNCs with the pendant quaternary ammonium salts. They evaluated the antimicrobial activity of quaternary ammonium modified CNCs against Staphylococcus and *E. coli* bacteria using agar and observed that modified CNCs with alkyl chain greater than ten carbons were effective in killing the bacteria. However, pristine CNC and quaternary ammonium modified CNCs with an alkyl chain length of smaller than 10 did not inhibit bacteria growth [158] (Fig. 5.7).

Feese et al. [159] reported on the synthesis of crystalline and water-insoluble CNCs, where the CNC surface was decorated with cationic porphyrins via the Cu(I)-catalyzed Huisgen–Meldal–Sharpless 'click' reaction. They reported that the CNC-Por systems suspended in an aqueous solution were capable of photodynamic inactivation of *Mycobacterium smegmatis* and *S. aureus*, but only displayed a slight activity against *E. coli* [159].

Tang et al. [160] described a sustainable approach to fabricate cellulose nanocrystal@polyrhodanine (CNC@PR) nanoparticles through the polymerization of rhodanine on negatively charged CNC surface using ferric chloride as the initiator and

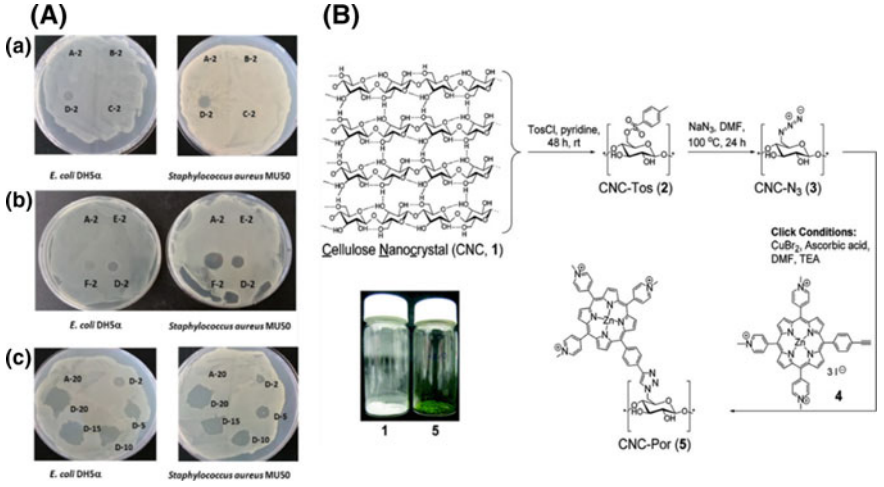

Fig. 5.7 **a** Agar diffusion method antibacterial test of different CNCs with varying chain length QAGs showing antibacterial effect. Reused with permission from [158]. **b** Reaction scheme of the synthesis of CNC-porphyrin conjugate CNC-Por. Reproduced from [159]

oxidant. The in vitro antimicrobial tests were evaluated against *E. coli* (Gram negative) and *Bacillus subtilis* (Gram positive) through the plate colony counting methods. They observed that the spherical nanocomposite particles (SiO_2@PR), rod-like nanosized CNC@PR nanoparticles possessed good antimicrobial properties toward both bacteria, which could be associated with the lower percolation threshold of the higher aspect ratio rod-like nanoparticles. They also evaluated the toxicity of CNC@PR nanoparticles against HeLa cells, which was negligible within the concentration of the antimicrobial activity [160].

De Castro et al. [161] reported on the functionalization of CNC by chemical grafting of natural rosin via a green, and a solvent free method. They evaluated the rosin-CNC (R-CNC) nanoparticles for antibacterial action against *E. coli* and *B. subtilis* bacteria, where the R-CNCs possessed strong antibacterial activity against *E. coli* bacteria. Due to the difference in cell membrane structure, the R-CNC only showed weak activity against the gram positive *B. subtilis* strains [161]. Furthermore, Niu et al. [162] reported on polylactic acid-chitosan (PLA/CS) based composite films reinforced with rosin functionalized cellulose nanofibers (R-CNFs) for active antibacterial food packaging application. Through the green solvent-free reaction process [161], they functionalized CNF using a natural rosin (which is a mixture of abietic acids and pimaric acids with characteristic hydrophenanthrene structures) to improve the compatibility of hydrophilic CNF with hydrophobic PLA, where the CNF acted as reinforcing filler for PLA. By utilizing layer by layer (LBL) process, the R-CNF reinforced film was coated with CHT to prepare a two-layer composite film and the in vitro antibacterial studies of such films demonstrated excellent antimicrobial performance against *E. coli* and *B. subtilis,* probably due to the synergistic antimicrobial effect of chitosan and rosin [162].

Zhang et al. [163] reported on the fabrication of polyethersulfone (PES) ultrafiltration membranes by incorporating cellulose nanocrystals (CNC) through the non-solvent induced phase inversion technique to improve their antibacterial/antifouling properties for the selective separation of protein from water. Such PES/CNC nanocomposite membranes possessed smaller pore size and thicker skin layer, offering improved antifouling property (quantified by measuring the flux recovery ratio) and hydrophilicity. They reported that after conditioning with polyhydroxyamines (PAHA), the fabricated PES-CNC-PAHA membranes displayed high antibacterial property against gram-positive bacteria *S. aureus* [163].

Yang et al. [164] reported on the preparation of melt extruded ternary PLA nanocomposite films, obtained by dispersing two lignocellulosic nanofillers: cellulose nanocrystals (CNC) and lignin nanoparticles (LNPs), in neat PLA and glycidyl methacrylate (GMA) grafted PLA (g-PLA). Due to the synergistic effect of LNPs and CNC nanoparticles in the composite, not only the films' transparency, mechanical properties, and UV light blocking capability were improved, but there were significant enhancement in the antibacterial activity with a reduction in the tomato bacterial plant pathogen *Pseudomonas syringae* pv. *tomato* (Pst). Such green functionality would potentially facilitate the development of innovative strategies in food packaging [164].

As the bacterial cellulose (BC) does not intrinsically possess antimicrobial properties, Fernandes et al. [165] showed that by introducing aminoalkyl groups to the BC nanofibrils using a silane chemical grafting approach, a novel antibacterial bioactive BC membrane was produced. In addition to improved mechanical and thermal properties, the bacterial cellulose nanostructured membranes (BC-NH_2) displayed lethal actions against *S. aureus* and *E. coli*, while remaining nontoxic to human adipose-derived mesenchymal stem cells (ADSCs) [165].

Antibacterial electrospun-cellulose nanofibers (ESCs) were prepared by electrospinning of quaternized materials or dipping the ESCs into a solution of quaternary ammonium compounds. For instance, ESC with excellent antibacterial activities against *E. coli* and *S. aureus* was obtained by electrospinning cellulose acetate which was modified by 3-amino propyl trimethoxysilane or 2,4-bi[(3-benzyl-3-bimethyl-ammonium) propylamino]-6-choro-1,3,5-triazine chloride (BBCTC). Dipping ESC mats into 3-(trimethoxysilyl) propyl-dimethyl-octadecyl-ammonium chloride would impart the ESC mats with excellent antibacterial activities against *S. aureus* [148, 166, 167] (Table 5.3).

There are some recent review articles on the metal-CNC hybrid nanocomposites, where these systems displayed antimicrobial/antibacterial characteristics [15, 19,

Table 5.3 Summary of cellulose-based antibacterial applications

Nanopolysaccharide	Antibacterial agent/compound	Synthesis method	Tested bacterial species	Reference
NFC	Aldehyde	Oxidization	*S. aureus* MDR	[150]
CNC	Quaternary ammonium	Chloroacetylation	Staphylococcus *E. coli*	[158]
CNC	Porphyrin	Cu(I)-catalyzed Huisgen–Meldal–Sharpless 'click' reaction	*Mycobacterium smegmatis* *S. aureus* *E. coli* (light effect)	[159]
CNC	Polyrhodanine	Polymerization of rhodanine using ferric chloride	*E. coli* *Bacillus subtilis*	[160]
CNCs	Natural rosin	Solvent free method	*E. coli* *B. subtilis*	[161]
CNC	PES, PAHA	Non-solvent induced phase inversion technique	*S. aureus*	[163]
CNC	LNPs, GMA	Dispersing two lignocellulosic nanofillers	*Pseudomonas syringae* pv *tomato*	[164]
BC	Aminoalkyl groups	A silane chemical grafting	*S. aureus* *E. coli*	[165]

168–171]. The antibacterial functions of these nanocomposite hybrid systems are afforded by metal nanoparticles, where the nanopolysaccharides served as support (template) during the preparation process. Numerous published literature on metal nanoparticles (Ag, Cu, Zn, Ni, Ti etc.) on CNC/CNF template indicated that these systems possessed antibacterial characteristics.

5.4 Tissue Engineering and Bio-Scaffolds for Cell Cultivation

5.4.1 Introduction

Tissue engineering (TE) has emerged as a promising solution to treat loss or damaged tissue or organ. Tissue engineered medical treatment, such as stem cell therapy and implantable bio-scaffolds are commonly prepared via three major steps: (1) preparation of scaffolds with biocompatible materials in the laboratory or bioreactor, (2) culture/grow stem cells or specific cell lines on the scaffolds, and (3) transplant cultured scaffolds with higher number of cells to the targeted area. The role of bio-scaffolds is to maintain desirable shape and environment for cell cultivation; therefore, those should have the mechanical properties to withstand the physiological environment with good biocompatible, non-toxicity and biodegradable characteristics. Furthermore, the strategies to improve cell proliferation are required to maximize medicinal efficiency for malfunctioned tissue and organ.

There are several fabrication techniques for TE scaffolds, such as freeze-drying, electrospinning, and crosslinking of hydrogels. A lyophilization (freeze-drying) technique is the most common and conventional method to prepare a spongy 3-D microporous scaffold structure. An electrospinning method has been widely adapted for scaffold fabrication due to higher mechanical strength and stability. Also, gel-based TE scaffolds have been actively investigated since they could be directly injected to damaged tissue, enabling a non-invasively surgery for patients.

In terms of biomaterials used for TE scaffolds, synthetic polymers have been widely used due to their good functionality, accessibility and price. For example, aliphatic polyesters, such as polylactide (PLA), polyglycolide (PGA), poly(lactic-co-glycolide) (PLGA), poly-ε-caprolactone (PCL) are common synthetic polymers for cartilage, bone, skin, neuronal, tendon, liver, vascular system, and cardiac TE application. However, their cell affinity is poor due to their hydrophobicity and lack of cell recognition sites on the surface. From this point of view, polysaccharide-based materials could be beneficial for TE applications since they enhance the biocompatibility, cell affinity, proliferation, and successful cultivation rate in scaffold [172]. This section will discuss the polysaccharide-based nanomaterials for bone, cartilage, cardiac, skin tissue engineering approaches for cell cultivation.

5.4.2 *Bone Tissue Engineering Application*

Bone tissue engineering is a pioneering field in the history of TE development [172]. From the earlier stage, scientists attempted to use cellulose-based materials, such as wood to mimic the bone structure. Recent advances have focused on promoting osteogenic differentiation using various stem cells, such as bone marrow mesenchymal, embryonic, umbilical cord blood, amniotic fluid stem cells. Polysaccharide based materials have been actively investigated to repair and enhance bone properties through TE approach in medical treatment. This section will focus on the use of chitosan, cellulose, alginate, and starch-based materials for bone TE applications (Fig. 5.8).

5.4.2.1 Chitosan (CS)-Based Bone TE Scaffolds

Chitosan (CS), a polycationic polysaccharide and a partially deacetylated derivative of chitin, have been widely investigated as biodegradable materials for bone TE applications due to its good cytocompatibility, biodegradability, and antimicrobial effect [172]. The role of CS scaffolds is to provide a stable platform of artificial extracellular matrix (ECM) to accommodate cell proliferation before implantation [174]. CS-based materials enhance the properties for bone generation, but limitations still exist due to its low mechanical strength, poor stability, and poor shape retention. Therefore, much efforts have been devoted to improve CS functionality by incorporating other materials, such as alginate [175], hydroxyapatite [176], and calcium phosphate to improve their mechanical properties [172].

Functionalized CS scaffolds with natural HAp (HAT) derived from *Thunnus obesus* bone (tuna bone) and carbon nanotube were reported by Venkatesan et al., and

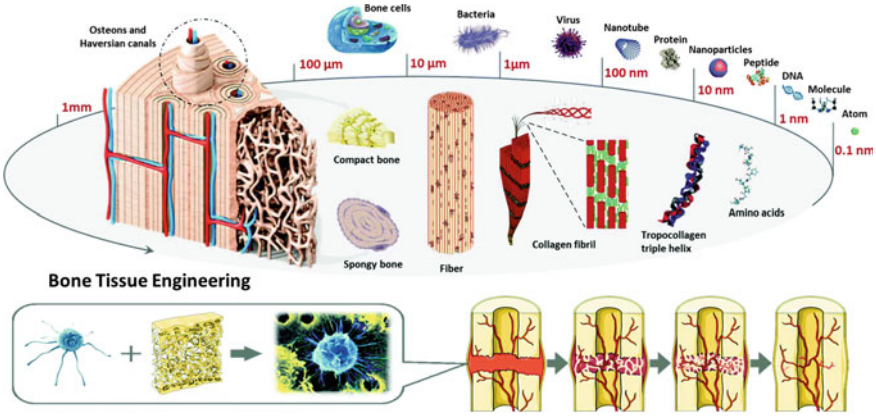

Fig. 5.8 The micro-composition of bone and bone regeneration by TE approached treatment. Reproduced from [173]

the MWCNT-g-CS/HAp possessed good thermal stability, interconnected porosity, biodegradability, and cell proliferation that mimic the properties of extracellular bone matrix [177]. Also, nanosized HAT, such as nanohydroxyapatite (nHAT) was synthesized together with CS to produce nanocomposite CS-nHAT scaffold that exhibited enhanced compression modulus, slower degradation time, better cell proliferation, and reduced water uptake. Interestingly, CS-nHAT scaffolds facilitated greater cellularity despite its similar pore size compared to CS scaffolds, suggesting that CS-nHAT nanocomposite could be a good candidate for bone regenerative materials [178].

CS-based scaffolds have also been used to deliver growth factors or proteins to enhance osteogenesis and angiogenesis in a timely fashion within the scaffold constructs. Porous CS/collagen scaffolds loaded with plasmid and adenoviral vector encoding human transforming growth factor (TGF-β1) exhibited an enhanced proliferation of human periodontal ligament cells, a collagen expression regulation, and better integration of surrounding tissues after implanted in vivo [179]. Fibrous CS scaffolds incorporated with PLGA and Poly(3-hydroxybutyrate-co-3-hydroxyvalerate) (PHBV) nanocapsules were examined for the delivery of bone morphogenetic protein BMP-2 and BMP-7 for osteogenic differentiation (Alkaline phosphatase (ALP) activity). The system incorporated with two population of nanocapsules induced more osteogenic differentiation than individual nanocapsules [180].

5.4.2.2 Cellulose-Based Bone TE Scaffolds

Nanocellulose materials (cellulose nanocrystals, bacterial nanocellulose, and cellulose nanofibrils) have excellent physical and biological properties for TE applications [181]. A natural bone has a complex organic-inorganic structure in which the hydroxyapatite (HAT) and collagen fibrils are organized into a hierarchical system. Many trials have been conducted to introduce HAT in bone TE scaffolds. Carboxymethyl cellulose (CMC) was conjugated to nano-hydroxypatite (n-HAT) and CS to prepare n-HAT/CS/CMC scaffolds for bone TE application. CMC was used as a crosslinker in composite scaffolds due to the strong ionic interaction between CMC and CS in the absence of agglomeration, and n-HAT/CS/CMC composite scaffolds showed highly-interconnected porous structure, compressive strength, and good structural stability that are favorable for TE applications [182]. Similarly, CMC based hydrogel loaded with HAT showed enhanced cell proliferation, metabolic activity of osteoblast MG63 cell line that promoted the production of mineralized extracellular matrix [183]. Also, CMC was blended with pectin and microfibrillated cellulose (MFC) to improve the tensile strength and stiffness [184]. Another interesting study on the modification of CS/CMC composite scaffolds with various concentrations of mesoporous wollastonite (m-WS) particles. The bio-mineralization and protein adsorption properties of CS/CMC/m-WS scaffold were significantly enhanced, and the addition of m-WS altered the physical properties of scaffolds by reducing swelling and degradation properties with osteogenic potential [185].

Cellulose nanocrystals (CNCs) that contain highly crystalline domains within the cellulose microfibrils have great potentials in TE applications [186]. Zhou et al. used CNCs with maleic anhydride (MAH) grafted poly(lactic acid) (PLA) by electrospinning method to prepare MPLA/CNC bone TE scaffolds. The tensile strength of MPLA/CNC scaffold loaded with 5 wt% CNC was increased by more than 10 MPa, and it was stable and the in vitro degradation was enhanced. Also, MPLA/CNC scaffolds were not cytotoxic to human mesenchymal stem cells and they promoted cell proliferation with good biodegradable and biocompatible properties [187].

Bacterial cellulose (BC), which is biosynthesized extracellularly by the bacterium *Acetobacter xylinum* have favorable properties, such as high purity, a fine fiber network, high crystallinity, and tissue compatibility, hence it has been used in many TE applications. However, BC scaffolds have a relatively small pore size due to the dense structure that limits cell infiltration for TE applications. In order to address this limitation, porogen materials consisting of starch and paraffin particles were incorporated during the fermentation process, which was then removed to successful control the porosity to achieve good proliferation and migration rate of smooth muscle cells [188]. Another microporous BC scaffolds for bone regeneration were fabricated using paraffin wax microsphere [189]. Also, BC scaffolds loaded with hydroxyapatite (HAp/BC) scaffolds increased both proliferation rate and osteoblastic differentiation of human bone marrow cells [190]. Most recently, collagen was combined with BC, and the hybrid not only displayed greater adhesion and phenotype maintenance of human osteoblasts, but also the in vivo results suggested that the modification with gelatin and HAT significantly promoted biocompatibility, and osteoinductivity of BC scaffolds [191].

5.4.2.3 Starch-Based Bone TE Scaffolds

A blend of starch with polycaprolactone (SPCL) and poly(lactic acid) (SPLC) was used to prepare bone TE scaffolds that possessed adequate porosity and mechanical properties for enzymatic degradation and cell proliferation [192]. Another study confirmed that sustained cell proliferation, osteogenic differentiation, and mineralization formation on human adipose stem cells (hASC) in 3D fiber meshes SPCL scaffolds treated with calcium silicate for in situ functionalization of Si–OH groups [193]. Also, electrospun hierarchical SPCL scaffolds comprising of parallel aligned microfibers and randomly blended nanofibers of polycaprolactone showed good cell proliferation and osteoblastic activity [194]. The immunogenicity of starch-based scaffolds incorporated with ethylene vinyl alcohol (SEVA-C), cellulose acetate (SCA), and SPCL composite with the presence of hydroxyapatite (HAT) was evaluated, and SEVA-C scaffolds presented a higher number of cells compared to SCA and SPCL composite, while SCA scaffolds induced a low level of toxicity that resulted in delayed cell proliferation [195]. SPCL and SCA scaffolds stimulated in vitro tissue response and angiogenic activation of outgrowth endothelial cells without supplementation of growth factors, as well as in vivo results showed greater vascularization after subcutaneous

implantation [196]. Another in vivo results of endosseous response to SCA, SEVA-C, and SEVA-C with phosphate layer (SEVA-C/CaP) scaffolds showed a favorable response for bone generation. However, SEVA-C scaffolds did not show any bone contact and SEVA-C/CaP exhibited only transitory bone contact after 3 weeks while SCA showed direct bone contact after 6 weeks of implantation [197].

Most recently, starch-derived nanographene oxide (nGO) was incorporated with starch-based nanofiber scaffolds in formic acid by electrospinning method, and the addition of nGO enhanced electrospinning ability, thermal stability, biodegradability, biocompatibility, and osteo-bioactivity of starch scaffolds [198]. A citric acid modification of starch-based hydrogel scaffolds have been used to mimic bone-like apatite layers, and primary heterogenous nucleation of apatitic calcium phosphate was observed due to greater chemical affinity of carboxyl group in citrate-starch hydrogel scaffolds [199].

5.4.3 Cartilage Tissue Engineering Applications

Most of the medical treatment for cartilage defect was leaning towards treating clinical symptoms rather than regeneration of damaged tissue. The first concept of cartilage TE approach was proposed by Green in 1977, suggesting that transplantation of chondrocytes cultured in an ex vivo environment would reinforce the functionality of damaged cartilage tissue [200]. The first clinical trial was achieved by implanting laboratory cultured chondrocytes into an injured knee [201]. Since then, TE approach to repair cartilage tissue have been actively investigated. We will discuss the use of CS, cellulose-based materials into cartilage TE engineering applications (Fig. 5.9).

5.4.3.1 Chitosan-Based Cartilage TE Scaffolds

Many studies have reported that CS modulates chondrocyte morphology, differentiation and facilitating chondrogenesis [203]. Injectable hydrogel provides less painful surgical interventions for patients as it can be directly injected into the damaged tissue. Water-soluble CS-based hydrogel grafted with glycolic acid and phloretic acid (PA) retained its shape after cultured with chondrocytes for 2 weeks, where it could be used as an artificial ECM for bone tissue engineering [204].

Hydrophilic fibrous CS scaffolds blended with polyhydroxybutyrate (PHB) were prepared by electrospinning for cartilage TE applications. The addition of CS with PHB decreased the hydrophobicity and tensile strength. The optimal concentration of CS was found to be between 15 and 20% and the chondrocytes were well-attached to the scaffold [205]. Most recently, CS-based hydrogel prepared with oligopyrrole was evaluated as an electroactive scaffold to facilitate tissue repair and regeneration. They reported that an increased concentration of oligopyrrole in CS hydrogel decreased the pore size, and increased the gelation time, swelling behavior, conductivity, and degradation time. The best optimized ratio of oligomer:chitosan ratio was at 0.1 w/w for

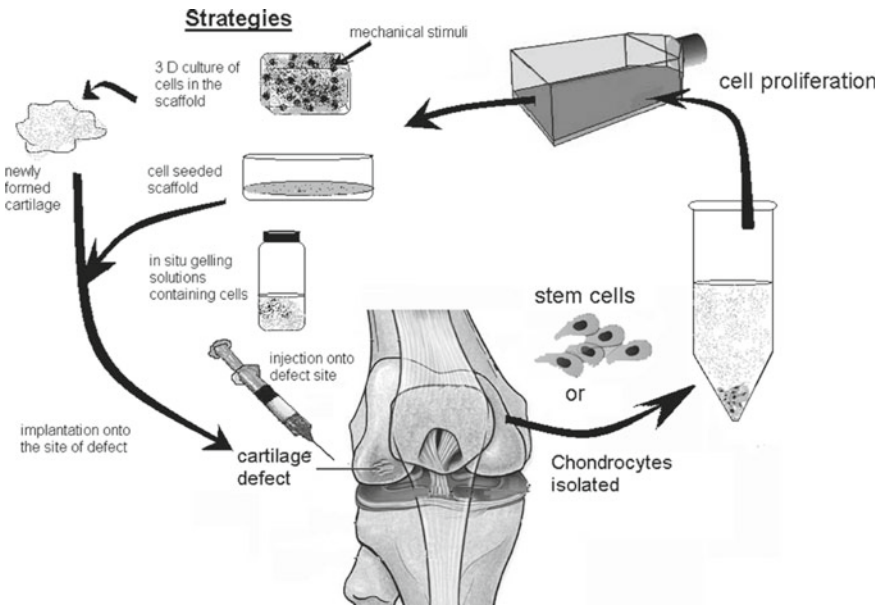

Fig. 5.9 The schematic illustration of TE approach for cartilage regeneration and treatment. Reproduced from [202]

cartilage TE scaffold, and it possessed a high porosity and low cytotoxicity [206]. The cartilaginous tissue formation in silk fibroin/chitosan scaffolds cultured with bovine chondrocytes was also examined, and the silk fibroin/chitosan scaffold promoted cell attachment, proliferation, and chondrogenic phenotype. Scaffolds with 1:1 ratio of silk fibroin:chitosan ratio displayed the highest glycosaminoglycan and collagen accumulation [207]. Gelatin was crosslinked with CS for cartilage TE scaffolds, and in vitro and in vivo studies of chitosan/gelatin polyelectrolyte scaffolds revealed a good proliferation rate of chondrocytes and an abundance of extracellular matrix secretion as well as evidence of cartilage regeneration after implantation [208]. Nanostructured 3-D scaffolds composed of CS and chondroitin sulphate were fabricated by LBL assembly, and these multilayered hierarchical scaffolds possessed viscoelastic properties with a 300% of water uptake capacity. Bovine chondrocytes and bone marrow derived stromal cells were well attached, proliferated, and metabolically active over the scaffold as well as cartilaginous ECM formation was confirmed.

5.4.3.2 Cellulose-Based Cartilage TE Scaffolds

Nanocellulose-based interpenetrating polymer network (IPN) hydrogels composed of sodium alginate (SA) and gelatin were fabricated for cartilage TE applications. Double-crosslinked structure formed by SA with calcium chloride (ionic crosslinking) and cellulose (hydrogen bonding), increased the tensile strength and strain. Also,

favorable properties for cartilage scaffolds, such as high porosity, water uptake, cytocompatibility toward mesenchymal stem cells were confirmed [209]. Recently, 3D printing technologies have revolutionized TE fields and several research studies with nanocellulose confirmed their feasibility for cartilage culture and implant. 3D printing bioink composed of nanocellulose and alginate provided excellent printability and biocompatible for cell culture [210]. Another nanocellulose/alginate bioink cultured with human-derived induced pluripotent stem cells (IPSCs) supported both cell proliferation and antitumorigenic properties for cartilage production with irradiated chondrocytes [211].

Bacterial nanocelluloses (BNC) comprising of highly hydrated fibrils are produced by the bacterium *Gluconacetobacter xylinus*, and they are novel materials for cartilage TE applications. Human primary chondrocytes were attached to 3-D porous BNC scaffold surface to yield cartilaginous matrix proteins [212]. Suitable mechanical properties of BNC scaffolds were reported by Nimeskern and coworkers for ear cartilage implant. The mechanical properties were tuned by varying the effective cellulose concentration, and the fluid flow resistance in the BNC scaffolds could be improved by chemical modification even after implantation [213]. Another biocompatible evaluation of BNC hydrogel scaffolds showed that BNC hydrogel with a cellulose content of 17% reduced endotoxin content, cytotoxicity, and host responses when compared to hydrogel with a lower cellulose content (15%) [214].

5.4.4 Skin TE and Wound Healing Applications

The skin is the largest organ of the human body consisting of three layers (epidermis, dermis and subcutaneous tissue). The use of nanotechnologies for skin repair is growing rapidly based on advances made over the 25 years. The cutaneous healing processes undergo three phases: inflammatory, proliferation, and maturation phases. Fibroblasts play a significant role in initiating wound healing in tissue matrix, and keratinocytes induced the inflammation and re-epithelization so that damaged skin tissue can fully recover with further re-vascularization, ECM deposition, angiogenesis, restoration and remodeling. There are many advances in the development of skin TE scaffolds promoting skin regenerative properties and wound healing process using synthetic or natural materials. Polysaccharide based nanomaterials, such as chitosan nanofiber and nanocellulose were evaluated for cell cultivation (fibroblast or keratinocytes) and re-epithelization. This section will focus on cellulose and CS-based nanomaterials that promote the cutaneous healing process.

5.4.4.1 Cellulose-Based Nanomaterials for Skin TE Applications

Bacterial nanocellulose (BNC), a natural nanomaterial synthesized by *Gluconacetobacter xylinus* have been applied to skin repair and TE applications due to its

biocompatibility, conformability, elasticity, transparency, and good moisture capturing capabilities. Fu et al. prepared uniform BNC wound dressing films for large area skin transplantation. In vitro results of BNC wound dressings showed good proliferation and adhesion of NIH/3T3 cells with low cytotoxicity. Also, pathologic studies on the back of C57BL/6 mice showed that BNC scaffolds provided better healing and tissue regeneration abilities, and lower inflammatory responses compared to a control group [215]. Keskin et al. incorporated keratin into BC nanocomposite to improve the attachment of dermal fibroblast cells. Keratin, a structural protein composed of eukaryotic cell matrices and protective tissues, such as nails, hair, and horn, has the capability to regulate cell penetration, adhesion, and migration in 3D matrices. The cell culture studies on BC/keratin nanocomposite scaffolds revealed better cell attachment profile of human skin keratinocytes by preserving its original epithelial morphology on the surface [216]. Azarniya et al. fabricated electrospun CS/BNC nanofibrous composite reinforced with graphene oxide. The introduction of GO nanosheets improved the mechanical properties (tensile strength and Young's modulus) and reduced the average size of polymeric fibers. Also, the addition of GO increased the hydrophobicity and water vapor permeability [217]. Hydroxyethyl cellulose (HEC), a non-ionic hydrophilic polysaccharide with ether linkages attached to hydroxyl groups of cellulosic structure, have been widely used for pharmaceutical and wound healing applications due to its desirable characteristics, such as biocompatible, biodegradable, and non-toxicity. Zulkifli et al. developed electrospun nanofibrous HEC/PVA scaffolds using glutaraldehyde as cross-linkers. By varying the ratio between HEC and PVA (30–50%), they found that HEC (5%) with PVA (15%) was the optimized condition for preparing smooth nanofibers. The mechanical, thermal and stability of HEC/PVA scaffolds increased due to the production of crosslinked network structure by glutaraldehyde. The in vitro studies with human A375 melanoma cells showed that HEC/PVA scaffolds possessed good biocompatibility, cell attachment, and cell proliferation rate over 7 days [218]. Zulkifli et al. incorporated silver nanoparticle with HEC (AgNPs/HEC) via a green synthesis approach under various concentrations of $AgNO_3$ (0.4–1.6%), and the AgNPs/HEC scaffolds showed good porosity, swelling ability, low toxicity, and thermal stability as well as good cytocompatibility with human fibroblast cells [219]. TEMPO oxidation is one of the common technique to chemically modify the surface of nanocellulose by oxidizing the C6 primary hydroxyl to carboxyl groups. Shefa et al. synthesized TEMPO oxidized cellulose nanofiber (TOCN) with silk fibroin for wound healing applications. In vitro studies of TOCN-silk fibroin scaffolds revealed good cell proliferation and attachment of L929 primary fibroblast cells. In vivo evaluation with rat skin revealed that the TOCN-silk fibroin scaffolds promoted wound healing in the presence of biological markers, and scaffolds with 2% concentration showed the fastest wound healing [220].

5.4.4.2 Chitosan-Based Nanomaterials for Skin TE Applications

CS is a good candidate for skin TE applications since it promotes wound healing, and it is biocompatible, biodegradable, non-toxic and possesses antibacterial property. The CS sponge scaffolds can retain water and they prevent infection and dehydration of the damaged skin tissue; therefore, many attempts to utilize CS-based nanosystem by the incorporation of various synthetic or natural compounds. Shalumon et al. developed CS/poly(caprolactone) (CS/PCL) nanofiber scaffolds fabricated by electrospinning that increased the hydrophilicity, bioactivity, and protein adsorption of the scaffold. Also, in vitro results showed that CS/PCL scaffolds displayed enhanced cell attachment, proliferation of human osteoscarcoma cells (MG63) without any evidence of cytotoxicity [221]. Electrospun CS based nano/micro fibrous scaffolds were prepared and incorporated into freeze dried collagen matrix to form a novel hierarchical system composed of both strong fibrous and porous structure for cell cultivation. Hierarchical CS-collagen scaffolds displayed satisfactory tensile strength, swelling behavior, and biodegradability as well as good cytocompatibility with fibroblasts and keratinocytes. Also, ex vivo results of CS-collagen scaffolds in human skin wound model revealed the migration of keratinocyte and re-epithelization that are essential for skin healing and regeneration [222]. Kumar et al. developed CS hydrogel/nanofibrin composite bandage (CFBs) for skin repair purpose. The physical properties of microporous, flexible, swelling ability, biodegradable, CFBs were desirable for skin repair bandage, and the introduction of nanofibrin improved the blood clotting and platelet activity of CFBs. In vitro studies with human umbilical vein endothelial cells and human dermal fibroblast cells showed good cell attachment to CFBs that promoted the proliferation rate of both cells. In vivo results showed that CFBs generated more deposition of collagen in the wound site [223].

5.4.5 Cardiac Tissue Engineering Applications

Heart functional diseases (HFD), such as myocardial infarction and heart stroke are mainly caused by cardiac cells/tissues damage due to blood vessels blockage by fatty acids, cholesterol or other compounds. HFD is among one of the more serious medical issues leading to sudden death of many people and the number of HFD patients are increasing. A cardiac TE treatment (cardiac patch) was proposed to prevent and cure serious HFD by implanting or injecting biomaterials cultured with cardiac cells. Many studies have showed the potentials of new engineered cardiac patches to repair heart functionality, damaged cardiac cells (cardiac myoblast or heart beating muscle cells) and tissue.

CS-based nanofiber scaffolds have been used for cardiac TE application using electrospinning method as they have many advantages, such as high surface area to volume ratio, good mechanical strength, wide capabilities for polymer conjugation, and mass production capabilities. Bioactive chitosan nanofiber scaffolds fabricated

by electrospinning are biocompatible, biodegradable, and they possessed desirable properties (e.g. cell attachment) that can retain cardiac structure and function [224]. Another group fabricated CS nanofiber scaffold and combined it with poly (lactic acid) (PLA) via electrospinning method, where the aligned nanofibers could promote cardiomyocyte proliferation and attachment. Compared to pure CS scaffolds, and CS nanofiber/PLA scaffolds with ratio of 7:1 (PLA:CS nanofiber) significantly enhanced cell-scaffold interaction as well as the synthesis of ECM [225]. Recently, efforts to increase conductivity for cardiac tissue engineered biomaterials have been attempted since cardiac muscle is an electroactive tissue that can transfer electrical signals from SA node to Purkinje fibers. CS scaffolds incorporated with carbon nanofibers enhanced the electrical properties, metabolic activity of neonatal rat heart cells, and expression of cardiac-specific genes that regulate muscle contraction and electrical coupling [226]. Another trial to increase conductivity was conducted by introducing selenium nanoparticle (SeNPs) into the CS-based film, which increased the electrical stimulation, mechanical strength, and proliferation of H9C2 cells [227]. CS-based injectable hydrogel scaffolds containing AuNP also supported viability, metabolism, migration, proliferation, and cardiomyogenic differentiation of MSCs, suggesting that the addition of GNP could promote the regenerative property of other electroactive tissues [228]. Chen et al. synthesized electrospun scaffolds composed of ethyl cellulose (EC) and polyurethane (PU), where their physical properties consisted of a 3D porous and uniform fibrous nanostructure for cardiac TE applications. The increased mechanical strength enables the fabricating of ultrathin cardiac patches that could support contractile cardiac tissue. The in vitro results with cardiac myoblast cells revealed good cell retentions and proliferation, suggesting that PU/EC scaffolds improved cell guidance and regulation as well as proliferation to mimic the extracellular matrix of myocardium [229].

5.5 Concluding Remarks

The use of nanopolysaccharides in biomedical science offers many advantages as the materials are derived from nature, and they are compatible with many biological systems. In this chapter, several examples on the use of nanopolysaccharides are described and discussed. The feasibility of using these materials is explored and examined, where advances in selected applications are outlined. There are increasing opportunities in the use and development of functional nanomaterials based on polysaccharides, and increasing research and development into the applications of these systems are being pursued in the academic and industrial laboratories.

References

1. Malam Y, Loizidou M, Seifalian AM (2009) Liposomes and nanoparticles: nanosized vehicles for drug delivery in cancer. Trends Pharmacol Sci 30:592–599
2. Debele TA, Mekuria SL, Tsai HC (2016) Polysaccharide based nanogels in the drug delivery system: application as the carrier of pharmaceutical agents. Mater Sci Eng C 68:964–981
3. Goldberg M, Langer R, Jia X (2007) Nanostructured materials for applications in drug delivery and tissue engineering. J Biomater Sci Polym Ed 18:241–268
4. Wilczewska AZ, Niemirowicz K, Markiewicz KH et al (2012) Nanoparticles as drug delivery systems. Pharmacol Rep 64:1020–1037
5. Swierczewska M, Han HS, Kim K et al (2016) Polysaccharide-based nanoparticles for theranostic nanomedicine. Adv Drug Deliv Rev 99:70–84
6. García-González CA, Alnaief M, Smirnova I (2011) Polysaccharide-based aerogels—promising biodegradable carriers for drug delivery systems. Carbohydr Polym 86:1425–1438
7. Mehling T, Smirnova I, Guenther U et al (2009) Polysaccharide-based aerogels as drug carriers. J Non Cryst Solids 355:2472–2479
8. Liu Z, Jiao Y, Wang Y et al (2008) Polysaccharides-based nanoparticles as drug delivery systems. Adv Drug Deliv Rev 60:1650–1662
9. Arora D, Rawal RK, Shankar R et al (2016) Polysaccharides based nanomaterials for targeted anti-cancer drug delivery. J Drug Target 25:1–16
10. Saravanakumar G, Jo D-G, Park JH (2012) Polysaccharide-based nanoparticles: a versatile platform for drug delivery and biomedical imaging. Curr Med Chem 19:3212
11. Zhang N, Wardwell PR, Bader RA (2013) Polysaccharide-based micelles for drug delivery. Pharmaceutics 5:329–352
12. Hu B, Huang Q (2013) Biopolymer based nano-delivery systems for enhancing bioavailability of nutraceuticals. Chin J Polym Sci 31:1190
13. Nitta SK, Numata K (2013) Biopolymer-based nanoparticles for drug/gene delivery and tissue engineering. Int J Mol Sci 14(1):1629–1654
14. Peng B, Tang J, Wang P et al (2018) Rheological properties of cellulose nanocrystal-polymeric systems. Cellulose 25:3229–3240
15. Islam MS, Chen L, Sisler J et al (2018) Cellulose nanocrystal (CNC)–inorganic hybrid systems: synthesis, properties and applications. J Mater Chem B 6:864–883
16. Mohammed N, Grishkewich N, Tam KC (2018) Cellulose nanomaterials: promising sustainable nanomaterials for application in water/wastewater treatment processes. Environ Sci Nano 5:623–658
17. Song Y, Zhang L, Gan W et al (2011) Self-assembled micelles based on hydrophobically modified quaternized cellulose for drug delivery. Colloids Surf B Biointerfaces 83:313–320
18. Tang J, Sisler J, Grishkewich N et al (2017) Functionalization of cellulose nanocrystals for advanced applications. J Colloid Interface Sci 494:397–409
19. Grishkewich N, Mohammed N, Tang J et al (2017) Recent advances in the application of cellulose nanocrystals. Curr Opin Colloid Interface Sci 29:32–45
20. Shukla RK, Tiwari A (2012) Carbohydrate polymers: applications and recent advances in delivering drugs to the colon. Carbohydr Polym 88:399–416
21. Luong JHT, Lam E, Leung ACW et al (2012) Applications of functionalized and nanoparticle-modified nanocrystalline cellulose. Trends Biotechnol 30:283–290
22. Li Z, Xu W, Zhang C et al (2015) Self-assembled lysozyme/carboxymethylcellulose nanogels for delivery of methotrexate. Int J Biol Macromol 75:166–172
23. Tan J, Kang H, Liu R et al (2011) Dual-stimuli sensitive nanogels fabricated by self-association of thiolated hydroxypropyl cellulose. Polym Chem 2:672–678
24. Hu B, Ting Y, Zeng X et al (2012) Cellular uptake and cytotoxicity of chitosan–caseinophosphopeptides nanocomplexes loaded with epigallocatechin gallate. Carbohydr Polym 89:362–370
25. Ghimire A, Kasi RM, Kumar CV (2014) Proton-coupled protein binding: controlling lysozyme/poly(acrylic acid) interactions with pH. J Phys Chem B 118:5026–5033

26. Li Z, Xu W, Xiong W et al (2015) Curcumin encapsulated in the complex of lysozyme/carboxymethylcellulose and implications for the antioxidant activity of curcumin. Food Res Int 75:98–105
27. Deng H, Li B, Peng Z et al (2012) Nanogels fabricated by lysozyme and sodium carboxymethyl cellulose for 5-fluorouracil controlled release. Int J Pharm 441:721–727
28. Qian H, Wang X, Yuan K et al (2014) Delivery of doxorubicin in vitro and in vivo using bio-reductive cellulose nanogels. Biomater Sci 2:220–232
29. Rahimian K, Wen Y, Oh JK (2015) Redox-responsive cellulose-based thermoresponsive grafted copolymers and in-situ disulfide crosslinked nanogels. Polymer 72:387–394
30. Wen Y, Oh JK (2015) Intracellular delivery cellulose-based bionanogels with dual temperature/pH-response for cancer therapy. Colloids Surf B Biointerfaces 133:246–253
31. Wang H, He J, Zhang M et al (2015) A new pathway towards polymer modified cellulose nanocrystals via a "grafting onto" process for drug delivery. Polym Chem 6:4206–4209
32. You J, Cao J, Zhao Y et al (2016) Improved mechanical properties and sustained release behavior of cationic cellulose nanocrystals reinforced cationic cellulose injectable hydrogels. Biomacromolecules 17:2839–2848
33. Lin N, Gèze A, Wouessidjewe D et al (2016) Biocompatible double-membrane hydrogels from cationic cellulose nanocrystals and anionic alginate as complexing drugs codelivery. ACS Appl Mater Interfaces 8:6880–6889
34. Dong S, Cho HJ, Lee YW et al (2014) Synthesis and cellular uptake of folic acid-conjugated cellulose nanocrystals for cancer targeting. Biomacromolecules 15:1560–1567
35. Ikkala O, Kontturi E, Rosilo H et al (2014) Cationic polymer brush-modified cellulose nanocrystals for high-affinity virus binding. Nanoscale 6:11871–11881
36. Cihova M, Altanerova V, Altaner C (2011) Stem cell based cancer gene therapy. Mol Pharm 8:1480–1487
37. Hu H, Yuan W, Liu FS et al (2015) Redox-responsive polycation-functionalized cotton cellulose nanocrystals for effective cancer treatment. ACS Appl Mater Interfaces 7:8942–8951
38. Hu H, Hou XJ, Wang XC et al (2016) Gold nanoparticle-conjugated heterogeneous polymer brush-wrapped cellulose nanocrystals prepared by combining different controllable polymerization techniques for theranostic applications. Polym Chem 7:3107–3116
39. Son Y, Jang JS, Cho YW et al (2003) Biodistribution and anti-tumor efficacy of doxorubicin loaded glycol-chitosan nanoaggregates by EPR effect. J Control Release 91 (1-2):135-145
40. Prabaharan M (2015) Chitosan-based nanoparticles for tumor-targeted drug delivery. Int J Biol Macromol 72:1313–1322
41. Agnihotri SA, Mallikarjuna NN, Aminabhavi TM (2004) Recent advances on chitosan-based micro- and nanoparticles in drug delivery. J Control Release 100:5–28
42. Luo Y, Wang Q (2014) Recent development of chitosan-based polyelectrolyte complexes with natural polysaccharides for drug delivery. Int J Biol Macromol 64:353–367
43. Shanmuganathan R, Edison TNJI, LewisOscar F et al (2019) Chitosan nanopolymers: an overview of drug delivery against cancer. Int J Biol Macromol 130:727–736
44. Kean T, Thanou M (2010) Biodegradation, biodistribution and toxicity of chitosan. Adv Drug Deliv Rev 62:3–11
45. Yu S, Xu X, Feng J et al (2019) Chitosan and chitosan coating nanoparticles for the treatment of brain disease. Int J Pharm 560:282–293
46. Bernkop-Schnürch A, Dünnhaupt S (2012) Chitosan-based drug delivery systems. Eur J Pharm Biopharm 81:463–469
47. Bhattarai N, Gunn J, Zhang M (2010) Chitosan-based hydrogels for controlled, localized drug delivery. Adv Drug Deliv Rev 62:83–99
48. Kumar MNVR, Muzzarelli RAA, Muzzarelli C et al (2004) Chitosan chemistry and pharmaceutical perspectives. Chem Rev 104:6017–6084
49. Anitha A, Sowmya S, Kumar PTS et al (2014) Chitin and chitosan in selected biomedical applications. Prog Polym Sci 39:1644–1667
50. Van der Lubben IM, Verhoef JC, Borchard G et al (2001) Chitosan and its derivatives in mucosal drug and vaccine delivery. Eur J Pharm Sci 14:201–207

51. Hejazi R, Amiji M (2003) Chitosan-based gastrointestinal delivery systems. J Control Release 89:151–165
52. Jayakumar R, Prabaharan M, Sudheesh Kumar PT et al (2011) Biomaterials based on chitin and chitosan in wound dressing applications. Biotechnol Adv 29:322–337
53. Du J, Dai J, Liu JL et al (2006) Novel pH-sensitive polyelectrolyte carboxymethyl Konjac glucomannan-chitosan beads as drug carriers. React Funct Polym 66:1055–1061
54. Il'ina AV, Varlamov VP (2005) Chitosan-based polyelectrolyte complexes: a review. Appl Biochem Microbiol 41:5–11
55. Torchilin V (2011) Tumor delivery of macromolecular drugs based on the EPR effect. Adv Drug Deliv Rev 63:131–135
56. Brigger I, Dubernet C, Couvreur P (2012) Nanoparticles in cancer therapy and diagnosis. Adv Drug Deliv Rev 64:24–36
57. Yu M, Lee I-H, Kim H et al (2008) Conjugated chitosan as a novel platform for oral delivery of paclitaxel. J Med Chem 51:6442–6449
58. Lee E, Lee J, Jon S (2010) A novel approach to oral delivery of insulin by conjugating with low molecular weight chitosan. Bioconjug Chem 21:1720–1723
59. Xiong F-L, Gu X-B, Zheng H et al (2012) Preparation, characterization and in vitro release study of a glutathione-dependent polymeric prodrug Cis-3-(9H-purin-6-ylthio)-acrylic acid-graft-carboxymethyl chitosan. Int J Pharm 436:240–247
60. Yang L, Chen L, Zeng R et al (2010) Synthesis, nanosizing and in vitro drug release of a novel anti-HIV polymeric prodrug: chitosan-O-isopropyl-5′-O-d4T monophosphate conjugate. Bioorg Med Chem 18:117–123
61. Yang L, Zeng R, Li C et al (2009) Novel synthesis and in vitro drug release of polymeric prodrug: chitosan-O-isopropyl-5′-O-d4T monophosphate conjugate. Bioorg Med Chem Lett 19:2566–2569
62. Sah AK, Dewangan M, Suresh PK (2019) Potential of chitosan-based carrier for periodontal drug delivery. Colloids Surf B Biointerfaces 178:185–198
63. Wolfbeis OS (2015) An overview of nanoparticles commonly used in fluorescent bioimaging. Chem Soc Rev 4743–4768
64. Ghoshal A, Goswami U, Raza A et al (2016) Recombinant sFRP4 bound chitosan–alginate composite nanoparticles embedded with silver nanoclusters for Wnt/β-catenin targeting in cancer theranostics. RSC Adv 85763–85772
65. Raveendran S, Poulose AC, Yoshida Y et al (2013) Bacterial exopolysaccharide based nanoparticles for sustained drug delivery, cancer chemotherapy and bioimaging. Carbohydr Polym 91:22–32
66. Hou X, Zhou H, Wang L et al (2017) Multifunctional near-infrared dye-magnetic nanoparticles for bioimaging and cancer therapy. Cancer Lett 390:168–175
67. Chowdhuri AR, Tripathy S, Haldar C (2015) Single step synthesis of carbon dot embedded chitosan nanoparticles for cell imaging and hydrophobic drug delivery. J Mater Chem B 47:9122–9131
68. Wang H, Di J, Sun Y et al (2015) Biocompatible PEG-chitosan @ carbon dots hybrid nanogels for two-photon fluorescence imaging, near-infrared light/pH dual-responsive drug carrier, and synergistic therapy. Adv Funct Mater 25:5537–5547
69. Tomak A, Bor G, Muhammed U (2017) BODIPY-conjugated chitosan nanoparticles as a fluorescent probe. Drug Chem Toxicol 40:375–382
70. Dong S, Roman M (2007) Fluorescently labeled cellulose nanocrystals for bioimaging applications. J Am Chem Soc 129:13810–13811
71. Mahmoud KA, Mena JA, Male KB et al (2010) Effect of surface charge on the cellular uptake and cytotoxicity of fluorescent labeled cellulose nanocrystals. ACS Appl Mater 2:2924–2932
72. Guo J, Liu D, Filpponen I et al (2017) Photoluminescent hybrids of cellulose nanocrystals and carbon quantum dots as cytocompatible probes for in vitro bioimaging. Biomacromolecules 18:2045–2055
73. Abitbol T, Palermo A, Moran-Mirabal JM et al (2013) Fluorescent labeling and characterization of cellulose nanocrystals with varying charge contents. Biomacromolecules 14:3278–3284

74. Drogat N, Granet R, Le Morvan C et al (2012) Chlorin-PEI-labeled cellulose nanocrystals: synthesis, characterization and potential application in PDT. Bioorg Med Chem Lett 22:3648–3652
75. Grate JW, Mo K, Shin Y et al (2015) Alexa fluor-labeled fluorescent cellulose nanocrystals for bioimaging solid cellulose in spatially structured microenvironments. Bioconjug Chem 26:593–601
76. Thakur B, Amarnath CA, Sawant SN (2014) Pectin coated polyaniline nanoparticles for an amperometric glucose biosensor. RSC Adv 77:40917–40923
77. Elmizadeh H, Soleimani M, Faridbod F et al (2018) Fabrication and optimization of a sensitive tetracycline fluorescent nano-sensor based on oxidized starch polysaccharide biopolymer-capped CdTe/ZnS quantum dots: Box–Behnken design. J Photochem Photobiol A Chem 367:188–199
78. Edwards JV, Fontenot KR, Prevost NT et al (2016) Preparation, characterization and activity of a peptide-cellulosic aerogel protease sensor from cotton. Sensors 16:1–19
79. Rejinold NS, Chennazhi KP, Tamura H et al (2011) Multifunctional chitin nanogels for simultaneous drug delivery, bioimaging, and biosensing. ACS Appl Mater 3:3654–3665
80. Anusha JR, Raj CJ, Cho B et al (2015) Amperometric glucose biosensor based on glucose oxidase immobilized over chitosan nanoparticles from gladius of *Uroteuthis duvaucelii*. Sens Actuators B Chem 215:536–543
81. Singh A, Sinsinbar G, Choudhary M et al (2013) Chemical graphene oxide-chitosan nanocomposite based electrochemical DNA biosensor for detection of typhoid. Sens Actuators B Chem 185:675–684
82. Liu S, Kang M, Yan F et al (2015) Electrochemical DNA biosensor based on microspheres of cuprous oxide and nano-chitosan for Hg(II) detection. Electrochim Acta 160:64–73
83. Li G, Xue Q, Feng J et al (2015) Electrochemical biosensor based on nanocomposites film of thiol graphene-thiol chitosan/nano gold for the detection of carcinoembryonic antigen. Electroanalysis 27:1245–1252
84. Nielsen LJ, Eyley S, Thielemans W et al (2010) Dual fluorescent labelling of cellulose nanocrystals for pH sensing. Chem Commun 46:8929–8931
85. Chen L, Cao W, Grishkewich N et al (2015) Synthesis and characterization of pH-responsive and fluorescent poly (amidoamine) dendrimer-grafted cellulose nanocrystals. J Colloid Interface Sci 450:101–108
86. Dong L, Zhang X, Ren S et al (2016) Poly(diallyldimethylammonium chloride)–cellulose nanocrystals supported Au nanoparticles for nonenzymatic glucose sensing. RSC Adv 6:6436–6442
87. Zhang L, Li Q, Zhou J et al (2012) Synthesis and photophysical behavior of pyrene-bearing cellulose nanocrystals for Fe^{3+} sensing. Macromol Chem Phys 213:1612–1617
88. Mehdi S, Min S, Sayed M et al (2019) Lipase-immobilized chitosan-crosslinked magnetic nanoparticle as a biocatalyst for ring opening esterification of itaconic anhydride. Biochem Eng J 143:141–150
89. Myra F, Manan A, Attan N et al (2018) Insight into the *Rhizomucor miehei* lipase supported on chitosan-chitin nanowhiskers assisted esterification of eugenol to eugenyl benzoate. J Biotechnol 280:19–30
90. Dhavale RP, Parit SB, Sahoo SC et al (2018) α-amylase immobilized on magnetic nanoparticles: reusable robust nano-biocatalyst for starch hydrolysis
91. Kim M, Cheol S, Sung J et al (2018) Anti-proliferative applications of laccase immobilized on super-magnetic chitosan-functionalized halloysite nanotubes. Int J Biol Macromol 118:228–237
92. Chandren S, Attan N, Mahat NA et al (2017) Structure and properties of oil palm-based nanocellulose reinforced chitosan nanocomposite for efficient synthesis of butyl butyrate. Carbohydr Polym 176:281–292
93. Asmat S, Husain Q (2018) Exquisite stability and catalytic performance of immobilized lipase on novel fabricated nanocellulose fused polypyrrole/graphene oxide nanocomposite: characterization and application. Int J Biol Macromol 117:331–341

94. Rad-Moghadam K, Dehghan N (2014) Application of cellulose/chitosan grafted nano-magnetites as efficient and recyclable catalysts for selective synthesis of 3-indolylindolin-2-ones. J Mol Catal A Chem 392:97–104
95. Yuan B, Yang XQ, Xue LW et al (2016) A novel recycling system for nano-magnetic molecular imprinting immobilised cellulases: synergistic recovery of anthocyanin from fruit and vegetable waste. Bioresour Technol 222:14–23
96. Koutinas AA, Sypsas V, Kandylis P et al (2012) Nano-tubular cellulose for bioprocess technology development. PLoS ONE 7:e34350
97. Kumar MN, Gialleli A, Bekatorou A et al (2016) Application of nano/micro-tubular cellulose of Indian origin for alcoholic fermentation and cold pasteurization of contaminated water. LWT Food Sci Technol 69:273–279
98. Moon RJ, Martini A, Nairn J et al (2011) Cellulose nanomaterials review: structure, properties and nanocomposites. Chem Soc Rev 40:3941–3994
99. Ates B, Cerkez I (2017) Dual antibacterial functional regenerated cellulose fibers. J Appl Polym Sci 134:1–8
100. Klevens RM et al (2007) Estimating health care-associated infections and deaths in U.S. hospitals, 2002. Public Health Rep 122:160–166
101. Hu Z, Gänzle MG (2018) Challenges and opportunities related to the use of chitosan as a food preservative. J Appl Microbiol 307:1–14
102. Chao D, Xin M, Jingru M et al (2019) Chitosan as a preservative for fruits and vegetables: a review on chemistry and antimicrobial properties. J Bioresour Bioprod 4:11–21
103. Raafat D, Sahl H-G (2009) Chitosan and its antimicrobial potential—a critical literature survey. Microb Biotechnol 2:186–201
104. Kong M, Chen XG, Xing K et al (2010) Antimicrobial properties of chitosan and mode of action: a state of the art review. Int J Food Microbiol 144:51–63
105. Rabea EI, Badawy MET, Stevens CV et al (2003) Chitosan as antimicrobial agent: applications and mode of action. Biomacromolecules 4:1457–1465
106. Je J-Y, Kim S-K (2006) Chitosan derivatives killed bacteria by disrupting the outer and inner membrane. J Agric Food Chem 54:6629–6633
107. Tao Y, Qian LH, Xie J (2011) Effect of chitosan on membrane permeability and cell morphology of *Pseudomonas aeruginosa* and *Staphylococcus aureus*. Carbohydr Polym 86:969–974
108. Helander IM, Nurmiaho-Lassila EL, Ahvenainen R et al (2001) Chitosan disrupts the barrier properties of the outer membrane of gram-negative bacteria. Int J Food Microbiol 71:235–244
109. Liu H, Du Y, Wang X et al (2004) Chitosan kills bacteria through cell membrane damage. Int J Food Microbiol 95:147–155
110. Raafat D, Von Bargen K, Haas A et al (2008) Insights into the mode of action of chitosan as an antibacterial compound. Appl Environ Microbiol 74:3764–3773
111. Shahid-Ul-Islam, Butola BS (2019) Recent advances in chitosan polysaccharide and its derivatives in antimicrobial modification of textile materials. Int J Biol Macromol 121:905–912
112. Shahid-Ul-Islam, Shahid M, Mohammad F (2013) Green chemistry approaches to develop antimicrobial textiles based on sustainable biopolymers—a review. Ind Eng Chem Res 52:5245–5260
113. Li P, Kwong TL, Lee DKL et al (2005) Novel core-shell particles with poly(n-butyl acrylate) cores and chitosan shells as an antibacterial coating for textiles. Polymer 46:10538–10543
114. Jung K-H, Huh M-W, Meng W et al (2007) Preparation and antibacterial activity of PET/chitosan nanofibrous mats using an electrospinning technique. J Appl Polym Sci 105:2816–2823
115. Ivanova NA, Philipchenko AB (2012) Superhydrophobic chitosan-based coatings for textile processing. Appl Surf Sci 263:783–787
116. Joshi M, Khanna R, Shekhar R et al (2011) Chitosan nanocoating on cotton textile substrate using layer-by-layer self-assembly technique. J Appl Polym Sci 119:2793–2799
117. Liu J, Liu C, Liu Y et al (2013) Study on the grafting of chitosan-gelatin microcapsules onto cotton fabrics and its antibacterial effect. Colloids Surf B Biointerfaces 109:103–108

118. Alonso D, Gimeno M, Sepúlveda-Sánchez JD et al (2010) Chitosan-based microcapsules containing grapefruit seed extract grafted onto cellulose fibers by a non-toxic procedure. Carbohydr Res 345:854–859
119. Abdel-Mohsen AM, Aly AS, Hrdina R et al (2012) Biomedical textiles through multifunctionalization of cotton fabrics using innovative methoxypolyethylene glycol-n-chitosan graft copolymer. J Polym Environ 20:104–116
120. Janjic S, Kostic M, Vucinic V et al (2009) Biologically active fibers based on chitosan-coated lyocell fibers. Carbohydr Polym 78:240–246
121. Sheikh J, Bramhecha I (2018) Multifunctional modification of linen fabric using chitosan-based formulations. Int J Biol Macromol 118:896–902
122. Suppakul P, Miltz J, Sonneveld K et al (2003) Active packaging technologies with an emphasis on antimicrobial packaging and its applications. J Food Sci 68:408–420
123. Quintavalla S, Vicini L (2002) Antimicrobial food packaging in meat industry. Meat Sci 62:373–380
124. Malhotra B, Keshwani A, Kharkwal H (2015) Antimicrobial food packaging: potential and pitfalls. Front Microbiol 6:1–9
125. Cha DS, Chinnan MS (2004) Biopolymer-based antimicrobial packaging: a review. Crit Rev Food Sci Nutr 44:223–237
126. Leceta I, Guerrero P, De La Caba K (2013) Functional properties of chitosan-based films. Carbohydr Polym 93:339–346
127. Mujtaba M, Morsi RE, Kerch G et al (2019) Current advancements in chitosan-based film production for food technology: a review. Int J Biol Macromol
128. Van Den Broek LAM, Knoop RJI, Kappen FHJ et al (2015) Chitosan films and blends for packaging material. Carbohydr Polym 116:237–242
129. Jianglian D (2013) Application of chitosan based coating in fruit and vegetable preservation: a review. J Food Process Technol 04:5–8
130. Elsabee MZ, Abdou ES (2013) Chitosan based edible films and coatings: a review. Mater Sci Eng C 33:1819–1841
131. Kerch G (2015) Chitosan films and coatings prevent losses of fresh fruit nutritional quality: a review. Trends Food Sci Technol 46:159–166
132. Xing Y, Xu Q, Li X et al (2016) Chitosan-based coating with antimicrobial agents: preparation, property, mechanism, and application effectiveness on fruits and vegetables. Int J Polym Sci
133. Leceta I, Peñalba M, Arana P et al (2015) Ageing of chitosan films: effect of storage time on structure and optical, barrier and mechanical properties. Eur Polym J 66:170–179
134. Siripatrawan U, Vitchayakitti W (2016) Improving functional properties of chitosan films as active food packaging by incorporating with propolis. Food Hydrocoll 61:695–702
135. Sun L, Sun J, Chen L et al (2017) Preparation and characterization of chitosan film incorporated with thinned young apple polyphenols as an active packaging material. Carbohydr Polym 163:81–91
136. Özen İ, Erim FB, Torlak E et al (2017) Antimicrobial and physical properties of chitosan films incorporated with turmeric extract. Int J Biol Macromol 101:882–888
137. Azizi S, Ahmad MB, Ibrahim NA et al (2014) Cellulose nanocrystals/ZnO as a bifunctional reinforcing nanocomposite for poly(vinyl alcohol)/chitosan blend films: fabrication, characterization and properties. Int J Mol Sci 15:11040–11053
138. Del Nobile MA, Conte A, Attianese I et al (2013) MMT-supported Ag nanoparticles for chitosan nanocomposites: structural properties and antibacterial activity. Carbohydr Polym 102:385–392
139. Vlacha M, Giannakas A, Katapodis P et al (2016) On the efficiency of oleic acid as plasticizer of chitosan/clay nanocomposites and its role on thermo-mechanical, barrier and antimicrobial properties—comparison with glycerol. Food Hydrocoll 57:10–19
140. Zhang L, Wang H, Jin C et al (2017) Sodium lactate loaded chitosan-polyvinyl alcohol/montmorillonite composite film towards active food packaging. Innov Food Sci Emerg Technol 42:101–108

141. Moghadas B, Dashtimoghadam E, Mirzadeh H et al (2016) Novel chitosan-based nanobiohybrid membranes for wound dressing applications. RSC Adv 6:7701–7711
142. Liu Y, Wang S, Lan W (2018) Fabrication of antibacterial chitosan-PVA blended film using electrospray technique for food packaging applications. Int J Biol Macromol 107:848–854
143. Stoica-Guzun A, Parvulescu O, Stroescu M et al (2015) Chitosan-vanillin composites with antimicrobial properties. Food Hydrocoll 48:62–71
144. Mohebi E, Shahbazi Y (2017) Application of chitosan and gelatin based active packaging films for peeled shrimp preservation: a novel functional wrapping design. LWT Food Sci Technol 76:108–116
145. Devlieghere F, Vermeulen A, Debevere J (2004) Chitosan: antimicrobial activity, interactions with food components and applicability as a coating on fruit and vegetables. Food Microbiol 21:703–714
146. Chien PJ, Sheu F, Yang FH (2007) Effects of edible chitosan coating on quality and shelf life of sliced mango fruit. J Food Eng 78:225–229
147. Sheikhi A, Hayashi J, Eichenbaum J et al (2019) Recent advances in nanoengineering cellulose for cargo delivery. J Control Release 294:53–76
148. Li J, Cha R, Mou K et al (2018) Nanocellulose-based antibacterial materials. Adv Healthc Mater 7:1–16
149. Sunasee R, Hemraz U (2018) Synthetic strategies for the fabrication of cationic surface-modified cellulose nanocrystals. Fibers 6:15
150. Mou K, Li J, Wang Y et al (2017) 2,3-Dialdehyde nanofibrillated cellulose as a potential material for the treatment of MRSA infection. J Mater Chem B 5:7876–7884
151. Montanari S, Roumani M, Heux L et al (2005) Topochemistry of carboxylated cellulose nanocrystals resulting from TEMPO-mediated oxidation. Macromolecules 38:1665–1671
152. Cao X, Ding B, Yu J et al (2013) In situ growth of silver nanoparticles on TEMPO-oxidized jute fibers by microwave heating. Carbohydr Polym 92:571–576
153. Tang J, Lee MFX, Zhang W et al (2014) Dual responsive pickering emulsion stabilized by poly[2-(dimethylamino)ethyl methacrylate] grafted cellulose nanocrystals. Biomacromolecules 15:3052–3060
154. Morits M, Hynninen V, Nonappa et al (2018) Polymer brush guided templating on well-defined rod-like cellulose nanocrystals. Polym Chem 9:1650–1657
155. Yi J, Xu Q, Zhang X et al (2009) Temperature-induced chiral nematic phase changes of suspensions of poly(N, N-dimethylaminoethyl methacrylate)-grafted cellulose nanocrystals. Cellulose 16:989–997
156. Grishkewich N, Akhlaghi SP, Zhaoling Y et al (2016) Cellulose nanocrystal-poly(oligo(ethylene glycol) methacrylate) brushes with tunable LCSTs. Carbohydr Polym 144:215–222
157. Sunasee R, Burdick JS, Boluk Y et al (2014) Cationic poly(2-aminoethylmethacrylate) and poly(N-(2-aminoethylmethacrylamide)) modified cellulose nanocrystals: synthesis, characterization, and cytotoxicity. Biomacromolecules 16:319–325
158. Bespalova Y, Kwon D, Vasanthan N (2017) Surface modification and antimicrobial properties of cellulose nanocrystals. J Appl Polym Sci 134:1–7
159. Feese E, Sadeghifar H, Gracz HS et al (2011) Photobactericidal porphyrin-cellulose nanocrystals: synthesis, characterization, and antimicrobial properties. Biomacromolecules 12:3528–3539
160. Tang J, Song Y, Tanvir S et al (2015) Polyrhodanine coated cellulose nanocrystals: a sustainable antimicrobial agent. ACS Sustain Chem Eng 3:1801–1809
161. De Castro DO, Bras J, Gandini A et al (2016) Surface grafting of cellulose nanocrystals with natural antimicrobial rosin mixture using a green process. Carbohydr Polym 137:1–8
162. Niu X, Liu Y, Song Y et al (2018) Rosin modified cellulose nanofiber as a reinforcing and co-antimicrobial agents in polylactic acid/chitosan composite film for food packaging. Carbohydr Polym 183:102–109
163. Zhang D, Karkooti A, Liu L et al (2018) Fabrication of antifouling and antibacterial polyethersulfone (PES)/cellulose nanocrystals (CNC) nanocomposite membranes. J Membr Sci 549:350–356

164. Yang W, Fortunati E, Dominici F et al (2016) Synergic effect of cellulose and lignin nanostructures in PLA based systems for food antibacterial packaging. Eur Polym J 79:1–12
165. Fernandes SCM, Sadocco P, Alonso-Varona A et al (2013) Bioinspired antimicrobial and biocompatible bacterial cellulose membranes obtained by surface functionalization with aminoalkyl groups. ACS Appl Mater Interfaces 5:3290–3297
166. Li R, Jiang Q, Ren X et al (2015) Electrospun non-leaching biocombatible antimicrobial cellulose acetate nanofibrous mats. J Ind Eng Chem 27:315–321
167. Hou A, Zhou M, Wang X (2009) Preparation and characterization of durable antibacterial cellulose biomaterials modified with triazine derivatives. Carbohydr Polym 75:328–332
168. Kaushik M, Moores A (2016) Review: nanocelluloses as versatile supports for metal nanoparticles and their applications in catalysis. Green Chem 18:622–637
169. Foresti ML, Vázquez A, Boury B (2017) Applications of bacterial cellulose as precursor of carbon and composites with metal oxide, metal sulfide and metal nanoparticles: a review of recent advances. Carbohydr Polym 157:447–467
170. Bethke K, Palantöken S, Andrei V et al (2018) Functionalized cellulose for water purification, antimicrobial applications, and sensors. Adv Funct Mater 28:1–14
171. Zhao S-W, Guo C-R, Hu Y-Z et al (2018) The preparation and antibacterial activity of cellulose/ZnO composite: a review. Open Chem 16:9–20
172. Khan F, Ahmad SR (2013) Polysaccharides and their derivatives for versatile tissue engineering application. Macromol Biosci 13:395–421
173. Hao Z, Song Z, Huang J et al (2017) The scaffold microenvironment for stem cell based bone tissue engineering. Biomater Sci 5:1382–1392
174. Costa-Pinto AR, Reis RL, Neves NM (2011) Scaffolds based bone tissue engineering: the role of chitosan. Tissue Eng Part B Rev 17:331–347
175. Li Z, Ramay HR, Hauch KD et al (2005) Chitosan—alginate hybrid scaffolds for bone tissue engineering. Biomaterials 26:3919–3928
176. Zhang Y, Reddy J, El-Turki A et al (2008) Electrospun biomimetic nanocomposite nanofibers of hydroxyapatite/chitosan for bone tissue engineering. Biomaterials 29:4314–4322
177. Venkatesan J, Qian Z, Ryu B (2011) Preparation and characterization of carbon nanotube-grafted-chitosan—natural hydroxyapatite composite for bone tissue engineering. Carbohydr Polym 83:569–577
178. Misra RDK (2009) Biomimetic chitosan—nanohydroxyapatite composite scaffolds for bone tissue engineering. Acta Biomater 5:1182–1197
179. Zhang Y, Cheng X, Wang J et al (2006) Novel chitosan/collagen scaffold containing transforming growth factor-β 1 DNA for periodontal tissue engineering. Biochem Biophys Res Commun 344:362–369
180. Yilgor P, Tuzlakoglu K, Reis RL et al (2009) Incorporation of a sequential BMP-2/BMP-7 delivery system into chitosan-based scaffolds for bone tissue engineering. Biomaterials 30:3551–3559
181. Jorfi M, Foster EJ (2015) Recent advances in nanocellulose for biomedical applications. J Appl Polym Sci 132:1–19
182. Liuyun J, Yubao L, Chengdong X (2009) Tissue engineering. J Biomed Sci 10:1–10
183. Pasqui D, Torricelli P, De Cagna M et al (2013) Carboxymethyl cellulose—hydroxyapatite hybrid hydrogel as a composite material for bone tissue engineering applications. J Biomed Mater Res A 102:1568–1579
184. Ninan N, Muthiah M, Park I et al (2013) Pectin/carboxymethyl cellulose/microfibrillated cellulose composite scaffolds for tissue engineering. Carbohydr Polym 98:877–885
185. Sainitya R, Sriram M, Kalyanaraman V et al (2015) Scaffolds containing chitosan/carboxymethyl cellulose/mesoporous wollastonite for bone tissue engineering. Int J Biol Macromol 80:481–488
186. Domingues RMA, Gomes ME, Reis RL (2014) The potential of cellulose nanocrystals in tissue engineering strategies. Biomacromolecules 15:2327–2346
187. Zhou C, Shi Q, Guo W et al (2013) Electrospun bio-nanocomposite scaffolds for bone tissue engineering by cellulose nanocrystals reinforcing maleic anhydride grafted PLA. ACS Appl Mater Interfaces 5:3847–3854

188. Henrik B, Esguerra M, Delbro D et al (2008) Engineering microporosity in bacterial cellulose scaffolds. J Tissue Eng Regen Med 2:320–330
189. Zaborowska M, Bodin A, Bäckdahl H et al (2010) Microporous bacterial cellulose as a potential scaffold for bone regeneration. Acta Biomater 6:2540–2547
190. Fang B, Wan Y, Tang T et al (2009) Proliferation and osteoblastic differentiation of human bone marrow stromal cells on hydroxyapatite/bacterial cellulose nanocomposite scaffolds. Tissue Eng Part A 15:1091–1098
191. Huang Y, Wang J, Yang F et al (2017) Modification and evaluation of micro-nano structured porous bacterial cellulose scaffold for bone tissue engineering. Mater Sci Eng C 75:1034–1041
192. Gomes ME, Azevedo HS, Moreira AR et al (2008) Starch–poly(ε-caprolactone) and starch–poly(lactic acid) fibre-mesh scaffolds for bone tissue engineering applications: structure, mechanical properties and degradation behaviour. J Tissue Eng Regen Med 2:243–252
193. Rodrigues AI, Gomes ME, Leonor IB et al (2012) Bioactive starch-based scaffolds and human adipose stem cells are a good combination for bone tissue engineering. Acta Biomater 8:3765–3776
194. Martins A, Chung S, Pedro AJ et al (2009) Hierarchical starch-based fibrous scaffold for bone tissue engineering applications. J Tissue Eng Regen Med 37–42
195. Marques AP, Reis RL (2005) Hydroxyapatite reinforcement of different starch-based polymers affects osteoblast-like cells adhesion/spreading and proliferation. Mater Sci Eng C 25:215–229
196. Fuchs S, Ghanaati S, Orth C et al (2009) Contribution of outgrowth endothelial cells from human peripheral blood on in vivo vascularization of bone tissue engineered constructs based on starch polycaprolactone scaffolds. Biomaterials 30:526–534
197. Slgado AJ, Coutinho OP, Reis RL et al (2006) In vivo response to starch-based scaffolds designed for bone tissue engineering applications. J Biomed Mater Res Part A 80A:983–989
198. Wu D, Samanta A, Srivastava RK et al (2017) Starch-derived nanographene oxide paves the way for electrospinnable and bioactive starch scaffolds for bone tissue engineering. Biomacromolecules 18:1582–1591
199. Nourmohammadi J, Shahriarpanah S, Asadzadehzanjani N et al (2016) Biomimetic apatite layer formation on a novel citrate starch scaffold suitable for bone tissue engineering applications. Starch/Staerke 68:1275–1281
200. Kang R, Marui T, Ghivizzani SC et al (1997) Ex vivo gene transfer to chondrocytes in full-thickness articular cartilage defects: a feasibility study. Osteoarthr Cartil 5:139–143
201. Brittberg M, Lindahl A, Nilsson A et al (1994) Treatment of deep cartilage defects in the knee with autologous chondrocyte transplantation. N Engl J Med 331:889–895
202. Biji Balakrishnan, R. Banerjee, (2011) Biopolymer-Based Hydrogels for Cartilage Tissue Engineering. Chemical Reviews 111 (8):4453-4474
203. Francis Suh JK, Matthew HWT (2000) Application of chitosan-based polysaccharide biomaterials in cartilage tissue engineering: a review. Biomaterials 21:2589–2598
204. Jin R, Moreira Teixeira LS, Dijkstra PJ et al (2009) Injectable chitosan-based hydrogels for cartilage tissue engineering. Biomaterials 30:2544–2551
205. Sadeghi D, Karbasi S, Razavi S et al (2016) Electrospun poly(hydroxybutyrate)/chitosan blend fibrous scaffolds for cartilage tissue engineering. J Appl Polym Sci 133:1–9
206. Kashi M, Baghbani F, Moztarzadeh F et al (2018) Green synthesis of degradable conductive thermosensitive oligopyrrole/chitosan hydrogel intended for cartilage tissue engineering. Int J Biol Macromol 107:1567–1575
207. Bhardwaj N, Nguyen QT, Chen AC et al (2011) Potential of 3-D tissue constructs engineered from bovine chondrocytes/silk fibroin-chitosan for in vitro cartilage tissue engineering. Biomaterials 32:5773–5781
208. Whu SW, Hung KC, Hsieh KH et al (2013) In vitro and in vivo evaluation of chitosan-gelatin scaffolds for cartilage tissue engineering. Mater Sci Eng C 33:2855–2863
209. Naseri N, Deepa B, Mathew AP et al (2016) Nanocellulose-based interpenetrating polymer network (IPN) hydrogels for cartilage applications. Biomacromolecules 17:3714–3723

210. Markstedt K, Mantas A, Tournier I et al (2015) 3D bioprinting human chondrocytes with nanocellulose-alginate bioink for cartilage tissue engineering applications. Biomacromolecules 16:1489–1496
211. Nguyen D, Hgg DA, Forsman A et al (2017) Cartilage tissue engineering by the 3D bioprinting of iPS cells in a nanocellulose/alginate bioink. Sci Rep 7:1–10
212. Feldmann EM, Sundberg JF, Bobbili B et al (2013) Description of a novel approach to engineer cartilage with porous bacterial nanocellulose for reconstruction of a human auricle. J Biomater Appl 28:626–640
213. Nimeskern L, Martínez Ávila H, Sundberg J et al (2013) Mechanical evaluation of bacterial nanocellulose as an implant material for ear cartilage replacement. J Mech Behav Biomed Mater 22:12–21
214. Martínez Ávila H, Schwarz S, Feldmann EM et al (2014) Biocompatibility evaluation of densified bacterial nanocellulose hydrogel as an implant material for auricular cartilage regeneration. Appl Microbiol Biotechnol 98:7423–7435
215. Fu L, Zhou P, Zhang S, Yang G (2013) Evaluation of bacterial nanocellulose-based uniform wound dressing for large area skin transplantation. Mater Sci Eng C 33:2995–3000
216. Keskin Z, Sendemir Urkmez A et al (2017) Novel keratin modified bacterial cellulose nanocomposite production and characterization for skin tissue engineering. Mater Sci Eng C 75:1144–1153
217. Azarniya A, Eslahi N, Mahmoudi N et al (2016) Effect of graphene oxide nanosheets on the physico-mechanical properties of chitosan/bacterial cellulose nanofibrous composites. Compos Part A Appl Sci Manuf 85:113–122
218. Zulkifli FH, Hussain FSJ, Rasad MSBA et al (2014) Nanostructured materials from hydroxyethyl cellulose for skin tissue engineering. Carbohydr Polym 114:238–245
219. Rasad MSBA, Yusuff MM, Zulkifli FH et al (2017) A facile synthesis method of hydroxyethyl cellulose-silver nanoparticle scaffolds for skin tissue engineering applications. Mater Sci Eng C 79:151–160
220. Jung H-I, Choi H, Amirian J et al (2017) In vitro and in vivo evaluation of effectiveness of a novel TEMPO-oxidized cellulose nanofiber-silk fibroin scaffold in wound healing. Carbohydr Polym 177:284–296
221. Shalumon KT, Anulekha KH, Chennazhi KP et al (2011) Fabrication of chitosan/poly(caprolactone) nanofibrous scaffold for bone and skin tissue engineering. Int J Biol Macromol 48:571–576
222. Sarkar SD, Farrugia BL, Dargaville TR et al (2013) Chitosan-collagen scaffolds with nano/microfibrous architecture for skin tissue engineering. J Biomed Mater Res Part A 101:3482–3492
223. Kumar PTS, Raj NM, Praveen G et al (2013) In vitro and in vivo evaluation of microporous chitosan hydrogel/nanofibrin composite bandage for skin tissue regeneration. Tissue Eng Part A 19:380–392
224. Hussain A, Collins G, Yip D et al (2013) Functional 3-D cardiac co-culture model using bioactive chitosan nanofiber scaffolds. Biotechnol Bioeng 110:637–647
225. Liu Y, Wang S, Zhang R (2017) Composite poly(lactic acid)/chitosan nanofibrous scaffolds for cardiac tissue engineering. Int J Biol Macromol 103:1130–1137
226. Martins AM, Eng G, Caridade SG et al (2014) Electrically conductive chitosan/carbon scaffolds for cardiac tissue engineering. Biomacromolecules 15:635–643
227. Kalishwaralal K, Jeyabharathi S, Sundar K et al (2018) A novel biocompatible chitosan–Selenium nanoparticles (SeNPs) film with electrical conductivity for cardiac tissue engineering application. Mater Sci Eng C 92:151–160
228. Baei P, Jalili-Firoozinezhad S, Rajabi-Zeleti S et al (2016) Electrically conductive gold nanoparticle-chitosan thermosensitive hydrogels for cardiac tissue engineering. Mater Sci Eng C 63:131–141
229. Chen PH, Liao HC, Hsu SH et al (2015) A novel polyurethane/cellulose fibrous scaffold for cardiac tissue engineering. RSC Adv 5:6932–6939

Chapter 6
Nanopolysaccharides in Emulsion Stabilization

Juntao Tang, Ning Lin, Zhen Zhang, Chunyue Pan and Guipeng Yu

Abstract Due to increasing pressure to adopt sustainable approaches to product design and manufacture, the requirement to develop sustainable products has become one of the most important challenges to industry. Currently, there is a growing trend in developing products that maintain the concept of being natural and "green". This has motivated the utilization of bio-based products to replace petrochemicals for the formulation of Pickering emulsions for food, cosmetic and other industries. Polysaccharide nanoparticles are an excellent choice for this application, as they are derived from nature and consistent with the demands for sustainable development. This chapter's content includes the definition of emulsions and Pickering emulsions, the instability mechanism of emulsions and the potential applications based on nanopolysaccharides stabilized emulsions and their derived functional materials.

Keywords Nanopolysaccharides · Pickering emulsions · Nanocomposites · Emulsion stability

J. Tang (✉) · C. Pan · G. Yu
College of Chemistry and Chemical Engineering, Central South University, Changsha 410083, Hunan, People's Republic of China
e-mail: Reynard.tangjuntao@gmail.com

N. Lin
School of Chemistry, Chemical Engineering and Life Sciences, Wuhan University of Technology, Wuhan 430070, People's Republic of China

Z. Zhang
SCNU-TUE Joint Lab of Device Integrated Responsive Materials (DIRM), National Center for International Research on Green Optoelectronics, South China Normal University, Guangzhou 510006, People's Republic of China

N. Lin et al. (eds.), *Advanced Functional Materials from Nanopolysaccharides*,
Springer Series in Biomaterials Science and Engineering 15,
https://doi.org/10.1007/978-981-15-0913-1_6

6.1 General Information on Pickering Emulsions

6.1.1 Definition

An emulsion is made up of two immiscible liquids, with one of the liquids being dispersed as small droplets in the other liquid. Usually the two immiscible liquids are water and oil, but this is not always necessary [1, 2]. Water-in-water (W/W) and oil-in-oil emulsion (O/O) have also been created and reported. The liquid that makes up the droplets is commonly referred to as the "internal phase", "dispersed phase", or "discontinuous phase", whereas the material that makes up the surrounding phase is referred to as the "external phase", "dispersing phase", or "continuous phase". An example of an emulsion would be an oil-in-water emulsion (O/W), wherein the oil is the dispersed phase, and water is the dispersion medium. It is also possible to produce various types of multiple emulsions, e.g. oil-in-water-in-oil (O/W/O), water-in-oil-in-water (W/O/W) [3]. In order to stabilize the emulsions, surface-active substances, or so-called emulsifiers are commonly applied in the formulations. The emulsifier can lower the interfacial tension and tend to adsorb to the surface of emulsion droplets to form a protective coating that impedes the coalescence of droplets by introducing electrostatic or steric repulsive force. When traditional surfactants are used as stabilizers, the emulsions are thermodynamically unstable, as the molecules undergo adsorption and desorption at the interface. Emulsions that are stabilized by solid nanoparticles possess better stability against coalescence in comparison to surfactant-based emulsions since the first report by Pickering in 1907 [4]. However, they were largely ignored for a long period of time due to limited research in the field. Pickering emulsions have attracted attention in recent years due to new insights and developments in material science and engineering [5, 6].

Pickering emulsions can be defined as emulsions of any type which are stabilized by solid particles in the place of surfactants, thus Pickering emulsions can replace classic emulsion in a variety of industries spanning food, pharmaceuticals, petroleum and etc. [7–10]. Additionally, they hold several advantages when compared to conventional emulsions stabilized by surfactants. The high resistance to coalescence is a major benefit because the particles were dynamically adsorbed at the interface. Furthermore, the "surfactant-free" characteristic make them idea candidates for biomedical applications as they possess better biocompatibility. Moreover, the versatility of nanomaterials enables a diverse design to meet the various needs of applications [4, 11, 12]. The preparation of Pickering emulsions involves the procedure of dispersing nanoparticles into the continuous phase and driving the nanoparticles to adsorb at the interface. Pioneering works have demonstrated that the type of emulsions formed depends on the partial wettability in each of the immiscible phases. This is related to the interfacial energies of three interfaces: oil-water, solid-oil and solid-water [13]. Analogous to the hydrophilic-lipophilic balance (HLB) parameter of a surfactant molecule, the three-phase contact angle of a solid particle situated at an oil/water interface can be given by the Young's equation shown below [6]:

$$\cos\theta_w = \frac{\gamma_{s/o} - \gamma_{s/w}}{\gamma_{o/w}} \tag{6.1}$$

where $\gamma_{s/o}$, $\gamma_{s/w}$, and $\gamma_{o/w}$ are the solid/oil, solid/water, and oil/water interfacial energies, respectively. For more lipophilic particles, θ_w is typically greater than 90° and the majority of the particle is wetted by the oil phase. For more hydrophilic particles, θ_w is typically less than 90° and more of the particle surface is wetted by the aqueous phase. Particles equally wetted by both phases result in θ_w being equal to 90° and the oil/water interface is effectively planar (Fig. 6.1). Complete wetting of the particle in either phase results in instability of the emulsions. It is generally accepted that more hydrophilic particles, such as silica and metal oxide, can stabilize o/w emulsions, and lipophilic particles, such as pristine carbon materials, can stabilize w/o emulsions. Kaptay [14] reported that the optimized contact angle in water for stabilizing w/o emulsions is 94–110° and 70–86° for stabilizing o/w emulsions respectively.

It was reported by Binks [4] that assuming the particle size is small enough (typically less than a few μm in diameter), and the effect of gravity can be neglected, the energy E required to remove a solid spherical particle with a radius r from the interface is:

$$\Delta E = \pi r^2 \gamma_{ow}(1 - |\cos\theta_{ow}|)^2 \tag{6.2}$$

where $\gamma_{o/w}$ is the interfacial tension between oil and water. From the equation, it may be concluded that the adsorption free energy is always larger than the thermal energy, even when the solid particles are very small. As an example, the energy of

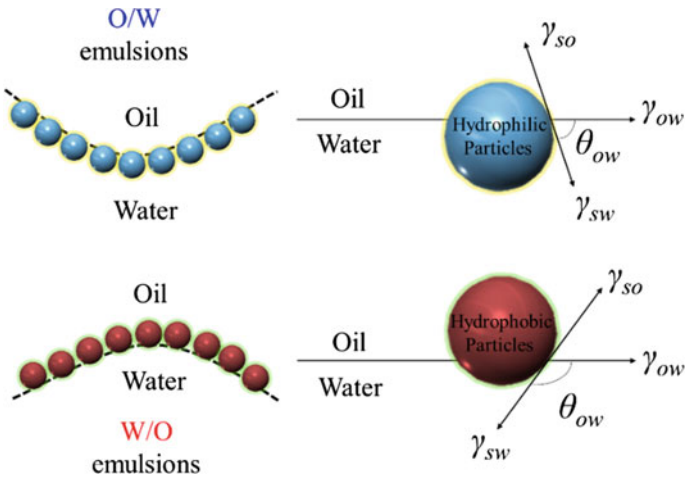

Fig. 6.1 Hydrophilic particles (in Blue) with contact angle less than 90° to stabilize oil-in-water emulsions; hydrophobic particles (in red) with contact angle higher than 90° to stabilize water-in-oil emulsions

a 10 nm solid spherical nanoparticles at the hydrocarbon-water interface ($\gamma_{o/w}$ = 50 mN m^{-1}) having a contact angle of 90° is $\Delta E = 1.6 \times 10^{-17}$ J, which is generally multiple orders of magnitude larger than kT (4×10^{-21} J at 293 K). Thus the solid particles, once attached to the interface, can be thought of as irreversibly adsorbed [5]. This is in contrast to surfactants, which adsorb and desorb on a relatively fast timescale.

6.1.2 *Instability Mechanism*

The term "emulsion stability" can be defined as the system's ability to resist changes in its physicochemical properties over time. The emulsions may become unstable due to a variety of mechanisms, such as creaming and sedimentation (gravitational separation), flocculation, coalescence, Ostwald ripening (Fig. 6.2) [15–17]. Gravitational separation refers to the process (creaming/sedimentation) whereby droplets move upward/downwards due to a lower/higher density than the surrounding phase. Flocculation refers to the process where droplets "stick" together to form a large aggregate and each of the initial droplets retains individual integrity. Coalescence refers to the process whereby the droplets merge together to form a single and large droplet. Ostwald ripening is the process whereby larger droplets grow at the expense

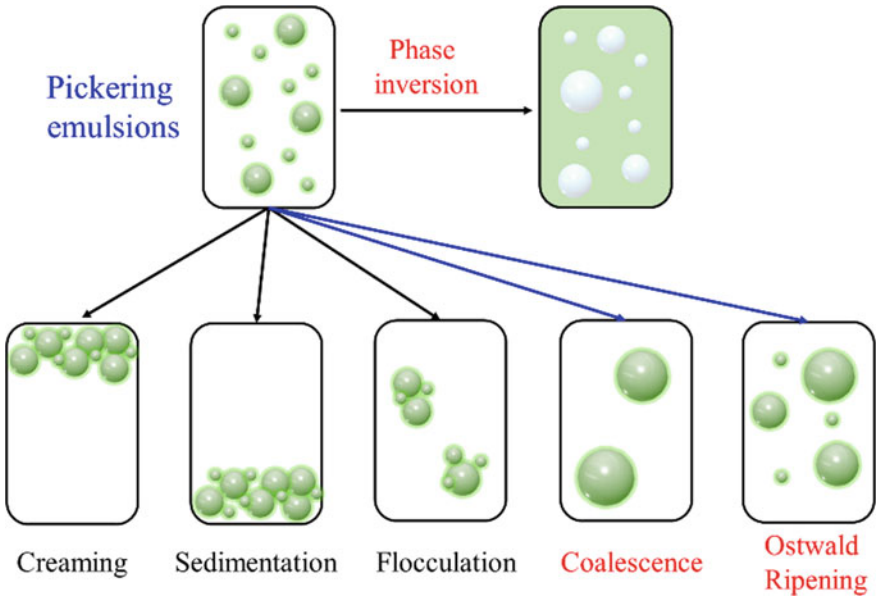

Fig. 6.2 Schematic diagram showing the common instability mechanisms that occur in Pickering emulsions: creaming, sedimentation, flocculation, coalescence, Ostwald ripening and phase inversion

of smaller droplets due to mass transport of dispersed phase material through the continuous phase. It should be noted that various instability mechanisms are often interrelated. For instance, an increase in droplet size due to flocculation, coalescence or Ostwald ripening usually result in an increase in the instability of the droplets to gravitational separation. If droplets come to close contact because of gravitational separation or flocculation they are often more susceptible to coalescence. Therefore, the mechanism responsible for the visible observation of emulsion breakdown may not necessarily be the reason that the emulsion became unstable. The rapid creaming behavior of the droplets, which occurs in an emulsion, may result from droplet aggregation. In this situation, it is typically more efficient to take measures to prevent the aggregation behavior, rather than the droplet creaming.

6.1.3 Surface Coverage

Surface coverage is an important parameter which reflects the adsorption behavior of nanoparticles at interfaces (taking a rod-like nanoparticle as an example). Coverage can be determined from the amount of stabilizing particles in the emulsion and the dispersed phase effectively trapped within the droplets. Usually, the nanoparticle contents in the continuous phase should be determined. The surface coverage C can then be given by the ratio of the theoretical maximum area covered by the particles S_p and the total surface area of the dispersed droplets S_d:

$$\mathrm{C} = \frac{S_p}{S_d} \tag{6.3}$$

where

$$S_p = N_p Ll = \frac{m_p}{h\rho_p} \tag{6.4}$$

And

$$S_d = 4\pi R^2 \frac{3V_{dis}}{4\pi R^3} = \frac{3V_{dis}}{R} \tag{6.5}$$

where N_p is the number of nanoparticles, L, l and h are the length, width and thickness of rod-like nanoparticles respectively, m_p is the mass of the nanoparticles, ρ_p is the density of the nanoparticles, R is the average drop radius, and V_{dis} is the volume of the dispersed phase. From the aforementioned equations, the total surface coverage can be shown to be

$$\mathrm{C} = \frac{m_p D}{6h\rho V_{dis}} \tag{6.6}$$

where D is the average radius of the dispersed droplets.

6.2 Emulsions Stabilized by Pristine Nanopolysaccharides

Unmodified or pristine nanocellulose, including cellulose nanocrystals (CNCs) and cellulose nanofibrils (CNFs), are one type of nanopolysaccharides that have been intensively investigated for stabilizing the emulsions. Numerous review articles related to this topic have been published [8, 45–47]. The stability of nanocellulose-stabilized emulsions originates from the amphiphilic character of nanocellulose, which has been demonstrated by molecular organization at crystalline surfaces. Kalashnikova et al. prepared CNCs through HCl-acid hydrolysis of BC and it was found that the nanoparticles can stabilize monodispersed oil (hexadecane) droplets of approximately 4 μm in water phase against coalescence for 4 months (Fig. 6.3a, b) [18]. Raw material (nata de coco) was chosen as they contain a high concentration of cellulose. The authors reported that by increasing the nanoparticle concentrations, an increase in surface coverage can be attained. The partitioning of nanoparticles at the oil-water interface and irreversible adsorption can significantly enhance the stability of oil droplets. In order to further understanding of the stabilization mechanism,

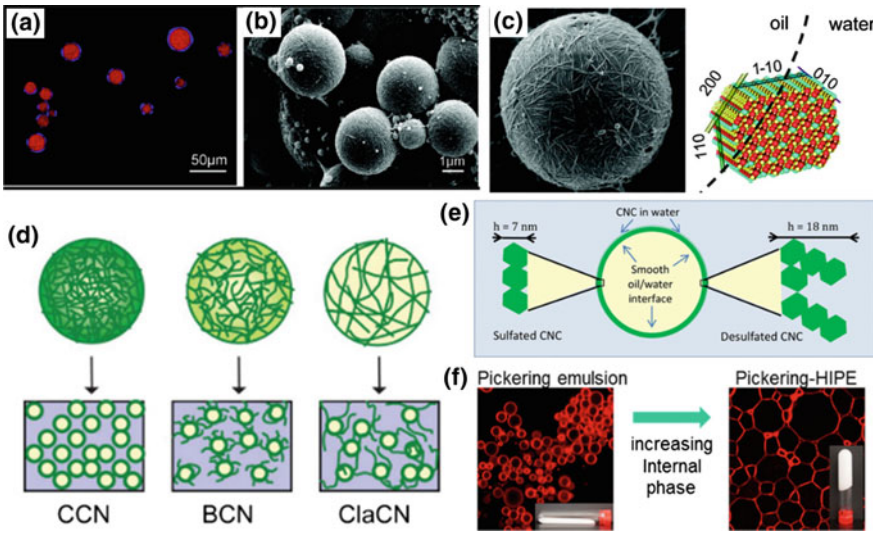

Fig. 6.3 **a** Confocal laser scanning micrograph of oil droplets stabilized by CNCs; **b**, **c** scanning electron micrographs (SEM) of styrene particles obtained from polymerization of Pickering emulsions stabilized by BCN (Reproduced from [18, 19]); **d** schematic representation of emulsions stabilized by CNCs with different aspect ratios (Reproduced from [20]); **e** schematic representation illustrating the packing behavior of pristine and desulfated CNC the oil-water interface (Reproduced from [21]); **f** confocal laser scanning micrograph of HIPE stabilized by CNCs (Reproduced from [22])

Kalashnikova et al. released another work and suggested that cellulose nanocrystals with a charge density greater than 0.03 e/nm^2 could not efficiently stabilize oil droplets [19]. The results showed that regardless of crystallinity of the cellulose nanomaterials, the electrostatic interactions between the nanoparticles at the oil-water interface was the critical factor governing the interface properties, as neutral CNCs extracted by HCl hydrolysis performed better than sulfated CNCs. It is postulated that the (2 0 0) crystalline plane of the nanoparticles directly interacts with the oil-water interface, which might account for the emulsion stabilization (Fig. 6.3c). They also demonstrated that the elongated shape or aspect ratio of cellulose nanocrystals has a direct impact on interfacial coverage, where a lower aspect ratio lead to a denser packing of nanoparticles at the interface (Fig. 6.3d) [20]. The packing behavior of CNCs (195 nm in length, 23 nm in width and 6 nm in thickness) with various surface charges at oil-water interface was also investigated by Capron and coworkers with the help of small angle neutron scattering (SANS) [21]. They reported that the average thickness of the layer around the oil droplets was 18 and 7 nm for uncharged and charged CNCs, respectively (Fig. 6.3e). This result lends credence to the conclusions drawn from the previous studies. Other systems, such as oil-in-water high internal phase emulsions (HIPE) [22] as well as water-in-water emulsions [27], have also reported to be produced by applying cellulose nanocrystals. The HIPE system can only be produced via a two-step method consisting of the formation of the primary Pickering emulsion and a subsequent swelling (Fig. 6.3f). CNFs have a higher axial ratio and flexibility, resulting from their lower degree of crystallinity than cellulose nanocrystals, which promotes entanglement and leads to gelation at low concentrations. As the chemical structure of CNFs resembles that of CNCs, one could expect CNFs to also possess the ability to stabilize emulsion droplets. Liu and coworkers found that flexible CNFs could curve towards the dodecane phase and results in O/W emulsions with droplet diameters ranging from 12 to 40 μm. [35] Increasing the concentration of nanoparticles will lead to higher probability of intermolecular "physical" cross-linking and consequently higher surface coverage. This is also evidenced by rheological studies, which showed a stabilizing network formed by cellulose nanofibrils [48]. However, the characteristics of the emulsions may vary in response to surface chemistries. Capron et al. showed that nanosized (sub-micro) droplets can be achieved with TEMPO oxidized CNF using HP-homogenizer, but this was not demonstrated for the less fibrillated pristine CNF.

For pristine CNF, the fibers formed a heterogeneous and scattered layer and the large droplets (in micro size) were lightly covered and interconnected by the agglomerated networks (Fig. 6.4a) [49]. Bai et al. described other interesting emulsion systems based on cellulose nanocrystals and cellulose nanofibrils [43]. CNF were used to induce the depletion stabilization of o/w emulsions stabilized by CNC. The stabilization was concentration-dependent and the creamed or flocculated emulsions became stable when the CNF concentration was increased up to 0.3 wt%. This can be ascribed to the increased propensity for entanglement of the cellulosic fibrils at high concentration, thereby forming dense networks in the aqueous phase. This work has demonstrates the potential of using biopolymers in all-natural Pickering colloidal dispersions.

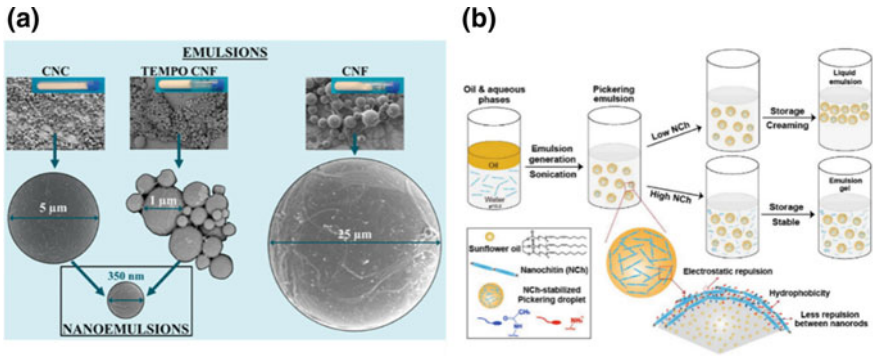

Fig. 6.4 **a** SEM images of droplets issued from emulsions stabilized by CNC, TEMPO-CNF and CNF (Reproduced from [49]); **b** schematic illustration of Pickering emulsion formation via nanochitin adsorption at sunflower oil-water interface (Reproduced from [44])

Pristine nanochitin and nanostarch has received less investigation than nanocellulose, although the mechanisms are quite similar to those applied for nanocellulose. Most of the reported systems have been summarized in Table 6.1. Biliaderis et al. have prepared chitin nanocrystals via acid hydrolysis of crude chitin from crab shells [38]. The obtained chitin nanocrystals were proven to be effective stabilizers for stabilizing corn oil droplets over a period of one month. By increasing the concentration of chitin nanocrystals, a gel-like structure formed and further improved the stability by immobilizing the oil droplets within the network structures. Bras et al. have comprehensively investigated the capabilities and differences between chitin nanocrystals and chitin nanofibers for stabilizing the Pickering emulsions [30]. Both of the nanomaterials were isolated and purified from the same source of chitin. Results demonstrated that the chitin nanofibrils exhibited better oil-in-water stabilization performance than chitin nanocrystals at the same concentrations, which may be attributed to the higher viscosity of the chitin nanofibrils suspensions. Bai and Rojas have reported an interesting sunflower oil-water system stabilized by short and long chitin nanoparticles [44]. They found out that the nanoparticles could effectively reduce the interfacial tension and stabilized the oil droplet by forming networks. Bearing surface hydrophobic *N*-acetyl groups and improved wetting properties, nanochitin proved to be a super-stabilizer at concentrations as low as 0.001 wt% in aqueous phase, demonstrating their ability to replace surfactants at ultra-low concentrations (Fig. 6.4b).

6.3 Emulsions Stabilized by Modified Nanopolysaccharides

Aside from their abundant and biocompatible properties, another advantage of using polysaccharide nanoparticles is that they can be readily modified. Diversified modification strategies, including non-covalent bonding and covalent bonding, have been

Table 6.1 Summary of Pickering emulsions stabilized by pristine polysaccharide nanoparticles

Materials	Oil phase	Emulsion type	Research highlights	Reference
CNCs	Hexadecane	O/W	Noteworthy early work investigating influencing factors	[18]
CNCs	Hexadecane	O/W	Mechanisms regarding to amphiphilic properties	[19]
CNCs with different aspect ratio	Hexadecane	O/W	Packing behavior with different aspect ratio	[20]
CNCs, desulfated CNCs	Hexadecane	O/W	Structural description of packing at the interface	[21]
CNCs	Hexadecane	O/W	High internal phase Pickering emulsion (HIPE)	[22]
CNCs, desulfated CNCs	Dodecane	O/W	Fundamental study towards adsorption	[23]
CNCs with different crystalline allomorph	Hexadecane	O/W	Influence of crystalline allomorph	[24]
CNCs	Corn oil	O/W	Effect of counter ions on stabilization	[25]
CNCs from acid and enzyme hydrolysis	Hexadecane	O/W	Fundamental study	[26]
CNCs	Dextran/PEO	W/W	Stabilizing low interfacial tension system	[27]
CNCs, adding salt	Dextran/PEO	W/W	Impact of ionic strength, Emulsion gels	[28]
CNCs extracted from sisal fiber	Different organic solvents	O/W	Fundamental study	[29]
CNCs or CNFs	Sunflower oil	O/W	Comparing the differences in toxicity and emulsion stabilization	[30]
CNCs from asparagus	Palm oil	O/W	Fundamental study	[31]

(continued)

Table 6.1 (continued)

Materials	Oil phase	Emulsion type	Research highlights	Reference
CNFs from banana peels	Sunflower oil	O/W	Impact of high-energy emulsification	[32]
CNFs from plant cells	Soybean oil	O/W	Stabilization and microstructure	[33]
CNFs	Almond oil	O/W	Origin and sources for producing	[34]
CNFs	Dodecane	O/W	Emulsification and Packing behavior	[35]
ChNCs from prawn shell	Corn oil	O/W	Origin and sources for producing	[36]
ChNCs	Styrene	O/W	High internal phase Pickering emulsion (HIPE)	[37]
ChNCs	Corn oil	O/W	Fundamental study towards adsorption	[38]
Starch-based Nanoparticles	n-Hexane	O/W	Fundamental study towards adsorption	[39]
SNCs	Soy oil	O/W	High internal phase Pickering emulsion (HIPE)	[40]
Starch nanoparticle	Soybean oil	O/W	Stabilized by starch nanoparticles: Influence of starch variety and particle size	[41]
Milled starch nanoparticle	Soybean oil	O/W	Influence of amylose/amylopectin ratios	[42]
CNCs and CNFs	Sunflower oil	O/W	Superstable emulsion at low concentration region	[43]
ChNCs and ChNFs	Sunflower oil	O/W	Depletion force induced stabilization	[44]

incorporated to tailor their properties to improve emulsion stability (Table 6.2). The term non-covalent bonds may refer to physical interactions such as van der Waals force, hydrogen bonding, electrostatic interaction and etc., whereas covalent bonding may vary and could be achieved through the installation of functional groups or surface active polymers.

In non-covalent bonding systems, various surface active components were utilized including cationic surfactants didecyldimethyl ammonium bromide (DMAB) [50], cetyltrimethylammonium bromide (CTAB) [50], hydrophobic quaternary ammonium salts [51], food grade food-grade cationic surfactant, ethyl lauroyl arginate (ELA) [53], cellulose derivatives (methyl cellulose, MC or hydroxyethyl cellulose, HEC) [54], protein molecules [55] and etc. Cranston and coworkers have introduced two types of cationic charged surfactants, DMAB and CTAB, on the surface of negatively charged CNC to tailor the hydrophobicity of the nanoparticles (Fig. 6.5a) [50]. The emulsion stabilizing capability of the modified nanoparticles was investigated. A double transitional phase inversion (from O/W to W/O and then back to O/W) for emulsions stabilized by CNCs with increasing amounts of DMAB (a more hydrophobic molecule) was observed. Similarly, Capron et al. have also reported a simple route to fabricate hydrophobic nanoparticles. This was achieved through adsorbing hydrophobic quaternary ammonium salts onto TEMPO-oxidized CNCs, which were capable of stabilizing inverse water-in-oil emulsions [51]. In addition, Cranston and coworkers have studied the effects of both water-soluble polymers (hydroxyethyl cellulose or methyl cellulose) and surfactants on the properties of Pickering emulsions stabilized by cellulose nanocrystals (Fig. 6.5b) [54]. The polymer coated CNC nanoparticles produced emulsions with smaller droplet sizes, and the emulsions could resist coalescence when subjected to multiple cycles of heating and cooling. Tang and coworkers have incorporated protein molecules (bovine serum albumin, BSA) onto the surface of CNCs via electrostatic interactions at pH 3 [55]. They claimed that very stable, gel-like HIPEs can be obtained with the emulsifying agent of 0.5% (w/v) CNCs covered with 0.01%-0.1% (w/v) BSA (Fig. 6.5c). This work has expanded the database of surface active components that can be readily used to manipulate the surface properties of cellulose nanocrystals in stabilizing emulsions for food and pharmaceutical applications. Rojas and his coworkers have reported a high-internal phase oil-in-water Pickering emulsion system based on CNCs and a food-grade cationic surfactant, ELA [53]. They found that CNCs played a critical role in achieving a synergistic effect and that the stabilization mechanism is highly related to the type of ELA structure adsorbed (in form of surfactants or admicelles), the presence of free ELA molecules, and the hydrophobic nature of the oil (Fig. 6.5d). Cellulose nanofibrils with higher aspect ratio and higher fraction of amorphous regions, exhibit substantially different behavior than cellulose nanocrystals in complex systems. Rojas and coworkers have investigated the impact of incorporating CNF into surfactant (sodium dodecyl sulfate, SDS)-based emulsions [57]. They found out that irregular droplets and “bi-continuous” morphologies were observed at medium and high salinity for systems including high CNF and SDS concentrations. Water-in-oil emulsions were only possible at high salinity and SDS concentrations

Table 6.2 Summary on Pickering emulsions stabilized by modified polysaccharide nanoparticles

Materials	Oil phase	Emulsion type	Research highlights	Reference
Cellulose nanocrystals and surfactant (CTAB, DMAB)	Dodecane	O/W, W/O	Fundamental study towards adsorption	[50]
Cellulose nanocrystals, small molecules adsorption	Hexadecane	O/W, W/O	Fundamental study towards adsorption	[51]
Hydrophobic modified CNC	Hexadecane	O/W	Fundamental study towards adsorption	[52]
Cellulose nanocrystal, food-grade cationic surfactant	Sunflower oils and Dodecane	O/W	Fundamental study towards adsorption	[53]
CNC, methyl cellulose or HEC	Dodecane	O/W	Fundamental study towards adsorption	[54]
Protein/BSA covered CNC	Soy oil	O/W	High internal phase Pickering emulsion (HIPE)	[55]
CNC, non-ionic surfactant (PG1.5SFR0.05), gum arabic	Rice bran oil	O/W	Fundamental study towards adsorption	[56]
CNF, ionic surfactant	Toluene	O/W, W/O, bi-continuous phase	Fundamental study towards adsorption	[57]
CNF, Triton X-100	Soybean oil	W/O, W/O/W	Fundamental study towards adsorption	[58]
Alkyl intercalated CNCs	Soybean oil	O/W	Fundamental study towards adsorption	[59]
Hydrophobic modified CNC and hydrophobic modified CNF	Hexadecane	W/O, O/W/O	Fundamental study towards adsorption	[60]
Acetylated cellulose nanofibril	Soybean oil	O/W	Fundamental study towards adsorption	[61]
CNCs, octenyl succinic anhydride	Soy oil	O/W	Surface modification to make HIPE	[62]

(continued)

Table 6.2 (continued)

Materials	Oil phase	Emulsion type	Research highlights	Reference
CNC, polystyrene	Toluene, Hexadecane	O/W	Enhanced stabilization by modification	[63]
Hydrophobic modified CNF	Toluene	W/O	Fundamental study towards adsorption	[64]
Ammonium persulfate treated corncob cellulose	d-Limonene	O/W	Fundamental study towards adsorption	[65]
Carboxylated CNC	Triglyceride oil	O/W	Effect of pH	[66]
TEMPO oxidized bacterial cellulose	Liquid paraffin	O/W	Investigating the rheological properties	[67]
TEMPO oxidized bacterial cellulose	Liquid paraffin	O/W	Fundamental study towards adsorption	[68]
CNC, CNF, TEMPO-CNF	Hexadecane	O/W	Fundamental study towards adsorption	[49]
CNC, CNF, TEMPO-CNF	Dodecane	O/W	Fundamental study towards adsorption	[69]
TEMPO oxidized chitin nanocrystal	Paraffin	O/W	pH-responsive emulsion	[70]
Modified maize starch-based nanoparticles	Triacylglycerol	O/W	Octenylsuccinylation treated soluble starch nanoparticle	[71]
Hydrophobic modified starch	Soybean oil	O/W	NaCl and sucrose concentrations had no obvious effect on the cream volumes	[72]
Acetylated starch phthalic ester	Glyceryl trioctanoate	O/W	Fundamental study towards adsorption	[73]
CNC, PNIPAM	Heptane	O/W	Thermal responsive emulsion	[74]
CNC, PDMAEMA	Hexane, Toluene	O/W	pH-responsive Pickering emulsion	[75]
CNC-POEGMA-PMAA	Heptane	O/W	Oil harvesting	[76]

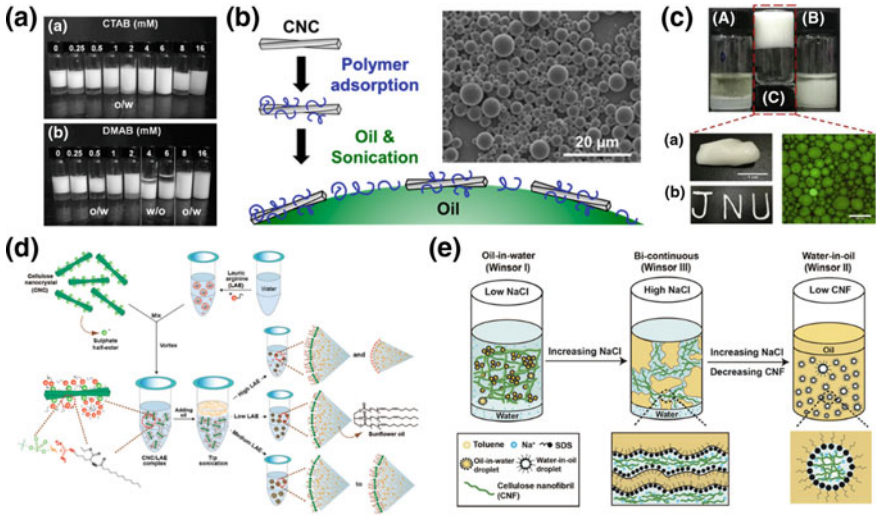

Fig. 6.5 **a** Water-dodecane emulsions stabilized by 0.25 wt% CNCs and surfactant (CTAB; DMAB) with concentrations from 0 to 16 mM (Reproduced from [50]); **b** schematic illustration of Pickering emulsion stabilized by CNC and adsorbed water-soluble polymers (Reproduced from [54]); **c** synergistic emulsifying action of BSA and CNCs and visual appearance of HIPE stabilized by them (Reproduced from [55]); **d** schematic illustration of the formulation, preparation, and oil droplet stabilization via electrostatic interactions involving CNC and ELA (Reproduced from [53]); **e** schematic illustration explaining the phase transition behavior of emulsions prepared with SDS in the presence of CNF and at increased salinity (Reproduced from [57])

in the presence of small amounts of CNF (Fig. 6.5e). All above suggested that CNF may possess interfacial activity that depends on the processing conditions.

The modified materials obtained by covalent bonds are typically more stable and the chemical structures of the nanoparticles are generally easier to understand. Extensive studies were carried out through hydrophobic modification by introducing long alkyl chains or benzylic containing molecules onto polysaccharide nanoparticles. They were commonly achieved by modifying the surfaces along the lengthwise direction with the help of abundant hydroxyl groups. Capron et al. have performed chemical modifications with lauroyl chloride (C12) on both CNCs and CNFs [60]. The resulting nanoparticles were more hydrophobic and capable of stabilizing water in hexadecane emulsions. Additionally, the authors also demonstrated that o/w/o double emulsions can be stabilized by the combination of C12-modified and pristine nanocellulose. Tang and coworkers have modified the CNC surface with octenyl succinic anhydride, which remarkably increased the surface hydrophobicity [62]. Consequently, an improved emulsification performance in o/w emulsions was obtained. The modifications can also facilitate the preparation of Pickering high-internal-phase-emulsions (HIPEs) (Fig. 6.6a). Aside from surface modifications, anisotropic modification can also be performed. This is achieved by taking advantage of decorated aldehyde groups at the end, allowing for the selective modification of the reducing

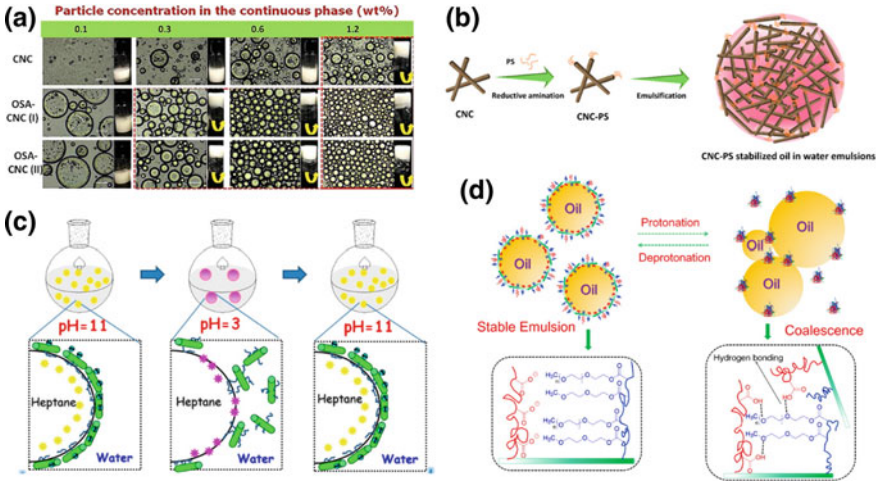

Fig. 6.6 **a** Optical micrographs and visual images of Pickering HIPEs stabilized by unmodified and OSA-modified CNCs (Reproduced from [62]); **b** schematic illustration of enhanced stabilization of the emulsion by end modified CNCs (Reproduced from [63]); **c** responsive behavior of emulsions stabilized by PDMAEMA-g-CNCs (0.5 wt%) with adjusting the pH values of the aqueous phase (Reproduced from [75]); **d** schematic illustrating the pH-responsive behavior of Pickering emulsions stabilized by CNCs-POEGMA-PMAA (Reproduced from [76])

ends of CNCs. Tang et al. have performed end-group modification by introducing hydrophobic polystyrene chains and the modified nanoparticles are more effective in emulsifying toluene and hexadecane than pristine CNC (Fig. 6.6b) [63]. However, due to the low aldehyde content present, only a small drop in surface tension was observed for modified nanoparticle. Similar or relevant hydrophobic modification have also applied to other nanopolysaccharides such as cellulose nanofibrils, starch nanoparticles and nanocrystals, which have been summarized in Table 6.2.

Another covalent modification would be to render the surface with specific functional groups. Specific functional groups were important parameters in determining the interfacial packing properties of nanoparticles. TEMPO or ammonium persulfate oxidation have been adopted to introduce carboxylate groups on polysaccharide nanoparticles. Zhong et al. found that TEMPO-oxidized bacterial cellulose (BC) was more effective than pristine BC in stabilizing the oil-water interface, which was attributed to the much smaller size [68]. They also reported that the dosage and degree of oxidation had significant influence on the stability and particle size distribution of emulsion samples. Capron and coworkers have compared the properties of emulsion droplets stabilized by CNCs, CNF and TEMPO-CNF [49]. Stable oil-in-water nanoemulsions with droplet sizes of 100–600 nm can be produced for CNCs and TEMPO-CNF, while micro- emulsions with average diameter of 5 μm were obtained for CNF.

Besides the incorporation of small molecules or specific functional groups, surface active or functional polymer chains are another type of entities that have been integrated onto the surface of polysaccharide nanoparticles via grafting from or grafting to methods. By applying simple grafting from methods, Tang et al. have performed interesting work on stimuli-responsive polymers modified cellulose nanocrystals [75]. With the installation of a weak polyelectrolyte poly[2-(dimethylamino) ethyl methacrylate] (PDMAEMA) on CNCs, the stability of emulsion droplets was further promoted and the controllable emulsification and demulsification process can be manipulated through changing the environment conditions such as pH and temperature (Fig. 6.6c). This can be explained by the chain conformation change of PDMAEMA in response to environment triggers. Further attempts of grafting binary brush (poly(oligoethylene glycol) methacrylate, POEGMA and poly(methacrylic acid), PMAA) onto the surface of CNC result in double (pH and thermo) responsive nanoparticles [76]. By virtue of the surface-active properties of polymer chains, the modified CNCs diffused to the oil-water interface and enhanced stabilization of the oil droplets was obtained at high pH. However, coalescence of the emulsion droplets was observed due to the detachment of nanoparticles from the interface at pH lower than 2, as strong hydrogen bonding between POEGMA and PMAA chains lead to aggregations of the nanoparticles (Fig. 6.6d). In another work, Rojas and coworkers also observed that the emulsions stabilized by poly(NIPAM)-g-CNCs break after heating at a temperature above the LCST of poly(NIPAM) [74]. This is yet another example of the responsiveness of the Pickering emulsions resulting from the properties of grafted polymers (Table 6.3).

6.4 Applications Based on Emulsions Stabilized by Nanopolysaccharides

6.4.1 Polymerizations

Adding nanoparticles to influence the emulsion polymerization process to prepare hybrid colloids is a concept that dates back to decades ago. Attention to this research topic has waned over the past 50 years, but recent revolutions in nanotechnology has revitalized the interest in polymerization with Pickering emulsifiers. However, an in-depth understanding of the mechanism and how it differs from the traditional emulsion polymerizations still requires attention. It is important to stress that Pickering emulsion polymerization is not the polymerization of emulsion droplets stabilized by solid particles. Thus, in this section, polymerizations occurring in the Pickering emulsions systems will be discussed, rather than Pickering emulsion polymerizations. Readers who are interested in concrete definitions and in-depth overviews of Pickering emulsion polymerization techniques are encouraged to refer to reviews written by Dr. Stefan Bon [89].

Table 6.3 Summary on emulsion polymerizations

Materials	Oil phase	Emulsion type	Applications	Reference
CNC	MMA, BA	O/W	Cationic initiator to ensure the adsorption of the negatively charged CNCs onto latex particle surface	[77]
CNC	MMA, BMA…	O/W	Emulsion polymerization, monomer on latex sizes	[78]
CNC	MMA	O/W	RAFT polymerization, emulsion polymerization	[79]
CNF	MMA	O/W	Emulsion polymerization	[80]
CNC, methyl cellulose	MMA	O/W	Emulsion polymerization	[81]
CNC modified with isobutyrate bromide moieties	n-BA	O/W, W/O	AGET-ATRP Polymerization of Pickering emulsions	[82]
CNC end modified with 18-Carbon Alkyl Chains	Styrene	O/W	Emulsion polymerization	[83]
Hydrophobic modified CNCs	Styrene	O/W	Emulsion polymerization, influence of HLB and aspect ratio of the nanoparticles	[84]
Hydrophobic modified SNPs	Ethyl acetate	W/O	Inverse emulsion polymerization of NIPAM	[85]
Acetylated cellulose nanocrystals	Styrene	O/W	Emulsions polymerization: impact of the polymerization initiator, impact of the ionic strength and mechanisms leading to the formation of the nanolatexes	[86]
Hydrophobic modified chitin nanofibers	Styrene	W/O	Composite and hollow particles from polymerization	[87]
PDMEMA-b-PGMA-b-PHFBA, CNC	MMA, BA	O/W	Soap free emulsion polymerization	[88]

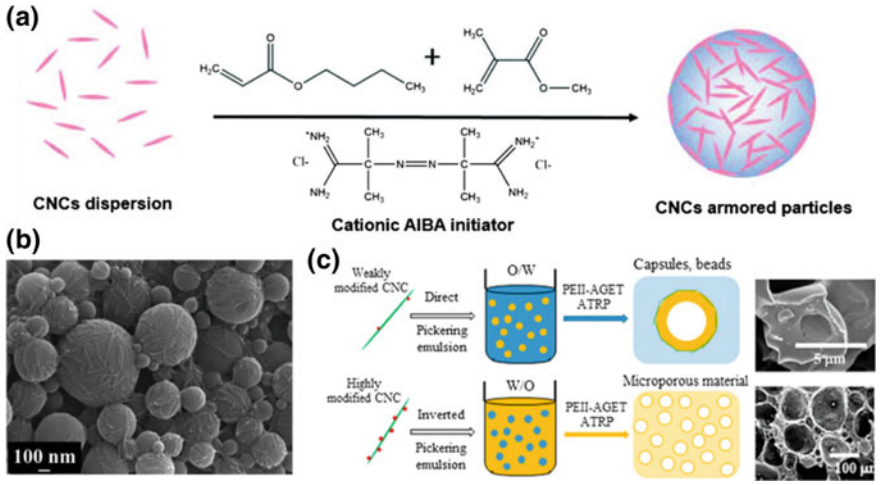

Fig. 6.7 **a** Schematic representation of the formation of CNCs armored poly(methyl methacrylate-co-butyl acrylate) particles with AIBA as initiator (Reproduced from [77]); **b** SEM images of polystyrene nanoparticles stabilized by CNCs (Reproduced from [78]); **c** Schematic illustration of various kinds of products obtained from Pickering emulsions stabilized by modified CNCs (Reproduced from [82])

Pristine nanopolysaccharides are intensively utilized as they are green, biodegradable and natural abundant. Also, through modification, enhanced stabilization may be obtained, which could cause the polymerization process to yield latex particles with different sizes and stability. Ballard et al. have reported a method to synthesize CNC-armored latex particles via emulsion polymerization process [77]. A cationic initiator (2,2′-azobis(2-methyl-propionamidine) dihydrochloride, AIBA) was added into the system, ensuring that the negatively charged particles were adsorbed on to the latex particle surface (Fig. 6.7a). Stable latexes with high conversion and low particle size ranged from 100 to 300 nm were obtained. They also found out that the relative amount of CNC to the cationic initiator was critical in the formation of stable latexes. Capron et al. have carried out work investigating the polymerization details in systems of unmodified CNC stabilized monomer (styrene, lauryl methacrylate, butyl methacrylate and etc.) droplets (Fig. 6.7b) [78]. The polymerizations produced latex particles with two distinct sizes through two concomitant mechanisms: (1) the microparticles were obtained by the suspension polymerization mechanism and (2) the nanoparticles were generated by the emulsion polymerization mechanism. They also pointed out that the solubility of the monomer in the continuous phases is the key parameter to tune the size distribution of latex particles. Bai and coworkers have reported a reversible addition-fragmentation chain transfer (RAFT) mediated emulsion polymerization using renewable CNCs as a sole stabilizer and methyl methacrylate as monomer [79]. Cellulose nanocrystals adsorbed at the oil-water interface to form stable emulsions. The RAFT polymerizations gave PMMA latex particles with well-controlled molecular weight and narrow molecular weight distributions. It is

interesting to note that the nanoparticles can be recycled and reused 5 times. Tingaut and coworkers have prepared nanoscale poly(methyl methacrylate) (PMMA) spheres by emulsion polymerization solely stabilized by cellulose nanofibrils network [80]. The obtained PMMA spheres were homogeneously distributed within the CNF network and the products were strongly influenced by several polymerization conditions, such as initiator, monomer to stabilizer ratios.

Similarly, polymerizations of emulsion systems stabilized by surface modified nanopolysaccharide have been reported. The impact of some critical synthetic conditions such as polymerization initiator, ionic strength and stabilizer concentrations on the properties of latex particles were discussed. It is interesting to note that the emulsion type is highly related to the degree of hydrophobic substitution. Héroguez et al. reported that Pickering emulsions of monomers stabilized by cellulose nanocrystals (CNCs) grafted with reactive isobutyrate bromide moieties (CNC-Br) could vary depending on different hydrophilic/hydrophobic balance [82]. Direct (o/w), inverted (w/o), or double emulsions of styrene orn-butyl acrylate were prepared by changing the formulation of the stabilizers. Interface-initiated Atom Transfer Radical Polymerization (PEII-AGET-ATRP) of different type of emulsions allowed producing various kinds of products, such as capsules, beads and open-cell solids (Fig. 6.7c). Gao et al. have modified the reducing end of cellulose nanocrystal with 18-carbon alkyl chains via Schiff-base reactions [83]. The obtained nanoparticle could be used for stabilizing o/w Pickering emulsions and subsequent polymerization could generate polystyrene microspheres covered with asymmetric modified CNCs. Further acid treatment can afford spheres with amine-rich surfaces, which may have potential industrial applications (Table 6.4).

6.4.2 Facile Route for Fabricating Composites

With features such as high mechanical strength mentioned in Chap. 1, nanopolysaccharides have been extensively studied as potential reinforcement filler for composites. However, incorporation of (mostly hydrophilic) polysaccharide nanoparticles in non-polar polymer matrices is challenging due to the incompatibility between the components, resulting in weak interfacial bonding. Thus, developing high-performance composite becomes a critical issue. In order to achieve homogeneous distribution of nanopolysaccharide in hydrophobic polymer matrix, complicated and time-consuming methods such as solvent exchange processes or modifications are necessary. Polymerizations with Pickering emulsions provide a simple and feasible route to disperse nanoparticles into the polymer matrix. Furthermore, modification of the nanoparticles can bring an enhanced emulsion stabilization effect and lower the interfacial energy by regulating the interactions between the fillers and matrix at the same time. To summarize, for this application, pristine or modified cellulose nanocrystal, cellulose nanofibrils, chitin nanocrystals and starch based particles have all been investigated and documented in literature. The polymer matrixes that are highly researched are poly(lactic acid) (PLA) [95], acrylated epoxy [96], polystyrene

Table 6.4 Summary on fabricating composites via Pickering emulsions route

Materials	Oil phase	Emulsion type	Applications	Reference
Acetylated CNCs	Various monomers	O/W	Polymerization for composite	[90]
Aldehyde functionalized CNCs	BMA	O/W	Polymerization for composite	[91]
Chitin nanocrystal	POFC	O/W	Degradable bioelastomers, composite	[92]
Chitin nanocrystal	Bioelastomer poly(1,8-octanediol-co-Pluronic F127 citrate)	O/W	Pickering emulsification approach for composite	[93]
CNF	Resin	O/W	Pickering emulsification approach for composite	[94]
CNF	CH_2Cl_2 and PLA	O/W	Pickering emulsification approach for composite	[95]
Bacterial cellulose nanofibril	Acrylated epoxidized soybean oil (AESO)	O/W	Pickering emulsification approach for composite	[96]
TEMPO-CNF	Styrene	O/W	Emulsion polymerization, transparent films	[97]
SMA modified cellulose nanofibril	Styrene	W/O/W	Emulsion polymerization, expansion of PS	[98]
CNF, Surfactant	PS in toluene	W/O/W	Compactisizer for composite	[99]
Starch nanocrystal	BMA	O/W	Emulsion polymerization for nanocomposites with improved performance	[100]

[97, 98], n-butyl methacrylate (BMA) [91, 100], methyl methacrylate (MMA) [90] and poly(1,8-octanediol citrate) (POC) [92]. Héroguez et al. reported a facile way to fabricate polymer composites via polymerizations in Pickering emulsions stabilized by acetylated CNCs [90]. They claimed that compared to the unfilled polystyrene sample, the Young's modulus of acetylated CNCs-reinforced composite obtained from Pickering emulsion approach was 50% higher (2.95 GPa). In addition, through incorporating acetylated CNCs, the fracture strength of poly(n-butyl methacrylate) composite was increased by 115%, again confirming the improved mechanical performance brought by this method. Fujisawa and coworkers communicated a facile aqueous polymerization process for nanostructured polystyrene (PS)/CNF composites via the formation of a TEMPO-CNF (1 wt%)-stabilized Pickering emulsion [97]. Transparent PS/CNF composite film was simply formed by melt pressing (Fig. 6.8a). The film showed high optical transparency with a transmittance of 88% at 600 nm, which is comparable to that of pristine CNF. An increase in mechanical strength were

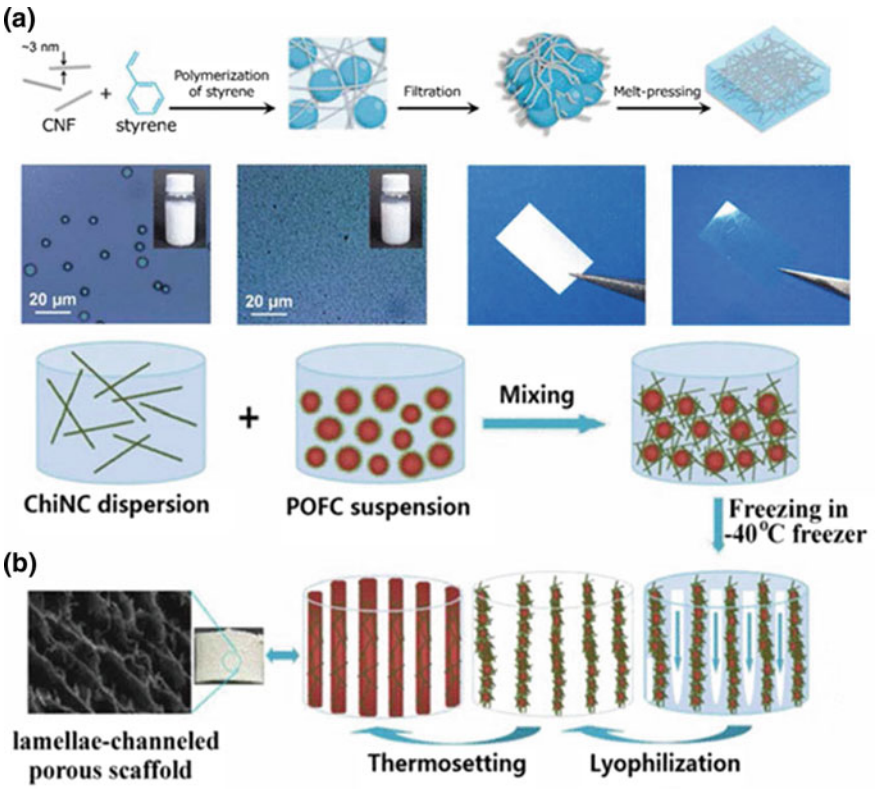

Fig. 6.8 **a** Schematic illustration of fabricating transparent PS/CNF composite films; photographs and optical micrographs of CNF-stabilized emulsion before and after polymerization (Reproduced from [97]); **b** schematic presentation of ChiNC supported emulsion-freeze-casting process to prepare porous scaffold (Reproduced from [92])

gained with a Young's modulus and ultimate strength reached up to 3.4 ± 0.1 GPa and 50.1 ± 2.6 M, respectively for the composite film. An interesting approach where chitin nanocrystal (ChNC) supported emulsion-freeze-casting was utilized to fabricate porous scaffolds of thermoset elastomer by Ji et al. [92]. ChNC can functionalized as a Pickering stabilizer, a supporting agent to prevent ice-templated pores from collapse during curing process, as well as a nanofiller to reinforce porous scaffold (Fig. 6.8b). The nanocomposite elastomer porous scaffold exhibited cyclable compressibility and elastic resilience, which would be beneficial in potential applications in tissue engineering (Table 6.5).

6.4.3 Encapsulation and Controlled Release Applications

Pickering emulsion based delivery systems are available for encapsulation of a wide variety of materials, such as lipids, essential oils, flavor, antimicrobial agents, drug and other substances. The emulsion itself and also the materials built from the platform of emulsions can offer chemical or physical protections and controlled release. For example, a simple emulsion system can be converted into a powdered form by spray drying, which could increase the long-term stability as well as facilitate their transport. Stimuli-responsive carriers can be designed and fabricated via polymerizations and composite formulations. The active components could then be retained within the delivery system until release in response to a specific environmental trigger such as ionic strength, temperature, light or pH values. Potential applications in food, biomedical and cosmetic sectors have been established. It is heavily agreed upon that the Pickering emulsion platform has several advantages for encapsulations: (a) improved physical stability to the surrounding stresses, such as dehydration, freezing, mechanical stirring and etc.; (b) improved chemical stability of encapsulated active components, such as oxidations; (c) general control over the release rate and the ability to change the rate in response to stimuli. Mackie et al. have prepared sunflower oil-in-water emulsions stabilized by cellulose nanocrystals and the emulsions were exposed to stimulated upper gastrointestinal tract digestion [104]. They claimed that the CNCs were entrapped in the intestinal mucus layer and failed to reach the underlying epithelium, which led to the reduced absorption of saturated lipids. They concluded that CNCs represented a safe and effective emulsifier, which could potentially lower plasma cholesterol. Redispersible Pickering emulsion powders have also been demonstrated by Cranston el al. [109] and Yue et al. [101] through the combination of cellulose nanocrystals with methyl cellulose-tannic acid multilayers (Fig. 6.9a) or hydroxypropyl methylcellulose, respectively. The surfactant free characteristics may help these edible emulsions in potential applications spanning food, cosmetic, and pharmaceutics. Pickering emulsions have also been incorporated into different hydrogel matrixes to address issues such as low loading capacity for hydrophobic drugs or compounds. Marquis and coworkers described a two-step approach to encapsulate oil-microdroplets within alginate microgels (Fig. 6.9b) [107]. They demonstrated that the double encapsulation protocol could provide better protection

Table 6.5 Summary on encapsulation and controlled release applications

Materials	Oil phase	Emulsion type	Application	Reference
CNC, NaCMC	Camellia oil	O/W	Redispersible Pickering emulsion powder, encapsulation	[101]
CNC, CNC	Chloroform	O/W	Pickering-emulsion solvent evaporation, drug delivery	[102]
CNC	CH_2Cl_2	O/W	Entrapment of Pickering emulsions in alginate beads, drug delivery	[103]
CNC	Sunflower oil	O/W	Gastrointestinal digestion and exposure to intestinal mucosa	[104]
Aminated nanocellulose (ECH and amine)	Natural coconut oil	O/W	Coumarin and curcumin encapsulation	[105]
Cellulose nanofibrils from mangosteen	Soybean oil	O/W	Encapsulation of vitamin D3	[106]
CNC	Hexadecane	O/W	Encapsulation and release control	[107]
Cinnamoyl chloride modified CNCs	Butyl alcohol	O/W	Turpentine encapsulation and release control	[108]
CNC-MC, Tannic acid	Corn oil	O/W	Encapsulation, redispersible powders	[109]
Taro starch nanoparticles-tea polyphenol complex	Medium chain triglyceride	O/W	Polyphenol encapsulation	[110]
Cinnamate modified CNCs	Toluene	W/O	Silica colloidsome, DNA encapsulation	[111]

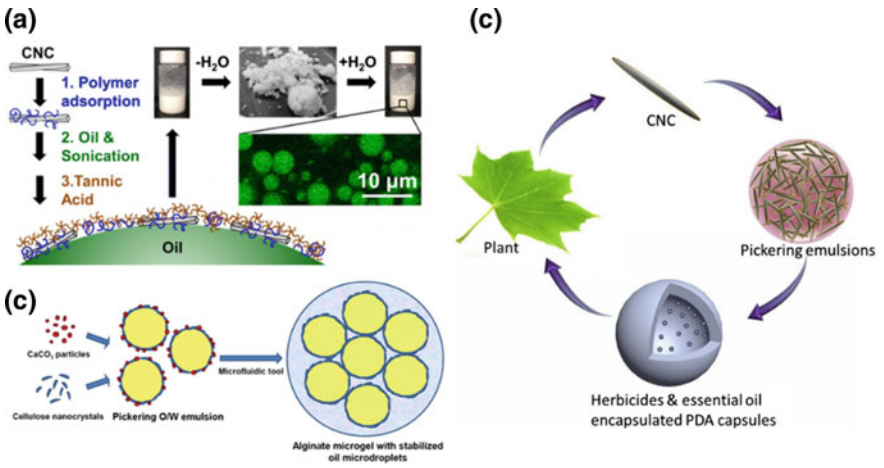

Fig. 6.9 **a** Illustration of a redispersible Pickering emulsion using tannic acid and HEC modified cellulose nanocrystals as stabilizer (Reproduced from [109]); **b** a two-step approach to encapsulate oil microdroplets within alginate microgels for controlled release application (Reproduced from [107]); **c** illustration of polydoapmine microcapsules obtained from Pickering emulsions stabilized by modified CNCs for herbicides and essential oil encapsulation (Reproduced from [108])

and sustained release when compared to conventional encapsulations. Furthermore, Tam et al. have performed dopamine polymerizations based on emulsions stabilized by cinnamoyl chloride modified cellulose nanocrystals to form capsules for essential oil and pesticides encapsulation (Fig. 6.9c) [108]. They found out that the loading and encapsulation efficiency of herbicide could be adjusted by controlling the monomer contents. This system showed a sustained release behavior, which indicates great potential in crop protection. It is anticipated that numerous encapsulating or controlled-release systems can be designed due to uncountable characteristics for the types of the existing materials. By taking advantage of their green and biorenewable nature, nanopolysaccharides will prove their value as a replacement for petroleum-based materials (Table 6.6).

6.4.4 Other Applications

Apart from the above mentioned categories, Pickering emulsions stabilized by nanopolysaccharides and their derived materials have also shown great potential in some emerging advanced applications. By incorporating stimuli-responsive properties, the stability of Pickering emulsion systems can be instantaneously controlled via external triggers, which offers a convenient platform for designing target or specified materials. Tang and coworkers have grafted binary polymer brush (poly(oligoethylene glycol) methacrylate (POEGMA) and poly(methacrylic acid)

Table 6.6 Summary on other applications based on Pickering emulsion systems

Materials	Oil phase	Emulsion type	Application	Reference
CNC-POEGMA-PMAA	Heptane	O/W	Oil harvesting	[76]
Starch based nanoparticle	Ethyl acetate	O/W	pH-responsive emulsion for recycling catalyst	[112]
Bacterial cellulose nanofibril	Dodecane	O/W	Template for organo hydrogel	[113]
CNF, alginate	PLA	O/W	3D-printing of low solids emulsion, composite	[114]
CNF	Acrylated epoxidized soybean oil	O/W	Foams from Pickering medium internal phase emulsions (Pickering-MIPEs)	[115]
TEMPO-CNF	Hexadecane	O/W	Thermo-insulation foam	[116]
CNC, NH_2-PS	Toluene	O/W	Adaptive structured Pickering emulsions and porous materials	[117]
CNF, zein protein		O/W	Aerogel for air filter	[118]
CNF	Acrylic resin	O/W	Nanocomposite-specific application	[119]
CNF	Paraffin wax	O/W	Thermal regulation nanocomposites	[120]
Starch granule modified with OSA	Parraffin and MCT oil	O/W	Barrier properties of heat-treated starch Pickering emulsions	[121]
CNC and chitosan	Oleic acid	O/W	Complex coating improves storability of pears during long-term cold storage	[122]
CNC form APS oxidation	Oregano essential oil	O/W	Antimicrobial application	[123]
Modified starch	Green coffee oil	O/W	Skin photo-protection	[124]

(PMAA)) onto the surface of cellulose nanocrystals [76]. The modified nanoparticles exhibited thermal and pH-responsive properties by inheriting the advantages from the physicochemical properties of the polymers, which in turn can be utilized to control the stability of Pickering emulsions stabilized by them. Successive stabilization-destabilization over 5 cycles was demonstrated by the authors by modulating the pH without any loss in efficiency. The strategy of combining stimuli-responsive properties with nanopolysaccharides provides a simple and effective route for oil harvesting applications. Luo et al. have also reported a pH-responsive Pickering emulsion system stabilized by poly [2-(dimethylamine)ethyl methacrylate] (PDMAEMA) modified starch nanoparticles [70]. Benefitting from the properties of polyelectrolyte, small size gold nanoparticles can be anchored onto the surface of starch nanoparticles. The pH-responsive emulsification/demulsification cycles along with the large interfacial area of the emulsion droplets can prove beneficial to catalytic systems with the oil droplet readily applied as micro-reactors. A high catalytic activity and good recyclability were obtained for the hydrogenation of p-nitroanisole at the oil-water interface, demonstrating their promising potential in green and sustainable chemistry.

Another typical example of materials that could be derived from Pickering emulsions is porous materials. They are important aspects of established research work such as catalysis and separations and in emerging technologies for energy and biomedical applications. Research related to this topic has been devoted into applications such as biomedical devices, thermal-insulating and environmental de-dusting. Bai and Rojas have reported a simple and feasible way to fabricate 3D porous scaffolds containing low-solid contents of cellulose nanofibrils and alginate via direct ink writing [114]. The nonadsorbing CNF in the aqueous phase acts as a costabilizer of emulsified PLA droplets and helps to build a gel-like network at the same time. The shrinkage of the scaffolds was minimized due to the incorporation of CNF, which can support or retain the shape upon processing. The swellable porous objects can be readily used in applications that require biocompatibility, including biomedical devices. Capron and coworkers have utilized strong gel-like TEMPO-CNF stabilized Pickering emulsions as template to form aerogels [116] (Fig. 6.10a). The freeze-dried samples had an extremely lightweight hierarchical architecture and exhibited a thermal conductivity down to 0.018 W/(m K), which was lower than that of stationary air. This work definitely opened a route to design sustainable and biosourced alternatives for super-insulating applications. Pan and coworkers fabricated a hierarchically structured all-biomass air filter based on Pickering emulsions stabilized by zein-protein-coated cellulose nanofibrils [118]. The porous structures were produced through the arrangement of wood pulps as well as the active composites particles from Pickering emulsions, which contribute to the high toxic gas removal efficiency and low air pressure during filtration (Fig. 6.10b). The modified nanoparticles, CNF/zein, not only helped to trap air pollutants including toxic gaseous molecules such as HCHO and CO through specific interactions, but also promoted the capturing capability for small particulate pollutants due to their high surface areas. The work addressesed the cost and production rate issues of electrospinning process used for making porous filtration membranes.

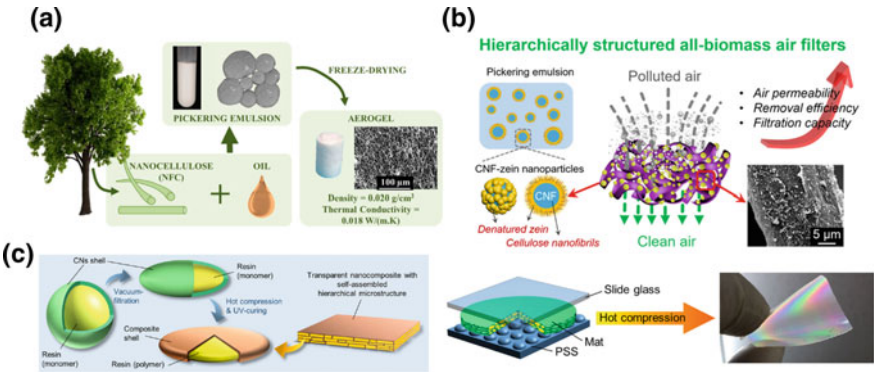

Fig. 6.10 **a** Illustration of thermal super-insulating materials made from nanofibrillated cellulose-stabilized Pickering emulsion (Reproduced from [116]); **b** illustration of the fabricating process for hierarchically structured all-biomass air filters based on Pickering emulsion (Reproduced from [118]); **c** schematic of evolution of the transparency and self-assembled hierarchical microstructure and the fabrication of a μLA on the surface of obtained nanocomposite (Reproduced from [119])

Except for the above mentioned aspects, some emerging applications based on Pickering emulsions stabilized by nanopolysaccharides have also been described in literature, such as thermo-regulating materials [120], composites with enhanced barrier properties [121], improved food storage [122], cosmetic and personal care products [124] and antimicrobial applications [123]. Li and Lars have developed a phase change materials (PCM) composite that may have potential use in energy-efficient smart buildings [120]. The PCM composite was created by encapsulating paraffin into Pickering emulsions stabilized by cellulose nanofibrils and then simultaneously gelled and dried. It is reported that the solid content of paraffin can reach up to 72 wt% and no obvious leakage was observed during heating/cooling cycles. High enthalpy and excellent thermal regulation performance were demonstrated in the form of a model roof under simulated sunlight. Biswas and coworkers have prepared a highly thermally stable transparent nanocomposite material via introduction of a load-bearing hierarchical network of the strong and stable cellulose nanorods as reinforcing agents [119]. By virtue of the Pickering emulsification process, the nanocomposites inherit the self-assembled structural hierarchy from the cellulose nanofibril-encapsulated resin (2,2-Bis[4- (acryloxypolyethoxy)phenyl] propane(ABPE-10) acrylic resin) droplets (Fig. 6.10c). The obtained nanocomposites exhibited good mechanical strength, toughness, and flexibility, providing advantages for fabricating photonic nano- or microstructures in high precision. By directly molding a highly thermally stable microlens array (μLA) on the surface of nanocomposites, the authors demonstrated the enhanced performance of fabricated nanocomposites in photonic and opto-electronic applications.

6.5 Concluding Remarks

Pickering emulsions stabilized by nanopolysaccharides have drawn increased attention recently as they possess numerous advantages over traditional surfactant stabilized emulsions, such as enhanced stability, biocompatibility, and environmental friendliness. The enhanced stability against coalescence mainly results from the dense barrier forming at the interface. This chapter offers an overview of Pickering emulsions stabilized by pristine and modified nanopolysaccharides and their potential applications in biomedical, cosmetic, pharmaceutical, energy-related and environmental sectors.

On the basis of plentiful research literatures regarding Pickering emulsion stabilization, the researchers working in this area should be aware of the physical and chemical properties of their polysaccharide nanomaterials. Careful attentions should be paid to several factors, including particle morphology, flexibility, surface charge and chemistry, purity, crystallinity and toxicity. For further modified materials, consistent, reliable and accurate material characterizations should be conducted to gain a comprehensive understanding regarding the changing of properties, such as morphology, hydrophobicity, surface active properties and etc. With the exponential growth in interest in Pickering emulsions, it is necessary to standardize the measurement protocols with respect to the quantification of emulsion stability. Only in this way can reliable and accurate data be obtained and compared. Additionally, future research should further strengthen the experimental and theoretical studies on stabilizing mechanisms. Comprehensive models and methods for validating the results should be developed. For instance, one should validate whether or not the nanoparticles were indeed adsorbed at the interface to stabilize the emulsions. One should also validate the surface coverage for specific stabilizing materials, and the bridging aspect or correlations between the amphiphilic property and particle wettability. Lastly, the combination of stimuli-responsive properties with emulsions can also be considered as it is particularly advantageous for improving the degree of precision control over a given system.

It is believed that Pickering emulsion systems with polysaccharide nanoparticles as stabilizers are useful in a number of applications. Although many efforts have been devoted to the development of Pickering emulsions, some other facets still need further advancement. For example, materials that can be identified as suitable for practical use in biomedical sectors require strict studies in vivo testing, including performance and toxicity studies. Correlation between physicochemical properties, Pickering emulsion derived materials, and their biological function will instruct the opportunities and limitations offered for each biomedical application. When applying nanoparticles to emulsion polymerizations, the effects of different parameters including the type of initiator, salt concentration and co-stabilizer should be studied in detail. There is also a need for a thorough mechanistic understanding towards the process, and further exploration is required to establish whether or not polymerizations with Pickering emulsions can lead to products in commercial sectors.

Stimuli-responsive Pickering emulsions utilized in controlled release systems or cosmetic and personal care products may increase the stability and shelf life of a given formulation, while permitting the rapid and controlled release of active components when desired in response to external stimuli. Therefore, a proper and wise design may be profitable for their further applications.

Sustainable nanomaterials have offered an attractive opportunity to produce Pickering emulsions using abundant, inert and biocompatible resources. With the help of functions and derived materials from suitable design, they may offer an attractive strategy to replace the products based on petro-chemicals. However, future research should pay more attention to finding better ways to reduce the costs and save energy in the process. Only in that way will sustainable nanomaterials finally find their use in solving the major crises of our time, such as access to food, water and sustainable energy.

Acknowledgements J. Tang wishes to acknowledge the funding from Hunan Provincial Natural Science Foundation of China (2019JJ60073).

References

1. Goodarzi F, Zendehboudi S (2019) A comprehensive review on emulsions and emulsion stability in chemical and energy industries. Can J Chem Eng 97:281–309
2. Kilpatrick PK (2012) Water-in-crude oil emulsion stabilization: review and unanswered questions. Energy Fuels 26:4017–4026
3. Patel AR (2018) Functional and engineered colloids from edible materials for emerging applications in designing the food of the future. Adv Funct Mater 1806809:1–34
4. Pickering SU (1907) CXCVI.—emulsions. J Chem Soc Trans 91:2001–2021
5. Aveyard R, Binks BP, Clint JH (2003) Emulsions stabilised solely by colloidal particles. Adv Colloid Interface Sci 100–102:503–546
6. Binks BP (2002) Particles as surfactants—similarities and differences. Curr Opin Colloid Interface Sci 7:21–41
7. Wu J, Ma GH (2016) Recent studies of Pickering emulsions: particles make the difference. Small 12:4633–4648
8. Salas C, Nypelö T, Rodriguez-Abreu C et al (2014) Nanocellulose properties and applications in colloids and interfaces. Curr Opin Colloid Interface Sci 19:383–396
9. Evans M, Ratcliffe I, Williams PA (2013) Emulsion stabilisation using polysaccharide–protein complexes. Curr Opin Colloid Interface Sci 18:272–282
10. Zhai J, Day L, Aguilar MI, Wooster TJ (2013) Protein folding at emulsion oil/water interfaces. Curr Opin Colloid Interface Sci 18:257–271
11. Zhu F (2019) Starch based Pickering emulsions: fabrication, properties, and applications. Trends Food Sci Technol 85:129–137
12. Yang Y, Fang Z, Chen X et al (2017) An overview of Pickering emulsions: solid-particle materials, classification, morphology, and applications. Front Pharmacol 8:1–20
13. Chevalier Y, Bolzinger MA (2013) Emulsions stabilized with solid nanoparticles: Pickering emulsions. Colloids Surf A Physicochem Eng Asp 439:23–34
14. Kaptay G (2006) On the equation of the maximum capillary pressure induced by solid particles to stabilize emulsions and foams and on the emulsion stability diagrams. Colloids Surf A Physicochem Eng Asp 282–283:387–401

15. Lam S, Velikov KP, Velev OD (2014) Pickering stabilization of foams and emulsions with particles of biological origin. Curr Opin Colloid Interface Sci 19:490–500
16. Calabrese V, Courtenay JC, Edler KJ et al (2018) Pickering emulsions stabilized by naturally derived or biodegradable particles. Curr Opin Green Sustain Chem 12:83–90
17. Lam RSH, Nickerson MT (2013) Food proteins: a review on their emulsifying properties using a structure-function approach. Food Chem 141:975–984
18. Kalashnikova I, Bizot H, Cathala B et al (2011) New Pickering emulsions stabilized by bacterial cellulose nanocrystals. Langmuir 27:7471–7479
19. Kalashnikova I, Bizot H, Cathala B et al (2012) Modulation of cellulose nanocrystals amphiphilic properties to stabilize oil/water interface. Biomacromol 13:267–275
20. Kalashnikova I, Bizot H, Bertoncini P et al (2013) Cellulosic nanorods of various aspect ratios for oil in water Pickering emulsions. Soft Matter 9:952–959
21. Cherhal F, Cousin F, Capron I (2016) Structural description of the interface of Pickering emulsions stabilized by cellulose nanocrystals. Biomacromol 17:496–502
22. Capron I, Cathala B (2013) Surfactant-free high internal phase emulsions stabilized by cellulose nanocrystals. Biomacromol 14:291–296
23. Pandey A, Derakhshandeh M, Kedzior SA et al (2018) Role of interparticle interactions on microstructural and rheological properties of cellulose nanocrystal stabilized emulsions. J Colloid Interface Sci 532:808–818
24. Li X, Li J, Gong J et al (2018) Cellulose nanocrystals (CNCs) with different crystalline allomorph for oil in water Pickering emulsions. Carbohydr Polym 183:303–310
25. Liu L, Hu Z, Sui X et al (2018) Effect of counterion choice on the stability of cellulose nanocrystal Pickering emulsions. Ind Eng Chem Res 57:7169–7180
26. Domingues AA, Pereira FV, Sierakowski MR et al (2016) Interfacial properties of cellulose nanoparticles obtained from acid and enzymatic hydrolysis of cellulose. Cellulose 23:2421–2437
27. Peddireddy KR, Nicolai T, Benyahia L et al (2016) Stabilization of water-in-water emulsions by nanorods. ACS Macro Lett 5:283–286
28. Ben Ayed E, Cochereau R, Dechancé C et al (2018) Water-in-water emulsion gels stabilized by cellulose nanocrystals. Langmuir 34:6887–6893
29. Liu H, Geng S, Hu P et al (2015) Study of Pickering emulsion stabilized by sulfonated cellulose nanowhiskers extracted from sisal fiber. Colloid Polym Sci 293:963–974
30. Larbi F, García A, del Valle LJ et al (2018) Comparison of nanocrystals and nanofibers produced from shrimp shell α-chitin: From energy production to material cytotoxicity and Pickering emulsion properties. Carbohydr Polym 196:385–397
31. Wang W, Du G, Li C et al (2016) Preparation of cellulose nanocrystals from asparagus (*Asparagus officinalis* L.) and their applications to palm oil/water Pickering emulsion. Carbohydr Polym 151:1–8
32. Costa ALR, Gomes A, Tibolla H et al (2018) Cellulose nanofibers from banana peels as a Pickering emulsifier: high-energy emulsification processes. Carbohydr Polym 194:122–131
33. Nomena EM, Remijn C, Rogier F et al (2018) Unravelling the mechanism of stabilization and microstructure of oil-in-water emulsions by native cellulose microfibrils in primary plant cells dispersions. ACS Appl Bio Mater 1:1440–1447
34. Buffiere J, Balogh-Michels Z, Borrega M et al (2017) The chemical-free production of nanocelluloses from microcrystalline cellulose and their use as Pickering emulsion stabilizer. Carbohydr Polym 178:48–56
35. Li Q, Wang Y, Wu Y et al (2019) Flexible cellulose nanofibrils as novel Pickering stabilizers: The emulsifying property and packing behavior. Food Hydrocoll 88:180–189
36. Barkhordari MR, Fathi M (2018) Production and characterization of chitin nanocrystals from prawn shell and their application for stabilization of Pickering emulsions. Food Hydrocoll 82:338–345
37. Perrin E, Bizot H, Cathala B et al (2014) Chitin nanocrystals for Pickering high internal phase emulsions. Biomacromol 15:3766–3771

38. Tzoumaki MV, Moschakis T, Kiosseoglou V et al (2011) Oil-in-water emulsions stabilized by chitin nanocrystal particles. Food Hydrocoll 25:1521–1529
39. Pei X, Zhai K, Liang X et al (2017) Interfacial activity of starch-based nanoparticles at the oil-water interface. Langmuir 33:3787–3793
40. Yang T, Zheng J, Zheng BS et al (2018) High internal phase emulsions stabilized by starch nanocrystals. Food Hydrocoll 82:230–238
41. Ge S, Xiong L, Li M et al (2017) Characterizations of Pickering emulsions stabilized by starch nanoparticles: Influence of starch variety and particle size. Food Chem 234:339–347
42. Lu X, Wang Y, Li Y et al (2018) Assembly of Pickering emulsions using milled starch particles with different amylose/amylopectin ratios. Food Hydrocoll 84:47–57
43. Bai L, Huan S, Xiang W et al (2018) Pickering emulsions by combining cellulose nanofibrils and nanocrystals: Phase behavior and depletion stabilization. Green Chem 20:1571–1582
44. Bai L, Huan S, Xiang W et al (2019) Self-assembled networks of short and long chitin nanoparticles for oil/water interfacial superstabilization. ACS Sustain Chem Eng 7:6497–6511
45. Fujisawa S, Togawa E, Kuroda K (2017) Nanocellulose-stabilized Pickering emulsions and their applications. Sci Technol Adv Mater 18:959–971
46. Bai L, Greca LG, Xiang W et al (2019) Adsorption and assembly of cellulosic and lignin colloids at oil/water interfaces. Langmuir 35:571–588
47. Tang J, Sisler J, Grishkewich N et al (2017) Functionalization of cellulose nanocrystals for advanced applications. J Colloid Interface Sci 494:397–409
48. Paximada P, Tsouko E, Kopsahelis N et al (2016) Bacterial cellulose as stabilizer of o/w emulsions. Food Hydrocoll 53:225–232
49. Jiménez Saelices C, Capron I (2018) Design of Pickering micro- and nanoemulsions based on the structural characteristics of nanocelluloses. Biomacromol 19:460–469
50. Hu Z, Ballinger S, Pelton R et al (2015) Surfactant-enhanced cellulose nanocrystal Pickering emulsions. J Colloid Interface Sci 439:139–148
51. Capron I, Guellec F, Perrin E et al (2016) Some modification of cellulose nanocrystals for functional Pickering emulsions. Philos Trans R Soc A Math Phys Eng Sci 374:20150139
52. Gong X, Wang Y, Chen L (2017) Enhanced emulsifying properties of wood-based cellulose nanocrystals as Pickering emulsion stabilizer. Carbohydr Polym 169:295–303
53. Bai L, Xiang W, Huan S et al (2018) Formulation and stabilization of concentrated edible oil-in-water emulsions based on electrostatic complexes of a food-grade cationic surfactant (ethyl lauroyl arginate) and cellulose nanocrystals. Biomacromol 19:1674–1685
54. Hu Z, Patten T, Pelton R et al (2015) Synergistic stabilization of emulsions and emulsion gels with water-soluble polymers and cellulose nanocrystals. ACS Sustain Chem Eng 3:1023–1031
55. Liu F, Zheng J, Huang CH et al (2018) Pickering high internal phase emulsions stabilized by protein-covered cellulose nanocrystals. Food Hydrocoll 82:96–105
56. Angkuratipakorn T, Sriprai A, Tantrawong S et al (2017) Fabrication and characterization of rice bran oil-in-water Pickering emulsion stabilized by cellulose nanocrystals. Colloids Surf A Physicochem Eng Asp 522:310–319
57. Huan S, Yokota S, Bai L et al (2017) Formulation and composition effects in phase transitions of emulsions costabilized by cellulose nanofibrils and an ionic surfactant. Biomacromol 18:4393–4404
58. Carrillo CA, Nypelö TE, Rojas OJ (2015) Cellulose nanofibrils for one-step stabilization of multiple emulsions (W/O/W) based on soybean oil. J Colloid Interface Sci 445:166–173
59. Guo J, Du W, Gao Y et al (2017) Cellulose nanocrystals as water-in-oil Pickering emulsifiers via intercalative modification. Colloids Surf A Physicochem Eng Asp 529:634–642
60. Cunha AG, Mougel JB, Cathala B et al (2014) Preparation of double Pickering emulsions stabilized by chemically tailored nanocelluloses. Langmuir 30:9327–9335
61. Xu HN, Li YH, Zhang L (2018) Driving forces for accumulation of cellulose nanofibrils at the oil/water interface. Langmuir 34:10757–10763
62. Chen QH, Zheng J, Xu YT et al (2018) Surface modification improves fabrication of Pickering high internal phase emulsions stabilized by cellulose nanocrystals. Food Hydrocoll 75:125–130

63. Tang C, Spinney S, Shi Z et al (2018) Amphiphilic cellulose nanocrystals for enhanced Pickering emulsion stabilization. Langmuir 34:12897–12905
64. Xhanari K, Syverud K, Chinga-Carrasco G et al (2011) Structure of nanofibrillated cellulose layers at the o/w interface. J Colloid Interface Sci 356:58–62
65. Wen C, Yuan Q, Liang H et al (2014) Preparation and stabilization of d-limonene Pickering emulsions by cellulose nanocrystals. Carbohydr Polym 112:695–700
66. Mikulcová V, Bordes R, Minařík A et al (2018) Pickering oil-in-water emulsions stabilized by carboxylated cellulose nanocrystals—effect of the pH. Food Hydrocoll 80:60–67
67. Jia Y, Zheng M, Xu Q et al (2019) Rheological behaviors of Pickering emulsions stabilized by TEMPO-oxidized bacterial cellulose. Carbohydr Polym 215:263–271
68. Jia Y, Zhai X, Fu W et al (2016) Surfactant-free emulsions stabilized by tempo-oxidized bacterial cellulose. Carbohydr Polym 151:907–915
69. Gestranius M, Stenius P, Kontturi E et al (2017) Phase behaviour and droplet size of oil-in-water Pickering emulsions stabilised with plant-derived nanocellulosic materials. Colloids Surf A Physicochem Eng Asp 519:60–70
70. Pang K, Ding B, Liu X et al (2017) High-yield preparation of a zwitterionically charged chitin nanofiber and its application in a doubly pH-responsive Pickering emulsion. Green Chem 19:3665–3670
71. Ye F, Miao M, Jiang B et al (2017) Elucidation of stabilizing oil-in-water Pickering emulsion with different modified maize starch-based nanoparticles. Food Chem 229:152–158
72. Song X, Pei Y, Qiao M et al (2015) Preparation and characterizations of Pickering emulsions stabilized by hydrophobic starch particles. Food Hydrocoll 45:256–263
73. Tan Y, Xu K, Niu C et al (2014) Triglyceride-water emulsions stabilised by starch-based nanoparticles. Food Hydrocoll 36:70–75
74. Zoppe JO, Venditti RA, Rojas OJ (2012) Pickering emulsions stabilized by cellulose nanocrystals grafted with thermo-responsive polymer brushes. J Colloid Interface Sci 369:202–209
75. Tang J, Lee MFX, Zhang W et al (2014) Dual responsive pickering emulsion stabilized by poly[2-(dimethylamino) ethyl methacrylate] grafted cellulose nanocrystals. Biomacromol 15:3052–3060
76. Tang J, Berry RM, Tam KC (2016) Stimuli-responsive cellulose nanocrystals for surfactant-free oil harvesting. Biomacromol 17:1748–1756
77. Limousin E, Ballard N, Asua JM (2019) Synthesis of cellulose nanocrystal armored latex particles for mechanically strong nanocomposite films. Polym Chem 10:1823–1831
78. Jiménez Saelices C, Save M, Capron I (2019) Synthesis of latex stabilized by unmodified cellulose nanocrystals: the effect of monomers on particle size. Polym Chem 10:727–737
79. Liu B, Yang D, Man H et al (2018) A green Pickering emulsion stabilized by cellulose nanocrystals via RAFT polymerization. Cellulose 25:77–85
80. Grüneberger F, Huch A, Geiger T et al (2016) Fibrillated cellulose in heterophase polymerization of nanoscale poly(methyl methacrylate) spheres. Colloid Polym Sci 294:1393–1403
81. Kedzior SA, Dubé MA, Cranston ED (2017) Cellulose nanocrystals and methyl cellulose as costabilizers for nanocomposite latexes with double morphology. ACS Sustain Chem Eng 5:10509–10517
82. Werner A, Schmitt V, Sèbe G et al (2019) Convenient synthesis of hybrid polymer materials by AGET-ATRP polymerization of Pickering emulsions stabilized by cellulose nanocrystals grafted with reactive moieties. Biomacromol 20:490–501
83. Du W, Guo J, Li H, Gao Y (2017) Heterogeneously modified cellulose nanocrystals-stabilized Pickering emulsion: preparation and their template application for the creation of PS microspheres with amino-rich surfaces. ACS Sustain Chem Eng 5:7514–7523
84. Zhang Y, Karimkhani V, Makowski BT et al (2017) Nanoemulsions and nanolatexes stabilized by hydrophobically functionalized cellulose nanocrystals. Macromolecules 50:6032–6042
85. Zhai K, Pei X, Wang C et al (2019) Water-in-oil Pickering emulsion polymerization of N-isopropyl acrylamide using starch-based nanoparticles as emulsifier. Int J Biol Macromol 131:1032–1037

86. Werner A, Schmitt V, Sèbe G et al (2017) Synthesis of surfactant-free micro-and nanolatexes from Pickering emulsions stabilized by acetylated cellulose nanocrystals. Polym Chem 8:6064–6072
87. Noguchi S, Sato K, Yamamoto K et al (2019) Preparation of composite and hollow particles from self-assembled chitin nanofibers by Pickering emulsion polymerization. Int J Biol Macromol 126:187–192
88. Zhou J, Li Y, Li H et al (2019) Cellulose nanocrystals/fluorinated polyacrylate soap-free emulsion prepared via RAFT-assisted Pickering emulsion polymerization. Colloids Surf B Biointerfaces 177:321–328
89. Lotierzo A, Bon SAF (2017) A mechanistic investigation of Pickering emulsion polymerization. Polym Chem 8:5100–5111
90. Werner A, Sèbe G, Héroguez V (2018) A new strategy to elaborate polymer composites: Via Pickering emulsion polymerization of a wide range of monomers. Polym Chem 9:5043–5050
91. Errezma M, Ben Mabrouk A, Magnin A et al (2018) Surfactant-free emulsion Pickering polymerization stabilized by aldehyde-functionalized cellulose nanocrystals. Carbohydr Polym 202:621–630
92. Tian Y, Liang K, Wang X et al (2017) Fabrication of nanocomposite bioelastomer porous scaffold based on chitin nanocrystal supported emulsion-freeze-casting. ACS Sustain Chem Eng 5:3305–3313
93. Wang X, Liang K, Tian Y et al (2017) A facile and green emulsion casting method to prepare chitin nanocrystal reinforced citrate-based bioelastomer. Carbohydr Polym 157:620–628
94. Biswas SK, Sano H, Shams MI et al (2017) Three-dimensional-moldable nanofiber-reinforced transparent composites with a hierarchically self-assembled "reverse" nacre-like architecture. ACS Appl Mater Interfaces 9:30177–30184
95. Zhang Y, Wu J, Wang B et al (2017) Cellulose nanofibril-reinforced biodegradable polymer composites obtained via a Pickering emulsion approach. Cellulose 24:3313–3322
96. Sousa AF, Ferreira S, Lopez A et al (2017) Thermosetting AESO-bacterial cellulose nanocomposite foams with tailored mechanical properties obtained by Pickering emulsion templating. Polymer 118:127–134
97. Fujisawa S, Togawa E, Kuroda K (2017) Facile route to transparent, strong, and thermally stable nanocellulose/polymer nanocomposites from an aqueous Pickering emulsion. Biomacromol 18:266–271
98. Nikfarjam N, Taheri Qazvini N et al (2015) Surfactant free Pickering emulsion polymerization of styrene in w/o/w system using cellulose nanofibrils. Eur Polym J 64:179–188
99. Carrillo CA, Nypelö T, Rojas OJ (2016) Double emulsions for the compatibilization of hydrophilic nanocellulose with non-polar polymers and validation in the synthesis of composite fibers. Soft Matter 12:2721–2728
100. Haaj SB, Thielemans W, Magnin A et al (2014) Starch nanocrystal stabilized pickering emulsion polymerization for nanocomposites with improved performance. ACS Appl Mater Interfaces 6:8263–8273
101. Xie J, Luo Y, Chen Y et al (2019) Redispersible Pickering emulsion powder stabilized by nanocrystalline cellulose combining with cellulosic derivatives. Carbohydr Polym 213:128–137
102. Li Y, Zhao X, Liu Y et al (2019) Melatonin loaded with bacterial cellulose nanofiber by Pickering-emulsion solvent evaporation for enhanced dissolution and bioavailability. Int J Pharm 559:393–401
103. Yan H, Chen X, Feng M et al (2019) Entrapment of bacterial cellulose nanocrystals stabilized Pickering emulsions droplets in alginate beads for hydrophobic drug delivery. Colloids Surfaces B Biointerfaces 177:112–120
104. MacKie A, Gourcy S, Rigby N et al (2019) The fate of cellulose nanocrystal stabilised emulsions after simulated gastrointestinal digestion and exposure to intestinal mucosa. Nanoscale 11:2991–2998
105. Asabuwa Ngwabebhoh F, Ilkar Erdagi S et al (2018) Pickering emulsions stabilized nanocellulosic-based nanoparticles for coumarin and curcumin nanoencapsulations: in vitro release, anticancer and antimicrobial activities. Carbohydr Polym 201:317–328

106. Winuprasith T, Khomein P, Mitbumrung W et al (2018) Encapsulation of vitamin D3 in pickering emulsions stabilized by nanofibrillated mangosteen cellulose: impact on in vitro digestion and bioaccessibility. Food Hydrocoll 83:153–164
107. Marquis M, Alix V, Capron I et al (2016) Microfluidic encapsulation of Pickering oil microdroplets into alginate microgels for lipophilic compound delivery. ACS Biomater Sci Eng 2:535–543
108. Tang C, Li Y, Pun J et al (2019) Polydopamine microcapsules from cellulose nanocrystal stabilized Pickering emulsions for essential oil and pesticide encapsulation. Colloids Surf A Physicochem Eng Asp 570:403–413
109. Hu Z, Marway HS, Kasem H et al (2016) Dried and redispersible cellulose nanocrystal Pickering emulsions. ACS Macro Lett 5:185–189
110. Shao P, Zhang H, Niu B et al (2018) Physical stabilities of taro starch nanoparticles stabilized Pickering emulsions and the potential application of encapsulated tea polyphenols. Int J Biol Macromol 118:2032–2039
111. Zhang Z, Tam KC, Wang X et al (2018) Inverse Pickering emulsions stabilized by cinnamate modified cellulose nanocrystals as templates to prepare silica colloidosomes. ACS Sustain Chem Eng 6:2583–2590
112. Qi L, Luo Z, Lu X (2018) Facile synthesis of starch-based nanoparticle stabilized Pickering emulsion: its pH-responsive behavior and application for recyclable catalysis. Green Chem 20:1538–1550
113. Zhang X, Wang Y, Luo X et al (2019) O/W Pickering emulsion templated organo-hydrogels with enhanced mechanical strength and energy storage capacity. ACS Appl Bio Mater 2:480–487
114. Huan S, Ajdary R, Bai L et al (2019) Low solids emulsion gels based on nanocellulose for 3D-printing. Biomacromol 20:635–644
115. Blaker JJ, Lee KY, Li X et al (2009) Renewable nanocomposite polymer foams synthesized from Pickering emulsion templates. Green Chem 11:1321–1326
116. Jiménez-Saelices C, Seantier B, Grohens Y et al (2018) Thermal superinsulating materials made from nanofibrillated cellulose-stabilized Pickering emulsions. ACS Appl Mater Interfaces 10:16193–16202
117. Li Y, Liu X, Zhang Z et al (2018) Adaptive structured Pickering emulsions and porous materials based on cellulose nanocrystal surfactants. Angew Chemie Int Ed 57:13560–13564
118. Fan X, Wang Y, Zhong W-H et al (2019) A hierarchically structured all-biomass air filter with high filtration efficiency and low air pressure drop based on Pickering emulsion. ACS Appl Mater Interfaces 11:acsami.8b21116
119. Biswas SK, Tanpichai S, Witayakran S et al (2019) Thermally superstable cellulosic-nanorod-reinforced transparent substrates featuring microscale surface patterns. ACS Nano 13:2015–2023
120. Li Y, Yu S, Chen P et al (2017) Cellulose nanofibers enable paraffin encapsulation and the formation of stable thermal regulation nanocomposites. Nano Energy 34:541–548
121. Sjöö M, Emek SC, Hall T et al (2015) Barrier properties of heat treated starch Pickering emulsions. J Colloid Interface Sci 450:182–188
122. Deng Z, Jung J, Simonsen J et al (2018) Cellulose nanocrystals Pickering emulsion incorporated chitosan coatings for improving storability of postharvest Bartlett pears (Pyrus communis) during long-term cold storage. Food Hydrocoll 84:229–237
123. Zhou Y, Sun S, Bei W et al (2018) Preparation and antimicrobial activity of oregano essential oil Pickering emulsion stabilized by cellulose nanocrystals. Int J Biol Macromol 112:7–13
124. Marto J, Gouveia LF, Gonçalves L et al (2016) Design of novel starch-based Pickering emulsions as platforms for skin photoprotection. J Photochem Photobiol B Biol 162:56–64

Chapter 7
Nanopolysaccharides in Environmental Treatments

Ge Zhu, Ning Lin and Alain Dufresne

Abstract In recent years, sustainable nanopolysaccharides, such as cellulose nanocrystals (CNC), cellulose nanofibrils (CNF) and chitin nanocrystals (ChNC) have been explored for improving the efficiency of environment prevention and purification. The potential application is attributed to their biodegradability, sustainability, renewability, biocompatibility, high aspect ratio and high capacity retention. Besides the outstanding advantages, the tailorability of the surface chemistry may enhance the binding efficiency. This review provides a detailed overview of pristine, surface-functionalized nanopolysaccharides and nanocomposites for applications in removal heavy metal ions, organic molecules, dyes and toxic gas in various wastewater treatment and gas adsorptions processes, such as adsorption, flocculation, and membrane filtration. It appears that abundant nanopolysaccharide materials have attracted increasing attention in promising environmental applications.

Keywords Cellulose nanocrystals · Cellulose nanofibrils · Chitin nanocrystals · Water treatments · Adsorption

7.1 Waste Water Treatment

Water and air are essential for our daily life, however, the pollution has raised serious concerns due to the rapid growth in population, industrialization and agricultural activities [1–6]. The pollutants contained various heavy metals, organic and inorganic particles, dyes and toxins. Researchers have developed many projects to remove pollutants from wastewater and purify air, such as adsorption, flocculation and membrane filtration [7–10]. Even though activated carbons of conventional wastewater treatment are widely used, but the greenhouse gas emissions and energy increase their

G. Zhu · A. Dufresne (✉)
Grenoble INP, Grenoble Alpes University, LGP2, 38000 Grenoble, France
e-mail: alain.dufresne@pagora.grenoble-inp.fr

N. Lin
School of Chemistry, Chemical Engineering and Life Sciences, Wuhan University of Technology, Wuhan 430070, People's Republic of China

N. Lin et al. (eds.), *Advanced Functional Materials from Nanopolysaccharides*,
Springer Series in Biomaterials Science and Engineering 15,
https://doi.org/10.1007/978-981-15-0913-1_7

cost. Hence, due to the environmentally friendly, low-cost and superior performance, the abundant polysaccharides materials for wastewater treatment and air purification have attracted increasing attention in promising applications [11–13].

7.1.1 Adsorption Materials

Adsorption is an effective and economical process for the removal of heavy metals and dyes from wastewater. There are various parameters of affecting the adsorption process, such as surface groups and charge characteristics. The adsorption conditions are also important, such as the temperature, contact time, pH, pollutant size, initial concentration of pollutant etc. The adsorption process includes Van der Waals forces and electrostatic attractions, while there are some chemical bonds between adsorbate molecules and the adsorbent [14, 15]. The development of polysaccharides adsorbents such as cellulose and chitin has gained popularity [16, 17].

7.1.1.1 Adsorbents for Heavy Metal Ions

Heavy metal ions are considered as a serious threat to humans and environment, which are found in industrial effluents such as metal plating and paint manufacture [18]. Polysaccharides and their derivatives showed high efficiency for removal of heavy metal ions from wastewater. The higher adsorption efficiency of polysaccharides can be attributed to high functionality, hydrophilicity and the highly reactive properties of the functional groups. Various polysaccharides adsorbents for the removal of heavy metals were shown in Table 7.1.

CNC, CNF and ChNC were used to remove Ag(I), Cu(II) and Fe(III) from contaminated water [19]. CNC was produced by sulfuric acid hydrolysis, CNF was isolated from cellulose sludge in the acidic and alkaline pH, and ChNC was isolated from crab shell residue. The specific surface area of CNC, CNF and ChNC were 138–226, 146–219 and 76–86 $m^2\ g^{-1}$, respectively. The q_{max} of CNC, CNF and ChNC for Ag(I) were 0.318, 0.143 and 0.183 mmol g^{-1}, respectively. Surface adsorption via electrostatic interactions was considered to be the prominent mechanism of heavy metal ion capture from wastewater. The surface modified CNC was also used for the removal of Cd(II), Pb(II) and Ni(II) [20]. The q_{max} of the surface modified CNC for Pb(II), Cd(II) and Ni(II) were 0.04, 0.09 and 0.15 mmol g^{-1}, respectively. The surface modification with more negatively charged groups significantly enhanced metal irons removal efficiency, which provided new ways as environment-friendly remediation for heavy metals. The adsorbents could be regenerated by using 0.5 M HNO_3 after three adsorption cycles. The succinic anhydride modified CNC (SCNC) was used for the adsorption of Cd(II) and Pb(II) [21]. CNC was modified with succinic anhydride to get SCNC, then treated with saturated $NaHCO_3$ to obtain NaSCNC. The q_{max} of SCNC and NaSCNC were 2.31 and 3.07 mmol g^{-1} for Cd(II); 1.77 and 2.24 mmol g^{-1} for Pb(II), respectively. The carboxylated CNF extracted from

Table 7.1 Various polysaccharide-based adsorbents for the removal of heavy metals

Polysaccharides-based adsorbent	Heavy metal ion	Equilibrium adsorption conditions	Q_{max} (mmol g^{-1})	Ref.
CNC, CNF, ChNC	Ag(I)	pH = 6.39, 5.45, 6.63 T = 25 °C, t = 12 h	0.32 [CNC], 0.14 [CNF], 0.18 [ChNC]	[19]
Modified CNC	Pb(II), Cd(II), Ni(II)	pH = 6.0, T = 25 °C, t = 40 min	0.04 [Pb(II)], 0.09 [Cd(II)], 0.15 [Ni(II)]	[20]
Modified CNC	Cd(II), Pb(II)	pH = 6.5 [Cd(II)], pH = 5.5 [Pb(II)], T = 25 °C, t = 150 min	2.31 [Cd(II)] 1.77 [Pb(II)]	[21]
Modified CNC	Cd(II), Pb(II)	pH = 6.5 [Cd(II)], pH = 5.5 [Pb(II)], T = 25 °C, t = 5 min	3.07 [Cd(II)] 2.24 [Pb(II)],	[21]
Modified CNF	Ni(II), Zn(II), Cu(II), Cd(II)	pH = 5.0, T = 25 °C, t = 24 h	0.74 [Ni(II)], 1.61[Zn(II)], 1.90 [Cu(II)], 2.06 [Cd(II)]	[22]
Carboxylated CNF	Cr(III), Ni(II), Cu(II), Zn(II)	pH = 6.2, T = 25 °C, t = 20 h	1.11 [Cr(III)], 0.83 [Ni(II)], 2.12 [Cu(II)], 1.01 [Zn(II)]	[23]
TEMPO-CNF	UO_2^{2+}	pH = 6.5, T = 25 °C, t = 2 h	0.62	[24]
Polymerized CNC	Pb(II), Ni(II), Cd(II), Cr(III)	pH = 6.5, T = 25 °C, t = 40 min	–	[25, 26]
AMEO-modified CNF	Cu(II), Ni(II), Cd(II)	pH = 5.0, T = 25 °C, t = 160 min [Cu(II)], 8 min [Cd(II)], 35 min [Ni(II)]	3.15 [Cu(II)], 2.73 [Ni(II)], 4.19 [Cd(II)]	[27]
CHA-modified CNF	Cd(II), Ni(II)	pH = 5.0, T = 25 °C, t = 5 min	1.22 [Cd(II)], 2.02 [Ni(II)]	[28]
Carboxylated CNF	Pb(II), Hg(II), Ag(I), Cu(II)	T = 25 °C, t = 3 days	0.53 [Pb(II)], 0.78 [Hg(II)], 1.06 [Ag(I)], 2.38 [Cu(II)]	[29]
TEMPO-CNF	Cu(II)	pH = 5.0, T = 30 °C, t = 20 h	0.82	[30]
Phosphorylated CNC	Cu(II), Ag(I), Fe(III)	pH = 3.5 to 4.5, T = 25 °C, t = 12 h [Cu(II) and Fe(III)], t = 6 h [Ag(I)]	1.84 [Cu(II)], 1.26 [Ag(I)], 2.06 [Fe(III)]	[31]

(continued)

Table 7.1 (continued)

Polysaccharides-based adsorbent	Heavy metal ion	Equilibrium adsorption conditions	Q_{max} (mmol g^{-1})	Ref.
Bisphosphonate CNC	V(V)	pH = 3, T = 25 °C, t = 24 h	1.98	[32]
Electrosterically CNC	Cu(II)	pH = 4.0, T = 25 °C, t = 210 s	2.91	[33]
Au-CNC composite	Hg(II)	pH = 7.0, T = 25 °C, t = 12 h	0.13	[34]
CNC nanocomposite	Co(II)	pH = 6.0, T = 30 °C, t = 120 min	5.95	[35]
CNC composite	Hg(II)	pH = 8.0, T = 30 °C, t = 60 min	1.19	[36]
FeNP-modified CNF	As(V)	pH = 2.0, T = 25 °C, t = 75 min	2.46	[37]
Carboxylated CNF	Pb(II)	pH = 4.5, T = 25 °C, t = 200 min	0.82	[38]
Sulfonated CNF	Pb(II)	pH = 5.0, T = 4 °C, t = 20 h	1.20	[39]

T temperature, *t* contact time, q_{max} maximum adsorption capacity

pulp residue could be used as efficient adsorbents for the removal of Ni(II), Zn(II), Cu(II) and Cr(III) from aqueous solutions, while the q_{max} were 0.74, 1.61, 1.90 and 2.06 mmol g^{-1}, respectively [22, 23]. The negatively charged TEMPO-CNF was very effective to adsorb UO_2^{2+} from wastewater, while the q_{max} was 0.62 mmol g^{-1} [24]. The high specific surface area, surface charge density and hydrophilicity of TEMPO-CNF contributed to the high UO_2^{2+} adsorption efficiency.

Graft polymerization CNC with monomeric acids introduced more negative carboxylate groups onto the surface of CNC [25, 26]. Amination of CNC with acryl amide was responsible to the incorporation of NH^{3+} cationic ligands on the surface. Esterification of CNC with succinic anhydride led to increase the binding sites with positively charged metal ions. The q_{max} for Cr(VI) and Cr(III) were 0.053 and 0.0055 mmol g^{-1}, respectively. Aminopropyltriethoxysilane (AMEO) modified CNF was prepared for removal of Cu(II), Ni(II) and Cd(II), while the q_{max} were 3.15, 2.73 and 4.19 mmol g^{-1}, respectively [27]. The amino ($–NH_2$) and hydroxyl (–OH) groups contributed to the higher adsorption efficiency due to the free electron doublets of the nitrogen and oxygen atoms. Carbonated hydroxyapatite modified CNF was reported to remove Cd(II) and Ni(II) from aqueous solution, while the q_{max} were 1.22 and 2.02 mmol g^{-1}, respectively [28]. The adsorption mechanism was mainly ionic interactions between adsorbates and modified CNF. The adsorption-desorption cycles proved that the 0.01 M HNO_3 was a highly effective regenerant for the adsorption. The cross-linked polyvinyl alcohol CNF (PVA-CNF) hybrid aerogels were used for removal of Pb(II), Hg(II), Ag(I) and Cu(II) from aqueous solutions, while the

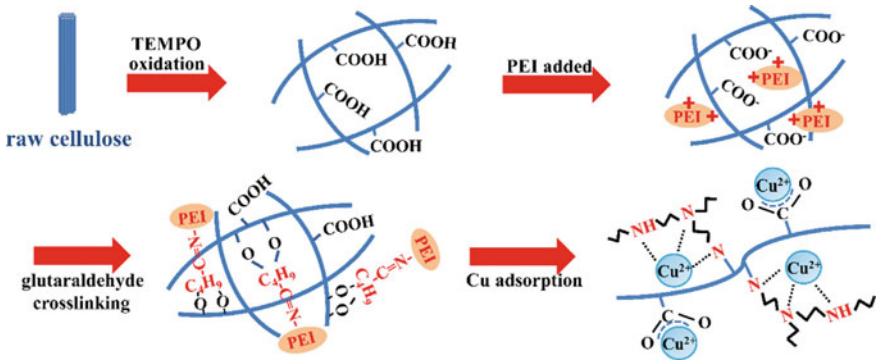

Fig. 7.1 General chemical routes of the adsorption of Cu(II) by polyethylenimine (PEI) modified TEMPO-CNF (Reproduced from [30])

q_{max} were 0.53, 0.78, 1.06 and 2.38 mmol g^{-1}, respectively [29]. The PVA-CNF aerogels were hydrophobic and oleophilic after being treated with methyltrichlorosilane. Polyethylenimine (PEI) modified TEMPO-CNF was reported for removal of Cu(II), as shown in Fig. 7.1 [30]. The abundant carboxyl and amino functional groups were introduced onto CNF, which acted as active sites for the binding of Cu(II).

Enzymatically phosphorylated CNC was reported to remove Cu(II), Ag(I) and Fe(III), while the q_{max} were 1.84, 1.26 and 2.06 mmol g^{-1}, respectively [31]. Phosphorylated CNC significantly improved the metal sorption capacity due to the high specific surface area. The bisphosphonate CNC was also used to remove vanadium(V) from aqueous solution, while the q_{max} was 1.98 mmol g^{-1} [32]. The electrosterically CNC (ECNC) was extracted from wood fibers through periodate/chlorite oxidation for removal of Cu(II) [33]. During the adsorption, ECNC aggregated into star-like particles at low Cu(II) concentration, and the aggregate morphology convert to raft-like particles at higher Cu(II) concentrations by the collapse between dicarboxylic cellulose chains and charge neutralization. The q_{max} for Cu(II) was 2.91 mmol g^{-1}, which was attributed to the highly charged dicarboxylic cellulose chains. The luminescent CNC composite could simultaneously sense and scavenge heavy metal ions, specifically for Hg(II) in water, as shown in Fig. 7.2 [34]. Nanocomposites were constructed by introducing bovine serum albumin-protected gold nanoclusters into the CNC alginate hydrogel beads, while the q_{max} for Hg(II) was 0.13 mmol g^{-1}. A poly grafted CNC composite with multi carboxyl functional group was developed for removal of Co(II) and Hg(II) from aqueous solutions [35, 36]. The adsorbents could be effectively reused more than five cycles with 0.1 M HCl.

Magnetic iron nanoparticles modified CNF was used for removal of As(V), while the q_{max} was 2.46 mmol g^{-1} [37]. The adsorbents could be effectively regenerated more than 98% after three cycles by 1 M NaOH solution. The carboxylated modified CNF magnetic hydrogels were reported for removal of Pb(II), while the adsorption capacity was much higher than that of without carboxylated CNF at the entire pH range [38, 39]. This could be attributed to the carboxyl groups on the carboxylated

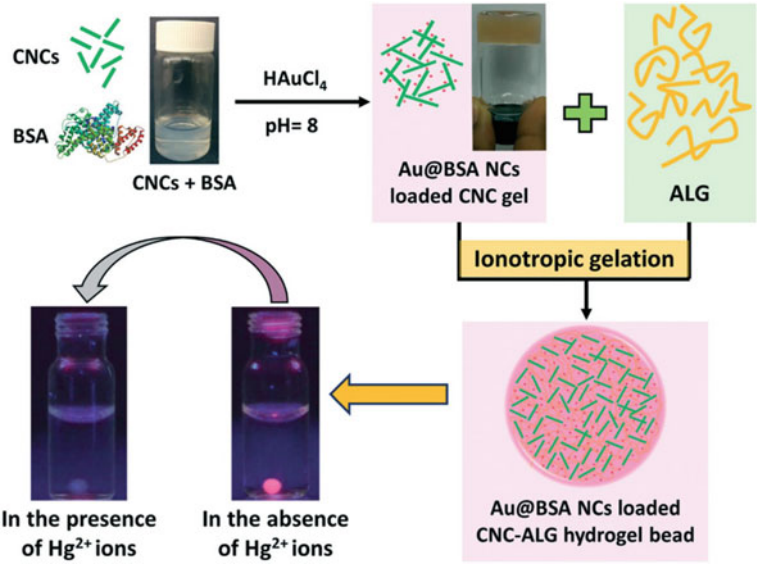

Fig. 7.2 Schematic representation showing the preparation of CNC nanocomposite and its simultaneous sensing and scavenging of Hg^{2+} ions in water (Reproduced from [34])

CNF surface, which significantly enhances the electrostatic interaction between the adsorbent and metal ions. Additionally, desorption experiments proved that the magnetic hydrogels could be easily regenerated with 0.01 M HNO_3 and the adsorption efficiency can be maintained more than 90% after four cycles.

7.1.1.2 Adsorbents for Dyes

Dyes have become one of the main sources of water pollution by the rapid development of the dyes, food, pharmaceutical and leather tanning industries [40–42]. The release of the dyes has attracted big concern on human health. It was very difficult to remove dyes from the wastewater. The conventional methods are either expensive or ineffective for removing dyes from wastewater, such as reverse osmosis, bacterial action and chemical oxidation. Recently, polysaccharides composites have been developed into conventional wastewater treatment adsorbents, as shown in Table 7.2.

The carboxylic CNC was extracted by citric acid/HCl hydrolysis, which showed remarkable coagulation flocculation performance to cationic dyes [43–45]. The q_{max} of CNC and carboxylic CNC for MB were 0.37 and 2.40 mmol g^{-1}, respectively. The higher content carboxyl groups of the carboxylic CNC could provide more active adsorption/flocculation sites during the adsorption process based on the charge neutralization mechanism. The amino-functionalized CNC (Amino-CNC) was prepared to remove anionic dyes (Congo red 4BS, acid red GR and reactive yellow K-4G) from aqueous solutions [46]. Amino-CNC were prepared by grafting ethylenediamine

Table 7.2 Various polysaccharide-based adsorbents for the removal of dyes

Polysaccharides-based adsorbent	Dye	Equilibrium adsorption conditions	q_{max} (mmol g^{-1})	Ref.
CNC	Methylene blue	pH = 7.5, T = 60 °C, t = 1 h	0.40	[43]
Carboxylated CNC	Methylene blue	pH = 7.0, T = 25 °C, t = 30 min	–	[44]
Carboxylated CNC	Methylene blue	pH = 9.0, T = 25 °C, t = 30 min	2.40	[45]
Amino-CNC	Acid red GR	pH = 4.7, T = 25 °C, t = 7 h	1.39	[46]
Imidazolium-CNC	Orange II	–	0.28	[47]
MA-grafted CNC	Crystal violet, methylene blue	pH = 6.0, T = 30 °C, t = 4 h	0.59	[48]
CNC/HPAM	Methylene blue	pH = 6.5, T = 25 °C, t = 4 h	–	[49]
CNC/HPAM	Methylene blue	pH = 5.0, T = 25 °C, t = 4 h	1.02	[50]
CNC/alginate hydrogels	Methylene blue	pH = 7.0, T = 25 °C, t = 1 h	0.80	[51, 52]
MnO_2/CNF hybrids	Methylene blue	pH = 9.6, T = 25 °C, t = 5 min	–	[53]
Silsesquioxane-modified CNF	Yellow B-4RFN, blue B-RN	pH = 7.0, T = 30 °C, t = 4 h	–	[54]
D-CNC/PVAm microgels	Congo red 4BS, acid red GR, yellow K-4G	pH = 3.5, T = 25 °C, t = 1, 8, 8 h	2.12, 2.17, 0.77	[55]
CNF	Congo red, Acid green 25	pH = 7.0, T = 21 °C, t = 1 min	0.95, 1.09	[56]
Magnetic CNC microbeads	Methylene blue	–	–	[57]

onto the sodium periodate oxidation CNC. The hydroxyl (–OH) and primary amine ($–NH_2$) groups with highly active adsorption sites contributed to be the high adsorption capacity. The q_{max} for acid red GR was 1.39 mmol g^{-1}. The imidazolium-grafted CNC was synthesized by using copper(I) catalyzed azide-alkyne cycloaddition and bromide anion, while the q_{max} for Orange II dye was 0.28 mmol g^{-1} [47]. The carboxylate modified CNC grafted by Microcystis aeruginosa (MA) was reported for removal of Crystal Violet and Methylene Blue [48]. Compared with raw cellulose, the adsorption capacity of modified CNC for cationic dyes was drastically improved, which was attributed to the high surface area and sulfate ester groups. High surface area provided more exposed hydroxyl reactive sites and the negative charged sulfate ester groups were favorable for cationic dyes removal. The adsorption capacity of

MA-CNC was much higher than that of pristine CNC, indicating that the carboxyl groups were easy to attract cationic dyes through electrostatic interaction.

The development of polymer adsorbent systems is highly encouraged due to their large removal efficiency and the spontaneous decontamination. The porous composite hydrogels fabricated by hydrolyzed polyacrylamide (HPAM) and CNC were reported for removal of Methylene Blue from aqueous solutions, while the q_{max} was 1.02 mmol g^{-1} [49, 50]. The composite hydrogels displayed high removal efficiency and rapid swelling rate at low concentrations. The composite hydrogels enhanced not only the formation of crosslinked network but also the dye adsorption efficiency. A new generation of recyclable adsorbents comprising of alginate and CNC (ALG-CNC) with superior adsorption capacity were reported for removal of Methylene Blue in aqueous solution [51, 52]. The q_{max} for Methylene blue was 0.80 mmol g^{-1} within 60 min, and the removal efficiency remained more than 97% after five cycles. The manganese dioxide (MnO_2)/CNF hybrids were reported for the removal of MB, which showed excellent adsorption and oxidation efficiency [53]. The CNF hybrids containing multi-*N*-methylol silsesquioxane were reported for removal of yellow B-4RFN and blue B-RN dyes from aqueous solution [54]. The removal capacity of CNF hybrids was significantly higher than that of pristine CNF. It can be attributed to organic functional groups and numerous cubic cores in CNF hybrids.

The nanocomposite microgel based on amphoteric polyvinylamine (PVAm) and CNC were prepared for the removal of anionic dyes (Congo red 4BS, Acid red GR and Yellow K-4G) [55]. The removal capacity of microgel was high at acid conditions. The q_{max} for Congo red 4BS, acid red GR and Yellow K-4G were 2.12, 2.17 and 0.77 mmol g^{-1}, respectively. The surface quaternized CNF was used for the removal of anionic dyes (Acid green 25 and Congo red) [56]. The transparent and viscous dispersion were obtained by strongly mechanical homogenization of the cellulose slurries. The q_{max} for Congo red and acid green 25 were 1.10 and 0.95 mmol g^{-1}, respectively. The magnetic microbeads were reported for the removal of MB, while the q_{max} was 0.006 mmol g^{-1} [57]. The magnetic particles and CNC banded together to form a structured layer, as shown in Fig. 7.3. The magnetic functionality enabled easy separation of substances immobilized on the beads.

7.1.1.3 Adsorbents for Oil/Water Separation

Oil from petrochemical industries has become a serious concern, and absorbents based on organic and inorganic porous materials have been developed for oil/water separation. Among these absorbents, polysaccharide absorbents have gained increasing attention due to their unique properties and sustainable character, as shown in Table 7.3.

The hydrazine-carboxyl CNC aerogels were high elasticity and fast oil/water separation, while the absorption capacity for water, dodecane, ethanol and toluene were 133, 54, 99 and 34 g g^{-1}, respectively [58]. Meanwhile, the results proved that the more carboxyl groups contributed to the excellent mechanical properties and shape recovery ability. The chemically cross-linked CNC aerogels based on

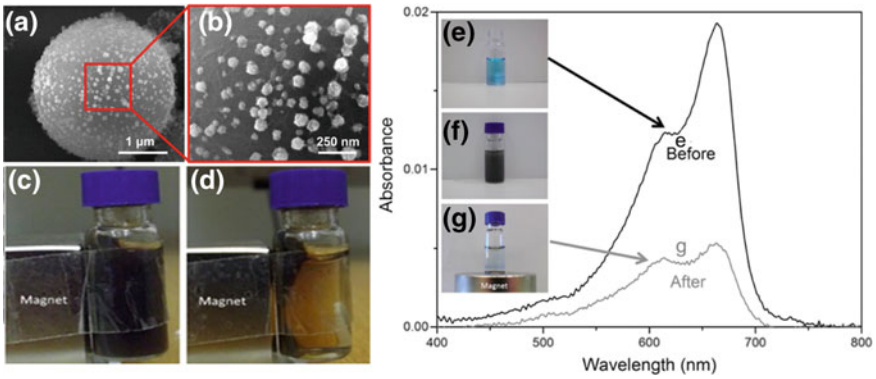

Fig. 7.3 SEM images of **a** an individual hybrid CNC-$CoFe_2O_4$-PS microbead; **b** close-up of the surface revealing the CNC hybrid mesh formation; **c**, **d** indicates that the microbeads can be separated by magnetic manipulation; **e**, **f**, **g** methylene blue removal from aqueous solution by introducing CNC-$CoFe_2O_4$-PS microbeads; UV-vis spectra of the methylene blue solution before (**e**) and after (**g**) adsorption (Reproduced from [57])

hydrazide and aldehyde-modified CNC were reported for oil/water separation [59]. The unique pore structure of the CNC aerogels contributed to the shape recovery ability. The absorption capacity of the CNC aerogels for water, dodecane, ethanol and dimethyl sulfoxide were 160, 72, 130 and 134 g g^{-1}, respectively. The cross-linked PVA-CNF hybrid aerogels were prepared for removing oil and organic solvents from wastewater [38]. The hydrophobic PVA-CNF aerogels exhibited excellent absorption capacity in the ranging of 44–96 g g^{-1} for various types of organic solvents (hexane, toluene, gasoline, chloroform) and oils (pump oil, crude oil, diesel oil, corn oil). The hydrophobic CNF aerogels were also prepared through vapor deposition with triethoxyl silane for oil/water separation [60, 61]. The resulting aerogels were ultralight (1.7–8.1 mg cm^{-3}) and ultra-porous (99.5–99.9%) features, which displayed excellent absorption capacity and good recyclability. The absorption capacity for water, chloroform, non-polar liquids were 210, 375, 139–356 g g^{-1}, respectively.

Composite aerogels were fabricated by silylated tunicate CNC and red mud for oil/water separation [62]. The absorption capacity of these composite aerogels for oil and 2,4-dichlorophenol were 33–36 and 5.5–6.0 g g^{-1}, respectively. A facile synthesis of hydrophobic and ultralight CNF aerogels were reported with a silylation process, as shown in Fig. 7.4 [63]. Compared with conventional inorganic porous materials, the shape recovery of silylated CNF aerogels was nearly to 96% in 50% compression strain, which displayed an excellent flexibility. In the basis of the hydrophobic properties, the aerogels were highly efficient in removing organic solvents from wastewater with an excellent selectivity and recyclability. The absorption capacity for oils (silicone oil, motor oil, mineral oil) and organic solvents (ethanol, acetone, dodecane, toluene) were 49–102 g g^{-1}. The highly porous CNF aerogels coated with titanium dioxide showed a selective oil-absorbing capacity, while the

Table 7.3 Various polysaccharide-based absorbents for oil/water separation processes

Polysaccharides-based adsorbent	Absorbent characteristics	Absorption capacity	Ref.
Carboxyl CNC aerogel	$\rho = 22.4–23.3$ mg cm^{-3} BET = 195–303 m^2 g^{-10} P = 96.3–97.2%	133 ± 6 g g^{-1} (water) 54 ± 6 g g^{-1} (dodecane) 99 ± 8 g g^{-1} (ethanol) 34 ± 4 g g^{-1} (toluene)	[58]
Hydrazine-CNC aerogel	$\rho = 5.6$ mg cm^{-3} BET = 250 ± 80 m^2 g^{-1} P = 99.6%	160 ± 10 g g^{-1} (water) 72 ± 5 g g^{-1} (dodecane) 130 ± 10 g g^{-1} (ethanol) 134 ± 8 g g^{-1} (dimethyl sulfoxide)	59]
Carboxylated-CNF/PVA aerogel	$\rho = 13$ mg cm^{-3}, BET = 172 ± 13 m^2 g^{-1} θ = 150.3 ± 1.2°, P = 98%	44–96 g g^{-1} (oil and organic solvents)	[38]
Triethoxy (octyl) silane-CNF aerogel	$\rho = 1.7–8.1$ mg cm^{-3} BET = 10.9 m^2 g^{-1} P = 99.5–99.9%	210 g g^{-1} (water) 375 g g^{-1} (chloroform) 139–356 g g^{-1} (non-polar liquids)	[60]
CNC scaffold composite	$\rho = 3.3–7.5$ mg cm^{-3} Pore diameter = 0.1–10 μm	100–200 g g^{-1} (organic solvents)	[61]
Silylated tunicate CNC	BET = 73.23 m^2 g^{-1}, θ = 134.5, P = 98.8%,	33–36 g g^{-1} (oil)	[62]
Methyltrimethoxysilane-CNF aerogel	$\rho = 5.07–17.3$ mg cm^{-3} BET = 3–25 m^2 g^{-1} θ = 110–150°, P = 99%	49–102 g g^{-1} (organic solvents)	[63]
TiO_2-CNF aerogel	$\rho = 20$-30 mg cm^{-3}, P = 98%, θ = 90°	20-40 g g^{-1} (non-polar liquids)	[64]

ρ density, *P* porosity, *BET* specific surface area, θ contact angle

absorption capacities were in the range of 20–40 g g^{-1} for non-polar liquids and oils [64].

7.1.2 Flocculation

Flocculation is a simple and efficient method for wastewater treatment, and it is widely used for the removal of suspended and dissolved solids in industrial wastewater [65–67]. During the addition of flocculants, the divided or dispersed particles are aggregated together to form large particles [68]. In recent years, polysaccharides flocculants have developed to be promising alternative flocculants to replace conventional materials. Compared with conventional flocculants, polysaccharides flocculants are biodegradable, renewable and sustainable [69]. Bio-flocculants can also destabilize the equilibrium of colloidal solution through increasing the ionic strength

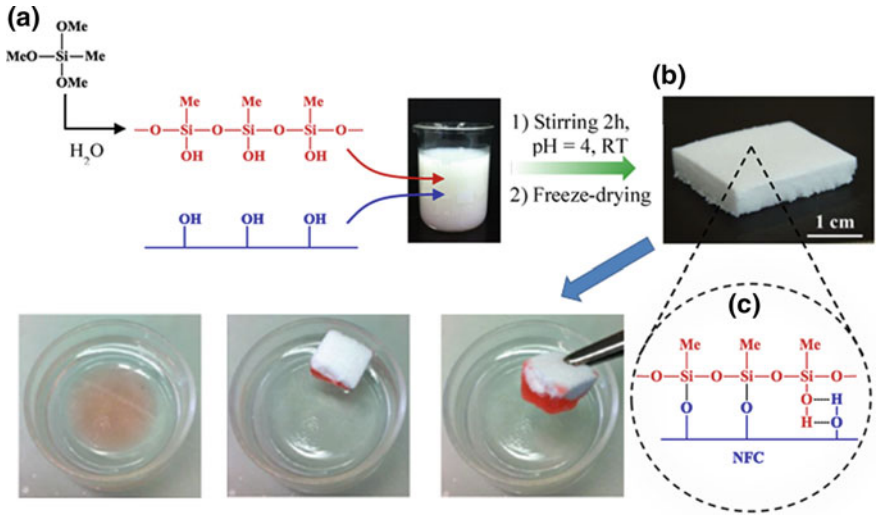

Fig. 7.4 Schematic diagram showing the general scheme for the synthesis of silylated CNF sponges and their simultaneous use in the removal of red-colored dodecane spill from water (Reproduced from [63])

or deducing the zeta potential according to the variety of carboxyl or hydroxyl groups [70]. Various polysaccharide flocculants for the flocculation of water contaminants were shown in Table 7.4.

The carboxymethyl cellulose prepared from agricultural waste was used as friendly flocculant with aluminum sulfate for wastewater treatment [71]. The turbidity removal efficiency was 95% in the optimum conditions. A novel CNC flocculant was presented for removing Chlorella vulgaris [72]. The cationic CNC was prepared by grafting cationic pyridinium groups onto CNC through nucleophilic substitution and esterification reactions. In contrast to conventional polymer flocculants, cationic CNC was relatively insensitive to inhibition of flocculation. Imidazole grafted CNC was also investigated by using one-pot modification strategy [73]. The surface charge of the imidazole CNC could be converted from negative to positive by protonation of the imidazole moieties. The Chlorella vulgaris were used to test the flocculation efficiency of the modified CNC. The maximum flocculation efficiency was more than 90% at pH 3.5. The flocculation of the Gram-negative bacterium was tested, while the CNC concentration was less than 0.1% [74]. The CNC nanoparticles were very effective for the phase separation, which was at very low concentrations of the CNC nanoparticles. The dicarboxylic acid nanocellulose flocculants were produced by nanofibrillation of periodate and chlorite-oxidized celluloses, which showed good performance in the coagulation-flocculation wastewater treatment, as shown in Fig. 7.5 [75]. The coagulation-flocculation treatment resulted in a low residual turbidity by the addition of ferric sulfate as coagulant. In the condition of high charge density and nanofibril content, the flocculant had the best flocculation performance. The dicarboxylic nanocellulose showed high stability in aqueous suspensions

Table 7.4 Various polysaccharide-based flocculants for the flocculation of water contaminants

Polysaccharides-based flocculants	Contaminant	Flocculation conditions	Flocculent performance	Ref.
Carboxymethyl cellulose	Solid particles	Stirring velocity = 30 r min^{-1}, pH = 8	T = 95%	[71]
Pyridinium grafted CNC	*Chlorella vulgaris*	f = 0.1 g g^{-1}, pH = 4–11, t = 30 min	F = 95%	[72]
Pyridinium grafted CNC	*Chlorella vulgaris*	f = 0.1 g g^{-1}, pH = 4–11, t = 30 min	F ≥ 95%	[72]
4-(1-bromo-methyl) benzoic acid modified CNC	*Chlorella vulgaris*	f = 200 mg L^{-1}, pH = 3.5, t = 30 min	F = 90%,	[73]
Pristine CNC	*Pseudomonas aeruginosa*	f = 0.1%, t = 24 h	T = 100%	[74]
Dicarboxylic acid CNF	Solid particles	f = 2.5–5.0 mg L^{-1}, pH = 6–8, t = 30 min	T = 40–80%, C = 40–60%	[75]
Sulfonated CNF	Solid particles	f = 2.5 mg L^{-1}, t = 30 min	–	[76]
Quaternized CNF	Reactive orange 16	f = 150 mg L^{-1}, t = 12 h	q_{max} = 0.477 mmol g^{-1}	[77]
Chitosan and alum	*Escherichia coli*	f = 0.5 mg L^{-1}	T = 99.99%	[80]
$Fecl_3$-chitosan	Arsenate and arsenite species	f = 0.5 mg L^{-1}, pH = 5.5–9, t = 50 min	F = 100% [As(V)], F = 80% [As(III)]	[81]
Kaolin-chitosan	Lipophilic extractives	f = 60 mg L^{-1}	F = 100%	[82]
$Ca(OH)_2$-chitosan	Cells	f = 0.075 g L^{-1}	F = 95–99%	[83]
Sulfonated chitosan	Bentonite, kaolinite, alumina	pH = 4.5–7.0 (bentonite), pH = 4.5–5.5 (kaolinite), pH = 7.0–8.0 (alumina)	F = 100%	[84]
Chitosan-g-PDMC	Pulp mill wastewater	f = 2.52 mg L^{-1}, t = 3 h	T = 99.4%, C = 90.7%	[85]
Chitosan-g-polyacrylamide	Methyl orange, basic bright yellow	f = 80 mg L^{-1} (pH = 4.0), f = 160 mg L^{-1} (pH = 11.0)	F = 92.9% (methyl orange), F = 95.0% (basic bright yellow)	[86]

(continued)

Table 7.4 (continued)

Polysaccharides-based flocculants	Contaminant	Flocculation conditions	Flocculent performance	Ref.
Chitosan-g-CTA	Kaolin suspension	f = 0.03–0.20 mg L^{-1} (pH < 6.5), f = 0.8–1.0 mg L^{-1} (pH > 6.5)	T = 88.4%	[87]
Montmorillonite-chitosan	*Microcystis aeruginosa*	f = 300–320 mg L^{-1}, t = 16–50 min	F = 94.7%	[88]

f flocculant dosage, *T* turbidity removal, *F* flocculation efficiencies, *C* COD removal

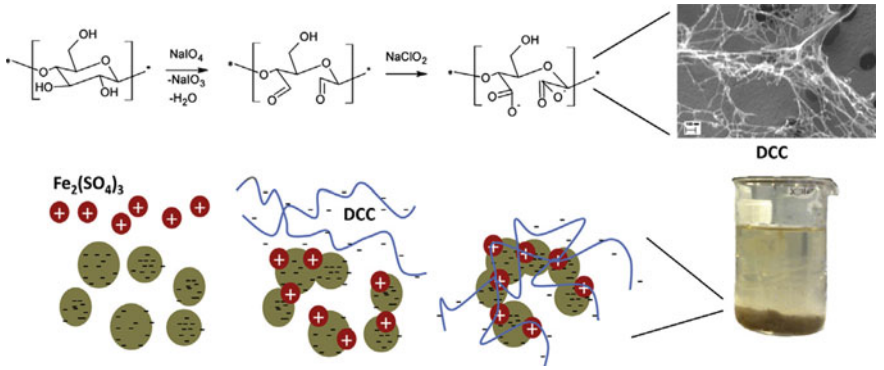

Fig. 7.5 Images showing the differences in floc morphology between the cationic reference flocculants and the nanofibrillar DCC flocculants (Reproduced from [75])

during a long period time. The flocculation performance of anionic sulfonated CNF was also tested with variable charge densities in combined coagulation-flocculation wastewater treatment [76]. The glycidyltrimethyl ammonium chloride (GTMAC) modified CNF flocculants were used for the removal of Reactive Orange 16, while the removal efficiency was 0.477 mol g^{-1} [77]. The modified CNF flocculants provided a sustainable and biodegradable alternative to traditional synthetic flocculants.

Chitosan is one of the most promising biopolymer, which is insoluble in either water or organic solvents but soluble in dilute organic acids such as formic and acetic acid [78]. The chitosan dissolved in acids not only produced protonated amine groups, but also facilitated electrostatic interactions between the negatively charged contaminants and polymer chains during the wastewater treatment [79]. According to the several intrinsic characteristics of the amino-chitosan such as high cationic charge density and long polymer chains, the amino-chitosan was an effective flocculant for the removal of contaminants. Therefore, the development of chitosan material was an expanding field in wastewater treatment.

The alum and chitosan were investigated for the removal of Escherichia coli from waste water, while the removal efficiency was 99.99% [80]. It was attributed to the anti-bacterial effect of chitosan related to its binding affinity of the microbe surface. The chitosan and $FeCl_3$ were prepared to remove As(III) and As(V) from wastewater, while the removal efficiency for As(III) and As(V) were 80% and 100%, respectively [81]. Kaolin and chitosan as adsorbents and coagulant aids were reported for the removal of lipophilic extractives, while the removal efficiencies were more than 91% [82]. The kaolin fraction could significantly increase the settling rate of the chitosan flocs, which led to the high removal efficiency. A double system containing chitosan and calcium hydroxide ($Ca(OH)_2$) as coagulant were reported to remove cells and toxins of Gymnodinium catenatum, while the removal efficiency was in the rang of 95–99% [83]. Sulfonated chitosan was synthesized by replacing the hydroxyl groups with sulfate for the removal of colloidal suspensions of alumina, bentonite and kaolinite [84]. The sulfonated chitosan showed variable surface charges depending on the pH of the solution and the electrostatic interactions contributed to the high removal efficiency between sulfonated chitosan and colloidal particles.

Chitosan grafted with poly (2-methacryloyloxyethyl) trimethyl ammonium chloride (chitosan-g-PDMC) were investigated for the pulp mill wastewater treatment, while the removal efficiency for turbidity and chemical oxygen demand were 99.4 and 90.7%, respectively [85] Carboxymethyl chitosan grafted with polyacrylamide (chitosan-g-PAM) were reported to remove various dyes from aqueous solutions, while the removal efficiencies for Methyl Orange and Basic Bright Yellow were 92.9 and 95.0%, respectively [86]. More importantly, the grafted polyacrylamide chains produced notably more compacted flocs, which contributed significantly to remove flocs from the wastewater. Amphoteric carboxymethyl chitosan grafted with 3-chloro-2-hydroxypropyl trimethyl ammonium chloride (CTA) (chitosan-g-CTA) as flocculants were reported [87]. Compared with chitosan and cationic chitosan, the amphoteric flocculants showed notable improvement in solubility and salt-resistance during the entire pH range. The morphology of the polymeric flocculants in solution also greatly affected the final flocculation performances. Chitosan modified nano-sized montmorillonite (chitosan-NMMT) were investigated for the removal of Microcystis aeruginosa, while the maximum removal efficiency was 94.7% [88]. The release rate of intracellular microcystins was caused by the damage of intact *Microcystis aeruginosa* cells during the flocculation and floc storage processes.

7.1.3 Membrane Separation

Membrane filtration is widely used in wastewater treatment, which are designed with well-defined pore size and tailored by surface chemistry [89]. According to the pore size, the separation forms of the membranes include microfiltration, ultrafiltration and nanofiltration [90]. There are many studies about the use of polysaccharide membranes for the removal of contaminants in wastewater, as shown in Table 7.5.

Table 7.5 Various polysaccharides-based membranes for the filtration of water contaminants

Polysaccharides-based membrane	Contaminant	Membrane operating conditions	Membrane characteristics	Ref.
CNF nanopaper	Swine influenza virus	p = 10–15 kPa	A = 19 nm, P = 35%, BET = 88 $m^2\ g^{-1}$	[91]
Citric acid-CNF nanopaper	Gold nanoparticles	p = 37 kPa	A = 15 nm, P = 35%	[92]
CNF nanopaper	Xenotropic murine leukemia virus	p = 10–15 kPa	A = 16 nm, P = 35%	[93]
CNF membrane	Oil/water emulsions	p = 30 psi	R = 99.7%, Pe = 185 L $m^{-2}\ h^{-1}$	[94]
PAN-CNF membrane	Bacteria, virus and organic dye	p = 19.3 kPa	Pe = 59 ± 2 L $m^{-2}\ h^{-1}\ kPa^{-1}$, q_{max} = 0.166 mmol g^{-1} (crystal violet)	[95]
PAN/PET CNF membrane	Bacteria, virus, Cr(VI), Pb(II)	pH = 6	Pe = 1300 L $m^{-2}\ h^{-1}\ psi^{-1}$, q_{max} = 0.875 [Pb(II)], 1.923 [Cr(VI)] mmol g^{-1}	[96]
Polymerization CNF membrane	Nanofiltration	p = 3.4 bar	R = 74–91%, Pe = 238 L $m^{-2}\ h^{-1}\ bar^{-1}$	[97]
PEG-CNF membrane	Ultrafiltration	p = 206.8 kPa	R = 90%	[98]
CNC membrane	Cationic dyes	p = 0.196 MPa	Pe = 64 L $m^{-2}\ h^{-1}\ MPa^{-1}$, q_{max} = 90% (methyl violet), 98% (victoria blue), 70% (rhodamine 6G)	[99]
CNC/CNF nanopaper	Ag^+, Cu^{2+}, Fe^{3+}/Fe^{2+}	p = 0.45 MPa	BET = 0.43–71 $m^2\ g^{-1}$, q_{max} = 100%	[100]
CNF-SF membranes	Dyes, heavy metal ions	P = 90 kPa	A = 1.8 ± 0.5 nm, q_{max} = 7.305 (Ag^+), 0.675 (Au^+), 0.293 (Ni^{2+}), 1.018 (Cu^{2+}) mmol g^{-1}	[101]
thiol-modified CNF membrane	Cr(VI), Pb(II)	p = 2 psi	q_{max} = 0.416 [Pb(II)], 1.682 [Cr(VI)] mmol g^{-1}	[102]
Silver CNF membrane	Water purification applications	p = 1 bar	R = 92.4–94.0%	[103]

(continued)

Table 7.5 (continued)

Polysaccharides-based membrane	Contaminant	Membrane operating conditions	Membrane characteristics	Ref.
PVDF-CNC membrane	Membrane distillation	p = 27 psi	P = 75%, Re = 99.9%	[104]

p pressure, *P* porosity, *BET* specific surface area, *A* average pore size, *R* rejection ratio, *Pe* permeability

Pristine CNF polymer membranes were reported for removal of viruses based on the size exclusion principle, as shown in Fig. 7.6 [91]. The facile heat-pressing manufacturing method could be used to the existing capacities for roll-to-roll paper making processes. Nanocellulose cross-linked with citric acid was efficient removal of 20 nm Au nanoparticles from the wastewater [92]. The citric acid route was particularly promising for enhancing the wet strength of nanocellulose filters for biotechnology

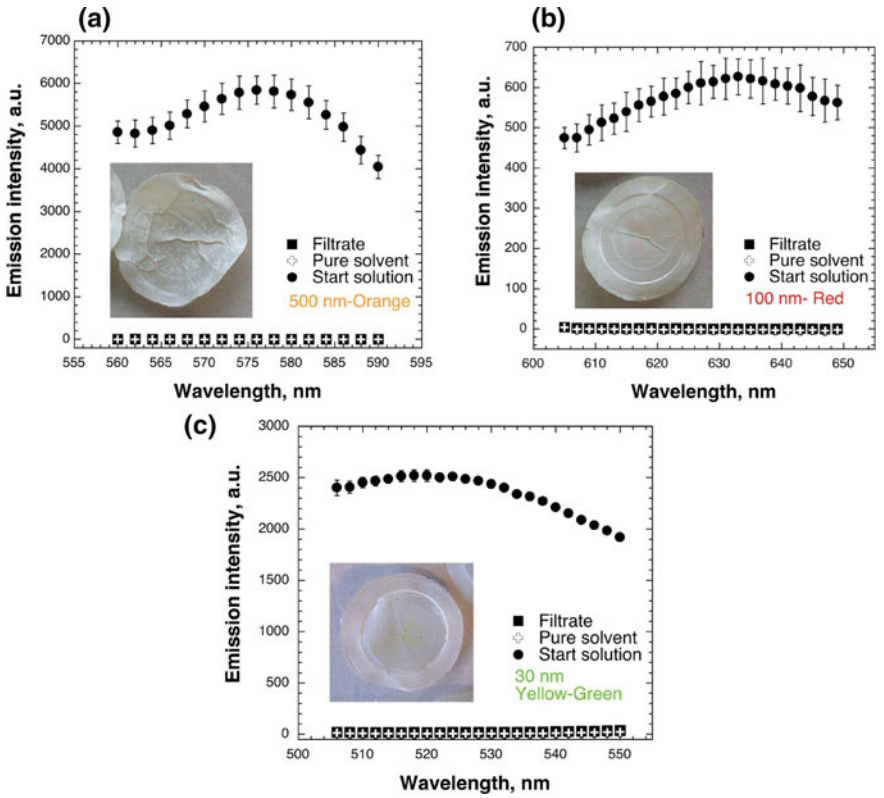

Fig. 7.6 Fluorospectrophotometric profiles of the starting latex bead dispersions and the filtrate: **a** 500 nm beads; **b** 100 nm beads; and **c** 30 nm beads (Reproduced from [91])

applications, which was facile, cost-efficient, and non-toxic. The size-exclusion filter paper was reported for the removal of xenotropic murine leukemia virus [93]. The average porosity and pore size of these nanopapers were 35% and 16 nm. The results suggested that the nanocellulose filter paper was useful for removal of endogenous rodent retroviruses and retrovirus-like particles during the production of recombinant proteins. The thin-film CNF membranes were reported for water purification [94]. The viscosity of CNF suspension was affected by pH and ionic strength. The permeation flux with above 99.5% rejection ratio of CNF membranes was 10-fold higher than commercial ultrafiltration membranes for ultrafiltration of oil/water emulsions. It was ascribed to the negatively charged surface and high specific surface area.

A multilayered microfiltration membrane system was reported with low pressure drop, high flux and retention capability [95]. The membrane was prepared by impregnating ultrafine CNC into polyacrylonitrile scaffold. The resulting membrane possessed a narrow pore size distribution and a high retention ratio against bacteria. A novel two-layered PAN/polyethylene terephthalate fibrous membrane was reported for removing viruses, bacteria and toxic heavy metal ions [96]. The resulting membrane was able to remove Escherichia coli completely, and the adsorption capability of Cr(VI) and Pb(II) were 100 and 260 mg g^{-1}, respectively. The development of these membranes was ascribed to the web-like structure with very high charge density and large surface area for adsorption of contaminant molecules. The CNF membranes based on composite barrier layer were prepared by interfacial polymerization of polyamide [97]. After being treated with 1% trimesoyl chloride, the resulting membranes showed better filtration performance with a higher NaCl rejection. This behavior could be ascribed to the decrease in pore size with the cross-linking reaction between trimesoyl chloride and amino groups. The cross-linked PEG-CNF ultrafiltration membranes showed hydrophilic and excellent anti-fouling properties [98]. The flux of the composite layer was twice than that of commercial membranes, while the rejection was maintained more than 90%.

CNC composite membranes were fabricated with chitosan matrix for water purification [99]. CNC and Chitosan membranes were in a stable and nanoporous structure, while the pore size was in the range of 10–13 nm. At the low water flux, the removal efficiency of these membranes for rhodamine 6G, methyl violet and victoria blue were 70%, 90% and 98%, respectively. The high removal efficiency was ascribed to the electrostatic attraction between positively charged dyes and negatively charged CNC. A multi-layered nanocellulose membrane was prepared by vacuum-filtration CNF suspensions and carboxylate CNC for removing Fe(III)/Fe(II), Cu(II) and Ag(I) [100]. The properties of these membranes such as specific surface area, pore structure and wet strength could be tailored through acetone treatment, which could increase the pores and decrease the hydrogen bonding capability. The silk fibroin and CNF (CNF-SF) membranes showed special "shish kebab" nanostructures, which enabled to improve properties of these membranes, such as excellent mechanical performance, fast water permeation and high rejection ratio [101]. The rejection rate of these membranes for malachite green, brilliant blue, methylene blue and gold nanoparticles were 80%, 94%, 85% and 100%, respectively. The negative surface potential of the CNF-SF membranes contributed to high retention of positively charged particles.

Thiol-modified CNF membranes were embedded in electrospun PAN scaffold for the removal of Pb(II) and Cr(VI) [102]. The q_{max} for Pb(II) and Cr(VI) were 0.416 and 1.682 mmol g^{-1}, respectively. The high concentration of thiol groups and large surface area contributed to the high adsorption capacity. In addition, the resulting membranes could be regenerated more than three times with high removal efficiency, indicating that the thiol-modified CNF membrane could be a promising candidate for water purification applications. The CNF composite membranes modified with silver and platinum nanoparticles were used for water purification applications [103]. The polyvinylidenefluoride (PVDF) CNC membranes were prepared by electrospining technique for application in membrane distillation [104]. The CNC-PVDF matrix could improve the Young's modulus and tensile strength of the membranes. The liquid entry pressure was improved significantly, which was an important parameter to ensure high salt rejection of the membranes in membrane distillation.

7.2 Gas Adsorption

7.2.1 Greenhouse Gas Adsorption (CO_2)

The global warming and climate changes have become the most serious environmental issue, which caused by the increase of greenhouse gases [105, 106]. In order to control the emission of the greenhouse gases, many gas-adsorbing materials have been developed throughout the world. Since polysaccharides are sustainability, biodegradability and renewability, they have been applied to adsorption of polluted gases [107, 108].

A new type of membrane was fabricated by incorporating NH_2-MIL-Al filler into cellulose acetate (CA) matrix for separation of CO_2/N_2 and CO_2/CH_4 gas mixtures [109]. Compared to the previous results, the presence of NH_2-MIL-Al in CA matrix showed higher CO_2 separation performance. The ZIF-90 (MOFs) and TEMPO-CNF films were synthesized based on strong interactions for the separation of CO_2/CH_4 mixture [110]. According to the results, these films could separate CO_2/CH_4 gas mixtures completely. Because the permeance of the films for CO_2/CH_4 was inversely, which was negligible for CH_4, on the country, was high and constant for CO_2. The combination of nanoporous and TEMPO-CNF showed high selectivity for separation of CO_2/CH_4 mixture, and was expected to a promising candidate for high performance gas-separation materials. Diaminosilane N-[3-(Trimethoxysilyl) propyl] ethylenediamine (DAMO) modified CNF films were used as CO_2 adsorbent materials [111]. The CO_2 adsorption capacity of the modified CNF films from oat hulls, kraft pulp and corn husks were 1.27, 2.11 and 0.90 mmol g^{-1}, respectively. The chemisorption mechanism between the reactivity of CO_2 and amine groups contributed to the high adsorption capacity. The high-porosity, ultra-lightweight amino-modified spherical CNF aerogels were developed for CO_2 absorption [112]. Compared with conventional inorganic porous CO_2 adsorbents, the amino-modified CNF

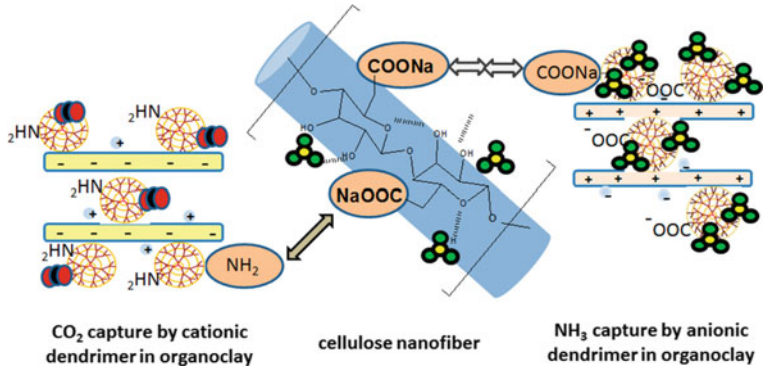

Fig. 7.7 Schematic representation of CO_2 and NH_3 gas adsorption on organoclay-TCNF film (Reproduced from [115])

aerogels showed excellent thermal stability and high CO_2 absorption capacity. The adsorption capacity of the modified CNF aerogels did not change significantly after ten cycles. The versatile functionalization method showed new opportunities for the design of novel advanced functional biomaterials in the CO_2 capture.

The application of cellulose acetate/silica (CA-SiO_2) fiber sorbents modified with polyethylenimine (PEI) was prepared for CO_2 capture [113]. The modified CA fibers were successfully proved in CO_2 capture with ultra-dilute suspension under both dry and humid conditions. The bamboo cellulose could adsorb CO_2 at relative humidity of 60–80% [114]. The TEMPO-CNF hybridized modified with organoclays were reported for gas adsorption due to the high adsorption capacity and selectivity on the gas adsorption, as shown in Fig. 7.7 [115]. The modified TEMPO-CNF films displayed higher adsorption and desorption of CO_2 gas in comparison with the other systems. The CO_2 gas was adsorbed and remained on cationic dendrimer sites in modified TEMPO-CNF films, which was easily desorbed from the films. The NH_3 adsorption was inversive to the CO_2 adsorption, while the CO_2 molecules adsorbed on the cationic dendrimers and the NH_3 molecules adsorbed on the anionic dendrimers were preferably captured in these adsorbents.

Polyethylenimine (PEI) modified CNF membranes were synthesized as adsorbents to separate CO_2 and H_2 gas mixture [116]. For the membrane separation technique, the concentration of PEI was from 3 to 15 wt%. According to the results, the CO_2 permeability was 16.72 bar and the corresponding selectivity of CO_2/H_2 was 0.15 with 3 wt% PEI coating. The Fe_3O_4 and TiO_2 modified cellulose via hydroxyl group interactions were reported for CO_2 separation [117]. The pressure decay technique demonstrated that Fe_3O_4 and TiO_2 increased the CO_2 sorption capacity and CO_2/N_2 selectivity of cellulose at all pressures. The CO_2 sorption ability of TiO_2-cellulose and Fe_3O_4-cellulose was 184.1 and 130.6 mg g^{-1}, respectively, in the condition of 30 bar and 298.15 K. The TiO_2-cellulose showed the best CO_2/N_2 selectivity capacity, which was approximately 270% higher than that of raw cellulose fibers. CO_2 sorption recycling experiments demonstrated high stability and reuse capacity

in CO_2 capture processes of TiO_2-cellulose. Due to their environmentally friendly nature and their excellent CO_2 sorption ability, these compounds deserved more attention in CO_2 capture.

The cross-linked carboxymethyl cellulose and ZIF nanosheets (CMC-ZIF) membranes were fabricated through a facile and organic-solvent-free method [118]. The anion charge repulsion effect between CMC and ZIF contributed to the high dispersion stability of the aqueous system. Based on the molecular sieving effect of ZIF and CMC matrix, gas permeation of the ZIF-CMC membranes showed a great improvement in gas selectivity such as CO_2, N_2, H_2 and CH_4 mixture. The content of the ZIF nanosheets in the CMC matrix was 30 wt% with the highest separation ability. The MOF-cellulose composite materials were prepared by MOF deposition onto precipitated calcium carbonate (PCC) filler in cellulose paper [119]. The PCC filler in the cellulose paper led to more hydroxyl groups available for facilitating the formation of small sized MOF crystals. According to the gas adsorption results, the MOF-cellulose paper exhibited a superior gas adsorption capacity including N_2, CO_2, H_2 and CH_4. The zeolite-chitosan composites were prepared by solvent exchange and calcination for adsorption and chemical fixation of CO_2 [120]. These results suggested that the mesoporous structure and interaction sites of the zeolite-chitosan composites contributed to CO_2 adsorption capacity and catalytic activity in chemical fixation of CO_2. The graphene oxide modified chitosan provided large surface area, high porosity and a large number of amine group, which facilitated the CO_2 adsorption [121]. The adsorption capacity of CO_2 was 0.257 mmol g^{-1} at 1 bar, which was significantly higher than the adsorption capacity of pure chitosan.

7.2.2 Toxic Gas Adsorption

With the rapid development of human community and industrialization, pollutions have induced serious impacts on public health [122]. Among various air pollutants, nitrogen oxides (NO_x), formaldehyde (HCHO), sulfur oxides (SO_x) and volatile organic compounds (VOC) can easily penetrate into human respiratory system [123, 124]. Researchers have paid more attention to develop green efficiency air filters for air purification [125–127].

The ZIF-CNF filters were fabricated for isolating pollutants, while the ZIF crystals enhanced composite filters with high gas adsorption capacity due to flexible adsorption structure and abundant open metal sites [128, 129]. The incorporation of ZIF increased the specific surface area of filter, strengthened the interactions between filter and particles. The filtration efficiencies of ZIF-CNF filters were 99.94% and 98.36% for 0.5 μm and 0.3 μm particles, respectively. Moreover, the N_2 adsorption efficiency of the filters was about 20-fold more than that of pure CNF filter. This multi-functional ZIF-CNF filter had great potential to be a high performance air filter for simultaneously purifying some toxic gases and PM2.5.

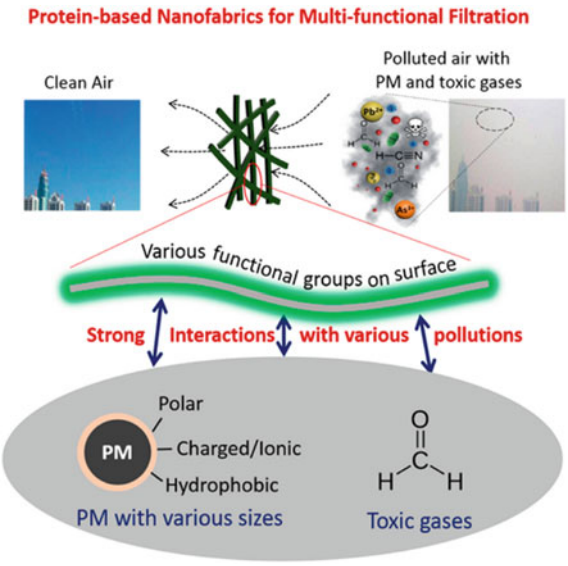

Fig. 7.8 Simplified representation of interaction-based filtration mechanism for SPI-based nanofabrics (Reproduced from [131])

A β-cyclodextrin (β-CD) modified chitosan was reported for the removal of HCHO pollution [130]. The abundant amino and hydroxyl groups of the β-cyclodextrin played an important role for the adsorption of HCHO. The adsorbent could be regenerated effectively, and the adsorption capacity remained above 95% after more than four cycles. The HCHO adsorption mechanism was a physicochemical adsorption with multi-molecular layer adsorption, which was the synergistic effect of the hydrogen bond interaction and Schiff base reaction. A poly(vinyl alcohol) (PVA) modified soy protein isolate (SPI) air filter was reported, as shown in Fig. 7.8 [131]. The resulting filter showed high adsorption capacity for both toxic gases (HCHO and CO) and pollutants particles, which were 90.90% and 62.50% for removal of CO and HCHO, respectively, and 99.80% for removal of PM2.5. The amino acids of proteins could significantly enhance the interactions between filter and pollutions. The SPI and bacterial cellulose (BC) composites also reported as high efficiency air filtering materials [132]. The network of BC contributed to the physical capturing of PM particles, while the functional groups of SPI further attracted the PM particles via electrostatic attraction. Removal efficiency of the resulting SPI/BC composite was 99.95% and 99.94% for PM10 and PM2.5, respectively. Activated carbon impregnated cellulose filters were fabricated to remove volatile organic compounds such as ethyl benzene, toluene and benzene [133]. The rapid removal efficiency was attributed to the high surface area of the activated carbon, which provided enough chance and time for the gases to be adsorbed.

7.3 Conclusions and Future Perspectives

In this review, we summarize and discuss various types of wastewater/gas adsorptions treatments. Polysaccharides nanomaterials exhibit well-known properties, such as low density, biodegradability, sustainability, renewability, nontoxicity and biocompatibility. Moreover, the increased specific surface area and nanosize effect of nanopolysaccharides not only increase the amount of adsorption sites but also offer the tailorability of the surface chemistry. Due to the high mechanical strength and dispersibility in water, they can be used as efficient adsorbent and flexible membranes to remove heavy metal ions, dyes, organic molecules and several other contaminants in wastewater. Membranes and flocculants based on polysaccharides displayed better performance in the filtration of a wide variety of contaminants. The combination of abundant polysaccharides provides a promising solution for air-filtration applications. The polysaccharides nanocomposites show high removal efficiency for both broad size range and toxic gases. However, we should focus more attention on reducing the cost of isolation of nanopolysaccharides as well as tailoring their surface functionalities for their development in wastewater/gas adsorptions treatment systems. Commercialization of nanopolysaccharides in environment treatment is seen as the next big step forward.

Acknowledgements The authors are grateful to the support of China Scholarship Council (CSC) under Grant No. 201806950016. LGP2 is part of the LabEx Tec 21 (Investissements d'Avenir—grant agreement n° ANR-11-LABX-0030) and of the PolyNat Carnot Institut (Investissements d'Avenir—grant agreement n° ANR-11-CARN-030-01).

References

1. Ali I, Gupta VK (2006) Advances in water treatment by adsorption technology. Nat Protoc 1:2661
2. Dich J, Zahm SH, Hanberg A et al (1997) Pesticides and cancer. Cancer Causes Control 8:420–443
3. Bhatnagar A, Sillanpää M (2010) Utilization of agro-industrial and municipal waste materials as potential adsorbents for water treatment—a review. Chem Eng J 157:277–296
4. Satyanarayana KG, Arizaga GG, Wypych F (2009) Biodegradable composites based on lignocellulosic fibers—an overview. Prog Polym Sci 34:982–1021
5. Ali I (2012) New generation adsorbents for water treatment. Chem Rev 112:5073–5091
6. Lin N, Huang J, Dufresne A (2012) Preparation, properties and applications of polysaccharide nanocrystals in advanced functional nanomaterials: a review. Nanoscale 4:3274–3294
7. Rajawat DS, Kardam A, Srivastava S et al (2013) Nanocellulosic fiber-modified carbon paste electrode for ultra trace determination of Cd(II) and Pb(II) in aqueous solution. Environ Sci Pollut Res 20:3068–3076
8. Roy D, Semsarilar M, Guthrie JT et al (2009) Cellulose modification by polymer grafting: a review. Chem Soc Rev 38:2046–2064
9. Dufresne A (2000) Dynamic mechanical analysis of the interphase in bacterial polyester/cellulose whiskers natural composites. Compos Interfaces 7:53–67

10. Dufresne A, Cavaillé JY, Helbert W (1997) Thermoplastic nanocomposites filled with wheat straw cellulose whiskers. Part II: effect of processing and modeling. Poly Compos 18:198–210
11. Favier V, Canova G, Cavaillé J et al (1995) Nanocomposite materials from latex and cellulose whiskers. Polym Adv Technol 6:351–355
12. Lin N, Dufresne A (2013) Supramolecular hydrogels from in situ host–guest inclusion between chemically modified cellulose nanocrystals and cyclodextrin. Biomacromol 14:871–880
13. Lin N, Dufresne A (2013) Physical and/or chemical compatibilization of extruded cellulose nano-crystal reinforced polystyrene nanocomposites. Macromolecules 46(14):5570–5583
14. Cui G, Liu M, Chen Y et al (2016) Synthesis of a ferric hydroxide-coated cellulose nanofiber hybrid for effective removal of phosphate from wastewater. Carbohydr Polym 154:40–47
15. Khajeh M, Laurent S, Dastafkan K (2013) Nanoadsorbents: classification, preparation, and applications (with emphasis on aqueous media). Chem Rev 113(10):7728–7768
16. Carpenter AW, de Lannoy CF, Wiesner MR (2015) Cellulose nanomaterials in water treatment technologies. Environ Sci Tech 49:5277–5287
17. Hokkanen S, Bhatnagar A, Sillanpää M (2016) A review on modification methods to cellulose-based adsorbents to improve adsorption capacity. Water Res 91:156–173
18. O'Connell DW, Birkinshaw C, O'Dwyer TF (2008) Heavy metal adsorbents prepared from the modification of cellulose: a review. Bioresour Technol 99:6709–6724
19. Liu P, Sehaqui H, Tingaut P et al (2014) Cellulose and chitin nanomaterials for capturing silver ions (Ag+) from water via surface adsorption. Cellulose 21:449–461
20. Kardam A, Raj KR, Srivastava S et al (2014) Nanocellulose fibers for biosorption of cadmium, nickel, and lead ions from aqueous solution. Clean Technol Environ Policy 16:385–393
21. Yu X, Tong S, Ge M et al (2013) Adsorption of heavy metal ions from aqueous solution by car-boxylated cellulose nanocrystals. J Environ Sc 25:933–943
22. Hokkanen S, Repo E, Sillanpää M (2013) Removal of heavy metals from aqueous solutions by succinic anhydride modified mercerized nanocellulose. Chem Eng J 223:40–47
23. Sehaqui H, de Larraya UP, Liu P et al (2014) Enhancing adsorption of heavy metal ions onto bi-obased nanofibers from waste pulp residues for application in wastewater treatment. Cellulose 21:2831–2844
24. Ma H, Hsiao BS, Chu B (2012) Ultrafine cellulose nanofibers as efficient adsorbents for removal of UO_2^{2+} in water. ACS Macro Lett 1:213–216
25. Kardam A, Rohit Raj K, Srivastava S (2012) Novel nano cellulosic fibers for remediation of heavy metals from synthetic water. Int J Nano Dimens 3:155–162
26. Srivastava S, Kardam A, Raj KR (2012) Nanotech reinforcement onto cellulosic fibers: green re-mediation of toxic metals. Int J Green Nanotechnol 4:46–53
27. Hokkanen S, Repo E, Suopajärvi T et al (2014) Adsorption of Ni(II): Cu(II) and Cd(II) from aqueous solutions by amino modified nanostructured microfibrillated cellulose. Cellulose 21:1471–1487
28. Hokkanen S, Repo E, Westholm LJ et al (2014) Adsorption of Ni^{2+}, Cd^{2+}, PO_4^{3-} and NO_3^- from aqueous solutions by nanostructured microfibrillated cellulose modified with carbonated hydroxyapatite. Chem Eng J 252:64–74
29. Kanel SR, Manning B, Charlet L et al (2005) Removal of arsenic(III) from groundwater by nanoscale zero-valent iron. Environ Sci Tech 39:1291–1298
30. Zhang N, Zang GL, Shi C et al (2016) A novel adsorbent TEMPO-mediated oxidized cellulose nanofibrils modified with PEI: Preparation, characterization, and application for Cu(II) removal. J Hazard Maters 316:11–18
31. Liu P, Borrell PF, Božič M et al (2015) Nanocelluloses and their phosphorylated derivatives for selective adsorption of Ag+, Cu^{2+} and Fe^{3+} from industrial effluents. J Hazard Maters 294:177–185
32. Sirviö JA, Hasa T, Leiviskä T et al (2016) Bisphosphonate nanocellulose in the removal of vanadium(V) from water. Cellulose 23:689–697
33. Sheikhi A, Safari S, Yang H et al (2015) Copper removal using electrosterically stabilized nano-crystalline cellulose. ACS Appl Mater Interfaces 7:11301–11308

34. Mohammed N, Baidya A, Murugesan V et al (2016) Diffusion-controlled simultaneous sensing and scavenging of heavy metal ions in water using atomically precise cluster-cellulose nanocrystal composites. ACS Sustain Chem Eng 4:6167–6176
35. Anirudhan TS, Deepa JR, Christa J (2016) Nanocellulose/nanobentonite composite anchored with multi-carboxyl functional groups as an adsorbent for the effective removal of cobalt(II) from nuclear industry wastewater samples. J Colloid Interface Sci 467:307–320
36. Anirudhan TS, Shainy F (2015) Effective removal of mercury(II) ions from chlor-alkali industrial wastewater using 2-mercaptobenzamide modified itaconic acid-grafted-magnetite nanocellulose com-posite. J Colloid Interface Sci 456:22–31
37. Hokkanen S, Repo E, Lou S et al (2015) Removal of arsenic(V) by magnetic nanoparticle activated microfibrillated cellulose. Chem Eng J 260:886–894
38. Zheng Q, Cai Z, Gong S (2014) Green synthesis of polyvinyl alcohol (PVA)–cellulose nanofibril (CNF) hybrid aerogels and their use as superabsorbents. J Mater Chem A 2:3110–3118
39. Zhou Y, Fu S, Zhang L et al (2014) Use of carboxylated cellulose nanofibrils-filled magnetic chitosan hydrogel beads as adsorbents for Pb(II). Carbohydr Polym 101:75–82
40. Mohammed N, Grishkewich N, Tam KC (2018) Cellulose nanomaterials: Promising sustainable nanomaterials for application in water/wastewater treatment processes. Environ Sci-Nano 5:623–658
41. Crini G (2006) Non-conventional low-cost adsorbents for dye removal: a review. Bioresour Technol 97:1061–1085
42. Rafatullah M, Sulaiman O, Hashim R et al (2010) Adsorption of methylene blue on low-cost ad-sorbents: a review. J Hazard Maters 177(1–3):70–80
43. He X, Male KB, Nesterenko PN et al (2013) Adsorption and desorption of methylene blue on porous carbon monoliths and nanocrystalline cellulose. ACS Appl Mater Inter 5:8796–8804
44. Yu HY, Zhang DZ, Lu FF et al (2016) New approach for single-step extraction of carboxylated cellulose nanocrystals for their use as adsorbents and flocculants. ACS Sustain Chem Eng 4:2632–2643
45. Batmaz R, Mohammed N, Zaman M et al (2014) Cellulose nanocrystals as promising adsorbents for the removal of cationic dyes. Cellulose 21:1655–1665
46. Jin L, Li W, Xu Q et al (2015) Amino-functionalized nanocrystalline cellulose as an adsorbent for anionic dyes. Cellulose 22:2443–2456
47. Eyley S, Thielemans W (2011) Imidazolium grafted cellulose nanocrystals for ion exchange appli-cations. Chem Commun 47:4177–4179
48. Qiao H, Zhou Y, Yu F et al (2015) Effective removal of cationic dyes using carboxylate-functionalized cellulose nanocrystals. Chemosphere 141:297–303
49. Zhou C, Lee S, Dooley K et al (2013) A facile approach to fabricate porous nanocomposite gels based on partially hydrolyzed polyacrylamide and cellulose nanocrystals for adsorbing methylene blue at low concentrations. J Hazard Maters 263:334–341
50. Zhou C, Wu Q, Lei T et al (2014) Adsorption kinetic and equilibrium studies for methylene blue dye by partially hydrolyzed polyacrylamide/cellulose nanocrystal nanocomposite hydrogels. Chem Eng J 251:17–24
51. Mohammed N, Grishkewich N, Berry RM et al (2015) Cellulose nanocrystal–alginate hydrogel beads as novel adsorbents for organic dyes in aqueous solutions. Cellulose 22:3725–3738
52. Mohammed N, Grishkewich N, Waeijen HA et al (2016) Continuous flow adsorption of methylene blue by cellulose nanocrystal-alginate hydrogel beads in fixed bed columns. Carbohydr Polym 136:1194–1202
53. Wang Y, Zhang X, He X et al (2014) In situ synthesis of MnO_2 coated cellulose nanofibers hybrid for effective removal of methylene blue. Carbohydr Polym 110:302–308
54. Xie K, Zhao W, He X (2011) Adsorption properties of nano-cellulose hybrid containing polyhedral oligomeric silsesquioxane and removal of reactive dyes from aqueous solution. Carbohydr Polym 83:1516–1520
55. Jin L, Sun Q, Xu Q et al (2015) Adsorptive removal of anionic dyes from aqueous solutions using microgel based on nanocellulose and polyvinylamine. Bioresour Technol 197:348–355

56. Pei A, Butchosa N, Berglund LA et al (2013) Surface quaternized cellulose nanofibrils with high water absorbency and adsorption capacity for anionic dyes. Soft Matter 9:2047–2055
57. Nypelö T, Rodriguez-Abreu C, Kolen'ko YV et al (2014) Microbeads and hollow microcapsules obtained by self-assembly of Pickering magneto-responsive cellulose nanocrystals. ACS Appl Mater Inter 6:16851–16858
58. Ma H, Wang S, Meng F et al (2017) A hydrazone-carboxyl ligand-linked cellulose nanocrystal aerogel with high elasticity and fast oil/water separation. Cellulose 24:797–809
59. Yang X, Cranston ED (2014) Chemically cross-linked cellulose nanocrystal aerogels with shape recovery and superabsorbent properties. Chem Mater 26:6016–6025
60. Jiang F, Hsieh YL (2014) Amphiphilic superabsorbent cellulose nanofibril aerogels. J Mater Chem A 2:6337–6342
61. Abraham E, Weber DE, Sharon S et al (2017) Multifunctional cellulosic scaffolds from modified cellulose nanocrystals. ACS Appl Mater Inter 9:2010–2015
62. Zhu G, Xu H, Dufresne A et al (2018) High-adsorption, self-extinguishing, thermal, and acoustic-resistance aerogels based on organic and inorganic waste valorization from cellulose nanocrystals and red mud. ACS Sustain Chem Eng 6:7168–7180
63. Zhang Z, Sèbe G, Rentsch D et al (2014) Ultralightweight and flexible silylated nanocellulose sponges for the selective removal of oil from water. Chem Mater 26:2659–2668
64. Korhonen JT, Kettunen M, Ras RH et al (2011) Hydrophobic nanocellulose aerogels as floating, sustainable, reusable, and recyclable oil absorbents. ACS Appl Mater Inter 3:1813–1816
65. Renault F, Sancey B, Charles J et al (2009) Chitosan flocculation of cardboard-mill secondary biological wastewater. Chem Eng J 155:775–783
66. Divakaran R, Pillai VS (2001) Flocculation of kaolinite suspensions in water by chitosan. Water Res 35:3904–3908
67. Nasser MS, James AE (2006) The effect of polyacrylamide charge density and molecular weight on the flocculation and sedimentation behaviour of kaolinite suspensions. Sep Purif Technol 52:241–252
68. Singh RP, Pal S, Mal D (2006) A high performance flocculating agent and viscosifiers based on cationic guar gum. Macromol Symp 242:227–234
69. Bolto B, Gregory J (2007) Organic polyelectrolytes in water treatment. Water Res 41:2301–2324
70. Özacar M, Şengil İA (2003) Evaluation of tannin biopolymer as a coagulant aid for coagulation of colloidal particles. Colloids Surf A 229:85–96
71. Khiari R, Dridi-Dhaouadi S, Aguir C et al (2010) Experimental evaluation of eco-friendly flocculants prepared from date palm rachis. J Environ Sci 22:1539–1543
72. Vandamme D, Eyley S, Van den Mooter G et al (2015) Highly charged cellulose-based nanocrystals as flocculants for harvesting Chlorella vulgaris. Bioresour Technol 194:270–275
73. Eyley S, Vandamme D, Lama S et al (2015) CO_2 controlled flocculation of microalgae using pH responsive cellulose nanocrystals. Nanoscale 7:14413–14421
74. Sun X, Danumah C, Liu Y et al (2012) Flocculation of bacteria by depletion interactions due to rod-shaped cellulose nanocrystals. Chem Eng J 198:476–481
75. Suopajärvi T, Liimatainen H, Hormi O et al (2013) Coagulation–flocculation treatment of munici-pal wastewater based on anionized nanocelluloses. Chem Eng J 231:59–67
76. Suopajärvi T, Koivuranta E, Liimatainen H et al (2014) Flocculation of municipal wastewaters with anionic nanocelluloses: Influence of nanocellulose characteristics on floc morphology and strength. J Environ Chem Eng 2:2005–2012
77. Quinlan PJ, Tanvir A, Tam KC (2015) Application of the central composite design to study the flocculation of an anionic azo dye using quaternized cellulose nanofibrils. Carbohydr Polym 133:80–89
78. Szyguła A, Guibal E, Palacín MA et al (2009) Removal of an anionic dye (Acid Blue 92) by coagulation–flocculation using chitosan. J Environ Manage 90:2979–2986
79. Renault F, Sancey B, Badot PM et al (2009) Chitosan for coagulation/flocculation processes—an eco-friendly approach. Eur Polym J 45:1337–1348

80. Bina B, Mehdinejad M, Nikaeen M et al (2009) Effectiveness of chitosan as natural coagulant aid in treating turbid waters. J Environ Health Sci Eng 6:247–252
81. Hesami F, Bina B, Ebrahimi A et al (2012) Arsenic removal by coagulation using ferric chloride and chitosan from water. Int J Environ Health Eng 1:1–6
82. Leiviskä T, Sarpola A, Tanskanen J (2012) Removal of lipophilic extractives from debarking wastewater by adsorption on kaolin or enhanced coagulation with chitosan and kaolin. Appl Clay Sci 61:22–28
83. Martínez TDCC, Rodríguez RA, Voltolina D et al (2016) Effectiveness of coagulants-flocculants for removing cells and toxins of Gymnodinium catenatum. Aquaculture 452:188–193
84. Rios-Donato N, Navarro R, Avila-Rodriguez M et al (2012) Coagulation–flocculation of colloidal suspensions of kaolinite, bentonite, and alumina by chitosan sulfate. J Appl Polym Sci 123:2003–2010
85. Wang JP, Chen YZ, Yuan SJ et al (2009) Synthesis and characterization of a novel cationic chi-tosan-based flocculant with a high water-solubility for pulp mill wastewater treatment. Water Res 43:5267–5275
86. Yang Z, Yang H, Jiang Z et al (2013) Flocculation of both anionic and cationic dyes in aqueous solutions by the amphoteric grafting flocculant carboxymethyl chitosan-graft-polyacrylamide. J Hazard Maters 254:36–45
87. Yang Z, Shang Y, Lu Y et al (2011) Flocculation properties of biodegradable amphoteric chitosan-based flocculants. Chem Eng J 172:287–295
88. Lu Y, Shang Y, Huang X et al (2011) Preparation of strong cationic chitosan-graft-polyacrylamide flocculants and their flocculating properties. Ind Eng Chem Res 50:7141–7149
89. Park HB, Kamcev J, Robeson LM et al (2017) Maximizing the right stuff: the trade-off between membrane permeability and selectivity. Science 356:eaab0530
90. Pearce G (2007) Introduction to membranes: filtration for water and wastewater treatment. Filtr Separat 44:24–27
91. Metreveli G, Wågberg L, Emmoth E et al (2014) A size-exclusion nanocellulose filter paper for virus removal. Adv Healthcare Mater 3:1546–1550
92. Quellmalz A, Mihranyan A (2015) Citric acid cross-linked nanocellulose-based paper for size-exclusion nanofiltration. ACS Biomater Sci Eng 1:271–276
93. Asper M, Hanrieder T, Quellmalz A et al (2015) Removal of xenotropic murine leukemia virus by nanocellulose based filter paper. Biologicals 43:452–456
94. Ma H, Burger C, Hsiao BS et al (2014) Fabrication and characterization of cellulose nanofiber based thin-film nanofibrous composite membranes. J Membr Sci 454:272–282
95. Ma H, Burger C, Hsiao BS et al (2011) Nanofibrous microfiltration membrane based on cellulose nanowhiskers. Biomacromol 13:180–186
96. Wang R, Guan S, Sato A et al (2013) Nanofibrous microfiltration membranes capable of remov-ing bacteria, viruses and heavy metal ions. J Membr Sci 446:376–382
97. Wang X, Yeh TM, Wang Z et al (2014) Nanofiltration membranes prepared by interfacial polymerization on thin-film nanofibrous composite scaffold. Polymer 55:1358–1366
98. Wang Z, Ma H, Hsiao BS et al (2014) Nanofibrous ultrafiltration membranes containing cross-linked poly (ethylene glycol) and cellulose nanofiber composite barrier layer. Polymer 55:366–372
99. Karim Z, Mathew AP, Grahn M et al (2014) Nanoporous membranes with cellulose nanocrystals as functional entity in chitosan: removal of dyes from water. Carbohydr Polym 112:668–676
100. Karim Z, Claudpierre S, Grahn M et al (2016) Nanocellulose based functional membranes for water cleaning: tailoring of mechanical properties, porosity and metal ion capture. J Membr Sci 514:418–428
101. Xiong R, Kim HS, Zhang S et al (2017) Template-guided assembly of silk fibroin on cellulose nanofibers for robust nanostructures with ultrafast water transport. ACS Nano 11:12008–12019

102. Yang R, Aubrecht KB, Ma H et al (2014) Thiol-modified cellulose nanofibrous composite membranes for chromium(VI) and lead(II) adsorption. Polymer 55:1167–1176
103. Cruz-Tato P, Ortiz-Quiles EO, Vega-Figueroa K et al (2017) Metalized nanocellulose composites as a feasible material for membrane supports: design and applications for water treatment. Environ Sci Tech 51:4585–4595
104. Lalia BS, Guillen E, Arafat HA et al (2014) Nanocrystalline cellulose reinforced PVDF-HFP membranes for membrane distillation application. Desalination 332:134–141
105. Karl TR, Trenberth KE (2003) Modern global climate change. Science 302:1719–1723
106. Nel A, Xia T, Mädler L et al (2006) Toxic potential of materials at the nanolevel. Science 311:622–627
107. Yoon K, Hsiao BS, Chu B (2008) Functional nanofibers for environmental applications. J Mater Chem 18:5326–5334
108. Bhardwaj R, Mohanty AK, Drzal LT et al (2006) Renewable resource-based green composites from recycled cellulose fiber and poly (3-hydroxybutyrate-co-3-hydroxyvalerate) bioplastic. Biom-acromolecules 7:2044–2051
109. Mubashir M, Yeong YF, Lau KK et al (2018) Efficient CO_2/N_2 and CO_2/CH_4 separation using NH_2-MIL-53 (Al)/cellulose acetate (CA) mixed matrix membranes. Sep Purif Technol 199:140–151
110. Matsumoto M, Kitaoka T (2016) Ultraselective gas separation by nanoporous metal–organic frameworks embedded in gas-barrier nanocellulose films. Adv Mater 28:1765–1769
111. Valdebenito F, García R, Cruces K et al (2018) CO_2 adsorption of surface-modified cellulose nanofibril films derived from agricultural wastes. ACS Sustain Chem Eng 6:12603–12612
112. Liu S, Zhang Y, Jiang H et al (2018) High CO_2 adsorption by amino-modified bio-spherical cellulose nanofibres aerogels. Environ Chem Lett 16:605–614
113. Sujan A, Pang SH, Zhu G et al (2019) Direct CO_2 capture from air using poly (ethyleneimine)-loaded polymer/silica fiber sorbents. ACS Sustain Chem Eng 33:1745–1752
114. Hou C, Wu Y, Wang T et al (2018) Preparation of quaternized bamboo cellulose and its implication in direct air capture of CO_2. Energ Fuel 33:1745–1752
115. Shah KJ, Imae T (2016) Selective gas capture ability of gas-adsorbent-incorporated cellulose nanofiber films. Biomacromol 17:1653–1661
116. Wu SY, Hsiao IC, Liu CM et al (2017) A novel bio-cellulose membrane and modified adsorption approach in CO_2/H_2 separation technique for PEM fuel cell applications. Int J Hydrogen Macromol 42:27630–27640
117. Campbell S, Bernard FL, Rodrigues DM et al (2019) Performance of metal-functionalized rice husk cellulose for CO_2 sorption and CO_2/N_2 separation. Fuel 239:737–746
118. Zhang F, Dou J, Zhang H (2018) Mixed membranes comprising carboxymethyl cellulose (as capping agent and gas barrier matrix) and nanoporous ZIF-L nanosheets for gas separation applications. Polymers 10:1340
119. Yang Q, Zhang M, Song S et al (2017) Surface modification of PCC filled cellulose paper by MOF-5 ($Zn_3(BDC)_2$) metal–organic frameworks for use as soft gas adsorption composite materials. Cellulose 24:3051–3060
120. Kumar S, Prasad K, Gil JM et al (2018) Mesoporous zeolite-chitosan composite for enhanced capture and catalytic activity in chemical fixation of CO2. Carbohydr Polym 198:401–406
121. Hsan N, Dutta PK, Kumar S et al (2019) Chitosan grafted graphene oxide aerogel: Synthesis, characterization and carbon dioxide capture study. Int J Biol Macromol 125:300–306
122. Zhang S, Tang N, Cao L et al (2016) Highly integrated polysulfone/polyacrylonitrile/polyamide-6 air filter for multilevel physical sieving airborne particles. ACS Appl Mater Inter 8:29062–29072
123. Zhang Y, Yuan S, Feng X et al (2016) Preparation of nanofibrous metal–organic framework filters for efficient air pollution control. J Am Chem Soc 138:5785–5788
124. Souzandeh H, Scudiero L, Wang Y et al (2017) A disposable multi-functional air filter: Paper towel/protein nanofibers with gradient porous structures for capturing pollutants of broad species and sizes. ACS Sustain Chem Eng 5:6209–6217

125. Nemoto J, Saito T, Isogai A (2015) Simple freeze-drying procedure for producing nanocellulose aerogel-containing, high-performance air filters. ACS Appl Mater Inter 7:19809–19815
126. Xu J, Liu C, Hsu PC et al (2016) Roll-to-roll transfer of electrospun nanofiber film for high-efficiency transparent air filter. Nano Lett 16:1270–1275
127. Zhang S, Liu H, Zuo F et al (2017) A controlled design of ripple-like polyamide-6 nanofiber/nets membrane for high-efficiency air filter. Small 13:1603151
128. Ma S, Zhang M, Nie J et al (2018) Multifunctional cellulose-based air filters with high loadings of metal–organic frameworks prepared by in situ growth method for gas adsorption and antibacterial ap-plications. Cellulose 25:5999–6010
129. Su Z, Zhang M, Lu Z et al (2018) Functionalization of cellulose fiber by in situ growth of zeolitic imidazolate framework-8 (ZIF-8) nanocrystals for preparing a cellulose-based air filter with gas ad-sorption ability. Cellulose 25:1997–2008
130. Yang Z, Miao H, Rui Z et al (2019) Enhanced formaldehyde removal from air using fully biodegradable chitosan grafted β-cyclodextrin adsorbent with weak chemical interaction. Polymers 11:276
131. Souzandeh H, Johnson KS, Wang Y et al (2016) Soy-protein-based nanofabrics for highly efficient and multifunctional air filtration. ACS Appl Mater Inter 8:20023–20031
132. Liu X, Souzandeh H, Zheng Y et al (2017) Soy protein isolate/bacterial cellulose composite membranes for high efficiency particulate air filtration. Compos Sci and Technol 138:124–133
133. Kim SY, Yoon YH, Kim KS (2016) Performance of activated carbon-impregnated cellulose filters for indoor VOCs and dust control. Int J Environ Sci Technol 13:2189–2198

Chapter 8
Nanopolysaccharides in Surface Coating

Hale Oguzlu and Feng Jiang

Abstract Surface coating represents a process that modifies the properties and functionalities of a bulk material by applying a thin layer of coating material. Depending on the coating material characteristics and targeted performance, the coating layer can range from a few nm to hundreds of μm or even mm thick. Nanopolysaccharides have been widely used as coating materials due to the interesting nanoscale dimension, abundant surface functional groups, low gas permeability, and excellent mechanical properties. This chapter summaries the most recent progress in coating techniques and applications of nanopolysaccharides as coating materials. The coating of nanopolysaccharides can be achieved either at the molecular/nanoscale level (Langmuir deposition, spin coating, and layer-by-layer deposition) or at large scale (dip coating and spray coating) and continuous production scale (roll-to-roll coating). In terms of coating applications, nanopolysaccharides can serve as rheology modifier for conventional coating materials, reinforcing filler in nanocomposites, or as standalone coating material for food packaging, photonic devices, biomedical devices, structural and building materials, as well as onto traditional substrates such as paper, plastic, and fabrics.

Keywords Nanopolysaccharides · Coating techniques · Applications · Rheology modifiers

8.1 Introduction

Surface coatings are utilized in numerous applications that offer protection and/or functionality, improvements in overall performance and lifetimes of products. The advantage of surface coating lies in several aspects including tuning the surface physical and chemical properties of the bulk materials, enhancing the physical performance of some intrinsically under-performed materials, and adding extra barrier and/or

H. Oguzlu · F. Jiang (✉)
Sustainable Functional Biomaterials Laboratory, Department of Wood Science, University of British Columbia, Vancouver, BC V6T1Z4, Canada
e-mail: feng.jiang@ubc.ca

N. Lin et al. (eds.), *Advanced Functional Materials from Nanopolysaccharides*,
Springer Series in Biomaterials Science and Engineering 15,
https://doi.org/10.1007/978-981-15-0913-1_8

functional layer for desired functionalities. In recent years, fossil fuel depletion and environmental concerns have driven the development of more ecologically friendly coating materials, to limit the use of either synthetic polymeric coating materials or organic solvent. Nanopolysaccharides are naturally derived polymeric nanomaterials that form stable aqueous suspension. The lateral dimension of nanopolysaccharides is around a few to tens of nm and the length can vary from a few hundred nm to microns. The nanoscale lateral dimension of nanopolysaccharides offers them high transparency, strong affinity to each other and other substrates, high packing density, small roughness and good film forming properties. Therefore, nanopolysaccharides have great potential to replace or supplement conventical coating materials, and have found numerous applications in food packaging, biomedical, electronics, and optical sensors. As waterborne coating material, nanopolysaccharides can be applied either by themselves or as additives into other natural or synthetic coating materials.

Nanopolysaccharides are typically extracted from biomass (cellulose, chitin and starch) by chemical/biological hydrolysis, surface oxidation/derivatization, and mechanical disintegration methods. One criterion for deriving nanopolysaccharides using these chemical/biological/mechanical processes should be the preservation of natural crystal structure, whereas the amorphous region could be largely or partially removed. Depending on source of the biomass, nanopolysaccharides can be classified into three categories (Fig. 8.1): (1) nanocellulose (NC) including cellulose nanocrystals (CNC), cellulose nanofibers (CNF) and bacterial nanocelluloses (BNC), (2) nanochitin (NCh) including chitin nanocrystals (ChNC) and chitin nanofibers (ChNF), and (3) nanostarches (NS). The source materials and preparation methods for synthesizing nanopolysaccharides can significantly affect the morphology, dimensions, surface functional groups, and charge density, and therefore lead to different physical properties of the coated layers. For detailed preparation methods and characteristics of the nanopolysaccharides, readers can refer to Chap. 1 of this book and other review articles [1, 2]. Physical properties, such as thickness, surface roughness, and packing density, could also be tuned by different coating methods, including

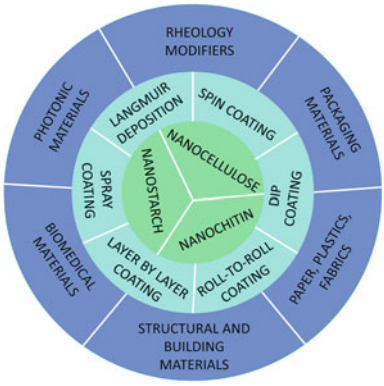

Fig. 8.1 Major coatings techniques and applications of nanopolysaccharides

spin coating, Langmuir deposition, dip coating, spray coating, layer-by-layer coating, roll-to-roll coating, and other coating methods such as screen and inject printing. These printing techniques will first be reviewed for their application in coating nanopolysaccharides, as well as some of the critical parameters used for controlling the properties of coating layers. The chapter will continue to develop on the application of nanopolysaccharides as coating materials, including using nanopolysaccharides as rheology modifier, for packaging materials with enhanced barrier and mechanical properties, as photonic and biomedical devices, and for structural and building materials, as well as onto other conventional substrates.

8.2 Coating Techniques and Theory

8.2.1 Spin Coating

Spin coating is a technique used to produce uniformly smooth and ultrathin film from polymer solution or nanoparticle dispersion by high speed centrifugal spinning. The process of spin coating starts by dispensing excess amount of solution/suspension to completely cover the substrate surface, followed by acceleration of the substrate to get rid of the liquid completely. Inertial centrifugal forces lead to flinging of the liquid from the edge of substrate until it reaches solid-like behavior due to a dramatic viscosity increase from solvent evaporation. The final thinning of the film depends on solvent evaporation [3]. Based on studies of Meyerhofer [4], Bornside et al. [5], and Lawrence and Zhou [6], the final thickness (h_f) of the spin-coated film can be predicted from the following assumptions: (1) solvent evaporation do not affect radial outflow driven convective thinning, (2) convective thinning equals to evaporation rate, and (3) enough time is given to complete the spinning process. The spin-coated final film thickness, h_f is then defined with the following expression:

$$h_f \propto \omega^{-1/2} \eta^{1/3} c_0^{1/3} \tag{8.1}$$

where ω denotes the spinning velocity, η is the viscosity of the coating solution while c_0 represents its initial concentration. This relationship shows that the final thickness of the spin-coated film depends on physical properties of the coating solution and spin speed of the disk [7]. In general, the spin-coated film thickness increases with the increasing concentration and decreases with the increasing spinning speed at fixed concentration (Fig. 8.2a), as being observed for cellulose nanofibrils (CNFs) [8] and chitin nanocrystals (ChNC) films [9, 10]. Study found that spin-coating cellulose nanocrystals (CNCs) with different concentrations (c) could result in smooth and colorless film at c < 1.7%, faint brown film at 3–4%, blue colored film at 7–8% (Fig. 8.2b), and then purple colored film at 11%, which has been identified as the highest possible concentration for spin coating [11]. In addition, due to the high radial velocity of the spin coating process, it is possible to orient the nanocrystals in the

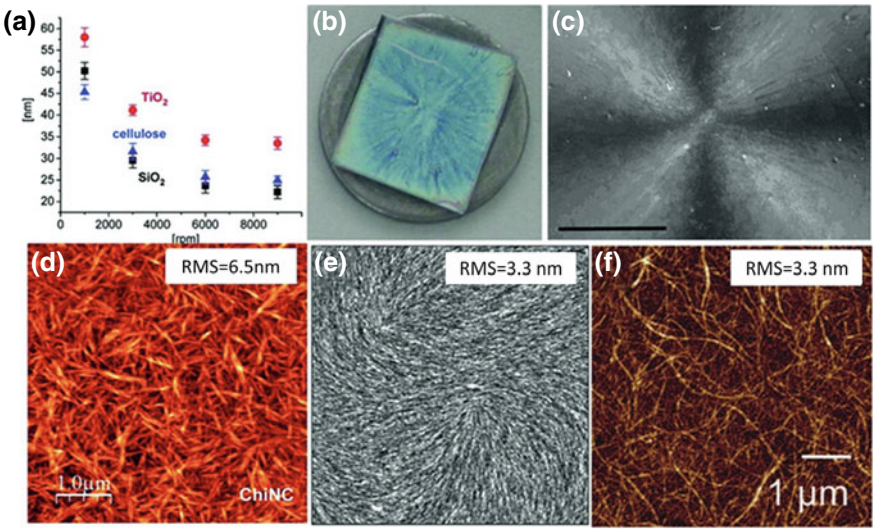

Fig. 8.2 **a** Film thickness as determined by ellipsometry of closed films (full coverage) spin coated from 20 g/L cellulose nanocrystal dispersion on silica, titania, and cellulose substrates as a function of different spinning speeds (Reproduced from [14]), **b** appearance of cellulose I film spin-coated from nanocrystal suspension on silicon wafer (Reproduced from [15]), **c** a digital image between crossed polarizers of a cellulose suspension spin-coated onto a glass surface, showing the radial orientation of the cellulose nanocrystals (Reproduced from [11]), and AFM height images of spin-coated, **d** ChNCs (Reproduced from [9]), **e** CNCs (Reproduced from [13]) and **f** CNFs (Reproduced from [16])

radial direction from the centre point to display a Maltese cross pattern (Fig. 8.2c) [12]. The surface roughness of the spin-coated nanocellulose and nanochitin films are generally in the range of a few nm (Fig. 8.2d–f), but it is highly dependent on the morphology and surface charge of the nanocrystals [13]. Other than the spin-coating parameters and nanocrystal characteristics, it has been found that the film properties also depend on the specific interaction between different substrates and nanocrystals [14]. It is discovered that CNCs tend to form a thicker film on Titania than those on silica and cellulose, which should be ascribed to the electrostatic adsorption of negatively charged CNCs on positively charged Titania substrate.

8.2.2 Langmuir Deposition

Langmuir deposition is a coating technique that transfer a monolayer of amphiphiles from air-liquid interface onto a solid substrate by dipping and withdrawing the substrate in a Langmuir trough under constant surface pressure. Due to the different polarities of the amphiphiles at the two ends, they tend to form a monolayer at the air-water interface with the hydrophobic tail pointing towards air, which can lower

the surface tension of water. The surface tension difference between the sub-phase solution without (γ_0) and with (γ) a monolayer is defined as surface pressure (π), $\pi = \gamma_0 - \gamma$. For Langmuir deposition, the monolayer property is generally defined by the surface pressure through a surface pressure/area isotherm, which could be facilely adjusted mechanically by controlling the area per molecule ($A_M = A/N_M$) with a moveable barrier. For efficient cohesion of the monolayer and homogeneous coated layer, surface pressure should be high enough for amphiphiles to pack closely and homogeneously cover the surface, as well as not exceed the collapse pressure where monolayer collapses into disordered multilayers. Once monolayer is formed at the air-water interface, deposition of monolayer film onto a solid substrate could be accomplished using two different methods, either vertically "dipping" or horizontally "lifting", named as Langmuir Blodgett (LB, Fig. 8.3a) deposition and Langmuir-Schaefer (LS, Fig. 8.3c) deposition, respectively [17].

Langmuir deposition of cellulose nanocrystals derived from tunicin, ramie, sisal and cotton were firstly investigated by Habibi et al. using both LB [18] and LS technique [19]. Although CNC is generally considered amphiphilic nanoparticles, negligible amount will adsorb at the air-water interface, as being previously demonstrated that CNC could only lower the surface tension of water to 67 mN/m at 1% [20]. In this first trial, cationic surfactant dimethyldioctadecylammonium (DODA) was added to interact with CNC through electrostatic interaction and carry the adsorbed CNC to the interface. The addition of CNC in the sub-phase leads to an increase in surface pressure due to better packing of DODA molecules at interface as the surface groups on CNC could screen the electrostatic repulsion between DODA head groups to decrease the repulsion. It is found that homogeneous and compact CNC monolayer could be formed at surface pressure greater than 40 mN/m and higher CNC concentration in

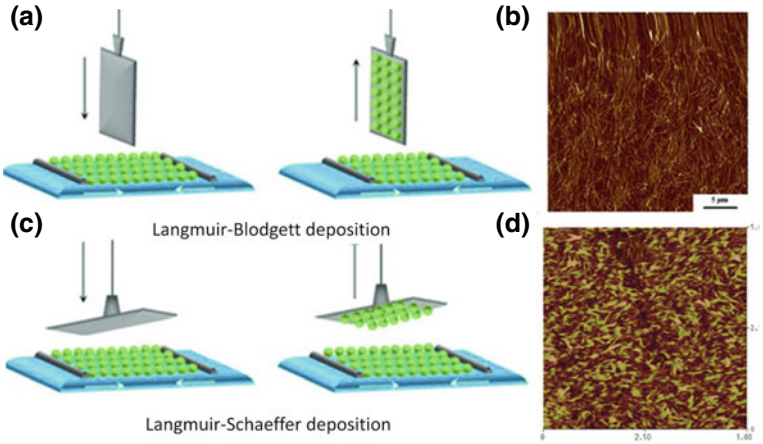

Fig. 8.3 Illustration of **a** Langmuir-Blodgett and **c** Langmuir-Schaefer deposition experimental setups (Reproduced from [22]) and AFM images of **b** LB deposited CNCs films at 55 mN/m surface pressure (Reproduced from [18]) and **d** LS deposited CNCs films at 60 mN/m surface pressure (Reproduced from [19])

the sub-phase, with the monolayer thickness of 7 nm for ramie CNCs and 9.3 nm for tunicin CNCs, corresponding to their respective thickness of individual CNC. The roughness of the coating CNCs monolayer is 1.8 and 3.1 nm for ramie and tunicin CNCs, respectively, indicating smooth surface by the LB technique. AFM image of the tunicin CNC LB film indicated preferentially aligned CNCs along the dipping direction (Fig. 8.3b). Due to the horizontal "lifting" method, LS technique has the advantages of coating the substrate only onto one surface through the hydrophobic interaction between the hydrophobic tail of DODA and the alkyl chain modified gold substrate, as well as no anchoring surfactant on the top surface of the deposited CNC monolayer, making it ideal monolayer for surface analysis. In addition, the packing and orientation of the CNC is strongly affected by the surface pressure, showing that a closely packed and well-organized CNC film could be formed at 60 mN/m surface pressure (Fig. 8.3d). Unmodified CNCs were also observed to adsorb at the air-water interface when the surface charges were screened by increasing salt concentration, which could increase the adsorption energy and reduce the exclude volume. The LS deposited film by unmodified CNC showed a CNC monolayer with surface coverage of 21% [21].

8.2.3 Dip Coating

Both spin-coating and Langmuir deposition are desired for coating nanometer thick or monolayer nanopolysaccharides onto smooth substrate using dilute suspension. For thicker coating in the micrometer range and onto more generalized substrate, it is necessary to explore other coating techniques that do not involve delicate setup and could be operated using wider solution concentration ranges. Dip coating is a simple technique to create uniform films onto both flat and heterogeneous substrates. A general dip-coating process involves immersing the substrate into a coating bath containing solution or dispersion of coating material, stabilizing the substrate in the coating bath, withdrawing the substrate from the coating bath at a constant speed, and then drying the film by evaporation of excess liquid (Fig. 8.4a). In the steady state flow regime, the coating thickness from Newtonian fluid could be predicted based on the balance between viscous force, surface tension (capillary force) and gravity, as being proposed by Landau and Levich [23] and then Derjaguin [24]. The coating thickness increases with increasing withdrawal velocity (Fig. 8.4b), which is confirmed by the study of Mendoza-Galvan et al. on dip coating of 5.7 wt% of CNC onto glass slides [25]. The dip-coated CNC films with a speed of 10 and 20 cm/min result film thickness of 2.8 and 6.0 μm, respectively. The withdrawal velocity during dip-coating has also been found to affect the orientation of CNCs as the drag of draining forces could align the CNC during drainage (Fig. 8.4c). Further concentrating CNC suspension under gravity could freeze the CNCs in a partial nematic ordering, resulting a linear polarizer film that could block the linearly polarized light emitted from a LCD screen [25]. In addition, as expected, both the coating thickness and surface coverage increase with increasing numbers of sequential dipping

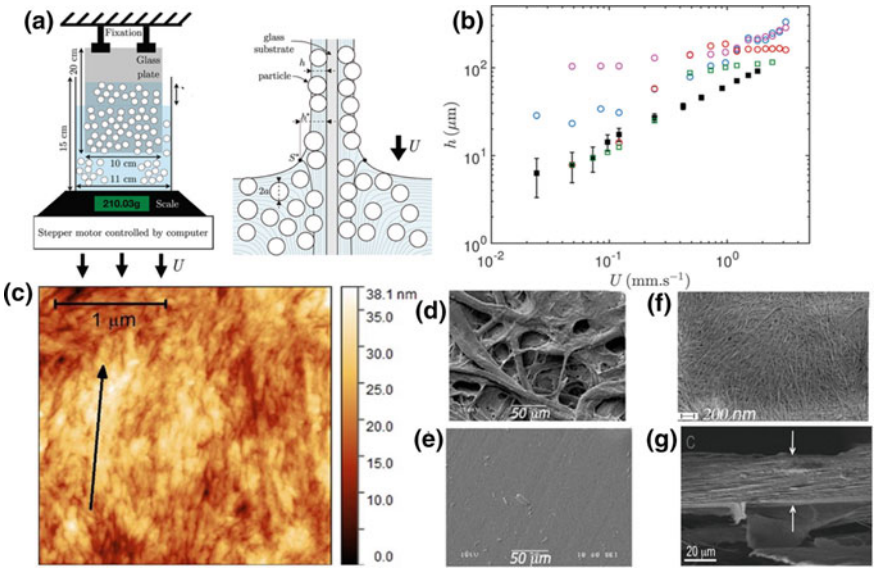

Fig. 8.4 **a** Illustration of the dip coating experimental setup [28], **b** average thickness of the coating layer after the withdrawal of the plate with respect to the withdrawal speed (Reproduced from [28]), **c** AFM images of dip-coated CNC films, SEM images of **d** uncoated coarse fiber substrate [27] and **e** dip-coated [27] samples with 5 layers of NCs , **f** dip-coated sample with 10 layers of NC [27] and **g** cross-sections of the fractured NC coatings (Reproduced from [27])

[26]. As previously described, one advantage of the dip-coating technique is that it could be used to coat heterogeneous and rough surface. In fact, it is observed that dip-coating is preferable for coating nanocellulose onto paper substrate that cover the coarse fibers with a uniform nanocellulose layer of thickness of 9 μm with 5 layers coating (Fig. 8.4d–g) [27].

8.2.4 Spray Coating

Spray coating is a common method for applying solution or suspension of the coating materials onto substrate at both laboratory and industrial scales. The process of spray coating has three steps: (1) atomization of coating fluid to droplets, (2) transportation of atomized droplets towards the substrate, and (3) film formation due to the impact of the droplets on the surface. During the atomization process, the bulk liquid is first transformed into a liquid sheet, then into liquid ligaments, at last into a droplet when the disruptive stresses exceed the cohesive stresses capable of holding it together for a sufficient duration. Atomization can be achieved through external pressure, supercritical process, electrostatic process, acoustic energy, or centrifugal force [29]. For instance, disruptive stress maintains by applying voltage in electrostatic process.

The characteristics of the coating film by spray coating can be manipulated by a numbers of process parameters including pressure of carrier gas, aperture of the spray nozzle, distance between nozzle and substrate, angle of impact, form of the spray jet, and the velocity of the nozzle and substrate. In addition, properties of coating solution and suspension including viscosity, particle size, and volatility of solvent also control the thickness and surface structure of the coatings [30]. The coating thickness of the cellulose nanofibrils defibrillated by Super Masscolloider ranges from 5.8–11.0 μm, which is directly correlated to basic weight and is determined by the synergistic effect of suspension concentration, nozzle pressure, distance to the substrate, and the spraying time [31]. Coating paper using CNF or CNF/nanoclay has shown to increase the tensile strength, and reduce both water and oxygen permeability [31, 32]. For continuous coating, spray coating could also be operated over a conveyor, where the thickness of spray-coated nanocellulose on a metal surface could be affected by the suspension concentration [33, 34], conveyor velocity [34], nozzle form [34], pressure [34] and set up configuration [34]. An increase in concentration of CNC suspension and a decrease in conveyor velocity result in an increase in basis weight and thicker films. Higher velocities and higher concentration lead to more uniform films.

8.2.5 Layer by Layer Coating

Layer by layer (LBL) is a basic technique for fabrication of multilayer coatings onto solid substrate from solution or dispersion based on physical bonds, mainly electrostatic interactions or other intermolecular interactions (e.g. Hydrogen bonding, π–π stacking forces, hydrophobic interactions, and charge-transfer interactions) between two or more different materials. LBL technique can be achieved with different coating technologies including solution dipping, spin coating, spray coating, electromagnetic and microfluidic coatings [35]. The advantages of this technique are simplicity and versatility, with the possibility of controlling the thickness at nanoscale or even molecular level [36].

Both sulfuric acid hydrolyzed CNCs and oxidized CNFs carry negative surface charge of sulfate and carboxylate (or carboxymethylate) groups, respectively, enabling them to interact with cationic polyelectrolyte such as poly (diallyl dimethyl ammonium chloride) (PDDA), Polyethylenimine (PEI), papaverine hydrochloride (PAHCl), poly (allylamine hydrochloride) (PAH) or chitosan (CS) to form multilayer films by layer-by-layer assembly (Table 8.1) [37–45]. As a common practice, LBL coating is achieved by alternately dipping the substrate into oppositely charged polyelectrolyte suspension or solution. LBL coating of CNCs and PDDA leads to consistent individual bilayer thickness of 11 nm (Fig. 8.5a) [37]. The rigid and long CNCs from tunicate can pile up during LBL assembly to create nanoporous structure showing strong antireflective characteristics (Fig. 8.5b) [46]. LBL coating has been found to transfer the ordered chiral nematic phases of CNCs onto substrates, resulting an ordered film by coating from the anisotropic phase of CNCs (Fig. 8.5c) [40] or under magnetic field for extended time [47]. Multilayer film assembled from PAH

Table 8.1 Review of LBL coatings of nano-polysaccharides

Nanopolysaccharides	Source, preparation method and dimension	Oppositely charged material	Substrate	Coating method	Number of layers	Layer thickness (nm)	References
CNC	Whatman paper Sulfuric acid hydrolysis d: 5 nm L: 100–300 nm	PDDA	Glass	Dip coating	1–10 bilayers	≈10–118	[37]
CNC	Whatman filter paper Sulfuric acid hydrolysis d: 5–10 nm, L: 100–200 nm	PAH	Silicon	Dip coating Spin coating	10–25 bilayers	10–500	[38]
CNC	Whatman filter paper Sulfuric acid hydrolysis d: 5–10 nm, L: 100–200 nm	PAH	Silicon	Dip coating	6–25 bilayers	108–480	[39]
CNC	Deuterated and unmodified cotton linters Sulfuric acid hydrolysis d: 5–10 nm, L: 100–200 nm	PEI PAH	Silicon	Dip coating	1–7 bilayers	30–206	[40]

(continued)

Table 8.1 (continued)

Nanopolysaccharides	Source, preparation method and dimension	Oppositely charged material	Substrate	Coating method	Number of layers	Layer thickness (nm)	References
CNC	Sulfite pulp Sulfuric acid and hydrochloric acid hydrolysis d: 3–7 nm, L: 300–500 nm	PAHCl	Glass Filter paper	Spin coating	25 alternate layers	265–425	[41]
CNC	Eucalyptus wood pulp Sulfuric acid hydrolysis d: 6 nm, L: 145 nm	CS	Glass	Dip coating	20 bilayers	140	[42]
CNC	Cotton linter Sulfuric acid hydrolysis	CS	Glass Silicon	Dip coating	5–40 bilayers	20–780	[43]
CNC	Deuterated cotton linters Sulfuric acid hydrolysis d: 5–10 nm, L: 100–200 nm	Xyloglucan	Silicon	Dip coating Spin coating Spray coating	6 bilayers	18–70	[50]

(continued)

Table 8.1 (continued)

Nanopolysaccharides	Source, preparation method and dimension	Oppositely charged material	Substrate	Coating method	Number of layers	Layer thickness (nm)	References
CNF	Sulfite softwood pulp High-pressure homogenization with carboxymethylation d: 5–15 nm, L: up to 1 μm	PEI PDADMAC PAH	Silicon	Dip coating Spraying coating	1–22 bilayers	2–300	[44]
CNF	Cationization with CHPTAC Carboxymethylation Micro-fluidization d: 5–10 nm L: up to 1 μm	PEI	Silica	SPAR QCM-D	1–5 bilayers	175 (4th bilayer)	[45]
Dopamine grafted CNF	Sulfite softwood pulp High-pressure homogenization with carboxymethylation d: 5–15 nm, L: up to 1 μm	PEI	Silicon wafer	QCM-D	3 bilayers	130	[55]
CNF	TEMPO oxidation d: 3–4 nm L: 0.5–1 μm	PAH	Silicon wafer	Dip coating	2–14 bilayers	5–250	[54]

(continued)

Table 8.1 (continued)

Nanopolysaccharides	Source, preparation method and dimension	Oppositely charged material	Substrate	Coating method	Number of layers	Layer thickness (nm)	References
CNF ChNF	Softwood kraft pulp TEMPO oxidation d: 3–4 nm, L: <1 μm Squid pens Hydrochloric acid hydrolysis d: 3–4 nm, L: <1 μm	–	Poly(ethylene terephthalate) PET	Spin coating	10 bilayers	70	[52]
ChNF	Crab shells Acid hydrolysis L: 160 nm d: 16 nm	Xyloglucan	Gold	Spin coating	1–10 bilayers	5–120	[9, 10]
ChNF	Dried crab shell powder Hydrochloric acid hydrolysis	PAA	Glass	Dip coating	1 bilayer	64–89	[60]
ChNF	Crab shell Hydrochloric acid hydrolysis dprimary: 156–201 nm dsecondary: 2070–4115 nm	PAA	Glass	Dip coating	6–14 bilayers	40–120	[61]

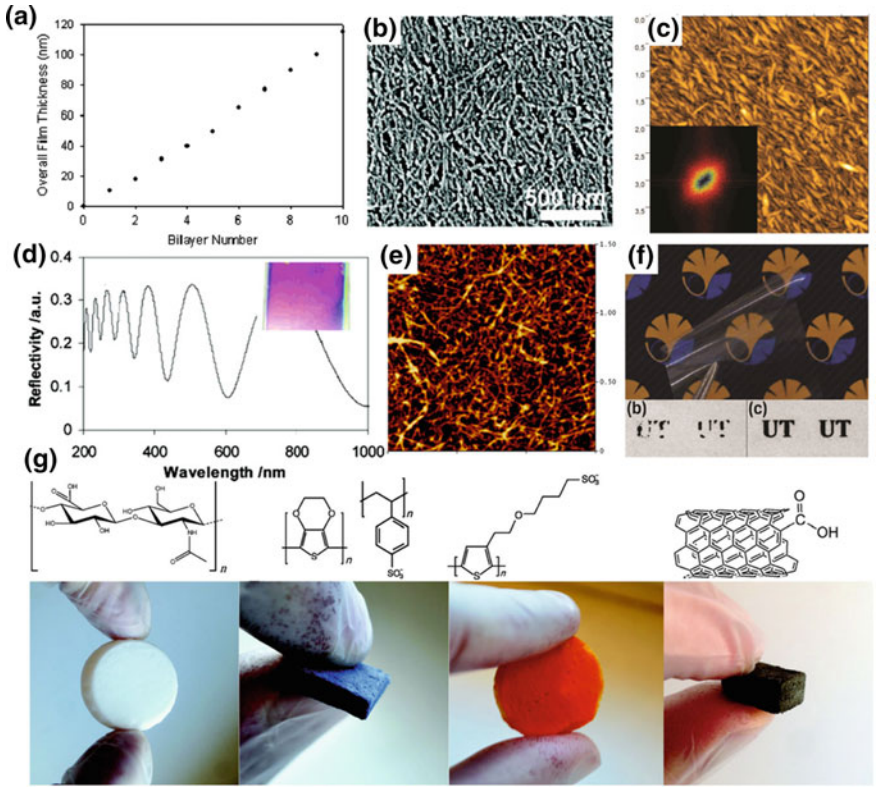

Fig. 8.5 **a** Overall thickness of LBL assembled PDDA/CNC with respect to bilayer number (Reproduced from [37]), **b** scanning electron microscopy images of the $(PEI/CNCs)_{20\ bilayers}$ (Reproduced from [46]), **c** AFM image and 2D Fourier transformations of the anisotropic phase of LBL coated CNC films (Reproduced from [40]), **d** wavelength-dependent reflectivity of spin-coated multilayered films of $(PAH/CNCs)_{25\ bilayers}$ (Reproduced from [38]), **e** AFM image of one bilayer of PEI/MFC on an oxidized silicon wafer (Reproduced from [44]), **f** Flexible LBL-coated PET film and comparison inkjet printability of an unmodified PET film (bottom left) and LBL-coated film (bottom right) (Reproduced from [52]), and **g** LBL-functionalized aerogels from left to right showing: $(PAH/HA)_{5\ bilayers}$, $(PEI/PEDOT:PSS)_{10\ bilayers}$, $(PEI/ADS2000P)_{10\ bilayers}$, $(PEI/SWCNT)_{5\ bilayers}$ (Reproduced from [59])

and CNCs were characterized in much detail by tuning different coating parameters such as drying between each adsorbed layer, adsorption time, ionic strength and CNC concentrations [48]. It is found that drying after each adsorption is essential in constructing highly homogeneous film and building up multilayers even with very short dipping time of 1 min. Adsorption of CNCs onto PAH has been found to be influenced by the chain conformation, presenting a single CNC layer at low ionic strength and double CNC layers when the charge on PAH was screened by high ionic strength to form a condensed and three-dimensional network structure. Alternative coating techniques such as spin-coating and spray-coating have also been used to assist LBL

construction. Cranston and Gray compared solution dipping and spinning coating assisted LBL assembly coating technique of negatively charged CNC with cationic PAH [38]. Compared to dip coating, spin-coating assisted LBL assembly can lead to smoother film with roughness of 4–5 nm, radial orientation of CNCs, much thicker film (7 times thicker than the dip coating film) showing intense color due to the interference between the light reflected from the air-film interface and film-substrate interface (Fig. 8.5d). Spin-coating assisted LBL assembly has also been applied to construct CNC/xyloglucan film of 16 nm thickness per bilayer [49], approximately twice the thickness of the film by dip coating (7–8 nm per bilayer) [50]. In contrast to the electrostatic interactions for polyelectrolyte assembly, hydrogen bonds and van der Waals force are the primary driving force between CNCs and xyloglucans. Spray coating of CNCs and chitin nanofibers was adopted to form a multilayer coating onto PLA substrate [51]. A five layer coating sample PLA-(ChNF-CNC)$_2$–ChNF shows a coating thickness of 3.7 μm and surface roughness of 11.8 nm.

As another type of nanocellulose, anionic cellulose nanofibrils have also been explored for constructing LBL film with cationic polyelectrolytes including PEI, polydiallyldimethylammonium chloride (PDDA), PAH, and chitin nanofibers (ChNFs) (Table 8.1) [44, 45, 52, 53]. LBL assembly between carboxymethylated CNFs and varied cationic polyelectrolytes showed clear influence of the chain conformation of polycations and ionic strength on the structure of the multilayers [44]. A bilayer of PEI/MFC surface showed distinguished fibrils on the surface with open fibrillar network structure (Fig. 8.5e). Compared to branched polyelectrolyte such as PEI, linear polyelectrolytes can result in thinner layers of CNFs. The assembled LBL structure showed nanoporous open network structure with interference color of violet to light blue depending on the thickness of the film. Similar to findings in other LBL system, ionic strength has been found to have a strong correlation to the assembled TEMPO oxidized CNF/PAH film characteristics such as porosity, swelling and optical properties [54]. Essentially, with increasing ionic strength of PAH solution and CNF suspension, much thicker layer with higher roughness could be formed due to the random coil configuration of the polyelectrolyte induced by charge screening, which leads to high porosity with antireflective properties. CNF based adhesive nanocoating was developed by grafting dopamine onto carboxymethylated CNF and then assembled with PEI, demonstrating much stronger adhesive force with silica in the presence of Fe^{3+} due to the catecholato-iron chelation [55]. Other than synthetic polyelectrolytes, LBL coating could be feasibly assembled from oppositely charged natural polymer electrolyte, such as anionically and cationically modified microfibrillated cellulose, [45] cellulose and chitin nanofibrils, [52] chitin nanocrystals and xyloglucan [9] and cellulose nanocrystals and chitosan [42, 43].

One advantage of LBL coating lies in its agnostic to the substrate, whether being flat surface such as plastic film (PET, Fig. 8.5f) [52] or 3D corrugated surface such as wood fibres [56, 57] wood, [58] or aerogels [59]. To this extent, cellulose serves as substrate instead of coating materials. LBL coating of CNF aerogel was demonstrated

using PAH/hyaluronic acid (HA) for biomedical applications, PEI/sodium poly[2-(3-thienyl)ethoxy-4-butyl-sulfonate] (ADS2000P) for confocal imaging, PEI/poly(3,4-ethylenedioxythiophene): poly(styrenesulfonate) (PEDOT:PSS), and PEI/single-wall carbon nanotubes (SWCNTs) for electronic applications (Fig. 8.5g) [59].

8.2.6 Roll to Roll Coating

Roll-to-roll (R2R) or web coating is a large-scale manufacturing system involving continuous coating of solution or suspension on flexible substrate transferring between two moving rolls. Various coating techniques could be integrated to R2R system including dip coating, knife-over-edge coating, slot-die coating, direct- and micro-gravure coating, and spray coating, [62] with the coating thickness depending on their respective coating parameters.

Roll-to-roll coating of CNF and CNC suspension are challenging due to several reasons: (1) the high viscosity of CNF and CNC suspensions even at low solid content could result in difficulties in thin and uniform film formation; (2) the high amount of water in suspension may damage the substrate and require excessive dewatering; and (3) high crystallinity of CNCs and strong inter-particle hydrogen bonding lead to brittle coating layer and inadequate adhesion to substrate. These challenges can be overcome by controlling coating process parameters and properties of CNC and CNF suspensions. Both slot-die and micro-gravure coating of CNF and CNC suspensions and their mixtures have been practiced focusing on the process parameters and coating properties. R2R spray coating has been discussed in previous section and will not be mentioned here.

Slot-die R2R coating of CNF [63, 64] and CNC [65] onto paperboard has been investigated and the coating characteristics are investigated by controlling the coating and suspension conditions including slot gap, slot-web gap, coating speed, additives, viscosity and surface tension of liquid [63, 65]. Both CNC and CNF present shear thinning properties with reduced viscosity at high shear rate, rendering its feasibility for R2R coating. Shear rate of slot-die could be adjusted by slot gap and pressure drop, independent of coating speed, which allows for relative high shear rate while maintaining the low coating speed for drying. CNF coating thickness could be enhanced by increasing the slot-web gap, showing very high coat weight of over 10 g/m^2 in a single step coating, indicating the advantage of slot-die R2R coating techniques [63]. Another issue in R2R coating is drying capacity, which can be controlled with suspension concentration, coating speed and additives. Both reduced coating speed and increased CNF concentration could improve the coating drying capacity. However, higher CNF concentration could lead to increased suspension viscosity to limit the coating process. Additive such as carboxymethyl cellulose (CMC) has been found to aid the coating process by enhancing the water retention and reducing viscosity [63]. Adding sorbitol to CNC suspensions does not show any effect on viscosity of CNC suspensions; however, it can act as a plasticizer for more flexible and adhesive coating layer [65]. Slot type R2R coating could also be used for foam coating, where CNF

foam containing over 90-95% air could be applied to the substrate forming coating of less than 1 μm and coat weight of 0.1–1 g/m^2 [66].

R2R gravure coating consists of immersing of engraved cylinder and pressing the coating layer between reversely rotating rolls (gravure and web). The coating quality largely depends on the interactions between coating material and the substrate, gravure speed, web speed, drying unit, and solvent type. Chowdhury et al. optimized R2R gravure coating of CNC suspensions on PET in terms of micro-gravure speed, web speed, speed ratio (micro-gravure speed to web speed), capillary number ($Ca = \eta U/\gamma$), and CNC concentration [67]. Although higher speed ratio can lead to thicker coating, it may cause de-wetting defects of suspension due to bubble formation and line defects due to Marangoni effect. Increase in CNC concentration, and therefore the viscosity and capillary number, also results in thicker and rougher coated layer, and adhesion strength will also be weaker to form cracks. In general, gravure speed, web speed and suspension viscosity control the viscous and inertia forces governing the coating thickness and roughness [67].

8.2.7 Other Coating Techniques

Printing is a process to reproduce text, images or patterns by transferring a pattern of liquid or semi-liquid ink from a master form or template to the substrate. Printing of nanocellulose onto varied substrates has been achieved by screen printing [68] and inkjet printing [69, 70]. Screen printing is an additive coating process to press the ink through a screen using a squeegee. Ink for screen coating needs to have shear thinning properties with high viscosity at rest to prevent spreading of ink during pre- and post-printing, and reduced viscosity under shear stress by squeegee to pass through the screen and deposit onto substrate [68, 71]. Due to the shear thinning properties of CNFs, it has been added into colloidal silver ink for screen printing to print conductive electrode onto PET substrate [68]. A photoelectrical ink was also developed using TEMPO oxidized CNF/CdS quantum dot/surfactant with both surface tension and viscosity close to the ink for screen printing [72]. However, actual screen printing was not reported using this ink. CNC and polyaniline emulsion ink was developed for flexographical printing, and the CNC was found to introduce shear thinning property and better penetration into the paper substrate [73]. Inkjet printing is an automated deposition technique that can eject fixed amount of ink from a nozzle via piezoelectric system. The drop spreading and the final printed shape are a function of the viscosity. In contrast to screen-printing, ink with lower viscosity is more processable due to the easiness in penetration into substrate. Therefore, CNF with much lower concentration (0.03%) was able to be printed on paper substrate [69]. Inkjet printing of nanocellulose is commonly used to modify porous substrate as a primer layer to increase the smoothness and prevent spreading of the functional ink.

Due to its easier operation and readily accessible setup, bar coating is commonly used for applying nanocellulose coating onto substrate, including alkyd

resin/nanocellulose onto paperboard [74], microfibirllated cellulose onto cardboard and paper [75], microfibrillated cellulose/shellac on paperboard [76] and cellulose nanofibrils on paper [76]. Details of bar coating will not be elaborated due to the simplicity of this process.

8.3 Applications

Application of nanopolysaccharides coating has been widely studied in areas including packaging, electronics, photonics, biomedical, sensors, energy storage, and water treatment. Due to its nanoscale dimension and available surface functional groups, very small amount of nanopolysaccharides coating can introduce dramatic improvement in rheological properties, mechanical properties, barrier performance, surface roughness, optical properties, and printability. In this section, the application of nanopolysaccharides in these areas and their performance will be reviewed.

8.3.1 Nanopolysaccharides as Rheology Modifiers

Nanopolysaccharides have been applied in coating formulations as rheology modifiers due to its high viscosity close to zero-shear and shear thinning properties with increased shear rate, which can help to improve the performance of the coating formulations. Nanopolysaccharide suspension usually behaves as a non-Newtonian fluid with shear thinning (pseudoplastic) properties, showing decreasing trend in viscosity with respect to increasing shear rate. This shear thinning property can lead to an ease of processing coating formulations such as mixing and transferring to the substrates. Another desired property of nanopolysaccharides is the high viscosity close to zero-shear, which can reduce settling and increase the stability of coatings. The stability of coatings is also governed by the yield stress, or resisting stress to flow, by inhibiting flow under relatively low stresses induced by gravity. The viscoelastic property of nanopolysaccharides is a complex phenomenon that is dependent on the dimension, aspect ratio, surface chemistry, charge density, and ionization degree.

The rheological behavior of CNF suspensions depends on preparation methods. In general, CNFs can be produced by shear force aided defibrillation to overcome the inter-fibrils hydrogen bonds. To aid the fibrillation, some chemical and biological pre-treatments are necessary, including: (1) enzymatic pre-treatment and (2) chemical modification such as carboxylation, carboxymethylation, quaternization or sulfonation. CNF suspensions behave like viscous gels and exhibit complex rheological behaviors at low concentration (<1%) due to the fibril network and the presence of surface polar groups (such as hydroxyl and carboxyl groups). CNF suspensions shows shear thinning [77–80] and thixotropic [81, 82] behavior due to breaking the entangled fibril network by shear and time (Fig. 8.6a) [83]. CNF suspensions also possess yield stress behavior, which prevents sedimentation in suspension. Cellulose

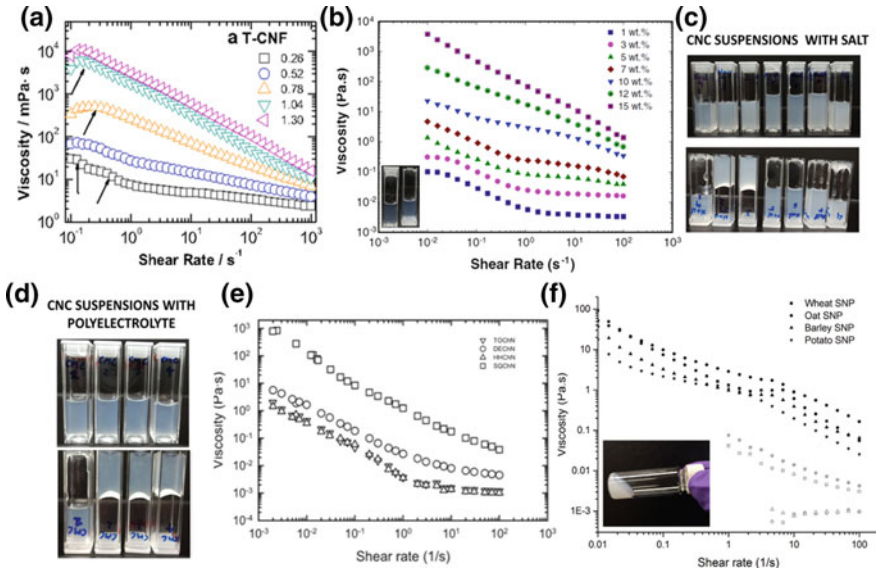

Fig. 8.6 Viscosity versus shear rate diagram of **a** TEMPO-oxidized CNF [83], **b** sulfated CNC (Reproduced from [81]), **e** ChNFs with various preparation method (Reproduced from [94]) and **f** SNCs suspensions (Reproduced from [96]); gelation behavior of CNC suspensions with **c** electrolyte (Reproduced from [93]) and **d** polyelectrolyte (Reproduced from [88])

nanocrystals (CNCs) are isolated from cellulose via sulfuric acid hydrolysis [2, 84] and oxidation [85, 86] resulting in negatively charged surface groups. In contrast to CNF, sulfated CNC [81, 87] suspensions exhibit non-Newtonian behavior with insufficient pseudoplasticity up to 7.0 wt% (Fig. 8.6b). However, rheology of CNC suspension can be modified by addition of electrolytes and macromolecules. Adding high concentration of electrolyte can form gel at low concentration of CNCs by screening electrostatic double layer [88, 89] (Fig. 8.6c). The presence of macromolecules may lead to either bridging flocculation or depletion flocculation. Addition of positively charge macromolecules such as quaternized hydroxyethylcellulose ethoxylate [90] to negatively charged CNCs lead to gelation due to electrostatic adsorption. Non-adsorbing macromolecules such as dextran [15], hydroxyethyl cellulose (HEC) [91] and carboxymethyl cellulose (CMC) [91–93] depleted CNCs in aqueous media (Fig. 8.6d). Therefore, CNC suspensions have potential to be used as rheological modifiers at low concentrations with the presence of adsorbing and non-adsorbing macromolecules. Chitin nanofibers (ChNFs) are extracted by TEMPO-oxidization, deacetylation or acid hydrolysis technique leading to highly stable suspensions with similar order of magnitude of zeta potential values (+65/−50 mV) [94]. Therefore, length of ChNFs dominates the rheological behavior (Fig. 8.6e). β-ChNFs are longer resulting in higher viscosity values at the same shear rates with pseudoplastic behavior. Deacetylation degree of ChNFs determines the zeta potential values and dimension. For instance, dimension of highly deacetylated ChNFs are reported

as 166–261 nm in length and 11 nm in diameter with zeta potential values relatively high as 105 mV [95]. Depending on the dimension, ChNFs could be potential competitor to CNFs. Similar to CNCs, rheological behavior of shorter ChNFs could be controlled with the addition of electrolytes and macromolecules. The rheological properties of starch nanocrystals (SNCs) change given to the starting source materials. The rheology of SNCs suspensions isolated from wheat, oat, barley, and potato all show relative low viscosity at close to zero-shear at 5% concentration (Fig. 8.6f), indicating that SNCs suspensions are not good candidate as rheology modifier [96]. This low viscosity of SNCs could be ascribed to their round and oval aggregates morphologies that limit the inter-particles interactions.

CNF/MFC are mainly used as rheology modifier for paper coatings, paints, and conductive inks [69, 97, 98]. Coating color or paint is a suspension consisting of particles, pigments and binders, which requires desired rheological properties for coating performance as well as the quality of the coated product. The effect of CNF on the rheology of coating color, dewatering, immobilized layer and coating coverage were investigated in several studies [99–103]. MFC/NFC has been used as partial co-binder replacement to improve strength of paper and phase separation and/or mobility of the coatings [99]. More porous coating could be obtained by partially relacing CMC with CNFs due to the gel-like nature of the CNFs and faster immobilization at lower solid content, but the permeability to water can be reduced [100]. Addition of CNF to coating colors also causes an enhancement in surface strength of coated paper and decrease in air permeability [102]. In contrast to the previous study showing reduced water permeability, this work showed that the water resistance will be decreased with addition of more hydrophilic CNFs [102].

In addition to coating colors and paint, CNFs have also been added as rheology modifier to improve coating efficiency and rheological properties in electronic applications. CNF as rheology modifier is used to print silver (Ag) nanowire-based electrodes [68, 104]. The presence of CNF thickens the Ag-nanowire suspensions while keeping thinning behaviour at higher shear rates. However, dynamic viscoelastic measurements indicated that CNF-Ag nanowire suspensions showed solid-like behaviour leading to a mottling defect during printing. Including hydroxypropyl methyl cellulose (HPMC) in CNF-Ag nanowire suspensions enables to print homogeneous layers because HPMC could induce depletion flocculation to modify viscoelastic properties of suspensions. Some other examples of using nanopolysaccharides to modify the rheological properties of conductive inks have been discussed in Sect. 8.2.7.

8.3.2 Coating for Packaging Materials

Food packaging materials provide the first barrier to protect food against influences and damage by outer environment, and it is essential to maintain the quality of the product and increase the shelf-life [105]. However, high demand in packaging causes serious problem in terms of negative environmental impact, and calls for the

development of biodegradable and sustainable packaging materials. Although free standing nanopolysaccharides film has proved to be excellent candidate for packaging materials with satisfactory barrier and mechanical properties, the high cost limits its application. To address these issues, coating of conventional packaging materials with thin layer nanopolysaccharides has drawn a wide interest for packaging applications due to their dispersibility in water, biodegradability, sustainability, improved physical properties such as barrier, mechanical and thermal properties, and multifunctionalities. Therefore, the focus of this section is on using nanopolysaccharides as a coating layer on top of conventional packaging materials such as plastic [43, 106, 107], paper [41, 108–110], and paperboard [76] to improve barrier, mechanical and optical properties. The nanopolysaccharides used for coating can be in its pristine form or mixed with other natural or synthetic materials as a composite form. For complete and more detailed applications of using nanopolysaccharides as packaging materials, the readers are referred to some recent reviews [111–114].

8.3.2.1 Barrier Properties

Water vapor permeability, gas permeability including oxygen, carbon dioxide and air, microorganisms, and grease resistance all play essential roles in packaging application. Molecules permeation through substrates depends highly on the microstructures. For solid dense films, the permeation mechanism is governed by the solution diffusion mechanisms, where the permeates adsorb onto the surface, diffuse and penetrate through the substrate and then desorb through the opposite surface (Fig. 8.7) [115]. In contrast, depending on both the pore and gas molecules sizes, permeation through porous films is more complicated and follows different diffusion mechanisms of Fickian diffusion, Knudsen diffusion, surface diffusion, molecular sieving, and capillary condensation [115]. Fickian diffusion is the permeation of gas molecules through very large pores. When the mean free path of the molecule is greater than

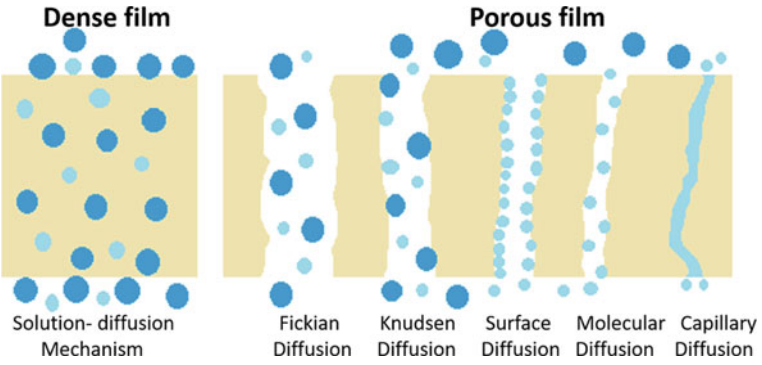

Fig. 8.7 Illustration of diffusion mechanism through non-porous and porous films. Reproduced from [116]

the pore size, permeation of molecules follows Knudsen diffusion mechanism. In surface diffusion mechanism, gas molecules with high polarity will pass through membrane through adsorption-diffusion mechanism. In capillary condensation, gas molecules condense in pores, and then diffuse as a liquid followed by evaporation through the film. Molecular sieving works for small pores where gas molecules could be separated by their sizes [41]. Therefore, control over adsorption and solubility of molecules onto substrate surfaces, tortuosity path, porosity and polarity allow tuning permeability of nanopolysaccharides-based coating.

Low oxygen permeability is desired for food packaging, and the oxygen transmission rate (OTR) is negatively correlated to the coating thickness, crystallinity, and packing density of the coating materials. TEMPO oxidized CNF coating has shown to reduce OTR of Polylactide (PLA) film by over 750 times [106], as the carboxyl groups of TEMPO oxidized CNF lead to higher cohesive energy, and therefore denser packing films with enhanced oxygen barrier properties. It is also found that the OTR will significantly decrease when the surface carboxylate groups are in the deprotonated COONa form (Fig. 8.8a), which is explained by the closer packing structure with smaller free volume due to more electrostatic repulsion between COONa CNF [117, 118]. Higher oxidation degree can also lead to more homogeneous and thinner CNFs that can increase the packing density and reduce the porosity. Therefore, the OTR decreases significantly for PET film coated with CNF carrying more carboxylate groups even at very thin coating thickness, leading to more than 350 time

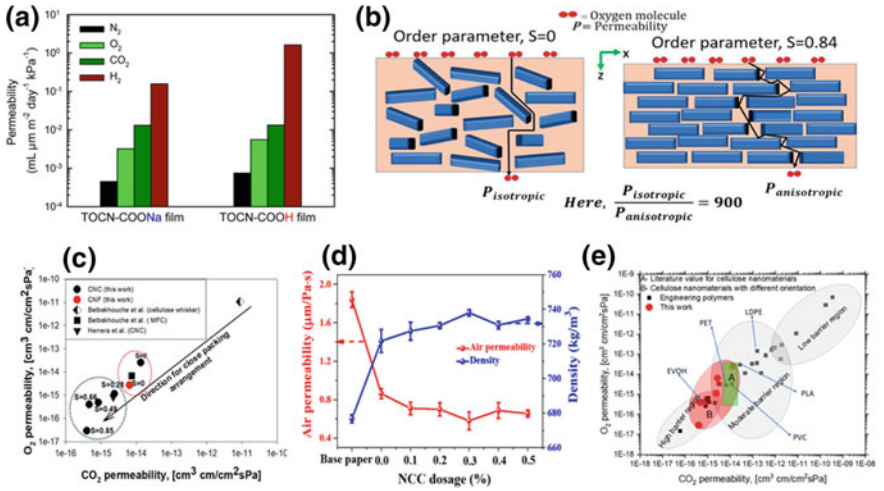

Fig. 8.8 **a** Gas permeabilities of PET films coated with TOCN-COONa or TOCN-COOH, (Reproduced from [117]), **b** isotropic and anisotropic configuration of CNCs, (Reproduced from [121]), **c** oxygen permeabilities of cellulose nanomaterials with respect to orientation or packing density, (Reproduced from [121]), **d** effect of NCC dosage on air permeability and density of surface-sized paper, (Reproduced from [137]) and **e** Ashby plot of gas permeability response of cellulose films with various structural arrangements with respect to other engineering polymers (Reproduced from [121])

reduction with 1 μm coating as compared to the uncoated one [119]. Higher surface charge density has also been observed for rod-like CNC, as being demonstrated by the much lower OTR for PET coating with ammonium persulfate (APS) oxidized CNCs as compared to the sulfuric acid hydrolyzed CNCs, with the former carrying more negatively charged groups [107]. The benefit of nanocellulose surface charge on the reduced oxygen permeability could be ascribed to the charge-charge repulsion that could delay the strong adhesion between nanocellulose and allow them to pack more densely during drying process [113]. This is further proved by the fact that uncharged microfibrillated cellulose (MFC) coating did not show effective oxygen permeation reduction, possibly due to the presence of nano-heterogeneity in the coating induced by the strong inter-fibrils attractions [75, 120]. Due to its high crystallinity, CNC coating demonstrates over 900 times improvement in oxygen barrier properties with anisotropic oriented arrangement (Fig. 8.8b). The oxygen permeability decreases with the increasing anisotropy (Fig. 8.8c), which is due to high packing density, low free volume, and tortuous path for gas diffusion [121]. However, as CNC coating is brittle and can form crack on the surface, it has been shown that paper coated with CNCs did not show reduced OTR [108]. In addition, due to the hydrophilic nature of nanocellulose, both CNC and CNF coatings showed increased OTR with increasing relative humidity [122–124]. A composite barrier coating containing both CNF and CNC have been fabricated to be benefited from the flexibility and high packing density of CNF and low water sensitivity of CNCs. The composite coating on paper showed over 260 times reduction in OTR [125]. Other than moisture, the nanocellulose coating layer is also sensitive to the storage time, showing significantly increased OTR after 8 month storage, which suggests another protective layer on top of nanocellulose coating layer is necessary [27].

Similar to oxygen permeability, the air permeability of nanocellulose coating also decreases with increasing coating thickness [122, 126]. Coating with CNC/starch composite showed reduced air permeability with increasing CNC dosage (Fig. 8.8d) [26]. The reduced air permeability for CNC coating on paper is due to the impermeability of highly crystalline CNCs and increased tortuous path formed by them [127]. However, it should be also emphasized that the low air permeability does not directly translate into low oxygen permeability. Coating calendared paper using MFC with bar coater has shown to reduce the air permeability by 97% [75]. Much lower air permeability could be achieved by coating with carboxymethylated MFC [122], due to the much finer dimension and strong hydrogen bonding by surface carboxylate groups. The CO_2 permeability also increases with increasing relative humidity, showing much stronger effect as compared to oxygen permeability due to the higher solubility of CO_2 in water than O_2 [128]. The CO_2 permeability of CNC coating also decreased with the increasing of degree of anisotropy (Fig. 8.8c) [121]. CNC coating with high anisotropic order presented both CO_2 and O_2 permeability lower than PET and EVOH (Fig. 8.8e).

Water and moisture resistance are critical for packaging used in high-moisture environment, as the gas permeability will dramatically increase at high relative humidity. The hydrophilic nature and polar surface functional groups make the water

vapor transmission rate (WVTR) of CNF much higher compared to synthetic polymer coatings [112]. There has been report that coating microfibrillated cellulose onto cardboard leads to increase in water absorption due to its hydrophilicity and high surface area [120]. However, the presence of nanocellulose in polymer coating layers decreased WVTR, such as in PLA [109] and Polyhydroxybutyrate (PHB)[109, 129, 130], as the presence of nanocellulose in matrix may lead to resistance to swelling and water vapor impermeability at the crystalline regions. Although the high crystallinity of nanocellulose and its dense packing have shown to reduce the WVTR of coarse paper substrate, the actual WVTR value is still as high as over 200 g/m^2 day [123]. A two-step coating of nanocellulose and alkyd resin onto paperboard has shown to reduce the WVTR from 517 to 73 g/m^2 day at 50% RH [74]. This indicates that nanocellulose itself could not serve as effective coating for water and moisture resistance. In order to improve the moisture barrier properties of the MFC coating, shellac resin has been applied on top of the MFC coating to reduce the WVTR to around 6 g/m^2 day, which could be considered as high moisture barrier. Other than water, both CNC and CNF coatings have shown increased oil and grease resistance [125]. Increased grease resistance was observed using Turpentine oil for CNC coated paper, showing good correlation to the low air permeability [108]. Oil resistance of MFC coating was also observed and the resistance can be improved by increasing the coating thickness and homogeneity [75, 122].

Alternating spray-coated chitin nanofibers (ChNF) and CNC on PLA showed over 73% reduced O_2 permeability, although the individual ChNF and CNC coating with the same number of layers did not show reduced O_2 permeability [51]. This has been explained by the much denser film formed by coating oppositely charged ChNF and CNC. Starch nanocrystals (SNC) can be added into thermoplastic starch coating to reduce the WVTR to up to 41%, due to the induced crystallinity and tortuosity by the platelet-like SNC [131]. In addition to coating for packaging materials, nanopolysaccharide coatings have also been directly applied onto foods or placed between its components to provide a barrier against water vapor, gases, aroma compounds and control the oxidation process leading to longer shelf-life [132–136].

8.3.2.2 Mechanical Properties

Mechanical properties of packaging material are essential for maintaining its durability and desired gas permeability. In essence, the coating layer should at least match the mechanical properties of the base substrate and should adhere and adapt to the substrate to prevent cracks or interfacial failure, which will negatively affect the barrier properties. Due to the high aspect ratio and abundant surface areas and functional groups, nanopolysaccharides, especially nanocellulose, have shown to improve tensile strength of papers as additive [138]. In general, nanocellulose coating has shown to improve varied mechanical properties of the substrate, including tensile strength [110, 123, 126, 139], Young's modulus [126, 139], breaking length [110, 140], burst index [140], internal cohesion [140], and bending stiffness [141]. Addition of sorbitol plasticizer along with CNC has shown to have a positive effect on both the

strength and toughness, possibly due to the formation of hydrogen bond between CNC and sorbitol [123]. Reinforcing effect of CNC on starch coating layer was investigated showing that an addition of 0.3 wt% CNC into starch coating could increase the tensile index, tear index, folding endurance, and burst index to 10, 13, 36, and 5%, respectively [137]. This enhancement has been ascribed to the reduced moisture sensitivity and excellent interfacial adhesion between CNC and starch molecules.

Albeit benefiting effects have been reported for nanopolysaccharides coating, several cases also demonstrated reduced mechanical properties with nanopolysaccharides coating. The reduction in mechanical properties for CNC and chitin nanofibers on PLA substrates was ascribed to the mismatch in thermal and mechanical properties at the polymer/nanopolysaccharide interface [51]. Successive wetting/drying onto paper substrate has shown to reduce the mechanical properties due to weakened network structure by water penetration [75, 108, 120].

8.3.2.3 Active Releasing Coating

Packaging coating with controlled active releasing properties is beneficial for antibacterial application, which is crucial for inhibiting the growth of microorganisms under suitable temperature and humidity conditions to enhance safety in packaged food, pharmaceutical, healthcare and personal-care products. The high surface area of nanopolysaccharides and nanoporous coating structure can benefit the drug releasing and antibacterial performance [142]. To obtain the active releasing and antibacterial properties, varied active reagents such as chitosan [143], silver nanoparticles [144], lysozyme [145] and chlorhexidine digluconate (CHX) [146] have been incorporated into nanocellulose coating. Gradual and slower release of CHX can be achieved when it is imbedded in MFC network, showing a reduction in the releasing amount by 20% [146]. The coating showed a sustained antibacterial property towards *Bacillus subtilis* even after the CHX was released. CNF/Ag nanoparticles coated paper with 20 ppm Ag showed 100% reduction towards *E. coli* and *S. aureus* [144]. Although CNC does not show antifungal properties, it has been found to improve the antifungal properties of chitosan due to its electrostatic interaction to immobilize chitosan [143].

8.3.3 Coating for Photonic Applications

Coatings for photonic applications refer to coatings that can tune the transmission, reflection, and/or polarization of the incident light. Anisotropic rod-like CNCs can assemble into periodically ordered structure under ambient drying, showing iridescent color caused by the light interference by the periodic structure. The structural coloration is promising for applications in anti-counterfeiting, anti-reflection and colorimetric sensors. Iridescent color from CNCs has been observed from free-standing film assembled from CNCs with chiral nematic liquid crystal phase (Fig. 8.9a), [38] where constructive interference occurs when the helical pitch matches the wavelength

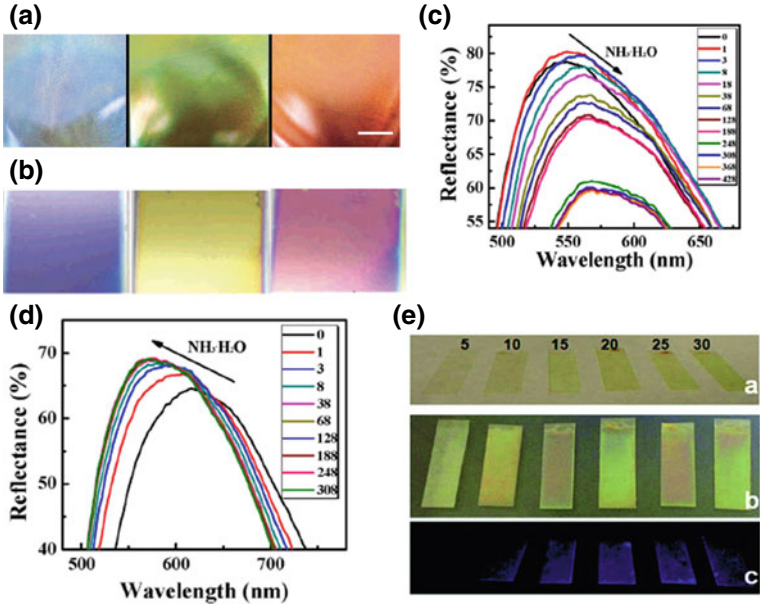

Fig. 8.9 **a** CNC films prepared from suspensions with the increase in sonication energy from left to right, showing structural color derived from constructive interference (Reproduced from [155]) **b** PAH/CNC films with the increase in number of bilayers from left to right, showing color derived from destructive interference (Reproduced from [38]), fiber optical spectroscopy of **c** CNC photonic coating exposure to vapors of $NH_3 \cdot H_2O$ (Reproduced from [153]) and **d** time dependent recovery with the release of $NH_3 \cdot H_2O$ vapors at 50 °C (Reproduced from [153]), and **e** CdS quantum dot functionalized CNC onto PET films (Reproduced from [154])

of certain visible light. Colored coating could also be obtained from spin-coated CNC model film onto a solid substrate (Fig. 8.9b), where the color was created due to the destructive interference between the light reflected from air-film interference and from the film-substrate interference [38].

The iridescent color has been found to respond to external stimuli such as moisture [147], organic solvent [148, 149], and gas [150], resulting from the change of the helical pitch under these stimuli. Free standing CNC film is brittle and difficult to handle, and therefore coating on substrates has been explored to fabricate iridescent film with better flexibility and durability. A flexible iridescent CNC coating has been applied to different polymeric substrate using CNC/PEG (poly(ethylene glycol)) mixture, and the addition of PEG could tune the helical pitch, and enhance the flexibility and adhesion strength on the polymer substrate [151]. Similarly, iridescent coating onto acrylonitrile butadiene styrene (ABS) and wood was demonstrated using CNC/glycerol, showing improved adhesion with the addition of glycerol even on hydrophobic ABS substrate [152]. Spin-coated CNCs on silicon substrate showed increased red-shift with increasing coating layers due to the Fabry-Perot fringes destruction interferences, and the coating is responsive to the vapors of NH_3H_2O,

H_2O, HAc, and HCl [153]. When exposed to vapor, the film color showed red-shift due to increased interlayer distance, and the color will recover after heating to release the molecules from the film (Fig. 8.9c, d). LBL coating of CdS quantum dot functionalized CNC onto PET showed both structural color from CNCs and the photoluminescence of the quantum dots, which has demonstrated application as anti-counterfeiting application for currency (Fig. 8.9e) [154].

8.3.4 Coating for Biomedical Applications

Coating of nanopolysaccharides in biomedical devices has been explored in areas of tissue engineering, wound dressing, and drug delivery, and has demonstrated potential in promoting cell growth, epithelialization, and drug delivery. A bioactive coating containing CNCs and bioactive glass (BG) has been developed by electrophoretic deposition method on stainless steel for bone substitutes [156]. CNC can assist the deposition of bioactive glass by adsorbing on the BG surface and then migrate under electric field. Co-deposition of CNC with BG on stainless steel has shown to stabilize the BG, improve adhesion strength, expedite biomineralization process, as well as accelerate cell attachment, proliferation, and differentiation. CNF was coated onto 3D printed polycaprolactone (PCL) scaffolds by immersing and freeze-drying, which could tune its hydrophobic surface to hydrophilic [157]. In addition, CNF coating can also enhance the differentiation of human bone marrow stromal cells (hBMSC), as evidenced from the elevated ALP activity, mineral formation and collagen Type-I production. CNF coating has also been found to promote the growth of more elongated cells due to its micronanoscale fibrillary structure. Directed growth of skeletal muscle cells by oriented CNCs from spin-coating has also been reported [158, 159]. Spin-coating can assist the orientation of CNCs along the local radial axis, and the orientation of myoblast cells on the CNC coated surface increases with the increasing orientation degree, suggesting that CNCs can direct the terminal differentiation of mammalian cells to produce tissue-like structures. For wound dressing applications, cotton gauze was coated with bacterial cellulose in *Acetobacter Xylinium* culture medium, which demonstrates high capability of medical liquid absorption and greater dry time that are both ideal for wound dressing application [160]. NFC sandwiched polyester-viscose based gauze was also reported [161], and it shows increased saline solution absorption and enhanced epithelialization rate, but did not show antimicrobial properties but also did not support bacterial growth.

8.3.5 Coating for Structural and Building Materials

Coatings in construction and building material such as metal and wood are aimed to provide protective and decorative function at the same time. For instance, applied coating should resist to loss of grip, embrittlement, corrosive spotting, changes in

modulus and optical properties due to weathering conditions including solar radiation, humidity and temperature. Application of stains, finishes, sealants, varnishes and paints in building materials has been primarily used owing to their positively perceived characteristics including enhancement in mold resistance, water repellence, and protection against wear. Nano-polysaccharides are promising to enhance anti-weathering properties of traditional coatings while acting as rheology modifiers.

Photoinduced weathering is undesirable for exterior building materials as it will lead to both performance and appearance deterioration, such as loss of modulus, strength, and adhesion, discoloration, embrittlement, chalking, loss of shine, and corrosive spotting. Photo-initiated oxidation and hydrolysis leads to degradation of coated layers due to the exposure of light, air and water. CNF has been used to disperse and stabilize zinc oxide in anionic acrylic emulsions, and shown to reduce crack formation and reduce gloss [162]. However, zinc oxide did not show sufficient effect on color stability and the addition of CNF does not improve the color stability. Although CNC does not absorb UV light or affect the color stability, adding unmodified CNCs into waterborne polyurethane acrylate resin coating has shown to enhance the color stability due to increased roughness to scatter UV light [163]. Hydrophobic CNC decreases the UV stability as the roughness is reduced. Protective polysimethylsiloxane (PDMS) space coating was developed with added varied surface modified CNCs by anchoring polysiloxane, cinnamate, chloroacetate, trifluoroacetate and vinyl esters with silylation and acylation to improve the dispersion of CNCs in the hydrophobic PDMS matrix [164]. Chlorinated CNCs improved the UV stability while not affecting mechanical properties and transparency of the films. At the same time, thermal stability of the coating was found to be improved with addition of CNCs. It has been previously discussed that nano-polysaccharides coating can serve as oxygen barriers in packaging, and oxygen has been responsible for photo oxidation of lignin that leads to discoloration. Addition of CNC into tung oil wood finishes has shown to reduce the oxygen permeability and therefore enhanced blocking of UV degradation [165].

Adding native and modified nanocellulose into waterborne coatings and solvent-based varnishes also improved mechanical properties including tensile strength, elongation at break, hardness, and impact strength [165–172]. Both impact strength and hardness increased simultaneously with the addition of CNCs into tung oil coating being attributed to good filler-matrix interactions and high Young's modulus of the structure [165]. The high aspect ratio of CNF makes it difficult to be homogeneously dispersed even in waterborne coating resin, which could be improved by grafting amine terminated silane (γ-aminopropyltriethoxysilane, APS) [166]. APS-modified CNF could be well dispersed in waterborne acrylic coatings and the Young's modulus could be increased 6 times. Hardness and abrasion resistance of the coating are also increased. CNF was added into waterborne polyurethane coating showing increase in tensile strength, Young's modulus, and hardness [173]. The increase in the Young's modulus follows a linear trend that could fit to Halpin-Tsai model with increasing CNF content up to 0.7 vol.%, and then increases drastically to follow Ouali model above the percolation threshold. Polar CNC has been added into polyols for synthesis polyurethane prepolymer coating and showed that CNC can function

as adhesion promoter to increase the pull-off adhesion strength of the coating to 154% [170]. For non-polar coating resin, nanocellulose needs to be modified with hydrophobic functional groups to enhance the miscibility. Non-covalent modification such as electrostatic adsorption of cationic surfactant hexadecyltrimethylammonium bromide (HDTMA) onto CNCs has shown to increase the tensile strength, modulus, hardness, and abrasion resistance of a UV curable acrylate coating [168]. Comparison between HDTMA adsorbed CNC and acrylated CNC from acryloyl chloride showed that acrylated CNC can lead to higher modulus as compared to the HDTMA adsorbed ones, although both modified CNC can increase the mechanical properties of the acrylated epoxidized soybean oil coating [172].

8.3.6 Coating for Paper, Plastic and Fabrics

Paper and plastic substrates have been coated with nanopolysaccharide for packaging materials with improved barrier and mechanical properties as discussed in Sect. 8.3.2. In this section, coating on paper, plastic, and fabrics by nanopolysaccharides for other purposes including painting restoration, dyeing color, and improving printing resolution will be further discussed. Application of nanopolysaccharides on conventional substrates is desirable considering its nanoscale dimension and roughness, abundant surface functional groups, mechanical performance, hydrophilicity, and affinity to the substrate or other active materials.

Oxidative and hydrolytic degradation of cellulose during aging leads to weakened structure of cotton canvas and historical papers that need to be consolidated or restored for preservation. Owing to its chemical structure similarity to cotton canvas and paper, nanocellulose has been considered ideal for the restoration, and this application has been widely accepted by the conservators. Advantages of using nanocellulose for canvas and paper restoration include high strength, transparency, lightweight, and reversibility, where cellulose at the nanoscale was used to bind together the worn cellulose microfibers in paper and fabric, instead of using synthetic resin. For restoration purpose, the substrate (historical paper or cotton canvas) has been coated with cellulose nanofibrils [174–177], cellulose nanocrystals [178], bacterial cellulose [177, 179–181], and chitin nanofibers [182]. Treating historical paper using these nanopolysaccharides has been found to stabilize and repair the substrate with low optical and haptic change [177].

Some clear and obvious advantages of coating these conventional substrates using nanopolysaccharides include reducing surface roughness and increasing mechanical strength. Coating paper with cellulose nanofibrils has shown to improve the printability of A4 paper by preventing random spreading of the ink droplet, and shown promising effects for printing supercapacitors on paper [69]. Similarly, aligned CNCs coating can be transferred onto polystyrene and found to enhance the printing resolution [183]. Coating cotton fabric with CNFs has also shown to prevent ink penetrating into to the fabric bulk and the conductive ink could be localized on the surface to improve the printing resolution [70]. NFC coating on cotton fabrics has also shown

to be a more sustainable way of dyeing cotton fabrics, which can reduce the salt and water consumption by one order of magnitude compared to the traditional exhaust dyeing method [184]. This high efficiency dyeing by NFC bearing reactive dyes can be ascribed to its strong affinity to cellulosic surfaces induced by hydrogen bonding, van der Waals force, and mechanical interlocking mechanisms.

8.4 Perspectives

This chapter aims to summarize the current state of using nanopolysaccharides as coating materials while leading new research and development directions. As being described in this chapter, coating with nanopolysaccharides shows great promise for broad applications and can introduce enhanced performance and interesting functionalities. However, it should also be mentioned that there is still unmet performance that need to be addressed and areas that need to be further explored. With this section, I hope to discuss some ideas that could raise more research activities in nanopolysaccharides coating.

Firstly, most of current research are focusing on cellulosic nanomaterials (CNCs and CNFs), and the research activities in other nanopolysaccharides (ChNC, ChNF, and SNCs) are apparently lacking. Using other types of nanopolysaccharides may provide benefits that cannot be obtained by nanocellulose, such as antibacterial properties of the deacetylated nanochitin, and therefore warrant more research activities.

Secondly, water sensitivity of nanopolysaccharides is a critical issue that needs to be addressed. The hydrophilic nature of nanopolysaccharides makes it unstable under high humidity environment. Although the nanopolysaccharides coating showed satisfactory performance regarding to low gas permeability, the water permeability and gas permeability at high RH does not satisfy its need as packaging materials. There are also conflicting results regarding to the effect of nanopolysaccharides on the water resistivity.

Thirdly, the majority of the published research work on using nanopolysaccharides coating are limited to conventional areas such as protection, packaging, and decoration. The future research should divert to more advanced application such as electronic, biomedical, and energy conversion and storage areas.

Acknowledgements This work was undertaken, in part, thanks to funding from the Canada Research Chair program. The authors also acknowledge the support of the Natural Sciences and Engineering Research Council of Canada (NSERC) [RGPIN-2018-06818].

References

1. Lin N, Huang J, Dufresne A (2012) Preparation, properties and applications of polysaccharide nanocrystals in advanced functional nanomaterials: a review. Nanoscale 4:3274–3294
2. Habibi Y, Lucia LA, Rojas OJ (2010) Cellulose nanocrystals: Chemistry, self-assembly, and applications. Chem Rev 110:3479–3500
3. Sahu N, Parija B, Panigrahi S (2009) Fundamental understanding and modeling of spin coating process: a review. Indian J Phys 83:493–502
4. Meyerhofer D (1978) Characteristics of resist films produced by spinning. J Appl Phys 49:3993–3997
5. Bornside DE, Macosko CW, Scriven LE (1987) Modelling of spin coating. J Imaging Technol 13:122–130
6. Lawrence CJ, Zhou W (1991) Spin coating of non-Newtonian fluids. J Non-Newtonian Fluid Mech 39:137–187
7. Rehg TJ, Higgins BG (1992) Spin coating of colloidal suspensions. AIChE J 38:489–501
8. Wilson BP, Yliniemi K, Gestranius M et al (2018) Structural distinction due to deposition method in ultrathin films of cellulose nanofibres. Cellulose 25:1715–1724
9. Villares A, Moreau C, Capron I et al (2014) Chitin nanocrystal-xyloglucan multilayer thin films. Biomacromol 15:188–194
10. Villares A, Moreau C, Capron I et al (2014) Impact of ionic strength on chitin nanocrystal-xyloglucan multilayer film growth. Biopolymers 101:924–930
11. Lefebvre J, Gray DG (2005) AFM of adsorbed polyelectrolytes on cellulose I surfaces spin-coated on silicon wafers. Cellulose 12:127–134
12. Edgar CD, Gray DG (2003) Smooth model cellulose I surfaces from nanocrystal suspensions. Cellulose 10:299–306
13. Jiang F, Kittle JD, Tan X et al (2013) Effects of sulfate groups on the adsorption and activity of cellulases on cellulose substrates. Langmuir 29:3280–3291
14. Kontturi E, Johansson LS, Kontturi KS et al (2007) Cellulose nanocrystal submonolayers by spin coating. Langmuir 23:9674–9680
15. Edgar CD, Gray DG (2002) Influence of dextran on the phase behavior of suspensions of cellulose nanocrystals. Macromolecules 35:7400–7406
16. Ahola S, Turon X, Österberg M et al (2008) Enzymatic hydrolysis of native cellulose nanofibrils and other cellulose model films: effect of surface structure. Langmuir 24:11592–11599
17. Hann RA (1990) Molecular structure and monolayer properties. In: Roberts G (ed) Langmuir-blodgett films, 1st edn. Springer, New York
18. Habibi Y, Foulon L, Aguie-Beghin V et al (2007) Langmuir-Blodgett films of cellulose nanocrystals: preparation and characterization. J Colloid Interface Sci 316:388–397
19. Habibi Y, Hoeger I, Kelley SS et al (2010) Development of Langmuir-Schaeffer cellulose nanocrystal monolayers and their interfacial behaviors. Langmuir 26:990–1001
20. Jiang F, Hsieh Y-L (2015) Holocellulose nanocrystals: Amphiphilicity, oil/water emulsion, and self-assembly. Biomacromol 16:1433–1441
21. Bertsch P, Diener M, Adamcik J et al (2018) Adsorption and interfacial layer structure of unmodified nanocrystalline cellulose at air/water interfaces. Langmuir 34:15195–15202
22. Capron I, Rojas OJ, Bordes R (2017) Behavior of nanocelluloses at interfaces. Curr Opin Colloid Interface Sci 29:83–95
23. Landau L, Levich VG (1942) Dragging of a liquid by a moving plate. Acta Physicochim USSR 17:42–54
24. Derjaguin BV (1943) Thickness of liquid layer adhering to walls of vessels on their emptying and the theory of photo- and motion-picture film coating. C R Acad Sci URSS 39:13–16
25. Mendoza-Galvan A, Tejeda-Galan T, Dominguez-Gomez AB et al (2019) Linear birefringent films of cellulose nanocrystals produced by dip-coating. Nanomaterials 9:45
26. Meulendijks N, Burghoorn M, van Ee R et al (2017) Electrically conductive coatings consisting of Ag-decorated cellulose nanocrystals. Cellulose 24:2191–2204

27. Herrera MA, Sirvio JA, Mathew AP et al (2016) Environmental friendly and sustainable gas barrier on porous materials: nanocellulose coatings prepared using spin- and dip-coating. Mater Des 93:19–25
28. Gans A, Dressaire E, Colnet B et al (2019) Dip-coating of suspensions. Soft Matter 15:252–261
29. Pawlowski L (2009) Suspension and solution thermal spray coatings. Surf Coat Technol 203:2807–2829
30. Ashgriz N (2011) Handbook of atomization and sprays theory and application Springer Science Business Media, London
31. Mirmehdi S, de Oliveira MLC, Hein PRG et al (2018) Spraying cellulose nanofibrils for improvement of tensile and barrier properties of writing & printing (W&P) paper. J Wood Chem Technol 38:233–245
32. Mirmehdi S, Hein PRG, Sarantopoulos C et al (2018) Cellulose nanofibrils/nanoclay hybrid composite as a paper coating: effects of spray time, nanoclay content and corona discharge on barrier and mechanical properties of the coated papers. Food Packag Shelf 15:87–94
33. Shanmugam K, Varanasi S, Garnier G et al (2017) Rapid preparation of smooth nanocellulose films using spray coating. Cellulose 24:2669–2676
34. Shanmugam K, Doosthosseini H, Varanasi S et al (2018) Flexible spray coating process for smooth nanocellulose film production. Cellulose 25:1725–1741
35. Richardson JJ, Björnmalm M, Caruso F (2015) Technology-driven layer-by-layer assembly of nanofilms. Science 348:aaa2491
36. Bertrand P, Jonas A, Laschewsky A et al (2000) Ultrathin polymer coatings by complexation of polyelectrolytes at interfaces: suitable materials, structure and properties. Macromol Rapid Commun 21:319–348
37. Podsiadlo P, Choi S-Y, Shim B et al (2005) Molecularly engineered nanocomposites: layer-by-layer assembly of cellulose nanocrystals. Biomacromol 6:2914–2918
38. Cranston ED, Gray DG (2006) Morphological and optical characterization of polyelectrolyte multilayers incorporating nanocrystalline cellulose. Biomacromol 7:2522–2530
39. Cranston ED, Gray DG (2008) Birefringence in spin-coated films containing cellulose nanocrystals. Colloids Surf A 325(1–2):44–51
40. Jean B, Dubreuil F, Heux L et al (2008) Structural details of cellulose nanocrystals/polyelectrolytes multilayers probed by neutron reflectivity and AFM. Langmuir 24:3452–3458
41. Herrera MA, Mathew AP, Oksman K (2014) Gas permeability and selectivity of cellulose nanocrystals films (layers) deposited by spin coating. Carbohydr Polym 112:494–501
42. de Mesquita JP, Donnici CL, Pereira FV (2010) Biobased nanocomposites from layer-by-layer assembly of cellulose nanowhiskers with chitosan. Biomacromol 11:473–480
43. Li F, Biagioni P, Finazzi M et al (2013) Tunable green oxygen barrier through layer-by-layer self-assembly of chitosan and cellulose nanocrystals. Carbohydr Polym 92:2128–2134
44. Wagberg L, Decher G, Norgren M et al (2008) The build-up of polyelectrolyte multilayers of microfibrillated cellulose and cationic polyelectrolytes. Langmuir 24:784–795
45. Aulin C, Johansson E, Wågberg L et al (2010) Self-organized films from cellulose i nanofibrils using the layer-by-layer technique. Biomacromol 11:872–882
46. Podsiadlo P, Sui L, Elkasabi Y et al (2007) Layer-by-layer assembled films of cellulose nanowires with antireflective properties. Langmuir 23:7901–7906
47. Cranston ED, Gray DG (2006) Formation of cellulose-based electrostatic layer-by-layer films in a magnetic field. Sci Technol Adv Mater 7:319–321
48. Moreau C, Beury N, Delorme N et al (2012) Tuning the architecture of cellulose nanocrystal-poly(allylamine hydrochloride) multilayered thin films: influence of dipping parameters. Langmuir 28:10425–10436
49. Cerclier CV, Guyomard-Lack A, Cousin F et al (2013) Xyloglucan-cellulose nanocrystal multilayered films: effect of film architecture on enzymatic hydrolysis. Biomacromol 14:3599–3609
50. Jean B, Heux L, Dubreuil F et al (2009) Non-electrostatic building of biomimetic cellulose-xyloglucan multilayers. Langmuir 25:3920–3923

51. Satam CC, Irvin CW, Lang AW et al (2018) Spray-coated multilayer cellulose nanocrystal—chitin nanofiber films for barrier applications. ACS Sustain Chem Eng 6:10637–10644
52. Qi ZD, Saito T, Fan Y et al (2012) Multifunctional coating films by layer-by-layer deposition of cellulose and chitin nanofibrils. Biomacromol 13:553–558
53. Pillai KV, Renneckar S (2016) Dynamic mechanical analysis of layer-by-layer cellulose nanocomposites. Ind Crops Prod 93:267–275
54. Azzam F, Moreau C, Cousin F et al (2014) Cellulose nanofibril-based multilayered thin films: effect of ionic strength on porosity, swelling, and optical properties. Langmuir 30:8091–8100
55. Karabulut E, Pettersson T, Ankerfors M et al (2012) Adhesive layer-by-layer films of carboxymethylated cellulose nanofibril dopamine covalent bioconjugates inspired by marine mussel threads. ACS Nano 6:4731–4739
56. Lin ZY, Renneckar S, Hindman DP (2008) Nanocomposite-based lignocellulosic fibers 1. Thermal stability of modified fibers with clay-polyelectrolyte multilayers. Cellulose 15:333–346
57. Eriksson M, Torgnysdotter A, Wagberg L (2006) Surface modification of wood fibers using the polyelectrolyte multilayer technique: effects on fiber joint and paper strength properties. Ind Eng Chem Res 45:5279–5286
58. Renneckar S, Zhou Y (2009) Nanoscale coatings on wood: polyelectrolyte adsorption and layer-by-layer assembled film formation. ACS Appl Mater Interfaces 1:559–566
59. Hamedi M, Karabulut E, Marais A et al (2013) Nanocellulose aerogels functionalized by rapid layer-by-layer assembly for high charge storage and beyond. Angew Chem Int Ed 52:12038–12042
60. Tanaka C, Shiratori S (2013) Fabrication of the durable low refractive index thin film with chitin-nanofiber by LBL method. In: MATEC web of conferences
61. Manabe K, Tanaka C, Moriyama Y et al (2016) Chitin nanofibers extracted from crab shells in broadband visible antireflection coatings with controlling layer-by-layer deposition and the application for durable antifog surfaces. ACS Appl Mater Interfaces 8:31951–31958
62. Park J, Shin K, Lee C (2016) Roll-to-roll coating technology and its applications: a review. Int J Precis Eng Manuf 17:537–550
63. Kumar V, Elfving A, Koivula H et al (2016) Roll-to-roll processed cellulose nanofiber coatings. Ind Eng Chem Res 55:3603–3613
64. Ottesen V, Kumar V, Toivakka M et al (2017) Viability and properties of roll-to-roll coating of cellulose nanofibrils on recycled paperboard. Nord Pulp Pap Res J 32:179–188
65. Koppolu R, Abitbol T, Kumar V et al (2018) Continuous roll-to-roll coating of cellulose nanocrystals onto paperboard. Cellulose 25:6055–6069
66. Kinnunen-Raudaskoski K, Hjelt T, Kentta E et al (2014) Thin coatings for paper by foam coating. Tappi J 13:9–19
67. Chowdhury RA, Clarkson C, Youngblood J (2018) Continuous roll-to-roll fabrication of transparent cellulose nanocrystal (CNC) coatings with controlled anisotropy. Cellulose 25:1769–1781
68. Hoeng F, Denneulin A, Reverdy-Bruas N et al (2017) Rheology of cellulose nanofibrils/silver nanowires suspension for the production of transparent and conductive electrodes by screen printing. Appl Surf Sci 394:160–168
69. Choi K-H, Yoo J, Lee CK et al (2016) All-inkjet-printed, solid-state flexible supercapacitors on paper. Energy Environ Sci 9:2812–2821
70. Nechyporchuk O, Yu J, Nierstrasz VA et al (2017) Cellulose nanofibril-based coatings of woven cotton fabrics for improved inkjet printing with a potential in e-textile manufacturing. ACS Sustain Chem Eng 5:4793–4801
71. Banks CE, Foster CW, Kadara RO (2016) Screen-printing electrochemical architectures. Springer Briefs in Applied Sciences and Technology, Springer, Cham
72. Tang AM, Liu Y, Wang QW et al (2016) A new photoelectric ink based on nanocellulose/CdS quantum dots for screen-printing. Carbohydr Polym 148:29–35
73. Latonen RM, Maattanen A, Ihalainen P et al (2017) Conducting ink based on cellulose nanocrystals and polyaniline for flexographical printing. J Mater Chem C 5:12172–12181

74. Aulin C, Strom G (2013) Multilayered alkyd resin/nanocellulose coatings for use in renewable packaging solutions with a high level of moisture resistance. Ind Eng Chem Res 52:2582–2589
75. Lavoine N, Desloges I, Khelifi B et al (2014) Impact of different coating processes of microfibrillated cellulose on the mechanical and barrier properties of paper. J Mater Sci 49:2879–2893
76. Hult EL, Iotti M, Lenes M (2010) Efficient approach to high barrier packaging using microfibrillar cellulose and shellac. Cellulose 17:575–586
77. Pääkkö M, Ankerfors M, Kosonen H et al (2007) Enzymatic hydrolysis combined with mechanical shearing and high-pressure homogenization for nanoscale cellulose fibrils and strong gels. Biomacromol 8:1934–1941
78. Saarikoski E, Saarinen T, Salmela J et al (2012) Flocculated flow of microfibrillated cellulose water suspensions: an imaging approach for characterisation of rheological behaviour. Cellulose 19:647
79. Lasseuguette E, Roux D, Nishiyama Y (2008) Rheological properties of microfibrillar suspension of TEMPO-oxidized pulp. Cellulose 3:425
80. Martoïa F, Perge C, Dumont PJJ et al (2015) Heterogeneous flow kinematics of cellulose nanofibril suspensions under shear. Soft Matter 11:4742
81. Shafiei-Sabet S, Hamad WY, Hatzikiriakos SG (2012) Rheology of nanocrystalline cellulose aqueous suspensions. Langmuir 28:17124–17133
82. Iotti M, Gregersen ØW, Moe S et al (2011) Rheological studies of microfibrillar cellulose water dispersions. J Polym Environ 19:137–145
83. Du L, Zhong T, Wolcott MP et al (2018) Dispersing and stabilizing cellulose nanoparticles in acrylic resin dispersions with unreduced transparency and changed rheological property. Cellulose 25:2435–2450
84. Hamad WY, Hu TQ (2010) Structure-process-yield interrelation in nanocrystalline cellulose extraction. Can J Chem Eng 88:392
85. Habibi Y, Chanzy H, Vignon MR (2006) TEMPO-mediated surface oxidation of cellulose whiskers. Cellulose 13:679–687
86. Leung ACW, Hrapovic S, Lam E et al (2011) Characteristics and properties of carboxylated cellulose nanocrystals prepared from a novel one-step procedure. Small 7:302–305
87. Lu A, Hemraz U, Khalili Z et al (2014) Unique viscoelastic behaviors of colloidal nanocrystalline cellulose aqueous suspensions. Cellulose 21:1239–1250
88. Oguzlu H, Danumah C, Boluk Y (2017) Colloidal behavior of aqueous cellulose nanocrystal suspensions. Curr Opin Colloid Interface Sci 29:46–56
89. Shafiei-Sabet S, Hamad WY, Hatzikiriakos SG (2014) Ionic strength effects on the microstructure and shear rheology of cellulose nanocrystal suspensions. Cellulose 21:3347–3359
90. Lu A, Song Y, Boluk Y (2014) Electrolyte effect on gelation behavior of oppositely charged nanocrystalline cellulose and polyelectrolyte. Carbohydr Polym 114:57–64
91. Boluk Y, Zhao L, Incani V (2012) Dispersions of nanocrystalline cellulose in aqueous polymer solutions: structure formation of colloidal rods. Langmuir 28:6114–6123
92. Oguzlu H, Boluk Y (2017) Interactions between cellulose nanocrystals and anionic and neutral polymers in aqueous solutions. Cellulose 24:131–146
93. Oguzlu H, Danumah C, Boluk Y (2016) The role of dilute and semi-dilute cellulose nanocrystal (CNC) suspensions on the rheology of carboxymethyl cellulose (CMC) solutions. Can J Chem Eng 94:1841–1847
94. Fan Y, Fukuzumi H, Saito T et al (2012) Comparative characterization of aqueous dispersions and cast films of different chitin nanowhiskers/nanofibers. Int J Biol Macromol 50:69–76
95. Bai L, Huan S, Xiang W et al (2019) Self-assembled networks of short and long chitin nanoparticles for oil/water interfacial superstabilization. ACS Sustain Chem Eng 7:6497–6511
96. Perez Herrera M, Vasanthan T, Chen L (2017) Rheology of starch nanoparticles as influenced by particle size, concentration and temperature. Food Hydrocolloids 66:237–245
97. Tuukkanen S, Lehtimäki S, Jahangir F et al (2014) Printable and disposable supercapacitor from nanocellulose and carbon nanotubes. In: 5th electronics system-integration technology conference

98. Torvinen K (2017) Flexible pigment-cellulose nanofibril composites for printed electronics applications. Åbo Akademi University, Finland
99. Dimic-Misic K, Gane PAC, Paltakari J (2013) Micro- and nanofibrillated cellulose as a rheology modifier additive in CMC-containing pigment-coating formulations. Ind Eng Chem Res 52:16066–16083
100. Dimic-Misic K, Ridgway C, Maloney T et al (2014) Influence on pore structure of micro/nanofibrillar cellulose in pigmented coating formulations. Transp Porous Media 103:155–179
101. Dimic-Misic K, Hummel M, Paltakari J et al (2015) From colloidal spheres to nanofibrils: extensional flow properties of mineral pigment and mixtures with micro and nanofibrils under progressive double layer suppression. J Colloid Interface Sci 446:31–43
102. Xu Y, Kuang Y, Salminen P et al (2016) The influence of nano-fibrillated cellulose as a coating component in paper coating. BioResources 11:4342–4352
103. Oh K, Lee J-H, Im W et al (2017) Role of cellulose nanofibrils in structure formation of pigment coating layers. Ind Eng Chem Res 56:9569–9577
104. Hoeng F, Denneulin A, Krosnicki G et al (2016) Positive impact of cellulose nanofibrils on silver nanowire coatings for transparent conductive films. J Mater Chem C 4:10945–10954
105. Marsh K, Bugusu B (2007) Food packaging—roles, materials, and environmental issues. J Food Sci 72:R39–R55
106. Fukuzumi H, Saito T, Wata T et al (2009) Transparent and high gas barrier films of cellulose nanofibers prepared by TEMPO-mediated oxidation. Biomacromol 10:162–165
107. Mascheroni E, Rampazzo R, Ortenzi MA et al (2016) Comparison of cellulose nanocrystals obtained by sulfuric acid hydrolysis and ammonium persulfate, to be used as coating on flexible food-packaging materials. Cellulose 23:779–793
108. Gicquel E, Martin C, Yanez JG et al (2017) Cellulose nanocrystals as new bio-based coating layer for improving fiber-based mechanical and barrier properties. J Mater Sci 52:3048–3061
109. Song Z, Xiao H, Zhao Y (2014) Hydrophobic-modified nano-cellulose fiber/PLA biodegradable composites for lowering water vapor transmission rate (WVTR) of paper. Carbohydr Polym 111:442–448
110. Syverud K, Stenius P (2008) Strength and barrier properties of MFC films. Cellulose 16:75–85
111. Azeredo HMC, Rosa MF, Mattoso LHC (2017) Nanocellulose in bio-based food packaging applications. Ind Crops Prod 97:664–671
112. Ferrer A, Pal L, Hubbe M (2017) Nanocellulose in packaging: Advances in barrier layer technologies. Ind Crops Prod 95:574–582
113. Hubbe MA, Ferrer A, Tyagi P et al (2017) Nanocellulose in thin films, coatings, and plies for packaging applications: a review. BioResources 12:2143–2233
114. Lavoine N, Desloges I, Dufresne A et al (2012) Microfibrillated cellulose—its barrier properties and applications in cellulosic materials: a review. Carbohydr Polym 90:735–764
115. Nagy E (2019) Chapter 3—Mass transport through a membrane layer. In: Nagy E (ed) Basic equations of mass transport through a membrane layer, 2nd edn. Elsevier, Netherlands, pp 21–68
116. Shindo R, Nagai K (2014) Gas separation membranes. In: Kobayashi S, Müllen K (eds) Encyclopedia of polymeric nanomaterials. Springer, Berlin, pp 1–8
117. Fukuzumi H, Fujisawa S, Saito T et al (2013) Selective permeation of hydrogen gas using cellulose nanofibril film. Biomacromol 14:1705–1709
118. Fujisawa S, Okita Y, Fukuzumi H et al (2011) Preparation and characterization of TEMPO-oxidized cellulose nanofibril films with free carboxyl groups. Carbohydr Polym 84:579–583
119. Rodionova G, Saito T, Lenes M et al (2012) Mechanical and oxygen barrier properties of films prepared from fibrillated dispersions of TEMPO-oxidized Norway spruce and Eucalyptus pulps. Cellulose 19:705–711
120. Lavoine N, Bras J, Desloges I (2014) Mechanical and barrier properties of cardboard and 3D packaging coated with microfibrillated cellulose. J Appl Polym Sci 131:40106
121. Chowdhury R, Nuruddin MD, Clarkson C et al (2018) Cellulose nanocrystal (CNC) coatings with controlled anisotropy as high-performance gas barrier films. ACS Appl Mater Interfaces

122. Aulin C, Gallstedt M, Lindstrom T (2010) Oxygen and oil barrier properties of microfibrillated cellulose films and coatings. Cellulose 17:559–574
123. Herrera MA, Mathew AP, Oksman K (2017) Barrier and mechanical properties of plasticized and cross-linked nanocellulose coatings for paper packaging applications. Cellulose 24:3969–3980
124. Li F, Biagioni P, Bollani M et al (2013) Multi-functional coating of cellulose nanocrystals for flexible packaging applications. Cellulose 20:2491–2504
125. Tyagi P, Lucia LA, Hubbe MA et al (2019) Nanocellulose-based multilayer barrier coatings for gas, oil, and grease resistance. Carbohydr Polym 206:281–288
126. Beneventi D, Chaussy D, Curtil D et al (2014) Highly porous paper loading with microfibrillated cellulose by spray coating on wet substrates. Ind Eng Chem Res 53:10982–10989
127. Gicquel E, Martin C, Garrido Yanez J et al (2016) Cellulose nanocrystals as new bio-based coating layer for improving fiber-based mechanical and barrier properties. J Mater Sci 52:3048–3061
128. Fotie G, Amoroso L, Muratore G et al (2018) Carbon dioxide diffusion at different relative humidity through coating of cellulose nanocrystals for food packaging applications. Food Packag Shelf 18:62–70
129. Cozzolino CA, Cerri G, Brundu A et al (2014) Microfibrillated cellulose (MFC): pullulan bionanocomposite films. Cellulose 21:4323–4335
130. El-Wakil NA, Hassan EA, Abou-Zeid RE et al (2015) Development of wheat gluten/nanocellulose/titanium dioxide nanocomposites for active food packaging. Carbohydr Polym 124:337–346
131. LeCorre D, Dufresne A, Rueff M et al (2014) All starch nanocomposite coating for barrier material. J Appl Polym Sci 131:39826
132. Deng Z, Jung J, Simonsen J et al (2017) Cellulose nanocrystal reinforced chitosan coatings for improving the storability of postharvest pears under both ambient and cold storages. J Food Sci 82:453–462
133. Azeredo HMC, Miranda KWE, Rosa MF et al (2012) Edible films from alginate-acerola puree reinforced with cellulose. LWT Food Sci Tech 46:294–297
134. Fakhouri FM, Casari ACA, Mariano M et al (2014) Effect of a gelatin-based edible coating containing cellulose nanocrystals (CNC) on the quality and nutrient retention of fresh strawberries during storage. IOP Conf. Series: Mater Sci Eng 64:012024
135. Sahraei Khosh Gardesh A, Badii F, Hashemi M et al (2016) Effect of nanochitosan based coating on climacteric behavior and postharvest shelf-life extension of apple cv. Golab Kohanz. LWT Food Sci Tech 70:33–40
136. Slavutsky AM, Bertuzzi MA (2014) Water barrier properties of starch films reinforced with cellulose nanocrystals obtained from sugarcane bagasse. Carbohydr Polym 110:53–61
137. Yang S, Tang Y, Wang J et al (2014) Surface treatment of cellulosic paper with starch-based composites reinforced with nanocrystalline cellulose. Ind Eng Chem Res 53:13980–13988
138. Taipale T, Osterberg M, Nykanen A et al (2010) Effect of microfibrillated cellulose and fines on the drainage of kraft pulp suspension and paper strength. Cellulose 17:1005–1020
139. Seoane IT, Luzi F, Puglia D et al (2018) Enhancement of paperboard performance as packaging material by layering with plasticized polyhydroxybutyrate/nanocellulose coatings. J Appl Polym Sci 135:46872
140. Tarres Q, Delgado-Aguilar M, Pelach MA et al (2016) Remarkable increase of paper strength by combining enzymatic cellulose nanofibers in bulk and TEMPO-oxidized nanofibers as coating. Cellulose 23:3939–3950
141. Ridgway CJ, Gane PAC (2011) Constructing NFC-pigment composite surface treatment for enhanced paper stiffness and surface properties. Cellulose 19:547–560
142. Lavoine N, Desloges I, Sillard C et al (2014) Controlled release and long-term antibacterial activity of chlorhexidine digluconate through the nanoporous network of microfibrillated cellulose. Cellulose 21:4429–4442
143. Amirabad LM, Jonoobi M, Mousavi NS et al (2018) Improved antifungal activity and stability of chitosan nanofibers using cellulose nanocrystal on banknote papers. Carbohydr Polym 189:229–237

144. Amini E, Azadfallah M, Layeghi M et al (2016) Silver-nanoparticle-impregnated cellulose nanofiber coating for packaging paper. Cellulose 23:557–570
145. Cozzolino CA, Nilsson F, Iotti M et al (2013) Exploiting the nano-sized features of microfibrillated cellulose (MFC) for the development of controlled-release packaging. Colloids Surf B Biointerfaces 110:208–216
146. Lavoine N, Desloges I, Manship B et al (2015) Antibacterial paperboard packaging using microfibrillated cellulose. J Food Sci Technol 52:5590–5600
147. He YD, Zhang ZL, Xue J et al (2018) Biomimetic optical cellulose nanocrystal films with controllable iridescent color and environmental stimuli-responsive chromism. ACS Appl Mater Interfaces 10:5805–5811
148. Giese M, Blusch LK, Khan MK et al (2014) Responsive mesoporous photonic cellulose films by supramolecular cotemplating. Angew Chem Int Ed 53:8880–8884
149. Gao YL, Jin ZX (2018) Iridescent chiral nematic cellulose nanocrystal/polyvinylpyrrolidone nanocomposite films for distinguishing similar organic solvents. Acs Sustainable Chem Eng 6:6192–6202
150. Song W, Lee JK, Gone MS et al (2018) Cellulose nanocrystal-based colored thin films for colorimetric detection of aldehyde gases. ACS Appl Mater Interfaces 10:10353–10361
151. Gu MY, Jiang CY, Liu DG et al (2016) Cellulose nanocrystal/poly(ethylene glycol) composite as an iridescent coating on polymer substrates: structure-color and interface adhesion. ACS Appl Mater Interfaces 8:32565–32573
152. Xu MC, Li W, Ma CH et al (2018) Multifunctional chiral nematic cellulose nanocrystals/glycerol structural colored nanocomposites for intelligent responsive films, photonic inks and iridescent coatings. J Mater Chem C 6:5391–5400
153. Zhao Y, Gao G, Liu D et al (2017) Vapor sensing with color-tunable multilayered coatings of cellulose nanocrystals. Carbohydr Polym 174:39–47
154. Chen L, Lai C, Marchewka R et al (2016) Use of CdS quantum dot-functionalized cellulose nanocrystal films for anti-counterfeiting applications. Nanoscale 8:13288–13296
155. Beck S, Bouchard J, Berry R (2011) Controlling the reflection wavelength of iridescent solid films of nanocrystalline cellulose. Biomacromol 12:167–172
156. Chen Q, Garcia RP, Munoz J et al (2015) Cellulose nanocrystals-bioactive glass hybrid coating as bone substitutes by electrophoretic co-deposition: in situ control of mineralization of bioactive glass and enhancement of osteoblastic performance. ACS Appl Mater Interfaces 7:24715–24725
157. Rashad A, Mohamed-Ahmed S, Ojansivu M et al (2018) Coating 3D printed polycaprolactone scaffolds with nanocellulose promotes growth and differentiation of mesenchymal stem cells. Biomacromol 19:4307–4319
158. Dugan JM, Collins RF, Gough JE et al (2013) Oriented surfaces of adsorbed cellulose nanowhiskers promote skeletal muscle myogenesis. Acta Biomater 9:4707–4715
159. Dugan JM, Gough JE, Eichhorn SJ (2010) Directing the morphology and differentiation of skeletal muscle cells using oriented cellulose nanowhiskers. Biomacromol 11:2498–2504
160. Meftahi A, Khajavi R, Rashidi A et al (2010) The effects of cotton gauze coating with microbial cellulose. Cellulose 17:199–204
161. Hakkarainen T, Koivuniemi R, Kosonen M et al (2016) Nanofibrillar cellulose wound dressing in skin graft donor site treatment. J Controlled Release 244(Part B):292–301
162. Grüneberger F, Künniger T, Huch A et al (2015) Nanofibrillated cellulose in wood coatings: dispersion and stabilization of ZnO as UV absorber. Prog Org Coat 87:112–121
163. Vardanyan V, Galstian T, Riedl B (2014) Effect of addition of cellulose nanocrystals to wood coatings on color changes and surface roughness due to accelerated weathering. J Coat Technol Res 12:247–258
164. Planes M, Brand J, Lewandowski S et al (2016) Improvement of the thermal and optical performances of protective polydimethylsiloxane space coatings with cellulose nanocrystal additives. ACS Appl Mater Interfaces 8:28030–28039
165. Yoo Y, Youngblood JP (2017) Tung oil wood finishes with improved weathering, durability, and scratch performance by addition of cellulose nanocrystals. ACS Appl Mater Interfaces 9:24936–24946

166. Tan Y, Liu Y, Chen W et al (2016) Homogeneous dispersion of cellulose nanofibers in waterborne acrylic coatings with improved properties and unreduced transparency. ACS Sustain Chem Eng 4:3766–3772
167. Virtanen S, Jämsä S, Talja R et al (2017) Chemically modified cellulose nanofibril as an additive for two-component polyurethane coatings. J Appl Polym Sci 134
168. Kaboorani A, Auclair N, Riedl B et al (2017) Mechanical properties of UV-cured cellulose nanocrystal (CNC) nanocomposite coating for wood furniture. Prog Org Coat 104:91–96
169. Jabbar A, Militký J, Ali A et al (2017) Mechanical behavior of nanocellulose coated jute/green epoxy composites. IOP Conf Series: Mater Sci Eng 254
170. Hubmann M, Kong X, Curtis JM (2019) Kinetic stabilization of cellulose nanocrystals in a photocurable prepolymer for application as an adhesion promoter in UV-curable coatings. Prog Org Coat 129:101–115
171. Veigel S, Lems E-M, Grüll G et al (2017) Simple green route to performance improvement of fully bio-based linseed oil coating using nanofibrillated cellulose. Polymers 9:425
172. Auclair N, Kaboorani A, Riedl B et al (2018) Influence of modified cellulose nanocrystals (CNC) on performance of bionanocomposite coatings. Prog Org Coat 123:27–34
173. Cheng D, Wen YB, An XY et al (2016) TEMPO-oxidized cellulose nanofibers (TOCNs) as a green reinforcement for waterborne polyurethane coating (WPU) on wood. Carbohydr Polym 151:326–334
174. Bridarolli A, Odlyha M, Nechyporchuk O et al (2018) Evaluation of the adhesion and performance of natural consolidants for cotton canvas conservation. ACS Appl Mater Interfaces 10:33652–33661
175. Kolman K, Nechyporchuk O, Persson M et al (2018) Combined nanocellulose/nanosilica approach for multiscale consolidation of painting canvases. ACS Appl Nano Mater 1:2036–2040
176. Nechyporchuk O, Kolman K, Bridarolli A et al (2018) On the potential of using nanocellulose for consolidation of painting canvases. Carbohydr Polym 194:161–169
177. Volkel L, Ahn K, Hahner U et al (2017) Nano meets the sheet: adhesive-free application of nanocellulosic suspensions in paper conservation. Heritage Sci 5:23
178. Cataldi A, Berglund L, Deflorian F et al (2015) A comparison between micro- and nanocellulose-filled composite adhesives for oil paintings restoration. Nanocomposites 1:195–203
179. Santos SM, Carbajo JM, Quintana E et al (2015) Characterization of purified bacterial cellulose focused on its use on paper restoration. Carbohydr Polym 116:173–181
180. Santos SM, Carbajo JM, Gomez N et al (2016) Use of bacterial cellulose in degraded paper restoration. Part I: application on model papers. J Mater Sci 51:1541–1552
181. Wu SQ, Li MY, Fang BS et al (2012) Reinforcement of vulnerable historic silk fabrics with bacterial cellulose film and its light aging behavior. Carbohydr Polym 88:496–501
182. Wijesena RN, Tissera N, Perera R et al (2014) Side selective surface modification of chitin nanofibers on anionically modified cotton fabrics. Carbohydr Polym 109:56–63
183. Prathapan R, Glatz BA, Ghosh AK et al (2019) Enhancing printing resolution on hydrophobic polymer surfaces using patterned coatings of cellulose nanocrystals. Langmuir 35:7155–7160
184. Kim Y, McCoy LT, Lee E et al (2017) Environmentally sound textile dyeing technology with nanofibrillated cellulose. Green Chem 19:4031–4035

Chapter 9
Nanopolysaccharides in Barrier Composites

Martin A. Hubbe, Preeti Tyagi and Lokendra Pal

Abstract The purpose of a barrier layer or film in a packaging product is to slow down or essentially eliminate the progress of oxygen, water vapor, or other molecules, thereby extending the shelf life, safety, and maybe also the taste of products—especially in the case of foods. This chapter discusses progress in the preparation of barrier composite films that include nanopolysaccharides, such as nanochitin, nanostarch, and nanocellulose. The reviewed research shows that these eco-friendly components in the resulting films often can improve barrier properties. While nanocellulose has attracted more research attention, nanostarch particles can be prepared under less aggressive chemical conditions, and particles related to chitin might possibly be preferred when one of the goals is to achieve antimicrobial effects. Nanopolysaccharides are also likely to find future applications in barrier films containing montmorillonite clay (nanoclay) and in multi-layer barrier film systems.

Keywords Nanocellulose · Nanochitin · Nanostarch · Barrier composites · Barrier mechanism

9.1 Architecture of Barrier Systems

9.1.1 Focus: Nanoreinforcements in Matrix Polymers

This chapter reviews progress in the use of nanopolysaccharides to enhance the barrier properties of a wide range of polymer matrix materials. There is great potential for such combinations to improve both the performance characteristics and also to minimize the environmental impacts of packaging materials for food products. Worldwide, the annual value of food packaging production has been estimated at about $161 billion [1], which is presumed to be just a fraction of the value in terms of preventing food spoilage and to feed the ever-growing population.

M. A. Hubbe (✉) · P. Tyagi · L. Pal
Department of Forest Biomaterials, College of Natural Resources, North Carolina State University, Campus Box 8005, Raleigh, NC 27695-8005, USA
e-mail: hubbe@ncsu.edu

N. Lin et al. (eds.), *Advanced Functional Materials from Nanopolysaccharides*, Springer Series in Biomaterials Science and Engineering 15,
https://doi.org/10.1007/978-981-15-0913-1_9

The present chapter builds upon earlier work in which different aspects of the topic have been reviewed [1–27]. In addition, other authors have reviewed related topics including the broader topic of food packaging [28], nanocomposites in food packaging [29–32], cellulose-based composites for various uses [33–36], antimicrobial aspects of nanocomposites for food packaging [37], the use of nanoclay in barrier films [38–40], barrier films formed from solutions of polysaccharides [41], polysaccharide-based edible films and coatings [42–44], barrier films prepared from nanocellulose without a matrix polymer [45], barrier films for packaging in general [46], and nanocellulose usage in packaging [47].

The present chapter distinguishes itself from the above-listed works, not only in its inclusion of very recent publications, but also in its emphasis on the usage of nanoparticles from starch, chitin, and chitosan, which provide alternatives to the more commonly studied nanocellulose options, which include cellulose nanocrystals (CNC), nanofibrillated cellulose (NFC), and bacterial cellulose (BC). By considering a wide range of nanopolysaccharides reported in the literature, the formulator of the future will have many options from which to choose in order to fine-tune the barrier layers for food packaging to meet different goals, which can range from processing and packaging efficiencies to enhanced safety. Also, in the final section of the article, an attempt is made to reexamine the mechanisms that can explain the often-reported ability of nanopolysaccharides to enhance the barrier properties of various matrix polymers. Emphasis will be placed here on the ability of nanopolysaccharide particles to decrease the permeability of various films to oxygen and to water vapor, along with the related topics of the physical strength and integrity of the nano-reinforce films.

9.1.2 Assembly Procedures

This section deals with the ways in which different researchers have prepared their barrier composite films that contained various nanopolysaccharides. Depending on the nature of the continuous phase in the composite (often called the “matrix”), some of the most widely used methods of composite film preparation can be called “casting”, “extrusion”, and various forms of coating onto porous substrates such as paper. In each case, the properties of the nano-filled composite films, i.e. nanocomposites, can be expected to be very much related to the manner of distribution of the nanoparticles within the matrix, which ultimately depends on the way in which the nanocomposite was assembled.

In 1995, Favier et al. [48] were the first to report the use of nanopolysaccharides as reinforcing agents in films. Their work employed cellulose whiskers obtained by acid hydrolysis of the spines taken from tunicates, which are sea creatures, to stiffen films prepared by the slow evaporation of water from latex suspensions. The pioneering work of Favier et al. [48] employed a film-casting and solvent evaporation approach, which continues to be the most-used way to form nanocomposites in the laboratory [17, 49–81]. Film-casting means that the reinforcing particles are first mixed with a

low-viscosity solution of the matrix polymer, the suspension is poured into a suitable mold, and then the suspending liquid is allowed to evaporate. The general procedure is shown schematically in Fig. 9.1. As a general rule, casting methods can achieve outstanding performance results, which can be attributed to the opportunity to achieve highly uniform particle distributions (see later) and avoid mechanical damage to the reinforcing particles. However, the time and energy required for the evaporation of a solvent are disadvantages of casting procedures. Thus, there are practical reasons to consider other approaches when the goal is to achieve high-speed processing on an industrial scale.

Melt extrusion is a process that is widely used in industry to apply films based on matrix polymers that liquefy upon heating. Figure 9.2 shows a schematic diagram of how this can be achieved. The incorporation of nanopolysaccharide particles into the melt extrusion processes has been considered in various studies [17, 57, 82–91]. As noted by Kargarzadeh et al. [17] and Vasile [27], such processing tends to reduce the size of elongated nanoparticles due to the effects of shearing.

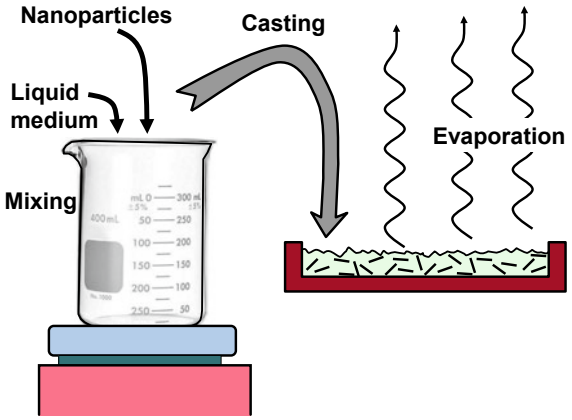

Fig. 9.1 Schematic diagram of a lab-scale casting process to make a barrier film

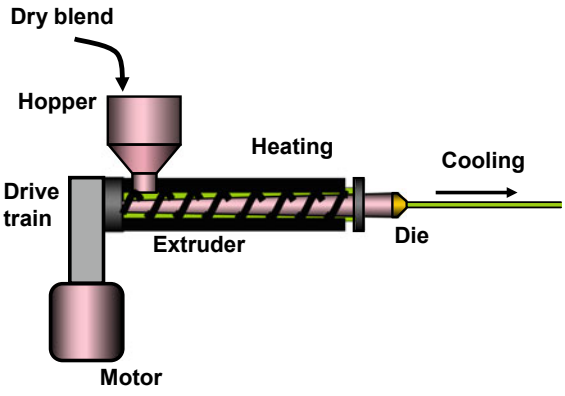

Fig. 9.2 Schematic diagram of a film extrusion process

Some additional promising strategies for assembling nanoparticle-reinforced polymer films can be mentioned briefly. Curing-type polymer formulations, such as epoxy resins, have the advantage of allowing the mixing to take place at a relatively low viscosity, thus minimizing the breakage of reinforcing particles. The following articles describe the application of such strategies to prepare nanopolysaccharide particle reinforced composites [92, 93]. Other researchers have developed procedures whereby a skeleton, composed of nanopolysaccharide fibrils, is formed first, and then a polymer solution or melt is infused into it (see Hubbe et al. [45]). Finally, as will be emphasized at the very end of this chapter, part of the take-away message will be that some of the most promising options to consider for packaging can be expected to involve separate layers of nanopolysaccharides, with or without additives, sandwiched between layers of other materials, such as plastic films.

9.1.3 Selection of Matrix

9.1.3.1 Base Properties

A matrix can be defined as the continuous phase within a two-phase solid mixture, which taken together is a composite. A majority of matrix polymers currently used for the barrier layers of food packages are single-phase petroleum-based polymers such as polyethylene, polyethylene terephthalate, or polyurethane [17, 37, 65, 66, 91, 94–102]. There is a mature technology to manufacture containers, as well as barrier films, from such feedstocks at high rates of speed and relatively low cost. Key limitations with such polymers are their persistence in the environment [103] and their moderate permeability to oxygen [104].

The polymer materials can have various deficiencies, and some of these may present motivations to consider the use of reinforcements. For instance, in some cases the particle-free films may be too brittle to fulfill their intended role, and the following articles suggest that such brittleness sometimes can be overcome using formulations that include nanoreinforcements [8, 16, 105]. Other polymers may be too stretchy, which again can be addressed through the addition of fibrillar or plate-like reinforcing particles [50, 106–109].

9.1.3.2 Ideal Attributes

A focus on ideal attributes provides another approach to selecting matrix polymers for different applications. For instance, recently there has been a lot of attention to replace petroleum-based polymers with bio-based polymers, either as single-phase packaging films or as the matrix of a composite [13, 96]. The idea is to minimize society's reliance on petroleum products, which are non-renewable. For example, there has been major attention paid to poly-(lactic acid) (PLA), which is a hydrophobic,

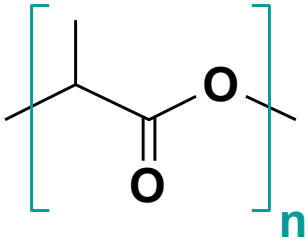

Fig. 9.3 Chemical structure of poly(lactic acid) (PLA)

meltable polymer that can be synthesized from biomaterials. The chemical structure of PLA is shown in Fig. 9.3. Many authors have reported results with PLA that has been reinforced with nanopolysaccharides, often in combination with plasticizers, to overcome problems such as brittleness [15, 57, 70, 72, 73, 83, 85, 86, 89, 107, 109–121]. At the other extreme, there has been an accelerated interest in hydrophilic matrix materials, which tend to have an inherent interfacial compatibility with nanopolysaccharides. Thus, alginates, chitosan, and polyvinyl alcohol are among various hydrophilic polymers that have been the focus of studies aimed at nanocomposite applications for possible use in food packaging [10, 51, 53, 58, 61, 63, 64, 72, 76–79, 81, 82, 122–155]. As a subset of the hydrophilic polymers, there has also been increasing interest on the use of nanopolysaccharides in films composed of edible polymers, including starch products [42–44, 69, 80, 102, 123, 124, 126, 131, 135, 148, 156–160]. There are opportunities to apply barrier coatings directly to food products, thereby increasing their shelf life. Though edible polymers such as starches can be readily made into films, such films, in their pure form, are often too brittle or too weak on their own to serve as effective barrier coatings [75, 80, 108, 147, 158, 161–163]. Other researchers have focused on the incorporation of antimicrobial or antioxidant features into the barrier films prepared with nanopolysaccharides, which is also known as active packaging [3, 8, 54, 122, 131, 160, 164–167].

9.1.4 Selection of Nanopolysaccharide

9.1.4.1 Suitability

The characteristics of different nanopolysaccharide particles are considered in detail in the first chapter of this volume. The emphasis here is the multiple options that these diverse nanoparticles provide for the preparation of barrier films. Some of the criteria by which one might select a nanopolysaccharide for use in barrier coatings are the same as those discussed in the previous section related to selection of the matrix polymer. As noted by Ferreira et al. [13], some of the over-arching issues are cost, environmental impact, and the amounts available at a given location. Criteria of likely interest also include edibility, biodegradability, interfacial compatibility (with

the matrix polymer selected), strength of the nanoparticle itself, and the ease by which the nanopolysaccharide can be obtained from the source material.

Whereas nanocellulose has been recognized as having superior strength properties [13], it is well known that severe conditions such as high energy or concentrated sulfuric acid solutions are typically used in its preparation. Though nanocrystals prepared from starch are not as strong, there are many barrier film applications in which only moderate particle strength is needed. In addition, the chemical conditions needed to selectively solubilize the non-crystalline parts of a starch material, thus releasing just the nanocrystals, are less severe and therefore safer and less expensive [11, 27, 47, 80, 105, 128, 147, 161, 168, 169].

9.1.4.2 Starch

In addition to the relatively mild conditions of their preparation, as mentioned above, starch nanoparticles also have a potential advantage, in some applications, of being readily hydrolyzed by amylase enzymes, which are present in saliva, for instance [170]. It is important to note that different kinds of starch nanoparticles can be obtained, depending not only on the source material, but also on the processing strategy employed. Starch nanocrystals have been reported to have diameters of 20–100 nm [47, 108, 128]. Kristo and Biliaderis [168] estimated that plate-like starch nanocrystals having thicknesses of 6–8 nm may initially form and then quickly agglomerate, such that somewhat larger particles might be present in nanocomposites. An alternative form of starch nanoparticles was prepared by Ma et al. [162], who used ethanol addition to precipitate the particles from a starch paste. The resulting particles were 50–100 nm. Nasseri and Mohammadi [147] reported nanostarch particles, obtained by acid hydrolysis, as being spherical in shape. Other authors have described certain starch nanoparticles as plate-like [27, 80, 168], which could be more favorable for inhibition of diffusion through a barrier film (see later). A variety of starch nanoparticle shapes can be obtained, depending on the source and other factors [171].

9.1.4.3 Chitin

The chemical structure of chitin is similar to that of cellulose except that one of the positions that would have been occupied by an –OH group (carbon 2 of the glucose monomeric unit) has an acetylamine group instead [172]. Chitin nanofibers can be prepared by acid hydrolysis, followed by ultrasonic treatment [51], or alternatively by KOH treatment to remove pectin, followed by bleaching with $NaClO_2$ [173]. The particle diameters have been reported to be in the range 2.5–2.8 nm [174] or 5–70 m [78], or alternatively 10–80 nm [173], depending on the preparation details. Lengths of 100–800 nm were reported [78, 173]. The shape has been described as slender parallelepiped rods with an aspect ratio of about 16 [175]. Chitin nanoparticles can also be produced by oxidation of chitin with ammonium persulfate, after which a

diameter of 15 nm and length of 400–500 nm was reported [150]. In cases where the preparation procedure includes treatment with strong base, one can expect a net positive charge at the particle surfaces at low to neutral pH values due to partial deacetylation, giving rise to amine groups at the surface.

9.1.4.4 Chitosan-Based

Chitosan is industrially produced by treating crustacean shells with a strong base [172]. Different grades of chitosan can be obtained having different degrees of deacetylation, depending on the severity of treatment. The degree of deacetylation is usually in the range of 0.05–0.3 [176]. Chitosan is most widely used under acidic conditions, whereby the amine groups become protonated and the polyelectrolyte goes into aqueous solution. Chitosan-based nanoparticles are prepared by changing the conditions of such solutions to bring about precipitation. Several groups of researchers prepared nanoparticles by adding sodium tripolyphospate (STPP) to chitosan solutions [52, 123, 156, 177]. A positive zeta potential, indicative of a net positive surface charge, has been reported for such nanoparticles [177]. Liu et al. [166] employed similar chemistry to encapsulate an antimicrobial agent, followed by using the capsules as a kind of reinforcement and additive in agar films. The nanoparticles formed from chitosan and STPP have been shown as spherical and with diameters in the range 85–1100 nm, depending on the conditions of preparation [156].

9.1.4.5 Cellulose Nanocrystals (CNC)

Because cellulose nanocrystals are relatively well known, the reader is referred to Chap. 1 of this volume for a general description and further citations. In general terms, CNC particles are rod-like and small (about 3.5–15 nm diameter by 100–300 nm lengths) for the most commonly prepared materials [178]. Though especially long CNCs, often called “whiskers”, can be obtained by acid hydrolysis of cellulose obtained from tunicates (sea creatures), such particles have been used in only a few notable cases for preparation of nanocomposite films [48, 179, 180]. Most researchers have employed concentrated sulfuric acid as a medium to hydrolyze the amorphous regions of the source cellulose material; as a consequence, the surfaces of the produced CNCs become substituted with sulfate half-ester groups, which impart a negative charge. The repulsion between like charges then serves to stabilize the particles in an aqueous suspension. Figure 9.4 contrasts the typical size and shape of a CNC particle with the next type of nanocellulose to be dicussed.

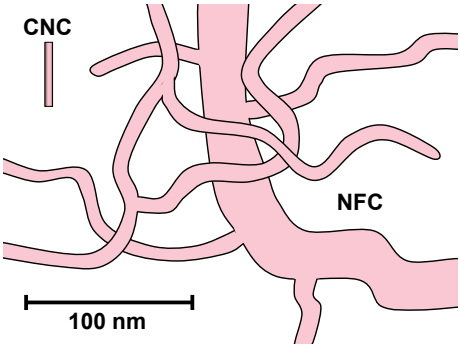

Fig. 9.4 Illustrations comparing typical sizes of cellulose nanocrystals (CNC) and nanofibrillated cellulose (NFC)

9.1.4.6 Nanofibrillated Cellulose (NFC)

When mechanical shearing is used as a primary means of separating cellulosic source material into nanoparticles, the resulting materials can be regarded as NFC. To earn the term "nano", it is understood that the fibrils need to be 100 nm or less in diameter. Typical diameters of NFC are about 20–30 nm [181], and their lengths are seldom quantified. Characteristics of NFC and related products are described in detail in the first chapter of this book. Outstanding features of NFC include a very high thickening tendency in aqueous suspensions and an irregular, branched structure and web-like structure in suspension [178]. Many of the researchers who have used NFC as an additive for barrier film enhancement have used TEMPO-mediated oxidation of the source cellulosic material [77, 116, 126, 140, 155, 182, 183]; such treatment renders a negative charge to the resulting NFC, promotes separation of fibrils, and decreases the amount of mechanical energy that needs to be applied to produce the NFC.

9.1.4.7 Bacterial Cellulose (BC)

The subject of bacterial cellulose is closely related to "nanocellulose" due to the fact that the cellulosic material produced at the surfaces of certain bacteria are already at a nano-scale at the time of their production [184]. Due to a wide variety of source microbes, growth conditions, and other factors, such as post-shearing, the range of diameters can range from about 4 nm, with no definable upper limit [14, 25]. Also, it is rare to see any ends of bacterial cellulose fibrils in published micrographs, which is suggestive of very long fibrils with high aspect ratios.

9.1.5 Options for Compatibilization

Before discussing the contributions of nanopolysaccharides to barrier properties of composite films, it is important to consider certain treatments that have been

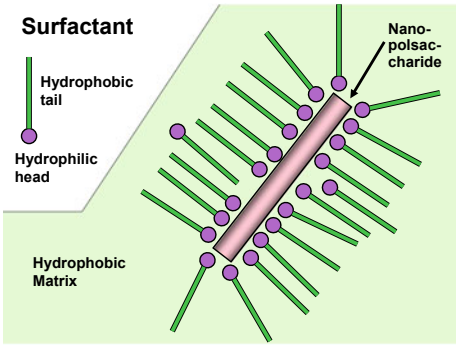

Fig. 9.5 Illustration of a proposed stabilizing role of surfactants when preparing composites with hydrophilic nanopolysaccharides in an oleophilic matrix

employed to achieve better compatibility between the surfaces of nanopolysaccharides and certain matrix materials [13]. Such treatments can be particularly important when the goal is to improve the mechanical or barrier properties of hydrophobic polymers such as polyethylene. Two main approaches have been used to enhance the wetting and dispersion of nanopolysaccharide particles in oleophilic polymer matrices—addition of surfactants and surface modification by covalent reactions.

9.1.5.1 Surfactants

Since nanopolysaccharides generally have water-loving surfaces with an abundance of –OH groups, it makes sense to use molecules in which a hydrophilic group is attached to a hydrophobic group, i.e. a surfactant. Thus, it has been widely reported that surfactants can help achieve better dispersion of nanopolysaccharides in oleophilic matrices, thus improving various film properties [65, 66, 83, 110, 113, 185]. Since surfactants do not stay fixed at surfaces to which they adsorb, some of their effects can be regarded as weak or temporary. But they are simple to use, and evidently they can be quite effective for preparation of some nanocomposites. Figure 9.5 illustrates how surfactant molecules might be expected to help compatibilize the interface between the hydrophilic surfaces of nanopolysaccharides and the hydrophobic surface of a typical plastic material in a hypothetical composite.

9.1.5.2 Surface Modification

Chemical approaches to modify the surface of cellulosic materials have been discussed in detail in other reviews [186–188]. Derivatization of the surfaces of nanoparticles can be tricky, since the particles are generally too small for ordinary filtration procedures. Thus, chemical byproducts of covalent reactions need to be removed by multiple centrifugation and rinsing steps or by dialysis. The following articles describe cases in which nanopolysaccharide particles were rendered hydrophobic,

and thus better able to serve as reinforcements in hydrophobic polymer matrices [9, 50, 66, 85, 101, 107, 111, 112, 114, 115, 118, 121, 142, 151, 185, 189–191].

9.2 Water Vapor and Oxygen Permeability

This section deals with both the criteria used to evaluate nanopolysaccharide-reinforced barrier films and their performance relative to these criteria.

9.2.1 Performance Indicators

Various protocols have been used to assess the barrier performance of reported nanopolysaccharide-reinforced composite films. Of the various criteria that have been considered, it appears that the most challenging objectives are to resist the permeation of both water vapor and oxygen, and to continue to resist such permeation even when the film is exposed to a wide range of humidity. In addition, the film needs to have sufficient strength, elastic modulus, and ability to stretch so that it does not break during typical usage. The film also needs to have sufficient integrity to avoid simple leakage of water vapor, oxygen, bacteria, or aromas, either into or out from the food package.

9.2.1.1 Water Vapor Barrier

In principle the water vapor permeability of a film or multi-layer packaging structure can be determined by maintaining different levels of relative humidity on the two sides and monitoring the gain or loss of mass in a reservoir of water or a selected solution on one of the sides [74, 148, 192–200]. Figure 9.6 shows a schematic illustration

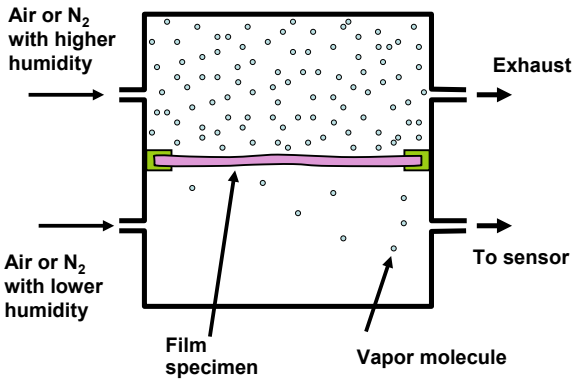

Fig. 9.6 Shematic illustration of one type of measuring system for water vapor permeability

of one type of equipment for such measurements. For example, Aulin et al. [196] studied the effect of relative humidity on water vapor permeability (WVP) values through a nanocellulose/alkyd resin bilayer film. They obtained WVP values of nanocellulose films at 50%, 80%, and 90% RH as 1.3, 13.6, and 36.6 g mm/m^2/day, respectively. Standard methods are available to measure water vapor permeability such as the gravimetric or the cup test method (ASTM E96 and ASTM F1249) using Mocon Perma-tran models. Advantages and disadvantages of the various methods have been discussed [192, 198, 199, 201].

Details need to be specified strictly, since the results are often dependent on the local values of relative humidity, and not just the computed gradient of relative humidity. Due to the abundant content of water-loving hydroxyl groups present on all polysaccharides, the nanomaterials can be expected to swell with increasing relative humidity. Thus, it is well known that the ability of polysaccharide-based films to resist water vapor will fall sharply with increasing relative humidity [45, 202]. Some other factors such as the chemical composition of sources [203], addition of plasticizers [204], and crystallinity of the matrix polymer also affect the water barrier function of polysaccharide films and coatings. Though the emphasis here will be on the effects of added nanopolysaccharides to a wide range of matrix polymers, which usually comprise about 95–99% of the dry weight of such films, one still needs to be concerned by water-vapor permeability of the nanoparticles themselves.

9.2.1.2 Oxygen Permeability

The permeability of nanocellulose-based barrier films relative to oxygen has been reviewed [205]. Test methods are available for evaluating permeability by oxygen [195–197, 206–212]. The permeability of gases through a substrate is defined as the quantification of permeate (gas and vapor) transmission through a resisting material [213, 214]. In a film without any defects such as pinholes or cracks, the primary mechanism of gas flow is solubilization of gas molecules on a film surface (Henry's law) followed by diffusion through the bulk (Fick's law), and finally desorption of gas molecules from the opposite surface. Permeability standard test methods such as ASTM standard F1927 and ASTM D3985 using MOCON's OTR (oxygen transmission rate) testers Ox-Tran 2/21 and Ox-Tran 1/50 respectively follow the same solubilization and diffusion principle [196, 207]. Further permeate diffusion across the substrate depends upon the type of gas molecules, temperature, difference in pressure, concentration gradient, film thickness, and area. According to Henry's law theory, gas molecules are unable to permeate a substrate if they are insoluble into the substrate material [215]. The other oxygen permeability test methods may include examining Gurley porosity, which provides information regarding air resistance through the films [216].

Strong correlations have been observed between a film's ability to impede passage of oxygen gas and its ability to block passage of nonpolar organic compounds, either in the gaseous or liquid state [217]. It appears that in each case, one of the keys to achieving effective resistance to nonpolar substances is a high energy cohesive

energy density of the film material [218]. The cohesive forces, which can arise due to extensive hydrogen bonding within dense films of cellulose and other polysaccharides, resist the solubilization and diffusion of the nonpolar molecules. However, as already mentioned, those same hydrogen bonds, which are holding the barrier film components together, are also strongly affected by the presence of humidity or moisture.

9.2.1.3 Leakage

Problems related to structural integrity of a barrier film can sometimes be revealed by microscopy and sometimes by testing of the strength properties. For instance, some polysaccharide films may crack during drying [105]. In an effort to increase the toughness of films prepared with CNC, McKee et al. [219] derivatized the surfaces of the nanoparticles with a glassy polymethacrylate polymer having side groups of ureido-pyrimidone. This in a case in which the reinforcing particles were covalently bonded to the polymer chains, which served as the matrix polymer in the resulting films. Alternatively, the incorporation of nanoreinforcements into a film can sometimes induce defects, especially when the contact of nanoparticles is high [68, 189, 220].

9.2.1.4 Antimicrobial

The antibacterial aspects of packaging materials can involve not only barrier issues, but also the inhibition of microbial growth, inhibition of colonization, or even killing of micro-organisms [221, 222]. In many cases the polymer matrix material plays a major role with respect to antimicrobial performance. For instance, many researchers have reported the tendency of chitosan to resist bacteria [3, 37, 123, 160, 165, 176, 223–226]. In addition, chitosan-based nanoparticles have been used to enhance the antibacterial properties of barrier films [76, 123, 166, 167]. It has been suggested that such antibacterial tendencies are related to the positive ionic charge of chitosan [227].

9.2.1.5 Other Performance Indicators

Effects of nanopolysaccharide particles on the strength of composite films have been reviewed elsewhere [14, 228]. Such issues can be important in the case of barrier properties in cases where a barrier film may be too weak (low tensile strength) or too brittle (low elongation to breakage) in order to avoid gross passage of vapors and even liquid.

9.2.2 Research Findings

In an effort to emphasize options that are in addition to the best-known nanopolysaccharide (nanocellulose), this section first considers research results pertaining to barrier films reinforced by nanostarch, nanochitin, and chitosan-based nanoparticles. Nanocellulose options are considered thereafter.

9.2.2.1 Nanostarch

Reported results for nanostarch incorporation in various composite films are listed in Table 9.1. As shown, in only a few cases did the authors report results for water vapor permeability testing. Three of those articles [47, 105, 162] reported significant reductions in the water vapor permeability of films that were mostly comprised of thermoplastic starch. Contrary results were reported by Kristo and Biliaderis [168], who added starch nanocrystals to a pullulan matrix. The cited authors speculated that in their system the starch nanoparticles may provide continuous pathways for water vapor diffusion. The results reported by Nasseri and Mohammadi [147] are especially worth noting, since it is logical to expect rod-like particles to be better reinforcing agent than spheres. Unexpectedly, more promising effects on barrier performance were achieved when adding the spherical nanoparticles. These authors attributed their findings to inherent excellent compatibility between the starch nanospheres and the starch matrix.

9.2.2.2 Nanochitin

Chitin also has been used as a source of nanoparticles, which have been used as reinforcements in barrier films. Table 9.2 lists relevant articles. Sriupayo et al. [78, 79] found that the water-vapor-permeability of both chitosan and polyvinyl alcohol films was substantially reduced by autoclave heat treatment at 110 °C. A relative further reduction in permeability, due to the addition of about 22% nanochitin particles, was still observed, as shown by the second values reported for permeability in the last two lines of Table 9.2.

9.2.2.3 Nanochitosan

As was noted earlier, despite their chemical similarity, nanoparticles based on chitosan differ in form from nanochitin, since the chitosan-based nanoparticles are formed by precipitation of the chitosan from aqueous solution. Published results from studies of chitosan-related nanoparticles (mostly precipitated with sodium tripolyphosphate) are listed in Table 9.3. Most of the results for water vapor per-

Table 9.1 Nanostarch particles and their reported effects on barrier film performance

Matrix type	NPs level (%)[a]	Relative change in permeability (%)		Research highlights	References
		Water vapor	Oxygen		
Starch	5–15	–	–	A reinforcing effect of the starch nano-crystals was attributed to hydrogen bonding with the matrix polymer	[161]
Poly-urethane	2–5	–	–	Enhanced mechanical performance was observed	[95]
PVOH	5–10	–	–	Lower moisture uptake was observed after adding starch nanocrystals	[128]
Pululan	20%+	1.3 at 20%	–	Water vapor permeability increased up to 20% NP; then it decreased	[168]
Starch	5, 30%	0.6	–	The starch nanocrystals also helped avoid cracking during drying of the film	[105]
Starch	5	0.38	–	Decreased performance was observed at >7% starch nanoparticles	[47]
Starch	4	0.57	–	The nanostarch also increased the tensile strength and modulus of the films. Most benefits were already achieved with the first 1% of nanostarch	[162]

(continued)

Table 9.1 (continued)

Matrix type	NPs level (%)[a]	Relative change in permeability (%)		Research highlights	References
		Water vapor	Oxygen		
Starch	10–20	–	–	Quasi-spherical starch nanoparticles gave greater strength benefit than rod-like CNC	[147]
Starch	5–25	–	–	Increasing nanostarch addition gave the composites higher modulus and less elongation	[80]

[a]NPs level (%): Nanoparticle content in film, mass percentage

meability were in the range of 0.4–0.81 in comparison to unfilled matrix material in different cases.

The most unusual result shown in the table involved the relatively hydrophobic polylactic acid (PLA) matrix polymer, for which a very strong improvement in oxygen barrier performance was found [119]. Such a result suggests that the nanoparticles helped to hold the relatively brittle PLA together in a contiguous layer. However, the hydrophilic nature of the nanochitosan evidently promoted the diffusion of water vapor, which is consistent with water's expected tendency to associate with polysaccharides.

9.2.2.4 Cellulose Nanocrystals (CNC)

When considering the preparation of barrier films containing nanocellulose, it is important to draw a distinction between cellulose-rich films [178] versus films in which the nanocellulose serves as reinforcement within a continuous matrix phase, which is the present focus. Table 9.4 lists results from studies in which CNC was included during the preparation of barrier films in a variety of continuous phases. Consistent with the results shown in the previous tables, the most frequent results for relative change in water vapor permeability due to the addition of CNC particles were in the range of about 0.5–0.9. However, there were some exceptions. Certain researchers obtained outstanding barrier performance in systems where solution-casting was employed [72, 73, 75]. Results for oxygen barrier performance were reported less often, and the relative permeabilities were often in the range of about

Table 9.2 Nanochitin particles and their reported effects on barrier film performance

Matrix type	NPs level (%)	Relative change in permeability (%)		Research highlights	References
		Water vapor	Oxygen		
Starch	3–5	0.6	–	Above 5% loading, the nanochitin particles adversely affected properties	[51]
Polyoct-anediol citrate	10–30	–	–	Decreased swelling in water was observed with increased nanochitin addition	[59]
Poly-propylene	1–2	0.25	–	Performance was better when the nano-chitin was derivatized with MAPP	[97]
Soy protein	5–30	–	–	The nanoparticles stiffened the films; agglomerates forms at higher content	[173]
Natural rubber	10	–	–	The diffusion rate of toluene was decreased by the nanochitin's presence	[175]
Carboxy methyl cellulose	1–10	0.9	–	The best resistance to water vapor was at 1% nanochitin content	[150]
Poly-lactic acid	–	1	–	Layers of nanochitin and CNC applied to the PLA surface did not decrease water vapor permeability	[120]

(continued)

Table 9.2 (continued)

Matrix type	NPs level (%)	Relative change in permeability (%)		Research highlights	References
		Water vapor	Oxygen		
Chitosan	22	0.66, 0.80	–	The nanochitin improved water resistance and decreased swelling	[78]
Polyvinyl alcohol	0–30	0.66, 0.52	–	The nanochitin improved water resistance and decreased swelling	[79]

0.25–1. Low values of oxygen permeability were obtained by the same group of researchers just cited [72, 73, 75] in addition to Deng et al. [131].

9.2.2.5 Nanofibrillated Cellulose (NFC)

The next type of nanopolysaccharide reinforcing particle to consider is NFC, the particles of which tend to be larger and more complex in comparison to CNC. Results reported for barrier films based on NFC within various matrix polymers are listed in Table 9.5. The results shown in Table 9.5 are notable for their diversity. In a few cases the NFC addition was very effective for decreasing the relative permeability of water vapor. The exceptional results reported by Nair et al. [92] can be attributed to the ability of an epoxy matrix to be formed at low viscosity, such that the reinforcing nanocellulose structure remains intact. The uncured epoxy resin was allowed to permeate into the dry nanocellulose film, followed by curing. In a couple of cases listed in the table, the best barrier results were achieved with NFC at very high levels, including 100% NFC [77, 163]. Not shown in the figure are a couple of related examples in which particularly promising reductions in oxygen permeability were achieved by coating pure NFC on top of another material of interest [116, 195, 229]. Such results are consistent with what has been reported in work related to pure NFC films and such films including minor amounts of other additives [45, 217].

9.2.2.6 Bacterial Cellulose (BC)

The last nanopolysaccharide to consider is bacterial cellulose. Like NFC, bacterial cellulose can be described as long and flexible in the wet state, though it can be expected to be highly diverse due to the wide variety of sources and culture conditions employed. Tome et al. [191] considered the permeability of water through films

Table 9.3 Nanochitosan particles and their reported effects on barrier film performance

Matrix type	NPs level (%)	Relative change in permeability (%)		Research highlights	References
		Water vapor	Oxygen		
Tara gum	10	0.77	–	Antimicrobial activity was reduced at high nanochitosan content	[123]
Starch	6	0.56	–	Higher than 8% nanoparticles led to a decrease in performances	[52]
HPMC	10	0.42	–	Hydroxypropyl methylcellulose became less permeable to water vapor	[156]
Agar	10	–	–	Mechanical properties of the films were enhanced	[166]
Alginate	10	–	–	Mechanical properties of the films were enhanced	[167]
Pectin	10	0.81	–	There was a minor decrease in water vapor permeability only for low-density methyl pectin, not for high density	[177]
Chitosan quinoa protein	1	0.83	–	The film was applied to a polyester (PET) clamshell package	[102]
Polylactic acid	5	1.6	0.1	Though the nanoparticles resisted oxygen, they promoted water vapor permeation	[119]

Table 9.4 Cellulose nanocrystal particles and their reported effects on barrier film performance

Matrix type	NPs level (%)	Relative change in permeability (%)		Research highlights	References
		Water vapor	Oxygen		
Alginate	1–10	0.83	–	Strength was highest at a 5% loading of the nanoparticles	[49]
HPMC	13.3	0.86	–	Hydroxymethylpropyl cellulose films with CNC resisted water vapor	[126]
Whey protein	4	0.69	–	The nanoparticles were well dispersed at up to 4% content	[127]
Chitosan	1	0.66	–	Slightly better resistance to water permeability was at 5% loading	[54]
Chitosan	10	1.05	0.14	Coatings applied to pears extended their shelf life	[131]
PHB	2	–	0.35	Poly(3-hydroxybutyrate) films became more resistant to oxygen gas	[132]
Polylactic acid	1–2	–	0.36–0.54	PLA chains were grafted onto the CNC to achieve higher performance	[85]
CMC and starch	0.5	0.6	–	A CMC-starch blend resisted water vapor better than pure CMC	[55]
Polylactic acid	2	0.67	0.63	A slightly higher oxygen barrier was observed with 6% CNC content	[111]
Polylactic acid	2–6	0.57	0.59	Grafted CNC, to achieve better compatibility, gave different results	[111]
Polylactic acid	2.5–15	1 or higher	1 or higher	Water vapor performance improved with grafting of the CNC	[112]

(continued)

Table 9.4 (continued)

Matrix type	NPs level (%)	Relative change in permeability (%)		Research highlights	References
		Water vapor	Oxygen		
Polylactic acid	1–5	0.66	0.52	Oxygen barrier was best at the higher CNC level. Surfactant helped	[113]
Polyvinyl acetate	2.5	0.38	–	High humidity disrupts CNC-polymer interactions	[94]
Gelatin	4	0.75	–	Tensile strength was also highest at 4% CNC	[135]
Alginate	5	0.69	–	Mechanical properties also were improved	[139]
PPC/PEC	0.3	–	0.24	The polyethylene glycol was used as a carrier for poly(propylene carbonate)	[263]
Polylactic acid	1	0.59	0.25	Water vapor permeability was observed at 85% relative humidity; O_2 evaluation was under dry conditions	[86]
Chitosan	5	0.73	–	Incorporation of CNC also decreased swelling	[60]
Tara gum	6	–	0.3	The water contact angle increased with increasing CNC up to 4%	[145]
Polyvinyl alcohol	5	0.3	–	Water vapor permeability was estimated by weight gain	[146]
Polylactic acid	1	–	0.74–0.83	Non-grafted CNC became less effective with increasing relative humidity	[118]
Polylactic acid	5	–	0.68–0.95	Grafted CNC was more affected by relative humidity	[118]

(continued)

Table 9.4 (continued)

Matrix type	NPs level (%)	Relative change in permeability (%)		Research highlights	References
		Water vapor	Oxygen		
Polylactic acid	1–3	0.57	–	Best results, slightly, were at 3% loading	[89]
Starch	2	0.60	–	The presence of lignin enhanced film properties also	[256]
Carboxy methyl cellulose	1	0.90	–	Increasing CNC decreased the water contact angle moderately	[148]
Carboxy methyl cellulose	5	0.74–0.81	–	CNC particles from three different plant sources were compared	[149]
Polyvinyl alcohol	10	0.36	–	Crosslinking treatment also decreased water vapor permeability	[151]
Gluten	7.5	0.64	–	Mechanical properties were also best at 7.5% CNC	[264]
Agar	3	0.75	–	Mechanical properties were optimized at 5% CNC	[265]
Agar	5	0.88	–	Best results were with CNC isolated using 45% concentration sulfuric acid	[266]
Carra-geenan	3	0.29	–	The carrageenan became less water-soluble in the presence of CNC	[71]
Polylactic acid	1–3	0.18	0.10	The CNC was prepared by freeze-drying before film casting	[72]
Carra-geenan	1–5	0.1	0.1	Films were prepared by solution casting	[73]

(continued)

Table 9.4 (continued)

Matrix type	NPs level (%)	Relative change in permeability (%)		Research highlights	References
		Water vapor	Oxygen		
Starch	3	0.1	0.08	CNC was incorporated into thermo-plastic starch by solution casting	[75]
Carra-geenan	5	0.81	–	Mechanical properties also increased significantly up to 5% of CNC content	[76]
Polyvinyl alcohol	9	0.71	–	Tensile strength also was greatly increased	[152]
Starch	3	0.28–0.87	–	Various different humidity levels on each side of the film were evaluated; the greatest advantage of the CNC was at the most humid conditions	[158]
Starch	0.3	0.7	–	Air permeability of paper coated with a CNC-reinforces starch layer was tested	[249]
PU/PVDC	0.1	0.4	–	Rod-shaped CNC was more effective than sphere-like CNC	[100]

Table 9.5 Nanofibrillated cellulose and its reported effects on barrier film performance

Matrix type	NPs level (%)	Relative change in permeability (%)		Research highlights	References
		Water vapor	Oxygen		
Polylactic acid	1	1.07	–	At higher levels, the performance of NFC was even poorer	[50]
HPMC	13.2	0.89	–	Slightly more promising results were obtained with CNC in parallel tests	[126]
Hydroxy-propyl guar	30	1.2	0.9	The oxygen barrier performance of a pure nanocellulose film was far superior to the nanocomposites	[209]
Guar gum	8	1.1	0.75	Much worse results for water vapor resistance were observed at 4% CNC	[183]
Mushroom polysacch.	–	0.52	–	Results are shown in comparison to the NFC film by itself, without the polysaccharide particles	[133]
Starch	10	0.62	–	Best barrier properties were at 10% NFC, but physical properties continued to rise with further NFC	[141]

(continued)

Table 9.5 (continued)

Matrix type	NPs level (%)	Relative change in permeability (%)		Research highlights	References
		Water vapor	Oxygen		
Epoxy	35	0.05	–	The composite far surpassed the barrier properties of the nanocellulose film by itself, and also of the epoxy	[92]
Carra-geenan	0.4–0.5	0.05	0.2	Solution casting exhibited positive effects of NFC on strength properties	[74]
Alginate	10–50	1+	–	NFC-reinforced films were no better than alginate alone in resisting water vapor after thickness normalization	[153]
Polylactic acid	1–10	1	–	No significant effects were demonstrated for barrier performance	[121]
Chitosan	15–25	0.2	0.15	Effects of NFC on barrier properties were slight at low NFC contents	[77]
Arabino–xylan	50	–	0.81	The pure xylan films were excellent oxygen barriers, and the NFC at the 20% level did not help	[194]

(continued)

Table 9.5 (continued)

Matrix type	NPs level (%)	Relative change in permeability (%)		Research highlights	References
		Water vapor	Oxygen		
Starch	1–100	0.5	–	Best results were with the nanocellulose alone	[163]
Polylactic acid	1–5	0.5–0.9	0.25–0.7	Excellent performance already at 1% content in the PLA	[197]
Collagen	10–20	0.63	–	The NFC also yielded higher tensile strength and less elongation	[267]

prepared from pure BC in water. Results were improved by heterogeneous esterification. No publications were found in which researchers used BC as the reinforcement for a polymer matrix.

9.3 Barrier Mechanism and Characterization

This section will review ideas that have been proposed to account for the barrier properties, as were listed in Tables 9.1, 9.2, 9.3, 9.4 and 9.5 of the previous section. In other words, various mechanistic concepts will be considered. This is the first time that such a comparison has been made based on such a large amount of relevant information. Notably, in the present work the collected data are presented together using a relative scale, comparing by what factor the nanopolysaccharide particles were able to change the permeabilities of a wide range of plastic films. The discussion that follows is organized into the subtopics of "opportunities", "challenges", and "prospects".

9.3.1 Opportunities

In the context of this chapter, an "opportunity" may consist of a mechanism by which the barrier properties of an eco-friendly, relatively inexpensive, and practical film can be enhanced. Focus will be placed on potential roles of nanopolysaccharides including nanostarch, nanochitin, chitosan-related nanoparticles, cellulose nanocrystals,

nanofibrillated cellulose, and bacterial cellulose. Three main categories of mechanistic explanation have appeared repeatedly in the related literature. In simple terms, these three types of explanation can be grouped according to the headings "tortuosity", "degree of crystallinity of the matrix", and "structural integrity of the matrix".

9.3.1.1 Tortuosity

Suppose that you were able to choose a material that was extremely thin, flat, and almost completely impervious to the passage of gas molecules. Suppose further that you were able to disperse suitably sized flakes of that material randomly and almost uniformly throughout a polymer film of interest. To the degree that both of those goals are achieved, one can then compute the extra distance that a monomer would need to diffuse in order to pass through the film. In fact, the tortuosity can be defined as the ratio of the actual mean distance that a molecule is required to diffuse in comparison to the same polymer film in the absence of the particles [12, 111, 230]. The concept is illustrated schematically in Fig. 9.7.

The situation that best corresponds to the description given in the previous paragraph is when a barrier film is filled with a mineral such as sodium montmorillonite, which often goes by the informal term "nanoclay" [38, 231, 232]. In fact, there are numerous accounts of the high effectiveness of nanoclay and related mineral products for achieving high levels of resistance to permeation through polymer films [27, 31, 108, 197, 230, 232–238].

Though the concept of tortuosity seems easily justified in the context of flat, very thin particles such as montmorillonite, it also has been invoked as a way to account for effects due to the inclusion of cellulose nanocrystals in a polymer film [86, 163]. Doubts related to application of tortuosity concepts as a main explanation for effects of nanocellulose were expressed by Mondal [20]. Citing results from Khan et al. [60], who reported a permeability reduction of 25% (relative permeability 0.75) due to the presence of 1% CNC, Mondal argued that the CNC was at much too low a

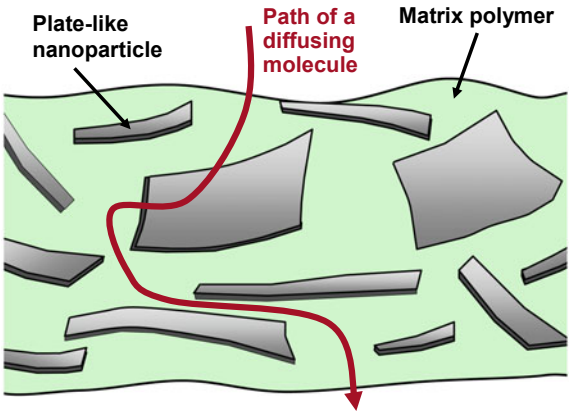

Fig. 9.7 Schematic depiction of increased tortuosity due to the presence of thin, relatively flat particles within a polymer matrix

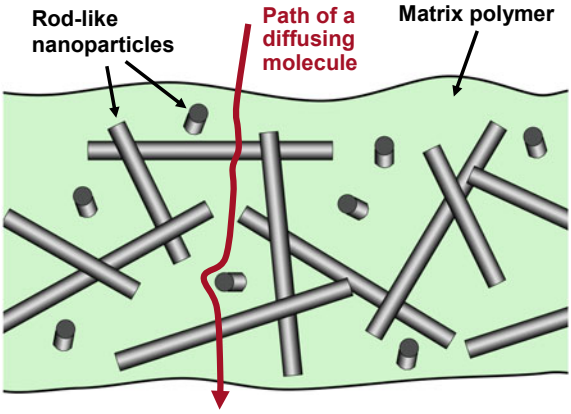

Fig. 9.8 Schematic depiction of minor increases in tortuosity due to the presence of thin, rod-like particles within a polymer matrix

concentration and of the wrong shape to possibly account for such a large change in permeability. Indeed, only a minor change in the path of diffusion would be needed for a molecule of gas to avoid the presence of a CNC particle due to its tiny diameter (often about 4–10 nm) and rod-like shape. This point is illustrated schematically in Fig. 9.8.

One can estimate that a 5% content of impervious rod-like particles in a matrix will increase the tortuosity value by only of the order of magnitude of 5% [239, 240]. This is not nearly enough to account of the water vapor barrier results reported in, for instance, Table 9.4.

A definitive study of reported literature related to the tortuosity issue, and its relationship to particle shape, was reported by Wolf et al. [220]. Results of hundreds of investigations were tabulated and then plotted on normalized scales. Though very large levels of seemingly random variation were found in all categories of the data, some general trends were very clear. In particular, flat particles such as montmorillonite have as a rule shown high correlation with strong decreases in permeability. By contrast, no clear trend was evident in dozens of studies involving rod-like or whisker-like reinforcing particles in composite films. It follows that any claims of large contributions to tortuosity due to the presence of nanopolysaccharides need to be regarded with skepticism. The take-away message is that if one wants to take advantage of tortuosity to reduce the permeability of a polymeric film, the fillers to consider ought to be plate-like particles.

When researchers choose to use montmorillonite nanoparticles in a composite, this does not necessarily rule out the use of nanopolysaccharide particles in the same structure. A few studies have used both nanocellulose and montmorillonite in the same nanocomposite film [197, 235]. Such usage of two contrasting types of particles simultaneously to reinforce a matrix is called a hybrid composite [241]. Presumably the platy nanoparticles would be used to increase the tortuosity, thus improving barrier performance. The additional use of a nanopolysaccharide ingredient would have to be justified in terms of other properties, such as strength. Yet another promising

approach is to use a platy clay-type nanoparticle in combination with nanofibrillated cellulose in the absence of any matrix polymer [242, 243].

9.3.1.2 Degree of Crystallinity of the Matrix

Many researchers have proposed that the presence of nanoparticles can positively affect the degree of crystallinity in a matrix polymer during such processes as evaporation of a solvent (in the case of cast films) or cooling of a melted polymer (in the case of extruded films) [58, 66, 107, 109, 112, 114, 119]. In other words, it has been hypothesized that the nanoparticles serve as points of nucleation for crystal formation and that a higher proportion of crystalline volume within a matrix polymer will mean fewer or more restricted passages for the permeation of gas molecules. The concept is illustrated schematically in Fig. 9.9. Evidence to support the inducement of crystallinity mechanism includes differential scanning calorimetry [93, 114, 244]. Further evidence may involve increases in the glass transition temperature of a matrix polymer in the vicinity of nanoparticles [50, 52, 93, 110, 162, 168, 245]. Karkhanis et al. [86] reported a favorable correlation between permeability and crystallinity of polylactic acid (PLA) films, where the increases in crystallinity were induced by the presence of CNC.

A related mechanism appears to play a role in the case of cellulose films when they are heated in the absence of a matrix polymer [246, 247], and it seems likely that something similar might happen in some cases even when a matrix polymer is present. The heat treatment appears to be effective in reducing the gas permeability of cellulose-rich films by promoting the development of crystallinity at the planes of cellulose-to-cellulose contact within the nanostructure [248].

Though it seems reasonable to suppose that induced increases in crystallinity of matrix polymers could account for some of the decreases in permeability due to

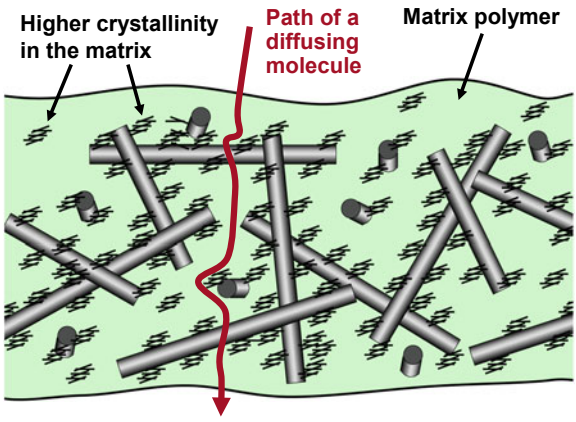

Fig. 9.9 Schematic drawing representing a hypothetical tendency of certain nanoparticles to induced increased crystallization within the matrix polymer, where the crystalline zones are assumed to have decreased permeability to oxygen or other monomers

inclusion of nanopolysaccharides (see Tables 9.1, 9.2, 9.3, 9.4 and 9.5), there seems to be a need for research focused more directly at elucidating such issues.

9.3.1.3 Structural Integrity of the Matrix

Most published studies of nanocomposite barrier films make an implicit assumption that the observed rates of permeation are indicative of average film properties rather than being dominated by local defects such as cracks or holes. However, another way to try to account for positive effects of nanopolysaccharides on barrier film performance is to hypothesize that their presence improves the integrity of the films by resisting cracking or tearing, etc. Alternatively, the role of nanocellulose in such films has been described as improving the cohesiveness of the barrier films [6]. As was noted earlier, various studies found evidence of cracking or other defects likely to hurt barrier performance of films [68, 105, 189, 220]. Because cracks or pinholes may remain undetected during typical experimentation, it is very difficult to estimate what kind of impact such defects will have in typical applications of barrier films. On the other hand, it is reasonable to consider reinforcement with relatively low levels (usually below 3%) of nanopolysaccharides as a strategy to attempt to promote barrier film integrity. Figure 9.10 presents a schematic illustration of the concept of using nanoparticles to reinforce a thin film so that it is less likely to develop cracks.

9.3.2 Challenges

In the present context a "challenge" can be understood as something that may explain a failure of barrier properties, in a certain case, to meet expectations, as might have been expected based on what was described in the previous subsection. Two types of

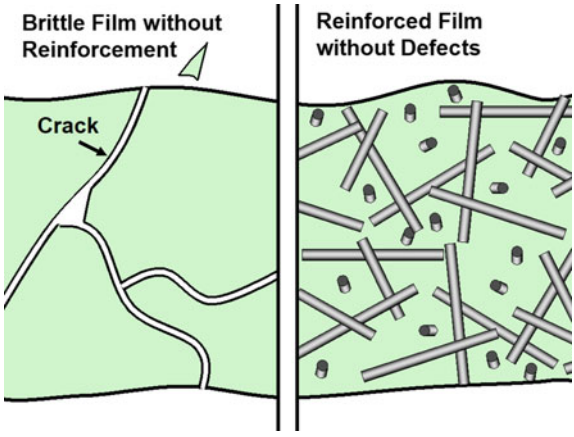

Fig. 9.10 Schematic illustration of the concept that the presence of nanoreinforcements may help to preserve the integrity of a barrier film during its preparation, processing, storage, and utilization

such challenges will be highlighted here: effects related to nonuniform distributions of nanoparticles and effects related to plasticization phenomena.

9.3.2.1 Nonuniformity

When considering the results shown in Tables 9.1, 9.2, 9.3, 9.4 and 9.5, representing about 70 studies that have dealt with the barrier properties of nanopolysaccharide-reinforced polymer films, some adjectives that might be used to summarize the combined findings may include "fussy", "marginal", and "exceptional". The word "fussy" is used here because of the wide range of findings, which seems to reflect a high sensitivity of barrier-enhancing mechanisms to various experimental details, such as the proportion of nanoparticles employed, details in how the system is mixed, the manner in which the film is formed, and maybe even differences in the detailed shapes of particles when comparing the results of studies that fall into a given category. When considering the suitability of a technology for industrial application, the manufacturing teams will require that the selected technology should work with high reliability to achieve a narrow range of outcomes.

The word "marginal" can be used when describing the most frequently reported ranges of relative permeability shown in Tables 9.1, 9.2, 9.3, 9.4 and 9.5. As noted already, many of the results related to water vapor permeability changes have fallen into the range of about 0.5–0.9. Though such improvements would be expected to have some value in extending the shelf life of certain food products, questions may arise as to whether implementation of the technology would be worth the trouble in comparison to some other approaches that could be implemented quickly with existing technology. For example, the thickness of a default barrier layer, not incorporating nanopolysaccharides, could just be increased by a moderate proportion. Or the temperatures of refrigeration during storage and transportation might be adjusted downwards by a moderate amount. There is an understanding among industrial process engineers that the most favorable results achieved in the laboratory are often not realized under the more constrained conditions of industrial processing. For example, the industrial equipment is likely to employ higher levels of hydrodynamic shear, which would be expected to result in more breakage of nanoparticles. Due to such considerations, highly promising results in the laboratory are often regarded as the basis for expecting marginally promising results at the scale of commercial production.

The word "exceptional" is used here to call attention to certain reported work in which the relative reductions in permeability to water vapor or oxygen were much greater than what was reported in most other work. The results reported by Nair et al. [92], Savadekar et al. [73–75], and Sanchez-Garcia and coworkers [71, 72] can be highlighted. Are such results merely reflective of the experimental skill and persistence of certain researchers, or are they reflective of some processing tricks that such researchers have selected to use? For example, is there some inherent advantage that can be gained by curing an epoxy resin after it has been infused into a pre-formed structure of nanocellulose [92]? Or is there something inherently advantageous that

can be achieved by providing time for nanoparticles to organize themselves during a gradual process of drying [17, 74]? Future researchers might consider further work related to some of the most promising findings tabulated in this review, with a goal to identifying what can make such results possible during routine production at an industrial scale.

9.3.2.2 Clusters as Defects

A great many researchers have reported the development of pronounced agglomeration of nanoparticles when attempting to prepare nanocomposites in which the proportion of nanoparticles is above a threshold, which is often in the range of about 3–5% [48, 50, 58, 71, 72, 74, 75, 82, 94, 97, 118, 148, 175, 249]. Clusters of particles seem to serve as defects in film structures, offering passages by which permeating gas molecules can pass relatively freely.

As noted by Kargarzadeh et al. [17], the threshold concentration of nanoparticles (as a volume fraction) needed to bring about significant agglomeration can be predicted from Eq. (9.1),

$$\text{Percolation concentration} = 0.7\,\mathrm{d/L} \tag{9.1}$$

where d is the particle diameter and L is its length. This equation predicts that long, slender particles, especially NFC and bacterial cellulose strands, will encounter serious clustering problems at very low contents. The equation also helps to make sense of the many articles that have reported the presence of notable agglomeration above various threshold levels [48, 50, 58, 71, 72, 74, 75, 82, 94, 97, 118, 148, 175, 249]. It is proposed here that clustering of nanopolysaccharide particles when they are present at levels above the percolation threshold is mainly a consequence of inter-particle collisions in shear flow. Such concepts have been well developed in the field of papermaking to predict the level of fiber flocculation, which affects the uniformity of manufactured paper [250, 251].

9.3.2.3 Self-assembly

Imagine a hypothetical mixture in which the nanoparticles act like highly obedient robots and organize themselves into patterns that maximize desired outcomes, which may include barrier properties. Such behavior is known in the literature as self-assembly, and there is some evidence that the idea may have some relevance for the formation of nanocomposites having superior barrier performance. For instance, it has been suggested that during casting of composites from a polymer solution, the particles may have time to self-organize into networks [17]. For this to happen effectively, there has to be sufficient available time and the viscosity needs to be suitably low. Also, the results can be expected to depend on the details of various forces acting between the solid surfaces in the suspension [252]. Capadona et al.

[253] worked towards achieving such advantages by allowing NFC first to assemble itself from aqueous suspension into a film, which was solvent-exchanged, dried, and then the nano-scaffold was filled with solutions of polymers such as polystyrene. Grande et al. [137, 138] used the term "self-assembly" to describe the formation of a nanocellulose film by bacterial synthesis, which is another way that such results could be achieved. Also, the term self-assembly has been used to describe some aspects of layer-by-layer assembly of barrier films, which may include nanopolysaccharides [144, 157]. However, the present search of the literature did not reveal any serious work in which credible progress has been made related to self-organization of nanoreinforcement particles within ordinary nanocomposite films. That is why self-assembly is included here in the subsection titled "challenges", rather than the previous subsection titled "opportunities". Courageous and inventive researchers are invited to consider this area of research.

9.3.2.4 Plasticizer Action Versus Permeability

The urge to formulate using multiple, contrasting ingredients can be almost irresistible. You need strength, so you add something strong. You need something to resist oxygen permeation, so you use some nanocellulose, which when used alone can give superior oxygen barrier performance [45, 217]. You need resistance to water, so you add something hydrophobic [64, 254]. As noted by Lindström and Aulin [36], the hydrophobic and hydrophilic ingredients will tend to phase-separate, making it challenging to achieve sufficient uniformity of the mixture. And finally, you need something to make the film less brittle, so you use a plasticizer. The most common plasticizers used for polysaccharides are glycerol, sorbitol or xylitol [255]. Indeed, many researches have used plasticizers in an effort to achieve a favorable balance of strength and flexibility of nanopolysaccharide composite films [8, 52, 62, 69, 81, 83, 124, 159, 161, 162, 168, 174, 179, 224, 229, 256–260]. Unfortunately, in addition to helping to achieve specific target properties, each additional ingredient is likely to have adverse effects on other desired attributes. When it comes to barrier properties, several studies have shown unfavorable effects of plasticizers [257–259]. On the other hand, Pereda et al. [69] found that CNC in combination with plasticizer can achieve favorable barrier performance in addition to flexibility. The frequently observed decreases in oxygen barrier performance with the addition of plasticizers can be related to the changes in secondary relaxations, leading to increased diffusion of oxygen molecules. In summary, this seems to be a topic that could use some well-focused research.

As was noted in an earlier review, relatively pure films composed of NFC can give superior resistance to oxygen permeation, but only at low to moderate relative humidity [45]. This is almost the opposite from the approach of using a multicomponent mixture, as in the examples cited in the previous paragraph. The challenge is to find some way to keep the purity of such a hydrophilic layer—as required for resistance to oxygen, when somehow protecting that layer with a hydrophobic barrier. Thus, rather than aiming for a composite structure, several research teams have

employed layered film structures as a strategy to achieve favorable combinations of barrier performance against both permeants. The following articles reported use of hydrophobic layers in combination with nanopolysaccharide layers [29, 45, 64, 88, 98, 116, 157, 195, 205, 261, 262].

9.3.3 Prospects

A "prospect" will be defined here as a prediction or educated guess of possible future developments based on the consideration of a large number of recent research studies, as have been considered already in this chapter.

With respect to lines of research and paths to industrial implementation, the collected findings summarized in this chapter show that many options are available to the researcher or developmental engineer. Depending on the balance that one is seeking with respect to such goals as strength, barrier properties, edibility, and many others, one can first choose from among nanostarch, nanochitin, chitosan-based nanoparticles, and various kinds of nanocellulose as the reinforcing phase. Thus, starch nanoparticles may be an ideal choice for reinforcement of starch films applied directly to food. Chitin or chitosan-based nanoparticles might have advantages for achieving specific property goals, maybe related to microbial resistance. Cellulose-based nanoparticles might be the best choice in situations where the strength of the nanoparticles is expected to be important. The nanopolysaccharides may be combined with a wide selection of matrix polymers by use of many contrasting assembly strategies, chief among which would be casting from solution and melt-extrusion. A number of alternative strategies of assembly need to be considered seriously, such as pre-forming of the nanopolysaccharide skeletal framework followed by infusion and curing of the matrix phase.

A second lesson that one can take from the general findings from many research accounts is that one ought to be modest in one's expectations regarding the relative change in permeability to water vapor and oxygen that is likely to be achieved by addition of the nanopolysaccharide particles. The modest gains that typically can be expected from the addition of about 0.5–5% of nanopolysaccharide content can be attributed to the relative ineffectiveness of fibrilar particles in the physical blocking of permeating molecules. If high tortuosity in a film is one's goal, then it is recommended to work with very thin, plate-like nanoparticles such as montmorillonite and related mineral nanoparticles. Since rod-like or fibrillar nanoparticles present at minor levels in a composite cannot be expected to be very effective at increasing the tortuosity of typical composite film, it is recommended that future researchers place emphasis on examining the effects of nanopolysaccharides on the resulting levels of crystallization and film integrity as primary candidate explanations of improvements in barrier properties upon addition of the nanopolysaccharides.

A third take-away message is for researchers and developmental engineers to exercise caution in implementation of strategies that call for the combining of incompatible phases within nanocomposites. Ordinary nanopolysaccharide particles cannot

be expected to disperse well in many widely used plastic materials, including not only polyethylene, but also some emerging bio-based meltable polymers such as poly-lactic acid. Many studies have shown that the surfaces of nanopolysaccharides can be modified by surfactant addition or chemical derivatization to overcome such incompatibilities in the laboratory. But the very high surface areas per unit mass of nanoparticles implies a high cost for such approaches.

A final summary comment is to urge researchers not to restrict their attention to typical composite strategies such as single-layer solvent casting and single-layer extrusion. One should avoid slavish focus just on composites in situations where strategies based on more than one layer may provide more practical answers. One of the most promising ways to minimize problems inherent in the mixing of incompatible phases appears to be the assembly of such phases into separate layers. Although such barrier structures may not fit all the usual definitions of composites, it seems that they may offer promising paths to achieving challenging and economically practical goals for various food packaging applications.

References

1. Bharimalla AK, Deshmukh SP, Vigneshwaran N et al (2017) Nanocellulose-polymer composites for applications in food packaging: current status, future prospects and challenges. Polym-Plast Technol Eng 56:805–823
2. Abdul Khalil HPS, Bhat AH, Yusra AFI (2012) Green composites from sustainable cellulose nanofibrils: a review. Carbohydr Polym 87:963–979
3. Abdul Khalil HPS, Saurabh CK, Adnan AS et al (2016) A review on chitosan-cellulose blends and nanocellulose reinforced chitosan biocomposites: properties and their applications. Carbohydr Polym 15:216–226
4. Khalil HPSA, Tye YY, Sourabh CK et al (2017) Biodegradable polymer films from seaweed polysaccharides: a review on cellulose as a reinforcement material. eXPRESS Polym Lett 11:244–265
5. Azeredo HMC (2009) Nanocomposites for food packaging applications. Food Res Int 42:1240–1253
6. Azeredo HMC, Rosa MF, Mattoso LHC (2017) Nanocellulose in bio-based food packaging applications. Indust Crops Prod 97:664–671
7. Berglund LA, Peijs T (2010) Cellulose biocomposites—From bulk moldings to nanostructured systems. MRS Bull 35:201–207
8. Castro-Rosas J, Cruz-Galvez AM, Gomez-Aldapa CA et al (2016) Biopolymer films and the effects of added lipids, nanoparticles and antimicrobials on their mechanical and barrier properties: a review. Intl J Food Sci Technol 51:1967–1978
9. Chakrabarty A, Teramoto Y (2018) Review. Recent advances in nanocellulose composites with polymers: a guide for choosing partners and how to incorporate them. Polymers 10: article no 517
10. Dufresne A (2010) Processing of polymer nanocomposites reinforced with polysaccharide nanocrystals. Molecules 15:4111–4128
11. Dufresne A, Castano J (2017) Polysaccharide nanomaterial reinforced starch nanocomposites: a review. Starch-Starke 69: article no 1500307
12. Feldman D (2013) Polymer nanocomposite barriers. J Macromol Sci Part A Pure Appl Chem 50:441–448

13. Ferreira FV, Dufresne A, Pinheiro IF et al (2018) How do cellulose nanocrystals affect the overall properties of biodegradable polymer nanocomposites: a comprehensive review. Eur Polym J 108:274–285
14. Ferrer A, Pal L, Hubbe M (2017) Nanocellulose in packaging: advances in barrier layer technologies. Indust Crops Prod 95:574–582
15. Freire CSR, Fernandes SCM, Silvestre AJD et al (2013) Novel cellulose-based composites based on nanofibrillated plant and bacterial cellulose: recent advances at the University of Aveiro—a review. Holzforschung 67:603–612
16. Ilyas RA, Sapuan SM, Sanyang ML et al (2018) Nanocrystalline cellulose as reinforcement for polymeric matrix nanocomposites and its potential applications: a review. Current Anal Chem 14:203–225
17. Kargarzadeh H, Mariano M, Huang J et al (2017) Recent developments on nanocellulose reinforced polymer nanocomposites: a review. Polymer 132:368–393
18. Khan A, Huq T, Khan RA et al (2014) Nanocellulose-based composites and bioactive agents for food packaging. Crit Rev Food Sci Nutr 54:163–174
19. Kumar N, Kaur P, Bhatia S (2017) Advances in bio-nanocomposite materials for food packaging: a review. Nutrition Food Sci 47:591–606
20. Mondal S (2018) Review on nanocellulose polymer nanocomposites. Polymer-Plastics Technol Eng 57:1377–1391
21. Paunonen S (2013) Strength and barrier enhancements of cellophane and cellulose derivative films: a review. BioResources 8:3098–3121
22. Paunonen S (2013) Strength and barrier enhancements of composites and packaging boards by nanocelluloses—a literature review. Nordic Pulp Paper Res J 28:165–181
23. Perez-Pacheco E, Canto-Pinto JC, Moo-Huchin VM et al (2016) Thermoplastic starch (TPS)-cellulosic fibers composites: mechanical properties and water vapor barrier: a review. In: Poletto M (ed) Composites from renewable and sustainable materials. INTEACH, pp 85–105
24. Sanchez-Garcia MD, Lopez-Rubio A, Lagaron JM (2010) Natural micro and nanobiocomposites with enhanced barrier properties and novel functionalities for food biopackaging applications. Trends Food Sci Technol 21(11):528–536
25. Siro I, Plackett D (2010) Microfibrillated cellulose and new nanocomposite materials: a review. Cellulose 17:459–494
26. Stark NM (2016) Opportunities for cellulose nanomaterials in packaging films: a review and future trends. J Renewable Mater 4:313–326
27. Vasile C (2018) Polymeric nanocomposites and nanocoatings for food packaging: A review. Materials 11: article no 1834
28. Robertson GL (2013) Food packaging principles and practice, 3rd edn. CRC Press. Taylor & Francis, Boca Raton, p 703
29. Arora A, Padua GW (2010) Review: nanocomposites in food packaging. J Food Sci 75:R43–R49
30. Duncan TV (2011) Applications of nanotechnology in food packaging and food safety: Barrier materials, antimicrobials and sensors. J Colloid Interface Sci 363:1–24
31. Silvestre C, Duraccio D, Cimmino S (2011) Food packaging based on polymer nanomaterials. Prog Polym Sci 36:1766–1782
32. Othman SH (2014) Bio-nanocomposite materials for food packaging applications: types of biopolymer and nano-sized filler. In: Chen NL, Man HC, Talib RA (eds) 2nd international conference on agricultural and food engineering (CAFE 2014)—new trends forward. Book series: agriculture and agricultural science procedia vol 2, pp 296–303
33. Bledski AK, Gassan J (1999) Composites reinforced with cellulose based fibres. Prog Polym Sci 24:221–274
34. Hubbe MA, Rojas OJ, Lucia LA et al (2008) Cellulosic nanocomposites. A review. BioResources 3:929–980
35. Moon RJ, Martini A, Nairn J et al (2011) Cellulose nanomaterials review: structure, properties, and nanocomposites. Chem Soc Rev 40:3941–3994

36. Lindstrom T, Aulin C (2014) Market and technical challenges and opportunities in the area of innovative new materials and composites based on nanocellulosics. Scand J Forest Res 29:345–351
37. Cagri A, Ustunol Z, Ryser ET (2004) Antimicrobial edible films and coatings. J Food Protection 67:833–848
38. Chivrac F, Pollet E, Avérous L (2009) Progress in nano-biocomposites based on polysaccharides and nanoclays. Mater Sci Eng: R Reports 67:1–17
39. Rhim JW, Park HM, Ha CS (2013) Bio-nanocomposites for food packaging applications. Prog Polym Sci 38(10–11):1629–1652
40. Mohanty F, Swain SK (2018) Bionanocomposites for food packaging applications. In: Oprea AE, Grumezescu AM (eds) Nanotechnology applications in food. flavor, stability, nutrition and safety. Elsevier BV, Amsterdam. (Ch 18)
41. Hansen NML, Plackett D (2008) Sustainable films and coatings from hemicelluloses: a review. Biomacromol 9(6):1493–1505
42. Tavassoli-Kafrani E, Shekarchizadeh H, Masoudpour-Behabadi M (2016) Development of edible films and coatings from alginates and carrageenans. Carbohydr Polym 137:360–374
43. Porta R, Mariniello L, Di Pierro P et al (2011) Transglutaminase crosslinked pectin- and chitosan-based edible films: a review. Crit Rev Food Sci Nutrition 51:223–238, article no PII 934350148
44. Hassan B, Chatha SAS, Hussain AI et al (2018) Recent advances on polysaccharides, lipids and protein based edible films and coatings: A review. Intl J Biol Macromol 109:1095–1107
45. Hubbe MA, Ferrer A, Tyagi P et al (2017) Nanocellulose in thin films, coatings, and plies for packaging applications: a review. BioResources 12:2143–2233
46. Lange J, Wyser Y (2003) Recent innovations in barrier technologies for plastic packaging—a review. Pack Technol Sci 16:149–158
47. Li F, Mascheroni E, Piergiovanni L (2015) The potential of nanocellulose in the packaging field: a review. Packag Technol Sci 28:475–508
48. Favier V, Chanzy H, Cavaille JY (1995) Polymer nanocomposites reinforced by cellulose whiskers. Macromol 28:6365–6367
49. Abdollahi M, Alboofetileh M, Behrooz R et al (2013) Reducing water sensitivity of alginate bio-nanocomposite films using cellulose nanoparticles. Int J Biol Macromol 54:166–173
50. Abdulkhani A, Hosseinzadeh J, Dadashi S et al (2015) A study of morphological, thermal, mechanical and barrier properties of PLA based biocomposites prepared with micro and nano sized cellulosic fibers. Cellulose Chem Technol 49(7–8):597–605
51. Chang PR, Jian RJ, Yu J et al (2010) Starch-based composites reinforced with novel chitin nanoparticles. Carbohyd Polym 80:420–425
52. Chang PR, Jian RJ, Yu JG et al (2010) Fabrication and characterisation of chitosan nanoparticles/plasticised-starch composites. Food Chem 120:736–740
53. Chang PR, Jian RJ, Zheng PW et al (2010) Preparation and properties of glycerol plasticized-starch (GPS)/cellulose nanoparticle (CN) composites. Carbohyd Polym 79:301–305
54. Corsello FA, Bolla PA, Anbinder PS et al (2017) Morphology and properties of neutralized chitosan-cellulose nanocrystals biocomposite films. Carbohydr Polym 156:452–459
55. El Miri N, Abdelouandi K, Barakat A et al (2015) Bio-nanocomposite films reinforced with cellulose nanocrystals: Rheology of film-forming solutions, transparency, water vapor barrier and tensile properties of films. Carbohydr Polym 129:156–167
56. Fernandes SCM, Freire CSR, Silvestre AJD et al (2010) Transparent chitosan films reinforced with a high content of nanofibrillated cellulose. Carbohydr Polym 81:394–401
57. Heshmati V, Kamal MR, Favis BD (2018) Cellulose nanocrystal in poly(lactic acid)/polyamide11 blends: Preparation, morphology and co-continuity. Eur Polym J 98:11–20
58. Hossain KMZ, Jasmani L, Ahmed I et al (2012) High cellulose nanowhisker content composites through cellosize bonding. Soft Matter 8:12099–12110
59. Ji YL, Wang XM, Liang K (2014) Regulating the mechanical properties of poly(1,8-octanediol citrate) bioelastomer via loading of chitin nanocrystals. RSC Advan 4:41357–41363

60. Khan A, Khan RA, Salmieri S et al (2012) Mechanical and barrier properties of nanocrystalline cellulose reinforced chitosan based nanocomposite films. Carbohydr Polym 90:1601–1608
61. Kord B, Malekian B, Yousefi H et al (2016) Preparation and characterization of nanofibrillated cellulose/poly (vinyl alcohol) composite films. Maderas Cienc Tecnol 18:743–752
62. Kvien I, Oksman K (2007) Orientation of nanowhiskers in polyvinyl alcohol. Appl Phys A Mater Sci Process 87:641–643
63. Lee SY, Mohan DJ, Kang IA et al (2009) Nanocellulose reinforced PVA composite films: effects of acid treatment and filler loading. Fibers Polymers 10:77–82
64. Li DF, Moriana R, Ek M (2016) From forest residues to hydrophobic nanocomposites with high oxygen-barrier properties. Nordic Pulp Paper Res J 31:261–269
65. Ljungberg N, Bonini C, Bortolussi F et al (2005) New nanocomposite materials reinforced with cellulose whiskers in atactic polypropylene: Effect of surface and dispersion characteristics. Biomacromol 6:2732–2739
66. Ljungberg N, Cavaillé JY, Heux L (2006) Nanocomposites of isotactic polypropylene reinforced with rod-like cellulose whiskers. Polymer 47:6285–6292
67. Ma L, Wang LL, Wu LX et al (2014) Cellulosic nanocomposite membranes from hydroxypropyl cellulose reinforced by cellulose nanocrystals. Cellulose 21:4443–4454
68. Pereda M, Amica G, Rácz I et al (2011) Structure and properties of nanocomposite films based on sodium caseinate and nanocellulose fibers. J Food Eng 103:76–83
69. Pereda M, Dufresne A, Aranguren ME et al (2014) Polyelectrolyte films based on chitosan/olive oil and reinforced with cellulose nanocrystals. Carbohydr Polym 101:1018–1026
70. Petersson L, Kvien I, Oksman K (2007) Structure and thermal properties of poly(lactic acid)/cellulose whiskers nanocomposite materials. Composites Sci Technol 67(11–12):2535–2544
71. Sanchez-Garcia MD, Hilliou L, Lagaron JM (2010) Morphology and water barrier properties of nanobiocomposites of k/i-hybrid carrageenan and cellulose nanowhiskers. J Agric Food Chem 58:12847–12857
72. Sanchez-Garcia M, Lagaron J (2010) On the use of plant cellulose nanowhiskers to enhance the barrier properties of polylactic acid. Cellulose 17:987–1004
73. Savadekar NR, Karande VS, Vigneshwaran N et al (2014) Preparation of cellulose nanowhiskers and its effect on performance properties of k-carrageenan. J Biomased Mater Bioenergy 8:618–626
74. Savadekar NR, Karande VS, Vigneshwaran N et al (2012) Preparation of nanocellulose fibers and its application in kappa-carrageenan based film. Intl J Biol Macromol 51:1008–1013
75. Savadekar NR, Karande VS, Vigneshwaran N et al (2015) Preparation of cotton linter nanowhiskers by high-pressure homogenization process and its application in thermoplastic starch. Appl Nanosci 5:281–290
76. Shankar S, Reddy JP, Rhim JW et al (2015) Preparation, characterization, and antimicrobial activity of chitin nanofibrils reinforced carrageenan nanocomposite films. Carbohydr Polym 117:468–475
77. Soni B, Hassan E, Schilling MW et al (2016) Transparent bionanocomposite films based on chitosan and TEMPO-oxidized cellulose nanofibers with enhanced mechanical and barrier properties. Carbohydr Polym 151:779–789
78. Sriupayo J, Supaphol P, Blackwell J et al (2005) Preparation and characterization of α-chitin whisker-reinforced chitosan nanocomposite films with or without heat treatment. Carbohydr Polym 62:130–136
79. Sriupayo J, Supaphol P, Blackwell J et al (2005) Preparation and characterization of alpha-chitin whisker-reinforced poly(vinyl alcohol) nanocomposite films with or without heat treatment. Polymer 46:5637–5644
80. Viguie J, Molina-Boisseau S, Dufresne A (2007) Processing and characterization of waxy maize starch films plasticized by sorbitol and reinforced with starch nanocrystals. Macromol Biosci 7:1206–1216
81. Zarina S, Ahmad I (2015) Biodegradable composite films based on κ-carrageenan reinforced by cellulose nanocrystal from kenaf fibers. BioResources 10:256–271

82. Alloin F, D'Aprea A, Dufresne A et al (2011) Poly(oxyethylene) and ramie whiskers based nanocomposites: Influence of processing: Extrusion and casting/evaporation. Cellulose 18:957–973
83. Bondeson D, Oksman K (2007) Dispersion and characteristics of surfactant modified cellulose whiskers nanocomposites. Compos Interfaces 14(7–9):617–630
84. Charlon S, Follain N, Chappey C et al (2015) Improvement of barrier properties of bio-based polyester nanocomposite membranes by water-assisted extrusion. J Membrane Sci 496:185–198
85. Dhar P, Gaur SS, Soundararajan N et al (2017) Reactive extrusion of polylactic acid/cellulose nanocrystal films for food packaging applications: Influence of filler type on thermomechanical, rheological, and barrier properties. Indust Eng Chem Res 56:4718–4735
86. Karkhanis SS, Stark NM, Sabo RC et al (2018) Water vapor and oxygen barrier properties of extrusion-blown poly(lactic acid)/cellulose nanocrystals nanocomposite films. Compos Part A Appl Sci Manuf 114:204–211
87. Lemahieu L, Bras J, Tiquet P et al (2011) Extrusion of nanocellulose-reinforced nanocomposites using the dispersed nano-objects protective encapsulation (DOPE) process. Macromol Mater Eng 296:984–991
88. Lu P, Xiao HN, Zhang WW et al (2014) Reactive coating of soybean oil-based polymer on nanofibrillated cellulose film for water vapor barrier packaging. Carbohyd Polym 111:524–529
89. Martinez-Sanz M, Lopez-Rubio A, Lagaron JM (2012) Optimization of the dispersion of unmodified bacterial cellulose nanowhiskers into polylactide via melt compounding to significantly enhance barrier and mechanical properties. Biomacromol 13:3887–3899
90. Natterodt JC, Shirole A, Sapkota J et al (2018) Polymer nanocomposites with cellulose nanocrystals made by co-precipitation. J Appl Polym Sci 135(24), article no 445648
91. Sapkota J, Natterodt JC, Shirole A et al (2017) Fabrication and properties of polyethylene/cellulose nanocrystal composites. Macromol Mater Eng 302: article no 1600300
92. Nair SS, Kuo PY, Chen HY, Yan N (2017) Investigating the effect of lignin on the mechanical, thermal, and barrier properties of cellulose nanofibril reinforced epoxy composite. Indust Crops Prod 100:208–217
93. Kong XH, Wolodko J, Zhao LY et al (2018) The preparation and characterization of polyurethane reinforced with a low fraction of cellulose nanocrystals. Prog Organic Coatings 125:207–214
94. Garcia de Rodriguez NLG, Thielemans W, Dufresne A (2006) Sisal cellulose whiskers reinforced polyvinyl acetate nanocomposites. Cellulose 13:261–270
95. Chen C, Wei M, Chen J et al (2008) Simultaneous reinforcing and toughening: New nanocomposites of waterborne polyurethane filled with low loading level of starch nanocrystals. Polymer 49:1860–1870
96. Mittal V (2011) Nanocomposites with biodegradable polymers. Synthesis, properties, and future perspectives. Oxford Scholarship Online, 1020
97. Li SCY, Sun YC, Guan Q et al (2016) Effects of chitin nanowhiskers on the thermal, barrier, mechanical, and rheological properties of polypropylene nanocomposites. RSC Advan 6:72086–72095
98. Fotie G, Rampazzo R, Ortenzi MA et al (2017) The effect of moisture on cellulose nanocrystals intended as a high gas barrier coating on flexible packaging materials. Polymers 9: article no 415
99. Majeed K, Hassan A, Abu Bakar A (2017) Barrier, biodegradation, and mechanical properties of (rice husk)/(montmorillonite) hybrid filler-filled low-density polyethylene nanocomposite films. J Vinyl Additive Technol I23:162–171
100. Yuwawech K, Wootthikanokkhan J, Tanpichai S (2018) Transparency, moisture barrier property, and performance of the alternative solar cell encapsulants based on PU/PVDC blend reinforced with different types of cellulose nanocrystals. Mater Renew Sustain Energy 7: article no 21

101. Forsgren L, Sahlin-Sjovold K, Venkatesh A et al (2019) Composites with surface-grafted cellulose nanocrystals (CNC). J Mater Sci 54:3009–3022
102. Medina E, Caro N, Abugoch L et al (2019) Chitosan thymol nanoparticles improve the antimicrobial effect and the water vapour barrier of chitosan-quinoa protein films. J Food Eng 240:191–198
103. Barnes DKA, Galgani F, Thompson RC et al (2009) Accumulation and fragmentation of plastic debris in global environments. Phil Trans Royal Soc B - Biol Sci 364(1526):1985–1998
104. Mrkic S, Galic K, Ivankovic M et al (2006) Gas transport and thermal characterization of mono- and di-polyethylene films used for food packaging. J Appl Polym Sci 99:1590–1599
105. LeCorre D, Dufresne A, Rueff M et al (2014) All starch nanocomposite coating for barrier material. J Appl Polymer Sci 131: article no 39826
106. Xu XZ, Liu F, Jiang L et al (2013) Cellulose nanocrystals vs cellulose nanofibrils: a comparative study on their microstructures and effects as polymer reinforcing agents. ACS Appl Mater Interfac 5:2999–3009
107. Yu HY, Zhang H, Song ML et al (2017) From cellulose nanospheres, nanorods to nanofibers: various aspect ratio induced nucleation/reinforcing effects on polylactic acid for robust-barrier food packaging. ACS Appl Mater Interfaces 9:43920–43938
108. Abdullah ZW, Dong Y (2018) Recent advances and perspectives on starch nanocomposites for packaging applications. J Mater Sci 53:15319–15339
109. Bagheriasl D, Carreau PJ, Riedl B et al (2018) Enhanced properties of polylactide by incorporating cellulose nanocrystals. Polym Compos 39:2685–2694
110. Chi K, Catchmark JM (2017) Enhanced dispersion and interface compatibilization of crystalline nanocellulose in polylactide by surfactant adsorption. Cellulose 24:4845–4860
111. Espino-Perez E, Bras J, Almeida G et al (2018) Designed cellulose nanocrystal surface properties for improving barrier properties in polylactide nanocomposites. Carbohydr Polym 183:267–277
112. Espino-Perez E, Bras J, Ducruet V et al (2013) Influence of chemical surface modification of cellulose nanowhiskers on thermal, mechanical, and barrier properties of poly(lactide) based bionanocomposites. Eur Polym J 49:3144–3154
113. Fortunati E, Peltzer M, Armentano I et al (2012) Effects of modified cellulose nanocrystals on the barrier and migration properties of PLA nano-biocomposites. Carbohydr Polym 90:948–956
114. Frone AN, Berlioz S, Chailan JF et al (2013) Morphology and thermal properties of PLA-cellulose nanofibers composites. Carbohyd Polym 91:377–384
115. Frone AN, Berlioz S, Chailan JF et al (2011) Cellulose fiber-reinforced polylactic acid. Polym Compos 32:976–985
116. Fukuzumi H, Saito T, Wata T et al (2009) Transparent and high gas barrier films of cellulose nanofibers prepared by TEMPO-mediated oxidation. Biomacromol 10:162–165
117. Iwataki A, Nogi M, Yano H (2008) Cellulose nanofiber-reinforced polylactic acid. Compos Sci Technol 68:2103–2106
118. Martinez-Sanz M, Abdelwahab MA, Lopez-Rubio A et al (2013) Incorporation of poly(glycidylmethacrylate) grafted bacterial cellulose nanowhiskers in poly(lactic acid) nanocomposites: improved barrier and mechanical properties. Eur Polym J 49:2062–2072
119. Pal AK, Katiyar V (2016) Nanoamphiphilic chitosan dispersed poly(lactic acid) bionanocomposite films with improved thermal, mechanical, and gas barrier properties. Biomacromol 17:2603–2618
120. Satam CC, Irvin CW, Lang AW et al (2018) Spray-coated multilayer cellulose nanocrystal-chitin nanofiber films for barrier applications. ACS Sustain Chem Eng 6:10637–10644
121. Song ZP, Xiao HN, Zhao Y (2014) Hydrophobic-modified nano-cellulose fiber/PLA biodegradable composites for lowering water vapor transmission rate (WVTR) of paper. Carbohydr Polym 111:442–448
122. Annamalai PK, Depan D (2015) Nano-cellulose reinforced chitosan nanocomposites for packaging and biomedical applications. In: Thakur VK, Kessler MR (eds) Green biorenewable biocomposites: from knowledge to industrial applications. CRC Press, Taylor and Francis, Boca Raton, pp 489–506

123. Antoniou J, Liu F, Majeed H et al (2015) Characterization of tara gum edible films incorporated with bulk chitosan and chitosan nanoparticles: a comparative study. Food Hydrocolloids 44:309–319
124. Azeredo HMC, Miranda KWE, Rosa MF et al (2012) Edible films from alginate-acerola puree reinforced with cellulose whiskers. LWT-Food Sci Technol 46: 294–297
125. Barud. HS, Souza JL, Santos DB et al (2011) Bacterial cellulose/poly(3-hydroxybutyrate) composite membranes Carbohydr Polym 83: 1279–1284
126. Bilbao-Sainz CB, Bras J, Williams T (2011) HPMC reinforced with different cellulose nanoparticles. Carbohyd Polym 86:1549–1557
127. Carvalho RA, Santos TA, de Azevedo VM et al (2018) Bio-nanocomposites for food packaging applications: effect of cellulose nanofibers on morphological, mechanical, optical and barrier properties. Polym Intl 67:386–392
128. Chen Y, Cao X, Chang PR et al (2008) Comparative study on the films of poly(vinyl alcohol)/pea starch nanocrystals and poly(vinyl alcohol)/native pea starch. Carbohydr Polym 73:8–17
129. Chi K, Catchmark JM (2018) Improved eco-friendly barrier materials based on crystalline nanocellulose/chitosan/carboxymethyl cellulose polyelectrolyte complexes. Food Hydrocolloids 80:195–205
130. Deepa B, Abraham E, Pothan LA et al (2016) Biodegradable nanocomposite films based on sodium alginate and cellulose nanofibrils. Materials 9:1–11 article no 9010050
131. Deng ZL, Jung J, Simonsen J et al (2017) Cellulose nanocrystal reinforced chitosan coatings for improving the storability of postharvest pears under both ambient and cold storages. J Food Sci 82:453–462
132. Dhar P, Bhardwaj U, Kumar A et al (2015) Poly (3-hydroxybutyrate)/ cellulose nanocrystal films for food packaging applications: barrier and migration studies. Polym Eng Sci 55:2388–2395
133. Fang DL, Deng ZL, Jung J et al (2018) Mushroom polysaccharides-incorporated cellulose nanofiber films with improved mechanical, moisture barrier, and antioxidant properties. J Appl Polymer Sci 135: article no 46166
134. Gea S, Bilotti E, Reynolds CT, Soykeabkeaw N et al (2010) Bacterial cellulose-poly(vinyl alcohol) nanocomposites prepared by an in-situ process. Mater Lett 64:901–904
135. George J, Siddaramaiah (2012) High performance edible nanocomposite films containing bacterial cellulose nanocrystals. Carbohydr Polym 87:2031–2037
136. Gicquel E, Martin C, Yanez JG et al (2017) Cellulose nanocrystals as new bio-based coating layer for improving fiber-based mechanical and barrier properties. J Mater Sci 52:3048–3061
137. Grande CJ, Torres FG, Gomez CM et al (2009) Nanocomposites of bacterial cellulose/hydroxyapatite for biomedical applications. Acta Biomater 5:1605–1615
138. Grande CJ, Torres FG, Gomez CM et al (2009) Development of self-assembled bacterial cellulose-starch nanocomposites. Mater Sci Eng, C 29:1098–1104
139. Huq T, Salmieri S, Khan A et al (2012) Nanocrystalline cellulose (NCC) reinforced alginate based biodegradable nanocomposite film. Carbohyd Polym 90:1757–1763
140. Johnson RK, Zink-Sharp A, Renneckar SH et al (2009) A new bio-based nanocomposite: fibrillated TEMPO-oxidized celluloses in hydroxypropylcellulose matrix. Cellulose 16:227–238
141. Kaushik A, Singh M, Verma G (2010) Green nanocomposites based on thermoplastic starch and steam exploded cellulose nanofibrils from wheat straw. Carbohydr Polym 82:337–345
142. Li MC, Mei CT, Xu XW et al (2016) Cationic surface modification of cellulose nanocrystals: toward tailoring dispersion and interface in carboxymethyl cellulose films. Polymer 107:200–210
143. Li W, Wu Q, Zhao X, Huang Z et al (2014) Enhanced thermal and mechanical properties of PVA composites formed with filamentous nanocellulose fibrils. Carbohydr Polymers 113:403–410
144. Li W, Zhao X, Huang Z, Liu S (2013) Nanocellulose fibrils isolated from BHKP using ultrasonication and their reinforcing properties in transparent poly (vinyl alcohol) films. J Polymer Res 20: article no 210

145. Ma Q, Hu D, Wang L (2016) Preparation and physical properties of tara gum film reinforced with cellulose nanocrystals. Intl J Biol Macromol 86:606–612
146. Mandal A, Chakrabarty D (2014) Studies on the mechanical, thermal, morphological and barrier properties of nanocomposites based on poly(vinyl alcohol) and nanocellulose from sugarcane bagasse. J Indust Eng Chem 20:462–473
147. Nasseri R, Mohammadi N (2014) Starch-based nanocomposites: a comparative performance study of cellulose whiskers and starch nanoparticles. Carbohydr Polym 106:432–439
148. Oun AA, Rhim JW (2015) Preparation and characterization of sodium carboxymethyl cellulose/cotton linter cellulose nanofibril composite films. Carbohydr Polym 127:101–109
149. Oun AA, Rhim JW (2016) Isolation of cellulose nanocrystals from grain straws and their use for the preparation of carboxymethyl cellulose-based nanocomposite films. Carbohydr Polym 150:187–200
150. Oun AA, Rhim JW (2017) Effect of oxidized chitin nanocrystals isolated by ammonium persulfate method on the properties of carboxymethyl cellulose-based films. Carbohydr Polym 175:712–720
151. Paralikar SA, Simonsen J, Lombardi J (2008) Poly(vinyl alcohol)/cellulose nanocrystal barrier membranes. J Membrane Sci 320:248–258
152. Silverio HA, Neto WPF, Pasquini D (2013) Effect of incorporating cellulose nanocrystals from corncob on the tensile, thermal and barrier properties of poly(vinyl alcohol) nanocomposites. J Nanomater, article no 289641
153. Sirviö JA, Kolehmainen A, Liimatainen H et al (2014) Biocomposite cellulose-alginate films: promising packaging materials. Food Chem 151:343–351
154. Shrestha S, Montes F, Schueneman GT et al (2018) Effects of aspect ratio and crystal orientation of cellulose nanocrystals on properties of poly(vinyl alcohol) composite fibers. Composites Sci Technol 167:482–488
155. Zhou YM, Fu SY, Zheng LM et al (2012) Effect of nanocellulose isolation techniques on the formation of reinforced poly(vinyl alcohol) nanocomposite films, eXPRESS Polymer Lett 6:794–804
156. De Moura MR, Aouada FA, Avena-Bustillos RJ et al (2009) Improved barrier and mechanical properties of novel hydroxypropyl methylcellulose edible films with chitosan/tripolyphosphate nanoparticles. J Food Eng 92:448–453
157. Kerch G (2015) Chitosan films and coatings prevent losses of fresh fruit nutritional quality: a review. Trends Food Sci Technol 46:159–166
158. Slavutsky AM, Bertuzzi MA (2014) Water barrier properties of starch films reinforced with cellulose nanocrystals obtained from sugarcane bagasse. Carbohydr Polym 110:53–61
159. Viera da Silva ISV, Neto WPF, Silverio HA et al (2017) Mechanical, thermal and barrier properties of pectin/cellulose nanocrystal nanocomposite films and their effect on the storability of strawberries (Fragaria ananassa). Polym Advan Technol 28:1005–1012
160. Wang HX, Qan J, Ding FY (2018) Emerging chitosan-based films for food packaging applications. J Agric Food Chem 66:395–413
161. Angellier H, Molina-Boisseau S, Dole P et al (2006) Thermoplastic starch-waxy maize starch nanocrystals nanocomposites. Biomacromol 7:531–539
162. Ma XF, Jian RJ, Chang PR et al (2008) Fabrication and characterization of citric acid-modified starch nanoparticles/plasticized-starch composites. Biomacromol 9:3314–3320
163. Svagan AJ, Hedenqvist MS, Berglund L (2009) Reduced water vapour sorption in cellulose nanocomposites with starch matrix. Compos Sci Technol 69:500–506
164. Atef M, Rezaei M, Behrooz R (2015) Characterization of physical, mechanical, and antibacterial properties of agar-cellulose bionanocomposite films incorporated with savory essential oils. Food Hydrocolloids 45:150–157
165. Elsabee MZ, Abdou ES (2013) Chitosan based edible films and coatings: a review. Mater Sci Eng, C 33:1819–1841
166. Liu K, Lin X, Chen L et al (2014) Dual-functional chitosan-methylisothiazolinone/microfibrillated cellulose biocomposites for enhancing antibacterial and mechanical properties of agar films. Cellulose 21:519–528

167. Liu K, Lin X, Chen L et al (2013) Preparation of microfibrillated cellulose/chitosan-benzalkonium chloride biocomposite for enhancing antibacterium and strength of sodium alginate films. J Agric Food Chem 61:6562–6567
168. Kristo E, Biliaderis CG (2007) Physical properties of starch nanocrystal reinforced pullulan films. Carbohydr Polym 68:146–158
169. LeCorre D, Bras J, Dufresne A (2010) Starch nanoparticles: a review. Biomacromol 11:1139–1153
170. Walsh NP, Blannin AK, Clark AM et al (1999) The effects of high-intensity intermittent exercise on saliva IgA, total protein and alpha-amylase. J Sports Sci 17:129–134
171. Herrera MP, Vasanthan T, Hoover R (2016) Characterization of maize starch nanoparticles prepared by acid hydrolysis. Cereal Chem 93:323–330
172. Rinaudo M (2006) Chitin and chitosan: properties and applications. Prog Polym Sci 31:603–632
173. Lu Y, Weng L, Zhang L (2004) Morphology and properties of soy protein isolate thermoplastics reinforced with chitin whiskers. Biomacromol 5:1046–1051
174. Revol JF, Marchessault RH (1993) In-vitro chiral nematic ordering of chitin crystallites. Int J Biol Macromol 15:329–335
175. Nair KG, Dufresne A (2003) Crab shell chitin whisker reinforced natural rubber nanocomposites 1 processing and swelling behavior. Biomacromol 4:657–665
176. van den Broek LAM, Knoop RJI, Kappen FHJ et al (2015) Chitosan films and blends for packaging material. Carbohydr Polym 116:237–242
177. Lorevice MV, Otoni CG, de Moura MR et al (2016) Chitosan nanoparticles on the improvement of thermal, barrier, and mechanical properties of high- and low-methyl pectin films. Food Hydrocolloids 52:732–740
178. Hubbe MA, Tayeb P, Joyce M et al (2017) Rheology of nanocellulose-rich aqueous suspensions: a Review. BioResources 12:9556–9661
179. Mathew AP, Dufresne A (2002) Morphological investigation of nanocomposites from sorbitol plasticized starch and tunicin whiskers. Biomacromol 3:609–617
180. Samir MASA, Alloin F, Gorecki W et al (2004) Nanocomposite polymer electrolytes based on poly(oxyethylene) and cellulose nanocrystals. J Phys Chem B 108:10845–10852
181. Chinga-Carrasco G, Syverud K (2010) Computer-assisted quantification of the multi-scale structure of films made of nanofibrillated cellulose. J Nanoparticle Res 12:841–851
182. Bideau B, Bras J, Adoui N et al (2017) Polypyrrole/ nanocellulose composite for food preservation: barrier and antioxidant characterization. Food Packag Shelf Life 12:1–8
183. Dai L, Long Z, Chen J et al (2017) Robust guar gum/cellulose nanofibrils multilayer films with good barrier properties. ACS Appl Mater Interfaces 9:5477–5485
184. Jonas R, Farah LF (1998) Production and application of microbial cellulose. Polym Degrad Stab 59:101–106
185. Olsson RT, Fogelström L, Martínez-Sanz M et al (2011) Cellulose nanofillers for food packaging. In: Jagarón JM (ed) Multifuctional and nanoreinforced polymers for food packaging. Woodhead Publ Ltd., Elsevier BV, Amsterdam, pp 86–107
186. Missoum K, Belgacem MN, Bras J (2013) Nanofibrillated cellulose surface modification: a review. Materials 6:1745–1766
187. Eyley S, Thielemans W (2014) Surface modification of cellulose nanocrystals. Nanoscale 6:7764–7779
188. Hubbe MA, Rojas OJ, Lucia LA (2015) Green modification of surface characteristics of cellulosic materials at the molecular or nano scale: a review. BioResources 10:6095–6229
189. Follain N, Belbekhouche S, Bras J et al (2018) Tunable gas barrier properties of filled-PCL film by forming percolating cellulose network. Colloids Surf. A - Physicochem Eng Aspects 545:26–30
190. Kalia S, Dufresne A, Cherian BM et al (2011) Cellulose-based bio- and nanocomposites: a review. Intl J Polym Sci 2011, article no 837875
191. Tome LC, Brandao L, Mendes AM et al (2010) Preparation and characterization of bacterial cellulose membranes with tailored surface and barrier properties. Cellulose 17:1203–1211

192. Wiles JL, Vergano PJ, Barron FH et al (2000) Water vapor transmission rates and sorption behavior of chitosan films. J Food Sci 65:1175–1179
193. Salleh E, Muhamad II, Khairuddin N (2009) Structural characterization and physical properties of antimicrobial (AM) starch-based films. World Acad Sci Eng Technol 55:432–440
194. Stevanic JS, Bergström EM, Gatenholm P et al (2012) Arabinoxylan/nanofibrillated cellulose composite films. J Mater Sci 47:6724–6732
195. Österberg M, Vartiainen J, Lucenius J et al (2013) A fast method to produce strong NFC films as a platform for barrier and functional materials. ACS Appl Mater Interfaces 5:4640–4647
196. Aulin C, Karabulut E, Tran A et al (2013) Transparent nanocellulose multilayer thin films on polylacktic acid with tunable gas barrier properties. ACS Appl Mater Interfaces 5:7352–7359
197. Trifol J, Plackett D, Sillard C et al (2016) A comparison of partially acetylated nanocellulose, nanocrystalline cellulose, and nanoclay as fillers for high-performance polylactide nanocomposites. J Appl Polym Sci 133: article no 43257
198. Liu YX, Sun B, Wang ZL et al (2016) Mechanical and water vapor barrier properties of bagasse hemicellulose-based films. BioResources 11:4226–4236
199. Tyagi P, Lucia LA, Hubbe MA et al (2019) Nanocellulose-based multilayer barrier coatings for gas, oil, and grease resistance. Carbohydr Polym 206:281–288
200. Zhang. R, Wang X, Cheng M (2018) Preparation and characterization of potato starch film with various size of nano-SiO2, Polymers 10: article no 1172
201. Amini E, Azadfallah M, Layeghi M et al (2016) Silver-nanoparticle-impregnated cellulose nanofiber coating for packaging paper. Cellulose 23:557–570
202. Bedane AH, Eić M, Farmahini-Farahani M et al (2015) Water vapor transport properties of regenerated cellulose and nanofibrillated cellulose films. J Membrane Sci 493:46–57
203. Spence KL, Venditti RA, Rojas OJ et al (2010) The effect of chemical composition on microfibrillar cellulose films from wood pulps: water interactions and physical properties for packaging applications. Cellulose 17:835–848
204. Minelli M, Baschetti MG, Doghieri F et al (2010) Investigation of mass transport properties of microfibrillated cellulose (MFC) films. J Membrane Sci 358:67–75
205. Wang JW, Gardner DJ, Stark NM et al (2018) Moisture and oxygen barrier properties of cellulose nanomaterial-based films. ACS Sustain Chem Eng 6:49–70
206. Aiba S, Ohashi M, Huang SY (1968) Rapid determination of oxygen permeability of polymer membranes. Indust Eng Chem Fund I7:497–502
207. Rodionova G, Roudot S, Eriksen Ø et al (2012) The formation and characterization of sustainable layered films incorporating microfibrillated cellulose (MFC). BioResources 7:3690–3700
208. Villani C, Loser R, West MJ et al (2014) An inter lab comparison of gas transport testing procedures: oxygen permeability and oxygen diffusivity. Cement Concrete Composites 53:357–366
209. Dai L, Wang B, Long Z et al (2015) Properties of hydroxypropyl guar/TEMPO-oxidized cellulose nanofibrils composite films. Cellulose 22:3117–3126
210. Kisonen V, Prakobna K, Xu CL et al (2015) Composite films of nanofibrillated cellulose and O-acetyl galactoglucomannan (GGM) coated with succinic esters of GGM showing potential as barrier material in food packaging. J Mater Sci 50:3189–3199
211. Naderi A, Lindström T, Weise CF et al (2016) Phosphorylated nanofibrillated cellulose: production and properties. Nordic Pulp Paper Res J 31:20–29
212. Tyagi P, Hubbe MA, Lucia L et al (2018) High performance nanocellulose-based composite coatings for oil and grease resistance. Cellulose 25:3377–3391
213. Gajdoš J, Galić K, Kurtanjek Ž et al (2001) Gas permeability and DSC characteristics of polymers used in food packaging. Polym Testing 20(1):49–57
214. Siracusa V, Blanco I, Romani S et al (2012) Poly(lactic acid)-modified films for food packaging application: physical, mechanical, and barrier behavior. J Appl Polym Sci 125:E390–E401
215. Kofinas P, Cohen RE, Halasa AF (1994) Gas-permeability of polyethylene poly(ethylene propylene) semicrystalline diblock copolymers. Polymer 35:1229–1235
216. Kumar V, Elfving A, Koivula H et al (2016) Roll-to-roll processed cellulose nanofiber coatings. Ind Eng Chem Res 55:3603–3613

217. Aulin C, Gallstedt M, Lindstrom T (2010) Oxygen and oil barrier properties of microfibrillated cellulose films and coatings. Cellulose 17:559–574
218. Lagaron JM, Catala R, Gavara R (2004) Structural characteristics defining high barrier properties in polymeric materials. Mater Sci Technol 20:1–7
219. McKee JR, Huokuna J, Martikainen L et al (2014) Molecular engineering of fracture energy dissipating sacrificial bonds into cellulose nanocrystal nanocomposites. Angew Chem Intl Ed 53:5049–5053
220. Wolf C, Angellier-Coussy H, Gontard N et al (2018) How the shape of fillers affects the barrier properties of polymer/non-porous particles nanocomposites: a review. J Membrane Sci 556:393–418
221. Malhotra B, Keshwani A, Kharkwal H (2015) Antimicrobial food packaging: potential and pitfalls. Frontiers Microbiol 6: article no UNSP 611
222. Khaneghah AM, Hashemi SMB, Limbo S (2018) Antimicrobial agents and packaging systems in antimicrobial active food packaging: an overview of approaches and interactions. Food Bioprod Proc 111:1–19
223. Aider M (2010) Chitosan application for active bio-based films production and potential in the food industry: review. Food Sci Technol 43:837–842
224. Cazon P, Velazquez G, Ramirez JA et al (2017) Polysaccharide-based films and coatings for food packaging: a review. Food Hydrocolloids 68:136–148
225. Rhim JW, Hong SI, Park HM et al (2006) Preparation and characterization of chitosan-based nanocomposite films with antimicrobial activity. J Agric Food Chem 54:5814–5822
226. Velasquez-Cock J, Ramirez E, Betancourt S et al (2014) Influence of the acid type in the production of chitosan films reinforced with bacterial nanocellulose. Int J Biol Macromol 69:208–213
227. Raafat D, Sahl HG (2009) Chitosan and its antimicrobial potential—a critical literature survey. Microbial Biotech 2:186–201
228. Rhim JW, Ng PKW (2007) Natural biopolymer-based nanocomposite films for packaging applications. Crit Rev Food Sci Nutrition 47:411–433
229. Herrera MA, Mathew AP, Oksman K (2017) Barrier and mechanical properties of plasticized and cross-linked nanocellulose coatings for paper packaging applications. Cellulose 24:3969–3980
230. Giannakas A, Grigoriadi K, Leontiou A et al (2014) Preparation, characterization, mechanical and barrier properties investigation of chitosan-clay nanocomposites. Carbohydr Polym 108:103–111
231. Abdollahi M, Rezai M, Farzi G (2012) A novel active bionanocomposite film incorporating rosemary essential oil and nanoclay into chitosan. J Food Eng 111:343–350
232. Muller CMO, Laurindo JB, Yamashita F (2011) Effect of nanoclay incorporation method on mechanical and water vapor barrier properties of starch-based films. Indust Crops Prod 33:605–610
233. Abdorreza MN, Abd Karim A (2013) Mechanical, barrier, physicochemical, and heat seal properties of starch films filled with nanoparticles. J Nano Res 25:90–100
234. Bardet R, Reverdy C, Belgacem N et al (2015) Substitution of nanoclay in high gas barrier films of cellulose nanofibrils with cellulose nanocrystals and thermal treatment. Cellulose 22:1227–1241
235. Gamelas JAF, Ferraz E (2015) Composite films based on nanocellulose and nanoclay minerals as high strength materials with gas barrier capabilities: key points and challenges. BioResources 10:6310–6313
236. Mohan TP, Devchand K, Kanny K (2017) Barrier and biodegradable properties of corn starch-derived biopolymer film filled with nanoclay fillers. J Plastic Film Sheeting 33(3):309–336
237. Rhim JW (2011) Effect of clay contents on mechanical and water vapor barrier properties of agar-based nanocomposite films. Carbohydr Polym 86:291–699
238. Saurabh CK, Gupta S, Bahadur J et al (2015) Mechanical and barrier properties of guar gum based nano-composite films. Carbohydr Polym 124:77–84

239. Wolf JR, Strieder W (1990) Surface and void tortuosities for a random fiber bed - Overlapping, parallel cylinders of several radii. J Membrane Sci 49:103–115
240. Zalc JM, Reyes SC, Iglesia E (2004) The effects of diffusion mechanism and void structure on transport rates and tortuosity factors in complex porous structures. Chem Eng Sci 59:2947–2960
241. Hubbe MA (2017) Hybrid filler (cellulose/noncellulose) reinforced nanocomposites. In: Kargarzadeh H, Ahmad I, Thomas S, Dufresne A (eds) Handbook of nanocellulose and cellulose nanocomposites. Vol 1, Wiley, pp 273–299. (Ch 8)
242. Liu AD, Walther A, Ikkala O et al (2011) Clay nanopaper with tough cellulose nanofiber matrix for fire retardancy and gas barrier functions. Biomacromol 12:633–641
243. Mirmehdi S, Hein PRG, Sarantopoulos CIGD et al (2018) Cellulose nanofibrils/nanoclay hybrid composite as a paper coating: effects of spray time, nanoclay content and corona discharge on barrier and mechanical properties of the coated papers. Food Packag Shelf Life 15:87–94
244. Wang YX, Cao XD, Zhang LN (2006) Effects of cellulose whiskers on properties of soy protein thermoplastics. Macromol Biosci 6:524–531
245. Soykeabkaew N, Laosat N, Ngaokla A et al (2012) Reinforcing potential of micro- and nano-sized fibers in the starch-based biocomposites. Composites Sci Technol 72:845–852
246. Sharma S, Zhang X, Nair SS et al (2014) Thermally enhanced high performance cellulose nano fibril barrier membranes. RSC Adv 4(85):45136–45142
247. Xia JY, Zhang Z, Liu W et al (2018) Highly transparent 100% cellulose nanofibril films with extremely high oxygen barriers in high relative humidity. Cellulose 25:4057–4066
248. Ponni R, Vuorinen T, Kontturi E (2012) Proposed nano-scale coalescence of cellulose in chemical pulp fibers during technical treatments. BioResources 7:6077–6108
249. Yang SJ, Tang YJ, Wang JM et al (2014) Surface treatment of cellulosic paper with starch-based composites reinforced with nanocrystalline cellulose. Indust Eng Chem Res 53:13980–13988
250. Kerekes RJ, Schell CJ (1992) Characerization of fiber flocculation regimes by a crowding factor. J Pulp Paper Sci 18:J32–J38
251. Hubbe MA (2007) Flocculation and redispersion of cellulosic fiber suspensions: a review of effects of hydrodynamic shear and polyelectrolytes. BioResources 2:296–331
252. Habibi Y, Lucia LA, Rojas OJ (2010) Cellulose nanocrystals: chemistry, self-assembly, and applications. Chem Rev 110:3479–3500
253. Capadona JR, Van Den Berg O, Capadona LA et al (2007) A versatile approach for the processing of polymer nanocomposites with self-assembled nanofibre templates. Nature Nanotech 1:765–769
254. Gontard N, Duchez C, Cuq JL et al (1994) Edible composite films of wheat gluten and lipids—water-vapor permeability and other physical properties. Intl J Food Sci Technol 29:39–50
255. Talja RA, Helén H, Roos YH et al (2007) Effect of various polyols and polyol contents on physical and mechanical properties of potato starch-based films. Carbohydr Polym 67:288–295
256. Miranda CS, Ferreira MS, Magalhães MT et al (2015) Mechanical, thermal and barrier properties of starch-based films plasticized with glycerol and lignin and reinforced with cellulose nanocrystals. Mater Today Proc 2:63–69
257. Arvanitoyannis IS, Nakayama A, Aiba S (1998) Chitosan and gelatin based edible films: state diagrams, mechanical and permeation properties. Carbohydr Polym 37:371–382
258. Caner C, Vergano PJ, Wiles JL (1998) Chitosan film mechanical and permeation properties as affected by acid, plasticizer, and storage. J Food Sci 63:1049–1053
259. Olivas GI, Barbosa-Cánovas GV (2008) Alginate-calcium films: water vapor permeability and mechanical properties as affected by plasticizer and relative humidity. LWT-Food Sci Technol 41:359–366
260. Peng XW, Ren JL, Zhong LX et al (2011) Nanocomposite films based on xylan-rich hemicelluloses and cellulose nanofibers with enhanced mechanical properties. Biomacromol 2011:3321–3329

261. Lagarón JM (2011) Multifunctional and nanoreinforced polymers for food packaging. In: Jagarón JM (ed) Multifuctional and nanoreinforced polymers for food packaging. Woodhead Publ Ltd., Elsevier BV, Amsterdam, pp 1–28
262. Lu P, Xiao HN, Pan YF (2015) Improving water vapor barrier of green-based nanocellulose film via hydrophobic coating. In: Chung SL (ed), proceedings of the 2014 international conference on materials science and energy engineering (CMSEE 2014), pp 148–153
263. Jiang G, Zhang MD, Feng J et al (2017) High oxygen barrier property of poly(propylene carbonate)/polyethylene glycol nanocomposites with low loading of cellulose nanocrystals. ACS Sustain Chem Eng 5:11246–11254
264. Rafieian F, Shahedi M, Keramat J et al (2014) Mechanical, thermal and barrier properties of nano-biocomposite based on gluten and carboxylated cellulose nanocrystals. Indust Crops Prod 53:282–288
265. Reddy JP, Rhim JW (2014) Characterization of bionanocomposite films prepared with agar and paper- mulberry pulp nanocellulose. Carbohydr Polym 110:480–488
266. Rhim JW, Reddy JP, Luo X (2015) Isolation of cellulose nanocrystals from onion skin and their utilization for the preparation of agar-based bio-nanocomposites film. Cellulose 22:407–420
267. Wang WH, Zhang XL, Li C et al (2018) Using carboxylated cellulose nanofibers to enhance mechanical and barrier properties of collagen fiber film by electrostatic interaction. J Sci Food Agric 98:3089–3097

Chapter 10
Nanopolysaccharides-Based Green Additives

Jianxiang Chen, Chuang Tang, Defeng Wu and Juntao Tang

Abstract Due to their unique and excellent properties, nanopolysaccharides have been widely used in a variety of areas, including stabilizing agents in diet meals, active components in cosmetic products and important substances in polymer composites. This chapter covers the contents of nanopolysaccharides as green additives and the corresponding disciplines. Their roles in achieving enhanced performances in food, cosmetics, construction, paper industry, and some emerging fields will be discussed in general.

Keywords Green additives · Food additives · Coating additives · Polymer additives

10.1 Introduction

Recent research has highlighted the application of nanopolysaccharides as green additives in a number of potential applications. Cellulose nanocrystals (CNCs), produced from natural cellulose by various methods, have been added into polymer matrix to produce high-performance functional custom materials. Chitin nanocrystals (ChNCs), derived from chitin, have been employed into soil to increase the grain yield and quality of winter wheat. This is owing to the three-dimensional network formation among chitin nanocrystals. However, the above mentioned examples are just a glimpse of the tremendous applications of nanopolysaccharides. They can also find

J. Chen (✉) · C. Tang
Department of Materials Engineering, Jiangsu University of Technology, Changzhou 213001, Jiangsu, China
e-mail: Chenjianxiang888@hotmail.com

D. Wu
Department of Chemistry and Chemical Engineering, Yangzhou University, Yangzhou 225002, Jiangsu, China

J. Tang (✉)
College of Chemistry and Chemical Engineering, Central South University, Changsha 410083, Hunan, People's Republic of China
e-mail: Reynard.tangjuntao@gmail.com

N. Lin et al. (eds.), *Advanced Functional Materials from Nanopolysaccharides*,
Springer Series in Biomaterials Science and Engineering 15,
https://doi.org/10.1007/978-981-15-0913-1_10

their suitable fit in the area of high-efficiency solar cells, lightweight batteries, as well as environmental remediation. Due to their unique properties, using nanopolysaccharides as additives may greatly promote the development of technologies that intend to solve global sustainability problems.

Among those literatures, nanocellulose-related contents seem to account for most of the reporting work. However, it should be emphasized that the utilization of other nanopolysaccharides cannot be neglected as they may have specific or superior effects in certain applications. This chapter picked up some of the recent examples to summarize the use of nanopolysaccharides as green additives in several main aspects, spanning food, construction and ceramics, inks, drilling fluid, adhesive and aqueous coating, cosmetics, paper, polymer and lubricant additives. Emphasis will be placed on their ability for the enhanced performance, along with the basic mechanism associated with the corresponding aspect. Given the importance of the reported systems, only the significant and illustrative examples in recent years are described herein.

10.2 Food Additives

Though the use of cellulose as a food additive has been proposed thirty years ago [1], food added with cellulose is not widely commercialized yet due to high production cost and uncertain biological issues. With the development of nanocellulose industrial production methods, the reduced cost enables nanocellulose to be a commercial product. Nowadays, nanocellulose, especially CNCs have been manufactured by various companies in the world [2]. The potential utilization of nanocellulose products as food additives in different aspects has been showed in Fig. 10.1.

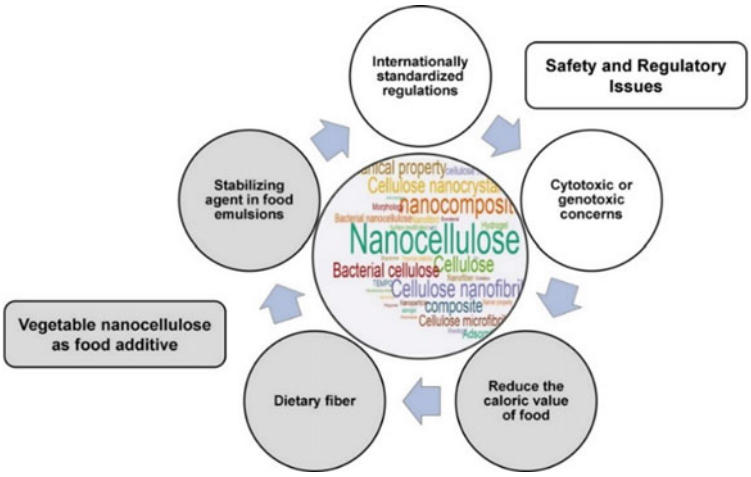

Fig. 10.1 Vegetable nanocellulose in food science. Reproduced from [3]

CNCs have been used as a stabilizer for food emulsions, and use CNCs as dietary fibers can lower the calories of food [3]. Hamburgers with CNCs exhibited similar structure and taste when comparing to common hamburgers, and they can hold more water without any side effects. As CNCs have a good stabilizing effect in oil-in-water emulsions and can be used as a thickener in the formulation, they can replace fats to make calorie reduced toppings. Adding a certain amount of CNCs in fruit-filled cookies will lead to a crispy structure without destroying the shape of the cookies.

Cellulose nanofibrils (CNFs) made from peach palm residue have been used as food additive to reduce the risk of non-transmitting of chronic diseases and prevent constipation. The biological tests have been carried out on mice. Results shown that with the addition of CNFs to the diet given to mice, the mice tended to gain weight. The blood sugar and lipid profile of all mice did not show significant difference and there was no relevant physiological loss of mineral nutrients [4]. As cellulose materials have been added to foods to reduce calorie commonly, DeLoid et al. [5] investigated the ability of CNFs to control the absorption of intake fat. Scanning electron microscopy (SEM) photos of digestion of cream with or without CNFs at different intestinal phase were shown in Fig. 10.2. In the samples with cream only, fat presented in the appearance of small droplets in the initial stage of digestion. In samples containing CNFs, a honeycomb-like lattice was formed. The fat droplets become larger and adhere to the finer CNF fibers. After digestion, the fat droplets disappeared in the cream only samples while they remained the same but droplet size slightly decreased in samples containing CNFs. It suggested that adding CNFs in food can reduce the fat absorption. In Gao's work [6], cellulose extracted from brown algae (BA) waste was used as milk thickener. In the milk system, casein micelles were adsorbed to the surface of BA cellulose nanofibers. A gel like structure was formed due to hydrogen-bond interaction and the milk system exhibited superior thickening behavior. 3-(4, 5-dimethyl-2-thiazolyl)-2, 5-diphenyl-2-H-tetrazolium bromide (MTT) test confirmed that BA cellulose nanofibers are safe and non-toxic when used as food additives, without sacrificing biocompatibility. There is an application prospect for CNCs and CNFs used as a food additive. But the related standards should be built to qualify the property and safety when they are used in food section in future studies.

Despite CNCs and CNFs, bacterial cellulose (BC) has become a new and important food base and dietary fiber due to its unique properties. BC has the same molecular structural unit with natural cellulose produced by plants or algae, but BC exhibits better physical, mechanical and biological properties. Due to purity, high porosity, strong water imbibition, ultrafine structure and other good properties, BC can be used as a food forming agent, thickener, dispersant, anti-solvent, and improve the taste of certain foods [7]. Since 1992, BC has been recognized as safe by the US Food and Drug Administration (FDA) [8]. BC can act as a functional additive in both conventional food and modern functional food, including pastries, vegetarian diets, custom food for patients and other novel products [9]. The effects of BC on the baking quality of wheat flours have been investigated by Corral et al. [10]. Results showed that BC increased the moisture retention while reduced the firmness and browning index of the bread crumb. And the BC crumb has larger average porous

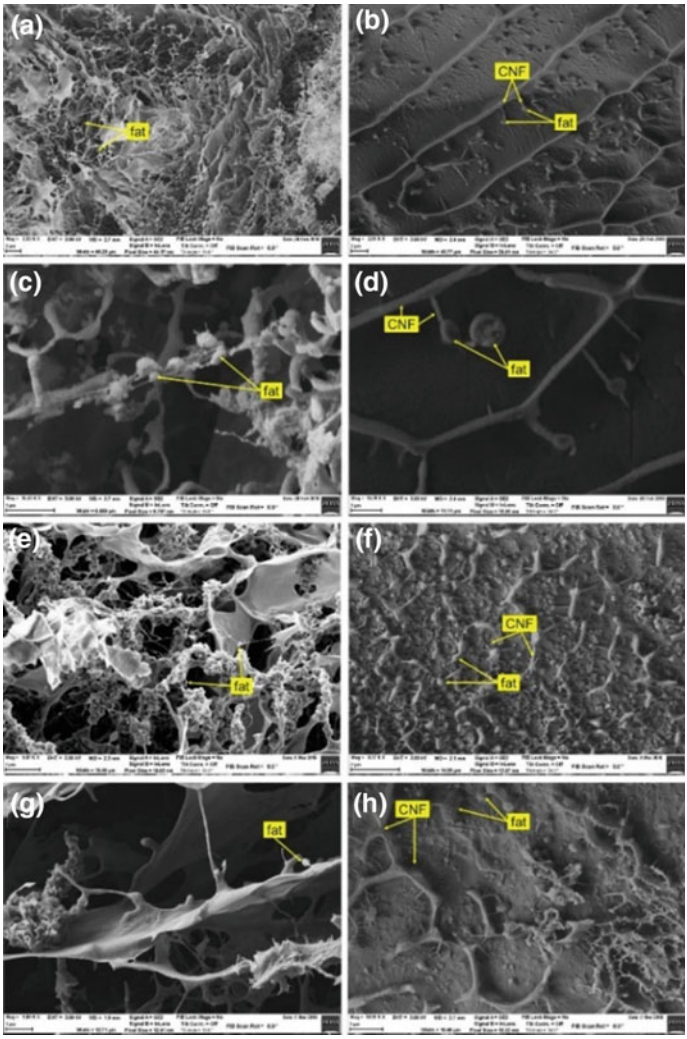

Fig. 10.2 SEM images of digesta: **a**, **c** cream only (13.3%), **b**, **d** cream (13.3%) plus 0.75% CNF-50 at start of small intestinal phase, **e**, **g** cream only, **f**, **h** cream plus CNF at end of small intestinal digestion. Reproduced from [5]

size than that of the control sample. Shapes of the BC incorporated wheat bread and the normal wheat bread are shown in Fig. 10.3. BC can also be added into meat emulsions to prepare low lipid and low sodium meat sausages [11].

Besides, as the second most abundant biomass material in nature, starch is also attractive and active in our daily life. Their derived starch nanoparticles (SNPs) can also be used as fat replacers in food. Add SNPs in food can form a smooth cream-like substance which tastes like fat and reduce the calorie in food at the same time [12].

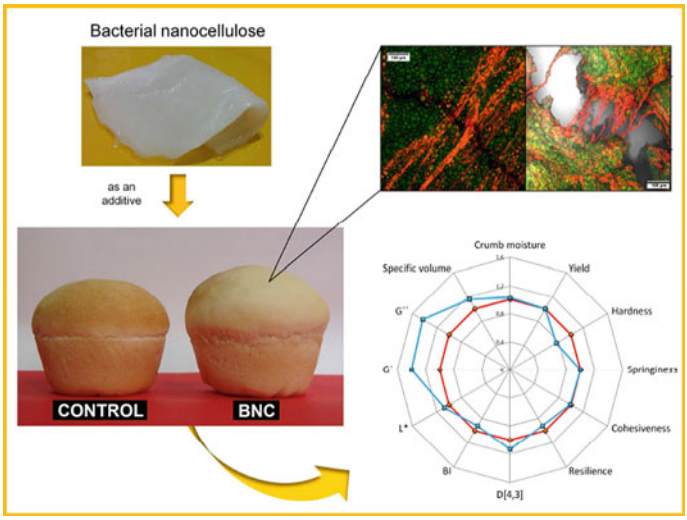

Fig. 10.3 BC used as a potential additive for wheat bread. Reproduced from [10]

10.3 Construction and Ceramics Additives

Cellulosic materials can be used not only in the food industry, but also in the construction sector. So far, a variety of wood-based structural modules have been used in the construction sector [13]. Because of natural abundance and low cost, the use of wood-derived materials in composites has great prospects. Wood is a versatile building material. It has been widely used because of its structural properties and aesthetic value. As a natural material, the performance of wood is affected by the environment. Changes in ambient temperature and humidity affect the moisture absorption and moisture content of wood. With the change of surrounding environment, wood may shrink and crack during use. CNCs can be used as an additive in consolidation of wood without losing performance even after aging [14]. Results showed that the addition of CNCs increased penetration within wood structure and compression strength of the treated samples.

As CNFs can increase the flexural strength, toughness, and impact resistance of cement-based material, cellulose-cement composites have been widely used in the field of architecture and agriculture. BC can be used as a green additive for production of bio-based cement composites. With the addition of BC, the organic part on the surface increases, and the cement composites become more susceptible to humidity [15]. The porosity becomes lower, and the surface becomes rougher. BC incorporation can make the fiber-cement composite surface more reactive. They can also decrease the fiber mineralization as well as the surface porosity of cellulose-cement composite. Incorporation of BC in gel form greatly decreases the surface basicity of the composite while incorporation of BC on fibers significantly increases the surface basicity [15].

10.4 Ink Additives

Smooth writing experience made gel pen to be the most popular writing instruments nowadays [16–18]. During writing process, the ball at the gel pen tip rolls and produces a certain amount of friction with the ink. The ink will appear "shear thinning" (viscosity decreases) when the shear begins and the state of ink changes from gel to solution [19–21]. Writing with a gel pen can avoid ink accumulation and leakage that occurred in ordinary ballpoint pen and water-based ink pen [22–24]. But the production of gel pen inks produces a number of toxic gas that can be inhaled by workers and pollute the environment [25–27]. In order to tune the rheological properties, nanopolysaccharides can be incorporated. Wang et al. found that the rheological and thixotropic properties of CNC were similar to that of the gel pen inks [28–31]. As is shown in Fig. 10.4, the viscosity of both ordinary ink and CNC decreased immediately with shear and recovered back rapidly without shear. This means that CNC is the good substitute for some organic solvents. Mixing CNC with dyestuff and surfactants in water can produce a novel gel pen ink and no toxic gas generated during the preparation process. The prepared new eco-ink kept the polarization properties of CNC, which can be used for security applications (shown in Fig. 10.5) [32].

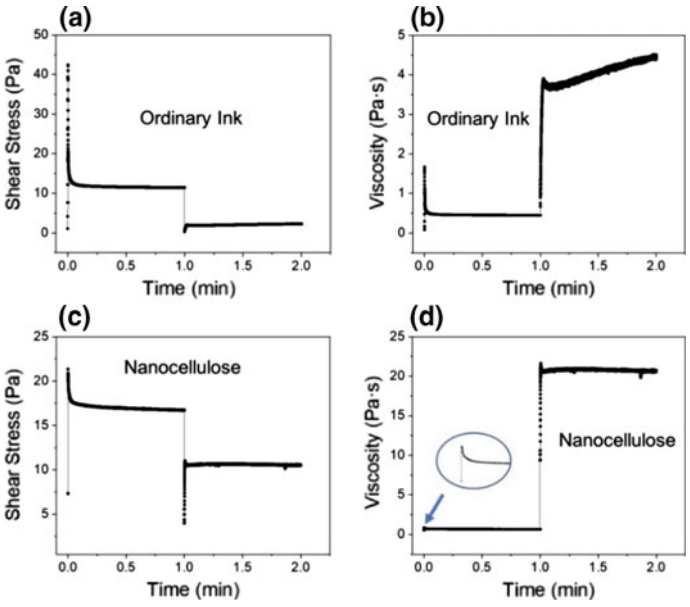

Fig. 10.4 Rheological data of commercial gel pen inks and CNCs. Reproduced from [32]

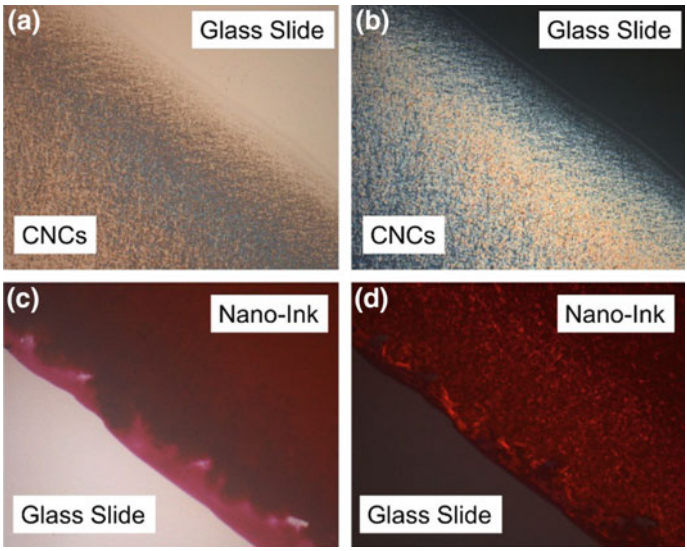

Fig. 10.5 Polarizing photos of CNCs and new nano-ink. Reproduced from [32]

10.5 Drilling Fluid Additives

The drilling fluid is the circulating flushing medium used in the well during the drilling process. The drilling fluid plays a very important role as it cools and lubricates the drill bit, clean the bottom of the well, bring out the cuttings, protect the well wall from collapse as well as transport the core [33–35]. The rheological and filtration properties of the drilling fluid affect the drilling operation. Improper drilling fluids can cause serious problems such as reservoir damage, drilling speed limit, increased costs and circulation lost. These problems become more serious in high temperature and high pressure environment. Drilling fluid is mainly composed of a solid phase, a liquid phase and other chemical additives. The liquid phase can be water, oil or emulsion. The solid phase can be bentonite (BT), weighting materials and rocks. BT has been used in water-based drilling fluid for many years due to its excellent colloidal properties. With the development of drilling fluids, high-quality drilling fluids with different functions have been developed and BT is no longer the only solid phase material. Lately, nanoparticles including graphene oxide, carbon nanotubes, nanometallic oxide and nanosilica have been added into the drilling fluid for better performance [36–44]. The nanoparticle added drilling fluids exhibit better properties. However, most of the nanoparticles are not environmental-friendly and nonrenewable. The addition of cellulose nanoparticles can reduce the cost of drilling fluids and help promoting the development of environmentally friendly materials. Biodegradable polysaccharides nanoparticles have been used in drilling fluids to control the viscosity of system and have been added in cement to improve the strength [45–47]. Employing a small amount of cellulose nanoparticles in traditional drilling

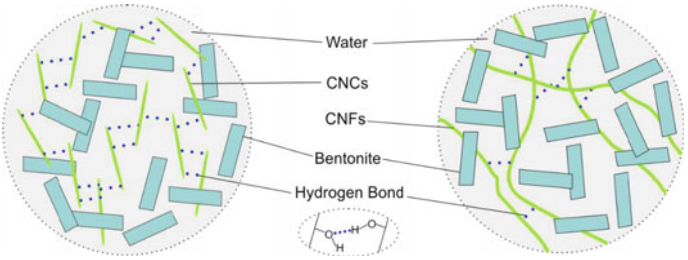

Fig. 10.6 Schematic diagram of the formations of hydrogen bonding among CNCs and CNFs in fluids. Reproduced from [33]

fluids can improve rheological properties, decrease drilling fluid loss and reduce formation damage [33]. The size of cellulose nanoparticles affected the viscosity, gel strength and yield point of the drilling fluid. As CNCs have smaller size than CNFs, the CNCs added fluids have better flow properties and exhibit lower viscosity, gel strength and yield point than that of the CNFs added fluids [33]. The improved properties of the drilling fluids with cellulose nanoparticles are ascribed to the hydrogen bond formation between cellulose nanoparticles as shown in Fig. 10.6.

Liu et al. [48] have produced a new chemical treatment agent for drilling fluid. 2-acrylamido-2-methylpropane sulfonic acid (AMPS) and *N, N*-dimethylacrylamide (DMA) were used to make the new cross-linked hydrogels (PADC-Fe^{3+}). The hydrogels were designed to load with different amounts of CNFs. They found out that the incorporation of CNFs helps to improve the salt resistance, high temperature resistance and shear resistance. Adding CNFs incorporated PADC-Fe^{3+} hydrogels in water-based drilling fluids can reduce filtrate loss at high temperatures and reduce the size of cement particles. By now, modified and unmodified cellulose materials have been widely studied and used in drilling fluids. Except for cellulose materials, starch-based nanoparticles have also been studied to prepare oil-based drilling fluid due to its low cost, extensive sources and biodegradability. As density, chemical reactivity, filtrate efficiency and rheological behaviors affect the performance of drilling fluid, phase separation and deposition of the drilling fluid can cause serious problems in the well, starch nanoparticles can improve the rheological properties and filtration reduction of drilling fluid [49]. However, starch based nanoparticles works only below 121 °C, when the temperature is higher than this, the thermal stability of starch in water-based drilling fluid declines. In such drilling conditions, starch products should be modified chemically, or substances that can increase the thermal stability of starch nanoparticles should be added into the drilling fluid [50].

10.6 Adhesive and Aqueous Coating Additives

There is a large number of reactive functional groups (−OH or −COOH or $-NH_2$) on the surface of nanopolysaccharides, which are convenient for developing adhesives. These reactive functional groups can adhere to different surfaces via different chemical reactions or hydrogen bonds. For example, Rose et al. [51] have demonstrated that rapid (within 30 s) and strong adhesion between two hydrogels can be obtained by using modified CNC dispersion as the effective glue. This is because the CNC nanoparticle can be used as a bridge to connect different polymer molecular chains, which could dissipate energy under stress [51]. They demonstrated that the fast and effective way to cohere tissues or gels may find potential application in medical fields. Besides, nanocellulose is usually used as additive of cobinder as it can regulate the rheological properties and water content [52]. In Veigel's work, CNCs have been added to a waterborne wood coating, test results reveal that CNCs ameliorate the internal cohesive property of the acrylate/polyurethane based wood coating layer [53].

Recently polysaccharides combined with fruit purees have also been used to make edible films and coatings. CNCs have been used to reinforce acerola puree and alginate and form nanocomposites edible films and coatings. CNCs can reduce the H_2O vapor penetration of packaging films, thus the quality of the product can be improved. When used as a fruit coating additive, CNCs have isolated the contact between fruits and the ambient environment. Without the interaction caused by water and oxygen in the air, the process of water loss, maturation and decay of the fruits were slowed down. And vitamin C of the fruits can be retained at the same time [54]. The synergistic effect of bioenvironmental composite coating on the preservation of cucumber is investigated by Dong et al. [55]. The composite coating is composed of water, 5% CNC and 1% chitosan. For comparative study, cucumbers are immersed in three different solutions to get different coatings, including pure H_2O coating, chitosan coating and CNC/chitosan composite coating. After stored at low temperature for 14 days, the weight loss of cucumbers in CNC/chitosan composite solution decreased significantly. All the experimental data show that the quality of cucumbers can be maintained longer with the use of CNC/chitosan composite coating and the shelf life of cucumbers can be prolonged [55]. Polysaccharides coatings, other than CNC/chitosan composite coating, have also been used to prolong the shelf life and keep the quality of fresh fruit during storage. Starch has been used to prepare coating for fruits as well, results showed that the starch composite coating can effectively reduce weight loss and inhibit the endogenous ethylene production of the fruits kept at room temperature [56, 57]. Polysaccharides can not only be used to keep the fruits fresh, but also can be used to keep the seafood fresh. In Chantarasataporn's work [58], chitin nanocrystals were used as seafood-based additives for pacific white shrimp. After soaking fresh shrimps in the soaking solution, the quality, color and texture of pacific white shrimp can be maintained for 2 days under storage at low temperature [58].

In Hubmann's work [59], CNCs have a potential use as an adhesion promoter. A small amount of CNCs can reinforce a UV-cured coating and improve the adhesion [59]. Moreover, CNCs derived from corncob residue can be added into paper coatings to improve rheological properties. As a green and renewable additive, CNCs have been produced by various methods. In Liu's work [60], CNCs were produced by acid hydrolysis and TEMPO mediated oxidation. Sulfuric acid and formic acid were used respectively in the acid hydrolysis process. CNCs obtained by sulfuric acid hydrolysis had better thickening function when compared with other CNCs products. The surface of the sulfuric acid hydrolyzed CNCs carries a large amount of sulfonic acid groups, the highly charged surface has stronger interactions with other molecules.

10.7 Cosmetic Additives

The coatings discussed above are mainly focused on the area of packaging, health care and chemical industry. In daily life, some cosmetics that people often used like sun scream, BB cream and foundation can be regarded as special coatings. Cosmetics are used for the purpose of beautifying, retaining or changing a person's appearance. People usually use cosmetics to clean, dye, rub, correct or protect the skin, hair, nails, eyes or teeth. As the petrochemical synthesis industry was well developed in last century, the price of raw materials from the chemical industry was low. Most cosmetic manufacturers use chemical raw materials to produce cosmetics. With the development of cosmetic industry and extraction technology, natural ingredients gradually can be found in the skin care cosmetics on the market. Researchers found that CNFs can replace traditional surfactants to stabilize cosmetic emulsion. BC has also been used in cosmetics such as facial masks and personal care products [61, 62]. The functions of BC in cosmetic formulations could be emulsion stabilizer, moisturizer or viscosity enhancer [63–65]. Nanochitin is also a good candidate for cosmetic products and can be found in lotions, creams, foundation, lipsticks, eye shadow and cleansing agents. Nanochitin and its derivatives have been used in hair care to reduce static electricity in hair, in oral care to prevent tooth damage and in skin care to treat acne and maintain skin moisture [66].

10.8 Paper Additives

In the papermaking industry, there are three ways to enhance the paper strength, including adding reinforcements, refining pulp and modifying paper fibers. Cellulose nanomaterials can act as a strength additive in the paper making process and can improve barrier properties of paper [67–73]. Due to its various unique characteristics, it is likely to be widely used as a sustainable reinforcing agent in the papermaking industry [74–78]. Shivyari et al. [79] prepared a novel laminate system composed of paper sheets and CNFs. The laminate manufacturing process was illustrated in

Fig. 10.7. Papers were first cut into strips and mix with the desired amount of CNF suspension. Then the paper strips were dip into diluted CNF suspension and they were stacked together in different ways as showed in Step 4 in Fig. 10.7. The obtained two samples with different structures were alternatively stacked together for water removal by cold pressing. Finally, the laminate was hot pressed for desired time [79]. Results showed that elastic modulus and strength of the obtained laminate system were much better than that of short glass fiber reinforced polypropylene or some wood or paper based laminates [79]. Balea et al. [80] have prepared CNFs from an agricultural waste-corn stalk and the nanoparticles were added into the pulping process. The results showed that the tensile index of recycled paper increased by 20% with the presence of 0.5% CNF originated from the corn waste [80]. The content of cellulose fiber and the raw material, as well as the production process, are all factors that affect the performance of recycled paper [81]. The tensile strength of paper can be correlated to the size of cellulose fiber. When the cellulose fiber is finer, the tensile strength is larger [82]. CNF can not only change paper properties but also affect the production process. After the addition of CNF, the drainage time of recycled paper decreased remarkably [83].

Chen et al. [84] produced BC from fiber sludge and the BC was used in paper-making. The cross-linked BC covered the surface of pulp fibers, acting as an outer reinforcement. The mechanical properties of the paper changed with varying the BC content. When the content is 10%, the tear resistance of the paper was increased by 1.4 times [84]. Different cellulose nanomaterials like CNC, CNF, cationic cellulose nanofibril (CCNF) and anionic cellulose nanofibril (ACNF) have been used in the presspaper to enhance the insulating performance. Owing to the electrostatic attraction between CNF and softwood fiber, the tensile strength of the insulating presspaper can be remarkably enhanced [85]. Ligno-nanocellulosic fibers can be made from triticale straws and the obtained fibers can significantly increase the elongation at break

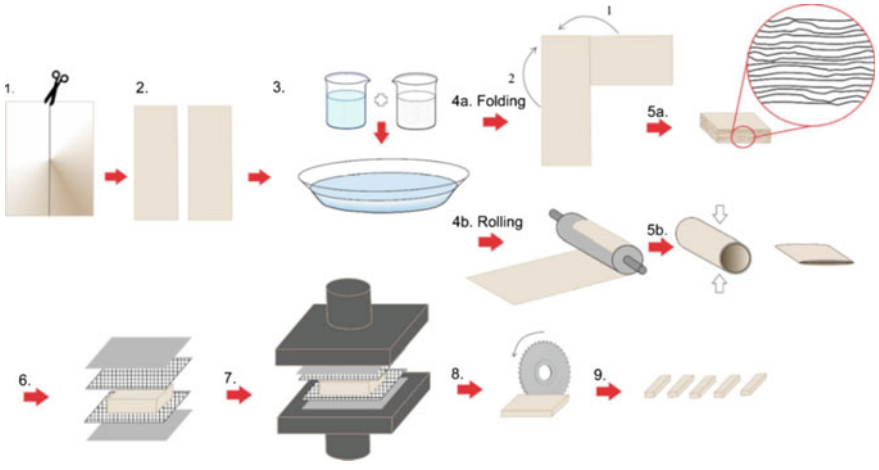

Fig. 10.7 Laminate manufacturing procedure. Reproduced from [79]

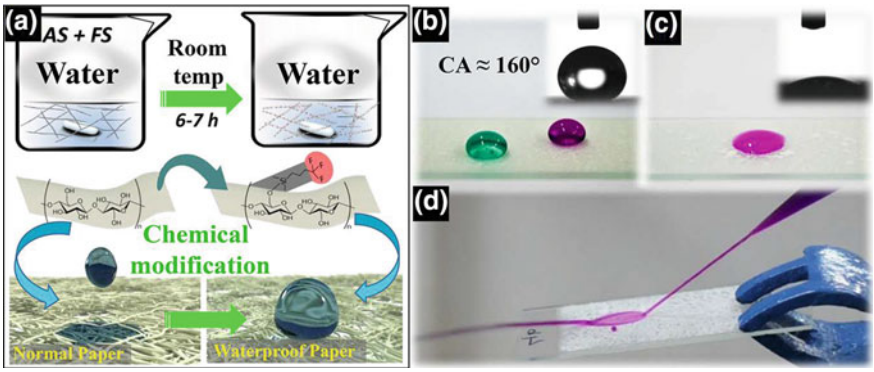

Fig. 10.8 **a** Schematic representation of CNF-based waterborne superhydrophobic material, **b**, **c** Water droplet on modified and native CNF-coated surface and **d** Continuous jet flow on coated glass. Reproduced from [87]

of test-liner paper [86]. Hydrogen bonding in cellulose causes aggregation problems when CNF and CNC used as reinforcing additives in papermaking. The aggregation would affect the mechanical properties of paper. Chemical modification of CNF can be made through various methods as reported by researchers. Among the modifications, a wet chemical process was employed to modify CNF by using functional silanes [87]. And the modification process and results were illustrated in Fig. 10.8.

The paper made from chemical functionalized CNF exhibits good waterproof performance, the abrasion and chemical resistance were improved at the same time. Superhydrophobicity of the modified CNF also made the waterproof paper showing good antibacterial properties, making it have a broader application prospects. Campano et al. [88] tried to improve the dispersion of CNC in pulp suspension through changing pulping conditions and using dispersing agents. Results found that a small amount of dispersing agent can significantly increase the tensile index.

10.9 Polymer Additives

To promote the development of sustainable and high-performance materials, nanopolysaccharides have been increasingly used as additives in polymer materials for different purposes [89]. Nanocellulose offers promising properties when used as reinforcing agents in polymer composites. With favorable mechanical characteristics and hygroscopic properties, CNFs have the potential to be used in facilitated transport membranes. Adding phosphorylated CNFs into polyvinyl alcohol membranes can promote gas separation [90, 91]. CNFs doped polymer precursor material has been made by Jiang et al. [92]. The addition of high aspect-ratio CNFs changes the crystalline and graphitic structure of the polyacrylonitrile (PAN) based material. Except for cellulose nanomaterials, nanochitin and starch have also been used as polymer

additives for specific purpose [93–103]. Nanochitin can be added into poly(ethylene oxide) (PEO) to increase the ionic conductivity. They can be mixed with poly(lactic acid) (PLA) to exploit the anti-microbial and skin regenerating properties [94, 95]. Nanostarch can enhance the cell viability and blood compatibility of poly(vinyl pyrrolidone) (PVP)/nanostarch bio-nanocomposite that suitable for wound dressing application [101].

10.9.1 Rheology Modifier

Nanopolysaccharides have been added into polymers to improve the properties of polymer or polymer blends. CNC is incompatible with most polymers. In order to detect the final dispersion of CNC in polymer matrix and the interfacial interaction between CNC and polymer, rheological test is an effective method. More importantly, rheological data can be used to optimize the process conditions and design the applications of composites, such as the CNC filled polymer composites [104]. As the CNC content increases, the nanoparticle-nanoparticle hydrodynamic interactions and the polymer-nanoparticle interactions become stronger. In the meantime, the low-frequency modulus significantly increases while the frequency dependence decreases.

Wu et al. [105] prepared PLA nanocomposites by mixing PLA with pristine, coupled and acetylated CNFs. Compared with the coupled CNFs, the acetylated CNFs exhibited better affinity to the polymer matrix. And the CNFs loadings have great influence on the rheological behavior of PLA. As showed in Fig. 10.9, the presence of 3 wt% CNFs results in an increased low-frequency response by about 2 orders of magnitude [105].

10.9.2 Crystallization Properties

CNCs can be used as fillers to fabricate bio-based nanocomposites. In the bio-based poly(β-hydroxybutyrate) (PHB)/CNCs nanocomposite, CNCs can accelerate the crystallization process of PHB as a good heterogeneous nucleating agent. At the same time, the incorporation of CNC can affect the texture and ring-banded structure of PHB spherulite, as well as the average band space, which is shown in Fig. 10.10 [106].

The corresponding intensity profiles of PHB and PHB/cellulose composite samples are shown in Fig. 10.11. Compared with pristine CNC, the surface modified CNC (CNC-*g*-PLA) shows enhanced interaction with PHB matrix. The stronger interaction between nanoparticles and polymer matrix, accompanied with the modified surface structure, changed the role of CNC-*g*-PLA during PHB crystallization. Unlike the pristine CNC, CNC-*g*-PLA retards the crystallization process of PHB as an anti-nucleation agent, which can be proven by Mo model. The parameters

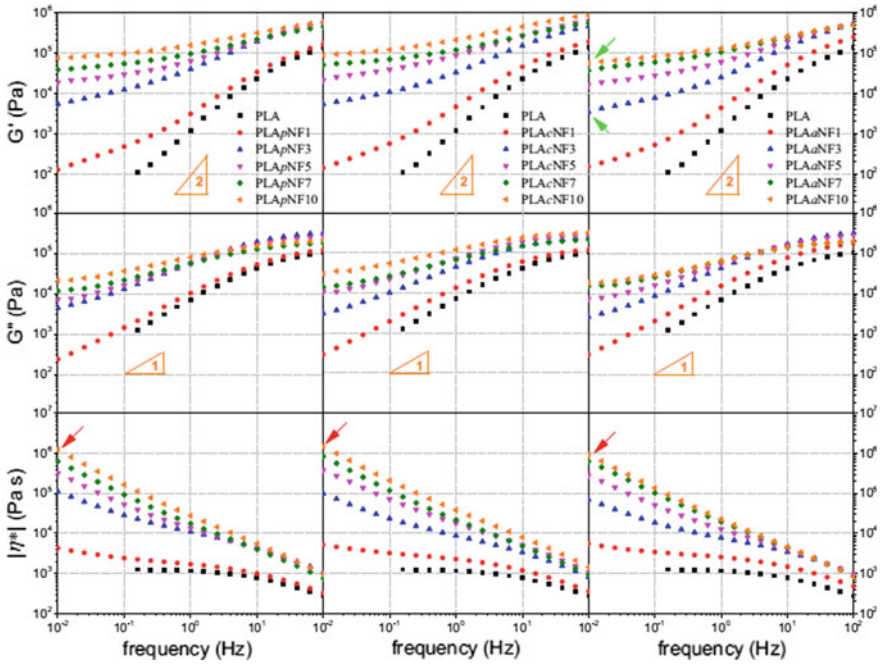

Fig. 10.9 The SAOS responses (storage modulus G' and loss modulus G'' as well as complex viscosity $|\eta^*|$) for PLA nanocomposites. Reproduced from [105]

obtained from Mo model further confirmed the different roles of CNC-*g*-PLA and pristine CNC [107].

10.9.3 Flame Retardant Properties

Biodegradable nanomaterials are gradually emerging in the filed of advanced materials. In Luo's work [108], CNC is used to prepare a kind of novel flame retardant with ammonium polyphosphate for polyurethane. The novel flame retardant with shell of dicyandiamide-formaldehyde on CNC shows more efficient flame retardancy than ammonium polyphosphate when applied to polyurethane [108]. The reason for this may be that dicyandiamide-formaldehyde produces non-flammable gas during the combustion process and dilute the concentration of oxygen. Meanwhile, CNC acts as carbonization agent to promote the formation of carbonized layers. Riehle et al. [109] have used surface-deacetylated ChNFs to fabricate multi-functional nanopapers, embracing the properties of flame-retardant and self-extinguishing. The flammability of the produced nanopapers could be tailored by exchanging counterions. The prominent flame retardant property and other specific properties of the novel high-performance nanopapers have been confirmed by experiments [109].

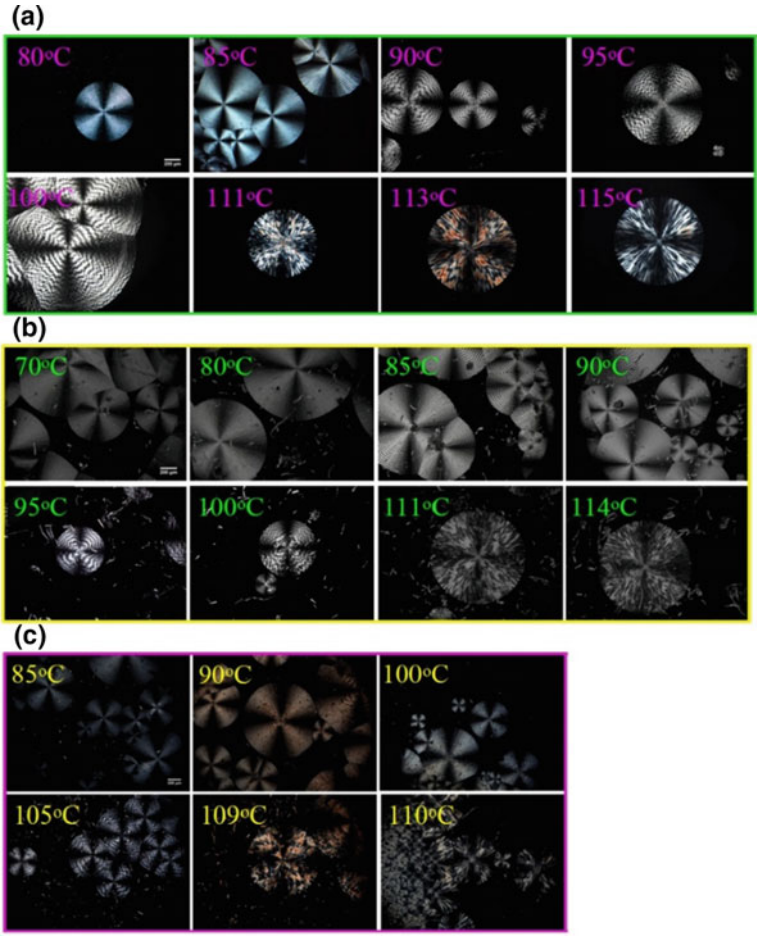

Fig. 10.10 Spherulite morphologies of **a** neat PHB, **b** PHBM2 and **c** PHBN2 at different temperatures during isothermal crystallization. Reproduced from [106]

10.10 Lubricant Additive

It is generally accepted that friction in mechanical operating systems has adverse impact on durability and efficiency. In order to reduce the friction between mechanical parts, lubricants, especially lubricant oil, are widely applied into the systems to lubricate the friction parts to reduce frictional resistance and power consumption. In addition to lubrication, lubricant oils also have the functions of cooling, rust prevention, cleaning, sealing and cushioning. Very recently, nanolubricants, combining nanoparticles and lubricant oil, have attracted increased attentions in tribology management. However, the materials employed have being restricted with the concerns on cost and environmental issues. Nanopolysaccharides possess unique advantages

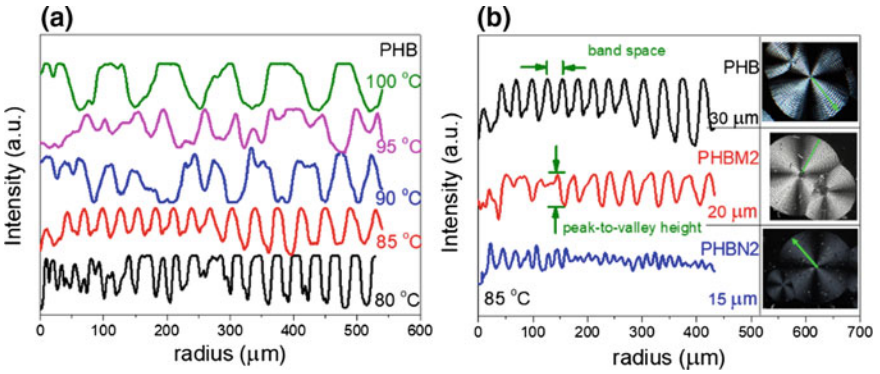

Fig. 10.11 Spherulite band spaces of **a** PHB at different temperatures and **b** PHB and its composites at the temperature of 85 °C. Reproduced from [106]

when comparing to traditional inorganic and metallic nanoparticle additives. The lightweight, environmental friendly and tunable surface properties make them great candidate as lubricant additives. Very recently, Awang et al. reported a work on cellulose nanocrystals as novel ecofriendly lubricant additives in engine oil [110]. They found out that the reduction of wear rate value can reach up to 69% when a small amount (0.1%) of CNCs were added into engine oil at a certain load and speed. The mechanical parts lubricated by CNC contained engine oil exhibit less friction than the parts lubricated by CNC-free engine oil. However, the compatibility between CNCs and hydrophobic engine oil still exist as an issue that have to be addressed. Lin and coworkers have explored the potentials of hydrophobic (C18) modified CNC in polyalphaolefin base oil as the lubricant additive [111]. A reduction on the coefficient of friction by 30% was obtained by the introduction of 2 wt% modified nanoparticles. They attributed the superior performance to the good dispersity and stability of the hydrophobic modified CNC. The presence of CNC modifies the oil viscosity and improves the boundary lubrication as showed in Fig. 10.12.

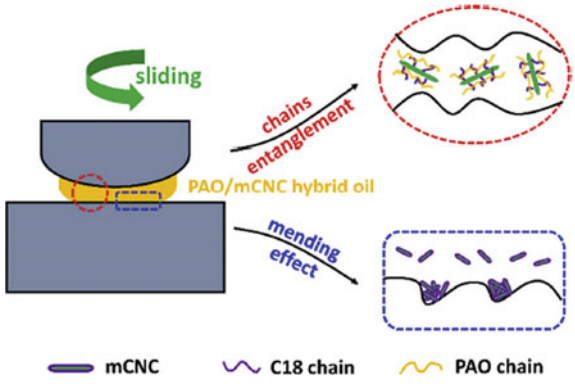

Fig. 10.12 Proposed lubricating mechanisms for modified cellulose nanocrystal and polyalphaolefin oil mixture. Reproduced from [111]

Moreover, the modified CNC has a mending effect on the defects of the friction surface, suggesting their important role in lubricating. The above work will pave the ways for designing ecofriendly and effective lubricant additive based on functional nanopolysaccharides. Various modification methods and friction reduction design strategies associated with different mechanisms could be expected in future studies.

10.11 Summary

Nanopolysaccharides, including nanocellulose, nanochitin, nanostarch have already been used as green additives in food, construction, coatings, cosmetics, pharmaceuticals, paper and other fields. The incorporation of nanopolysaccharides made the final products better and more controllable. With the aim of producing renewable and environmental friendly products, nanopolysaccharides-based green additives have great potentials in various applications. The biodegradable and renewable nanopolysaccharides-based material can partially replace fossil fuel based polymers to be used in daily life. With the development of scientific strategies and the achievement in research, nanostructured polysaccharides have gradually occupied a certain market in our daily life. Though some of the research is still in its infancy, we can foresee a broad application in the near future.

Acknowledgements J. Tang wishes to acknowledge the funding from Hunan Provincial Natural Science Foundation of China (2019JJ60073). J. Chen wishes to acknowledge the financial support from Jiangsu University of Technology (KYY18027).

References

1. Turbak AF, Snyder FW, Sandberg KR (1983) Microfibrillated cellulose, a new cellulose product: properties, uses, and commercial potential. J Appl Polym Sci Appl Polym Sympos 37:815–827
2. Charreau HL, Foresti M, Vazquez A (2013) Nanocellulose patents trends: a comprehensive review on patents on cellulose nanocrystals, microfibrillated and bacterial cellulose. Recent Pat Nanotech 7:56–80
3. Gómez HC, Serpa A, Velásquez-Cock J et al (2016) Vegetable nanocellulose in food science: a review. Food Hydrocolloids 57:178–186
4. Andrade DRM, Mendonça MH, Helm CV et al (2015) Assessment of nanocellulose from peach palm residue as potential food additive: part II: preliminary studies. J Food Sci Tech 52:5641–5650
5. DeLoid GM, Sohal IS, Lorente LR et al (2018) Reducing intestinal digestion and absorption of fat using a nature-derived biopolymer: interference of triglyceride hydrolysis by nanocellulose. ACS Nano 12:6469–6479
6. Gao HM, Duan B, Lu A et al (2018) Fabrication of cellulose nanofibers from waste brown algae and their potential application as milk thickeners. Food Hydrocolloids 79:473–481

7. Cerrutti P, Roldan P, Galvagno MA et al (2016) Production of bacterial nanocellulose from wine industry residues: importance of fermentation time on pellicle characteristics. J Appl Polym Sci 133:43109 (1–9)
8. Shi Z, Zhang Y, Phillips GO et al (2014) Utilization of bacterial cellulose in food. Food Hydrocolloids 35:539–545
9. Ullah H, Santos HA, Khan T (2016) Applications of bacterial cellulose in food, cosmetics and drug delivery. Cellulose 23:2291–2314
10. Corral ML, Cerrutti P, Vázquez A et al (2017) Bacterial nanocellulose as a potential additive for wheat bread. Food Hydrocolloids 67:189–196
11. Marchetti L, Muzzio B, Cerrutti P et al (2017) Bacterial nanocellulose as novel additive in low-lipid low-sodium meat sausages. Effect on quality and stability. Food Struct 14:52–59
12. Kaur J, Kaur G, Sharma S et al (2018) Cereal starch nanoparticles-a prospective food additive: a review. Crit Rev Food Sci 58:1097–1107
13. Lindström T, Aulin C (2014) Market and technical challenges and opportunities in the area of innovative new materials and composites based on nanocellulosics. Scand J Forest Res 29:345–351
14. Hamed SAAKM, Hassan ML (2019) A new mixture of hydroxypropyl cellulose and nanocellulose for wood consolidation. J Cult Herit 35:140–144
15. Mohammadkazemi F, Aguiar R, Cordeiro N (2017) Improvement of bagasse fiber-cement composites by addition of bacterial nanocellulose: an inverse gas chromatography study. Cellulose 24:1803–1814
16. Giles A (1997) An introduction to the gel pen-commentary. J Forensic Sci 42:759
17. Mazzella WD, Buzzini P (2005) Raman spectroscopy of blue gel pen inks. Forensic Sci Int 152:241–247
18. Roux C, Novotny M, Evans I et al (1999) A study to investigate the evidential value of blue and black ballpoint pen inks in Australia. Forensic Sci Int 101:167–176
19. Bei GX, Sheng HE, Liu SH et al (2015) Green design study of gel pen. Mech Electr Eng Technol 44:43–46
20. Qian JJ, Chen AP, Liu ZX et al (2009) The rheological characterization of the writing performance of carbon black gel ink. Adv Mater Res 66:139–142
21. Kito T, Senga K (1998) Preparation method for shear-thinning water-based ball-point pen inks compositions and ball-point pens employing the same. US patent
22. Williams RS, Fisher PC (1998) Pressurized roller pens and inks for such pens. US patent
23. Osada T (1999) Aqueous gel ink-filled ball point pen. US patent
24. Hanke DE, Gindelberger B, Heiman S (1995) Water-based ink composition for ballpoint pen. US patent
25. Reed G, Savage K, Edwards D et al (2014) Hyperspectral imaging of gel pen inks: an emerging tool in document analysis. Sci Justice 54:71–80
26. Liu ZX, Chen AP, Qian JJ et al (2009) Effect of surfactant on the properties of gel ink. Adv Mater Res 66:143–146
27. Yu PU, Chen AP, Qian JJ et al (2009) Rheological properties of gel ink with composite thickening agents. Mater Mech Eng 33:72–75
28. Puisto A, Illa X, Mohtaschemi M et al (2012) Modeling the rheology of nanocellulose suspensions. Nord Pulp Pap Res J 27:277–281
29. Chen Y, Xu CJ, Huang J et al (2017) Rheological properties of nanocrystalline cellulose suspensions. Carbohyd Polym 157:303–310
30. Wang WB, Fu SY, Leu SY et al (2018) A Nano-ink for gel pens based on scalable CNC preparation. Cellulose 25:6465–6478
31. Tseng WJ, Chen CN (2006) Dispersion and rheology of nickel nanoparticle inks. J Mater Sci 41:1213–1219
32. Wang WB, Fu SY (2019) Strategy for manufacturing a deep-red ink based on nanocellulose and reactive red 120. ACS Sustain Chem Eng 7:7233–7240
33. Song KL, Wu QL, Li MC et al (2016) Water-based bentonite drilling fluids modified by novel biopolymer for minimizing fluid loss and formation damage. Colloid Surf A Physicochem Eng Aspects 507:58–66

34. González J, Quintero F, Arellano J et al (2011) Effects of interactions between solids and surfactants on the tribological properties of water-based drilling fluids. Colloid Surf A Physicochem Eng Aspects 391:216–223
35. Li M, Wu Q, Song K et al (2015) Soy protein isolate as fluid loss additive in bentonite-water based drilling fluids. ACS Appl Mater Inter 7:24799–24809
36. Sun F, Lin M, Dong Z et al (2015) Nanosilica-induced high mechanical strength of nanocomposite hydrogel for killing fluids. J Colloid Interf Sci 458:45–52
37. Farboda M, Asl RK, Abadi ARN (2015) Morphology dependence of thermal and rheological properties of oil-based nanofluids of CuO nanostructures. Colloid Surf A Physicochem Eng Aspects 474:71–75
38. Li M, Wu Q, Song K et al (2015) Cellulose nanocrystals and polyanionic cellulose as additives in bentonite water-based drilling fluids: rheological modeling and filtration mechanisms. Ind Eng Chem Res 55:133–143
39. William JKM, Ponmani S, Samuel R et al (2014) Effect of CuO and ZnO nanofluids in xanthan gum on thermal, electrical and high pressure rheology of water-based drilling fluids. J Petroleum Sci Technol 117:15–27
40. Ponmani S, Nagarajan R, Sangwai JS (2016) Effect of nanofluids of CuO and ZnO in polyethylene glycol and polyvinylpyrrolidone on the thermal, electrical, and filtration-loss properties of water-based drilling fluids. SPE J 21:405–415
41. Cheraghian G, Hemmati M, Masihi M et al (2013) An experimental investigation of the enhanced oil recovery and improved performance of drilling fluids using titanium dioxide and fumed silica nanoparticles. J Nanostruct Chem 3:78–87
42. Kosynkin DV, Ceriotti G, Wilson KC et al (2011) Graphene oxide as a high-performance fluid-loss-control additive in water-based drilling fluids. ACS Appl Mater Inter 4:222–227
43. Mao H, Qiu Z, Shen Z et al (2015) Novel hydrophobic associated polymer based nano-silica composite with core-shell structure for intelligent drilling fluid under ultra-high temperature and ultra-high pressure. Prog Nat Sci 25:90–93
44. Fazelabdolabadi B, Khodadadi AA, Sedaghatzadeh M (2015) Thermal and rheological properties improvement of drilling fluids using functionalized carbon nanotubes. Appl Nanosci 5:651–659
45. Rincon-Torres MT, Hall LJ (2013) Cellulose nanowhiskers in well services. US patent
46. Hall LJ (2014) Chitin nanocrystal containing wellbore fluids. US patent
47. Lafitte V, Lee JC, James SG et al (2015) Fluids and methods including nanocellulose. US patent
48. Liu XL, Qu JL, Wang A et al (2019) Hydrogels prepared from cellulose nanofibrils via ferric ion-mediated crosslinking reaction for protecting drilling fluid. Carbohyd Polym 212:67–74
49. Dias F, Souza R, Lucas E (2018) Rheological behavior of drilling fluids containing hydrophobically modified starch for filtrate reduction. Chem Chem Technol 12:86–92
50. Alireza N, Javad ASM, Amin SNM et al (2018) Influence of monoethanolamine on thermal stability of starch in water based drilling fluid system. Petrol Explor Dev 45:167–171
51. Rose S, Prevoteau A, Elzie're P et al (2014) Nanoparticle solutions as adhesives for gels and biological tissues. Nature 505:382–385
52. Dimic-Misic K, Gane PAC et al (2013) Micro- and nanofibrillated cellulose as a rheology modifier additive in CMC-containing pigment-coating formulations. Ind Eng Chem Res 52:16066–16083
53. Veigel S, Grüll G, Pinkl S et al (2014) Improving the mechanical resistance of waterborne wood coatings by adding cellulose nanofibres. React Funct Polym 85:214–220
54. Azeredo HMC, Miranda KWE, Miranda HL et al (2012) Nanoreinforced alginate-acerola puree coatings on acerola fruits. J Food Eng 113:505–510
55. Dong F, Li SJ, Jin CD et al (2016) Effect of nanocellulose/chitosan composite coatings on cucumber quality and shelf life. Toxicol Environ Chem Rev 98:450–461
56. Thakur R, Pristijono P, Golding JB et al (2018) Development and application of rice starch based edible coating to improve the postharvest storage potential and quality of plum fruit (Prunus salicina). Sci Hortic-Amsterdam 237:59–66

57. Thakur R, Pristijono P, Scarlett CJ et al (2019) Starch-based films: major factors affecting their properties. Int J Biol Macromol 132:1079–1089
58. Chantarasataporn P, Yoksan R, Visessanguan W et al (2013) Water-based nano-sized chitin and chitosan as seafood additive through a case study of pacific white shrimp (Litopenaeus vannamei). Food Hydrocolloids 32:341–348
59. Hubmann M, Kong XH, Curtis JM (2019) Kinetic stabilization of cellulose nanocrystals in a photocurable prepolymer for application as an adhesion promoter in UV-curable coatings. Prog Org Coat 129:101–115
60. Liu C, Du HS, Dong L et al (2017) Properties of nanocelluloses and their application as rheology modifier in paper coating. Ind Eng Chem Res 56:8264–8273
61. Ougiya H, Watanabe K, Morinaga Y et al (1997) Emulsion-stabilizing effect of bacterial cellulose. Biosci Biotechnol Biochem 61:1541–1545
62. Amnuaikit T, Chusuit T, Raknam P et al (2011) Effects of a cellulose mask synthesized by a bacterium on facial skin characteristics and user satisfaction. Med Devices 4:77–81
63. Almeida IF, Pereira T, Silva NHCS et al (2014) Bacterial cellulose membranes as drug delivery systems: An in vivo skin compatibility study. Eur J Pharm Biopharm 86:332–336
64. Aramwit P, Bang N (2014) The characteristics of bacterial nanocellulose gel releasing silk sericin for facial treatment. BMC Biotechnol 14:104
65. Hasan N, Biak DRA, Kamarudin S (2012) Application of bacterial cellulose (BC) in natural facial scrub. Int J Adv Sci, Eng Inf Technol 2:1–4
66. Barikani M, Oliaei E, Seddiqi H et al (2014) Preparation and application of chitin and its derivatives: a review. Iran Polym J 23:307–326
67. Tozluoglu A, Poyraz B (2016) Effects of cellulose micro/nanofibers as paper additives in kraft and kraft-NaBH4 pulps. Nord Pulp Pap Res J 31:561–572
68. Hubbe MA (2006) Bonding between cellulosic fibres in the absence and presence of dry-strength agents: a review. Bioresour Technol 1:281–318
69. Ahola S, Österberg M, Laine J (2008) Cellulose nanofibres-adsorption with poly(amideamine) epichlorohydrin studied by QCM-D and application as a paper strength additive. Cellulose 15:303–314
70. Molin U, Daniel G (2004) Effects of beating on the fibre structure of kraft pulps as revealed by FE-SEM and TEM: influence of alkaline degradation. Holzforschung 58:226–232
71. Minor JL, Atalla RH, Harten TM (1993) Improving interfiber bonding of recycled fibers. J Pulp Pap Sci 19:J152–J155
72. Lindström T, Aulin C (2014) Market and technical challenges and opportunities in the area of innovative new materials and composites based on nanocellulosics. Scand J For Res 29:345–351
73. Herrera MA, Mathew AP, Oksman K (2017) Barrier and mechanical properties of plasticized and cross-linked nanocellulose coatings for paper packaging applications. Cellulose 24:3969–3980
74. González I, Boufi S, Pèlach MA et al (2012) Nanofibrillated cellulose as paper additive in eucalyptus pulps. Bioresource 7:5167–5180
75. Adel AM, El-Gendy AA, Diab MA et al (2016) Microfibrillated cellulose from agricultural residues. Part I: papermaking application. Ind Crop Prod 93:161–174
76. Taipale T, Österberg M, Nykänen A et al (2010) Effect of microfibrillated cellulose and fines on the drainage of kraft pulp suspension and paper strength. Cellulose 17:1005–1020
77. González I, Boufi S, Pèlach MA et al (2012) Nanofibrillated cellulose as paper additive in eucalyptus pulps. BioResources 7:5167–5180
78. Petroudy SRD, Syverud K, Chinga-Carrasco G et al (2014) Effects of bagasse microfibrillated cellulose and cationic polyacrylamide on key properties of bagasse paper. Carbohyd Polym 99:311–318
79. Shivyari NY, Tajvidi M, Bousfield DW et al (2016) Production and characterization of laminates of paper and cellulose nanofibrils. ACS Appl Mater Inter 8:25520–25528
80. Balea A, Merayo N, Fuente E et al (2016) Valorization of corn stalk by the production of cellulose nanofibers to improve recycled paper properties. BioResources 11:3416–3431

81. Manninen M, Kajanto I, Happonen J et al (2011) The effect of microfibrillated cellulose addition on drying shrinkage and dimensional stability of wood-free paper. Nord Pulp Pap Res J 26:297–305
82. Eriksen O, Syverud K, Gregersen O (2008) The use of microfibrillated cellulose produced from kraft pulp as strength enhancer in TMP paper. Nord Pulp Pap Res J 23:299–304
83. Merayo N, Balea A, Elena DLF et al (2017) Synergies between cellulose nanofibers and retention additives to improve recycled paper properties and the drainage process. Cellulose 24:2987–3000
84. Chen GQ, Wu GC, Alriksson B et al (2017) Bioconversion of waste fiber sludge to bacterial nanocellulose and use for reinforcement of CTMP paper sheets. Polymers-Basel 9:458
85. Huang JW, Zhou YX, Dong LY et al (2017) Enhancement of mechanical and electrical performances of insulating presspaper by introduction of nanocellulose. Compos Sci Technol 138:40–48
86. Tarrés Q, Ehman NV, Vallejos ME et al (2017) Lignocellulosic nanofibers from triticale straw: the influence of hemicelluloses and lignin in their production and properties. Carbohyd Polym 163:20–27
87. Baidya A, Ganayee MA, Ravindran SJ et al (2017) Organic solvent-free fabrication of durable and multifunctional superhydrophobic paper from waterborne fluorinated cellulose nanofiber building blocks. ACS Nano 11:11091–11099
88. Campano C, Merayo N, Balea A et al (2017) Mechanical and chemical dispersion of nanocelluloses to improve their reinforcing effect on recycled paper. Cellulose 25:269–280
89. Sharma A, Thakur M, Bhattacharya M et al (2019) Commercial application of cellulose nanocomposites-a review. Biotechnol 21:00316–00331
90. Jahan Z, Niazi MBK, Hagg M et al (2019) Phosphorylated nanocellulose fibrils/PVA nanocomposite membranes for biogas upgrading at higher pressure. Sep Sci Technol 177:258–268
91. Torstensen J, Helberg RML, Deng LY et al (2019) PVA/nanocellulose nanocomposite membranes for CO_2 separation from flue gas. Int J Greenh Gas Con 81:93–102
92. Jiang E, Amiralian N, Maghe M et al (2017) Cellulose nanofibers as rheology modifiers and enhancers of carbonization efficiency in polyacrylonitrile. ACS Sustain Chem Eng 5:3296–3304
93. Stephan AM, Kumar TP, Kulandainathan MA et al (2009) Chitin-incorporated poly(ethylene oxide)-based nanocomposite electrolytes for lithium batteries. J Phys Chem B 113:1963–1971
94. Coltelli MB, Cinelli P, Gigante V et al (2019) Chitin nanofibrils in poly(lactic acid) (PLA) nanocomposites: dispersion and thermo-mechanical properties. Int J Mol Sci 20:504–524
95. Shamshina JL, Zavgorodnya O, Berton P et al (2018) An ionic liquid platform for spinning composite chitin-poly(lactic acid) fibers. ACS Sustain Chem Eng 6:10241–10251
96. Mikhailov GM, Lebedeva MF (2005) Preparation and modification of chitin-based fibers. Russ J Appl Chem 78:1479–1485
97. Koh JJ, Zhang XW, He CB (2018) Fully biodegradable poly(lactic acid)/starch blends: a review of toughening strategies. Int J Biol Macromol 109:99–113
98. Mirab F, Eslamian M, Bagheri R (2018) Fabrication and characterization of a starch-based nanocomposite scaffold with highly porous and gradient structure for bone tissue engineering. Biomed Phys Eng Express 4:055021
99. Fourati Y, Tarrés Q, Mutjé P et al (2018) PBAT/thermoplastic starch blends: effect of compatibilizers on the rheological, mechanical and morphological properties. Carbohyd Polym 199:51–57
100. Garrido-Miranda KA, Rivas BL, Pérez MA et al (2018) Antioxidant and antifungal effects of eugenol incorporated in bionanocomposites of poly-(3-hydroxybutyrate)-thermoplastic starch. Food Sci Technol 98:260–267
101. Poonguzhali R, Basha SK, Kumari VS (2017) Nanostarch reinforced with chitosan/poly (vinyl pyrrolidone) blend for in vitro wound healing application. Polym-Plast Technol 57:1400–1410
102. Poonguzhali R, Basha SK, Kumari VS (2018) Fabrication of asymmetric nanostarch reinforced Chitosan/PVP membrane and its evaluation as an antibacterial patch for, in vivo, wound healing application. Int J Biol Macromol 114:204–213

103. Mol AS, Martins I, Oréfice RL (2015) Surface-pegylated chitin whiskers as an effective additive to enhance the mechanical properties of recycled ABS. J Appl Polym Sci 132:42463 (1–8)
104. Wang YK, Xu CJ, Wu DF et al (2018) Rheology of the cellulose nanocrystals filled poly(ε-caprolactone) biocomposites. Polymer 140:167–178
105. Ying ZR, Wu DF, Wang ZF et al (2018) Rheological and mechanical properties of polylactide nanocomposites reinforced with the cellulose nanofibers with various surface treatments. Cellulose 25:3955–3971
106. Chen JX, Xu CJ, Wu DF et al (2015) Insights into the nucleation role of cellulose crystals during crystallization of poly(β-hydroxybutyrate). Carbohyd Polym 134:508–515
107. Chen JX, Wu DF, Tam KC et al (2016) Effect of surface modification of cellulose nanocrystal on nonisothermal crystallization of poly(β-hydroxybutyrate) composites. Carbohyd Polym 157:1821–1829
108. Luo FB, Wu K, Li DF et al (2015) A novel intumescent flame retardant with nanocellulose as charring agent and its flame retardancy in polyurethane foam. Polym Composite 38:2762–2770
109. Riehle F, Hoenders D, Guo JQ et al (2019) Sustainable chitin nanofibrils provide outstanding flame-retardant nanopapers. Biomacromol 20:1098–1108
110. Awang N, Ramasamy D, Kadirgama K et al (2019) Study on friction and wear of Cellulose Nanocrystal (CNC) nanoparticle as lubricating additive in engine oil. Int J Heat Mass Transfer 131:1196–1204
111. Li K, Zhang X, Du C et al (2019) Friction reduction and viscosity modification of cellulose nanocrystals as biolubricant additives in polyalphaolefin oil. Carbohyd Polym 220:228–235

Chapter 11
Nanocellulose in High-Value Applications for Reported Trial and Commercial Products

Bolang Wu, Sunan Wang, Juntao Tang and Ning Lin

Abstract Despite abundant academic studies reported their diverse applications (as discussed in previous chapters), the practical products of nanocellulose are launched only during recent five years by several companies. In view of most cases concerning nanocellulose-based products, this chapter first summarizes the scale-up production of two types nanocelluloses, cellulose nanofibrils and cellulose nanocrystals all over the world. The introduction of various nanocellulose commercial products is based on its properties and functions, including the high mechanical strength and rigidity for composite additives, water retention for personal care products, rheological modification for writing ink, adsorption and barrier for paper and packaging application. It is unfortunate that some critical information and parameters of processing techniques and products can't be obtained because of the confidential consideration of some companies. However, the commercial products of nanocellulose (particularly in the cases of cellulose nanofibrils) introduced in this chapter can inspire the future commercialization of these renewable nanomaterials for the development of competitive commodity in industry.

Keywords Cellulose nanocrystals · Cellulose nanofibrils · High-value application · Commercial products

B. Wu · S. Wang · N. Lin (✉)
School of Chemistry, Chemical Engineering and Life Sciences, Wuhan University of Technology, Wuhan 430070, People's Republic of China
e-mail: ninglin@whut.edu.cn

J. Tang
College of Chemistry and Chemical Engineering, Central South University, Changsha 410083, China

N. Lin et al. (eds.), *Advanced Functional Materials from Nanopolysaccharides*, Springer Series in Biomaterials Science and Engineering 15,
https://doi.org/10.1007/978-981-15-0913-1_11

11.1 Scale-up Production of CNC and CNF

11.1.1 Worldwide Companies for CNC and CNF Production

Two important factors promote the commercial production of nanocellulose, concerning on non-renewable fossil resources and environment issues of synthesized polymers. With the global attention to the depletion of non-renewable resources such as oil, coal, natural gas and global environmental warming, nanocellulose as the renewable biomass resource, is expected to be transformed and utilized in our daily consumer good. In fact, plentiful academic research reported the remarkable advantages of nanocellulose in packaging barrier materials, high-performance composite materials, food and cosmetic additives, electronic products, biomedical materials, etc., which further drives the interest of global scale-up production of nanocellulose.

The reported commercial production of nanocellulose generally includes two types, viz. the rod-like cellulose nanocrystals (CNC) and semi-flexible cellulose nanofibrils (CNF). Despite the fact that numerous academic studies reported the preparation of CNC with the hydrolysis of inorganic acids [1], organic acids [2], enzymes [3] and deep eutectic solvents (DES) [4], the sulfuric acid hydrolysis to native cellulose is the prevailing method for CNC production in both laboratory and industry. In comparison with the other methods, the sulfuric acid hydrolysis is high efficiency (40–70% yield in 1–2 h), good reproductive, low-cost and can obtain the stable CNC product (surface negative charges) with a narrow size distribution and good dispersion stability. The preparation of CNF mainly adopts the methods of mechanical treatment such as high-pressure homogenization [5], ultrafine grinding [6] and microfluid method [7]. However, different conditions of mechanical treatments result in the wide scales of produced CNFs with 5–100 nm diameters and 1–100 μm lengths. It should be mentioned that the preparation of CNF generally includes a pretreatment process with the purpose of reducing the energy consumption, such as TEMPO oxidation [8], carboxymethylation [9] and enzymatic hydrolysis [10].

Since the first report on the commercial production of CNC by CelluForce company in 2011, the industrial technology on nanocellulose production was gradually advanced from laboratory to industrialization in order to obtain the high output at low cost. The scale-up production and pilot plants of CNC and CNF have been established in global companies, as summarized in Tables 11.1 and 11.2. Based on the traditional theory of strong acid hydrolysis to release CNCs, some companies invented the novel techniques to increase the yield and reduce the energy consumption. Canada's Blue Goose Biorefineries Inc. reported the transition metal catalyzed oxidation of lignocellulosic biomass to increase the CNC production. This technique is similar as pulp bleaching with material handling common in food production, taking the high quality and yield of the reported CNC production (10 kg/d). Compared with the traditional sulfuric acid hydrolysis, the reported CNC production by this process has no sulfonic group on CNC surface. Regarding the scale-up production

Table 11.1 Major industrial manufacturers of CNC in the world

Country	Region	Company	Reported capacity	Ref.
Canada	Windsor, Quebec	CelluForce	300 ton/y	[11]
	Calgary	Alberta Innovates (AITF)	100 kg/d	[12]
	Saskatoon	Blue Goose Biorefineries Inc.	10 ton/d	[13]
	Quebec	FPInnovations	10 kg/w	[14]
USA	–	American Process Inc.	–	[15]
	Madison	USDA-Forest Service-Forest Products Laboratory (FPL)	–	[16]
Sweden	Örnsköldsvik	MoRe Research	–	[17]
Israel	Rehovot	Melodea Ltd.	–	[18]

of CNF, Norwegian Borregaard reported the world's largest commercial-scale production facility for MFC (Exilva) production from Norwegian spruce in 2016, with a capacity of 10,000 tons suspension and 10% concentration (1000 tons dry weight). The commercial interest on CNF production is attracted by Japan's paper industry, including the Daio Paper, Sugino Machine, Chuetsu Pulp & Paper, Nippon Paper Industries, Oji Holdings and many other companies reported their pilot plants of CNF production. The Nippon Paper Industries is the largest paper company in Japan and reported the capacity of 500 tons/y of CNF production to meet the needs of research institutions and downstream companies.

According to the data listed in two tables, the number of CNC production companies worldwide is relatively small compared with CNF production companies. Furthermore, due to the relative high production cost and policy restrictions, the commercial production of CNC and CNF is mainly concentrated in North America, Europe and Japan. A possible reason for more popularity of CNF production than CNC production in industrial may be the different processing techniques. The relative complicated production process of CNC production and special production equipment (use of toxic and corrosive strong acid) may increase the cost and restrict the large-scale production of CNC. As a contrast, the mechanical treatment to produce CNF receives less pressure of environmental protection and equipment requirement than those of CNC production. It is worth noting that the advancement of scale-up production also promotes the commercialization of nanocellulose-based products in these regions, which will be discussed in the next section.

Table 11.2 Major industrial manufacturers of CNF and related products in the world

Country	Region	Company	Product (Brand)	Reported capacity	Ref.
Canada	–	Performance BioFilaments, Inc.	Cellulose filament	–	[19]
	Toronto	GreenCore Composites Inc.	CNF (NCell™)	–	[20]
USA	Atlanta	American Process Inc. (AVAPCO)	CNF	–	[15]
	Wisconsin	USDA-Forest Service-Forest Products Laboratory (FPL)	CNF	–	[16]
Norway	Sarpsborg	Borregaard	MFC (Exilva)	1000 ton/y	[21]
Sweden	Stockholm	InnventiaAB	Nanocellulose	100 kg/d	[22]
Finland	–	UPM-Kymmene Ltd.	Cellulose fibres	–	[23]
	Helsinki	Stora Enso Ltd.	MFC	–	[24]
	–	VTT	CNF	–	[25]
UK	–	ZelfoTechnology GmbH	NFC	–	[26]
	–	CelluComp	CNF (Curran)	–	[27]
France	–	InTechFibres	MFC	–	[28]
Germany	–	J. Rettenmaier & Söhne GmbH	CNF	–	[29]
Netherlands	Sittard-Geleen	Sappi	CNF	–	[30]
Japan	Tokyo	Dai-ichi Kogyo Seiyaku Co., Ltd	CNF	–	[31]
	Mishima	Daio Paper	CNF	100 ton/y	[32]
	Toyama	Sugino Machine	CNF (BiNFi-s)	1 ton/d	[33]
	Sendai	Chuetsu Pulp & Paper	CNF (nanoforest)	100 ton/y	[34]
	Ishinomaki	Nippon Paper Industries	CNF (cellenpia)	500 ton/y	[35]
	Tomioka	Oji Holdings	CNF	30 ton/y	[36]

11.1.2 Typical Cases of Scale-up Production for CNC and CNF

With the change from laboratory to commercial production of nanocellulose, the production condition and key equipment are important factors to affect the quality of products. In the CNC commercial production, the hydrolysis conditions need to be strictly controlled, including the factors of feedstock sources, hydrolysis duration and temperature, acid type and concentration, feedstock to acid ratio and mixing conditions. Optimizing the conditions can effectively increase the yield, reduce the cost, and obtain the products with the narrow size distribution and stable properties of CNC production. In the case of InnoTech Alberta's pilot plant (Canada), the acid hydrolysis is reported to occur in the reactor, where 110–155 kg of 63.5 or 64 wt% H_2SO_4 is pumped into the reactor from the acid storage tank. Sulfuric acid is then stirred at 200 rpm and heated up to 45 °C by low-pressure steam. Then, 10–13.5 kg of raw feedstock (bleached softwood or hardwood kraft pulps) is added into the reactor and reacts at this stirring speed for 2 h. After the reaction, 50 kg of water is pumped into the reactor to quench the acid hydrolysis reaction. The hydrolysate mixture is then transferred from the reactor to a 7500 L storage tank containing approximately 1200 kg of water to complete the reaction quenching, and finally neutralized by the slow addition of sodium hydroxide solution. In order to ensure the quality of CNC product, it is necessary to rapidly purify the hydrolyzed mixture, and the separation treatment (centrifugation) is the first step of the purification treatment. In this process, a centrifuge was reported to be used with a speed of 6500 rpm to separate the produced CNC from acid solution. After centrifugation, the CNC appears as a viscous paste-like solid, and the resulting centrifuge liquid (containing diluted H_2SO_4 solution) is sent to the spent acid treatment center for recycle. The paste-like CNC is sent to a storage tank, and diluted with 1500 L of water to produce the homogeneous and stable suspension. This CNC suspension is pumped back into the centrifuge for the water washing purification to remove high molecular weight cellulosic materials, large particles, dirt and unreacted materials. The purified CNC product is treated again as the aqueous suspension, and followed the second purification by ultrafiltration system to remove any sodium sulfate, glucose, oligomers and other impurities in the suspension. After the concentration to 3 wt%, the CNC suspension is dried into a powder. In this process, three key equipment viz. the reactor for hydrolysis reaction, the centrifuge for purification, and the dryer for CNC powders should be noted. In fact, the hydrolysis conditions and steps for the CNC production in industry is similar as those in the laboratory research. However, the equipment requirement is more rigid due to the large quantity of reactants. In the InnoTech Alberta's pilot plant for CNC production, the Pfaudler 50-gallon glass-lined reactor is used for the acid hydrolysis, and the GEA Westfalia SC-35 disk stack centrifuge is used for the solid-liquid separation. Regarding the last drying step, the spray drying (spx-anhydro ms-400 spray dryer) is used to remove water from some materials up to 37 kg per hour, which is one of the most widely used drying technologies in the food industry [37].

Several industrial CNC products are shown in Fig. 11.1. Specifically, the CNC product from CelluForce company is obtained by H_2SO_4 hydrolysis of wood pulp, and exhibits a nominal average length of 150 nm and a nominal average diameter of 7.5 nm with the nominal aspect ratio of 20 (image A). Another industrial CNC product prepared by Blue Goose Biorefineries Inc. using the transition metal catalyzed oxidation of lignocellulosic biomass have the similar morphology and dimensions (100–150 nm length and 9–14 nm diameter) as that of H_2SO_4 hydrolysis (image B). The InnoTech Alberta company produced the spray-dried CNC powders with a good re-dispersion to save the storage and transportation costs (image C).

The commercial production of CNF is concerned with the strong mechanical treatment, with the equipment of high-pressure homogenization, mechanical grinding, water jet [38] or microfluid processing to treat the purified cellulose fibers. The basic mechanism during these treatments is the introduction of high-energy process to destroy the interaction between cellulose chains and peel off cellulose

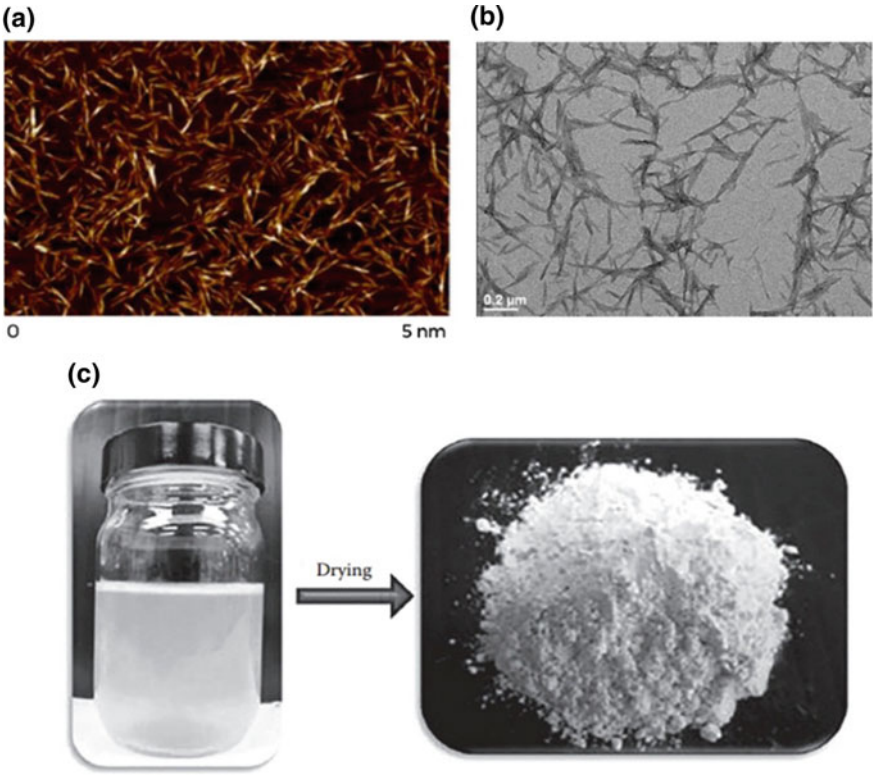

Fig. 11.1 **a** AFM image of CNC product from CelluForce company (reproduced from [11]); **b** TEM image of CNC product from Blue Goose Biorefineries Inc. (reproduced from [13]); **c** photos of CNC aqueous suspension and spray-dried powders from InnoTech Alberta company (reproduced from [37])

chains to obtain the nanoscale CNF products. In the case of MKZA10-15JIV supermasscolloider ultra-fine grinder produced from Masuko Sangyo co., Ltd. (Japan), the supermasscolloider ultra-fine grinders feature two ceramic nonporous grinders, which are adjustable at any clearance between the upper and lower grinder. Setting grinder clearance is important because it determines grain size, or the quality of products. The handle left and right rotation can be adjusted, with 1/100 mm gap up and down to adjust the clearance of the grinders. The porosity of traditional grinders is about 40%, and these pores will promote the growth of numerous bacteria, and may also cause cracks of grinder due to uneven heat distribution or thermal stress. The Supermasscolloider have nonporous grinders solves these problems completely, there is no growth of bacteria and no crack due to thermal stress. Meanwhile, the grinders have a 250 mm diameter and unique geometric geometry, which ensures an intensive dispersing effect and defibrillation of fibers by applying compression, circulation and abrasive shear forces. When using this equipment to prepare CNF, the fibers slurry (wood pulp, cotton, bamboo, etc.) was first soaked at 2% consistency and adequate mixing. The suspension was then fed into the supermasscolloider ultra-fine grinder, the feedstocks were passed 3–5 times through the grinder using gap width increasing operating power. The rotation speed was fixed at 1300 rpm in the first pass and at 1500 rpm in the following passes. The quality of the fibrillated cellulose was controlled by moving the lower grinder to set the clearance between the grinders. The fiber suspension was subjected to compression and shear forces between the grinders, which determined the particle size of the output material. The yield of the final product is 95% after the feedstock is treated by Masuko supermasscolloider ultra-fine grinder for 3–5 passes and the energy consumption during refining was 20.9 MWh/t [39–41].

Attributed to the strong hydrogen bonding interaction between cellulose chains, the scale-up CNF production by mechanical processes generally requires much energy and therefore results in the high costs. A high-efficiency approach to reduce the energy consumption during the industrial CNF production is the development of chemical pretreatment to the feedstock, and then followed by the mechanical treatments. Currently, the pretreatment methods of cellulose feedstock are reported to be the TEMPO oxidation, carboxymethylation, cationation, acetylation, phosphorylation, sulfonation, enzymatic hydrolysis, and the TEMPO oxidation pretreatment is widely used in both laboratory and industrial CNF production. In fact, performing the TEMPO oxidation pretreatment, the negative charges are introduced on the surface of cellulose fibers, and therefore the hydrogen bond interaction between cellulose chains can be reduced by repulsive effect from the introduced charges, which promotes the disintegration of aggregated nanofibrils. Furthermore, the pretreatment to the cellulose feedstock can make the cellulose less prone to flocculation, and more conducive to be peeled of chains, accompanied by the reduction of energy consumption and blockage risk for the equipment during the mechanical process. The UPM-Kymmene Ltd. (France) reported the different appearances and size distributions of prepared CNF by several techniques [42]. As shown in Fig. 11.2, the hardwood kraft pulp is treated by the supermasscolloider and microfluidizer with or without the TEMPO oxidation or carboxymethylation pretreatment to produce the CNF. It is apparent

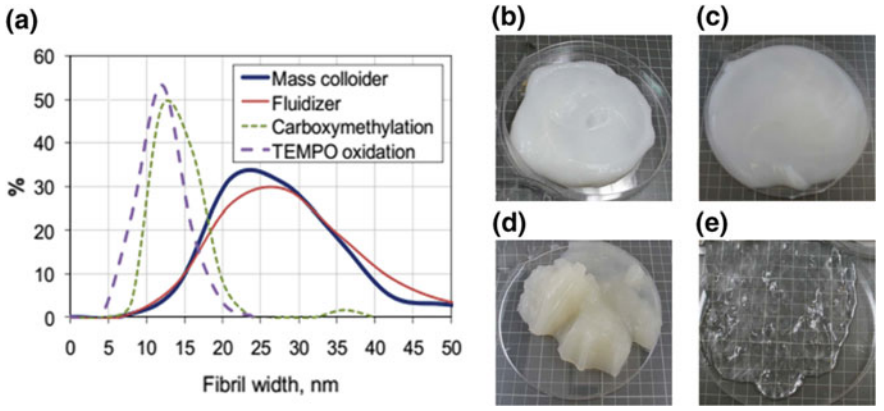

Fig. 11.2 The CNF fibril products from UPM-Kymmene Ltd. (France): width distribution (**a**) and appearances of products prepared by masscolloider (**b**), fluidizer (**c**), carboxymethylation pretreatment (**d**) and TEMPO oxidation pretreatment (**e**). Reproduced from [42]

that the CNF products prepared by the pretreatment have the smaller nanofibrils diameter (2.5–25 nm) and narrower diameter distribution than those CNFs produced only by mechanical processes (5–50 nm diameter). Furthermore, the CNF product prepared by the TEMPO oxidation pretreatment is more transparent than that of carboxymethylation pretreatment due to the additional surface charges.

11.2 Reported Products of Nanocellulose as Mechanical Enhancement

Derived from its superior mechanical property with specific modulus 4–5 times higher than steel, nanocellulose has been proved the promising nanofiller for various matrices with the purpose of enhancing their mechanical performances. In fact, some research institutes and experts regard the mechanical enhancement of nanocellulose as its most potential property for the commercial applications. Many academic attempts and studies have reported the use of this light-weight and high-strength nanomaterial as reinforcing nanofiller, and proposed the critical factors of composition, processing, compatibility and interfacial adhesion to determine the resultant properties of nanocellulose-enhanced composites [43]. In most of cases a chemical modification on nanocellulose is necessary to regulate its surface properties for the improvement of compatibility with hydrophobic matrix. However, these chemical treatments are generally complicated and high-cost, and therefore only several commercial products on nanocellulose in this application are reported.

The ASICS company (Japan) released the first-ever shoe containing CNF as reinforcing fillers (GEL-KAYANO™) in 2018 for the improvement of long-distance running performance [44], as shown in Fig. 11.3. This new shoe is reported to

Fig. 11.3 The product of running shoe GEL-KAYANO™ 25 with the reinforcement of CNF in midsole from Japanese ASICS company. Reproduced from [44]

use a foamed material FlyteFoam™Lyte1 in the midsole containing the surface hydrophobized CNF to offer extra mechanical reinforcement. The introduction of modified CNF into the elastomer matrix can effectively improve the tensile strength and Young's modulus of the composite, and achieve a simultaneous strengthening and toughening effect for the foamed composite. In comparison with those of the unfilled FlyteFoam material developed by ASICS, the mechanical strength and durability of new FlyteFoam™Lyte material reinforced by modified CNF are reported to be enhanced by approximately 20 and 7%, while keeping the lightweight for the application in midsole.

Nanocellulose could potentially replace some of the synthetic fiber composites with a natural and renewable alternative. In 2018, the Ideas2cycles company (Finland) produced the world's first bicycle with the mechanical enhancement of CNF to fabricate the frame in order to partly replace the synthetic fiber and enhance the overall performance of the bicycle [45]. As shown in Fig. 11.4, this company develops a technology and process to build up the CNF layer on a mandrel and further used for the manufacture of tubes. The tubes are then cut and mitered to the desired

Fig. 11.4 The product of bonded joints containing CNF in the assembled bicycle from Finland Ideas2cycles company. Reproduced from [45]

length, and further adhesively bonding the tubes at correct angles with the help of 3D-printed fixtures. The bonded joints are reinforced by laminating carbon fiber on top (overmoulding). The laminate is cured in a vacuum bag and the smooth outer surface is achieved with the help of 3D-printed moulds. Finally, a clear coat was applied on the surface and the bicycle was assembled using standard components.

The Green Science Alliance Co., Ltd. (Japan) launched a nanocomposite called "Nano Sakura" for the purpose of ultimate environmentally friendly material [46]. The composite material is prepared from nanocellulose enhancement and various type of resins including biodegradable resins and thermoplastic plastics. This new generation of composites hold the necessary mechanical strength to meet the practical application and is reported as the truly sustainable and recyclable materials (Fig. 11.5). This company attempts to the combination of nanocellulose with four kinds of matrices to produce the novel composites. (i) Biodegradable materials. Based on its biodegradability, nanocellulose is used to enhance the biodegradable resins to make disposable products such as food tray, food containers, beverage container, straw, cutlery etc. (ii) Conventional synthetic materials. Molding products of mechanical strength will be stronger with lighter weight from nanocellulose enhancement so that application can expand to various type of purpose including automotive, construction material, film, container etc. In addition, gas barrier property, crystallinity, dimensional stability will be improved as well as low thermal expansion. (iii) Recycle materials. This category of material is made by mixing nanocellulose and thermoplastic waste with the applications of film, container, home electrics, automotive, construction. (iv) Hybrid materials. This material is composed of nanocellulose, biodegradable resins and inorganic materials such as calcium carbonate ($CaCO_3$).

The bottom plate of the table tennis racket is made of multi-layer plywood with adhesive to improve the softness and comprehensive performance of the racket. However, the addition of the traditional adhesive will make the feel of the racket hitting the ball hard, and the ball stretch will disappear after hitting the ball, that is the efficiency of the fly-in speed converted to the ball by the racket is reduced. In order to eliminate this shortcoming, Darker company (Japan) reported the "Sakura"

Fig. 11.5 The products of "Nano Sakura" polymeric masterbatch containing nanocellulose: CNF PLA composite (PLA + 23% of CNF, composite) (**a**), CNF color masterbatch (PLA + 23% of CNF + yellow pigment 25%, composite masterbatch) (**b**) and related commodities (mold product composed of PLA + 2% of CNF) (**c**) from Green Science Alliance Co., Ltd. Reproduced from [46]

Fig. 11.6 The product of table tennis bats with the "Sakura" containing nanocellulose as adhesive from Darker company. Reproduced from [47]

[47] as a binder for the racquet bottom plate, using the light weight and high strength of nanocellulose to eliminate the adverse effects of the adhesive on the table tennis racket (Fig. 11.6).

As discussed before, the development of nanocellulose as the reinforcing filler to enhance the mechanical properties for the composites is widely expected to be the most prospective application in industry, particularly if only considering its superior mechanical properties. However, the practical application of nanocellulose as the mechanical reinforcing filler for the composites is not widely accepted by the industry like the commercial glass fiber, Kevlar fiber and inorganic additives. Several basic issues may restrict the practical enhancing effect of nanocellulose in the development of commercial products, involving the dispersibility and compatibility of nanocellulose with matrices, costs of processing and modification, and trade-off between different enhancing effects on strength, modulus and toughness.

11.3 Reported Products of Nanocellulose as High-Rigidity Component

Nanocellulose is a kind of typical rigid nanomaterial with the complete removal (CNC) or partial removal (CNF) of amorphous regions of cellulose chains, and therefore the high crystallinity and rigidity are their intrinsic features. Generally, the crystalline index and longitudinal modulus of CNF are reported as 60–80% and 100 GPa, which are even higher for CNC as 80–95% and 130 GPa [48]. This special physical property allows nanocellulose to be applied in the acoustic equipment, such as the diaphragm for headphone and audio speaker. As the sound unit of the headset, the diaphragm is very sensitive to the change of the magnetic field. When the electrical signal passes through the coil, the magnetic field changes, causing the diaphragm to deformation change under force. Meanwhile, the rapid change of electrical signal will cause the diaphragm to vibrate at high speed; thus, the vibration is transmitted to the air through the vibration of the diaphragm, and sound waves are generated. The quality of the diaphragm determines the overall quality of the headphone. Therefore,

the design of the diaphragm is required to be lighter in weight and better in rigidity. Such a diaphragm can completely convert the kinetic energy of the coil into sound. Nanocellulose is an ideal material for the preparation of diaphragm due to its light weight and high rigidity. As shown in Fig. 11.7, the Onkyo company (Japan) invented the world's first audio speaker "SC-3(B)" using the CNF diaphragm [49]. "SC-3(B)" is reported to be equipped with the "non-press ONF (Onkyo Nano Fiber)" vibrator plate which is the rigid nanomaterial developed by CNF. With the addition of CNF, this CNF-based diaphragm is both powerful and low-gravity, to achieve good bass playback, reproduce the shock of live performance, with the sense of air for players and the venue.

Another Japanese corporation "Pioneer" launched a headphone "SE-MONITOR5", using the lightweight but high-strength CNF as the diaphragm component (Fig. 11.8) and edge free structure providing users with a better auditory experience. The CNF-based diaphragm headphones developed by "Pioneer" have independently developed a driver with a diameter of 50 mm that supports broadband

Fig. 11.7 The product of audio speaker "SC-3(B)" containing the CNF diaphragm from the Onkyo company (Japan). Reproduced from [49]

Fig. 11.8 The product of headphone "SE-MONITOR5" containing the CNF diaphragm from the Pioneer corporation (Japan). Reproduced from [50]

playback of high definition audio sources (5 Hz–85 kHz) and clear audio images, allowing the headphones to bring in fine and detailed sound quality [50].

11.4 Reported Products of Nanocellulose as Water Retention Additives

Nanocellulose is a type of nanoparticles derived from natural cellulose, possessing abundant hydroxyl groups in the structure, and therefore the water molecules can be locked inside the formed hydrogen-bonding network by nanocellulose. The good biocompatibility and low toxicity together with the super moisturizing property endow the nanocellulose with a potential moisturizing ingredient in cosmetics and skin care products. In 2017, the Asia NanoTech company (Korea) announced a new series of whitening cosmetic with the addition of the palm tree extracted CNF [51], as shown in Fig. 11.9. These products are reported to have a much more longer moisturizing effect, safer on skin and a competitive price than others. The CNF is regarded to be safe for human body, and easy to penetrate the skin with the excellent moisturizing performance. Furthermore, the introduction of 10 nm CNF in these cosmetics is reported to maintain the skin physiological activity for a long time, disperse moisture and nutrition composition equably at the same time, and therefore exhibit an excellent effect on skin protection. After the addition of CNF, the moisture content of these cosmetics can be kept at 30–40% for 24 h, in comparison with only 2–4% moisture retention for the traditional products made from collagen or hyaluronic acid.

The Japanese Koyo Kasei Co., Ltd. reported three styles of cosmetics (ingredient gel, cream and water) using rose essence and CNF (provided by the Nippon Paper company) as the moisturizing ingredient [52], as shown in Fig. 11.10. These products containing hydrophilic CNF components are reported to be effective to enhance the moisturizing property easily absorbed by the skin to lock the water molecules.

The FABULA company (Taiwan) released their latest facial mask product—"Bio Fiber Nanocellulose Mask" (Fig. 11.11), which was made from nanocellulose with a diameter of about 20 nm, a hundred times smaller than the fiber of traditional nonwoven fabric. This mask was reported to be composed of nanocellulose fermented

Fig. 11.9 The series cosmetics products using CNF as the moisturizing ingredient from the Asia NanoTech company (Korea). Reproduced from [51]

Fig. 11.10 The three cosmetics products of "rose fragrance gel", "rose body & hand cream", and "rose skin water" using CNF as the moisturizing ingredient from the Koyo Kasei Co., Ltd. (Japan). Reproduced from [52]

Fig. 11.11 The product of "Bio Fiber Nanocellulose Mask" from the FABULA company (Taiwan). Reproduced from [53]

by microorganisms containing various face essence with the function to bleach, tranquilize the skin and eliminate wrinkles. The good hydrophilic and water retention of nanocellulose endow this mask with 200 times more moisture retaining than typical nonwoven mask. Attributed to the nanosized fiber and large specific surface area, it was reported that this nanocellulose-based mask can infuse 50% more nutrition essence, and deeply penetrate to skin's pore, grasp skin and moisture and not drop off. The three-dimensional network formed by the hydrogen bonds from nanocellulose can provide the extra tiny aperture for holding the water molecules and slowly evaporation of the essence. Moreover, the FABULA nanocellulose-based mask was

reported to remove 49% of sebum (skin's natural oil) after applying the mask for 20 min, and also possess good air permeability to provide the protection for injured skin [53].

11.5 Reported Products of Nanocellulose as Rheological Modifier

Cellulose and its derivatives are widely used as rheological thickeners with regulating thixotropy behaviors in many applications. Different from the native cellulose, nanocellulose have some unique rheological properties, which can be used as a novel rheology modifier to regulate the rheological behaviors of fluids by the change of its loading level, size distribution and temperature [54]. Typically, with the increase of the concentration, the nanocellulose suspension exhibits varied rheological behaviors as the liquid crystal polymer solution. Moreover, the shear rate significantly affects the viscosity of the nanocellulose suspension. It has been reported that at low shear rates, the viscosity of the nanocellulose suspension decreases with the increase of shear rate, indicating its shear thinned behavior at this stage. However, at high shear rates (above the critical shear rate), the viscosity of the nanocellulose suspension increases with the increase of shear rates.

A novel gel ink ballpoint pens using the oxidized CNF as the ink tackifier is released by the Mitsubishi Pencil Co., Ltd. (Japan) [55]. The viscosity of composite ink is reported to be reduced by about 50% compared with the traditional products, and even if writing quickly there will be no instability problem (as shown in Fig. 11.12). In the developed aqueous ink composition, the introduced oxidized CNF provides a high viscosity even at a low viscosity of 0.05–1.5 wt% and the composite inks show the high thixotropy index. The introduction of oxidized CNF exerts a rheology controlling effect as a thickener and gelling agent for the aqueous ink compositions in a smaller amount than those of a conventional fine cellulose (carboxymethyl cellulose) and xanthan gum.

In the aqueous ink composition, the content (solid content) of the oxidized CNF is optimized as 0.05–1.5 wt%, preferably 0.1–1.0 wt% based on the total amount of ink. If the content of CNF is less than 0.05 wt%, the satisfactory thickening action cannot be obtained, and meanwhile the solid matters such as the pigment will settle down in some cases. On the other hand, if the content of CNF exceeds 1.5 wt%, the viscosity of composite ink grows much high, and therefore a splitting phenomenon of the drawn lines and inferior discharge of the ink will appear. Another important component for this composite ink is the sugar's additive. The sugars (non-reducing sugars, particularly sugar alcohols) having an average molecular weight of 5000 or less used in the aqueous ink composition are a component which inhibits time-dependent heterogeneity (difference in viscosity between up- and down-sides) in viscosity distribution. The content of sugar should be ranged from 0.001 to 30 wt%, preferably 0.01–10 wt% based on the total amount of the aqueous ink. From the

Fig. 11.12 Gel ink ballpoint pen uni-ball "Signo 307" developed by the Mitsubishi Pencil Co., Ltd. (Japan) using CNF as the ink tackifier; and the pictures of lines drawn by the conventional product and uni-ball Signo 307. Reproduced from [55]

viewpoint of dispersion stability, the oxidized CNF has more preferably a number average fiber diameter of 3–80 nm. Controlling a number average fiber diameter of the oxidized CNF to 2 nm or more makes it possible to allow the oxidized CNF to exert a function of a dispersion medium, and on the contrary, controlling the number average fiber diameter to 150 nm or less makes it possible to further enhance dispersion stability of the cellulose fibers themselves [56, 57].

11.6 Reported Products of Nanocellulose as Adsorption Materials

The features of high aspect ratio and specific surface area of nanocellulose endow its good air permeability and strong adsorption performance based on the formed three-dimensional and porous network structure by the intertwining of nanofibers, which can be applied to the functional paper, disposable diapers and other daily necessities. In 2015, the Nippon Paper Industries Co., Ltd. (Japan) developed the "Hada Care Acty" series of adult diapers containing CNF (Fig. 11.13), exhibiting some functions of absorbing metal ions, deodorizing and sterilizing properties. It was reported that this kind of CNF-based diaper held three times of deodorizing effect in comparison with the traditional adult diapers [58]. Meanwhile, this diaper has the antibacterial performance, superior water absorption and good air permeability, which provides the better user experience than the traditional products.

Fig. 11.13 The product of adult diapers containing CNF from the Nippon Paper Industries Co., Ltd. (Japan). Reproduced from [58]

Another Japanese company Daio Paper Corp. reported the combination of CNF with pulp fibers to produce the functional paper toilet cleaner [59]. The CNF prepared from wood are tightly entangled with the pulp fibers, and provides two times mechanical enhancement to this paper toilet cleaner than that of the ordinary paper. Furthermore, this new CNF-based toilet paper also exhibits the deodorization and bacteriostasis under the premise of meeting basic cleaning requirements (Fig. 11.14). It was reported that one such paper toilet cleaner can make the whole toilet clean. In order to meet the various needs of consumers, the company recently launched some

Fig. 11.14 The product of functional paper toilet cleaner containing CNF from the Daio Paper Corp. (Japan). Reproduced from [59]

advanced products with the pure fragrance, rose, perilla, lemon and other fragrance paper toilet cleaner.

11.7 Reported Products of Nanocellulose as Packaging and Barrier Materials

With the advantages of lightweight, high-strength and nontoxicity, nanocellulose is a promising candidate for the preparation of lighter and stronger packaging materials. In order to replace the non-renewable materials, the Stora Enso company (Finland) launched its new packaging product prepared by microfibrillated cellulose (MFC) reinforced cardboard, which was reported to be widely used in fast-food packaging, liquid packaging (milk cartons, as shown in Fig. 11.15), barrier coating films etc. The Stora Enso company is supporting Canadian Elopak with renewable innovations on the New Natura Concept (NNC) mainly based on MFC, aiming to make packaging as light as possible [60]. By converting a small portion of wood pulp to MFC and mixing it into the composite, it can make paperboard with the same strength, opacity and brightness but use less original fibers. Therefore, the introduction of MFC allows for the stronger composites, weight saving and renewability. In addition, the introduction of MFC as the enhancing fillers for the folding box board can increase its bending strength, which can make a stronger board or reduce the package's total weight. According to the report of this company, the MFC can also create coatings and films featuring excellent barrier properties to preserve aromas and to protect against gases like oxygen, and even grease and oil. Besides the mechanical enhancement of MFC,

Fig. 11.15 The lightweight packaging product containing MFC for the storing of milk and beverage from the Stora Enso company (Finland). Reproduced from [61]

the barrier films fabricated by this nanomaterial exhibited the remarkable reduction of metals, CO_2 footprint and bacterial in stores of food and beverage products [61].

11.8 Concluding Remarks

The inherent properties of a substance determine its potential applications. The numerous advantages of renewability, nontoxicity, good biocompatibility and biodegradability together with the lightweight, high modulus and specific surface area make nanocellulose as a type of promising nanomaterial to replace traditional inorganic and metal particles in various applications, particularly with the requirement of environmental protection. Despite the fact that abundant academic studies reported diverse potential applications during last twenty years, the commercial products of nanocellulose were really developed until recent five years. As discussed in this chapter, some companies are very interested in these natural nanomaterials, and have attempted various applications based on the properties of nanocellulose as the mechanical and rigid enhancing fillers, water retention additives, liquid rheological modifier, adsorption and barrier components. Regarding the family of nanocellulose, the industrial interests on cellulose nanofibrils (CNF) are much higher than cellulose nanocrystals (CNC), which may be resulted from the relative low-cost and green preparation techniques of CNF than the strong acid hydrolysis for the preparation of CNC. Although several practical products on nanocellulose have been launched by some companies, the challenges still remain until the wide applications of these renewable nanomaterials in the development of competitive commodity. (i) A more high-efficiency, economical and "green" production technique of nanocellulose is required by the industry, which is strongly associated with the cost of prepared nanocellulose and price competition of the resultant products. One theory from the nanocellulose industry is the cost of commercial CNF should be controlled as 2–3 and 8–10 $/ton for commercial CNC, which can be competitive as other similar products. (ii) The exploration of new functional properties of nanocellulose is demanded to create the high added-value for the related products. In comparison with the traditional polysaccharide-based commercial derivatives and synthesized polymers, the new functional properties of nanocellulose may be the solution for its irreplaceability on the road of commercialization.

Acknowledgements The authors would like to acknowledge the support of the National Natural Science Foundation of China (51603159).

References

1. Beck-Candanedo S, Roman M, Gray DG (2005) Effect of reaction conditions on the properties and behavior of wood cellulose nanocrystal suspensions. Biomacromolecules 6:1048–1054

2. Filson PB, Dawson-Andoh BE (2009) Sono-chemical preparation of cellulose nanocrystals from lignocellulose derived materials. Bioresour Technol 100:2259–2264
3. Siqueira G, Tapin-Lingua S, Bras J et al (2010) Morphological investigation of nanoparticles obtained from combined mechanical shearing, and enzymatic and acid hydrolysis of sisal fibers. Cellulose 17:1147–1158
4. Sirviö JA, Visanko M, Liimatainen H (2016) Acidic deep eutectic solvents as hydrolytic media for cellulose nanocrystal production. Biomacromolecules 17:3025–3032
5. Turbak A, Snyder F, Sandberg K (1983) Microfibrillated cellulose, a new cellulose product: properties, uses and commercial potential. J Appl Polym Sci 37:815
6. Masuko Sangyo Co Ltd (2018) http://www.masuko.com/English/index.html. Accessed 20 Mar 2019
7. Zimmermann T, Pöhler E, Geiger T (2004) Cellulose fibrils for polymer reinforcement. Adv Eng Mater 6:754–761
8. Saito T, Kimura S, Nishiyama Y et al (2007) Cellulose nanofibers prepared by TEMPO-mediated oxidation of native cellulose. Biomacromolecules 8:2485–2491
9. Wågberg L, Decher G, Norgren M et al (2008) The build-up of polyelectrolyte multilayers of microfibrillated cellulose and cationic polyelectrolytes. Langmuir 24:784–795
10. Tibolla H, Pelissari FM, Menegalli FC (2014) Cellulose nanofibers produced from banana peel by chemical and enzymatic treatment. LWT-Food Sci Technol 59:1311–1318
11. CelluForce (2019) https://www.celluforce.com. Accessed 10 Apr 2019
12. Alberta Innovates (2016) https://albertainnovates.ca. Accessed 7 Apr 2019
13. Blue Goose Biorefineries Inc (2012) https://bluegoosebiorefineries.com. Accessed 20 Mar 2019
14. FPInnovations (2012) https://fpinnovations.ca/Pages/index.aspx. Accessed 25 Mar 2019
15. American Process Inc (1995) https://www.americanprocess.com. Accessed 24 Mar 2019
16. USDA Forest Products Laboratory (2012) https://www.fpl.fs.fed.us/index.php. Accessed 10 Apr 2019
17. MoRe Research (2013) http://www.more.se/en. Accessed 6 Apr 2019
18. Melodea Ltd (2018) http://www.melodea.eu. Accessed 22 Mar 2019
19. Performance BioFilaments Inc (2014) http://www.performancebiofilaments.com. Accessed 12 Apr 2019
20. GreenCore Composites Inc (2014) http://www.greencorenfc.com/technology.htm. Accessed 5 Apr 2019
21. Borregaard (2011) https://borregaard.com. Accessed 1 Apr 2019
22. InnventiaAB (2018) http://www.innventia.com. Accessed 10 Apr 2019
23. UPM-Kymmene Ltd (2019) https://www.upm.com. Accessed 24 Mar 2019
24. Stora Enso Ltd (2019) https://www.storaenso.com/en. Accessed 29 Mar 2019
25. VVT (2019) https://www.vttresearch.com. Accessed 9 Apr 2019
26. ZelfoTechnology GmbH (2010) http://www.zelfo-technology.com. Accessed 3 Apr 2019
27. CelluComp (2013) https://www.cellucomp.com. Accessed 27 Mar 2019
28. InTechFibres (2015) http://intechfibres.com. Accessed 21 Mar 2019
29. J. Rettenmaier & Söhne GmbH (2019) https://www.jrs.eu/jrs_en. Accessed 1 Apr 2019
30. Sappi (2019) https://www.sappi.com. Accessed 7 Apr 2019
31. Dai-ichi Kogyo Seiyaku Co Ltd (2003) https://www.dks-web.co.jp. Accessed 5 Apr 2019
32. Daio Paper (2015) https://www.daio-paper.co.jp/en. Accessed 21 Mar 2019
33. Sugino Machine (2001) http://www.sugino.com. Accessed 5 Apr 2019
34. Chuetsu Pulp & Paper (2000) http://www.chuetsu-pulp.co.jp. Accessed 20 Mar 2019
35. Nippon Paper Industries (2001) https://www.nipponpapergroup.com. Accessed 7 Apr 2019
36. Oji Holdings (2019) https://www.ojiholdings.co.jp. Accessed 2 Apr 2019
37. Lee KY (2018) Nanocellulose and sustainability: production, properties, applications, and case studies. CRC Press, Florida
38. Sugino Machine (2001) http://www.sugino.com/site/biomass-nanofiber-e/what-is-waterjetprocess.html. Accessed 2 Apr 2019
39. Solala I, Volperts A, Andersone A et al (2012) Mechanoradical formation and its effects on birch kraft pulp during the preparation of nanofibrillated cellulose with Masuko refining. Holzforschung 66:477–483

40. Lehmonen J, Pere J, Hytönen E et al (2016) Effect of cellulose microfibril (CMF) addition on strength properties of middle ply of board. Cellulose 24:1041–1055
41. Lahtinen P, Liukkonen S, Pere J et al (2014) A comparative study of fibrillated fibers from different mechanical and chemical pulps. BioResources 9:2115–2127
42. Pöhler T, Lappalainen T, Temmelin T et al (2012) Influence of fibrillation method on the character of nanofibrillated cellulose (NFC). Paper presented at TAPPI international conference on nanotechnology for renewable materials, Montreal, 5–7 June 2012
43. Kargarzadeh H, Mariano M, Huang J et al (2017) Recent developments on nanocellulose reinforced polymer nanocomposites: a review. Polymer 132:368–393
44. ASICS Company (2018) https://corp.asics.com/en/press/article/2018-06-01-3. Accessed 7 Apr 2019
45. Ideas2cycles Company (2018) http://ideas2cycles.com/prototypes/nanocellulose-bicycle. Accessed 5 Apr 2019
46. The Green Science Alliance Co., Ltd (2018) https://www.nano-sakura.com/product-1?tdsourcetag=s_pcqq_aiomsg. Accessed 4 Apr 2019
47. Darker Company (2019) https://tabletennisshop.com.au/index.php?main_page=page&id=40. Accessed 6 Apr 2019
48. Dufresne A (2013) Nanocellulose: a new ageless bionanomaterial. Mater Today 16:220–227
49. Onkyo Company (2016) https://www.jp.onkyo.com/audiovisual/speaker/sc3/index.htm. Accessed 25 Mar 2019
50. Pioneer Corporation (2018) https://pioneer-headphones.com/japanese/se-monitor5. Accessed 8 Apr 2019
51. Asia NanoTech Company (2017) https://www.personalcare1.com/articles/new-whitening-cosmetics-applying-nanocellulose-technology. Accessed 5 Apr 2019
52. Koyo Kasei Co Ltd (2018) https://baraio.jp/shop. Accessed 22 Mar 2019
53. FABULA Company (2011) http://www.theeggyolks.com/2011/12/fabula-bio-fiber-nano-cellulose-mask.html. Accessed 28 Mar 2019
54. Dufresne A (2017) Nanocellulose: from nature to high performance tailored materials. Berlin/Boston, Walter de Gruyter GmbH, p 649
55. Mitsubishi Pencil Co Ltd (2010) https://www.mpuni.co.jp/products/ballpoint_pens/gel/signo_rt/307.html. Accessed 10 Apr 2019
56. Nishijima C, Sakane N, Takeuchi Y (2016) Aqueous ink composition for writing instruments. US patent 0264800A1, Sept 2016
57. Takeuchi Y, Nishijima C, Sakane N (2016) Aqueous ink composition for writing tools. EU patent 3070131A1, Sept 2016
58. Nippon Paper Industries Co Ltd (2001) https://www.nipponpapergroup.com/english/research/organize/cnf.html. Accessed 28 Mar 2019
59. Daio Paper Corp (2018) https://www.elleair.jp/products/clean/kirekira.php. Accessed 28 Mar 2019
60. New Natura Concept (2003) https://www.storaenso.com/en/products/bio-based-materials/mfc-for-packaging. Accessed 28 Mar 2019
61. Stora Enso Company (2016) https://www.storaenso.com/en/newsroom/news/2016/2/more-with-less-with-mfc. Accessed 12 Apr 2019

Chapter 12
Conclusion Remarks and Likely Future Trends

Juntao Tang and Ning Lin

Abstract Based on the previous chapters on diverse topics of nanopolysaccharides, this chapter provides a brief conclusion for each topic and proposes some challenges and trends for the future study in this field. These challenges can serve as the inspiration to drive the research on nanopolysaccharides in functional materials, and we look forward to more rich fruits in this field in the following 10 years.

Keywords Nanopolysaccharides · Potential application · Future challenges

Replacing the widespread use of petroleum-derived chemicals with sustainable and biodegradable materials are in high demand by our "green and sustainable" life pursuit. Especially when "white pollutions" has become a global threat to aquatic and marine ecosystems, characteristics such as eco-friendly and biodegradability have highlighted the importance of nanomaterials derived from bio-renewable polysaccharides. Nowadays, the market has driven the research community to make newly prepared materials into practical use, and this may associate to the functions that have potential for certain applications. The functionality of nanopolysaccharides can be well designed from a "target-motivated" approach, through which the properties are tuned and adjusted to serve a specific purpose. This monograph has covered the majority of research topics in this field that are related to functional nanopolysaccharides in a variety of applications, with specific attentions paid on the work in recent 10 years. The development of nanotechnology has intrigued the research community to explore this new "sustainable gold" by modifications and functionalizations. We also would like to emphasize that the research on the functionalization of nanopolysaccharide is at its early stage and the novel properties and value-added applications are not just

J. Tang (✉)
College of Chemistry and Chemical Engineering, Central South University, Changsha 410083, China
e-mail: reynard.tangjuntao@gmail.com

N. Lin (✉)
School of Chemistry, Chemical Engineering and Life Sciences, Wuhan University of Technology, Wuhan 430070, People's Republic of China
e-mail: ninglin@whut.edu.cn

N. Lin et al. (eds.), *Advanced Functional Materials from Nanopolysaccharides*, Springer Series in Biomaterials Science and Engineering 15,
https://doi.org/10.1007/978-981-15-0913-1_12

limited to the contents we discussed in previous 11 chapters of this monograph. Yet there are a lot of potentials for these wonderful nanomaterials, we should pay more attentions to the design principles or cost regarding the processing methods. Also the functions or applications that take fully advantages of the intrinsic properties of nanopolysaccharides should be given priority to. This is not limited to their nanosize, colloidal suspension, particle morphology, flexibility, surface charge and chemistry. Interesting topics and challenges in this field that may bring further attraction include the following aspects.

Preparation of nanopolysaccharide (Chap. 1) through mechanical disintegration or acid hydrolysis are popular and widely accepted by research community. Especially, hydrolysis with sulfuric acid for obtaining cellulose nanocrystals have been commercialized by Celluforce. However, the processing development depends on environmental and economic conditions. Simply, green and feasible candidates may be more financially attractive. Research trend on extractions have moved from finding different kinds of resources to explore the novel processing conditions and large-scale productions. Environmental-friendly and sustainable acid, ionic liquids and deep eutectic solvents are receiving increased attentions in recent reports. More importantly, we should pay special attention to the quality of the products such as specific aspect ratio, size distributions, surface properties, dispersion and etc.

Harvesting pure and mono-dispersed nanopolysaccharide has being a challenging task and interesting topic for the researchers all over the world. The functional modifications on nanopolysaccharide (Chap. 2) is a hot area that have intensively explored. Numerous modification methods such as surface hydrophobic modification, fluorescent modification and grafting of antibacterial agents have been reported and their efficiency have been well investigated. Future studies on modification methods should consider more about the possibility of industrialization. In addition, the advantages brought by the intrinsic properties of nanopolysaccharide have to be emphasized once again.

The self-assembly behavior of polysaccharide nanocrystals suspensions (Chap. 3) is a fascinating research field that attracted significant attentions. The fundamental issues related to the sensitive balance between liquid crystal formation and gelation/glass formation (influenced by the aspect ratio of nanocrystals) have yet to be fully understood. The precisely controlling over the alignment of nanocrystals, in helical or non-helical states, also deserves more investigation. Control of the helix axis orientation and the pitches using appropriated approaches have to be explored. Their photonic properties can be well tuned, which may be suitable for several applications such as lasers, security papers, sensors and chiral separations. It should be noted that many analogies can be drawn from many other liquid crystalline colloidal suspensions, such as rod-like viruses, inorganic nanoparticles or carbon nanotubes.

Although nanopolysaccharide has been well established in constructing a variety of advanced materials/devices for high-performance energy related applications (Chap. 4), there are some issues that need to be addressed in future studies. First of all, big challenges are still existed for continuous and large-scale fabrication of materials and devices for energy-related applications. Secondly, in order to meet the

requirement for conductivity, high-temperature treatments are commonly incorporated. In-deep understanding is a blank area that have to be explored. We suggested that careful attention should be paid to the pyrolysis processes of nanopolysaccharide as the evolution in elemental composition and morphology is critical for evaluating their subsequent performance. Nanopolysaccharide are not just a class of organic source for carbon materials. Through careful design and regulations, specific nanostructures, tailorable atom-scale compositions and tunable physicochemical properties can be obtained. Thus the functions affected by all of the above can be controlled and optimized. Last, insight into the structure-function relationship should be gained and empirical conclusions should be drawn, which is of significant importance to guide the design principles.

Research focus on the biomedical applications of nanopolysaccharide (Chap. 5) seems to be a downward trend in the latest 5 years. It is generally accepted that biocompatibility and biodegradability are unique properties for nanoparticles that derived from sustainable resources. However, reliable in vivo and toxicity studies should be performed to pave the way for greater acceptance as commercially available materials in this specific applications. Special attentions can be paid on creating targeted and controlled properties, understanding the mechanisms for cell and nanopolysaccharide interactions as well as developing commercial available formulations. Other considerations such as covalent attaching with biologically active ligand molecules for specific applications can also be examined. In addition, the accumulation and interaction of nanopolysaccharides with the immune system in the cells, organs and blood vessels is a critical factor affecting their future application in biomedical materials, for instance.

The use of pristine or modified nanopolysaccharides as Pickering stabilizers (Chap. 6) are emerging applications in recent years. The vast development has promoted the researchers to gain deep understanding towards adsorption and desorption behaviors and mechanisms at the interface. Also it is necessary to standardize the measurement protocols towards the quantification of emulsion stability. The combination of stimuli-responsive properties with emulsions can also be considered as it is particularly advantageous for improving the degree of precise control over a given system. Although the applications brought from the emulsions, such as polymerizations, encapsulations and biomedical sectors offer promising potentials for industrialization, efforts in finding ways to reduce the costs and save energy is in highly demand.

The specific surface area and nanosize of nanopolysaccharides make them ideal materials in environmental applications (Chap. 7). The surface area provide abundant adsorption sites and the versatile surface chemistries offer diversify modifications in wastewater/gas adsorptions treatment. However, to reiterate, recovery of such nanomaterials would be problematic in practical use. Integrating those materials into membranes or devices will be more promising in scalable chemical engineering processes. Also great efforts should be spared on reducing the cost of production and tuning the surface functionalities when comparing to other non-sustainable alternatives.

The study on the application of nanopolysaccharide for coating (Chap. 8) may focus on finding feasible universal methods for preparing the formulations. Precise characterization and systematic understanding for the interactions between substrate and coating materials should be included in future investigations. The adhesion forces, matching and mechanisms between nanopolysaccharides-based coatings and diverse substrates are the critical factors of this topic, which deserves an in-depth study for the practical applications.

Extensive report or studies have focus on the use of nanopolysaccharides to enhance the barrier properties of a wide range of polymer matrix materials (Chap. 9). The ultimate purpose of this part is to slow down or essentially eliminate the progress of oxygen, water vapor, or other molecules, thereby extending the shelf life of products. One of the most difficult issues to address is the compatibility between different mixing phases. Thus novel modification methods and processing strategies should be adopted to achieve better performance. Also it should be noted that nanostarch can be prepared under less harsh conditions, and particles related to chitin might possibly be preferred when one of the goals is to achieve antimicrobial effects.

When come to the applications as additives (Chap. 10), great achievements have been made in food, construction, cosmetics, pharmaceuticals, paper and other fields. Yet there are several critical concerns including the cost and feasibility towards commercialization. As cellulose is the most abundant resource in the world, their derived materials including cellulose nanocrystals and cellulose nanofibrils may considered to have the highest possibility to commercialize. However, when comparing to starch nanoparticles, their cost is an obstacle that have to minimize in order to go forward. Nanomaterials derived from chitin contain certain functional groups, which might be possible for specific applications, for example, antimicrobial formulations.

Overall, research on nanopolysaccharide has motivated the forestry and agriculture industry to reconsider the pre-competitive technologies to secure a respectable return-on-investment and healthy growth. Developing such functional materials based on nanopolysaccharide could find enhanced applications in a multitude of fields. In addition, evolutionary nanotechnology processes to manufacture new high value-added products of superior performance hold significant promise of reviving the forestry industry. However, we have to keep searching for more efficient methods for process optimization and commercialization and scalable synthetic protocols for modifications. We believe that the products are extremely essential for addressing two critical issues confronting our world, namely energy and the environment.